



Transient Modelling of Heat Pipe Heat Exchangers with Vertical Thermosyphons for the Purpose of Waste Heat Recovery from Industrial Exhaust Gases

Daniel J. Brough

A submission presented in fulfilment of the requirements of
Brunel University London
for the degree of Doctor of Philosophy

January 2022

ABSTRACT

Heat Pipe Heat Exchangers (HPHEs) can be effectively installed within challenging waste heat streams where traditional heat exchangers fail or the heat from the stream is deemed 'unrecoverable'. Waste heat recovery using HPHEs in energy intensive industries can enhance energy efficiency, decrease fuel consumption and reduce emissions. Traditional methods of predicting HPHE performance rely on steady state or averaged input values, although the majority of process streams have fluctuating characteristics and, as such, it is important to determine the transient performance of a heat exchanger. The software, TRNSYS, has been used to achieve this capability for multiple configurations by creating a dedicated simulation component with personally developed internal coding. This component has been validated against two full-scale industrial units and a laboratory-scale unit, all of which have been installed and tested over the lifetime of this PhD programme. Alongside this work, a steady state model developed in MATLAB has been produced. The models can predict heat source and sink outlet temperatures, heat transfer rate, the conductance value and the pressure drop of the fluids across the heat exchanger.

The end use for the recovered waste heat is a site-specific decision and there may not be the capacity in one process to reintroduce all of the recovered heat. Consequently, HPHEs have been developed with various heat sink fluids or even to function with multiple streams in one system to fully utilise the waste heat across a site. The TRNSYS component was not created just for the validation of the experimental installations tested, but to be as useful and versatile as possible to the wider scientific community; to scale to any size of architecture design required for the quantity of energy recoverable, with the potential to simulate exhaust inlet gases across a wide range of temperatures and flow rates and with the ability to perform calculations on heat pipes that are finned or unfinned (smooth). The development of this simulation methodology aids visualising energy recovery transiently and can use real collected data as inputs, allowing specific examples to be tested and evaluated. This aids the design process and provides increased confidence in the expected performance prior to installation, as well as assessing the applications for the energy content recovered.

When comparing the temperature outlets between simulation predictions and experimental results, for the ceramic kiln exhaust-to-air full-scale unit, the component achieved an average accuracy of +3.76% for the exhaust and +1.30% for the air. In other words, the outlet

temperatures were higher for the simulation than for the experiment. For the aluminium furnace exhaust-to-air finned full-scale demonstration, an average simulated outlet temperature accuracy of +10.17% for the exhaust and +3.55% for the air was achieved. In this case, thermal losses had a larger influence due to higher temperature inlets, which reduced the experimental outlet temperatures. The laboratory-scale exhaust-to-water unit achieved an average accuracy of +0.67% for the exhaust with a spread of $\pm 6\%$, and +2.97% average accuracy with a spread of -8 to +9% for the water condenser section, more than sufficient for engineering applications. This experimental validation has ensured that the TRNSYS component can now be used confidently in overall system simulations.

Keywords: Waste Heat Recovery; Heat Pipe Heat Exchangers; Thermosyphons; Transient Modelling; TRNSYS.

DECLARATION

No part of this thesis has been submitted in support of an application for any degree or qualification of Brunel University London or any other University or Institute of learning.

AUTOBIOGRAPHY

The Author graduated in Natural Sciences from University College London in 2015 and has subsequently worked as the Site Engineer for a secondary aluminium smelter. Since 2019, he has been a Project Manager and Doctoral Researcher at the College of Engineering, Design and Physical Sciences at Brunel University London working on the topics of heat pipe-based heat exchangers and waste heat recovery as part of the Heat Pipe and Thermal Management Group.

During his studies, he was the Industrial Liaison Officer for the Greater London Region Northwest Institute of Mechanical Engineers. Additionally, he was the Brunel contact for both the ETEKINA and SMARTREC EU funded Horizon 2020 projects.

ACKNOWLEDGMENTS

The author acknowledges with sincere gratitude and appreciation Prof. Hussam Jouhara. Without the perseverance over multiple attempts to convince me to undertake a PhD programme, I would not have been exposed to the fascinating topics of thermodynamics and heat pipe heat exchangers. The lessons learnt and mindset taught throughout will be invaluable.

Special thanks go to Mr. Miles Brough at JBM International Ltd. for persuading me to broaden my horizons by pursuing the programme as well as the support given throughout.

Appreciation goes to:

Dr. Helen Brough for building the foundations allowing me to pursue this dream and her unwavering support.

Dr. Bertrand Delpech for being a fantastic and thought-provoking housemate and colleague, as well as teaching me 3D drawing.

Dr. Sulaiman Almahmoud for providing assistance with reviewing the coding process as well as being a brilliant fountain of fundamental thermodynamic knowledge.

Miss Jenny Sheppard for the love and understanding whilst working away from home.

All the talented and dedicated Brunel team members for their support and the fun that makes it all worthwhile, in particular, Mrs. Lujean Ahmad, Mr. Valentin Guichet and Dr. Amisha Chauhan.

Finally, the entire ETEKINA and SMARTREC consortiums, for tackling head on and overcoming all the hurdles that emerged throughout the projects and ensuring successful project completions on all sites.

PUBLICATIONS

[1] **Brough D**, Jouhara, H. The Aluminium Industry: A Review on State-of-the-Art Technologies, Environmental Impacts and Possibilities for Waste Heat Recovery. **International Journal of Thermofluids**, Volumes 1-2, February 2020. <https://doi.org/10.1016/j.ijft.2019.100007>

[2] **Brough D**, Mezquita A, Ferrer S, Segarra S, Chauhan A, Almahmoud S, Khordehgah N, Ahmad L, Middleton D, Sewell H. Isaac, Jouhara H. An Experimental Study and Computational Validation of Waste Heat Recovery from a Lab Scale Ceramic Kiln Using a Vertical Multi-Pass Heat Pipe Heat Exchanger. **Energy**, Volume 208, October 2020. <https://doi.org/10.1016/j.energy.2020.118325>

[3] **Brough D**, Ramos J, Delpech B, Jouhara H. Development and Validation of a TRNSYS Type to Simulate Heat Pipe Heat Exchangers in Transient Applications of Waste Heat Recovery. **International Journal of Thermofluids**, Volume 9, February 2021. <https://doi.org/10.1016/j.ijft.2020.100056>

[4] Jouhara H, Almahmoud S, **Brough D**, Guichet V, Delpech B, Chauhan A, Ahmad L, Serey N. Experimental and Theoretical Investigation of the performance of an Air to Water Multi-Pass. Heat Pipe-Based Heat Exchanger. **Energy**, Volume 219, March 2021. <https://doi.org/10.1016/j.energy.2020.119624>

[5] Venturelli M, **Brough D**, Milani M, Montorsi L, Jouhara H. Comprehensive Numerical Model for the Analysis of Potential Heat Recovery Solutions in a Ceramic Industry. **International Journal of Thermofluids**, Volume 10, May 2021. <https://doi.org/10.1016/j.ijft.2021.100080>

LIST OF FIGURES

<i>Figure 1: Graph showing the number of articles containing “Waste heat recovery” and “Waste Heat” on ScienceDirect.....</i>	<i>5</i>
<i>Figure 2: Graph showing the potential energy savings by subsector in the UK [15].....</i>	<i>8</i>
<i>Figure 3: Graph showing potential emissions savings by reusing surplus generated heat by technology [15].</i>	<i>8</i>
<i>Figure 4: Graph showing the percentage fuel reduction by using preheated combustion air [17].....</i>	<i>10</i>
<i>Figure 5: Photograph of an aluminium sow preheater using exhaust gases [24].....</i>	<i>12</i>
<i>Figure 6: Schematic of a thermosyphon (A) in comparison to a wicked heat pipe (B) [40].</i>	<i>15</i>
<i>Figure 7: Schematic of mesh, powder and grooved wick designs [49].....</i>	<i>17</i>
<i>Figure 8: Schematic showing a selection of heat pipe wick structures [40].</i>	<i>18</i>
<i>Figure 9: Graph showing the useful working temperature range for heat pipes depending on working fluid, adapted from [52]. At normal pressure and temperature: light grey- gaseous, grey – liquid, black – solid.</i>	<i>19</i>
<i>Figure 10: A generic phase diagram.</i>	<i>20</i>
<i>Figure 11: Graph showing figure of merit curves for common working fluids in a thermosyphon [57].</i>	<i>22</i>
<i>Figure 12: Heat pipe interaction between zones. Table remade from [45].</i>	<i>28</i>
<i>Figure 13: A graph showing the various heat pipe limitations [40].</i>	<i>33</i>
<i>Figure 14: 2D slice of parallel and counterflow HPHE configurations with fluid temperature profiles.</i>	<i>34</i>
<i>Figure 15: Photograph of a counterflow HPHE for an aluminium furnace [39].....</i>	<i>40</i>
<i>Figure 16: 3D drawing of a multi-sink, water and combustion air HPHE.</i>	<i>41</i>
<i>Figure 17: Photograph of an exhaust-to-coke gas HPHE unit [39].</i>	<i>42</i>
<i>Figure 18: Photograph of a pressurised HPHE for recovering energy from a ceramic roller kiln.</i>	<i>43</i>
<i>Figure 19: Photograph of an exhaust-to-thermal oil HPHE tied to an ORC cycle [98].....</i>	<i>44</i>
<i>Figure 20: Photograph of a HPHE used to cleanly dry mate tea leaves.</i>	<i>45</i>
<i>Figure 21: Graphs showing heat transfer rate and temperature comparisons between the conductance model and ϵ-NTU method for experimental and simulated results [134].</i>	<i>53</i>
<i>Figure 22: Schematic and photograph of water-in-glass evacuated tube solar water heater.</i>	<i>54</i>
<i>Figure 23: Schematic of crossflow flow patterns for fluids passing across a cylinder with increasing Reynolds number, adapted from [143].....</i>	<i>58</i>
<i>Figure 24: Photographs of in-line tube bundle flow patterns [143].....</i>	<i>62</i>
<i>Figure 25: Photographs of staggered arrangement tube bundle flow patterns [143].....</i>	<i>62</i>
<i>Figure 26: Schematic of in-line tube bundle arrangement.</i>	<i>63</i>
<i>Figure 27: Schematic of staggered tube bundle arrangement.</i>	<i>64</i>
<i>Figure 28: Schematic showing the overall thermal resistances of a thermosyphon, adapted from [59].</i>	<i>68</i>
<i>Figure 29: Schematic showing the thermal resistances of a thermosyphon. Adapted from [59], to include further axial and external resistances.</i>	<i>68</i>
<i>Figure 30: Schematic showing simplified thermal resistances for a thermosyphon.</i>	<i>71</i>

Figure 31: Schematic of thermosyphon cross-sectional dimensions with the converging nature of heat in the wall.....	72
Figure 32: Schematic of the resistances in HPHEs with (a) and without (b) adiabatic sections [67].....	76
Figure 33: Schematic of thermosyphon resistances to include those through a separation plate.	76
Figure 34: Schematic of a thermal resistance network diagram for a HPHE.....	79
Figure 35: Illustration to show the treatment of a thermosyphon as a liquid-coupled indirect-transfer-type heat exchanger.	84
Figure 36: Graph showing the k_{Nr} correction factor for staggered tube bundles, data extracted from [168].	97
Figure 37: Graph showing the k_{Nr} correction factor for in-line tube bundles, data extracted from [168].	98
Figure 38: Graph showing heat flux against temperature difference for the case of water boiling at atmospheric pressure, adapted from [126].	99
Figure 39: 3D drawings of available finning options.	106
Figure 40: Diagram of helical finning with symbols.....	107
Figure 41: Graph showing the thermal conductivity of carbon steel against temperature.....	109
Figure 42: Graph used to find X and f values for in-line unfinned tube bundles [143].	112
Figure 43: Graph used to find X and f values for staggered unfinned tube bundles [143].	113
Figure 44: Flowchart of the TRNSYS code logic.	115
Figure 45: Experiment 1 laboratory-scale kiln photograph.....	118
Figure 46: Diagram of the laboratory-scale kiln.....	118
Figure 47: Experiment 1 HPHE photograph.....	119
Figure 48: Experiment 1 HPHE general arrangement, showing thermosyphons and design parameters.....	121
Figure 49: Experiment 1 HPHE side elevations with external dimensions and flange detail.	122
Figure 50: Experiment 1 detail of separation plate and thermosyphon spacing.	123
Figure 51: Experiment 1 thermosyphon detail.	124
Figure 52: Experiment 1 P&ID of the installed system.	125
Figure 53: Experiment 1 labelled photographs of HPHE and location.	126
Figure 54: Diagram of a continuous roller kiln [2].	128
Figure 55: Experiment 2 installed HPHE photograph.....	129
Figure 56: Experiment 2 general arrangement of the HPHE and design parameters.	131
Figure 57: Experiment 2 HPHE dimensions and side elevations.	132
Figure 58: Experiment 2 detail of separation plate and thermosyphon arrangement.....	133
Figure 59: Experiment 2 detail of thermosyphon and finning.	134
Figure 60: Experiment 2 P&ID of the installed system.	135
Figure 61: Experiment 3 photograph of HPHE during installation.....	137
Figure 62: Experiment 3 photograph of finned thermosyphons in condenser and evaporator sections.	137
Figure 63: Experiment 3 HPHE general arrangement and design parameters.....	139
Figure 64: Experiment 3 HPHE dimensions and side elevations.	140
Figure 65: Experiment 3 detail of separation plate and spacing.	141

Figure 66: Experiment 3 detail of separation plate and thermosyphon type location.....	142
Figure 67: Experiment 3 detail of Dowtherm A thermosyphon.....	143
Figure 68: Experiment 3 detail of distilled water thermosyphon.....	144
Figure 69: Experiment 3 3D of installation [214].....	145
Figure 70: Schematic of heat paths during HPHE operation. SOL being the solution furnace and ENV the ageing furnace [214].....	146
Figure 71: Experiment 3 P&ID of system installation [214].....	147
Figure 72: A view of the standard TRNSYS component library and the location of the newly developed HPHE components.	150
Figure 73: Flowchart of the TRNSYS component coding process.....	151
Figure 74: Icons of Parallel Studio XE 2019 and Visual Studio 2019.	152
Figure 75: Code starting the subroutine for Type204.	160
Figure 76: Code to call external TRNSYS constants and functions.....	160
Figure 77: Code for exporting Type204 to an external DLL.	160
Figure 78: Code to declare all variables that Type204 uses throughout the subroutine.....	167
Figure 79: Code to set global simulation variables.....	167
Figure 80: Code to set version of component to TRNSYS 17.....	168
Figure 81: Code for last call manipulations.....	168
Figure 82: Code for end of timestep manipulations.....	168
Figure 83: Code to set the total number of parameters, inputs, derivatives, outputs, number of stored variables, number of discrete controls and the iteration mode.	169
Figure 84: Code to provide input and output values their unit type.	169
Figure 85: Code to fetch initial values for all parameters given by user.	170
Figure 86: TRNSYS pop-up message example if parameter errors are found during the simulation.	170
Figure 87: Code to provide error notification if parameters are outside correct ranges for calculations to function.....	172
Figure 88: Example of error messages when simulation is run with out-of-range parameters.....	172
Figure 89: Code to set initial values of outputs.	173
Figure 90: Code to allow multiple Type204 components to function in a simulation independently.	173
Figure 91: Code to set initial input values and the value used for pi.	174
Figure 92: Code to provide an error notification if out of range inputs are entered.....	174
Figure 93: Code for the equations that dictate outlet values.....	174
Figure 94: Code to set output values.	175
Figure 95: Code to return control to kernel and end the subroutine for Type204.	175
Figure 96: Flowchart for the process of compiling a component into a *.dll file to be used in TRNSYS.	176
Figure 97: View of Solution Explorer tab for Type204.....	177
Figure 98: Property page for MyDll where properties are configured for 'All configurations', 'Debug' and 'Release' according to Table 26.....	177

<i>Figure 99: Schematic of Type204 HPHE created in Microsoft PowerPoint.....</i>	<i>179</i>
<i>Figure 100: View of 'General' tab for HPHE component in Simulation Studio.....</i>	<i>180</i>
<i>Figure 101: View of Type204 component 'Parameter' tab in Simulation Studio.....</i>	<i>180</i>
<i>Figure 102: View of Type204 component 'Input' tab in Simulation Studio.....</i>	<i>181</i>
<i>Figure 103: View of Type204 component 'Output' tab in Simulation Studio.....</i>	<i>181</i>
<i>Figure 104: Model for Experiments 1 and 2.....</i>	<i>182</i>
<i>Figure 105: Connection between HPHE and Temperatures online graphical plotter.....</i>	<i>183</i>
<i>Figure 106: Model for Experiment 3.....</i>	<i>183</i>
<i>Figure 107: TRNSYS temperature output results for test 1.....</i>	<i>187</i>
<i>Figure 108: Transient results of test 1 showing the experimental and simulated inlet and outlet temperatures of water and exhaust streams.....</i>	<i>188</i>
<i>Figure 109: Heat transfer rate comparison for test 1 exhaust, water and simulation.....</i>	<i>190</i>
<i>Figure 110: Heat transfer rate comparison for test 1 experimental against simulation results.....</i>	<i>191</i>
<i>Figure 111: Transient results of test 2 showing the experimental and simulated inlet and outlet temperatures of water and exhaust streams.....</i>	<i>192</i>
<i>Figure 112: Heat transfer rate comparison for test 2 exhaust, water and simulation.....</i>	<i>194</i>
<i>Figure 113: Heat transfer rate comparison for test 2 experimental against simulation results.....</i>	<i>195</i>
<i>Figure 114: Transient results of test 3 showing the experimental and simulated inlet and outlet temperatures of water and exhaust streams.....</i>	<i>196</i>
<i>Figure 115: Heat transfer rate comparison for test 3 exhaust, water and simulation.....</i>	<i>197</i>
<i>Figure 116: Heat transfer rate comparison for test 3 experimental exhaust and simulation results.....</i>	<i>198</i>
<i>Figure 117: Transient results of test 4 showing the experimental and simulated inlet and outlet temperatures of water and exhaust streams.....</i>	<i>199</i>
<i>Figure 118: Heat transfer rate comparison for test 4 exhaust, water and simulation.....</i>	<i>201</i>
<i>Figure 119: Heat transfer rate comparison for test 4 experimental against simulation results.....</i>	<i>202</i>
<i>Figure 120: Transient results of test 5 showing the experimental and simulated inlet and outlet temperatures of water and exhaust streams.....</i>	<i>203</i>
<i>Figure 121: Heat transfer rate comparison for test 5 exhaust, water and simulation.....</i>	<i>205</i>
<i>Figure 122: Heat transfer rate comparison for test 5 experimental against simulation results.....</i>	<i>206</i>
<i>Figure 123: Transient results of test 6 showing the experimental and simulated inlet and outlet temperatures of water and exhaust streams.....</i>	<i>207</i>
<i>Figure 124: Heat transfer rate comparison for test 6 exhaust, water and simulation.....</i>	<i>209</i>
<i>Figure 125: Heat transfer rate comparison for test 6 experimental against simulation results.....</i>	<i>210</i>
<i>Figure 126: Transient results of test 7 showing the experimental and simulated inlet and outlet temperatures of water and exhaust streams.....</i>	<i>211</i>
<i>Figure 127: Heat transfer rate comparison for test 7 exhaust, water and simulation.....</i>	<i>213</i>
<i>Figure 128: Heat transfer rate comparison for test 7 experimental against simulation results.....</i>	<i>214</i>

<i>Figure 129: Transient results of test 8 showing the experimental and simulated inlet and outlet temperatures of water and exhaust streams.....</i>	<i>215</i>
<i>Figure 130: Heat transfer rate comparison for test 8 exhaust, water and simulation.....</i>	<i>216</i>
<i>Figure 131: Heat transfer rate comparison for test 8 experimental against simulation results.....</i>	<i>217</i>
<i>Figure 132: Transient results of test 9 showing the experimental and simulated inlet and outlet temperatures of water and exhaust streams.....</i>	<i>218</i>
<i>Figure 133: Heat transfer rate comparison for test 9 exhaust, water and simulation.....</i>	<i>219</i>
<i>Figure 134: Heat transfer rate comparison for test 9 experimental against simulation results.....</i>	<i>220</i>
<i>Figure 135: Pressure drop TRNSYS simulation output for test 9.....</i>	<i>221</i>
<i>Figure 136: TRNSYS graph outputs for heat transfer rate and conductance for each test.....</i>	<i>224</i>
<i>Figure 137: Experiment 1 heat transfer rate percentage difference between experiment and simulation.</i>	<i>226</i>
<i>Figure 138: Experiment 1 difference in temperature error between experiment and simulation outlet results.</i>	<i>227</i>
<i>Figure 139: Experiment 2 TRNSYS temperature output results.</i>	<i>234</i>
<i>Figure 140: Experiment 2 transient results showing the experimental and simulated inlet and outlet temperatures of water and exhaust streams.....</i>	<i>235</i>
<i>Figure 141: Experiment 2 heat transfer rate comparison for experimental and simulation results.</i>	<i>236</i>
<i>Figure 142: Experiment 2 mass flow rate measurements of exhaust gases and air.....</i>	<i>237</i>
<i>Figure 143: Experiment 2 heat transfer rate comparison for experimental against simulation results.....</i>	<i>238</i>
<i>Figure 144: Experiment 2 heat transfer rate percentage difference between experimental and simulation results.....</i>	<i>239</i>
<i>Figure 145: Experiment 2 percentage difference in outlet temperature error between experimental and simulation exhaust outlet results.</i>	<i>240</i>
<i>Figure 146: Experiment 2 percentage difference in outlet temperature error between experimental and simulation air outlet results.</i>	<i>240</i>
<i>Figure 147: Experiment 3 TRNSYS temperature output results.....</i>	<i>246</i>
<i>Figure 148: Experiment 3 transient results showing the experimental and simulated inlet and outlet temperatures of exhaust and air streams.....</i>	<i>247</i>
<i>Figure 149: Experiment 3 heat transfer rate comparison for experimental and simulation results.</i>	<i>250</i>
<i>Figure 150: Experiment 3 mass flow rate measurements of exhaust gases and air.....</i>	<i>251</i>
<i>Figure 151: Experiment 3 heat transfer rate comparison for experimental against simulation results.....</i>	<i>253</i>
<i>Figure 152: Experiment 3 heat transfer rate percentage difference between experimental and simulation results.....</i>	<i>254</i>
<i>Figure 153: Experiment 3 difference in temperature error between experimental and simulation exhaust outlet results.....</i>	<i>255</i>
<i>Figure 154: Experiment 3 air temperature difference error between experimental and simulation results.</i>	<i>255</i>
<i>Figure 155: Experiment 3 simulation pressure drop TRNSYS output.</i>	<i>259</i>
<i>Figure 156: Experiment 3 evaporator and condenser pressure drop measurements.</i>	<i>260</i>
<i>Figure 157: The prompt box that appears to enter the parameters in MATLAB.....</i>	<i>283</i>

<i>Figure 158: Density of exhaust gases against temperature.</i>	<i>374</i>
<i>Figure 159: Kinematic viscosity of exhaust gases against temperature.</i>	<i>375</i>
<i>Figure 160: Thermal conductivity of exhaust gases against temperature.</i>	<i>376</i>
<i>Figure 161: Specific heat capacity of exhaust gases against temperature.</i>	<i>377</i>
<i>Figure 162: Density of air against temperature.</i>	<i>379</i>
<i>Figure 163: Kinematic viscosity of air against temperature.</i>	<i>380</i>
<i>Figure 164: Thermal conductivity of air against temperature.</i>	<i>381</i>
<i>Figure 165: Specific heat capacity of air against temperature.</i>	<i>382</i>
<i>Figure 166: Density of water against temperature.</i>	<i>384</i>
<i>Figure 167: Kinematic viscosity of water against temperature.</i>	<i>385</i>
<i>Figure 168: Thermal conductivity of water against temperature.</i>	<i>386</i>
<i>Figure 169: Specific heat capacity of water against temperature.</i>	<i>387</i>
<i>Figure 170: Density of thermal oil against temperature.</i>	<i>390</i>
<i>Figure 171: Kinematic viscosity of thermal oil against temperature.</i>	<i>391</i>
<i>Figure 172: Thermal conductivity of thermal oil against temperature.</i>	<i>392</i>
<i>Figure 173: Specific heat capacity of thermal oil against temperature.</i>	<i>393</i>
<i>Figure 174: External dimensions of Experiment 3 HPHE.</i>	<i>394</i>

LIST OF TABLES

<i>Table 1: Available WHR technologies and their applicable temperature ranges [1].</i>	7
<i>Table 2: Percentage furnace efficiency improvement by preheating combustion air, adapted from [16].</i>	10
<i>Table 3: Working fluid and casing material compatibility, adapted from [46].</i>	25
<i>Table 4: Heat pipe components and their effect on its properties. Adapted from [42].</i>	27
<i>Table 5: Summary of advantages and disadvantages of HPHEs over traditional technologies.</i>	35
<i>Table 6: Further applications of heat pipe technology.</i>	39
<i>Table 7: Resistances and descriptions for Figure 29.</i>	69
<i>Table 8: Temperatures and descriptions for Figure 29.</i>	69
<i>Table 9: Thermosyphon maximum heat flux correlations [40].</i>	89
<i>Table 10: Available correlations for calculation of Nusselt numbers over unfinned tube bundles.</i>	92
<i>Table 11: Correction factor for Žukauskas correlations [166] with less than 16 rows of tubes [125].</i>	95
<i>Table 12: Available correlations for calculation of Nusselt numbers over finned tube bundles.</i>	95
<i>Table 13: Available correlations for calculation of heat transfer coefficient of pool boiling.</i>	100
<i>Table 14: Correlations for calculating heat transfer coefficient of falling film boiling [57].</i>	102
<i>Table 15: Available correlations for calculation of heat transfer coefficient of film condensation.</i>	103
<i>Table 16: Pressure drop equations for finned and unfinned banks of tubes.</i>	110
<i>Table 17: Cz correction factor for number of rows less than 5.</i>	111
<i>Table 18: Available correlations for calculation of Euler numbers over staggered tube bundles [143].</i>	114
<i>Table 19: Experiment 1 parameters, sensors and installation location.</i>	126
<i>Table 20: Experiment 1 test conditions.</i>	127
<i>Table 21: Experiment 2 parameters, sensors and installation location.</i>	136
<i>Table 22: Instrumentation used for Experiment 3.</i>	148
<i>Table 23: Inputs for HPHE TRNSYS component.</i>	152
<i>Table 24: Parameters for HPHE TRNSYS component.</i>	153
<i>Table 25: Internal calculated values within HPHE component.</i>	154
<i>Table 26: TRNDll settings required to be changed.</i>	178
<i>Table 27: Components and types used in the simulations.</i>	184
<i>Table 28: Test 1 average results summary.</i>	189
<i>Table 29: Test 2 average results summary.</i>	193
<i>Table 30: Test 3 average results summary.</i>	196
<i>Table 31: Test 4 average results summary.</i>	200
<i>Table 32: Test 5 average results summary.</i>	204
<i>Table 33: Test 6 average results summary.</i>	208
<i>Table 34: Test 7 average results summary.</i>	212
<i>Table 35: Test 8 average results summary.</i>	216

<i>Table 36: Test 9 average results summary.....</i>	<i>218</i>
<i>Table 37: Spearman correlation analysis for experimental exhaust heat transfer rate.....</i>	<i>228</i>
<i>Table 38: Collinearity tolerance for Experiment 1 variables.....</i>	<i>229</i>
<i>Table 39: Spearman correlation analysis for experimental water heat transfer rate.....</i>	<i>231</i>
<i>Table 40: Spearman correlation analysis for experimental exhaust heat transfer rate.....</i>	<i>241</i>
<i>Table 41: Spearman correlation analysis for experimental exhaust heat transfer rate.....</i>	<i>243</i>
<i>Table 42: Spearman correlation analysis for experimental exhaust heat transfer rate.....</i>	<i>256</i>
<i>Table 43: Spearman correlation analysis for experimental exhaust heat transfer rate.....</i>	<i>257</i>
<i>Table 44: Thermophysical properties of exhaust gases from natural gas combustion [216].</i>	<i>373</i>
<i>Table 45: Thermophysical properties of air [217].....</i>	<i>378</i>
<i>Table 46: Thermophysical properties of water [218].....</i>	<i>383</i>
<i>Table 47: Thermophysical properties of therminol-66 oil [219].</i>	<i>388</i>

NOMENCLATURE

Acronym	Description	
CFD	Computational Fluid Dynamics	
dll	Dynamic Link Library	
EIIs	Energy Intensive Industries	
EU	European Union	
GAHPHE	Gravity-Assisted Heat Pipe Heat Exchanger	
GHG	Greenhouse Gases	
HPHE	Heat Pipe Heat Exchanger	
HPTAM	Heat Pipe Transient Analysis Model	
HTC	Heat Transfer Coefficient	
HVAC	Heating, Ventilation and Air Conditioning	
LMTD	Logarithmic Mean Temperature Difference	
NTU	Number of Transfer Units	
ORC	Organic Rankine Cycle	
P&ID	Pipework and Instrumentation Diagram	
PAH	Polycyclic Aromatic Hydrocarbon	
ROI	Return On Investment	
THROUGHPUT	Thermal Hydraulic Response of Heat Pipes Under Transients	
TRNSYS	Transient System Simulation	
UK	United Kingdom	
WHR	Waste Heat Recovery	
Symbol	Description	Unit
A	Area	m^2
Bo	Bond number	Dimensionless
c_p	Specific heat capacity	$J.kg^{-1}.K^{-1}$
C	Heat capacity or Constant used in Ku or condensation correlations	$J.s^{-1}.K^{-1}$ Dimensionless
D	Diameter	m
e	Thickness	m
Eu	Euler number	Dimensionless

f	Friction factor	Dimensionless
\hat{f}	Modified friction factor	Dimensionless
g	Gravitational acceleration	m.s^{-2}
g_c	Proportionality constant	Dimensionless
G	Average core mass velocity	$\text{kg.m}^{-2}.\text{s}^{-1}$
Gr	Grashof number	Dimensionless
h	Heat transfer coefficient	$\text{W.m}^{-2}.\text{K}^{-1}$
H	Width or Enthalpy	m J
j	Colburn factor	Dimensionless
Ja	Jakob number	Dimensionless
K	Nusselt constants	Dimensionless
Ku	Kutateladze number	Dimensionless
n	Number of	Dimensionless
Nu	Nusselt number	Dimensionless
L	Length	m
L_b	Bubble scale length	m
M	Molecular weight	kg.kmol^{-1}
\dot{m}	Mass flow rate	kg.s^{-1}
h_{fg}	Latent heat	J.kg^{-1}
P	Pressure	Pa
Pr	Prandtl number	Dimensionless
P^*	Reduced pressure	Dimensionless
\dot{q}	Heat transfer rate	$\text{W (J.s}^{-1})$
q''	Heat flux	W.m^{-2}
R	Thermal resistance	K.W^{-1}
$R_{a,p}$	Average roughness parameter	m
R_g	Specific gas constant	$\text{J.kg}^{-1}.\text{K}^{-1}$
Re	Reynolds number	Dimensionless
S_T	Distance	m
T	Temperature	$\text{K or } ^\circ\text{C}$
U	Overall heat transfer coefficient	$\text{W.m}^{-2}.\text{K}^{-1}$

u	Flow velocity	m.s^{-1}
u	Tangential velocity	m.s^{-1}
v	Normal velocity	m.s^{-1}
V	Volume	m^3

Greek Symbol	Description	Unit
α , alpha	Accommodation coefficient or Thermal diffusivity	Dimensionless $\text{m}^2.\text{s}^{-1}$
β , beta	Coefficient of thermal expansion	K^{-1}
γ , gamma	Ratio of total surface area with fins to the surface area without fins	Dimensionless
δ , delta	Distance	m
ε , epsilon	Effectiveness or Emissivity	Dimensionless
η , eta	Efficiency	Dimensionless
θ , theta	Inclination	°
λ , lambda	Thermal conductivity	$\text{W.m}^{-1}.\text{K}^{-1}$
μ , mu	Dynamic viscosity	$\text{N.m}^{-2}.\text{s}$ or $\text{kg.m}^{-1}.\text{s}^{-1}$
ν , nu	Kinematic viscosity (momentum diffusivity)	$\text{m}^2.\text{s}^{-1}$
π , pi	Pi constant	Dimensionless
ξ , xi	Wick permeability	m^2
ρ , rho	Density	kg.m^{-3}
σ , sigma	Surface tension	N.m^{-1}
τ , tau	$1 - T_{red}$	
φ , phi	Angle from horizontal	°
χ , chi	Variable for maximum heat flux or Term for pressure drop calculations	Dimensionless
ω , omega	Pitzer acentric factor	Dimensionless
Γ , Gamma	Mass flow rate per unit periphery	$\text{kg.m}^{-1}.\text{s}^{-1}$
Δ , Delta	Difference	Dimensionless
Z , Zeta	Heat exchanger axial length	m
Υ , Upsilon	Pitch	m
Φ , Phi	Figure of merit	W.m^{-2}

X, Chi	Correction factor for pressure drop	Dimensionless
Ψ , Psi	Liquid film thickness scale	m

Subscript	Description
0	Standard conditions
a	Adiabatic
act	Actual
arr	Arrangement
atm	Atmospheric
ax	Axial
b	Boiling
c	Condenser
ch	Characteristic
cd	Condensation
cond	Conduction
conv	Convection
crit	Critical
cs	Cross-sectional
D	Relating to diameter
e	Evaporator
eff	Effective
ex	External or Exhaust
f	Film
fb	Film boiling
ff	Free flow
fin	Fin
fc	Forced convection
Fr	Frontal
H	Hydraulic
hl	Helical
i	Internal or inner
in	Inlet
inter	Interfacial

l	Liquid
L	Longitudinal
LM	Logarithmic mean
‘L	Diagonal between longitudinal centres
m	Mean
max	Maximum
min	Minimum
n	Relating to a row
nuc	Nucleation site
o	Outer
out	Outlet
p	Pool
pb	Pool boiling
r	Radial
rad	Radiation
rat	Ratio
red	Reduced
s	Surface
sat	Saturation
SB	Stefan-Boltzmann
sf	Surface finish
static	Static
t	Tubes
T	Transverse
tot	Total
TS	Thermosyphon
v	Vapour
VH	Volumetric hydraulic diameter
w	Wall
wf	Working fluid
wick	Wick
∞	Ambient or Bulk temperature of surroundings

TABLE OF CONTENTS

1. INTRODUCTION.....	1
1.1. RESEARCH GAP, AIMS AND OBJECTIVES.....	2
1.2. ORGANISATION AND STRUCTURE OF THE THESIS	3
2. STATE OF THE ART	5
2.1. ENERGY INTENSIVE INDUSTRIES.....	5
2.2. GENERAL APPLICATIONS OF WASTE HEAT RECOVERY IN INDUSTRIAL PROCESSES ...	6
2.2.1. <i>Preheating Combustion Air</i>	9
2.2.2. <i>Space and District Heating</i>	11
2.2.3. <i>Material Preheating</i>	11
2.2.4. <i>Decoating</i>	12
2.2.5. <i>Electricity Generation</i>	12
2.3. HEAT PIPES AND THERMOSYPHONS.....	13
2.3.1. <i>Brief Developmental History of the Heat Pipe</i>	16
2.3.2. <i>Wicks</i>	16
2.3.3. <i>Working Fluid</i>	18
2.3.4. <i>Casing Material and Compatibility</i>	24
2.3.5. <i>Heat Pipe Composition Influence on Design Requirements</i>	26
2.3.6. <i>Heat Pipe Operation and Interaction Between Regions</i>	28
2.4. HEAT PIPE OPERATING LIMITS	28
2.4.1. <i>Flooding and Entrainment Limit</i>	29
2.4.2. <i>Boiling Limit</i>	30
2.4.3. <i>Dryout Limit</i>	30
2.4.4. <i>Capillary or Hydrodynamic Limit</i>	30
2.4.5. <i>Viscous Limit</i>	31
2.4.6. <i>Sonic Limit</i>	31
2.4.7. <i>Condenser Limit</i>	32
2.4.8. <i>Summary</i>	32
2.5. HEAT PIPE HEAT EXCHANGERS.....	33
2.5.1. <i>Benefits and Drawbacks of Heat Pipe Heat Exchangers</i>	35
2.6. HEAT PIPE HEAT EXCHANGER INDUSTRIAL INSTALLATIONS	39

2.6.1.	<i>Aluminium Industry</i>	40
2.6.2.	<i>Steel Industry</i>	41
2.6.3.	<i>Ceramic Industry</i>	42
2.6.4.	<i>Incineration</i>	43
2.6.5.	<i>Tea Drying Industry</i>	44
2.7.	MODELLING WORK	45
2.7.1.	<i>Heat Pipe Transient Modelling</i>	45
2.7.2.	<i>Heat Pipe Heat Exchanger Modelling</i>	49
2.7.3.	<i>TRNSYS Work</i>	53
3.	THEORETICAL ANALYSIS	56
3.1.	THERMOPHYSICAL PROPERTIES OF HEAT SINK AND SOURCE FLUIDS.....	57
3.2.	KEY DIMENSIONLESS NUMBERS.....	57
3.2.1.	<i>Reynolds Number</i>	58
3.2.2.	<i>Prandtl Number</i>	59
3.2.3.	<i>Nusselt Number</i>	60
3.3.	ARRANGEMENT OF THERMOSYPHONS.....	61
3.3.1.	<i>Maximum Velocity, u_{max}</i>	62
3.4.	CONVECTION.....	65
3.5.	THERMOSYPHON THERMAL RESISTANCE NETWORK ANALOGY	66
3.5.1.	<i>Evaporator Section Resistances</i>	71
3.5.2.	<i>Adiabatic Section</i>	75
3.5.3.	<i>Condenser Section</i>	77
3.5.4.	<i>Vapour Region</i>	78
3.5.5.	<i>External Resistances</i>	78
3.6.	EXTENDED THERMAL RESISTANCE ANALOGY FOR THERMOSYPHON ROWS	79
3.7.	USING THE EFFECTIVENESS-NTU METHOD TO PREDICT HPHE PERFORMANCE.....	81
3.7.1.	<i>HPHE Conductance Value</i>	88
3.8.	MAXIMUM HEAT FLUX IN A THERMOSYPHON.....	88
3.9.	CALCULATING HEAT TRANSFER COEFFICIENTS	91
3.9.1.	<i>Heat Transfer Coefficient of Forced Convection</i>	91
3.9.2.	<i>Heat Transfer Coefficient of Boiling</i>	98
3.9.3.	<i>Heat Transfer Coefficient of Condensation</i>	102
3.9.4.	<i>Effect of Finning and Calculations</i>	105

3.10.	PRESSURE DROP	110
3.10.1.	<i>Unfinned Thermosyphons</i>	112
3.10.2.	<i>Finned Thermosyphons</i>	113
3.11.	RADIATION.....	114
3.12.	TRUE TRANSIENCE.....	115
3.13.	SUMMARY OF THEORETICAL ANALYSIS.....	115
4.	EXPERIMENTAL INVESTIGATION	116
4.1.	INTRODUCTION.....	116
4.2.	EXPERIMENT 1: LABORATORY-SCALE CERAMIC KILN	117
4.2.1.	<i>HPHE Design</i>	119
4.2.2.	<i>Experimental Apparatus and Instrumentation</i>	125
4.2.3.	<i>Test Conditions</i>	127
4.3.	EXPERIMENT 2: FULL-SCALE CERAMIC CONTINUOUS ROLLER KILN	128
4.3.1.	<i>Description of the Testing Facility</i>	128
4.3.2.	<i>HPHE Design</i>	129
4.3.3.	<i>Experimental Apparatus and Instrumentation</i>	135
4.4.	EXPERIMENT 3: FULL-SCALE ALUMINIUM HEAT TREATMENT FURNACE	136
4.4.1.	<i>Description of the Testing Facility</i>	136
4.4.2.	<i>HPHE Design</i>	137
4.4.3.	<i>Experimental Apparatus and Instrumentation</i>	145
5.	SIMULATION STUDIES.....	149
5.1.	PROCESS FOR CODING HPHE COMPONENT.....	150
5.1.1.	<i>HPHE Coding in Intel Visual Fortran</i>	159
5.1.2.	<i>Creating a *.dll File Using Intel Visual Fortran 19</i>	175
5.1.3.	<i>Type204 Component Skeleton</i>	179
5.2.	USING THE TYPE IN A SIMULATION	182
5.3.	MODEL LIMITATIONS.....	184
6.	EXPERIMENTAL AND THEORETICAL RESULTS AND DISCUSSION.....	186
6.1.	EXPERIMENT 1: LABORATORY-SCALE CERAMIC KILN	186
6.1.1.	<i>Test 1</i>	187

6.1.2.	<i>Test 2</i>	191
6.1.3.	<i>Test 3</i>	195
6.1.4.	<i>Test 4</i>	198
6.1.5.	<i>Test 5</i>	202
6.1.6.	<i>Test 6</i>	206
6.1.7.	<i>Test 7</i>	210
6.1.8.	<i>Test 8</i>	214
6.1.9.	<i>Test 9</i>	217
6.1.10.	<i>Graphical Heat Transfer Rate and Conductance Values</i>	221
6.1.11.	<i>Experiment 1 Error Analysis</i>	225
6.1.12.	<i>Statistical Analysis</i>	228
6.1.13.	<i>Experiment 1 Summary</i>	232
6.2.	EXPERIMENT 2: FULL-SCALE CERAMIC KILN.....	234
6.2.1.	<i>Statistical Analysis</i>	241
6.2.2.	<i>Experiment 2 Summary</i>	244
6.3.	EXPERIMENT 3: FULL-SCALE ALUMINIUM HEAT TREATMENT FURNACE	244
6.3.1.	<i>Statistical Analysis</i>	256
6.3.2.	<i>Pressure Drop Analysis</i>	258
6.3.3.	<i>Heat Loss Analysis</i>	260
6.3.4.	<i>Experiment 3 Summary</i>	261
7.	CONCLUSIONS AND FUTURE WORK	262
7.1.	CONCLUSIONS	262
7.2.	RECOMMENDATIONS FOR FUTURE WORK	264
8.	REFERENCES.....	266
9.	APPENDICES	282
A.	MATLAB CODE FOR HPHE	282
B.	FORTRAN CODE FOR TYPE204 TRNSYS COMPONENT.....	321
C.	THERMOPHYSICAL PROPERTIES.....	373
	<i>C1. Natural Gas Combustion Products</i>	373
	<i>C2. Air</i>	378
	<i>C3. Water</i>	383

<i>C4. Thermal Oil</i>	388
D. THERMAL LOSSES CALCULATIONS FOR EXPERIMENT 3	394

1. INTRODUCTION

HPHEs are a relatively unrecognised heat exchange technology that is increasingly being used by industry to recover energy from waste heat streams, with industrial exhaust gases primarily being targeted. Across industrial sectors, there are many challenging heat sources that are presently unexploited where a HPHE can be used to recover the waste heat, and traditional technologies have failed. This is a lost opportunity for companies to reduce primary energy consumption and lower overall emissions. Traditional technologies generally fail in challenging streams due to fouling by particulate content or by condensation of corrosive elements within the gases. The beneficial attributes of HPHEs, such as low pressure drop and isothermal operation, lend themselves to be a suitable technology for efficiently recovering currently wasted energy where streams have been deemed irrecoverable or too challenging for traditional technology.

Though these industrial HPHEs are being more widely recognised, manufactured and installed, there is limited awareness and publications on their use. Furthermore, their ongoing performance over time to fluctuating process conditions or evaluating their influence over time in an overall system simulation has not been conducted. Processes within companies, even if classed as continuous rather than batch processes, can still have highly fluctuating conditions. Assessing the performance of a HPHE over these varying conditions is crucial in their design and subsequent handling of the heat transfer fluids. Transient behaviour is important to consider as there are limitations in steady state analyses by averaging conditions. For example, extreme temperatures where material selection is affected by thermal expansion and stresses, or low temperatures where condensation of gases becomes an issue are not observed. Also, heat exchanger conductance values change with the varying conditions.

Currently, HPHEs are designed for operation based upon averaged values of: temperature, thermophysical properties of source and sink fluids, pressure, mass flow rate and composition of a waste heat stream. Maximum and minimum conditions observed can be evaluated to determine the range of operating parameters. The operating hours of the source of the waste heat stream can then be used to determine the potential saving. In reality, system performance and waste heat streams fluctuate over time. In order to increase accuracy, a transient model is proposed. For the manufacturer, this will aid in the design of a HPHE by more fully analysing

the performance. For the end user, this will provide a greater confidence in realising savings; hopefully seeing this technology adopted more frequently.

The heat transfer mechanisms within single heat pipes have been studied extensively for steady-state analyses, less so for HPHEs. Transient models are available for single heat pipes, particularly to determine start-up but nothing is available on transient performance of a HPHE over time. to transiently predict the performance of HPHEs, or to evaluate WHR systems incorporating HPHEs. The main relevance to science is filling this gap in knowledge with a novel developed tool. This thesis presents the work that has been conducted to develop a novel and versatile tool for predicting transient behaviour of HPHEs, building upon previous published heat transfer mechanisms and empirically derived correlations. The outputs of the model are the temperature of the stream outlets, conductance value of the HPHE, heat transfer rate and pressure drop across the banks of thermosyphons.

The Author developed the model as well as the test conditions and methodology of two of the presented HPHEs. A further full scale installation's data was also available and this has been used to further validate the tool using different test conditions and geometry.

1.1. Research Gap, Aims and Objectives

Three primary research gaps have been found in relation to this work, these being:

- a) A significant gap in awareness, knowledge, and published literature on full and laboratory-scale HPHE units for WHR from low-grade heat sources.
- b) Available transient models for heat pipe technology are extremely limited; mostly being used to determine start-up characteristics with single heat pipes. No transient models on heat exchange performance using bundles of thermosyphons in a HPHE are available. Therefore, the performance of a HPHE over time cannot be fully evaluated.
- c) Batch processes do not have steady state conditions so traditional modelling methodologies that use averaged conditions, such as temperature and mass flow rate, are not applicable and can be misrepresentative.

The aim of the experimental study was to demonstrate and characterise the potential for WHR using HPHEs with different heat sinks. The results obtained could then be used to empirically validate the computational models developed, as far as possible. The aim of the computational

study was to develop and publicise a versatile transient model that can accurately predict HPHE performance. Finalising this work in the software, TRNSYS, provides a platform where simulating overall WHR systems using HPHEs can be achieved. To fulfil these aims, five objectives of the research were set:

Objective 1: Develop a working knowledge of the heat transfer processes within a HPHE.

Objective 2: Develop a novel and versatile model for predicting transient behaviour of HPHEs.

Objective 3: Demonstrate the advantage of the tool over existing models.

Objective 4: Validate the model using experimental results from a laboratory-scale installation.

Objective 5: Validate the model using experimental results from a full-scale installation.

1.2. Organisation and Structure of the Thesis

This thesis is organised into seven Chapters, followed by the References and Appendices:

Chapter 1- Introduction. Provides an overview of the structure of the thesis, the research gap, aims and objectives of the published work with relevance to science and industry.

Chapter 2- State of the Art. Reviews: previous work on waste heat recovery (WHR) in energy intensive industries, the potential end uses for recovered waste heat, heat pipe and thermosyphon technology, installed HPHEs and previous modelling and simulation work with a latter focus on TRNSYS.

Chapter 3- Theoretical Analysis. Detail is provided on available heat exchanger performance calculation methodologies and the equations dictating the HPHE performance depending on its architectural design. Emphasis is given to key dimensionless numbers; the thermal network analysis and effectiveness-NTU methodologies; heat transfer coefficients; the effect of finning and pressure drop analysis.

Chapter 4- Experimental Investigation. Provides the P&IDs, drawings, experimental apparatus and test conditions used in the laboratory-scale and full-scale installations to obtain the HPHE performance results.

Chapter 5- Simulation Studies. Provides information on how the transient model has been coded using the theory provided in Chapter 3. The software used, terminology and logic are provided to show how the theoretical results were obtained. The limitations of the model are also outlined.

Chapter 6- Experimental and Theoretical Results and Discussion. Provides data and analysis of the experimental systems' simulation results in comparison with experimental results. Error analysis is provided for heat transfer rates and outlet temperatures. Statistical analysis has been conducted to highlight outliers and to determine confidence in the results.

Chapter 7- Conclusions and Future Work. Final conclusions are drawn from the experimental and theoretical results, and recommendations are made for future work.

References- Contains the compiled list of references used throughout the thesis.

Appendix- Contains the complete MATLAB and TRNSYS codes for steady state and transient modelling, thermophysical properties and thermal loss calculations for the third experiment.

2. STATE OF THE ART

This chapter provides a state of the art on waste heat recovery (WHR) from energy intensive industries (EIIs); a general background on heat pipes and thermosyphons, WHR applications of heat pipe heat exchangers (HPHEs); previous modelling on heat pipes and HPHEs and then, more specifically, Transient System Simulations (TRNSYS). Focus is given to examples involving the recovery of heat from exhaust gases. Certain sections of this chapter have been written with particular reference to [1] and [3]; both published by the author.

2.1. Energy Intensive Industries

WHR and waste heat are topics of rapidly growing research focus; Figure 1. The previous decade has shown a particularly dramatic increase in publications regarding these topics. WHR is primarily of importance to EIIs, usually within the industrial sector. EIIs are classified as industries whose energy usage makes up a significant part of production costs. More than half of European Union (EU) industrial energy consumption originates from EIIs [6].

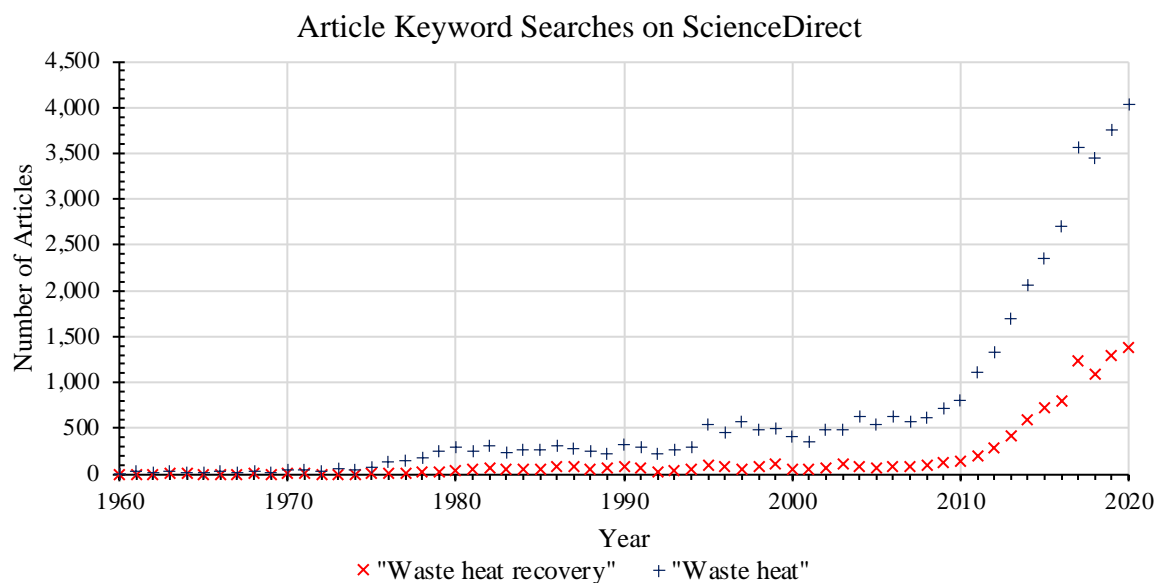


Figure 1: Graph showing the number of articles containing “Waste heat recovery” and “Waste Heat” on ScienceDirect.

In tandem, global thoughts are turned towards the conservation of natural resources and reducing emissions contributed by human activity, evidenced by the 195 signatories to the 2016

Paris agreement [7] and EU 2030 energy targets [8] with the aim to reduce GHG emissions to 80-95% below 1990 levels by 2050 [9]. The United Kingdom (UK) government has gone one step further by committing to net zero GHG emissions by 2050 [10]. In 2017, industrial production in the UK increased by 3.4% and was responsible for 20.2% of GDP. 15.2% of the labour force was employed by industry and natural gas consumption was 79.17 billion cubic metres [11]. Moreover, worldwide, 33% of GHG emissions were a result of industrial sector activities and the sector was also responsible for 26% of primary energy consumption [12,13].

More recently, at COP26 in 2021, 153 countries have proposed or updated their emission targets, which cover approximately 80% of the global GHG emissions. Predictions show that, if effected, GHG emission will be around 5 billion tonnes lower by 2030 [14].

2.2. General Applications of Waste Heat Recovery in Industrial Processes

There are two primary purposes for recovering waste heat in industrial processes: firstly, the cost benefit of minimising the use of natural resources by reducing energy or fuel consumption and, secondly, reducing emissions to hit governmental targets. This also has the added benefit of providing a healthier view of a company in regard to social and corporate responsibility.

The number of WHR technologies is extensive and growing. Table 1 provides a summary of available WHR technologies and their corresponding applicable temperature range.

Table 1: Available WHR technologies and their applicable temperature ranges [1].

High Temperature (>400°C)	Medium Temperature (400-100°C)	Low Temperature (<100°C)
<ul style="list-style-type: none"> • Ceramic recuperators • Heat pipes • Material preheating • Radiation/ convective/ hybrid recuperators • Regenerative/ recuperative burners • Rotary regenerators • Steam generation • Thermionic devices • Waste heat boilers • Thermodynamic cycles 	<ul style="list-style-type: none"> • De-coating • Economisers • Heat pipes • Material preheating • Radiation/ convective/ hybrid recuperators • Recuperative burners • Rotary regenerators • Shell and tube • Thermo-compressors • Thermoelectric devices • Waste heat boilers • Thermodynamic cycles 	<ul style="list-style-type: none"> • Air preheaters • Compact heat exchangers • Piezoelectric devices • Plate heat exchanger • Thermoelectric devices • Run around coils • Shell and tube heat exchangers • Heat pumps

Recovering the energy content within a waste heat stream is only the first stage. Afterwards, the end use of the recovered waste heat must be determined and linked to the recovery stage. A multitude of applications are possible, with a selection of commonly chosen applied end uses discussed in this section. Hammond and Norman [15] conducted a study of WHR options in the UK. The authors determined the annual potential energy savings by EII (Figure 2) and CO₂ reduction by method of reuse (Figure 3). Heat recovered from a piece of equipment in a process may not require the heat to be reintroduced back into that particular process, as in the case of recuperative or regenerative burners. Furthermore, the quantity of energy recovered could be larger than can be feasibly reintroduced. To increase versatility, the possibility may exist in a facility for another process or piece of equipment to use this recovered energy. ‘On-site recovery’ combines these two options.

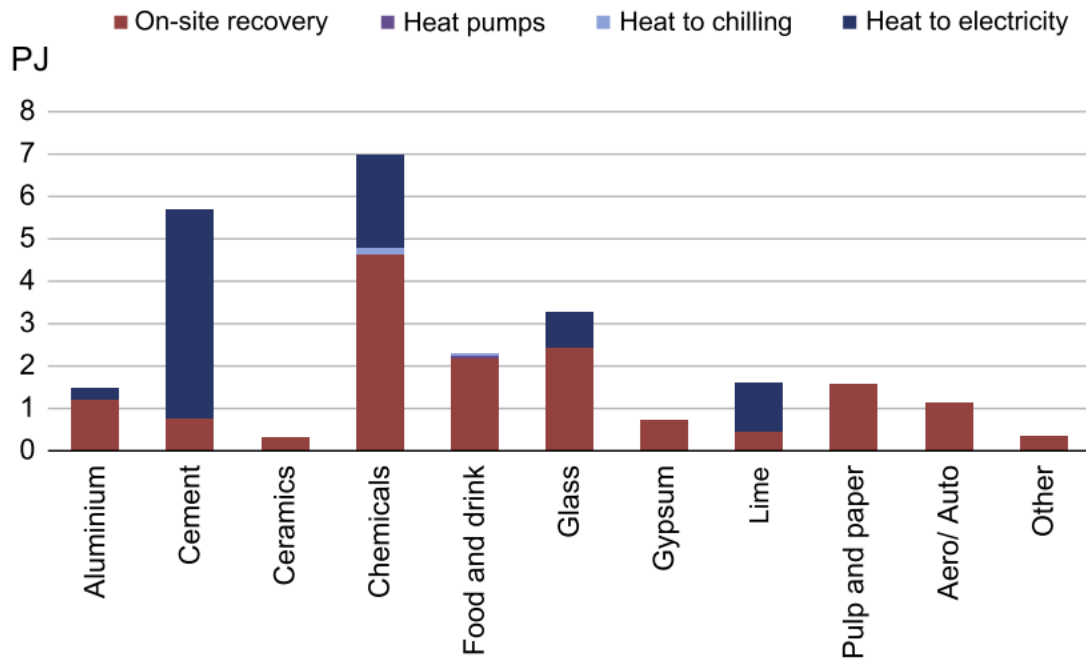


Figure 2: Graph showing the potential energy savings by subsector in the UK [15].

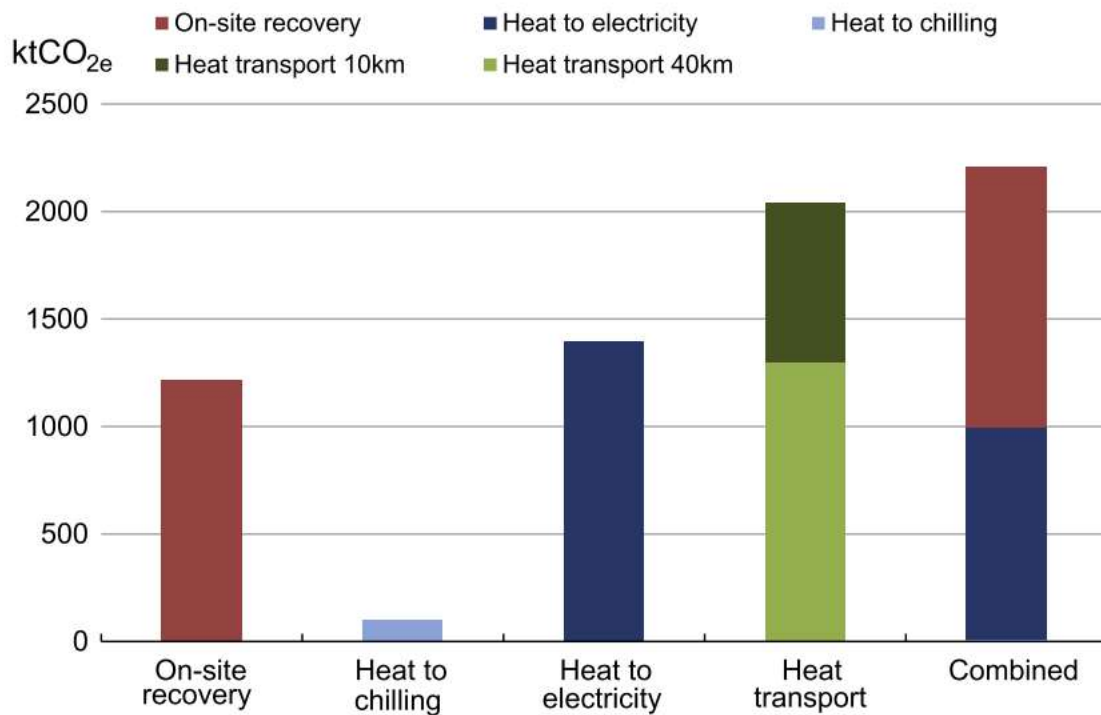


Figure 3: Graph showing potential emissions savings by reusing surplus generated heat by technology [15].

2.2.1. Preheating Combustion Air

Combustion is an exothermic reaction where the released energy is used to heat, melt, chemically alter or treat materials. Many EIs use combustion as part of their processes and, consequently, preheating combustion air is an extremely common application for WHR. This is due to numerous quantifiable benefits, including the ability for cost reduction on process overheads and emissions reduction. Generally, the combustion process uses a fuel, such as natural gas, that reacts with oxygen from air (known as combustion air), air enriched with oxygen or pure oxygen.



The combustion products are released alongside enthalpy (ΔH), primarily in the form of heat energy, to the process and are vented away as exhaust gases, post-process. By raising the ambient temperature of the combustion air, less energy is required to reach the activation energy of the reaction, leading to more efficient, complete combustion and increased total released energy. This leads to a hotter flame and an overall reduction in requisite fuel consumption as there is more heat output per fuel unit. Secondly, more energy is returned to the process so the CO₂ and GHG emissions per unit of heat is less.

Table 2 shows the percentage efficiency increase in a typical aluminium furnace, quantified by transfer of energy from the combustion reaction to the metal, by preheating the combustion air temperature introduced for the reaction. It can be seen in this example that a 48% efficiency improvement can be achieved by increasing the temperature of the combustion air.

Table 2: Percentage furnace efficiency improvement by preheating combustion air, adapted from [16].

Furnace Outlet Temperature, °C	Combustion Air Preheat Temperature, °C				
	204	316	427	538	649
1,427	22%	30%	37%	43%	48%
1,316	18%	26%	33%	38%	43%
1,204	16%	23%	29%	34%	39%
1,093	14%	20%	26%	31%	36%
982	13%	19%	24%	29%	33%
871	11%	17%	22%	26%	30%
760	10%	16%	20%	25%	28%

Figure 4 shows the potential fuel consumption reduction by preheating combustion air from various exhaust gas temperatures in comparison to using ambient temperature air. The legend refers to the temperature of the exhaust gases. For example, preheating combustion air to 1,400°C from 1,600°C exhaust gases (red line) can achieve an over 70% fuel reduction.

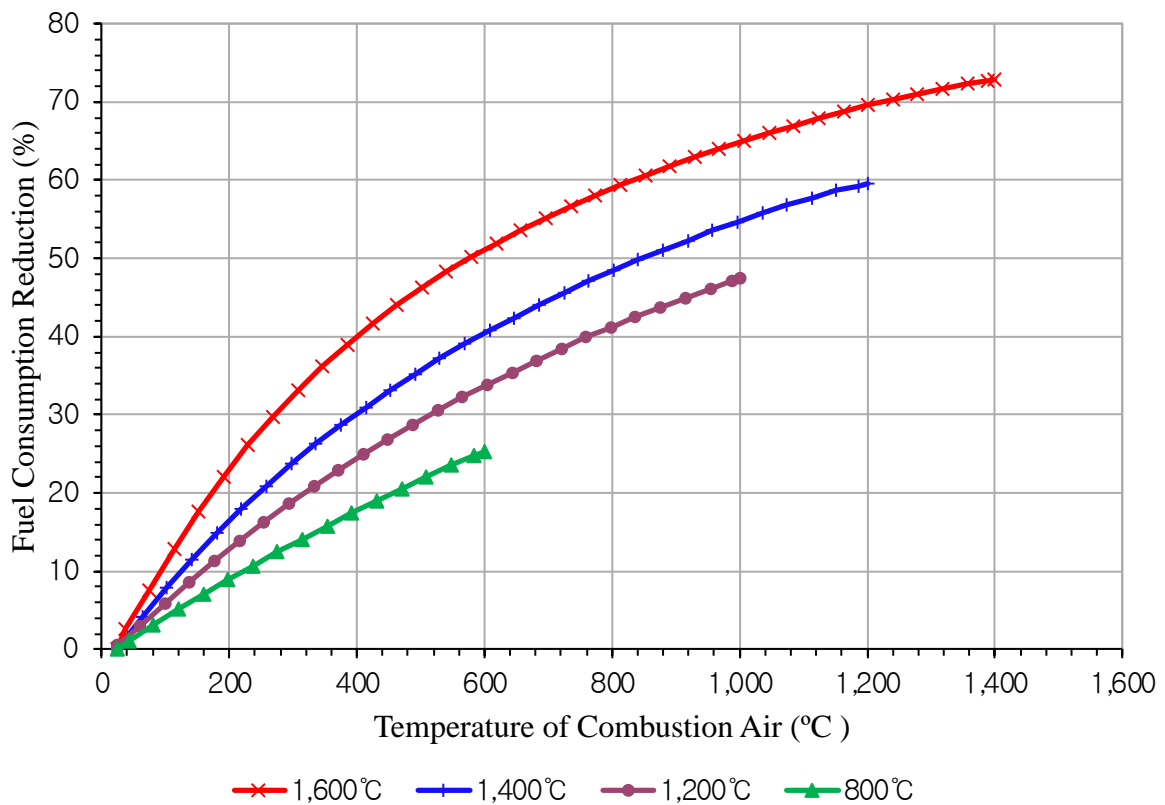


Figure 4: Graph showing the percentage fuel reduction by using preheated combustion air [17].

2.2.2. Space and District Heating

Many companies use fuel or electricity in central heating systems to provide a higher ambient temperature in offices or site buildings to make the space more comfortable. Also, hot water needs to be generated for available water facilities. Waste heat generated can be used to negate or reduce primary energy consumption for heating systems, reducing overheads. However, in geographically warm and mild climates, the benefits of space heating may be limited or perhaps not required all year round.

Larger producers of waste heat have extended this concept by heating neighbouring towns and villages, in either an altruistic manner or for revenue. A prominent example is the city of Copenhagen in Denmark, where 98% of the city's district heating is provided by waste heat from incineration or combined heat and power plants. The four largest cities in Denmark have 95% of their heating needs covered by district heating. This has led to a 70% reduction in CO₂ emissions. Remarkably, across Denmark, there are one billion litres of hot water within the 60,000 km district heating network that arise from recovering waste heat. [18]

Further studies have been conducted to provide a 40 MW district heating plant in Iceland with Alcoa Fjarðaál, a primary aluminium smelter, providing the source of waste heat [19] and, additionally, a study on a steel casting factory in Udine, Italy, to heat the most densely populated areas of the city [20].

2.2.3. Material Preheating

In the case of the aluminium industry, melting and holding furnaces have solid material introduced to them periodically. If there is a molten bath of metal in the furnace during charging, wet material can generate superheated steam and cause devastating explosions. This can be overcome by using exhaust gases from the furnaces to dry the material and increase its ambient temperature prior to charging [21,22]. The benefit of raising the material over ambient temperature is that less energy is then required to melt the material and, as such, it will reduce fuel consumption and decrease cycle times; improving productivity. Arink and Hassan [21] demonstrate that preheating aluminium scrap to 100°C prior to charging can reduce cycle time by 8 minutes. A 25.5% increase in production with a 21.1% energy saving by preheating material prior to charging can be realised [23]. One immeasurable advantage of installing these

systems is the health and safety benefit attributed to avoiding explosions by introducing wet material. An example of a typical aluminium sow preheater is shown in Figure 5.



Figure 5: Photograph of an aluminium sow preheater using exhaust gases [24].

2.2.4. Decoating

Another process where waste heat can be introduced is the decoating of scrap metal. Various scrap is coated with paint, polymers, or lacquer, and when this is introduced into a furnace, the amount of oxidised material (dross) produced is higher, leading to reduced recovery yields. By decoating scrap prior to charging, yield recovery increases [25]. In practice, this has been done with exhaust gases from rotary kilns. In addition, the calorific value of the coating can be returned to the furnace [26]. A novel method developed by [27] uses the organic material present on the scrap as a fuel to supply the energy to propagate further decoating.

2.2.5. Electricity Generation

Waste heat can be partnered with thermodynamic cycles, such as Rankine or Kalina cycles, to produce electricity. These methods use expansion or the phase change of a fluid to produce a rotary movement (usually a turbine) to generate AC current. Electricity distributed through a site can reduce operating costs or be returned to the grid to generate an income. Rankine examples include water desalination and steel production [28]. The cement industry [29], steel

mills [30] and power plants [31] have all used the Kalina cycle to generate electricity, among numerous other examples. Low recovery rates and high installation costs are seen in comparison to other WHR technologies [32]. Peris et al. [33] produced net 18.51 kW of electricity using an Organic Rankine Cycle (ORC) in the ceramics industry from a thermal power input of 128 to 180 kW. This equates to 115 MWh produced per year, in turn, saving 31 tonnes of CO₂ emissions per year.

On top of pure Rankine cycles, other technology can be introduced, which is referred to as a hybrid system. Radiative and convective recuperators have been tied to the Rankine cycle in this manner [34,35]. Another example of a hybrid system utilises a gas turbine [36,37] as part of a cogeneration system. The authors proposed a 4.4 MW gas turbine from a ceramic roller kiln with 20% efficiency.

Thermoelectric and thermionic generators are emerging technologies that can be used to generate electricity [1,38]. Thermoelectric generation during silicon casting [32] has been studied. Low efficiencies and material limitations are current challenges.

2.3. Heat Pipes and Thermosyphons

The direction of this research relates to the use of heat pipes for WHR, which are recognised as an extremely efficient heat transfer technology. A heat pipe is a sealed tube which, in manufacture, is initially evacuated and then charged and sealed with a small quantity of a working fluid. The majority of heat pipes produced have a cylindrical cross section, but other configurations are seen. A heat pipe uses the phase change of the working fluid, specifically liquid to vapour, to extract, transport and then release energy. For high temperature applications, solid metals at room temperature can be used, which then melt and evaporate at high temperatures. There are no moving parts, so the heat exchange works completely passively.

The operation of a heat pipe depends on a two-phase cycle across three recognised sections of a heat pipe: the evaporator, condenser and adiabatic sections. Heat is introduced to the evaporator section, where the working fluid boils and evaporates. The vapour travels through the adiabatic section, where there is no heat input or output, to the condenser section due to the minimal pressure difference between the sections. Heat is extracted from the vapour and upon

condensing, the liquid falls by gravity or is assisted by capillary forces provided by a wick structure to return the condensed working fluid to the evaporator. This cycle continues all the while heat is applied and extracted. Heat pipes are the generic name for the technology; a subsection of heat pipes are wicked and wickless heat pipes, with the latter being referred to as thermosyphons. Figure 6 provides a schematic of this two-phase cycle in both wicked and wickless heat pipes. The wicked heat pipe is shown operating vertically in this Figure, but it can operate in any orientation, whereas a thermosyphon solely relies on gravity to return the working fluid to the evaporator. The function of a heat pipe leads to numerous advantages, these include: very high thermal conductivity, an entire surface considered isothermal, long transportation distances with small temperature differences, large overall energy transfer due to the extra latent heat of vaporisation energy transported, long life expectancy (20 years) without the need for maintenance and passive heat transfer. [31,39]

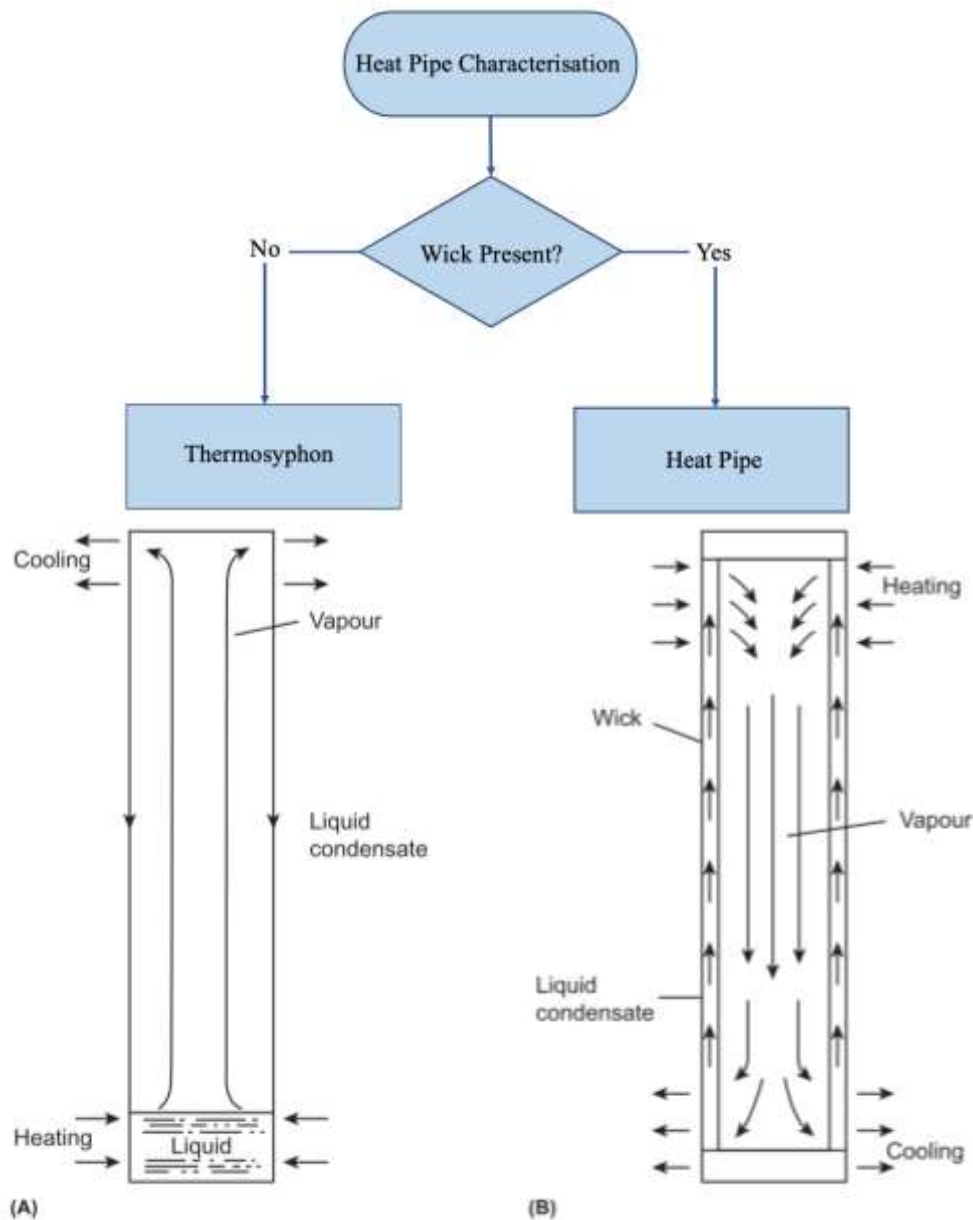


Figure 6: Schematic of a thermosyphon (A) in comparison to a wicked heat pipe (B) [40].

Heat pipe technology, in particular banks of heat pipes in HPHEs, were chosen as the primary technology to model over the course of this research programme as their benefits are being more readily recognised by industry and research on them is less prevalent than with traditional technologies, even though they have existed for some time. HPHEs tend to be used in challenging streams where traditional technologies would fail and increasing work is required to demonstrate and expose their potential.

2.3.1. Brief Developmental History of the Heat Pipe

The invention of the heat pipe has been traced back to the development of the Perkins tube [41]. The first designs in the 19th century used single phase heat transfer, which was exceeded by a new development that used two-phase cycles. Jacob Perkins filed UK Patent No. 7039 in April 1936 for this two-phase heat transfer tube. Initial applications were found in locomotive boilers.

In 1942, Gaugler, whilst working with refrigeration, proposed a closed tube which worked by two-phase heat transfer, where the liquid evaporates to a higher position and condenses and travels back to the evaporative location [42].

Also in 1942, the first example of a HPHE in the configuration recognised today was patented by Frazier Gay [43]. The HPHE developed was a gas-to-gas unit with a separation plate between the evaporator and condenser sections. External fins were added to increase the heat transfer surface area. Alternative internal working fluids to water, depending on the working temperature, were recognised, such as mercury and methanol. Mercury is largely discounted nowadays due its toxicity and potential for environmental harm.

The first article published using the term ‘heat pipe’ was in 1964 by Grover, Cotter and Erickson [44]. Nowadays, heat pipes are ubiquitously used in laptops and computers as a processor heat sink. Also, for microgravity applications, such as in space programmes, for the thermal equalisation of satellite transponders or thermal control of panels to equalise thermal stresses in structures caused by large temperature gradients where one side is continuously exposed to solar radiation and the other is exposed to deep space [42]. Faghri [45] and Jouhara et al. [39,46] provide reviews on the multitude of current applications for heat pipes. WHR using HPHEs is becoming a more prominent area of focus.

2.3.2. Wicks

A wick is the primary difference between a heat pipe and a thermosyphon. Reay and Kew [40] state for a thermosyphon: “a wick or wicks may be incorporated in at least part of the unit to reduce entrainment and improve liquid distribution within the evaporator”. However, it is commonly seen in literature that a thermosyphon is distinguished by no incorporated wick. This is the distinguishing feature that the author uses to discriminate between heat pipes and

thermosyphons. As a thermosyphon only uses gravity to maintain the two-phase cycle, they are seen primarily in vertical applications, though it should be noted that the highest heat transfer can also occur at inclination angles of 60-80° to the horizontal [40,47,48].

Wicked heat pipes use the wick structure to draw the working fluid by capillary action back to the evaporator so can be used in horizontal or antigravity applications where the evaporator is above the condenser. Figure 7 and Figure 8 show a selection of internal wicks.

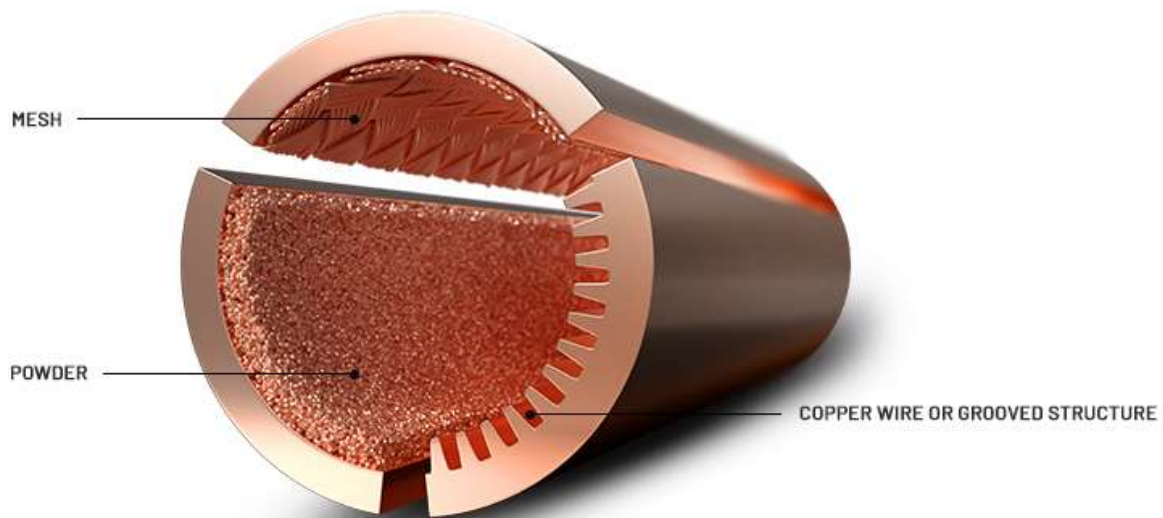


Figure 7: Schematic of mesh, powder and grooved wick designs [49].

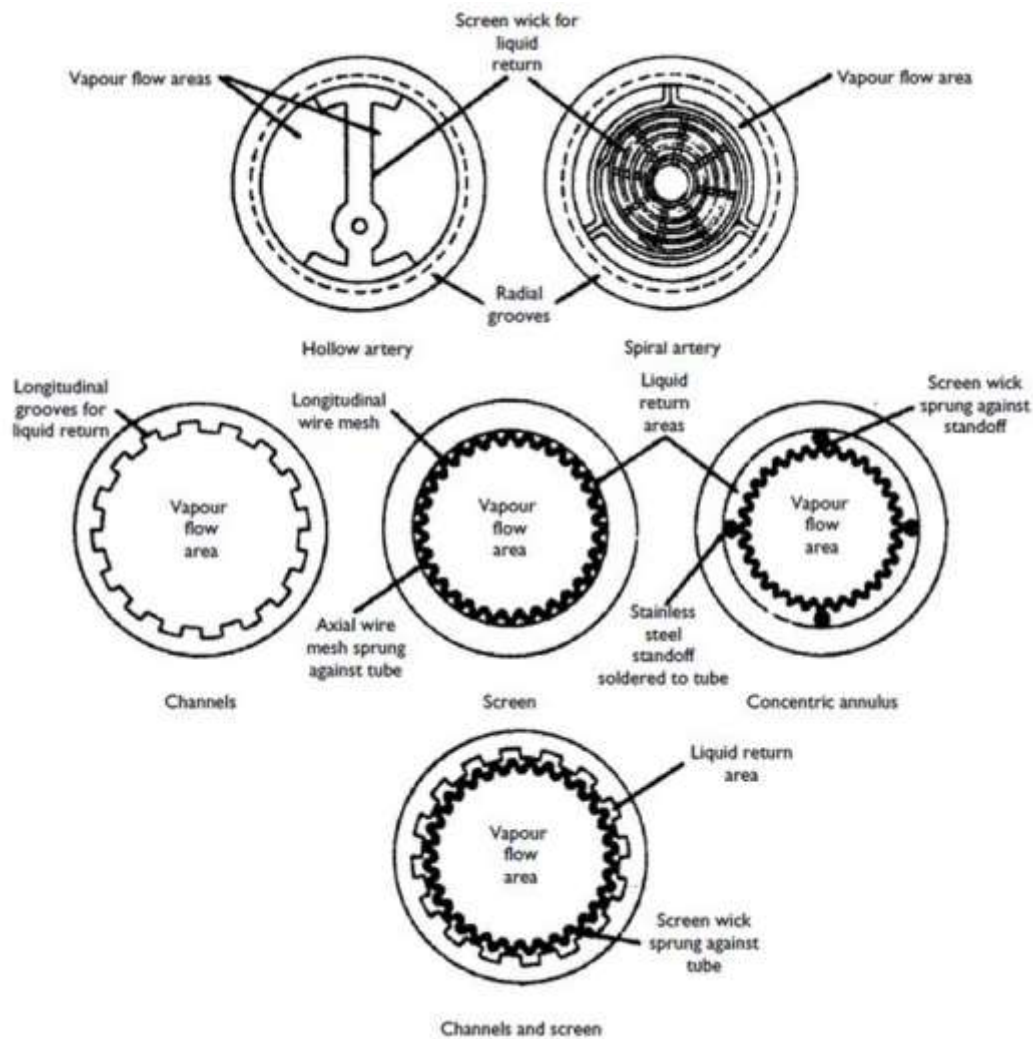


Figure 8: Schematic showing a selection of heat pipe wick structures [40].

In recent years, work has been conducted on the development of novel wick structures in which nanoparticles are introduced, for example by coating [50,51].

2.3.3. Working Fluid

The type and volume of working fluid in a heat pipe are crucial to its operation and this choice depends on the temperature range of the waste heat stream. The overarching factors for use are the liquid boiling and vapour condensation temperatures. Figure 9 shows the useful working temperature ranges of different heat pipe working fluids, although it has been truncated by removing cryogenic fluids to show the most commonly used fluids applicable for WHR.

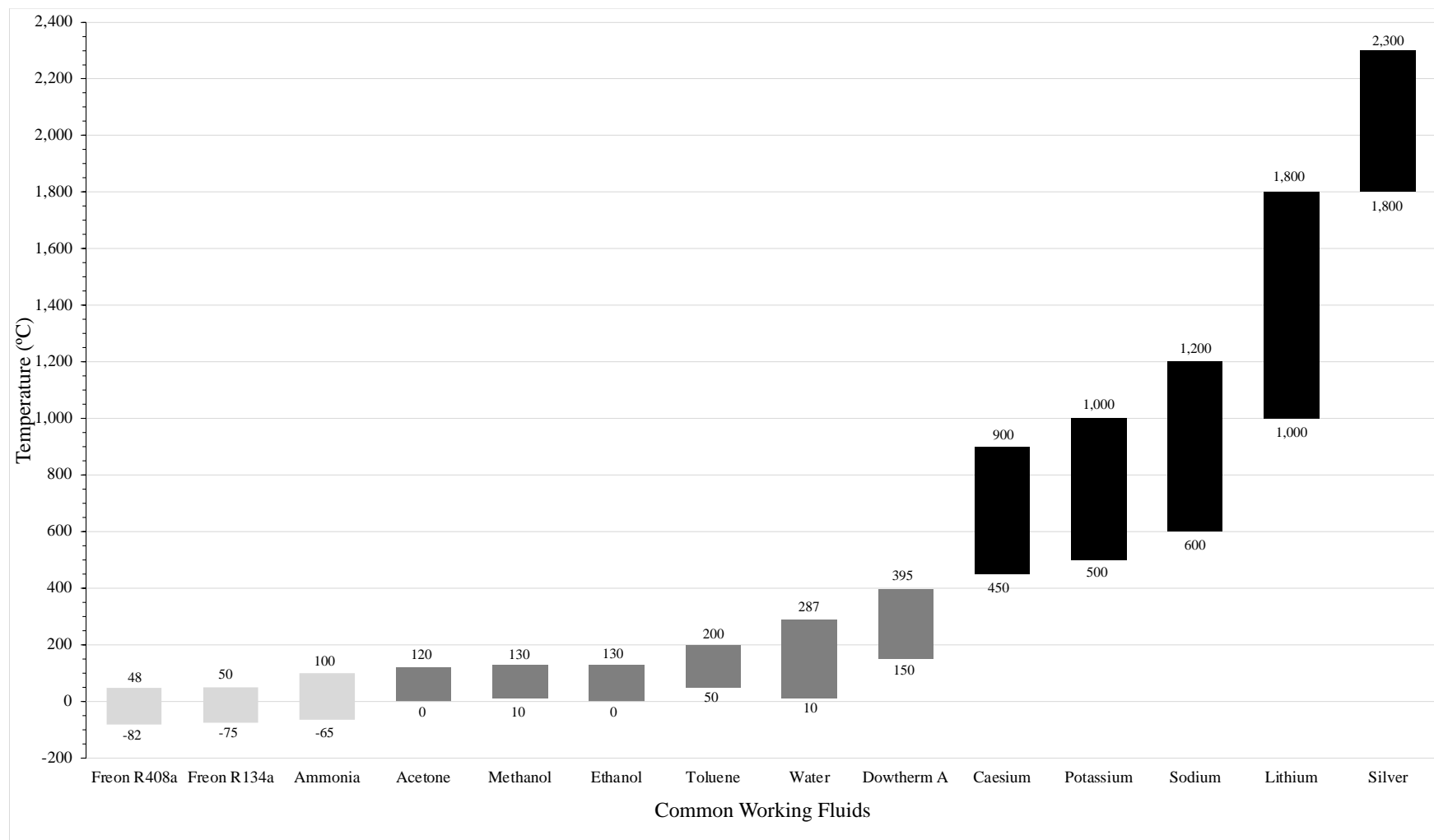


Figure 9: Graph showing the useful working temperature range for heat pipes depending on working fluid, adapted from [52]. At normal pressure and temperature: light grey- gaseous, grey – liquid, black – solid.

It is important to maintain the working temperature range as straying outside can break the two-phase heat transfer cycle where boiling or condensation cannot occur. This is best explained using a phase diagram, shown in Figure 10. The axes are pressure and temperature. The solid green line shows the freezing curve, blue the boiling curve and red the sublimation curve. The dotted blue line shows the irregular behaviour of water. The triple point is defined as the temperature and pressure where a substance can coexist in all phases in thermodynamic equilibrium and where all three curves meet. The critical point is defined as the condition where liquid and gas can coexist and have the same density, in essence, they are indistinguishable. This phase state is defined as a supercritical fluid. This leads to the values for critical temperature and critical pressure, located at the end of the boiling curve.

In the context of a heat pipe, it is a sealed unit, so as more liquid evaporates, the internal vapour pressure will increase. If the temperature is too low, or the pressure is too high, the working fluid will not evaporate. Vice versa, the fluid will not condense. If both the pressure and or temperature increase to such extent that the critical point is exceeded, the working fluid will exist in a supercritical state, assuming the heat pipe structure does not fail beforehand. Any of these conditions described above will break the two-phase cycle required for operation.

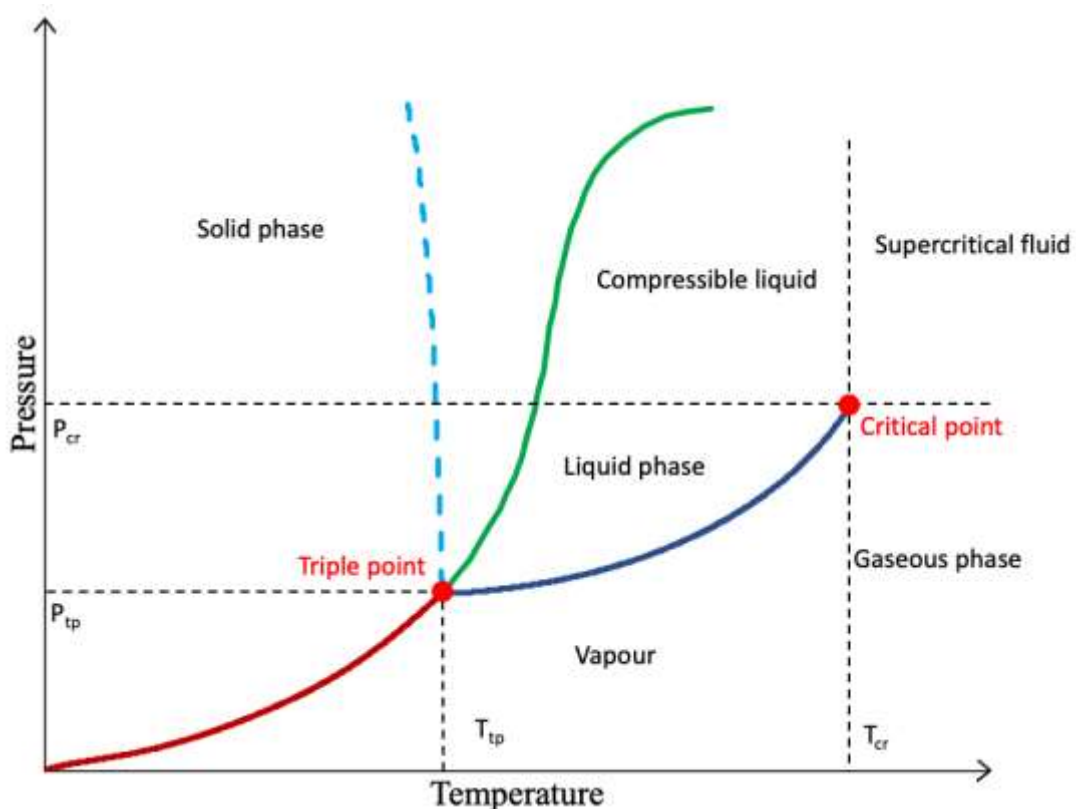


Figure 10: A generic phase diagram.

The choice of a working fluid is not solely down to the temperature range, as these can overlap. Further properties, characteristics and criteria are considered when selecting a working fluid [40]. Positive or considered attributes include:

- a) Good thermal stability.
- b) Good wettability.
- c) High thermal conductivity.
- d) Good compatibility with wick and container material.
- e) Reasonable vapour pressure at operating temperatures.
- f) High latent heat of evaporation.
- g) Low viscosity of both liquid and vapour phases.
- h) Liquid and vapour densities.
- i) Liquid and vapour dynamic viscosities.
- j) High vapour specific heat capacity.
- k) High surface tension, if antigravity.
- l) Freezing and pour point acceptable for range of application.
- m) Low toxicity.
- n) Low cost and easily available.

As well as incorporating nanoparticles into the wick structure, substantial research has been conducted on the introduction of nanoparticles into the working fluid, known as a nanofluid. Many experiments have been conducted on the heat transfer characteristics of various nanofluids in different heat pipe configurations. A large number of these experiments have been compiled in [53].

2.3.3.1. Figure of Merit

A measure of a heat pipe's working fluid efficiency is the figure of merit. Even though a functioning heat pipe is considered to be isothermal along its length, in practice, there is a small temperature gradient from the evaporator to the condenser. A measure of the working fluid properties' influence on the temperature drop is provided by the figure of merit. A high figure of merit value implies a small temperature difference between the two ends and vice versa. Accordingly, heat pipes with an internal working fluid with a high figure of merit value achieve better performance as there is a lower thermal resistance and higher heat transfer capability

[54]. The figure of merit also depends on the operating temperature of the heat pipe. Equation (2.2) calculates figure of merit values for typically used working fluids in wickless heat pipes [55,56]

$$\Phi = \left(\frac{h_{fg} \lambda_l^3 \rho_l^2}{\mu_l} \right)^{1/4} \quad (2.2)$$

where Φ is the figure of merit ($\text{kg.K}^{-3/4}.\text{s}^{-5/2}$), λ_l is the thermal conductivity of the liquid working fluid ($\text{W.m}^{-1}.\text{K}^{-1}$), h_{fg} is the specific latent heat of vaporisation (J.kg^{-1}), ρ_l is the density (kg.m^{-3}) and μ_l is the liquid viscosity (Pa.s). A visualisation of the application of this equation is shown in Figure 11.

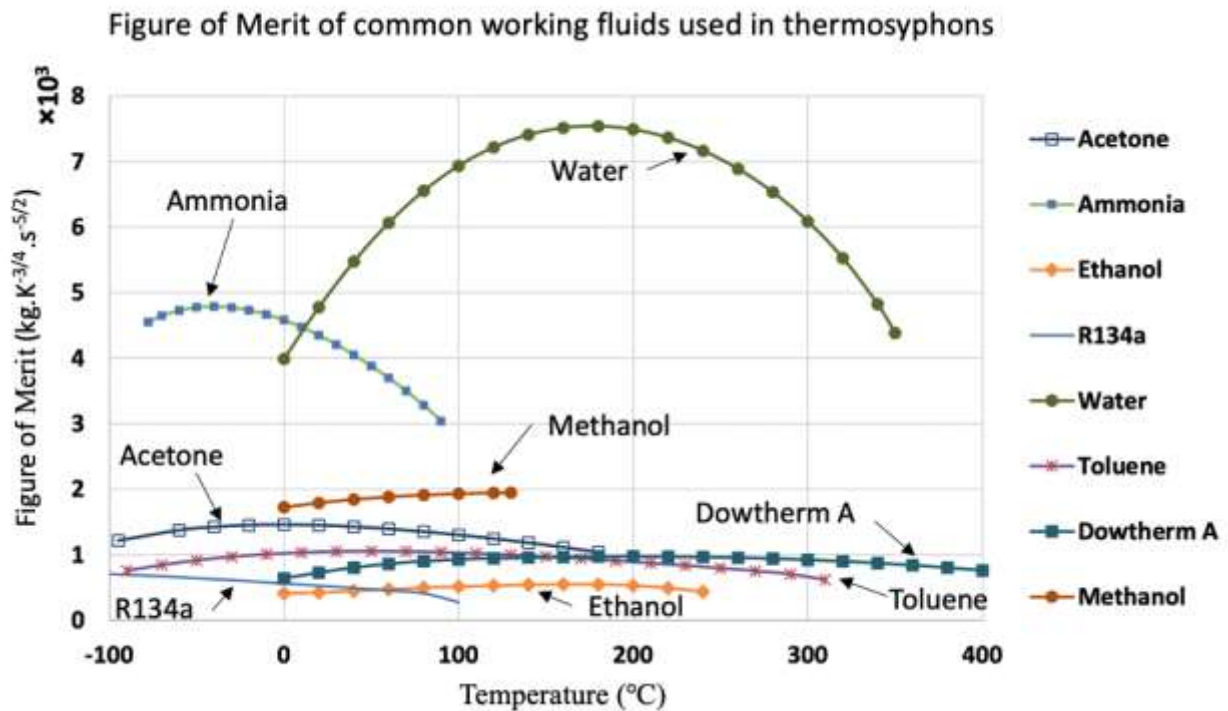


Figure 11: Graph showing figure of merit curves for common working fluids in a thermosyphon [57].

The figure of merit is calculated differently for wicked heat pipes, also available within [55].

2.3.3.2. Volume of Working Fluid

In the case of thermosyphons, it is imperative to achieve the correct filling ratio. Too much fluid can cause carriage of the liquid to the condenser section, blocking the available

condensation area, leading to reduced performance. Insufficient liquid can lead to dry out, which interrupts the two-phase cycle and prevents heat transfer. It is roughly recommended to fill the working fluid to at least half the volume of the evaporator section. A simple equation, using only geometry, to determine the minimum volume of working fluid, V_{wf} , in a thermosyphon is [58]:

$$V_{wf} > \frac{\pi D_i (L_e + L_a + L_c)}{1000} \quad (2.3)$$

where D_i is the internal diameter, L_e , L_a and L_c are the lengths of the evaporator, adiabatic and condenser sections. A more involved method developed by Bartsch and Unk and improved upon by Faghri [59], that includes fluid properties and various temperatures is:

$$V_{wf} = V_{wf,f} + V_{wf,p} \quad (2.4)$$

where the volume of the working fluid in the film, $V_{wf,f}$, is:

$$V_{wf,f} = \pi D_i \left(\frac{4\lambda\mu_l}{\rho_l^2 g h_{fg}} \right)^{1/4} \left[(T_{sat} - T_{w,c})^{1/4} \left(\frac{4}{5} L_c^{5/4} + L_a L_c^{1/4} \right) + \frac{4}{5} (T_{w,e} - T_{sat})^{1/4} (L_f^{5/4} - L_{f,p}^{5/4}) \right] \quad (2.5)$$

and working fluid in the pool, $V_{wf,p}$ is:

$$V_{wf,p} = \frac{\pi D_i^2}{4} L_p \quad (2.6)$$

where the length of the liquid pool, L_p is:

$$L_p = L_e - \left(\frac{1}{4\lambda} \right) \left(\frac{\mu_l}{\rho_l^2 g h_{fg}} \right)^{1/3} \left(\frac{3}{\pi D_i} \right)^{4/3} \left[\frac{\dot{q}_e^{4/3}}{T_{w,e} - T_{sat}} - \frac{\dot{q}_p^{4/3}}{T_{w,e} - T_p} \right] \quad (2.7)$$

The derivations of the equations are provided in [59] and symbols are given in the Nomenclature section. A simplified analysis conducted by Strel'tsov, by removing the liquid pool, gives:

$$V_{wf} = \left[\frac{4}{5}(L_c + L_e) + L_a \right] \left[\frac{3\dot{q}\mu_l(\pi D_i)^2}{\rho_l^2 g h_{fg}} \right]^{1/3} \quad (2.8)$$

Noie [60] conducted an experiment on the heat transfer rate depending on filling ratio and aspect ratio (the ratio of evaporator length to inside diameter) in a copper thermosyphon with distilled water as the working fluid. It was found that the maximum heat transfer rate took place at different filling ratios depending on the aspect ratio. This leads to the conclusion that there is not a generic optimum filling ratio, but this depends on the design of the thermosyphon. An optimal heat pipe has no liquid pool during operation, but a slight overfilling is recommended to ensure that there is not a breakdown in the liquid film.

2.3.3.3. *Removal of Non-Condensable Gases*

During the manufacturing process of heat pipes, cleaning, purification and charging of the working fluid is required [42]. If these steps are not completed meticulously, non-condensable gases can be produced in the heat pipe that limit performance. The gases are swept to the condenser section where they block performance of the section as only heat transfer by molecular diffusion can occur. The sources of non-condensable gases can be from fabrication oils, dissolved gases present in the working fluid, working fluid degradation, or generated by incompatibility between the working fluid and casing material. To prevent this, the heat pipes must be thoroughly degreased, the working fluid must be subjected to a period of boiling or cycles of flash freezing under vacuum conditions and the casing material must be compatible with the working fluid, discussed below.

2.3.4. **Casing Material and Compatibility**

The internal working fluid selected for the heat pipe must also be compatible with the casing material to avoid corrosion or production of non-condensable gases, which negatively affect the performance of the heat pipe. Table 3 provides an overview of compatibility from literature.

Table 3: Working fluid and casing material compatibility, adapted from [46].

Working Fluid	Casing Material					
	Aluminium	Copper	Ferritic Steel	Stainless Steels	Silicon	Polymers
Acetone	Acceptable	Y	Y	Y	-	PTFE
Ammonia	Y	Corrosive in presence of moisture	Y	Y	Y	Y
Argon	Y	Y	Y	Y	Y	Y
Carbon tetrafluoride	Y	Y	Y	Y	-	-
Dowtherm A	-	No	-	Y	-	-
Ethane	Y	Y	Y	Y	-	PTFE, PVDF
Ethanol	Acceptable	Acceptable	Acceptable	Y	Acceptable	-
Freon R11	Y	-	Y	Y	-	PTFE
Freon R113	-	Y	Y	Y	-	PTFE, PVDF
Freon R134a	-	Y	Y	-	-	-
Freon R21	Y	Y	Y	Y	-	PTFE, PVDF
Freon R22	-	-	-	Y	-	PTFE
Helium	Y	Y	Y	Y	Y	PCTFE, PVDF, PA
Heptane	Y	Y	Y	Y	-	PTFE, PVDF
Hydrogen	Y	Y	Y	Y	-	Y
Krypton	Y	Y	Y	Y	-	-
Methane	Y	Y	Y	Y	-	PTFE, PVDF
Methanol	No	Y	Y	Y	Y	Y
Neon	Y	Y	Y	Y	-	-
Nitrogen	Y	Y	Y	Y	Y	Y
Oxygen	Y	Y	Corrosive in presence of moisture	Y	Y	Y
Pentane	Acceptable	-	-	-	-	Y
Potassium	-	-	-	Y	-	-
Propane	Y	Y	Y	Y	-	Y

R410A	Y	Y	-	Y	-	PTFE, PVDF
R408A	-	Y	-	Y	-	-
Sodium	-	-	-	Y	-	-
Water	No	-	-	If heat treated	-	-
Xenon	Y	Y	Y	Y	-	-
<p>Y, Indicates compatibility of working fluid and casing material</p> <p>No, Casing material and working fluid are not compatible</p> <p>-, Not available in literature</p>						

2.3.5. Heat Pipe Composition Influence on Design Requirements

As discussed, the primary components of a heat pipe are the working fluid, case material and wick material. The choice of these components effects the heat pipe by a varying degree. Table 4 provides an overview of the importance of these components on different factors.

Table 4: Heat pipe components and their effect on its properties. Adapted from [42].

Property	Design Requirements	Working Fluid	Wick Material	Casing Material
Thermal Performance	Transport capacity	++	++	-
	Operating temperature range	++	-	-
	Temperature drop	+	-	-
Mechanical	Physical requirements	-	-	+
	Wall thickness-internal pressure	-	--	++
	Sink-source interface	--	--	++
	Dynamic/static loads	-	++	+
Reliability and Safety	Material compatibility	++	++	++
	External corrosion	--	--	++
	Fabrication	+	+	+
	Pressure containment/leakage	-	+	++
	Toxicity	++	-	-
<p>Key:</p> <p>++, strong influence</p> <p>+, moderate influence</p> <p>-, weak influence</p> <p>--, negligible influence</p>				

2.3.6. Heat Pipe Operation and Interaction Between Regions

Figure 12 shows a schematic of the transfer of heat from the source to the sink fluid. The variables, phenomena and governing equations are provided.

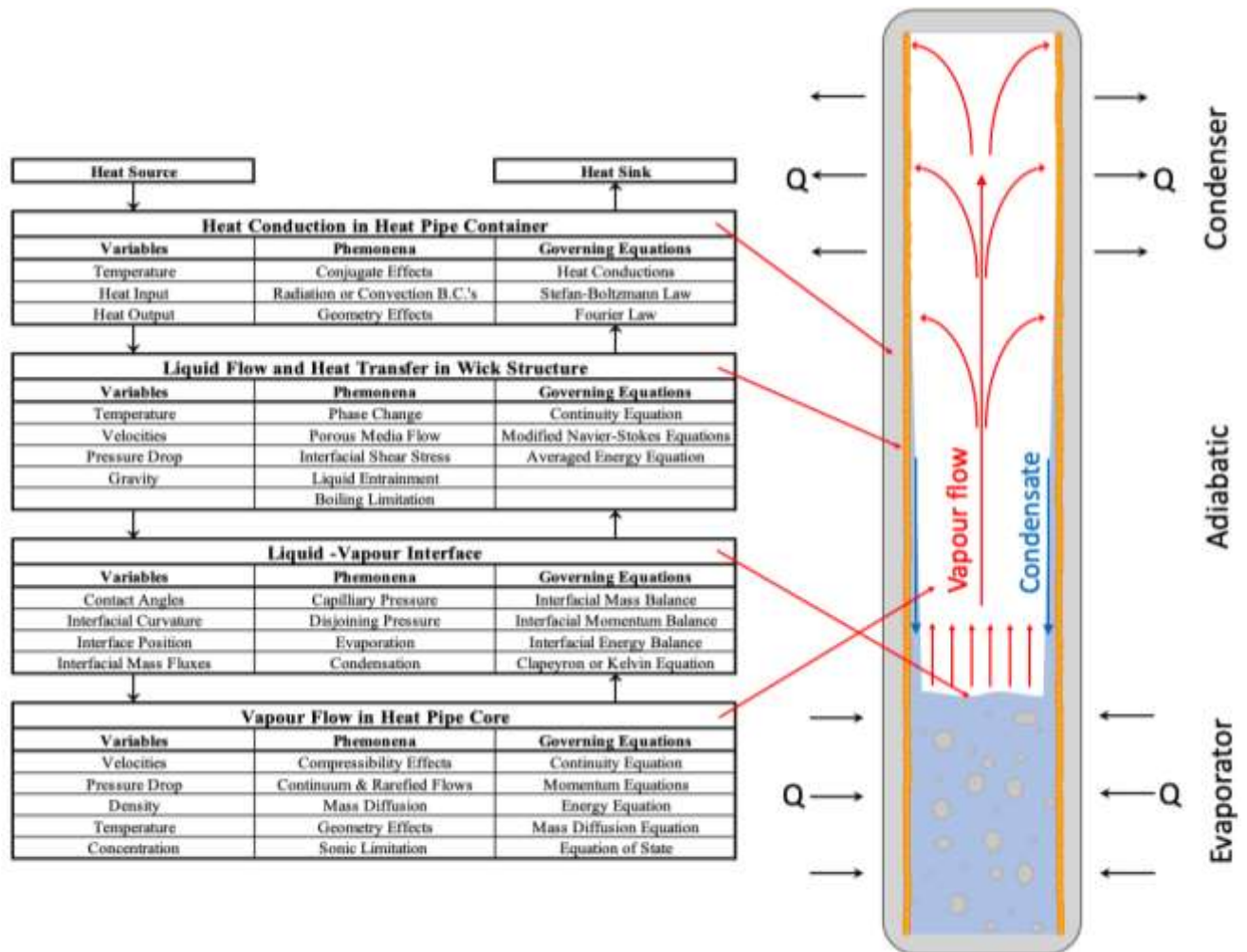


Figure 12: Heat pipe interaction between zones. Table remade from [45].

2.4. Heat Pipe Operating Limits

Wickless and wicked heat pipes are built to an operating design, and this operating design is built in consideration of the client's requirements. However, there are limits which need to be avoided during the design process. The specific limits for thermosyphons are the flooding, boiling and dryout limits. Other limits are present for wicked heat pipes such as the entrainment, capillary, viscous and sonic limits.

2.4.1. Flooding and Entrainment Limit

As vapour and liquid move in opposite directions in a thermosyphon, there is a shear force developed at the liquid-vapour interface. The flooding limit occurs when the vapour from the evaporator section is being released at such a high velocity that viscous shear forces overcome the surface tension forces of the condensate returning to the evaporator, which is then trapped in the adiabatic or condenser regions. The velocity of the vapour is much larger than that of the liquid, so the shear stress is mainly due to the vapour flow. This prevention of working fluid returning to the evaporator creates a break in the two-phase heat transfer cycle.

Faghri [61] developed a correlation that predicts the maximum heat transfer rate before flooding will occur. It includes the effect of geometry, surface tension and working fluid properties. It is recommended to operate at powers less than 75% of this limit.

$$\dot{q}_{flooding,max} = \left(\frac{\rho_l}{\rho_v}\right)^{0.14} \tanh^2\left(\frac{\sigma}{g(\rho_l - \rho_v)}\right)^{1/4} h_{fg} A_{cs} (g\sigma(\rho_l - \rho_v))^{1/4} \left(\rho_l^{-\frac{1}{4}} + \rho_v^{-\frac{1}{4}}\right)^{-2} \quad (2.9)$$

With wicked heat pipes, the equivalent of the flooding limit is known as the entrainment limit, where the shear forces cause the working fluid to be stripped away from the wick. A common methodology used to determine the entrainment limit is calculating the Weber number, We . It is a dimensionless number that defines the ratio of the viscous shear to surface tension forces and it is used when analysing fluid flows where there is an interface between two different fluids. The Weber number must be less than one to prevent liquid droplets in the vapour flow. [42]

$$We = \frac{2r_{H,wick}\rho_v v_v^2}{\sigma} \quad (2.10)$$

The heat transfer rate limit where entrainment will occur is given by [62]:

$$\dot{q}_{entrainment,max} = A_v h_{fg} \left(\frac{\sigma\rho_v}{2r_{H,wick}}\right)^{1/2} \quad (2.11)$$

2.4.2. Boiling Limit

The boiling limit is a phenomenon that occurs with heat pipes that have large fill ratios and experience a high radial flux. If a high flux is maintained, the working fluid generates bubbles at the wall. The critical heat flux is reached when the generated bubbles unite at the evaporator wall and there is boiling akin to film boiling, where there is a continuous vapour gap between the liquid working fluid and the heat pipe evaporator wall. As the vapour has a lower thermal conductivity than the liquid working fluid, there is a lower heat transfer rate leading to the wall of the heat pipe overheating, which can potentially lead to failure. There is also a large pressure increase, which can lead to casing failure.

Many correlations are proposed for the boiling limits. For a thermosyphon [63]:

$$\dot{q}_{boiling,max} = 0.16 \left[1 - e^{\left(-\frac{D_i}{L_e}\right)\left(\frac{\rho_l}{\rho_v}\right)^{0.13}} \right] \pi D_i L_e h_{fg} \rho_v^{0.5} [g\sigma(\rho_l - \rho_v)]^{1/4} \quad (2.12)$$

and for a wicked heat pipe [42]:

$$\dot{q}_{boiling,max} = \left[\frac{2\pi L_{eff} \lambda_{eff} T_{v,sat}}{h_{fg} \rho_v \ln\left(\frac{r_i}{r_v}\right)} \right] \left(\frac{2\sigma}{r_{crit,nuc}} - \Delta P_{c,max} \right) \quad (2.13)$$

2.4.3. Dryout Limit

If both the fill ratio of working fluid and the radial heat flux from the wall to fluid in the evaporator of a thermosyphon is small, a limit called dryout can be experienced. The entire working fluid volume is circulating but the falling liquid film thickness approaches zero towards the bottom of the evaporator. If all the working fluid is present as vapour or a falling film with no liquid pool, the wall temperature at the bottom of the evaporator increases as there is no evaporation. If the heat input continues to increase, the dry area will increase. This limit is simply overcome by ensuring sufficient working fluid volume. [59]

2.4.4. Capillary or Hydrodynamic Limit

The capillary limit, specific to a heat pipe, occurs when the net capillary forces from the condenser to the evaporator are insufficient to return liquid working fluid to the evaporator by overcoming gravitational, liquid and vapour flow pressure drops, i.e.:

$$\Delta P_{capillary,max} \geq \Delta P_l + \Delta P_v + \Delta P_g \quad (2.14)$$

This usually occurs in low temperature heat pipes. Breaching this limit will cause the phenomenon referred to as ‘dryout’, as in a thermosyphon, and this usually occurs when the power input is too high or if the wick is inappropriately designed for the heat pipe orientation or power. The maximum heat transfer limit in a circular heat pipe, the heat transfer rate where capillary action initially fails to provide working fluid to the evaporator, is described by [59]:

$$\dot{q}_{capillary,max} = \frac{\sigma_l \rho_l h_{fg}}{\mu_l} \left(\frac{\xi A_{wick}}{L_{eff}} \right) \left(\frac{2}{r_{eff}} - \frac{\rho_l g L}{\sigma_l} \cos \theta \right) \quad (2.15)$$

2.4.5. Viscous Limit

The viscous limit is reached when the viscous forces present in the vapour region are similar to or greater than the vapour pressure difference between the evaporator and condenser sections. This causes the vapour not to flow sufficiently and stagnate. This can occur when the heat pipe is operating at a temperature lower than design temperature. Furthermore, this limit can also occur when the triple point of the working fluid is being approached causing low vapour pressure. This limitation is usually seen in cryogenic heat pipes, those with very long condenser regions, or during start-up. Busse [64] developed the following expression to predict the viscous limit heat transfer rate in a heat pipe:

$$\dot{q}_{viscous,max} = \frac{A_v r_o^2 \lambda_v \rho_v P_v}{16 \mu_v L_{eff}} \quad (2.16)$$

2.4.6. Sonic Limit

The sonic limit describes when the vapour produced at the evaporator travels at the speed of sound. The vapour produced at the evaporator increases the velocity of the vapour travelling to and closer to the condenser section, as more vapour is produced behind it, with the fastest vapour seen at the end of the evaporator section. If the vapour flow reaches a sonic velocity, it causes the flow to be choked. The sonic vapour flow can cause the heat pipe to operate in a non-isothermal way and potentially lead to damage of the heat pipe. This primarily occurs when there is too much power at lower operating temperatures or during start-up. [42]

$$\dot{q}_{sonic,max} = 0.474A_v h_{fg} (\rho_v P_v)^{1/2} \quad (2.17)$$

2.4.7. Condenser Limit

Heat input to the evaporator section must be balanced by the ability to remove heat from the condenser section. At steady state, the heat input is equal to the heat output. The output of heat in the condenser section is transferred to the condenser fluid by different mechanisms, depending on the operating temperature and fluid phase. For lower temperature applications, convection is the dominant transfer mechanism and at higher temperatures, it is radiation. The condenser limit is reached when the heat input cannot be balanced by the heat output. This can be caused by a low flow rate in the condenser section or a small temperature difference between the heat pipe and the condenser fluid. For a cylindrical heat pipe, the condenser limit for radiation is described by [59]:

$$\dot{q}_{c,rad,max} = \iint_{A_c} \varepsilon_c \sigma_{SB} (T_c^4 - T_\infty^4) dA_c \quad (2.18)$$

which can be reduced to:

$$\dot{q}_{c,rad,max} = \pi D_o L_c \varepsilon_c \sigma_{SB} (T_c^4 - T_\infty^4) \quad (2.19)$$

The condenser convection heat transfer limit is:

$$\dot{q}_{c,conv,max} = A_c h (T_c - T_\infty) \quad (2.20)$$

ε_c is the emissivity of the outer surface of the condenser, σ_{SB} is the Stefan-Boltzmann constant, T_c is the temperature of the condenser section and T_∞ is the ambient temperature of the condenser fluid.

2.4.8. Summary

Figure 13 provides a graph showing where the various limitations of heat pipes and thermosyphons occur in respect to axial heat flux and temperature. Calculations, like those

presented above, are completed by the designer for the temperature range and parameters selected for the heat pipe to function. The area below the lines depicts where the heat pipe can operate.

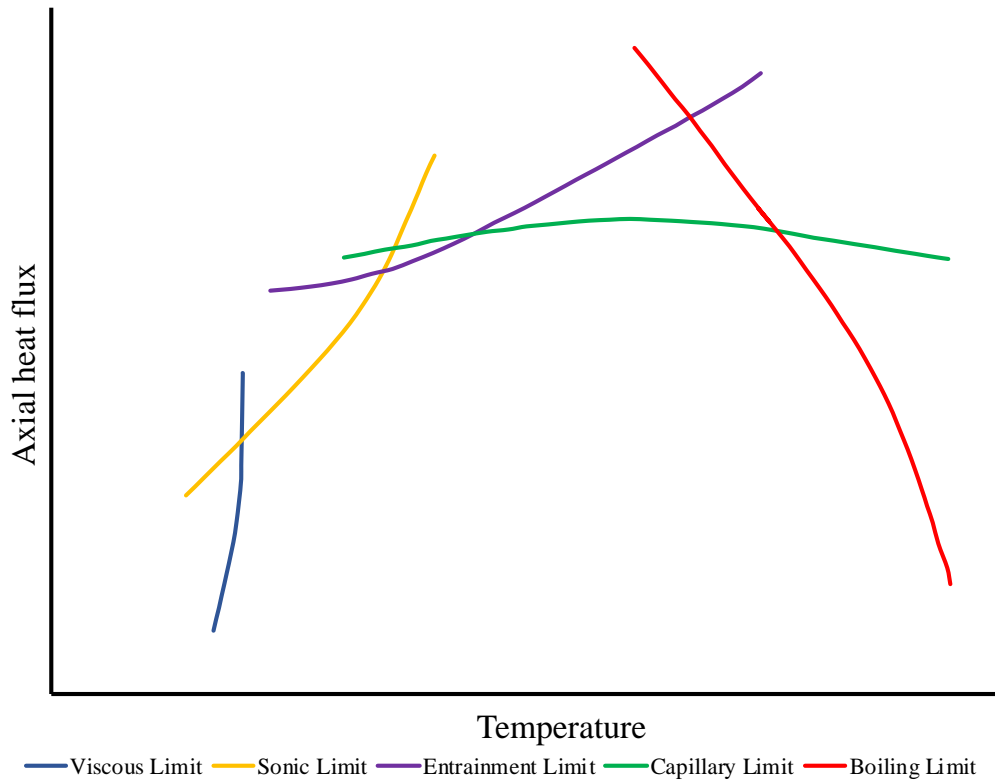


Figure 13: A graph showing the various heat pipe limitations [40].

2.5. Heat Pipe Heat Exchangers

Each heat pipe is an individual heat exchanger, but integrating many of them into a larger system forms a HPHE, which enhances the thermal performance and increases the quantity of heat transferred. Technological advancements and mass production methods have led to a significant reduction in the cost of manufacturing heat pipes, making HPHEs much more accessible. A HPHE comprises many individual heat pipes that are incorporated into banks of tubes in either a staggered or in-line conformation. All the heat pipes work in parallel to transfer heat from the heat source to the heat sink. The heat pipe evaporator ends sit in a hot stream and the condenser sections are placed in a cooler stream. A separation plate affixes the heat pipes and isolates the streams to prevent cross-contamination and as such is in the adiabatic section. There are many different configurations and inclinations possible for HPHEs. The work presented in this thesis is based around the most commonly seen configuration applied to WHR

in EIIs; vertical thermosyphons, surrounded by a casing with reducer ducts attaching the fluid carrying ducts to the core of the HPHE. Examples within Section 2.6 provide photographs of this particular design. Figure 14 provides a schematic of counterflow and parallel flow configurations. In counterflow, the temperature of the evaporator outlet can be lower than the condenser outlet. Counterflow is more commonly seen for this reason, but also to maintain a temperature difference between the condenser and evaporator sections. Even though these configurations are described as counter and parallel flow, they are physically a combination of two crossflow heat exchangers if divided between evaporator and condenser. The heat pipes are extracting and releasing heat crossflow to the direction of the incoming streams. Both crossflow and counterflow heat exchangers have a higher effectiveness than other heat exchanger geometries [65].

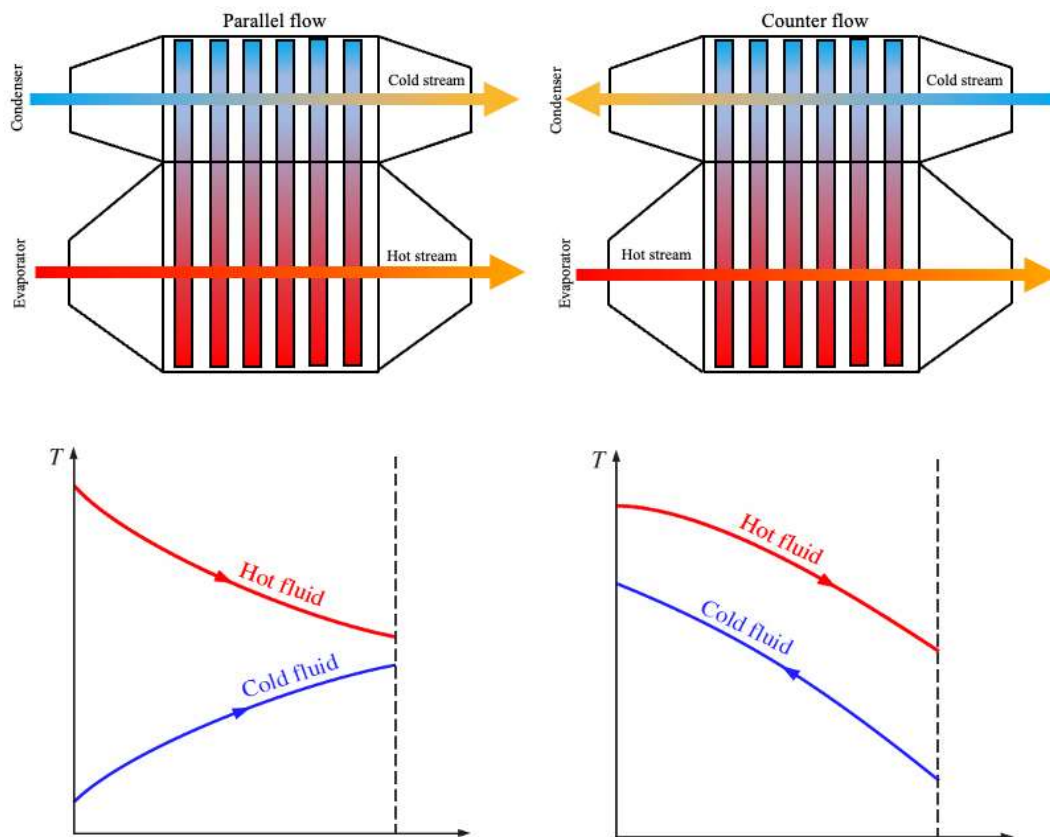


Figure 14: 2D slice of parallel and counterflow HPHE configurations with fluid temperature profiles.

In a parallel flow HPHE, as the condenser fluid progresses through the bank of tubes, heat is transferred into it and, therefore, it increases in temperature. The evaporator fluid decreases in temperature as it passes through the heat exchanger. This causes there to be a smaller temperature difference between the latter heat pipes and the condenser fluid, making the heat

transfer rate smaller. This can be overcome by using a counterflow configuration or multiple passes.

2.5.1. Benefits and Drawbacks of Heat Pipe Heat Exchangers

As with any technology, there are advantages and disadvantages of their use. The literature review conducted has indicated the numerous benefits of HPHEs over other WHR technology. The benefits and drawbacks are summarised in Table 5.

Table 5: Summary of advantages and disadvantages of HPHEs over traditional technologies.

Advantages	Disadvantages
Passive operation.	Using wicked heat pipes can be expensive so heat pipes tend to be thermosyphons.
Redundancy. One pipe failing does not affect the entire system. Easily replaced if so.	A limited temperature range determined by the working fluid selection.
Less chance of stream cross-contamination.	Compatibility of internal working fluid and external fluid stream with heat pipe case.
High thermal conductance, low thermal resistance (0.01-0.03 K.W ⁻¹).	Requires specialist thermodynamic knowledge to design.
Small footprint in comparison to traditional exchangers due to smaller surface area required.	Slow start-up period, with a careful procedure required.
Long life expectancy.	
Removes cold spots due to isothermal operation so condensation of corrosive gases leading to failure is eliminated.	
Evaporator and condenser sections can be of different sizes, meaning finning is not essential.	
Easy to install, scalable, versatile end-use.	
Low pressure drop so less fouling seen and lower parasitic cost to maintain stream flow rate.	

As discussed, heat pipes use two-phase heat transfer. The additional latent heat of vaporisation carried by the working fluid provides a high overall heat transfer in comparison to other technologies. The same energy can be transported as gas or single-phase liquid systems with smaller mass flow rates as HPHEs combine both the high sensible and latent heat capacity of the working fluid. Heat transport by latent heat is typically a few orders of magnitude higher than transport by sensible heat [39]. The conductance value of a heat exchanger (UA) is calculated from the overall heat transfer coefficient (U) and the heat transfer area (A). Both of these are relatively high in a HPHE leading to a high conductance value. A high conductance value means that the overall footprint of the heat exchanger can be relatively small. As such, HPHEs tend to be of a smaller footprint in comparison to a like for like heat exchanger. As the footprint is smaller, there can be significant weight savings and reduced structural, transportation and installation costs. With installations occurring offshore, where weight and size is a key factor, the structural ancillaries to the heat exchanger, such as platforms and support beams, can be of a lower specification and weight leading to further significant financial incentives.

The heat transfer fluids for the condenser and evaporator regions can be either liquid or gas in any configuration (i.e., gas-to-gas, liquid-to-gas, gas-to-liquid or liquid-to-liquid). This versatility is significant when choosing the waste heat stream to be recovered as well as the fluid which is linked to the end use. The direction of the heat transfer fluid streams entering the heat exchanger is also reversible, so heat can be transferred in either direction [66].

There are many choices seen for working fluid and casing materials. A heat pipe operates at an intermediate temperature between the heat source and sink. This allows very high temperature applications to be targeted [39]. Heat pipes have been designed to operate between 4 to 3,000K so a large range is possible [66].

The primary heat transfer mechanism in a HPHE is not conduction, so a comparatively thick separation plate can be used to isolate the source and sink fluid streams. If a single heat pipe fails, such as by splitting, corrosion or a weld failure, there is still a barrier between the two streams. This superior prevention of cross-contamination of the fluid streams is a significant benefit when streams must be isolated and there can be no risk of cross-contamination. In traditional heat exchanger technology, there must be a thin separation wall present in order to

enhance the heat transfer rate; this increases the risk of cross-contamination if a failure occurs at the separating walls. In addition, the heat transfer coefficient (HTC) is not largely affected by the heat pipe wall thickness. Thick walls can be used to provide a robust system, resisting erosion, corrosion and mechanical failure. The opportunity for thick heat pipe walls, along with a thick separation plate delivers a long lifespan in comparison to other technologies. Well-maintained HPHEs have been reported to be operating at 97% efficiency after 20 years. Maintenance of HPHE units can be conducted in situ, therefore dismantling and moving for maintenance is not required, reducing ongoing operating costs.

If one heat pipe fails, there is little effect on overall performance as there is just a slight reduction in overall heat transfer. This built-in redundancy allows continuous operation to a natural shut-down period where the failed heat pipe can be easily identified and replaced. Also, as they only contain a small quantity of work fluid, stream contamination is minimal. Compounding this, the heat pipe wall is an additional buffer between the source and sink fluids, reducing the chances of cross-contamination [39].

Historically, streams that are heavily laden with particulate, oils, or have corrosive elements present, have been deemed 'unrecoverable'. A core HPHE strength is that they can target these streams as they do not suffer from excessive fouling. Banks of tubes have a notoriously low pressure drop meaning the particulates do not build up quickly. Moreover, on board, automated, cleaning systems and easy access for maintenance can help combat this. Cylindrical unfinned heat pipes also do not provide a good surface for the build-up of particulates. Low pressure drops also ensure that relatively small extra fan or pump power is required.

Furthermore, as heat pipes operate isothermally, 'cold spots' are prevented whereby corrosive gases can condense leading to corrosion. The isothermal operation can also prevent degradation of thermal oils, if used, by preventing hot spots that accelerate the degradation process. With other technologies, there can be differential expansion of different parts that can lead to fatigue or stress fractures, causing failure and maintenance. HPHEs operate isothermally and the separation plate also increases in temperature, so this failure mode is eliminated. Temperature gradients can be reduced where parts are required to work in isothermal conditions.

Heat exchange using a heat pipe is completely passive with no internal or external mechanical operations, such as pumps and fans. The heat transfer process within the heat pipes also requires no pumping energy. This leads to lower wear or parasitic electricity costs. For example, rotary regenerators require constant rotary movement to transfer heat. Eventually wear parts such as seals and bearings will need replacement, requiring dismantling. This also means that ongoing maintenance costs are lower and the unit is more reliable [39]. However, fans or pumps are needed with HPHEs to move the heat transfer fluids through the unit.

Once start-up has been achieved, heat pipes can adapt to the changing conditions within the operating range and have a fast reaction time to changing conditions [39].

The design of the units is extremely customisable and scalable so many applications can be targeted. Also with the modular design, future expansion can be catered for and on-site assembly can be conducted.

Even with the benefits outlined, there are disadvantages to this technology's application. Due to the lack of market share this technology currently holds, there is limited information available as to the installation and design of these heat exchangers, as well as availability for manufacture. Specialist manufacturers' knowledge is required for the design and manufacture. The limited awareness of HPHEs means that their use is sometimes not even considered, and their popularity is still not as high as traditional technologies.

In the past, heat pipe manufacture was expensive, particularly if advanced materials or working fluid were used or if finning was required. Mass production methods seen over the last decades have reduced this cost, but the units can still be expensive. Shabgard et al. [67] report that the cost of a heat pipe for laptop cooling has dropped from \$10-15 in the 1990s to less than \$1 nowadays.

The start-up of a HPHE unit can be slow and sometimes failure can occur if, initially, the heat transfer rate is lower than that which the heat pipe is designed to achieve at operating temperature. To overcome this issue, it is reported that the optimal way to start-up a HPHE is to slowly raise the temperature of the entire heat pipe sections to the design operating level. The heat transfer rate is then steadily increased whilst maintaining the average temperature of

the heat pipes. Care must be taken to avoid introducing the heat source to the rated value suddenly. [68]

2.6. Heat Pipe Heat Exchanger Industrial Installations

Many different industries have used HPHEs to recover waste heat. HPHEs tend to be installed in challenging streams and, as such, each unit is made bespoke for a specific plant's needs. This section provides an overview of the different configurations and applications. As there is a large quantity of applications of heat pipes and HPHEs, only the applications where specifically HPHEs have been applied to recover energy from exhaust gases have been included. Additionally, theoretical applications have not been included. References [57,69] provide a good overview of where heat pipes and HPHEs have been applied in non-industrial applications. Table 6 provides references for other applications of heat pipe technology not detailed.

Table 6: Further applications of heat pipe technology.

Further Applications	References
Domestic space heating applications	[70,71]
Heat pipe refrigeration shelves	[40,72]
Solar energy PV/T & solar water heating	[73–76]
Heating, ventilation and air conditioning (HVAC)	[77–81]
Desalination	[82,83]
Data centre cooling	[84–86]
Maintaining permafrost around oil pipeline supports	[40,66]
Melting snow and de-icing	[40,66]
Thermal energy storage systems	[40,66]
Nuclear	[87]
Space and aerospace	[42,66,88,89]
Recovering by radiation	[57,90–93]
Baking ovens	[94]
Metal (brass) forging	[95]

2.6.1. Aluminium Industry

A counterflow HPHE was installed at an aluminium die caster and recovers energy from a heat treatment furnace, which is reintroduced to an ageing furnace. The HPHE was an exhaust-to-air unit, scaled to 88.6 kW [96]. The exhaust temperature was lowered from 400°C to 240°C and the air temperature was increased from 145°C to 317°C. The average mass flow rates of the exhaust and air were 1,791 and 1,802 kg.hr⁻¹, respectively. There were 310 thermosyphons in 31 rows that were 1,518 mm long with a diameter of 28 mm. The evaporator length is 620 mm and the condenser section 830 mm. Both evaporator and condenser sections were fitted with helical fins 1 mm thick, 10 mm wide with a pitch of 6 mm. Interestingly, the unit incorporated thermosyphons with both Dowtherm A and distilled water as the working fluid to optimise and increase the overall heat recovery.

Figure 15 shows a 528 kW exhaust-to-combustion air unit installed to recover heat energy from the exhaust gases of an aluminium furnace. The exhaust stream temperature was lowered from 400°C to 266°C and the air temperature was increased from 30°C to 293°C. The average mass flow rates of the exhaust and air were 12,000 and 6,374 kg.hr⁻¹. Savings of \$155,000 were realised each year with a payback of 16 months. [39]



Figure 15: Photograph of a counterflow HPHE for an aluminium furnace [39].

2.6.2. Steel Industry

A multi-sink 350 kW HPHE unit (Figure 16) was installed at a steelworks facility in Slovenia [96]. The exhaust gases temperature of a heat treatment furnace was reduced from 360°C to 178.5°C, with a flow rate of 6,150 kg.hr⁻¹, to generate 180°C combustion air for the burners for a 30°C inlet at a flow rate of 6,590 kg.hr⁻¹. There was already a recuperator installed prior to the HPHE. The water section increased the temperature of hot water from 70°C to 90°C at 3,000 kg.hr⁻¹ for space heating and hot water requirements. Furthermore, as not all the hot water was required during the summer, some was sold for sanitation purposes. The company has the ability to bypass or use the exhaust-to-water second stage depending on the price of primary energy as well accounting for the additional requirement for space heating in the colder months. Managing the system in this way allows increased versatility for the company.

The 558 unfinned thermosyphons in the first counterflow section were 2,018 mm long with an outer diameter of 28 mm; the evaporation and condenser sections were 1,167 mm and 800 mm, respectively. The working fluids were Dowtherm A in the exhaust-to-air section and distilled water in the exhaust-to-water section. The 126 unfinned thermosyphons in the second crossflow section were 1,500 mm long with an outer diameter of 28 mm, the evaporation and condenser sections were 1,175 mm and 280 mm.

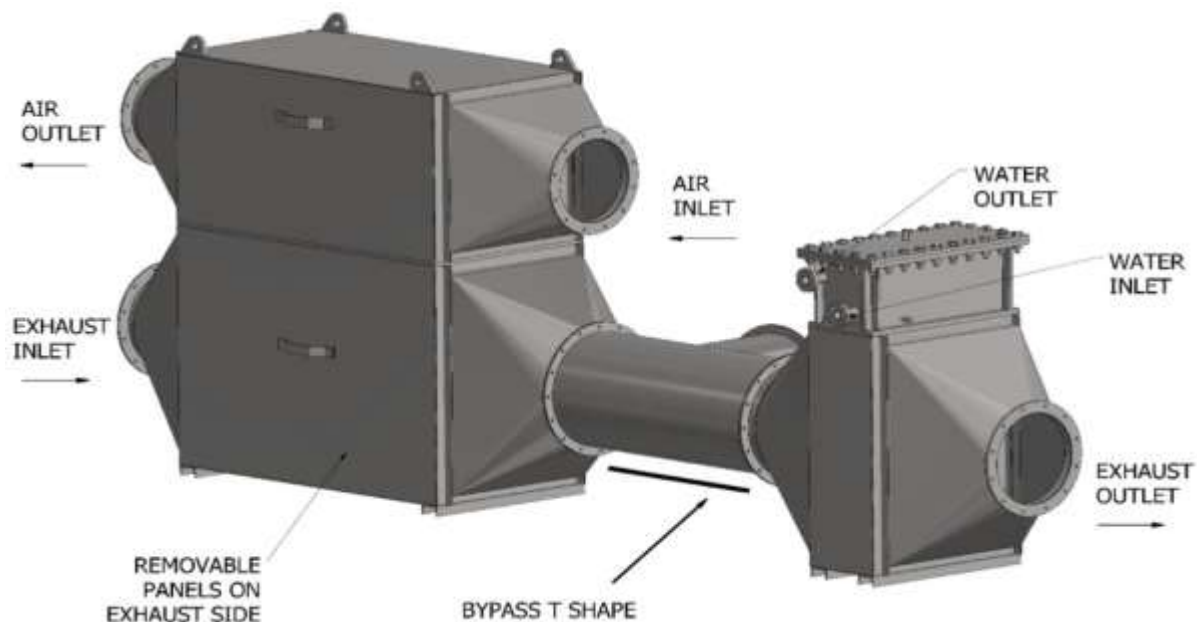


Figure 16: 3D drawing of a multi-sink, water and combustion air HPHE.

An example of a 12.6 MW counterflow HPHE installed to recover energy from exhaust gases from a steel mill blast furnace is shown in Figure 17. The unit comprised 1,575 stainless steel 7.6 m long helically finned distilled water thermosyphons. The exhaust temperature was reduced from 286°C at the inlet to 156°C at the outlet and the coke gas heat sink temperature was increased from 62°C to 197°C. The mass flow rate of each stream was 97,550 kg.hr⁻¹. The unit saves the company £800k per annum. [39]



Figure 17: Photograph of an exhaust-to-coke gas HPHE unit [39].

2.6.3. Ceramic Industry

In a ceramic tile production facility in Italy, Delpech et al. [97] installed an exhaust-to-air 99 kW HPHE on a ceramic roller kiln cooling stack to preheat fresh air which entered a spray dryer. 164 tonnes of CO₂ per annum were avoided by recovering 830 MWh equating to 110,000 m³ of natural gas consumption. This resulted in financial savings of €22k per year. Favourably, the unit return on investment (ROI) period was less than 2 years.

A 700 kW HPHE unit, of exhaust-to-water configuration, recovered energy from a ceramics roller kiln based in Italy and reused the energy after a second heat exchanger to preheat a spray dryer for a further process undertaken at the facility (Figure 18) [96]. The exhaust and pressurised water were at mass flow rates of 26,000 and 11,280 kg.hr⁻¹, respectively. The water was designed to increase from 115°C to 167°C and the exhaust temperature lowered from

245°C to 155°C. To cope with the high water temperature, the unit used pressurised water as the heat sink. There were 890 thermosyphons in total, 3 m in length and unfinned. The outer diameter was 40 mm and the working fluid was 1,360 ml of distilled water. The evaporator section and condenser section were 2,655 mm and 270 mm, respectively.



Figure 18: Photograph of a pressurised HPHE for recovering energy from a ceramic roller kiln.

2.6.4. Incineration

A very high temperature application is shown in Figure 19, a throughflow 940 kW exhaust-to-thermal oil HPHE unit. It cools the exhaust gases of a pyrolysis plant used for waste processing from 1,000°C to 250°C. Thermal oil is heated from 135°C to 280°C. The mass flow rates of the exhaust and oil are 4,150 and 9,200 kg.hr⁻¹, respectively. The energy saving equated to £150k per annum by generating electricity by an ORC. The ROI payback for the unit was less than 3 months as the unit was priced at 23 £.kW⁻¹.



Figure 19: Photograph of an exhaust-to-thermal oil HPHE tied to an ORC cycle [98].

2.6.5. Tea Drying Industry

The aforementioned examples have shown cases where HPHEs have been introduced to prevent primary energy costs and recover waste heat. In this case, a HPHE (Figure 20) was installed for health benefits by drying mate (yerba) tea leaves with clean hot air rather than direct exhaust gases from burning biomass fuel such as wood, wood chips and leaves. Mate is a caffeine-rich herbal drink consumed in South America, in particular Argentina and Brazil, where this unit was located. Drying the leaves using direct exposure to post-combustion exhaust gases leads to deposition of polycyclic aromatic hydrocarbons (PAHs). Prolonged consumption of mate has been linked to increased rates of various cancers and it is proposed that it is linked to increased PAH consumption, due to their carcinogenic properties. PAHs are fused aromatic rings that form during incomplete combustion or pyrolysis of organic matter. Leaves are initially dried by 25% by direct exposure to flame for 2 to 4 minutes and then by a further prolonged drying step at 100°C to 120°C until there is a 2 to 4% moisture content. In this application, the energy content from the exhaust gases was transferred to clean air, which was then introduced to the leaves to dry them. The counterflow unit took air from 30°C to 152°C by reducing exhaust gases from 356°C to 139°C. Drying using an uncontaminated clean heat source naturally led to less PAH deposition, leading to a cleaner and safer product. [99]

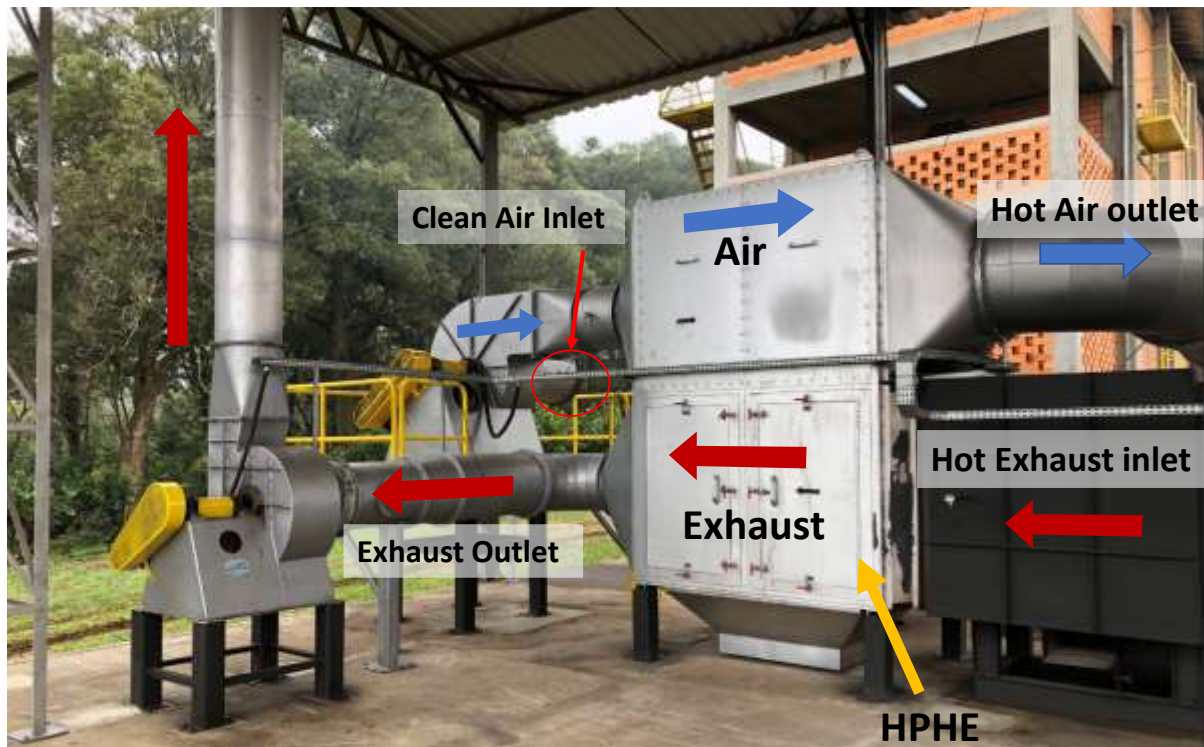


Figure 20: Photograph of a HPHE used to cleanly dry mate tea leaves.

2.7. Modelling Work

In this section, work is presented on transient heat pipe modelling, HPHE modelling and then specific examples relating to TRNSYS work, which is the ultimate direction and focus of this thesis.

2.7.1. Heat Pipe Transient Modelling

Transient modelling of single heat pipes has received significant interest in recent years. Transience has historically had different meanings in context to heat pipes. Many early ‘transient’ heat pipe models dealt with start-up, particularly the change of solid working fluids into liquid and eventually vapour. Transience is being used in the context of this research as change in performance over time with varying power from the source fluid with changing condenser and evaporator inlet parameters. However, both scenarios are presented here for completeness. Cryogenic heat pipes have not been included as they are outside of the scope of this work. Focus is directed to cylindrical heat pipes at room temperature and above. Steady state modelling theory of heat pipes is presented in [52,100,101].

Previous research on heat pipe modelling can be split into three approaches, in increasing order of complexity. Firstly, simplified generic analytical models can simulate energy transfer and vapour flow. Secondly, geometrically-based numerical models consider the different heat pipe regions and simulate vapour, wick and wall regions. Both of these overlook fluid flow dynamics in the wick. Thirdly, functional detailed numerical models are considered that couple the liquid and vapour hydrodynamics or predict the behaviour of the wick meniscus. Generally, more accurate predictions are given by numerical models but these take additional computational effort, coding and time. This is less important now computational power has increased but the generic analytical models are simpler and give good approximations. [102]

Deverall et al. [103] described the transient behaviour of water and metallic heat pipe start-up problems based upon experiments. They concluded that start-up was possible from a solid-state working fluid, however, it was highly dependent on the amount of heat rejected at the condenser. This is because the liquid had to return to the condenser to complete the two-phase cycle before solidifying. Colwell [104] is one of the first publications that model the complete transient start-up behaviour of a heat pipe at each stage of the process. In this work, a heat pipe is modelled with a metallic working fluid for high temperature applications, during start-up from a frozen state. A heat pipe cooled leading edge of a space shuttle wing was also modelled for purposes of re-entry. A more recent example, with a different application of start-up from frozen state, was performed by Yang et al. [105], who developed a transient analysis code for a flat heat pipe receiver in a solar power tower plant with sodium as the working fluid. The model was able to predict the temperature distributions reasonably well, and the experimental results showed promise for applications of flat heat pipes to solar towers. Hall and Doster [106] developed the THROHPUT code for transient liquid metal heat pipe start-up to steady state full power operation and presented comparisons with experimental data.

The above research was performed on higher temperature applications. In relation to room-temperature working fluids, even though frozen start-up is not commonly seen with water or ammonia, studies have been conducted on the modelling and testing [107]. Furthermore, in relation to room temperature working fluids, research widely shows that the transient hydraulic response of these working fluids happens in the order of a magnitude of a few seconds. However, the thermal response of the heat pipe wall can be several minutes to hours. Brocheny [108] modelled the transient behaviour of low-temperature heat pipes with room-temperature

working fluids. This contributed to previous work by including dry-out and recovery in the thermal predictions, but the effect of wick saturation was not considered.

The three groups of simplified generic models are: the lumped capacitance model [109–111], liquid transient behaviour [110,112] and thermal resistance network [113–115]. The lumped capacitance model assumes uniform internal temperature at any time, a saturated wick with vapour circulation established and applies an energy balance on the volume of the heat pipe. This methodology can only be used if the overall thermal resistance and capacitance of the heat pipe is low compared to the evaporator and condenser streams. The condenser heat transfer boundary conditions can be cooled by convection, or radiation if high temperature. Faghri and Harley [102], for conventional and non-condensable gas-loaded heat pipes, called this model a transient lumped heat pipe formulation. The authors looked to develop a more simplified and convenient method for designing heat pipes by making more approximations that reduced computational effort. This work presented a general formulation that compared well to full numerical solutions and experimental data. The boundary conditions were altered depending on whether the condenser heat output was increased or decreased with uniform heat input, also with steady cooling and altering the heat input.

The liquid transient behaviour models couple the liquid rewetting with the heat pipe temperature. This was done by Ambrose, Chow and Beam [110] to predict liquid rewetting behaviour with pulsed heat input, which allowed prediction of the dryout phenomena by tying liquid mass conservation with the lumped capacitance model. The authors introduced a time-lag term to account for the initial thermal inertia in the evaporator section to account for transient temperature profiles.

Tournier and El-Genk (1994) [116] built upon their previous research [117] and developed their own two-dimensional fully-thawed Heat Pipe Transient Analysis Model, known as HPTAM. The additional considerations were the liquid flow and hydrodynamic coupling of the liquid and vapour phases, the thermal expansion of the liquid pool and the receding and accumulation of the pool due to heat-up and cooldown transients. A two-dimensional treatment of the vapour flow was included. The results achieved were in reasonable agreement with the experiments, albeit the simulated transient response was found to be faster than in the

experiment due to time wasted as heat travels throughout the insulation. El-Genk, Huang and Tournier [118] went on to conduct transient experiments of an inclined copper-water heat pipe.

The thermal resistance network analysis is a proven way of viewing the thermal resistances in a heat exchanger [119] and considers the temperature difference between the evaporator and condenser streams as an important parameter. The method draws parallels with an electrical circuit. Resistance blocks the transfer of current, in a thermal energy analogy, current is heat flow and resistance is thermal resistance (R), defined as the difference in temperature (ΔT) divided by the heat transfer rate (\dot{q}), as shown in Equation (2.21). If the heat pipe is functioning correctly, the overall thermal resistance should be low. This method is described in more depth in Chapter 3.

$$R = \frac{\Delta T}{\dot{q}} \quad (2.21)$$

Zuo and Faghri (1998) [114] recognised the need for transient analysis over steady state and used first order, linear and ordinary differential equations to predict heat pipe operation using a network thermodynamic analysis based on the thermal network model. It is noted that the vapour and wall temperature transients have very different time scales, but the vapour flow thermal resistance can be neglected due to it being considerably less and spontaneous. The main transient behaviour of the heat pipe was determined to be the wall and wick heat conduction. Tests between 365 and 530 W from work conducted by El-Genk were analysed and the predictions were very similar to the measurements (maximum of 5% deviation). An overprediction in vapour temperature was seen, which was attributed to heat losses to the environment not accounted for. Moreover, the transient model reacted faster than the experimental heat pipe in both start-up and shutdown. However, transience is also described by a change in power; something that this study did not address.

Geometrically-based models are numerical models developed for increased accuracy and focus on the different heat pipe regions- the vapour, wall, liquid-wick. Zuo and Faghri (1997) [120], effectively modelled a transient heat pipe with quasi steady state one-dimensional vapour flow and a transient two-dimensional conduction in the wall and wick and compared the results to previous experimental and numerical studies. The authors used two methods to solve the vapour flow and wall and wick regions: the finite difference method and the boundary element

method. They show that assuming a quasi-steady state of the vapour flow is justified. However, the model was more valid for slow transients rather than rapid differences in heat fluxes.

Cao and Faghri [121] performed a numerical analysis of transient heat pipe performance on cylindrical and non-conventional heat pipes that had uniform and non-uniform heat distributions and compared it with available results. The authors coupled a transient compressible quasi-one-dimensional vapour flow model with a body-fitted grid system applied to a three-dimensional wall and wick model. They employed this design as it had been highlighted that radial temperature gradients highly affect transient results, particularly due to wall thickness and thermal conductivity.

2.7.2. Heat Pipe Heat Exchanger Modelling

Steady state modelling has been exhaustively conducted for HPHEs. Amode and Feldman [122], in 1975, and then Lee and Bedrossian [123], used a conductance model to estimate HTC's for small HPHE units, with heat pipes and thermosyphons in both in-line and staggered configurations. The latter presented an iterative calculation to predict acceptably the performance of heat exchangers with thermosyphons. Empirical information was presented with corrected surface HTC's. They also saw that the overall HTC increased, to a converging limit, by increasing Reynolds and Prandtl numbers. In addition, the authors presented a method for determining the optimum number of fins, as well as showing that inclination affected performance more with thermosyphons than heat pipes.

Following this work, Huang and Tsuei [124], in 1984, showed that the conductance model can be used to predict HPHE performance. Single heat pipe conductance was obtained experimentally and correlations for convective HTC's in tube banks were used to calculate the performance of an air-to-air HPHE. This was then tested with twelve experimental conditions. The HPHE size was small at four staggered longitudinal rows of eight pipes. The evaporator and condenser sections of the heat pipes were both 305 mm long. The evaporator inlet steam was between 238 and 301°C at flowrates between 8.2 to 12.9 m³.min⁻¹. The condenser inlet stream was between 24 and 35°C at flowrates between 6.8 to 13.2 m³.min⁻¹. Each longitudinal row was analysed for the temperature difference between experimental results and theory. The maximum average error for the evaporator air temperature was after the first row, where the experimental temperature was 6.2% higher than the theoretical results. For the condenser air

temperatures, the largest average error was after the second row, where the experimental results were 3.5% lower than the experimental results. The maximum average error for a row of heat pipe wall temperatures was 14.4°C for the evaporator and -14.7°C for the condenser wall temperatures. These were on the same rows where the highest average air temperature error was seen, as expected.

However, the above did not attempt transient modelling. There are three predominant methods used for predicting or characterising the performance of a heat exchanger. These are the Log Mean Temperature Difference (LMTD) method, the ϵ -NTU method and an extended version of the thermal network analysis method.

2.7.2.1. Extended Thermal Network Analysis Model

As each heat pipe is an individual miniature heat exchanger, they are all assumed to be heat transfer devices working in parallel with one another within a larger heat exchanger assembly. This methodology can be heavily used for performance predictions and is fully described in Chapter 3.

2.7.2.2. Logarithmic Mean Temperature Difference Method

The LMTD method can be used to quantify HPHE performance when inlet and outlet temperatures are known from experimentation or for design purposes when a desired outcome is required. This method can be used for steady state but cannot be applied in a model requiring a transient simulation. The LMTD method oversimplifies the model as averaged values need to be used, which does not reflect the real nature of energy intensive processes. Furthermore, this is not a predictive method as outlet temperatures must be known. This method can be used for HPHEs but relies on previously determined data for inlets and outlets of an existing unit and so it is not useful for predicting performance. For a counterflow heat exchanger, the equation to calculate LMTD (ΔT_{LM}) is [125]:

$$\Delta T_{LM} = \frac{(T_{h,in} - T_{c,out}) - (T_{h,out} - T_{c,in})}{\ln \left(\frac{T_{h,in} - T_{c,out}}{T_{h,out} - T_{c,in}} \right)} \quad (2.22)$$

For a crossflow heat exchanger or multipass, the flow conditions are too complex, leading to cumbersome equations. Therefore, a correction factor is introduced that can be taken from

empirically derived charts [126]. Weierman, Taborek and Marner [127] suggested that using the LMTD method for characterising in-line tube HPHEs was not suitable as there is a non-uniform temperature distribution in the direction of flow.

However, the LMTD method is useful in the model developed to determine heat transfer rate outputs by [128]:

$$\dot{q} = UA\Delta T_{LM} \quad (2.23)$$

2.7.2.3. Effectiveness-Number of Transfer Units Method

The ε -NTU method is used to predict outlet temperatures by calculating the effectiveness – a dimensionless parameter related to the heat transfer performance of the heat exchanger. It is a measure between 0 and 1 and it is the measure of the actual heat transfer rate compared to the maximum theoretical heat transfer rate for the heat exchanger. The general equation is shown below and has been developed for the evaporator, ε_e , and condenser, ε_c , sections of a HPHE [119]:

$$\varepsilon_e = \frac{\dot{q}_{act}}{\dot{q}_{max}} = \frac{C_e(T_{e,in} - T_{e,out})}{C_{min}(T_{e,in} - T_{c,in})} \quad (2.24)$$

$$\varepsilon_c = \frac{C_c(T_{c,out} - T_{c,in})}{C_{min}(T_{e,in} - T_{c,in})} \quad (2.25)$$

This method was determined to be the most useful for transient predictions and was used to create the TRNSYS component and is comprehensively discussed in Chapter 3.

To predict HPHE performance, numerous papers in literature have referenced using the Effectiveness Number of Transfer Units (ε -NTU) method. A limitation of this method is that it has only been applied to steady state conditions, which are often the exception in real life heat recovery systems unless significant control measures are implemented. A large proportion of the early work of modelling HPHEs focused on dehumidification and energy saving in HVAC systems. Krishman and Rao [129] and Chaudrone [130] in 1984, reported expressions of effectiveness for HPHEs by number of rows and for a single heat pipe.

Azad and Geoola [131] developed work presented by [65] in order to create a design procedure for counterflow HPHEs, which they call a Gravity-Assisted Heat Pipe Heat Exchanger (GAHPHE). There was a capillary wick present in the evaporator section to prevent issues caused by vapour-fluid shear stress and the heat source was waste moist air at 70°C. Variations of staggered tube spacing, aluminium fin parameters, and heat pipe section lengths were plotted. The resistances in the heat pipes were calculated using conductance equations for the outer wall, pipe wall, inner wall and saturated wick with thermal conductivity equations. The external HTC's were calculated from correlations for continuous fins with circular tubing by Rich [132] and the inner HTC by Rohsenow correlations. Calculation of the internal HTC in the condenser section was not fully outlined. Azad, Mohammadi and Moztarzadeh [133] theoretically built on this for a small HPHE with fixed characteristics but modelled 6 or 10 longitudinal rows. They used the ϵ -NTU to do an iterative row by row calculation to predict the performance of this HPHE at steady state.

Tan and Liu [134] report that the ϵ -NTU method is a viable alternative for predicting the performance of a HPHE. They went one step further than previous methods to mitigate iteration and hence reduce computation. They incorporated the thermal network analysis model to calculate convective HTC's from Whitaker [135] correlations. They compared the results to Huang and Tsuei's [124] conductance model, with good agreement. Unfortunately, no analysis was given on the accuracy of the results or any indication of the code. Figure 21 graphically outlines the results.

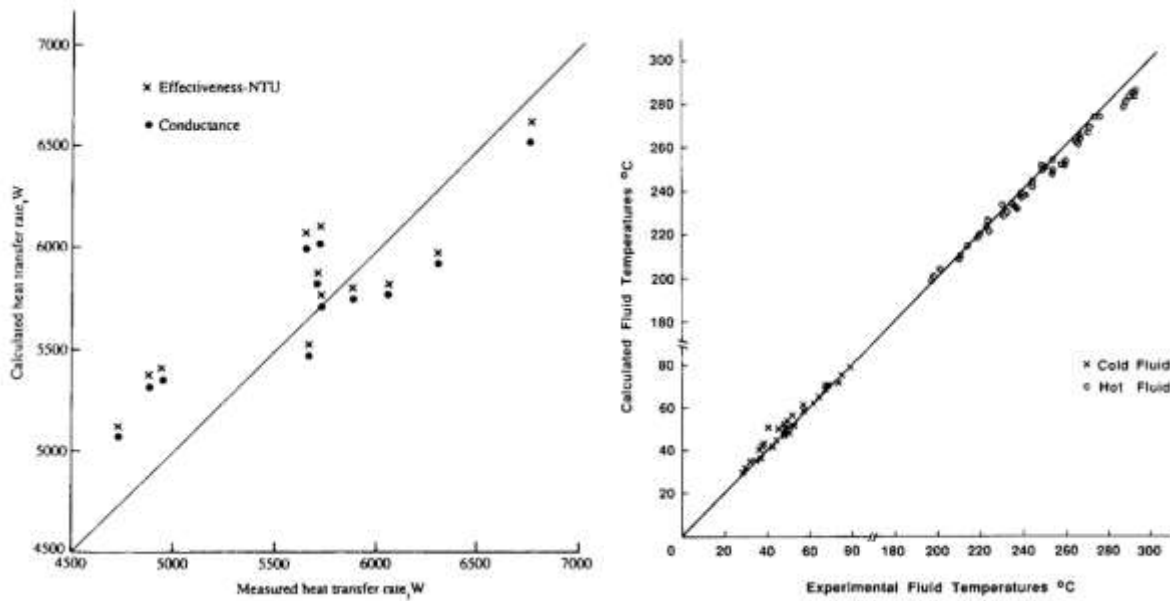


Figure 21: Graphs showing heat transfer rate and temperature comparisons between the conductance model and ϵ -NTU method for experimental and simulated results [134].

Ramos, Chong and Jouhara [119] used the ϵ -NTU method and thermal resistance network analogy to conduct a numerical investigation on a crossflow air-to-water HPHE equipped with thermosyphons. The authors coupled the ϵ -NTU method with CFD simulations in ANSYS to visualise the temperature distribution within the evaporator and condenser sections. The unit was only small, with six thermosyphons. For a range of flow conditions, the average temperature difference between numerical and experimental results was 5% in the evaporator section and 7% in the condenser section.

2.7.3. TRNSYS Work

To date, the vast majority of work on HPHEs has been steady state simulations conducted using traditional methods which use averaged input values and parameters. In order to create a transient simulation with varying inputs and parameters, the software TRNSYS (TRAnSient System Simulation) 17 was used. To date, TRNSYS has heavily been used primarily in the study of solar energy systems but some modelling has been conducted on heat recovery using heat pipe technology, described below. [2]

The earliest literature found regarding the use of TRNSYS and heat pipes was by Shariah and Shalabi in 1997 [136]. The authors optimised design parameters for a thermosyphon solar water heater in two regions of Jordan by using available weather data. At the time, 30% of households

in Jordan had these systems installed. However, averaged parameters were used for the thermal and optical properties of the solar collector, with simple equations to determine energy gain and the data input was hourly. The code was not provided.

Kalogirou and Papamarcou [137] also modelled a thermosyphon solar water heating system for Cyprus using TRNSYS and conducted simple experiments to validate with collected weather data to give an economic analysis. The solar water heater was of a fixed design. A more detailed model was made in 2003 by Budihardjo, Morrison and Behnia [138] for predicting the performance of water-in-glass evacuated tube solar water heaters (Figure 22). Again, though not WHR, this work highlighted the use of TRNSYS to simulate 21 inclined open thermosyphons. TRNSYS was used to simulate the collector efficiency and natural circulation flow rate. The Raleigh and Reynolds number correlations were given but no code was provided. Further TRNSYS work on water-in-glass evacuated tube solar water heaters was conducted by [76,139].

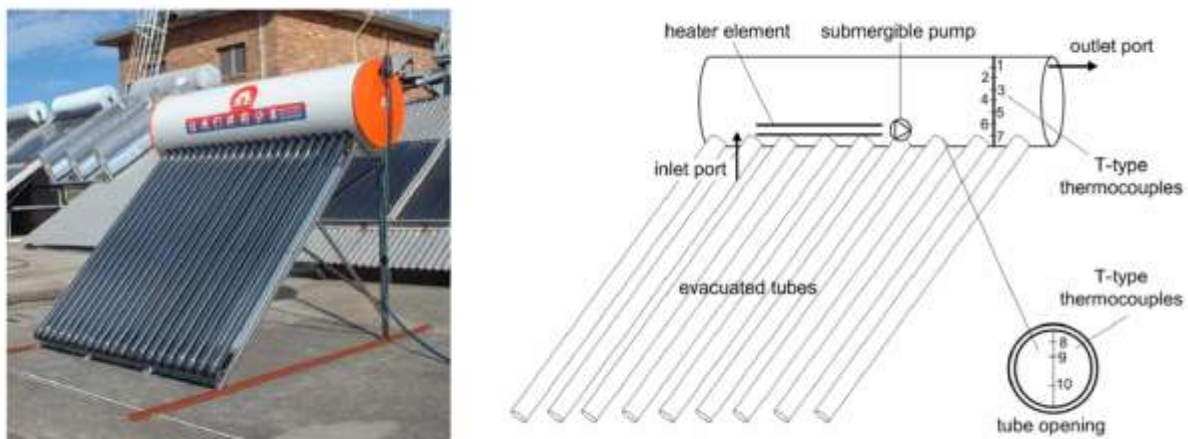


Figure 22: Schematic and photograph of water-in-glass evacuated tube solar water heater.

Yau and Tucker [80] calculated the overall effectiveness of a wet six-row wickless HPHE for a HVAC system. The main aim was to determine whether moisture content and film condensation on fins reduced the total effectiveness value of the HPHE. This was a very small laboratory-scale unit consisting of six copper heat pipes with an outer diameter of 9.55 mm. The heat pipes were finned with 0.33 mm thick aluminium at a spacing of 315 fins per metre. The TRNSYS model for the HPHE is the most relevant work to this presented work. The model is presented within the appendix of [140]. The model simulates a laboratory-scale HPHE,

equipped only with copper heat pipes and fins, to determine the overall effectiveness of this heat exchanger and specially requires an inclination angle and humidity of the air. This is an example of WHR, but focuses on HVAC systems and removing humidity for air, focusing on hospitals, and predicting the onset of film condensation. This model used hour-by-hour climatic data from Kuala Lumpur and dealt with low temperature ranges, less than 35°C. This work was built upon by Yau [79], in 2008, to analyse the hourly effects on a double HVAC HPHE system for treating ventilation air in an operating theatre. Further TRNSYS systems were studied by Ahmadzadehtalatapeh [141,142] who looked at HPHEs to replace conventional air conditioning systems. There was no mention of the use for the waste heat, the units were small three row configurations (2,4,6 rows) and there was no reference to the number of pipes in each row.

Previous work by Brough et al. [2] saw the use of TRNSYS to model a HPHE applied to a laboratory-scale ceramic kiln using exhaust gases to preheat water. The authors noted the necessity for a dedicated HPHE component to simulate the performance more accurately rather than the existing heat exchanger models available. Energy recovery rates were within $\pm 15\%$ with an error of $< 5.8\%$, though temperature prediction differences of up to around 35% were seen. The model could not be confidently used for simulation predictions and used averaged values of conductance taken from the experimental work. This was the catalyst for the present work that builds upon the conclusions previously published, whilst demonstrating validity on full-scale installations using a component that can be used to predict performance in the future.

To date there have been no publications for a dedicated transient simulation component of a versatile full-scale HPHE for recovering waste heat from industrial exhaust gases. The present research aims to fill this gap in knowledge using TRNSYS. This Thesis presents a HPHE component that can simulate multiple heat sinks, varying vertical thermosyphon configurations, and is configured for WHR from industrial exhaust gases.

3. THEORETICAL ANALYSIS

Faghri [59], a pioneer in heat pipe research, explains for the analysis of HPHEs: *‘The following assumptions are made in the analyses below: the [HPHE] operates at steady state, all thermophysical properties are constant and the vapor temperature drops within the heat pipes are negligible’*. Shabgard et al. [67] also state: *‘it is emphasized that representation of a thermosyphon and related [thermosyphon heat exchangers] in terms of thermal resistances is only accurate for steady state conditions.’*

A main contribution of this work is expanding on this traditional methodology by conducting analysis transiently and altering thermophysical properties and performance depending on the fluctuating conditions present. The hypothesis tested is that an adapted ϵ -NTU model can be used to predict HPHE performance quasi-transiently rather than relying on standard averaged models. The phenomena taken advantage of is the fact that heat pipes, once operational, have a relatively fast reaction time to changing thermal loads or flux.

Chapter 2 generally covered the available modelling techniques for heat pipes and HPHEs. This Chapter goes into detail about how available techniques and theory are used and adapted to create a transient predictor of HPHE performance. Two models have been developed in separate software, one a steady state in MATLAB_R2019b and the second a transient TRNSYS v17 model. The benefit of the MATLAB model is that the value of every parameter is visible at the end of a simulation and hence can be evaluated. When using the TRNSYS model, only the explicit outputs are visible, but the added benefit of transient analysis is gained. Details of the thermal network analysis, the extended analysis for HPHEs and ϵ -NTU method are given, also, how the following are calculated: maximum heat flux, applicable heat transfer coefficients, thermophysical properties, key dimensionless numbers and factors that are influenced by HPHE design geometry such as arrangement and presence of finning. Moving forward, the models for the HPHE are based upon wickless heat pipe (thermosyphon) equations. True heat pipe equations and wicks are no longer considered. The equations appearing below may not follow the same nomenclature as originally reported as they have been adapted to follow the nomenclature of this Thesis.

3.1. Thermophysical Properties of Heat Sink and Source Fluids

Common heat sink fluids for HPHEs are air, water and thermal oil. These fluids have varying thermophysical properties depending on the conditions present, mainly temperature and pressure. Key thermophysical properties for each of these fluids were found in literature, plotted and best fit equations extracted to determine the variation of thermal properties against temperature. The thermophysical property graphs and equations are provided in Appendix C for reference. As exhaust gases are predominantly the industrial waste heat source used to recover waste heat, the properties of natural gas combustion products are used for the heat source fluid entering the evaporator. Other exhaust gases from various combustion sources, or with different properties, can be easily exchanged, if required. It is necessary to calculate thermophysical properties at inlet and outlet conditions, which are then averaged to determine the properties for the centre of the unit. The properties are also evaluated at the wall temperatures in both the condenser and evaporator sections.

The exhaust streams referred to are, in fact, a mixture of gases; as is air. Exhaust and exhaust gases are considered synonymous throughout this thesis. In the calculations, the exhaust gases and air are treated as a single fluid, where their composition affects the properties. NO_x can also be present in exhaust gases, particularly at high temperature, but at the temperature ranges tested, their presence would be negligible.

The key properties required for calculations for each fluid are:

- Density, ρ (kg.m^{-3})
- Kinematic or momentum viscosity, ν ($\text{m}^2.\text{s}^{-1}$)
- Thermal conductivity, λ ($\text{W.m}^{-1}.\text{K}^{-1}$)
- Specific heat capacity, c_p ($\text{J.kg}^{-1}.\text{K}^{-1}$)

It should be noted for thermal oil that therminol-66 was used. Alternative oils' thermophysical properties can easily be introduced into the model, if required.

3.2. Key Dimensionless Numbers

Throughout this chapter, a few key dimensionless numbers appear across concepts, these being the Reynolds, Prandtl and Nusselt Numbers. They are outlined in this section.

3.2.1. Reynolds Number

The Reynolds number (Re) provides an indication of the flow regime and also the point where laminar flow transitions to turbulent flow. Laminar flow is synonymous with a smooth, ordered, and regular flow with little mixing where fluid layers slide over each other. Turbulent flow is described as an irregular, disordered flow with mixing. Large Reynolds numbers indicate turbulent flow and a quick transition from laminar to turbulent flow and *vice versa* for a small Reynolds number [125]. Figure 23 shows typical Reynolds numbers associated with crossflow fluid patterns for shell side fluids. Reynolds numbers analysis is also applied for fluid flow inside pipes or between fins.

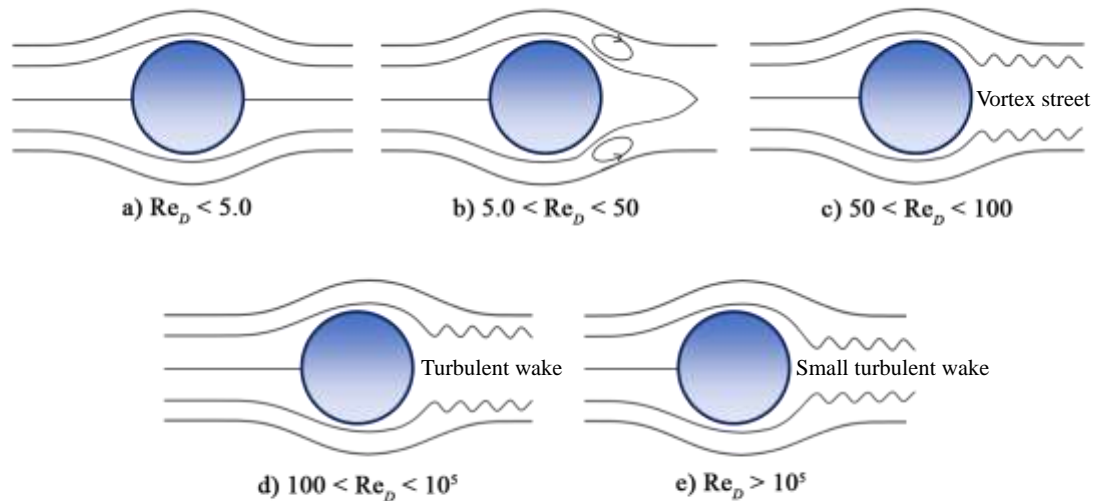


Figure 23: Schematic of crossflow flow patterns for fluids passing across a cylinder with increasing Reynolds number, adapted from [143].

Equation (3.1) is the general equation used to calculate the Reynolds number.

$$Re = \frac{\text{Inertial forces}}{\text{Viscous forces}} = \frac{\rho u L_{ch}}{\mu} = \frac{u L_{ch}}{\nu} \quad (3.1)$$

where, u is the flow velocity, μ is the dynamic viscosity, ν is the kinematic viscosity and L_{ch} is the characteristic length. When calculating the Reynolds number associated with banks of thermosyphons in a HPHE, the outer diameter of a tube (D_o) is the characteristic length, the velocity used is the maximum velocity, u_{max} , experienced (described in Section 3.3.1) and hence the Reynolds number associated with diameter, Re_D , is:

$$Re_D = \frac{u_{max} D_o}{\nu} \quad (3.2)$$

3.2.2. Prandtl Number

The Prandtl number, Pr , of a fluid is the ratio between momentum diffusivity and thermal diffusivity. It is necessary to calculate this in order to calculate the Nusselt number as the majority of Nusselt correlations include the Prandtl number as a term. A velocity and thermal boundary layer develops when a fluid flows over a surface with a different temperature. The number describes the relative sizes of the thicknesses of the thermal and velocity boundary layers. Gases typically have Prandtl numbers around 0.7 to 1.0, water is 1.7 to 13.7 and oils are 50 to 1×10^5 [125]. The Prandtl number can be determined by Equation (3.3) [126].

$$Pr = \frac{\text{Momentum diffusivity of momentum}}{\text{Thermal diffusivity of heat}} = \frac{\nu}{\alpha} = \frac{\mu/\rho}{\lambda/c_p\rho} = \frac{c_p\mu}{\lambda} \quad (3.3)$$

α is the thermal diffusivity ($\text{m}^2 \cdot \text{s}^{-1}$).

3.2.2.1. Prandtl Number Evaluated at Wall Temperature, Pr_s .

Another specific Prandtl number required for some Nusselt correlations is Pr_s , the Prandtl number evaluated at the external wall temperature of the thermosyphon. In this case, the wall temperatures of the thermosyphons are unknown and, as such, need to be calculated. This can be done using two methods, either the thermal network analysis described in Section 3.5 or by conducting a thermal energy balance at both the evaporator and condenser sections. In the case of the developed model, an initial approximation of the wall temperature is used to give initial outlet temperature values and calculated heat transfer rate values using:

$$\dot{q} = \dot{m}c_p\Delta T \quad (3.4)$$

where ΔT is the difference between the inlet and outlet temperature of the heat transfer fluid in either the evaporator or condenser stream. A second equation to find the heat transfer rate using initial calculated temperature values is:

$$\dot{q} = hA \frac{T_{in} - T_{out}}{\ln(T_{in} - T_w / T_{out} - T_w)} \quad (3.5)$$

These two equations are balanced against each other and a coded goal seek function alters the wall temperature, T_w , value by 0.001°C until a balance between the two heat transfer rates is reached. The max number of iterations is set to one million.

Once the heat transfer rate of Equations (3.4)(3.5 are balanced, the approximate value of wall temperature, T_w , is then found by rearranging Equation (3.5) which is then used to recalculate a more accurate heat transfer rate. The rearranged equation to give the wall temperature for either the evaporator or condenser section is shown by Equation (3.6, though in the model the wall temperature is saved as a variable in the memory:

$$T_w = \frac{T_{out}e^x - T_{in}}{e^x - 1} \quad (3.6)$$

where,

$$x = \frac{hA(T_{in} - T_{out})}{\dot{q}} \quad (3.7)$$

3.2.3. Nusselt Number

The Nusselt number is calculated from Equation (3.8) in order create a non-dimensional number from many contributing variables. In essence, the Nusselt number represents a ratio of heat transfer by convection to conduction across a fluid layer to quantify which mechanism contributes the most to heat transfer, and it is also a measure of the surface temperature gradient [125].

$$Nu = \frac{hL_{ch}}{\lambda} \quad (3.8)$$

where h is the heat transfer coefficient. In the case of HPHEs, this is adapted to:

$$Nu = \frac{h_{fc}D_o}{\lambda} \quad (3.9)$$

h_{fc} is the heat transfer coefficient of forced convection. An important note, worthy of mentioning, is that D is usually presented as the hydraulic diameter, D_H . In the case of cylindrical pipes, which is usually the case in HPHEs, the hydraulic diameter is replaced with the outer diameter as they are equivalent, D_o . The hydraulic diameter only comes into effect when non-standard pipes are used in order to perform calculations. For example, non-circular tubes or channels.

$$D_H = \frac{4A_{cs}}{\text{Wetted Perimeter}} = D_o \quad (3.10)$$

A_{cs} is the cross-sectional area.

The Nusselt number can be found using empirical correlations, detailed in Section 3.9.1.1 where the heat transfer coefficient can then be determined by rearranging Equation (3.9). These correlations rely on determining Prandtl and Reynolds Numbers as the Nusselt number is normally seen as a function of both. It can also depend on the inclination angle, φ , but only vertical pipes are presented here so this can be discounted.

$$Nu = f(Re, Pr, \varphi) \quad (3.11)$$

3.3. Arrangement of Thermosyphons

The arrangement of the thermosyphons can be staggered or in-line, as shown by Figure 24 and Figure 25. A staggered arrangement is usually preferable to in-line as there is increased coverage of the fluid streams by the staggered-tube bundles leading to higher effectiveness as the heat transfer coefficient is larger. This effect is stronger if the tube banks are tightly rather

than widely spaced [144]. Interestingly, Kuntysh and Stenin [145] show that, in a staggered configuration, the highest heat transfer rates are not seen in the first row. But for an in-line arrangement, the highest heat transfer coefficient was seen in the first row. The effect on arrangement on the forced convection heat transfer coefficient is described in Section 3.9.1 and the effect on the pressure drop across a bank of thermosyphons is outlined in Section 3.10.



Figure 24: Photographs of in-line tube bundle flow patterns [143].



Figure 25: Photographs of staggered arrangement tube bundle flow patterns [143].

3.3.1. Maximum Velocity, u_{max}

The calculation of u_{max} , the maximum velocity occurring in the minimum flow area between tubes can differ depending on whether the tubes are in a staggered or in-line arrangement. Tube

bundles comprising circular cross-section pipes are a commonly seen heat transfer surface with the heat transfer fluid predominantly flowing normal to the tubes. Cylindrical thermosyphons can be treated as tube bundles for this analysis. Staggered and in-line are the two most commonly applied configurations. As the fluid travels through a bundle, it converges in the spaces between the tubes causing a turbulent flow. Low relative pressure behind the tubes causes recirculation behind and in a tube bank, this recirculation region is smaller than behind a single tube and is influenced by geometrical positioning such as the relative pitches in transverse and longitudinal directions. The more compact a bundle, the smaller the recirculation. In a staggered bundle, the flow converges and then widens repeatedly. Flow through an inline bundle acts more akin to straight channels [146].

Figure 26 shows an in-line tube bundle arrangement with the varying parameters and Equation (3.13) provides the calculation for the maximum velocity. Figure 27 shows a staggered arrangement with the u_{max} calculations provided by Equations (3.14) to (3.16).

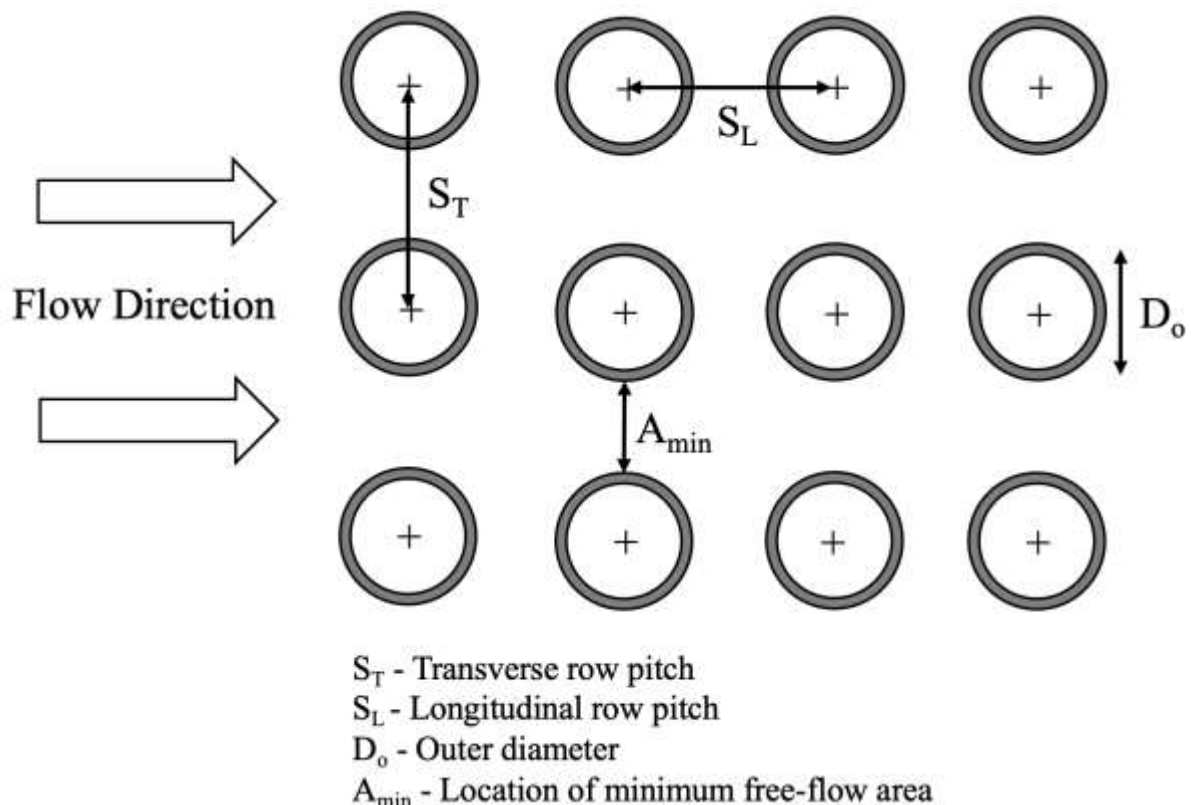


Figure 26: Schematic of in-line tube bundle arrangement.

$$A_{min} = S_T - D_o \quad (3.12)$$

$$u_{max} = \left(\frac{S_T}{S_T - D_o} \right) u_{ff} \quad (3.13)$$

where u_{ff} is the free-flow velocity at the inlet face area without tubes.

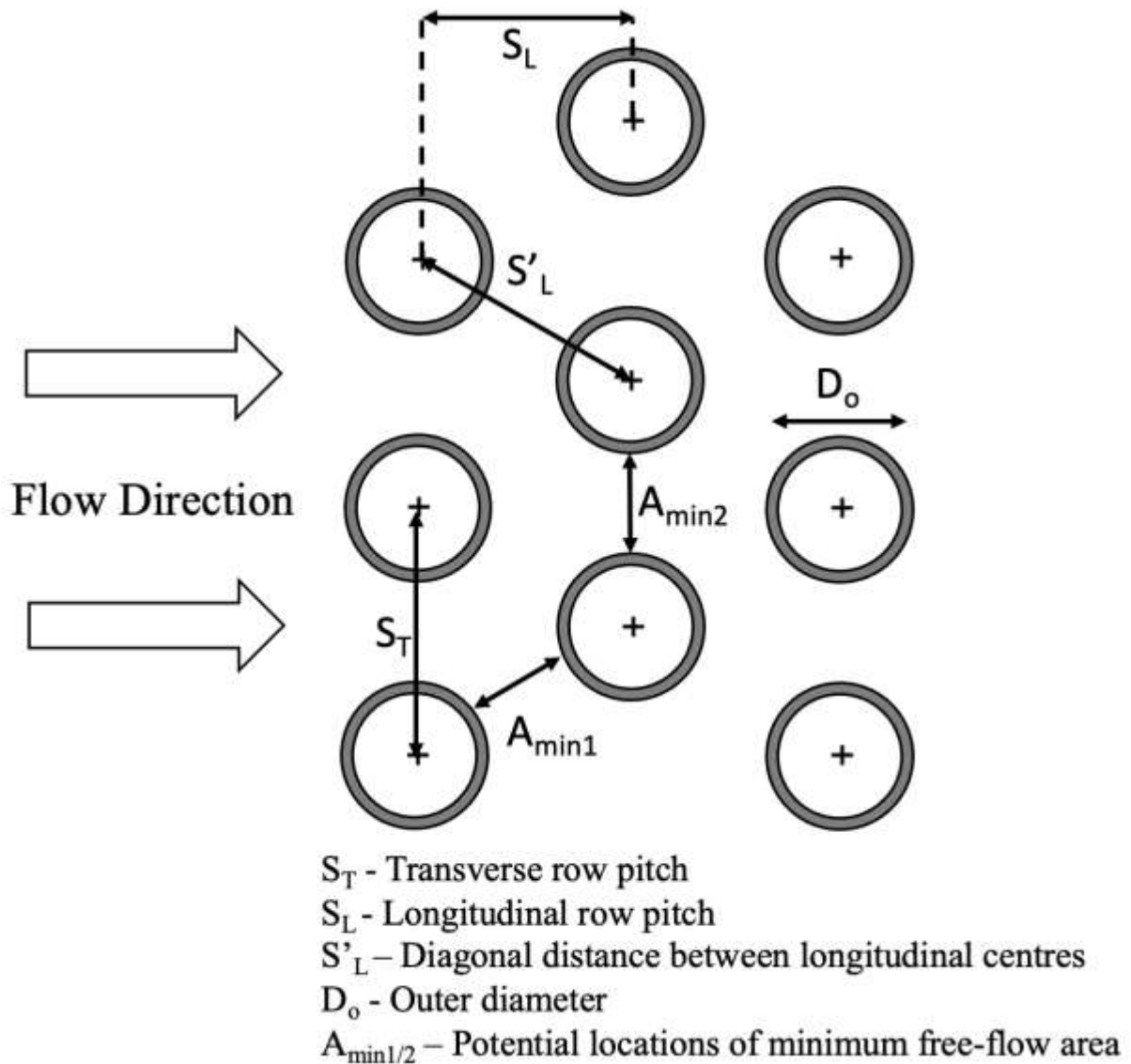


Figure 27: Schematic of staggered tube bundle arrangement.

The minimum free-flow area, A_{min} , can potentially occur in two places in staggered arrangements. It can be, as for Equation (3.12), transversely between the tube rows. However, if S_T is much larger than S_L such that:

$$\sqrt{\left(\frac{S_T}{2}\right)^2 + S_L^2} < \frac{S_T + D_o}{2} \quad (3.14)$$

according to [143]:

$$u_{max} = \left[\frac{S_T/2}{\sqrt{\left(\frac{S_T}{2}\right)^2 + S_L^2 - D_o}} \right] u_{ff} \quad (3.15)$$

The author has rearranged this to:

$$u_{max} = \frac{u_{ff}}{\sqrt{1 + \left(2\frac{S_L}{S_T}\right)^2 - 2\frac{D_o}{S_T}}} \quad (3.16)$$

3.4. Convection

There are two different recognised forms of convection; natural (or free) and forced convection. In the case of the presented model, only forced convection is considered as it substantially prevailed, as explained below.

Natural convection is fluid motion caused by natural phenomena such as buoyancy. This can be due to a change in density of a fluid due to a temperature change. Heat transfer by natural convection is found using the equation of motion.

$$u \frac{\partial u}{\partial x} + v \frac{\partial u}{\partial y} = \nu \frac{\partial^2 u}{\partial y^2} + g\beta(T - T_\infty) \quad (3.17)$$

β is the coefficient of thermal expansion. u is the tangential velocity and v is the normal velocity. ν is the kinematic viscosity. The Grashof number is a result of non-dimensionalising the above and represents a ratio between the buoyancy and viscous forces acting on a fluid. It is analogous to the Reynolds number in forced convection.

$$Gr = \frac{\text{bouyancy forces}}{\text{viscous forces}} = \frac{g\beta(T_s - T_\infty)L_{ch}^3}{\nu^2} \quad (3.18)$$

Forced convection is where the flow of a fluid is forced over a surface by any external means. In practise, this means fans for gases or pumps for liquids. Pumps and fans are used in HPHE recovery systems to provide this forced convection and to overcome the pressure drop across the bank of tubes.

The Richardson number (Ri) gives an indication of whether forced or natural convection prevails or if there is a combination of both in a system. A Richardson number close to unity indicates a combined regime. A value much greater than unity indicates that natural convection prevails. A value much less than unity indicates forced convection prevails. In this case, forced convection does prevail.

$$Ri = \frac{Gr}{Re^2} \quad (3.19)$$

Reference [56] state that a ratio of length to outside diameter greater than three results in natural convection being discounted. Convective heat transfer between a cylinder's outer surface and a heat transfer fluid can be expressed by a heat transfer coefficient in the form of:

$$h = \frac{\dot{q}}{\pi D_o L (T_{s,m} - T_\infty)} \quad (3.20)$$

where $T_{s,m}$ is the mean temperature on the surface of the cylinder and T_∞ is the bulk temperature of the fluid.

3.5. Thermosyphon Thermal Resistance Network Analogy

The thermal resistance network modelling of a thermosyphon can be used for a detailed analysis. The final model presented removes the need to determine the overall resistance, mainly to increase the versatility of the model. The justification for this approach is highlighted throughout the section. The methodology is outlined to illustrate what can be added to the

model if a more refined approach is required. Working out the thermal resistance of a single thermosyphon (R_{TS}) is critical to working out the heat transfer rate (\dot{q} , $\text{J}\cdot\text{s}^{-1}$) through the thermosyphon, using the temperature difference between the evaporator ($T_{e,ex-w}$) and condenser external walls ($T_{c,ex-w}$).

$$\dot{q}_{TS} = \frac{T_{e,ex-w} - T_{c,ex-w}}{R_{TS}} \quad (3.21)$$

When including the thermal resistance between the thermosyphon and the evaporator and condenser surroundings (Figure 28), the primary and secondary heat transfer fluids, you can obtain the total thermosyphon resistance, $R_{tot,TS}$, by summing the resistances, as they are in series. The eventual aim of working out the heat transfer rate of a single thermosyphon is that the value can then be extended for multiple heat pipes in a row as seen in a HPHE.

$$R_{tot,TS} = R_{c,ex} + R_{e,ex} + R_{TS} \quad (3.22)$$

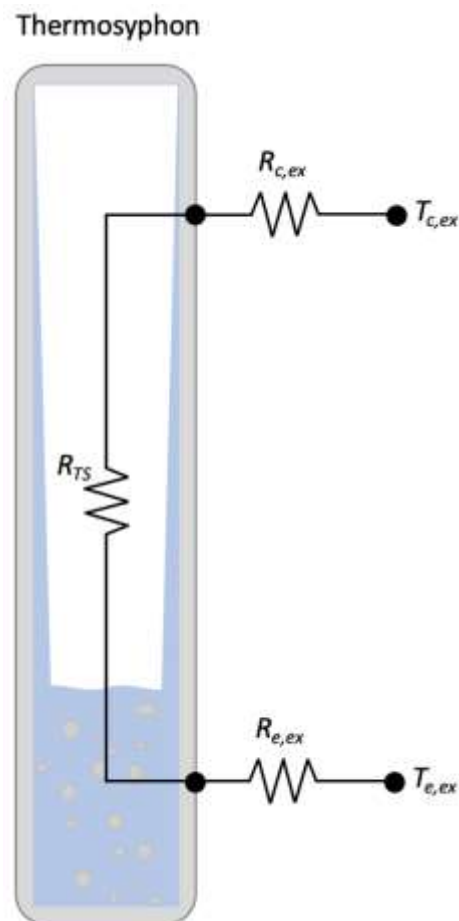


Figure 28: Schematic showing the overall thermal resistances of a thermosyphon, adapted from [59].

The thermal resistance for a thermosyphon is a combination of many resistances (Figure 29) [59]. The temperature terms can be determined and, hence, values can be used in later equations. The schematics show a two-dimensional representation of the resistances, but it should be noted that the resistances occur in a three-dimensional manner.

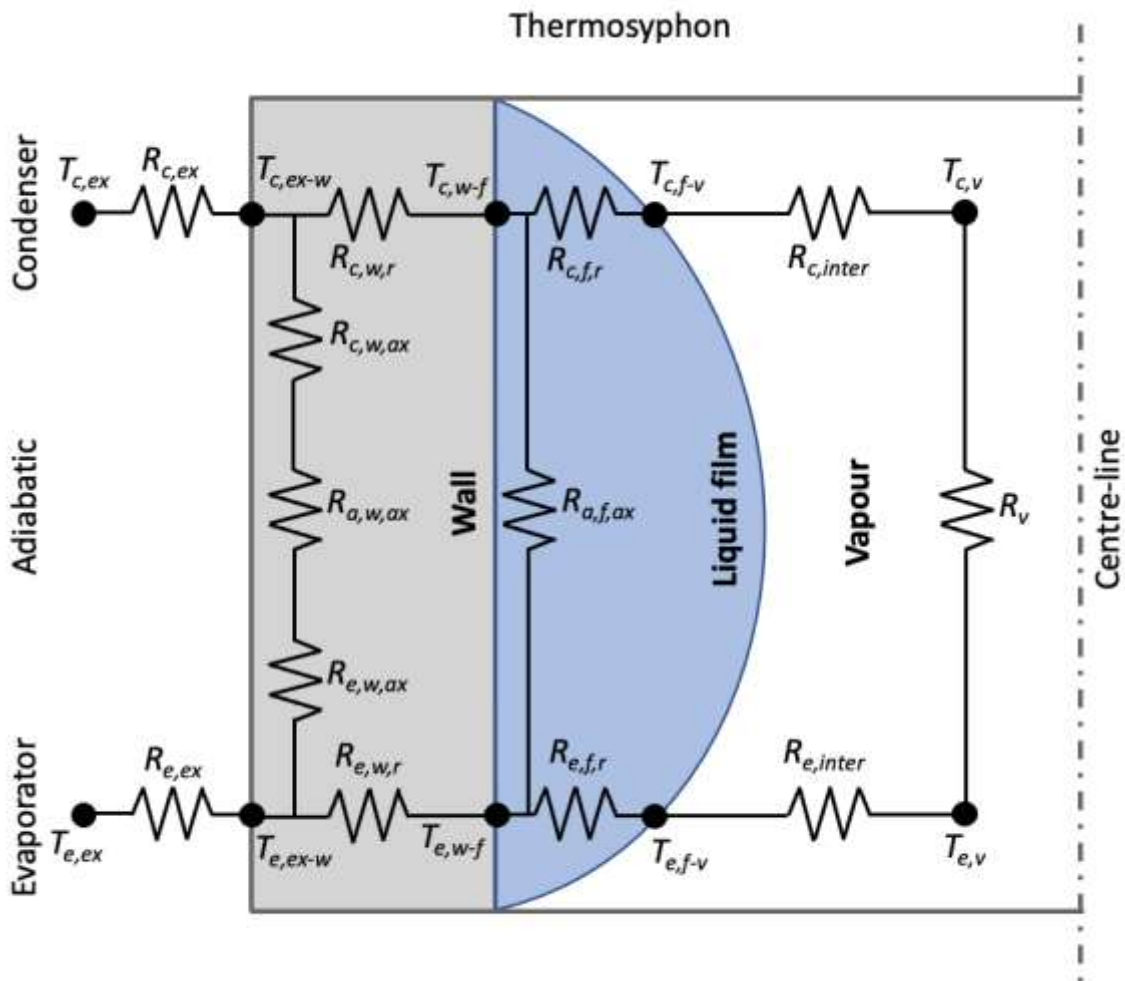


Figure 29: Schematic showing the thermal resistances of a thermosyphon. Adapted from [59], to include further axial and external resistances.

Table 7 and Table 8 provide the description of the resistances and temperatures shown by Figure 29.

Table 7: Resistances and descriptions for Figure 29.

Resistance	Description
$R_{e,ex}$	Evaporator, external
$R_{e,w,r}$	Evaporator, wall, radial
$R_{e,w,ax}$	Evaporator, wall, axial
$R_{a,w,ax}$	Adiabatic, wall, axial
$R_{c,w,ax}$	Condenser, wall, axial
$R_{w,ax}$	Wall, axial
$R_{e,f,r}$	Evaporator, film, radial
$R_{e,inter}$	Evaporator, interfacial
R_v	Vapour
$R_{c,inter}$	Condenser, interfacial
$R_{c,f,r}$	Condenser, film, radial
$R_{a,f,ax}$	Adiabatic, film, axial
$R_{c,ex}$	Condenser, external
R_{plate}	Plate (conduction)
$R_{e,ex,plate}$	Evaporator, external, plate
$R_{c,ex,plate}$	Condenser, external, plate
$R_{e,conv,ex}$	Evaporator, convection, external
$R_{e,cond}$	Evaporator, conduction
$R_{c,cond}$	Condenser, conduction
R_b	Boiling
R_{cd}	Condensation
$R_{c,conv,ex}$	Condenser, convection, external

Table 8: Temperatures and descriptions for Figure 29.

Temperature	Description
$T_{e,ex}$	Evaporator, external (heat source)
$T_{e,ex-w}$	Evaporator, external, wall
$T_{e,w-f}$	Evaporator, internal wall, film

$T_{e,f-v}$	Evaporator, film, vapour
$T_{e,v}$	Evaporator, vapour
$T_{c,v}$	Condenser, vapour
$T_{c,f-v}$	Condenser, film, vapour
$T_{c,w-f}$	Condenser, internal wall, film
$T_{c,ex-w}$	Condenser, external, wall
$T_{c,ex}$	Condenser, external (heat sink)

At the evaporator section, there is a resistance from the heat source fluid to the thermosyphon outer wall ($R_{e,ex}$). There is then a combination of three axial conduction terms through the evaporator, adiabatic and condenser thermosyphon wall sections; these are usually combined into a single axial wall conduction resistance, $R_{w,ax}$, Equation (3.23). There is also parallel radial conduction through the evaporator wall ($R_{e,w,r}$). Axial conduction through the wall is normally neglected on long thermosyphons [69]. The next resistances seen are from the inner wall into and through the film of working fluid. Again, this can be axially or radially. The axial term is normally neglected as the film is falling and it is minimal. The interface between the liquid film and the vapour is the next term, and then resistance through the vapour due to vapour pressure drop. The reverse process of resistances is then seen through the condenser section.

$$R_{w,ax} = R_{c,w,ax} + R_{e,w,ax} + R_{a,w,ax} \quad (3.23)$$

R_{TS} is then found using [59]:

$$R_{TS} = \frac{\left[R_{e,w,r} + R_{c,w,r} + \frac{(R_{e,f,r} + R_{e,inter} + R_v + R_{c,inter} + R_{c,f,r})(R_{f,ax})}{(R_{e,f,r} + R_{e,inter} + R_v + R_{c,inter} + R_{c,f,r}) + (R_{f,ax})} \right] R_{w,ax}}{\left[R_{e,w,r} + R_{c,w,r} + \frac{(R_{e,f,r} + R_{e,inter} + R_v + R_{c,inter} + R_{c,f,r})(R_{f,ax})}{(R_{e,f,r} + R_{e,inter} + R_v + R_{c,inter} + R_{c,f,r}) + (R_{f,ax})} \right] + R_{w,ax}} \quad (3.24)$$

A simplified equation (3.25) has been developed and can be used, that removes some of the more negligible terms and combines factors and it gives accurate results [69]. Figure 30 provides a simplified schematic of resistances with an exaggerated wall thickness.

$$R_{tot,TS} = R_{e,conv,ex} + R_{e,cond} + R_b + R_v + R_{cd} + R_{c,cond} + R_{c,conv,ex} \quad (3.25)$$

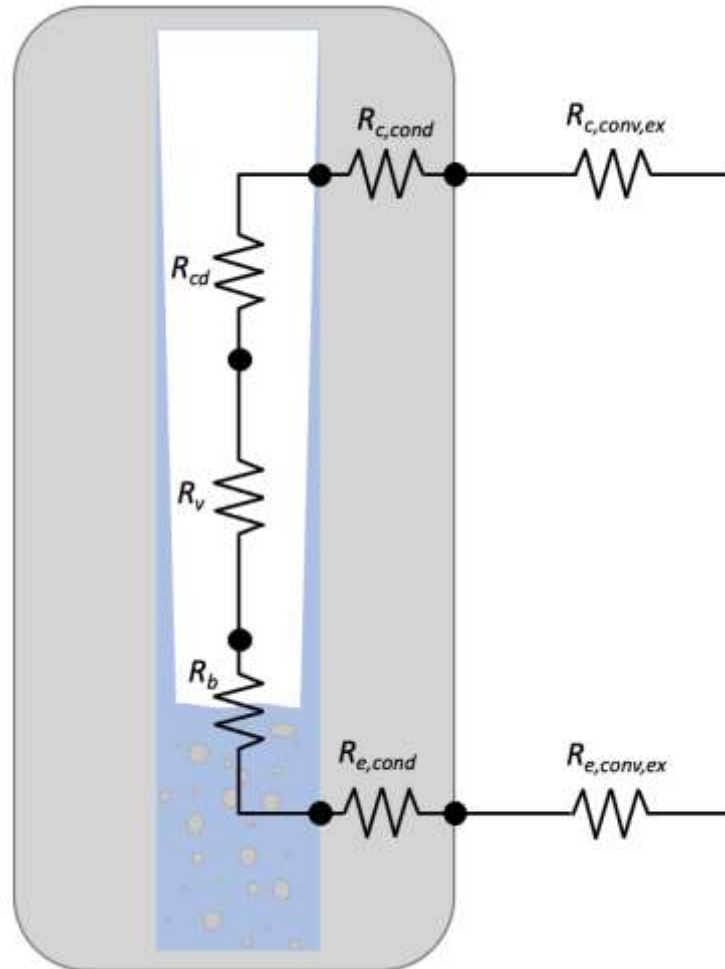


Figure 30: Schematic showing simplified thermal resistances for a thermosyphon.

Resistances of convection, boiling and condensation ($R_{e/c,conv,ex}$, R_b , R_{cd}) are analogous to the resistances seen in Figure 29. The subsections below describe the equations for each resistance seen [59,67,69].

3.5.1. Evaporator Section Resistances

3.5.1.1. Radial Conduction Through Wall

Typically, one of the largest resistances seen is radial conduction through the thermosyphon wall. The reason the natural log is used as a term is that heat transferring through the wall converges from the outer wall to the inner wall, as explained by Figure 31. Inside and outside diameters can be used instead of radius, if desired, as the term is equivalent.

$$R_{e,w,r} = \frac{\ln(r_o/r_i)}{2\pi\lambda_w L_e} \quad (3.26)$$

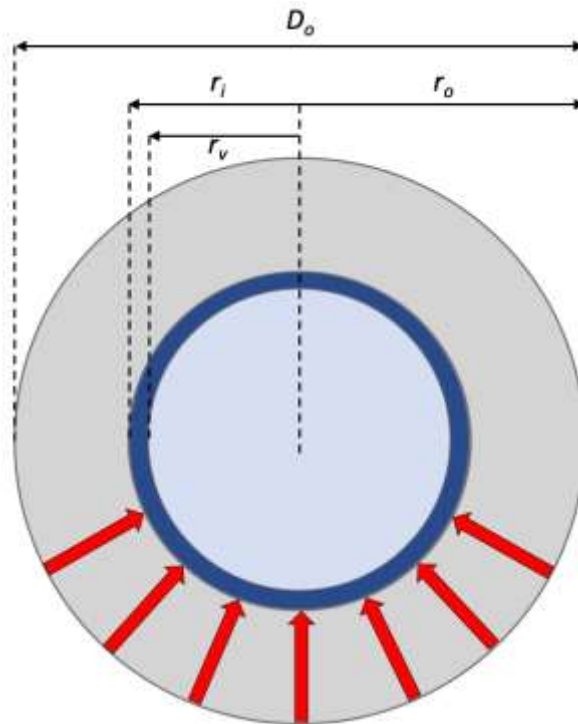


Figure 31: Schematic of thermosyphon cross-sectional dimensions with the converging nature of heat in the wall.

3.5.1.2. Axial Conduction Through Wall

With axial conduction through the wall, the heat does not converge so the inverse of Fourier's Law is used to find the resistance. Fourier's Law for conduction is:

$$\dot{q} = \frac{\lambda A_{cs} \Delta T}{\delta} \quad (3.27)$$

where δ is the distance or length travelled. Heat transfer rate, \dot{q} , in Equation (3.27) can be substituted into:

$$R = \frac{\Delta T}{\dot{q}} \quad (3.28)$$

to find resistance:

$$R = \frac{\delta}{\lambda A_{cs}} \quad (3.29)$$

For axial conduction in a circular cross section evaporator pipe wall, this becomes:

$$R_{e,w,ax} = \frac{0.5L_e}{\lambda_w \pi (r_o^2 - r_i^2)} \quad (3.30)$$

0.5 is used in the equation above as it can be assumed that heat is applied along the whole length of the evaporator uniformly and by integrating on the whole surface an approximation of 0.5 can be used. In essence, halfway along the length of the evaporator is the length where you can consider that the whole heat is applied.

3.5.1.3. Radial Conduction Through Film

Radial conduction in the liquid film ($R_{e,f,r}$) is found by using the heat transfer coefficients calculated for both the liquid film and, if present, pool:

$$R_{e,f,r} = \frac{1}{h_{pb}A_p + h_{fb}(A_{e,in} - A_p)} \quad (3.31)$$

where, according to [67], the heat transfer coefficient for the pool, h_{pb} , can be obtained from a correlation derived specifically for thermosyphons by Shiraishi, Kikuchi and Yamanishi [147]:

$$h_{pb} = 0.32q_p''^{0.4} \left(\frac{P_v}{P_{atm}} \right)^{0.23} \left(\frac{g^{0.2} \rho_l^{0.65} c_{p,l}^{0.7} \lambda_l^{0.3}}{\rho_v^{0.25} h_{fg}^{0.4} \mu_l^{0.1}} \right) \quad (3.32)$$

Other available boiling correlations are provided in Section 3.9.2 depending on the boiling regime and conditions present. h_{fb} , the heat transfer coefficient for the film is found as below or by Nusselt analysis, depending on the input heat flux. It should be mentioned that an ideal thermosyphon should not have a liquid pool during operation, but they are usually overfilled to prevent dryout by a sudden increase in heat flux and to maintain the two-phase cycle.

$$h_{fb} = 1.71 \sqrt[3]{\frac{g\rho_p(\rho_p - \rho_v)\lambda_p^3 h_{fg} r_i}{\mu_p \dot{q}_{TS}}} \quad (3.33)$$

q_p'' is the heat flux to the liquid pool, P_{atm} and P_v are the atmospheric and vapour pressures, g is gravitational acceleration, ρ_v , ρ_l and ρ_p are the vapour, liquid and liquid pool densities, $c_{p,p}$ is the specific heat capacity of the liquid pool, λ_p is the thermal conductivity of the liquid pool, h_{fg} is the latent heat of evaporation, μ_p is the dynamic viscosity of the liquid pool, \dot{q}_{TS} is the heat transfer rate of the thermosyphon.

3.5.1.4. Liquid-Vapour Interface

The evaporator fluid-vapour interface is again found by calculating a heat transfer coefficient.

$$R_{e,inter} = \frac{1}{h_{e,inter} A_{e,inter}} \quad (3.34)$$

where,

$$h_{e,inter} = \left(\frac{2\alpha}{1-\alpha} \right) \left(\frac{h_{fg}^2}{T_v v_{fg}} \right) \sqrt{\frac{1}{2\pi R_g T_v} \left(1 - \frac{P_v v_{fg}}{2h_{fg}} \right)} \quad (3.35)$$

α is the evaporation coefficient, also known as the accommodation coefficient, and it is selected depending upon which working fluid is selected and which heat transfer phase change process. These values, provided experimentally, are highly studied, as seen for water for both evaporation and condensation in [148]. Evaporation coefficients for multiple fluids can be found in [149]. Interfacial condensation heat transfer coefficients of vapours can be found in [150]. Condensation heat transfer in the condenser section can be based upon the Nusselt model (1916), other correlations are reported by Gross, Hahne, ESDU and Uehara et al. [151]. Guichet et al. [152] provide a thorough review on nucleate pool boiling heat transfer in wickless heat pipes. The thermal resistances at the interfaces are normally ignored as they are small and other resistances such as the external heat sink resistance are usually overriding.

3.5.2. Adiabatic Section

3.5.2.1. Axial Conduction Through Wall

There are only two resistances considered for the adiabatic section of a heat pipe both relating to axial conduction in the wall and liquid film as this section is defined as the region where there is no heat input or output. Respectively, these resistances are quite small. Axial conduction in the wall is obtained using:

$$R_{a,w,ax} = \frac{L_a}{\pi(r_o^2 - r_i^2)\lambda_w} \quad (3.36)$$

The whole length of the adiabatic section is used as it is considered that there is no heat input or output through the walls.

3.5.2.2. Axial Conduction Through Film

Axial conduction through the liquid film is calculating by using the cross-sectional area and length of the film and corresponding thermal conductivity:

$$R_{a,f,ax} = \frac{L_a}{\pi(r_i^2 - r_v^2)\lambda_f} \quad (3.37)$$

The adiabatic section is very small in the design of HPHEs presented as it is normally just a very small section connected to the separation plate as shown by Figure 32 (b) [67]. As such, the resistances are treated differently. In (b), there is a parallel path through the separation plate. The additional resistances are shown by Figure 33.

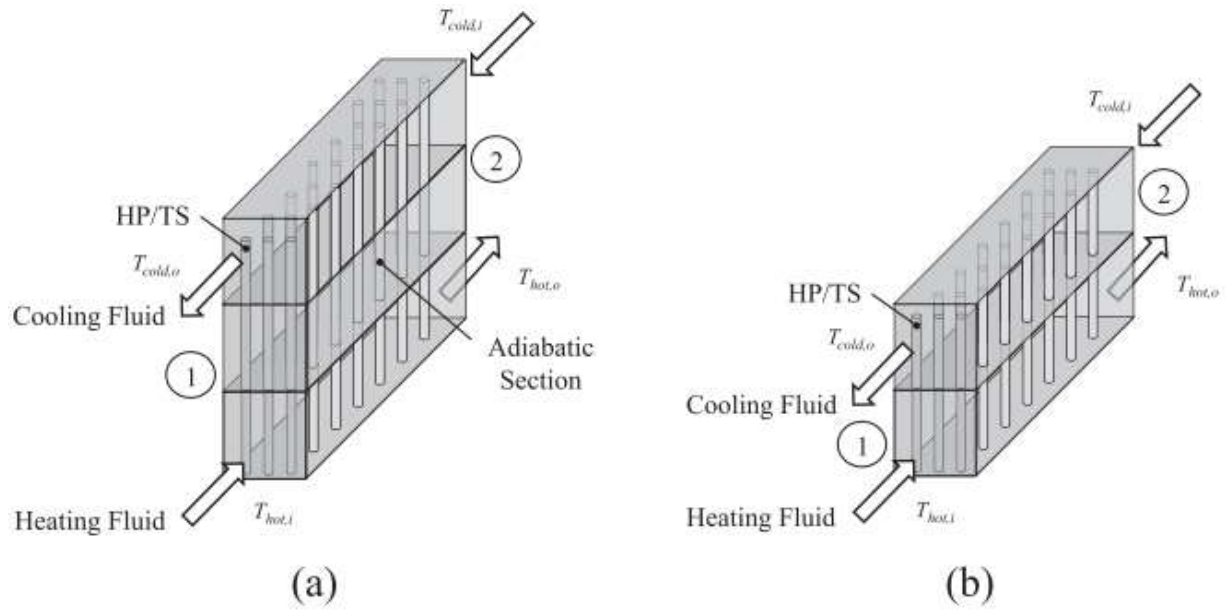


Figure 32: Schematic of the resistances in HPHEs with (a) and without (b) adiabatic sections [67].

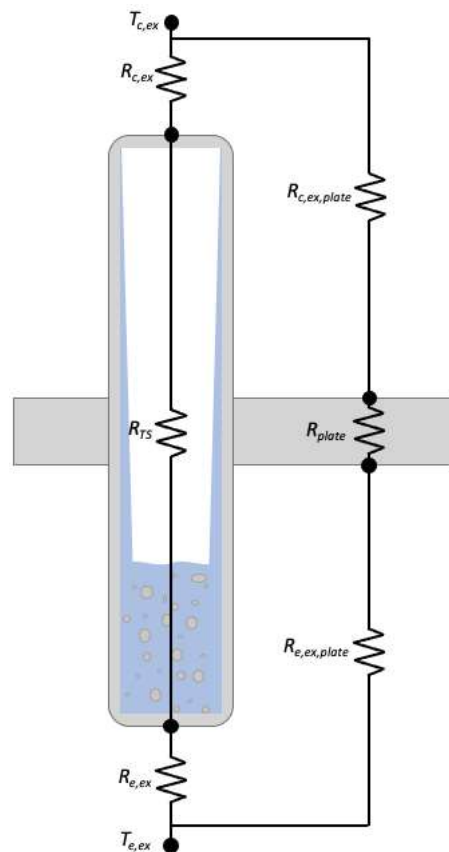


Figure 33: Schematic of thermosyphon resistances to include those through a separation plate.

The plate resistance can be found using traditional conduction analysis [67]:

$$R_{plate} = \frac{e_{plate}}{\lambda_{plate} A_{plate}} \quad (3.38)$$

where e_{plate} is the thickness of the plate.

Heat transfer from the primary fluid to the plate and to the secondary fluid can be found using convection analysis with correlations found in [153].

$$R_{e/c,ex,plate} = \frac{1}{h_{plate} A_{plate}} \quad (3.39)$$

3.5.3. Condenser Section

3.5.3.1. Radial Conduction Through Wall

The condenser section resistances are found in a similar way to the evaporator but are presented here for completeness. Radial conduction in the wall:

$$R_{c,w,r} = \frac{\ln(r_o/r_i)}{2\pi\lambda_w L_c} \quad (3.40)$$

3.5.3.2. Axial Conduction Through Wall

Axial conduction in the condenser wall:

$$R_{c,w,ax} = \frac{0.5L_c}{\pi(r_o^2 - r_i^2)\lambda_w} \quad (3.41)$$

3.5.3.3. Radial Conduction Through Film

Radial conduction in the liquid film is found as in the evaporator section Equations (3.31) to (3.33).

3.5.3.4. Fluid-Vapour Interface

The condenser fluid-vapour interface is found by:

$$R_{c,inter} = \frac{1}{h_{c,inter}A_{c,inter}} \quad (3.42)$$

with $h_{c,inter}$, found from Equation (3.35), though this is usually discounted as is negligible.

3.5.4. Vapour Region

3.5.4.1. Vapour Resistance Relating to Pressure Drop

The thermal resistance of the vapour is found using properties of the vapour and geometry of the thermosyphon. The properties of the vapour are related to the temperature. This can be calculated using the Clausius-Clapeyron relation between pressure and temperature by using a known reference.

$$\ln \frac{P_1}{P_2} = \frac{\Delta h_{fg}}{R_g} \left(\frac{1}{T_2} - \frac{1}{T_1} \right) \quad (3.43)$$

R_g is the specific gas constant. The pressure of the vapour drops as it travels to the condenser section and as such is treated as a thermal resistance. The equation used below assumes laminar vapour flow in a cylindrical heat pipe.

$$R_v = \frac{8R_g\mu_v T_v^2}{\pi h_{fg}^2 P_v \rho_v} \left[\frac{(L_e + L_c)/2 + L_a}{r_i^4} \right] \quad (3.44)$$

3.5.5. External Resistances

The condenser and evaporator external forced convection resistances are found using:

$$R_{e/c,ex} = \frac{1}{h_{e/c,ex}A_{c,ex}} \quad (3.45)$$

Calculating $h_{e/c,ex}$, the heat transfer coefficient is provided in Section 3.9.1.

3.6. Extended Thermal Resistance Analogy for Thermosyphon Rows

HPHEs are banks of thermosyphons, so finding a single thermosyphon resistance must then be translated into the transverse row and then longitudinally. This is achieved by assuming the thermosyphons are parallel to each other as shown by Figure 34. This process is of importance when determining the resistance of a row of thermosyphons for the ϵ -NTU method described in Section 3.7.

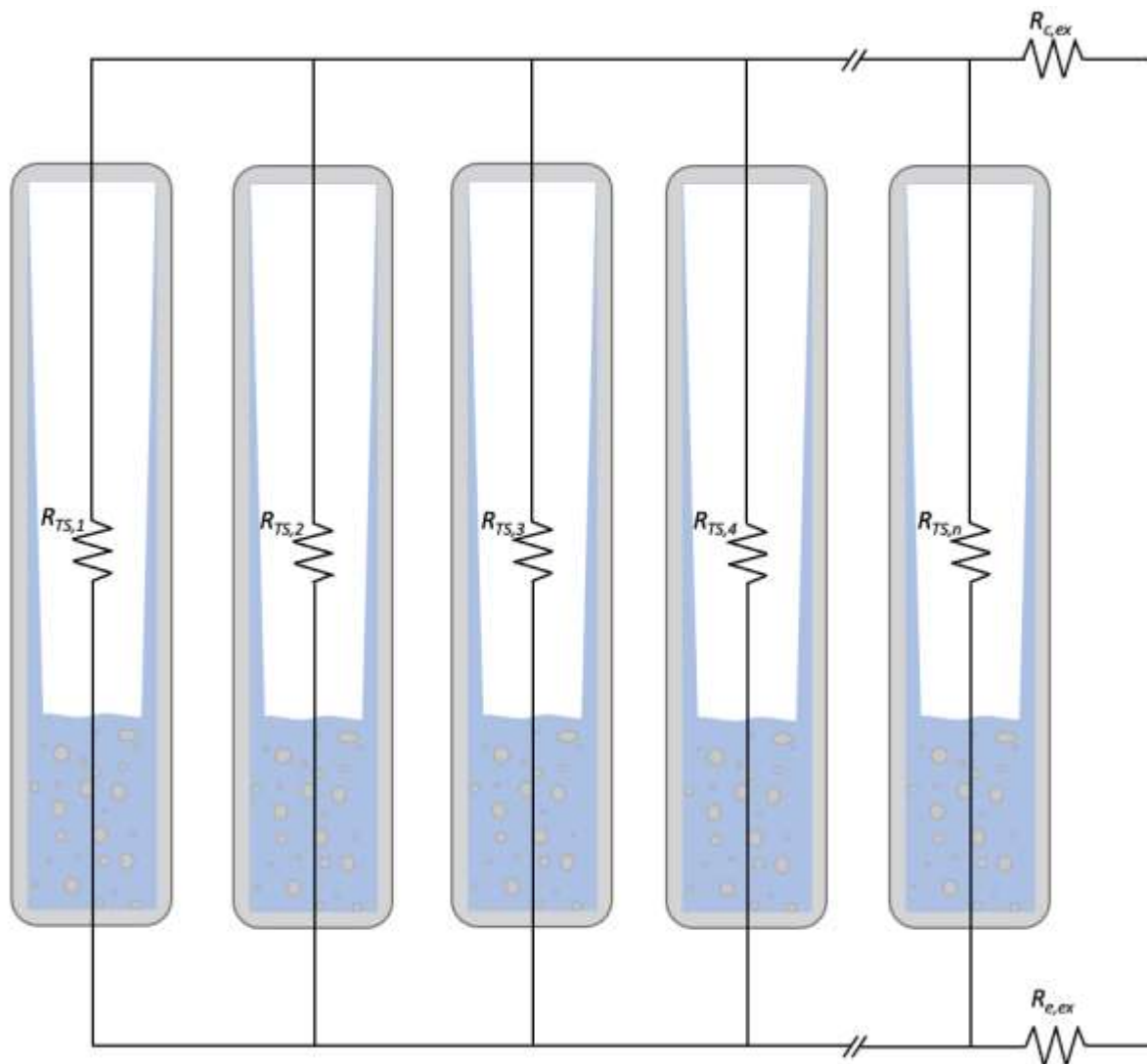


Figure 34: Schematic of a thermal resistance network diagram for a HPHE.

From this, an equation is derived to find the overall resistance for a number of thermosyphons:

$$(R_{n,TS})^{-1} = R_{TS,1}^{-1} + R_{TS,2}^{-1} + R_{TS,3}^{-1} + R_{TS,4}^{-1} + \dots + R_{TS,n}^{-1} \quad (3.46)$$

Previous research has assumed that all the thermosyphons in a row have the same thermal resistance [69], in order to simplify the equation to:

$$R_{n,TS} = \frac{R_{TS}}{n} \quad (3.47)$$

where n is the total number of thermosyphons. The resistance of the HPHE can then be obtained from:

$$R_{HPHE} = R_{n,TS} + R_{e,ex} + R_{c,ex} \quad (3.48)$$

However, as the fluids progress through the heat exchanger, they change in temperature and hence the calculated resistances change so they cannot be considered the same at all points. In the majority of cases, the same thermosyphon design is used in an entire bank, mainly for ease of manufacture in quantity. However, the design of the thermosyphon, such as the working fluid, may differ as you progress through the bank of tubes. Therefore, for a better approximation, the resistance calculations are conducted at the logarithmic mean temperature of the external fluids to average out the differences.

There are two reasons why, if there is a large bank of thermosyphons in a HPHE, as seen in industrial applications, the system can treat the thermosyphons as having negligible resistance. Firstly, by increasing the number of heat pipes, the heat transfer area increases and therefore:

$$R = \frac{1}{hA} \xrightarrow{A \rightarrow \infty} 0 \quad (3.49)$$

Secondly, it can be seen that, as the total number of thermosyphons increases, because they are in parallel, the overall resistance decreases and tends towards 0.

$$\frac{1}{R_{n,TS}} = \sum_{i=R_{TS,1}}^{R_{TS,n}} i^{-1} \xrightarrow{n \rightarrow \infty} \infty \quad (3.50)$$

Therefore,

$$R_{n,TS} \xrightarrow{n \rightarrow \infty} 0 \quad (3.51)$$

3.7. Using the Effectiveness-NTU Method to Predict HPHE Performance

This section describes the ε -NTU method for calculating the effectiveness of a HPHE and predicting outlet temperatures. It is very useful methodology as it allows the heat transfer rate to be calculated without knowing the outlet temperatures of the HPHE. It was first reported by Kays and London and has since been used in relation to HPHEs by [3,4,69,94,131,154,155] but only in a steady state manner. By calculating the heat transfer rate, the outlet temperatures can then be determined. The thermal network analysis is a very cumbersome method of calculating the heat transfer rate of a thermosyphon or HPHE and can lead to large differences between theoretical and experimental results. This can be attributed to the chaotic nature of the two phase boiling and condensation cycle [156] and an extensive iteration process is needed, for example, to calculate wall temperatures. Furthermore, the correlations used are empirically derived and, as such, are based on experimental conditions, heat flux, geometry and working fluid and are not applicable universally. The ε -NTU method can use the thermal resistances of the thermosyphons to calculate the overall heat transfer coefficient.

Effectiveness, ε , of a heat exchanger is a dimensionless ratio of actual heat transfer rate, \dot{q}_{act} , to the maximum heat transfer rate, \dot{q}_{max} , theoretically permitted [157], i.e.:

$$\varepsilon = \frac{\dot{q}_{act}}{\dot{q}_{max}} \quad (3.52)$$

\dot{q}_{max} is calculated by knowing the inlet temperatures of the heat transfer fluids and their mass flow rates. These are easily measured, though on industrial sites are normally logged or monitored so can be provided. The maximum possible heat transfer rate is calculated from the

maximum temperature difference, ΔT_{max} , that a heat exchanger can achieve, which is the difference in temperature between the hot and cold fluid at the evaporator and condenser inlets. The maximum heat transfer occurs when either the hot fluid cools to the inlet temperature of the cold fluid, or the cold fluid heats to the inlet temperature of the hot fluid. This is determined by whichever has the smaller heat capacity rate, C_{min} , as it will be the first to reach the maximum permitted temperature.

$$\Delta T_{max} = T_{e,in} - T_{c,in} \quad (3.53)$$

$$\dot{q}_{max} = C_{min} \Delta T_{max} \quad (3.54)$$

$T_{e,in}$ and $T_{c,in}$ are the inlet temperatures of the evaporator and condenser fluids. C_{min} is the smallest heat capacity rate of the two fluids, C_e or C_c .

$$C_e = \dot{m}_e c_{p,e} \quad (3.55)$$

$$C_c = \dot{m}_c c_{p,c} \quad (3.56)$$

\dot{m}_e and \dot{m}_c are the mass flow rates ($\text{kg}\cdot\text{s}^{-1}$) of the evaporator and condenser streams and $c_{p,e}$ and $c_{p,c}$ are the specific heat capacities of the respective fluids.

Effectiveness allows the thermal performance of a heat exchanger to be measured and benchmarked against other systems. The value of effectiveness ranges between zero and one, zero being no heat transfer and one being a perfect heat exchanger transferring the theoretical maximum amount of heat. Also, by calculating the effectiveness, the heat transfer rate can then be determined from the heat source to sink using, for a generic heat exchanger:

$$\dot{q}_{act} = \varepsilon C_{min} (T_{hot,in} - T_{cold,in}) \quad (3.57)$$

In the case of a HPHE, where the inlets are described at the evaporator and condenser sections:

$$\dot{q}_{act} = \varepsilon C_{min}(T_{e,in} - T_{c,in}) \quad (3.58)$$

The effectiveness depends on three main factors, the number of transfer units (NTU- a widely used dimensionless parameter for heat exchanger analysis), the flow arrangement and the heat capacity ratio; described below. The effectiveness for a counterflow heat exchanger has been provided by many sources [59,140,153,158]:

$$\varepsilon = \frac{1 - e^{-NTU(1-\frac{C_{min}}{C_{max}})}}{1 - \frac{C_{min}}{C_{max}} e^{-NTU(1-\frac{C_{min}}{C_{max}})}} \quad (3.59)$$

C_{max} is the larger heat capacity rate of the two heat transfer fluids of the evaporator and condenser, C_e or C_c . This equation can be used to give a single effectiveness value for the entire HPHE where only the source and sink stream inlet temperatures, flow arrangement and thermal resistance of the HPHE are needed. However, a further modified method can be used, by treating the evaporator and condenser section separately, where an effectiveness for both the sections can be obtained [59]. This is best illustrated by treating the HPHE as a liquid-coupled indirect-transfer-type heat exchanger [131], as shown by Figure 35.

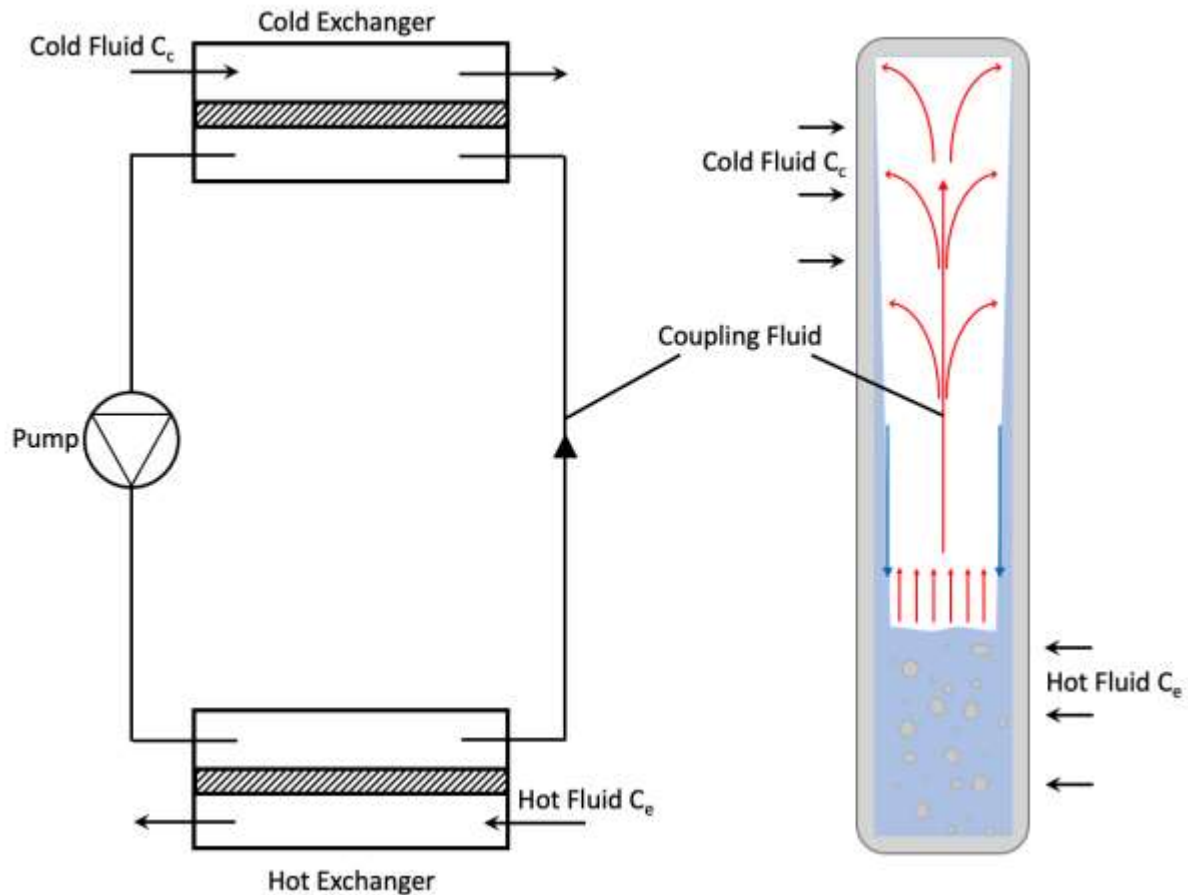


Figure 35: Illustration to show the treatment of a thermosyphon as a liquid-coupled indirect-transfer-type heat exchanger.

This is the method that was used and adapted to a thermosyphon equipped heat exchanger [69] by assuming the evaporator and condenser sections are two different heat exchangers, which are coupled by the thermosyphon working fluid. In this way, both the outlet temperatures of the evaporator and condenser sections can be calculated using Equations (3.60) and (3.61), allowing a predictor of performance for both streams.

$$T_{e,out} = T_{e,in} - \varepsilon_{tot} \frac{C_{min}}{C_e} (T_{e,in} - T_{c,in}) \quad (3.60)$$

$$T_{c,out} = T_{c,in} + \varepsilon_{tot} \frac{C_{min}}{C_c} (T_{e,in} - T_{c,in}) \quad (3.61)$$

which can, by substituting Equation (3.58), also be written as:

$$T_{e,out} = T_{e,in} - \frac{\dot{q}_{act}}{C_e} \quad (3.62)$$

$$T_{c,out} = T_{c,in} + \frac{\dot{q}_{act}}{C_c} \quad (3.63)$$

ε_{tot} is the total effectiveness of the heat exchanger, calculated using the equations below. Depending on which heat capacity is the larger of the condenser and evaporator fluids, the total effectiveness equation varies. Multiple methods for calculating ε_{tot} have been reported, the method below was deemed the correct version, reported by [69,155]:

$$\text{If } C_e > C_c \quad \varepsilon_{tot} = \left(\frac{1}{\varepsilon_{c,n}} + \frac{C_c/C_e}{\varepsilon_{e,n}} \right)^{-1} \quad (3.64)$$

$$\text{If } C_c > C_e \quad \varepsilon_{tot} = \left(\frac{1}{\varepsilon_{e,n}} + \frac{C_e/C_c}{\varepsilon_{c,n}} \right)^{-1} \quad (3.65)$$

[78,140,159], among others, have reported the following, but care should be taken to avoid this as it gives erroneous results:

$$\text{If } C_c > C_e \quad \varepsilon_{tot} = \left(\frac{1}{\varepsilon_{c,n}} + \frac{C_e/C_c}{\varepsilon_{e,n}} \right)^{-1} \quad (3.66)$$

$\varepsilon_{c,n}$ and $\varepsilon_{e,n}$ are the effectiveness of n number of longitudinal thermosyphons rows in the evaporator or condenser sections and are determined by Equations (3.70) and (3.71), respectively. These stem from the effectiveness of a multistage heat exchanger in counterflow for n number of rows [59]:

$$\varepsilon_{e,n} = \frac{\left(\frac{1 - C_{rat}\varepsilon_e}{1 - \varepsilon_e} \right)^n - 1}{\left(\frac{1 - C_{rat}\varepsilon_e}{1 - \varepsilon_e} \right)^n - C_{rat}} \quad (3.67)$$

$$\varepsilon_{c,n} = \frac{\left(\frac{1 - C_{rat}\varepsilon_c}{1 - \varepsilon_c}\right)^n - 1}{\left(\frac{1 - C_{rat}\varepsilon_c}{1 - \varepsilon_c}\right)^n - C_{rat}} \quad (3.68)$$

where,

$$C_{rat} = \frac{C_{min}}{C_{max}} \quad (3.69)$$

C_{rat} , the heat capacity ratio, between the shell side and working fluid, is effectively equal to 0. The working fluid is at a constant temperature and, as such, its capacity rate is infinite. Therefore, the simplified Equations (3.70) and (3.71) can be used for a HPHE.

$$\varepsilon_{e,n} = 1 - (1 - \varepsilon_e)^n \quad (3.70)$$

$$\varepsilon_{c,n} = 1 - (1 - \varepsilon_c)^n \quad (3.71)$$

where ε_e and ε_c are the effectiveness of a single transverse row of thermosyphons in the evaporator or condenser section and n is the number of longitudinal thermosyphons in a row. This can be applied only if the effectiveness of each row in the HPHE is equal. If they are not equal, the effectiveness of each row is multiplied [133]:

$$\varepsilon_{e/c,n} = \{1 - (1 - \varepsilon_{e/c,1})(1 - \varepsilon_{e/c,2}) \dots (1 - \varepsilon_{e/c,n})\} \quad (3.72)$$

The effectiveness of the evaporator and condenser sections of a thermosyphon can be determined by Equations (3.73) and (3.74).

$$\varepsilon_e = 1 - e^{-NTU_e} \quad (3.73)$$

$$\varepsilon_c = 1 - e^{-NTU_c} \quad (3.74)$$

where NTU_e and NTU_c are the number of transfer units for the evaporator and condenser. NTU refers to the nondimensional heat transfer size or thermal size of the heat exchanger and is defined as [160]:

$$NTU \equiv \frac{UA}{C_{min}} = \frac{1}{C_{min}} \int_A U dA \quad (3.75)$$

The number of transfer units of the evaporator and condenser sections (NTU_e and NTU_c) are equivalent to Equations (3.76) and (3.77).

$$NTU_e \equiv \frac{U_e A_e}{C_e} \quad (3.76)$$

$$NTU_c \equiv \frac{U_c A_c}{C_c} \quad (3.77)$$

where U_e and U_c are the overall heat transfer coefficients of the evaporator and condenser sections and A_e and A_c are the overall heat transfer areas.

In this analysis, the UA values are equivalent to the inverse of the thermal resistance of that section and U is equal to h_{fc} , the forced convection average heat transfer coefficient [3,4]. This is shown in Equations (3.83) and (3.84) [155].

$$U_e A_e = \frac{1}{R_{e,out}} = \frac{1}{h_{fc,e} A_{TS,e}} + R_{TS,e} \quad (3.78)$$

$$U_c A_c = \frac{1}{R_{c,out}} = \frac{1}{h_{fc,c} A_{TS,c}} + R_{TS,c} \quad (3.79)$$

A simplification can be made if the thermosyphons are considered to be superconductors, i.e.:

$$R_{TS,e/c} \approx 0 \quad (3.80)$$

and the heat transfer area of the outer surface of the thermosyphons equals the total heat transfer area:

$$A_e = A_{TS,e} \quad (3.81)$$

$$A_c = A_{TS,c} \quad (3.82)$$

Equations (3.78) and (3.79) can be reduced to:

$$U_e = h_{fc,e} \quad (3.83)$$

$$U_c = h_{fc,c} \quad (3.84)$$

where $R_{e,out}$ and $R_{c,out}$ are the thermal resistances of the evaporator section and the condenser section. The thermal resistance decreases as the number of thermosyphons increases, due to the increased surface area. Section 3.9.1 deals with how the heat transfer coefficient of forced convection, h_{fc} , is calculated.

3.7.1. HPHE Conductance Value

Conductance, UA ($W.K^{-1}$), is not just applicable to an individual thermosyphon but to the entire heat exchanger and is a measure of how much heat is transferred per Kelvin and is a good benchmark for performance in comparison to the total heat transfer area and other heat exchangers. To give this value as an output, the following equation was used.

$$U_{HPHE}A_{HPHE} = \frac{\dot{q}_{act}}{LMTD} \quad (3.85)$$

3.8. Maximum Heat Flux in a Thermosyphon

Thermosyphons have a maximum heat flux, q'' ($W.m^{-2}$), possible. This is an important factor to consider to limit heat transfer and prevent overprediction if a HPHE design cannot feasibly transfer the heat transfer rate predicted. The current model does not limit the maximum heat flux but this can be incorporated. It is recommended that thermosyphons should operate at less than 50% of the calculated maximum heat flux. The maximum heat flux uses the Kutateladze number, Ku , and fluid properties.

$$q'' = \frac{Ku}{\Delta h_{fg} p_v^{0.5} [g\sigma(\rho_l - \rho_v)]^{0.25}} \quad (3.86)$$

Many correlations are available for determining the Kutateladze number, summarised in Table 9.

Table 9: Thermosyphon maximum heat flux correlations [40].

Correlation	Reference	Equation
$Ku = \frac{0.725^2}{4} Bo^{0.5} \frac{(D_{e,o}/L_e)}{\left[1 + \left(\frac{\rho_v}{\rho_l}\right)^{0.25}\right]^2}$	Sakhuja	(3.87)
$Ku = 0.09Bo^{0.5} \frac{(D_{e,o}/L_e)^{0.9}}{\left[1 + \left(\frac{\rho_v}{\rho_l}\right)^{0.25}\right]^2}$	Nejat	(3.88)
$Ku = \frac{0.1}{1 + 0.491(L_e/D_{e,o})Bo^{-0.3}}$	Katto	(3.89)
$Ku = \frac{3.2}{4} \frac{(D_{e,o}/L_e)}{\left[1 + \left(\frac{\rho_v}{\rho_l}\right)^{0.25}\right]^2} ; Bo \geq 30$	Tien and Chung	(3.90)
$Ku = \frac{3.2}{4} [\tanh(0.5Bo^{0.5})]^2 \frac{(D_{e,o}/L_e)}{\left[1 + \left(\frac{\rho_v}{\rho_l}\right)^{0.25}\right]^2}$	Tien and Chung	(3.91)
$Ku = 9.64 (D_{e,o}/L_e) \rho_v h_{fg} C \left(\frac{\sigma}{\rho_v}\right)^{0.5} ; C \left(\frac{\sigma}{\rho_v}\right)^{0.5} \geq 0.079$	Harada et al.	(3.92)
$Ku = 14.1 (D_{e,o}/L_e) \rho_v h_{fg} \left[C \left(\frac{\sigma}{\rho_v}\right)^{0.5}\right]^{1.15} ; C \left(\frac{\sigma}{\rho_v}\right)^{0.5} < 0.079$		(3.93)
$Ku = 0.0093 \left(\frac{D_{e,o}}{L_e}\right)^{1.1} \left(\frac{D_{c,o}}{L_c}\right)^{-0.88} F_e^{-0.74} (1 + 0.03Bo)^2 ; 2 < Bo < 60$	Gorbis and Savchenkov	(3.94)
$Ku = 2.55 \left(\frac{D_{e,o}}{L_e}\right) \left\{ \frac{\sigma}{\rho} \left[\frac{g(\rho_l - \rho_v)}{\sigma} \right]^{0.5} \right\}^{0.17} ; \frac{\sigma}{\rho} \left[\frac{g(\rho_l - \rho_v)}{\sigma} \right]^{0.5} \geq 2.5 \times 10^{-5}$	Bezrodnyi	(3.95)
$Ku = 0.425 \left(\frac{D_{e,o}}{L_e}\right) ; \frac{\sigma}{\rho} \left[\frac{g(\rho_l - \rho_v)}{\sigma} \right]^{0.5} < 2.5 \times 10^{-5}$		(3.96)

$Ku = 0.747 \left(\frac{D_{e,o}}{L_e} \right) [g\sigma(\rho_l - \rho_v)]^{0.295} (h_{fg}\rho_v)^{-0.045}$	Prenger	(3.97)
$Ku = 2 \left(\frac{D_{e,o}}{L_e} \right)^{0.83} F_e^{0.03} \left\{ \frac{[g\sigma(\rho_l - \rho_v)]^{0.5}}{h_{fg}\rho_v} \right\}^{0.2}$	Fukano et al.	(3.98)
$Ku = 0.16 \left\{ 1 - e \left[- \left(\frac{D_{e,o}}{L_e} \right) \left(\frac{\rho_l}{\rho_v} \right)^{0.13} \right] \right\}$	Imura et al.	(3.99)
$Ku = 0.131 \left\{ 1 - e \left[- \left(\frac{D_{e,o}}{L_e} \right) \left(\frac{\rho_l}{\rho_v} \right)^{0.13} \cos^{1.8}(\varphi - 55^\circ) \right] \right\}^{0.8}$	Pirotto and Voroncova	(3.100)
<p>F_e = Fill ratio of liquid fill volume to evaporator volume, dimensionless φ = Inclination angle from horizontal, degrees g = Gravitational acceleration, m.s⁻² σ = Surface tension, N.m⁻¹ $C = 1.58 \left(\frac{D_{e,o}}{\sigma} \right)^{0.4}$; $\frac{D_{e,o}}{\sigma} < 0.318$. $C = 1$; $\frac{D_{e,o}}{\sigma} \geq 0.318$ $Bo, Bond Number = D_{e,o} \left[\frac{g(\rho_l - \rho_v)}{\sigma} \right]^{0.5}$</p>		

Golobič and Gašperšič [161] conducted a thorough review on the maximum heat flux in a two-phase closed vertical thermosyphon with against 436 experimental data for non-polar and polar solvents. Their attempt to simplify the equations by using molecular weight, critical temperature, critical pressure and the Pitzer acentric factor (ω - Equation (3.106)) rather than more complex thermodynamic and transport properties of a fluid at a given temperature was fairly successful. This approach can lead to predictions of a wide range of applications without the need to find thermodynamic and transport properties. The authors present a deviation of 25.3% from all the experimental data.

$$q'' = 0.131\chi_1 \left\{ 1 - e \left[-\chi_2 \left(\frac{D_{e,o}}{L_e} \right) \cos^{1.8}(\varphi - 55^\circ) \right] \right\}^{0.8} \quad (3.101)$$

where

$$\chi_1 = \frac{T_c^{\frac{1}{3}} \rho_c^{\frac{11}{12}} g^{\frac{1}{4}}}{M^{\frac{1}{4}}} \tau e(\chi_3) \quad (3.102)$$

and

$$\chi_2 = [(0.484\tau - 1.036)\omega + 0.984\tau - 1.076]^{-1} \quad (3.103)$$

and

$$\begin{aligned} \chi_3 = & 2.576 - 11.423\tau + 1.1146\omega + 21.610\tau^2 - 3.159\tau\omega^2 + 5.337\tau^2\omega^2 \\ & - 28.440\tau^3 - 22.224\omega^2 - 22.224\tau^3\omega \end{aligned} \quad (3.104)$$

and

$$\tau = 1 - T_{red} \quad (3.105)$$

$$\omega = -1 - \log\left(\frac{\rho}{\rho_{c(T_{red}=0.7)}}\right) \quad (3.106)$$

where ρ_c is the critical pressure at a reduced temperature (T_{red}) (temperature/ critical temperature) of 0.7. The Pitzer acentric factor is a standard for the phase characterisation. As its value increases, higher boiling points are seen.

3.9. Calculating Heat Transfer Coefficients

Many types of heat transfer coefficients can be considered for a HPHE. Methods for calculating those for external forced convection, boiling and condensation are presented in this section.

3.9.1. Heat Transfer Coefficient of Forced Convection

The heat transfer coefficient of forced convection, h_{fc} , is the most challenging variable to determine and it depends on a variety of flow properties and calculation of some key dimensionless numbers- Prandtl, Reynolds and Nusselt. Furthermore, it is an averaged value as the local flow properties, and hence value, fluctuate at every location on the thermosyphon. As such, the value is found exclusively from empirical studies. The main variables considered are temperature gradient at the surface, turbulence and thermal diffusivity. The calculations predominantly depend upon the design of the HPHE. The h_{fc} must be calculated for both the evaporator and condenser sections, as below:

$$h_{fc} = \frac{Nu_D \lambda}{D_o} \quad (3.107)$$

The Nu_D is the Nusselt number in respect to the outer diameter of the thermosyphon, D_o (characteristic length). The heat transfer rate of forced convection can be found for either the evaporator or condenser by:

$$\dot{q}_{fc} = h_{fc} A_{e/c} LMTD \quad (3.108)$$

3.9.1.1. Nusselt Correlations

This section provides the available correlations for calculating the Nusselt number from literature with the varying applications and conditions where they can be applied. Nusselt correlations developed for inclined cylinders have not been included as are they outside the scope. The model first chooses the most fitting correlation depending on geometry. There is some overlap between correlations so not all presented are used but are given here for completeness. Heat pipes can also be finned or unfinned, which changes the selection of the correlations to be used.

3.9.1.2. Unfinned correlations

Table 10 provides the correlations for unfinned tube bundles of varying arrangements, Prandtl and Reynolds Numbers. Reference [166] correlations are provided in the model code in the Appendix as were most fitting for the presented data and are widely recognised and reported in literature. The other correlations provided can be selected and incorporated as required depending on the conditions and HPHE geometry.

Table 10: Available correlations for calculation of Nusselt numbers over unfinned tube bundles.

Ref.	Correlation	Condition	Equation
[162]	$Nu_D = 0.33 Re_D^{0.6} Pr^{1/3}$	Staggered >10 rows $10 < Re_D < 40,000$	(3.109)
[163]	$Nu_D = K Re_D^n$	Air only	(3.110)

	K and n values are tabulated in [143,164]	>10 rows	
[65]	$Nu_D = K_1 Re_D^n$ K_1 and n values are tabulated in [143,164]	Air only <10 rows	(3.111)
[163]	$Nu_D = 0.32 F_a Re_D^{0.61} Pr^{0.31}$ F_a , an arrangement correction factor provided in [163]		(3.112)
[165]	$Nu_D = 0.34 \left[1 + \left(S_L + \frac{7.17}{S_L} - 6.52 \right) \left[\frac{0.266}{(S_T - 0.8)^2} - 0.12 \right] \sqrt{\frac{1000}{Re_D}} \right] Re_D^{0.61} Pr^{0.31}$	In-line	(3.113)
	$Nu_D = 0.35 F_a Re_D^{0.57} Pr^{0.31}$ $F_a = 1 + \frac{S_L}{10} + \frac{0.34}{S_T}$	Staggered	(3.114)
[166]*	$Nu_D = 0.9 Re_D^{0.4} Pr^{0.36} (Pr/Pr_s)^{0.25}$	In-line >16 rows 0-100 Re_D	(3.115)
	$Nu_D = 0.52 Re_D^{0.5} Pr^{0.36} (Pr/Pr_s)^{0.25}$	In-line >16 rows 100-1000 Re_D	(3.116)
	$Nu_D = 0.27 Re_D^{0.63} Pr^{0.36} (Pr/Pr_s)^{0.25}$	In-line >16 rows 1000-20,000 Re_D	(3.117)
	$Nu_D = 0.033 Re_D^{0.8} Pr^{0.4} (Pr/Pr_s)^{0.25}$	In-line >16 rows 20,000-200,000 Re_D	(3.118)
	$Nu_D = 1.04 Re_D^{0.4} Pr^{0.36} (Pr/Pr_s)^{0.25}$	Staggered >16 rows 0-500 Re_D	(3.119)
	$Nu_D = 0.71 Re_D^{0.5} Pr^{0.36} (Pr/Pr_s)^{0.25}$	Staggered >16 rows 500-1000 Re_D	(3.120)
	$Nu_D = 0.35 (S_T/S_L)^{0.2} Re_D^{0.6} Pr^{0.36} (Pr/Pr_s)^{0.25}$	Staggered >16 rows	(3.121)

		1000-20,000 Re_D	
	$Nu_D = 0.031(S_T/S_L)^{0.2} Re_D^{0.8} Pr^{0.36} (Pr/Pr_s)^{0.25}$	Staggered >16 rows 20,000-200,000 Re_D	(3.122)
[143]	$Nu_D = 0.8 Re_D^{0.4} Pr^{0.36} (Pr/Pr_s)^{0.25}$	In-line >10 rows 0.7 < Pr < 500 10 < Re_D < 100	(3.123)
	$Nu_D = 0.9 Re_D^{0.4} Pr^{0.36} (Pr/Pr_s)^{0.25}$	Staggered >10 rows 0.7 < Pr < 500 10 < Re_D < 100	(3.124)
	$Nu_D = 0.27 Re_D^{0.63} Pr^{0.36} (Pr/Pr_s)^{0.25}$	In line 0.7 < Pr < 500 1000 < Re_D < 10,000 $S_T/S_L \geq 0.7$	(3.125)
	$Nu_D = 0.35 \left(\frac{S_T}{S_L}\right)^{0.2} Re_D^{0.6} Pr^{0.36} (Pr/Pr_s)^{0.25}$	Staggered 0.7 < Pr < 500 1000 < Re_D < 10,000 $S_T/S_L < 2$	(3.126)
	$Nu_D = 0.4 Re_D^{0.6} Pr^{0.36} (Pr/Pr_s)^{0.25}$	Staggered 0.7 < Pr < 500 1000 < Re_D < 10,000 $S_T/S_L \geq 2$	(3.127)
	$Nu_D = 0.021 Re_D^{0.84} Pr^{0.36} (Pr/Pr_s)^{0.25}$	In-line 0.7 < Pr < 500 $Re_D > 10,000$	(3.128)
	$Nu_D = 0.022 Re_D^{0.84} Pr^{0.36} (Pr/Pr_s)^{0.25}$	Staggered 0.7 < Pr < 500 $Re_D > 10,000$	(3.129)
	$Nu_D = 0.019 Re_D^{0.84}$	Staggered Pr=0.7 $Re_D > 10,000$	(3.130)

	$Nu_D = 0.0131Re_D^{0.883} Pr^{0.36}$	Staggered 450,000 < Re_D < 700,000 $S_T/D=2$ $S_L/D=1.4$	(3.131)
[135]	$Nu_D = (0.5Re_D^{0.5} + 0.2Re_D^{2/3}) Pr^{1/3} \left(\frac{\mu_\infty}{\mu_w}\right)^{0.14}$	Staggered $30 \geq Pr$ $Re \geq 100$ $0.65 \geq$ Void faction	(3.132)

*For [166], if the number of longitudinal rows (Nr) is less than 16 and Re_D is greater than 1,000, a correction factor can be used, shown in Table 11.

Table 11: Correction factor for Žukauskas correlations [166] with less than 16 rows of tubes [125].

Nr	1	2	3	4	5	7	10	13
In-line	0.70	0.80	0.86	0.90	0.93	0.96	0.98	0.99
Staggered	0.64	0.76	0.84	0.89				

3.9.1.2.1. Finned correlations

For finned tube bundles, Table 12 provides Nusselt correlations for various arrangements, finning type and conditions. Reference [143] correlations were used in the presented model. Others can be selected depending on the HPHE geometry and conditions.

Table 12: Available correlations for calculation of Nusselt numbers over finned tube bundles.

Ref.	Correlation	Condition	Eq.
[167]	$Nu_D = 0.044 \left(\frac{S_T}{S_L}\right)^{0.2} \left(\frac{Y_{fin}}{D_o}\right)^{0.18} \left(\frac{H_{fin}}{D_o}\right)^{-0.14} Re_D^{0.8}$	Circular fins Staggered $20,000 \leq Re_D \leq 200,000$	(3.133)
	$Nu_D = 0.0067 \left(\frac{S_T}{S_L}\right)^{0.2} \left(\frac{Y_{fin}}{D_o}\right)^{0.18} \left(\frac{H_{fin}}{D_o}\right)^{-0.14} Re_D^{0.95}$	Circular fins Staggered $200,000 \leq Re_D \leq 1,300,000$	(3.134)
[168]	$Nu_s = 0.023k_{Nr} \left(\frac{A}{A_T}\right)^{0.2} \left(\frac{D_o}{Y_{fin}}\right)^{-0.54} \left(\frac{H_{fin}}{Y_{fin}}\right)^{-0.14} Re_s^{0.65}$	Circular fins Staggered $1,000 \leq Re_D \leq 20,000$	(3.135)

	$Nu_s = 0.105k_{Nr} \left(\frac{D_o}{Y_{fin}} \right)^{-0.54} \left(\frac{H_{fin}}{Y_{fin}} \right)^{-0.14} Re_s^{0.65}$	Circular fins In-line $1,000 \leq Re_D \leq 20,000$	(3.136)
[169]	$Nu_D = 0.45 \left(\frac{A_t}{A_{exposed}} \right)^{-0.375} Re_D^{0.625} Pr^{1/3}$	Staggered $1,000 \leq Re_D \leq 40,000$	(3.137)
	$Nu_D = 0.3 \left(\frac{A_t}{A_{exposed}} \right)^{-0.375} Re_D^{0.625} Pr^{1/3}$	In-line $1,000 \leq Re_D \leq 40,000$	(3.138)
[143] †	$Nu_D = 0.192 Re_D^{0.65} Pr^{0.36} \left(\frac{S_T}{S_L} \right)^{0.2} \left(\frac{Y_{fin}}{D_o} \right)^{0.18} \left(\frac{H_{fin}}{D_o} \right)^{-0.14} \left(\frac{Pr}{Pr_s} \right)^{0.25}$	Circular or helical Staggered $100 \leq Re_D \leq 20,000$	(3.139)
	$Nu_D = 0.0507 Re_D^{0.8} Pr^{0.4} \left(\frac{S_T}{S_L} \right)^{0.2} \left(\frac{Y_{fin}}{D_o} \right)^{0.18} \left(\frac{H_{fin}}{D_o} \right)^{-0.14} \left(\frac{Pr}{Pr_s} \right)^{0.25}$	Circular or helical Staggered $20,000 \leq Re_D \leq 200,000$	(3.140)
	$Nu_D = 0.0081 Re_D^{0.95} Pr^{0.4} \left(\frac{S_T}{S_L} \right)^{0.2} \left(\frac{Y_{fin}}{D_o} \right)^{0.18} \left(\frac{H_{fin}}{D_o} \right)^{-0.14} \left(\frac{Pr}{Pr_s} \right)^{0.25}$	Circular or helical Staggered $200,000 \leq Re_D \leq 1,400,000$	(3.141)
[170]	$j = 0.134 \left(\frac{Y_{fin} - e_{fin}}{H_{fin}} \right)^{0.2} \left(\frac{Y_{fin} - e_{fin}}{e_{fin}} \right)^{0.11} Re_D^{-0.319}$	Circular fins Equilaterally staggered $1,100 \leq Re_D \leq 1,800$	(3.142)
[171]	$j = 1.1184 Re_D^{-0.5183} \left(\frac{Y_{fin}}{D_o} \right)^{0.7147} Nr^{-0.1684}$	Helical fins Staggered $340 \leq Re_D \leq 1,050$	(3.143)
	$j = 0.3452 Re_D^{-0.3972} \left(\frac{Y_{fin}}{D_o} \right)^{0.6626} Nr^{-0.2026}$	Helical fins In-Line $340 \leq Re_D \leq 1,050$	(3.144)
	$Nu_D = 0.138 Re_D^{0.68} Pr^{0.33} \left(\frac{S_T}{D_o} \right)^{0.263} \left(\frac{S_L}{D_o} \right)^{-0.194} \left(\frac{Y_{fin}}{D_o} \right)^{0.168} \left(\frac{H_{fin}}{D_o} \right)^{-0.13}$	Circular or helical Staggered $D_o = 32 \text{ mm}$ $5,000 \leq Re_D \leq 55,000$	(3.145)
$\frac{A_t}{A_{exposed}}$ is the ratio of total heat transfer surface area per tube to exposed area of tube.			
†The following conditions also apply:			

$$0.06 \leq \frac{Y_{fin}}{D_o} \leq 0.36$$

$$0.07 \leq \frac{H_{fin}}{D_o} \leq 0.715$$

$$1.1 \leq \frac{S_T}{D_o} \leq 4.2$$

$$1.03 \leq \frac{S_L}{D_o} \leq 2.5$$

For equations giving the j , Colburn factor:

$$Nu_D = \frac{j, \text{ Colburn factor}}{Re_D Pr^{1/3}}$$

For [168], the correction factor, k_{Nr} is extracted from the graphs for both staggered (Figure 36) and in-line tube banks (Figure 37). The staggered correction factor is only applicable below 20 rows or else it defaults to 1.02 and only has a dramatic effect under around 12 rows. The correction factor for in-line banks is only needed if the number of rows is less than five, or else it defaults to 1. Note that even though the correction factor is presented as a line graph, only whole rows truly apply.

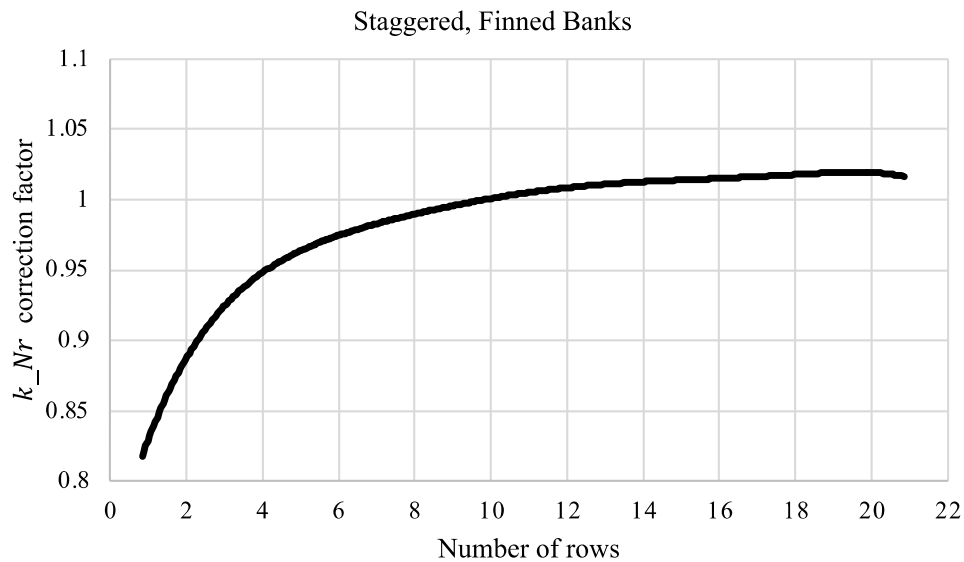


Figure 36: Graph showing the k_{Nr} correction factor for staggered tube bundles, data extracted from [168].

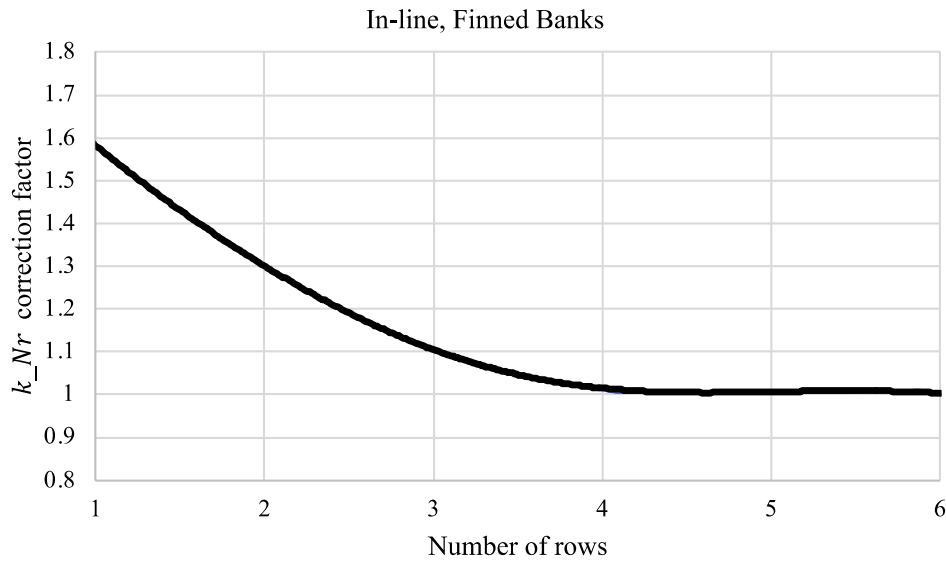


Figure 37: Graph showing the k_{Nr} correction factor for in-line tube bundles, data extracted from [168].

3.9.2. Heat Transfer Coefficient of Boiling

Two-phase heat transfer by boiling, liquid to gaseous phase, occurs when the temperature of the liquid is higher than the saturation temperature. The saturation temperature is also known as the boiling point of the liquid. Boiling depends upon the latent heat of vaporisation of the liquid and the surface tension at the interface between the liquid and vapour. In a heat pipe, the solid-liquid interface is the heat pipe casing to working fluid interface. Boiling occurs here if the liquid comes into contact with the casing at a higher temperature than that of the boiling point of the liquid. Four different boiling regimes are recognised: free convection, nucleate, transition and film. Nucleate boiling is the regime considered in effectively designed heat pipes.

A boiling curve is shown in Figure 38 to illustrate the different flow regimes, using water at atmospheric pressure for illustration. The temperature difference shown is between the heating surface temperature and the saturation temperature of the fluid in contact with it. With a small temperature difference, natural convection prevails with a small heat flux. As the temperature difference increases, bubbles generate but collapse in the fluid (A-B), particularly if the liquid is sub-cooled. The highest heat flux at Point C (maximum or critical heat flux) seen is when the bubbles rise to the surface (B-C), which occurs when the liquid is at saturated condition. After this point, transition boiling occurs where the presence of too many bubbles causes the

heat flux to drop as the heat transfer rate to a high temperature gas is lower than to a fluid, which blocks effective heat transfer. Continuous raising of the temperature difference reduces the heat flux until the Leidenfrost inversion point is reached (D), where film boiling then dominates, being where the fluid sits on a blanket of bubbles. Point E is defined as the burnout point, which is the melting point of the surface or heater and is variable.

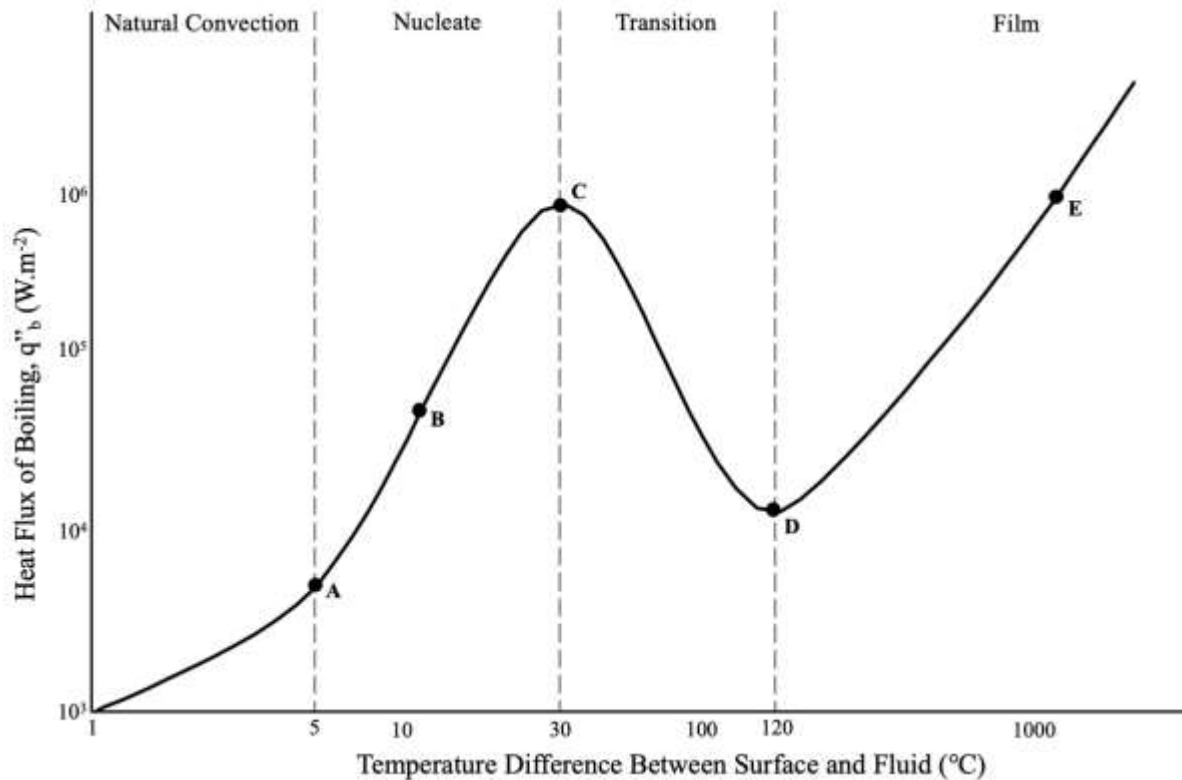


Figure 38: Graph showing heat flux against temperature difference for the case of water boiling at atmospheric pressure, adapted from [126].

Four flow regimes have been observed for the evaporating fluid in the evaporator section [172], namely, a smooth continuous film with surface evaporation, a series of rivulets with a breakdown of the smooth continuous film; a wavy film with unstable rivulets and a wavy film with bubble nucleation occurring in the unstable rivulets.

The two types of boiling seen in thermosyphons are pool boiling from the working fluid pool at the evaporator section of a thermosyphon and boiling of the returning condensate running down the sides of the heat pipe. The falling film boiling mechanism is similar to flow boiling with an annular flow regime. Depending on the size of the pool in the thermosyphon, one of the boiling types will dominate.

Of an abundant number of heat transfer correlations for boiling, Table 13 shows commonly seen correlations for pool boiling, Table 14 for falling film boiling, those that have been shown to be accurate, or those developed specifically for thermosyphons. For a more extensive list of correlations, [152] provides a thorough overview. The following correlations were not used in the model but are required for the thermal resistance network, if a more detailed analysis is conducted.

Table 13: Available correlations for calculation of heat transfer coefficient of pool boiling.

Ref.	Equation	Condition	Eq.
[173]	$h_{pb} = 0.082 \left(\frac{\lambda_l}{L_b} \right) \left(\frac{h_{fg} q''_{pb} \rho_v}{T_{sat} \lambda_l \rho_l - \rho_v} \right)^{0.7} \left(\frac{T_{sat} c_{p,l} \sigma \rho_l}{h_{fg}^2 \rho_v^2 L_b} \right)^{0.33} Pr_l^{-0.45}$		(3.146)
[174]	$h_{pb} = \left(\frac{q''_{pb}}{h_{fg}} \right)^{2/3} \left(\frac{\mu_l}{L_b} \right)^{1/3} \frac{c_{p,l}}{C_{sf}} Pr_l^{-1}$	Water	(3.147)
	$h_{pb} = \left(\frac{q''_{pb}}{h_{fg}} \right)^{2/3} \left(\frac{\mu_l}{L_b} \right)^{1/3} \frac{c_{p,l}}{C_{sf}} Pr_l^{-1.7*}$	Fluids other than water	(3.148)
[175]	$h_{pb} = 0.225 \left(\frac{q''_{pb} c_p}{h_{fg}} \right)^{0.69} \left(\frac{P \lambda_l}{\sigma} \right)^{0.31} \left(\frac{\rho_l}{\rho_v} - 1 \right)^{0.33}$		(3.149)
[176]	$h_{pb} = \frac{0.00122 \times \Delta T_{sat}^{0.24} \Delta P_{sat}^{0.75} c_{p,l}^{0.45} \rho_l^{0.49} \lambda_l^{0.79}}{\sigma^{0.5} h_{fg}^{0.24} \mu_l^{0.29} \rho_v^{0.24}}$		(3.150)
[177]	$h_{pb} = 61.3 \lambda_l Pr_l^{0.33} N_a^{0.5} \Delta T_{sat}$		(3.151)
[178]	$h_{pb} = 3.596 \times 10^{-5} P_{crit}^{0.69} q''_{pb}^{0.7} (1.8 P^{*0.17} + 4 P^{*1.2} + 10 P^{*10})$		(3.152)
[179]	$h_{pb} = 0.075 \left[1 + 10 \left(\frac{\rho_v}{\rho_l - \rho_v} \right)^{0.67} \right] \left(\frac{\lambda_l^2}{v_l \sigma T_{sat}} \right)^{0.33} q''_{pb}^{0.67}$		(3.153)
[180]	$h_{pb} = 0.32 \left(\frac{\rho_l^{0.65} \lambda_l^{0.3} c_{p,l}^{0.7} g^{0.2}}{\rho_v^{0.25} h_{fg}^{0.4} \mu_l^{0.1}} \right) \left(\frac{P_v}{P_{atm}} \right)^{0.23} q''_{pb}^{0.4}$		(3.154)
[181]	$h_{pb} = 0.246 \frac{\lambda_l}{D_d} \times 10^{-7} \times X_1^{0.673} X_2^{1.26} X_3^{-1.58} X_4^{5.22}$ $X_1 = \left(\frac{q''_{pb} D_d}{k_l T_v} \right), X_2 = \left(\frac{c_p T_v D_d^2}{\alpha^2} \right), X_3 = \left(\frac{h_{fg} D_d^2}{\alpha^2} \right), X_4 = \left(\frac{\rho_l - \rho_v}{\rho_l} \right)$	Water $10^{-4} \leq P^* \leq 0.88$	(3.155)
[147]	$h_{pb} = 0.32 \left(\frac{\rho_l^{0.65} \lambda_l^{0.3} c_{p,l}^{0.7} g^{0.2}}{\rho_v^{0.25} h_{fg}^{0.4} \mu_l^{0.1}} \right) \left(\frac{P_v}{P_{atm}} \right)^{0.23} q''_{pb}^{0.4}$	Specific for thermosyphons	(3.156)
[182]	$h_{pb} = 3.596 \times 10^{-5} P_{crit}^{0.69} (q''_{pb})^{0.7} \left[0.7 + 2 P^* \left(4 + \frac{1}{1 - P^*} \right) \right]$		(3.157)
[183]	$h_{pb} = 31.4 \frac{p_{crit}^{0.2}}{M^{0.1} T_{crit}^{0.9}} \left(8 \frac{R_p}{R_{p0}} \right)^{0.2(1-P^*)} \frac{P^{*0.23}}{(1 - 0.99 P^*)^{0.9}} q''_{pb}^{0.8}$		(3.158)
[184]	$h_{pb} = 55 q''_{pb}^{0.67} P^{*(0.12 - 0.21 \log R_{a,p})} (-\log P^*)^{-0.55} M^{-1/2}$		(3.159)

[185]	$h_{pb} = 0.0098^{-1} Pr_l^{-1.7} \left(\frac{c_{p,l}}{h_{fg}} q''_{pb} \right) \left(\frac{L_b}{h_{fg} \mu_l} q''_{pb} \right)^{-1/3}$	Water	(3.160)
	$h_{pb} = 0.0028^{-1} Pr_l^{-1.7} \left(\frac{c_{p,l}}{h_{fg}} q''_{pb} \right) \left(\frac{L_b}{h_{fg} \mu_l} q''_{pb} \right)^{-1/3}$	Methanol	(3.161)
[186]	$h_{pb} = 0.44 Pr_l^{0.35} \left(\frac{\lambda_l}{L_b} \right) \left(\frac{\rho_l}{\rho_l - \rho_v} \frac{P \times 10^{-4}}{\rho_v g h_{fg} \mu_l} q''_{pb} \right)^{0.7}$		(3.162)
	$h_{pb} = \left[3.37 \times 10^{-9} \frac{\lambda_l}{L_b} \left(\frac{q''_{pb} c_{p,l}}{h_{fg}} \right)^2 \frac{(P/\rho_v)^2}{\sigma g / (\rho_l - \rho_v)} \right]^{1/3}$		(3.163)
[187]	$h_{pb} = 55 q''_{pb}{}^{0.7} [P^{*0.12} / ((-\log_{10} P^*)^{0.55} M^{0.5})]$		(3.164)
[188]	$h_{pb} = 22 (\rho_v / \rho_l)^{0.4} R_{a,p}{}^{0.2(1-P^*)} 0.44 Pr_l^{0.35} \left(\frac{\lambda_l}{L_b} \right) \left(\frac{\rho_l}{\rho_l - \rho_v} \frac{P \times 10^{-4}}{\rho_v g i_{lv} \mu_l} q''_{pb} \right)^{0.7}$		(3.165)
[189]	$h_{pb} = 11.43 \left(\frac{q''_{pb} D_d}{\rho_v h_{fg} \nu_l} \right)^{0.72} (Pr_l)^{0.42} \left(\frac{\rho_v}{\rho_l} \right)^{0.5} \left(\frac{D_d}{D_i} \right) \left(\frac{\lambda_l}{D_d} \right)$	Specific for water thermosyphons	(3.166)
[190]	$h_{pb} = \left(1 + 4.95 \left(\frac{\rho_v}{\rho_l} \right)^{0.4} \left[\frac{P_v \nu_l}{\sigma} \left(\frac{\rho_l^2}{\sigma g (\rho_l - \rho_v)} \right)^{1/4} \right]^{1/4} \right) h_{pb,Ku}$ where, $h_{pb,Ku} = 0.44 Pr_l^{0.35} \left(\frac{\lambda_l}{L_b} \right) \left(\frac{\rho_l}{\rho_l - \rho_v} \frac{P \times 10^{-4}}{\rho_v g h_{fg} \mu_l} q''_{pb} \right)^{0.7}$		(3.167)
[191]	$h_{pb} = 18.688 \left(\frac{\mu h_{fg}}{L_b \Delta T_{sat}} \right) \left(\frac{c_p \Delta T_{sat}}{h_{fg} Pr} \right)^{1.0716}$	Water	(3.168)
	$h_{pb} = 17.625 \left(\frac{\mu h_{fg}}{L_b \Delta T_{sat}} \right) \left(\frac{c_p \Delta T_{sat}}{h_{fg} Pr} \right)^{0.99}$	Ethanol	(3.169)

C_{sf} values, depending on the surface finish, are tabulated in [126].

L_b is the bubble scale length:

$$L_b = \left[\frac{\sigma}{g(\rho_l - \rho_v)} \right]^{1/2}$$

P^* is the reduced pressure:

$$P^* = P / P_{crit}$$

D_d is the bubble departure diameter can be calculated in many ways [152], with the most recommended calculated by [192]:

$$D_d = 0.19 L_b \left\{ \left(1.8 + 10^5 \left(\frac{Ja}{Pr_l} \right) \left[\frac{g \rho_l (\rho_l - \rho_v)}{\mu_l} \right] \left[\frac{\sigma}{g(\rho_l - \rho_v)} \right]^{3/2} \right)^{-1} \right\}^{2/3}$$

where,

$$Ja = \frac{(T_s - T_{sat})c_p}{h_{fg}}$$

Table 14: Correlations for calculating heat transfer coefficient of falling film boiling [57].

Ref.	Equation	Eq.
[193]	$h_{fb} = 0.1 \left(\frac{\lambda_l h_{fg} \rho_v q''_{fb}}{\sigma T_{sat}} \right) \frac{1}{\lambda_l} \left(\frac{\mu_l^2}{\rho_l^2 g} \right)^2$	(3.170)
[194]	$h_{fb} = 0.606 \left(\frac{\dot{q}}{\pi D_i h_{fg} \mu_l} \right)^{-1/3}$	(3.171)
[195]	$h_{fb} = \left(\frac{4}{3} \right)^{1/3} \left(\frac{4\dot{q}}{\pi D_i h_{fg} \mu_l} \right)^{-1/3} \left[\left(\left(\frac{4}{3} \right)^{1/3} \left(\frac{4\dot{q}}{\pi D_i h_{fg} \mu_l} \right)^{-1/3} \left(\frac{\lambda_l}{\Psi^{1/3}} \right) \right)^3 + 1.155 \times 10^{-3} \left(\frac{\lambda_l}{L_b} \right) \left(\frac{\mu_l}{(\sigma \rho_l L_b)^{1/2}} \right)^{0.33} Pr_l^{0.35} \left(\frac{q''_{f, nb} L_b \rho_l}{\rho_v h_{fg} \mu_l} \right) \left(\frac{PL_b}{\sigma} \right)^{0.7} \right]^3$	(3.172)
[196]	$h_{fb} = 0.01 \left(\frac{\mu_l^2}{\rho_l^2 g} \right)^{1/3} \frac{1}{L_b} \left(\frac{4\dot{q}}{\pi D_i h_{fg} \mu_l} \right)^{0.8} Pr_l^{1/3} \left(1 + 10 \left(\frac{\rho_v}{\rho_l - \rho_v} \right)^{2/3} \right) \left(\frac{(h_{fg} \rho_v)^2 L_b}{T_{sat} c_{p, l} \sigma \rho_l} \right)^{0.4} \left(\frac{R_z}{L_f} \right)^{0.2} \left(\frac{\lambda_l c_{p, l} \rho_l}{\lambda_w c_{p, w} \rho_w} \right)^{-0.2}$	(3.173)
[59]	$h_{fb} = 1.71 \sqrt[3]{\frac{g \rho_p (\rho_p - \rho_v) \lambda_p^3 h_{fg} r_i}{\mu_p \dot{q}_{TS}}}$	(3.174)

3.9.3. Heat Transfer Coefficient of Condensation

In the reverse of boiling, condensation occurs when vapour temperatures are reduced below the saturation temperature. In thermosyphons, this occurs at the condenser wall or the falling liquid film. There are two main forms of condensation on a solid surface, these are film or dropwise condensation. Film condensation occurs when the condensate forms a film and totally wets the surface. Due to gravity, this falls and increases in thickness as additional condensation occurs on the film. In dropwise condensation, the vapour condenses to form droplets on the surface and does not form a film. When the droplets reach a certain size, they drop and clear the surface allowing a free condensation site directly on the surface, with a corresponding increase

in heat transfer rate. In practice, this does not occur continuously or sustainably so only film condensation is considered. [126]

Table 15 provides available condensation correlations that are applicable to thermosyphons; inclined thermosyphons have been omitted. For further reading, see [197]. The following correlations were not used in the model but are required for the thermal resistance network, if a more detailed analysis is conducted.

Table 15: Available correlations for calculation of heat transfer coefficient of film condensation.

Ref.	Equation	Condition	Eq.
[198]	$h_{Nu,cd} = 0.943 \left(\frac{\rho_l(\rho_l - \rho_v)h_{fg}g\lambda_l^3}{\mu_l L_c(T_{sat} - T_w)} \right)^{1/4}$		(3.175)
[199]	$h_{cd} = 1.13 \left(\frac{\rho_l(\rho_l - \rho_v)h_{fg}g\lambda_l^3}{\mu_l L_c(T_{sat} - T_w)} \right)^{1/4}$		(3.176)
	$h_{cd} = 0.943 \left(\frac{\rho_l(\rho_l - \rho_v)h_{fg}g\lambda_l^3}{\mu_l L_c(T_{sat} - T_w)} \right)^{1/4}$		(3.177)
[200]	$h_{cd} = 1.51 \left(\frac{P_v}{P_{crit}} \right)^{0.14} 0.943 \left\{ \frac{\rho_l(\rho_l - \rho_v)g\lambda_l^3}{\mu_l L_c(T_{sat} - T_w)} [h_{fg} + 0.375c_{p,l}(T_{sat} - T_w)] \right\}^{1/4}$ Thermophysical properties evaluated at temperature: $T = T_w + 0.31(T_{sat} - T_w)$	$20 \leq Re_f$ ≤ 600	(3.178)
[201]	$h_{cd} = \frac{\Gamma/\mu_l}{1.47(\Gamma/\mu_l)^{1.22} - 1.3} \lambda_l \Psi^{-1/3}$		(3.179)
[202]	$h_{cd} = 1.013 \left(\frac{4\Gamma}{\mu_l} \right)^{-0.22} \lambda_l \Psi^{-1/3}$		(3.180)
[203]	$h_{cd} = \left(\left(0.925(1 - 0.63(P_v/P_{crit})^{3.3})^{-1} \left(\frac{\dot{q}}{\pi D_i h_{fg} \mu_l} \right)^{-1/3} \right)^2 + \left(0.044 Pr_l^{2/5} \left(\frac{\dot{q}}{\pi D_i h_{fg} \mu_l} \right)^{1/6} \right)^2 \right)^{1/2} \lambda_l \Psi^{-1/3}$		(3.181)
[204]	$h_{cd} = 0.693 \left(\frac{1 - \rho_v/\rho_l}{\Gamma/\mu_l} \right)^{1/3} \lambda_l \Psi^{-1/3}$		(3.182)

[201]	$h_{cd} = \frac{\Gamma/\mu_l}{1.47(\Gamma/\mu_l)^{1.22} - 1.3} \lambda_l \Psi^{-1/3}$		(3.183)
[202]	$h_{cd} = 1.013 \left(\frac{4\Gamma}{\mu_l}\right)^{-0.22} \lambda_l \Psi^{-1/3}$		(3.184)
[205]	$h_{cd} = 1.013 \left(\frac{\dot{q}}{\pi D_i h_{fg} \mu_l}\right)^{-1/3} \lambda_l \Psi^{-1/3}$		(3.185)
[206]	$h_{cd} = \left[1.33 \left(\frac{4\Gamma}{\mu_l}\right)^{-1/3} + 9.56 \times 10^{-6} \left(\frac{4\Gamma}{\mu_l}\right)^{0.89} Pr_l^{0.94} + 8.22 \right. \\ \left. \times 10^{-2} \right] \lambda_l \Psi^{-1/3}$		(3.186)
[203]	$h_{cd} = \left(\left(0.925(1 - 0.63(P_v/P_{crit})^{3.3})^{-1} \left(\frac{\dot{q}}{\pi D_i h_{fg} \mu_l}\right)^{-1/3} \right)^2 \right. \\ \left. + \left(0.044 Pr_l^{2/5} \left(\frac{\dot{q}}{\pi D_i h_{fg} \mu_l}\right)^{1/6} \right)^2 \right)^{1/2} \lambda_l \Psi^{-1/3}$	$600 \leq Re_f$ $\leq 1,600$	(3.187)
[207]	$h_{cd} = 0.87 \left(\frac{4\Gamma}{\mu_l}\right)^{0.07} h_{Nu,cd}$		(3.188)
[204]	$h_{cd} = \left(\left[0.693 \left(\frac{1 - \rho_v/\rho_l}{\Gamma/\mu_l}\right)^{1/3} \lambda_l \Psi^{-1/3} \right]^2 \right. \\ \left. + \left[\frac{0.0283(\Gamma/\mu_l)^{7/24} Pr_l^{1/3}}{1 + 9.66(\Gamma/\mu_l)^{-3/8} Pr_l^{-1/6}} \lambda_l \Psi^{-1/3} \right]^2 \right)^{1/2}$		(3.189)
[208]	$h_{cd} = 0.85 \left(\frac{4\Gamma}{\mu_l}\right)^{0.1} e^{(-6.7 \times 10^{-5} \frac{\rho_l}{\rho_v} - 0.6)} h_{Nu,cd}$		(3.190)
[156]	$h_{cd} = 0.85 \left(\frac{4\dot{q}}{\pi D_i h_{fg} \mu_l}\right)^{0.1} e^{(-6.7 \times 10^{-5} \frac{\rho_l}{\rho_v} - 0.14)} h_{Nu,cd}$		(3.191)
[209]	$h_{cd} = 0.0306 \left(\frac{4\Gamma}{\mu_l}\right)^{1/4} Pr_l^{1/2} \lambda_l \Psi^{-1/3}$	$1,600$	(3.192)
[205]	$h_{cd} = 0.044 Pr_l^{2/5} \left(\frac{\dot{q}}{\pi D_i h_{fg} \mu_l}\right)^{1/6} \lambda_l \Psi^{-1/3}$	$\leq Re_f$	(3.193)

[206]	$h_{cd} = \left[1.33 \left(\frac{4\Gamma}{\mu_l} \right)^{-1/3} + 9.56 \times 10^{-6} \left(\frac{4\Gamma}{\mu_l} \right)^{0.89} Pr_l^{0.94} + 8.22 \right. \\ \left. \times 10^{-2} \right] \lambda_l \Psi^{-1/3}$	(3.194)
[203]	$h_{cd} = \left(\left(0.925(1 - 0.63(P_v/P_{crit})^{3.3})^{-1} \left(\frac{\dot{q}}{\pi D_i h_{fg} \mu_l} \right)^{-1/3} \right)^2 \right. \\ \left. + \left(0.044 Pr_l^{2/5} \left(\frac{\dot{q}}{\pi D_i h_{fg} \mu_l} \right)^{1/6} \right)^2 \right)^{1/2} \lambda_l \Psi^{-1/3}$	(3.195)
[204]	$h_{cd} = \frac{0.0283(\Gamma/\mu_l)^{7/24} Pr_l^{1/3}}{1 + 9.66(\Gamma/\mu_l)^{-3/8} Pr_l^{-1/6}} \lambda_l \Psi^{-1/3}$	(3.196)
[208]	$h_{cd} = 0.85 \left(\frac{4\dot{q}}{\pi D_i h_{fg} \mu_l} \right)^{0.1} e^{(-6.7 \times 10^{-5} \frac{\rho_l}{\rho_v} - 0.6)} h_{Nu,cd}$	(3.197)
[156]	$h_{cd} = 0.85 \left(\frac{4\dot{q}}{\pi D_i h_{fg} \mu_l} \right)^{0.1} e^{(-6.7 \times 10^{-5} \frac{\rho_l}{\rho_v} - 0.14)} h_{Nu,cd}$	(3.198)
<p>Ψ, the liquid film thickness scale, is described by:</p> $\Psi = \frac{\mu_l^2}{g \rho_l (\rho_l - \rho_v)}$		

3.9.4. Effect of Finning and Calculations

The final design factor that needs to be considered is whether the thermosyphons are finned in either or both the condenser or evaporator sections. External pipe finning is used to increase the heat transfer surface and increase turbulence and is primarily for gaseous applications, but can also be used for liquids, due to the inherent lower heat transfer coefficient, which depends upon the thermal conductivity, viscosity, density and specific heat capacity. Fins introduce an additional parallel thermal resistance to a pipe to further reduce the overall thermal resistance. HPHEs tested had helical fins both the evaporator and condenser sections. The total heat transfer area (A_{tot}) of a section with fins is found by adding the heat transfer area of the thermosyphon (A_{TS}) to the heat transfer area of the fins (A_f) whilst considering the efficiency of the fins. Heat transfer is reduced the further the fin section is from the pipe as the energy is passed by conduction originating from or to the outer wall. Therefore, a coefficient of efficiency for the fin is introduced (η_f). Figure 39 shows a selection of available fin designs. Annular (circular) and helical are the main two designs seen.



Figure 39: 3D drawings of available finning options.

Figure 40 shows a diagram of a helically finned pipe and the symbols used in the following equations. Determining the fin efficiency of annular fins is provided in [210]. Helical finning is presented here.

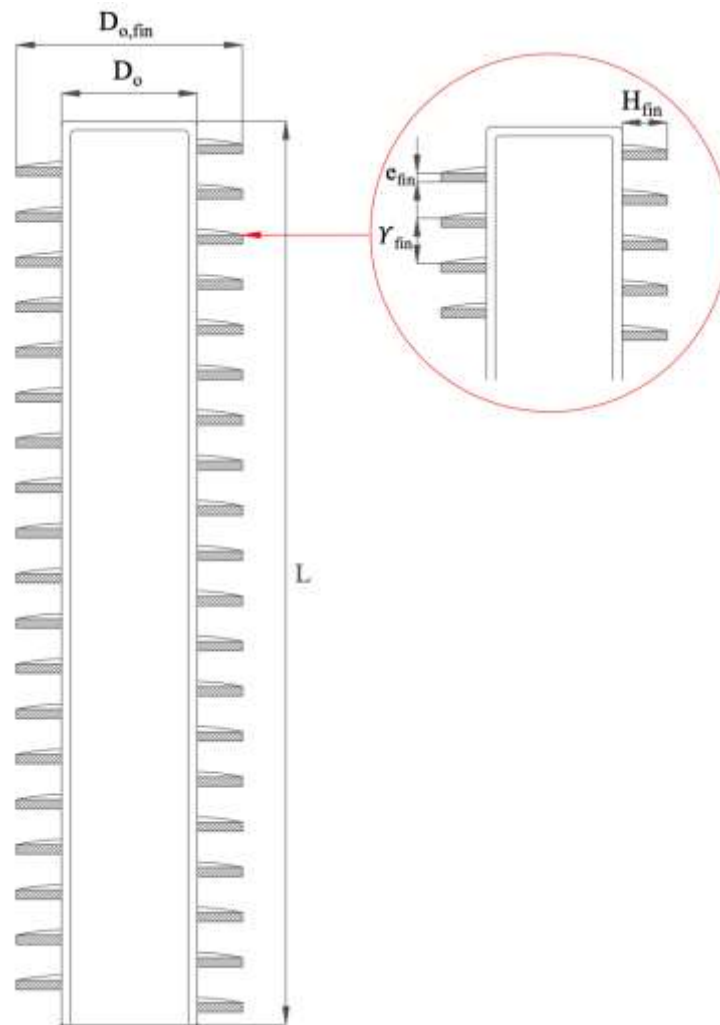


Figure 40: Diagram of helical finning with symbols.

The total heat transfer area for the evaporator or condenser section of a thermosyphon is found separately, in this case, using:

$$A_{tot} = A_{TS} + \eta_{fin} A_{fin} \quad (3.199)$$

where η_{fin} is:

$$\eta_{fin} = \frac{\tanh(xH_{fin})}{xH_{fin}} \quad (3.200)$$

H_{fin} is the width of the fins and x is:

$$x = \sqrt{\frac{2h_{fc}}{\lambda_{fin}e_{fin}}} \quad (3.201)$$

h_{fc} is the heat transfer coefficient of forced convection, found by correlations relating to the hydraulic diameter, λ_f is the thermal conductivity of the fin material, e_{fin} is the thickness of the fin.

The heat transfer area of the fins is:

$$A_{fin} = 2H_{fin}L_{hl} \quad (3.202)$$

L_{hl} is the average length of the helical found by:

$$L_{hl} = \frac{L}{Y_{fin}} \sqrt{\left(\pi \frac{D_{o,fin} + D_o}{2}\right)^2 + Y_{fin}^2} \quad (3.203)$$

L is the length of the finned thermosyphon section, whether it is either the evaporator and/or condenser. $D_{o,fin}$ is the outer diameter including the fins, D_o is the outer diameter of the thermosyphon and Y_{fin} is the pitch of the fins.

The heat transfer area of the bare surface of a thermosyphon (A_{TS}), without fins, is found by:

$$A_{TS} = \pi D_o L N_t \quad (3.204)$$

A HPHE consists of many individual heat pipes. The heat transfer area in the entire exchanger condenser A_c and evaporator A_e section is given by:

$$A_c = N_r N_t A_{tot} \quad (3.205)$$

$$A_e = N_r N_t A_{tot} \quad (3.206)$$

3.9.4.1. Thermal Conductivity of Fins

Other models seen use a fixed thermal conductivity value for fins. This was deemed not to be appropriate for transient analysis or wide temperature possibilities. Therefore, data from a graph within [211] was extracted to create Figure 41. The thermal conductivity equations are then provided with a more relevant value. Carbon steel is presented here though other materials such as stainless steels are applicable.

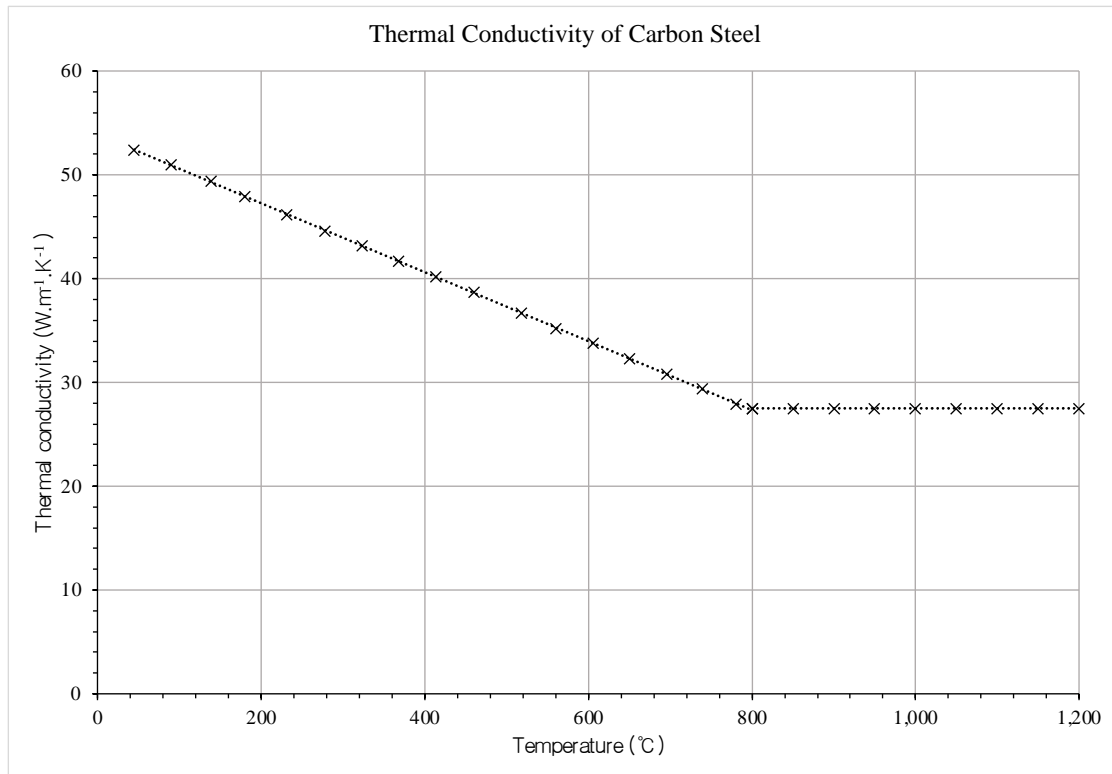


Figure 41: Graph showing the thermal conductivity of carbon steel against temperature.

If the temperature is less than 800°C:

$$\lambda = -0.0333T + 53.902 \quad (3.207)$$

If the temperature is between 800°C and 1,200°C:

$$\lambda = 27.5 \quad (3.208)$$

3.10. Pressure Drop

Pressure drop is a key indicator of performance for heat exchanger installations and a prediction is needed to assist in the selection of fans for gas, or pumps for liquid heat transfer fluids in order to overcome this pressure drop. Too high a pressure drop restricts flow and may require unnecessarily large equipment to overcome it, resulting in a less positive operating cost analysis. Pumping power is proportional to the pressure drop. Pressure drop calculations are needed for both the evaporator and condenser sections and the methodology depends on whether the thermosyphons are finned and the arrangement. An in-line arrangement of thermosyphons is not usually preferred, even though the pressure drop is less, as the overall heat transfer coefficient is reduced due to less exposure to flow and there is less development of turbulence than seen in a staggered arrangement.

With the design of a HPHE, the pressure drop is influenced by the inlet and outlet transition pieces as well as the core of the heat exchanger. The pressure reduction and increase relating to the inlet ducting or between fins have been assumed to be equal and the core being the dominating factor. The literature search conducted has found multiple methods used to determine pressure drop over a bank of tubes. A combination of the Žukauskas method, Yudin model and Shah and Sekulic models have been chosen to predict the pressure drop depending on the arrangement and presence of finning.

Table 16: Pressure drop equations for finned and unfinned banks of tubes.

Author	Equation	Eq.
Kays and London [65]	$\Delta P = \left(\frac{G^2}{\rho_{in} g_c} \right) \left[\left(1 + \left(\frac{A_{min}}{A_{Fr}} \right)^2 \right) \left(\frac{\rho_{in}}{\rho_{out}} - 1 \right) + f \frac{A_s}{A_{min}} \frac{\rho_{in}}{\rho_m} \right]$ $f = \frac{2 \rho_{in} \Delta P_c A_s}{G^2 A}$	(3.209)
Žukauskas [143]	$\Delta P = Nr X f \left(\frac{\rho u_{max}^2}{2 g_c} \right)$ <p>X and f are presented graphically in Section 3.10.1.</p>	(3.210)
Holman-Jakob [212]	$\Delta P = \left(\frac{G_{max}^2 N_L}{\rho (0.5g)} \right) \left(\frac{\mu_w}{\mu} \right)^{0.14} Re_{D,max}^{-0.16} \left[0.25 + \frac{0.118}{\left(\frac{S_T - D_o}{D_o} \right)} \right]$	(3.211)
Gunter-Shaw [212]	$\Delta P = \frac{f}{2g} \frac{1}{\mu} \left(\frac{\mu_w}{\mu} \right)^{0.14} \left(\frac{D_{VH}}{S_T} \right)^{0.4} \left(\frac{S_L}{S_T} \right)^{0.6} \left(\frac{G^2 Z}{D_{VH} \rho} \right)$	(3.212)

	$D_{VH} = \left(\frac{4 S_T S_L}{\pi D_o} - D_o \right)$ $\frac{f}{2} = \begin{cases} 90Re^{-1} & (Re \leq 200) \\ 0.96Re^{-0.145} & (Re > 200) \end{cases}$	
Shah and Giovannelli [59]	$\Delta P = 2N_r \hat{f} \frac{G^2}{\rho_{in}} + G^2 \left(\frac{1}{\rho_{out}} - \frac{1}{\rho_{in}} \right)$ $\hat{f} = 9.465 Re_D^{0.316} \left(\frac{S_T}{D_o} \right)^{-0.937}$	(3.213)
Shah and Sekulic [157]	$\frac{\Delta P}{P_{static}} = \left(\frac{G_m^2}{2g_c \rho_{in} P_{static}} \right) \left[Eu N_r \rho_{in} \left(\frac{1}{\rho} \right)_m + 2 \left(\frac{\rho_{in}}{\rho_{out}} - 1 \right) \right]$	(3.214)
Rich [132][131]	$\Delta P = \left(0.204 \frac{g_c}{g} \left(\frac{0.1}{((S_T/D_o) - 1)^{1/3}} \right) N_r \rho u^2 \right) + \left(1.7 Re_L^{-0.5} \left(\frac{A_{fin}}{2A_{min}} \right) \rho u^2 \right)$ $Re_L = G \frac{S_T}{\mu}$	(3.215)
Yudin [168] Lokshin and Fomina [213]	$\Delta P = Eu(\rho V_\infty^2 N_L) C_z$	(3.216)

For SI, $g_c = 1$, so can be removed.

G is the flow stream mass velocity, calculated at the inlet.

$$G = \frac{\dot{m}}{A_{Fr}}$$

G_m is the average core mass velocity:

$$G_m = \left(\frac{\rho_{in} + \rho_{out}}{2} \right) \left(\frac{u_{max,in} + u_{max,out}}{2} \right)$$

C_z , is a correction factor depending on if the number of longitudinal rows is less than 5 and is shown in Table 17.

Table 17: C_z correction factor for number of rows less than 5.

N_L	1	2	3	4	≥ 5
Staggered	1.45	1.25	1.10	1.05	1.00
In-line	2.25	1.60	1.20	1.05	1.00

3.10.1. Unfinned Thermosyphons

Finding the values of X and f for the Žukauskas pressure drop (Equation (3.210)) depends upon the Reynolds Number and the transverse and longitudinal pitch. X is a correction factor relating to the longitudinal and transverse pitches of the pipes, f is the friction factor obtained empirically. The data for X and f from Figure 42 and Figure 43 [143] have been extracted in order to code the values.

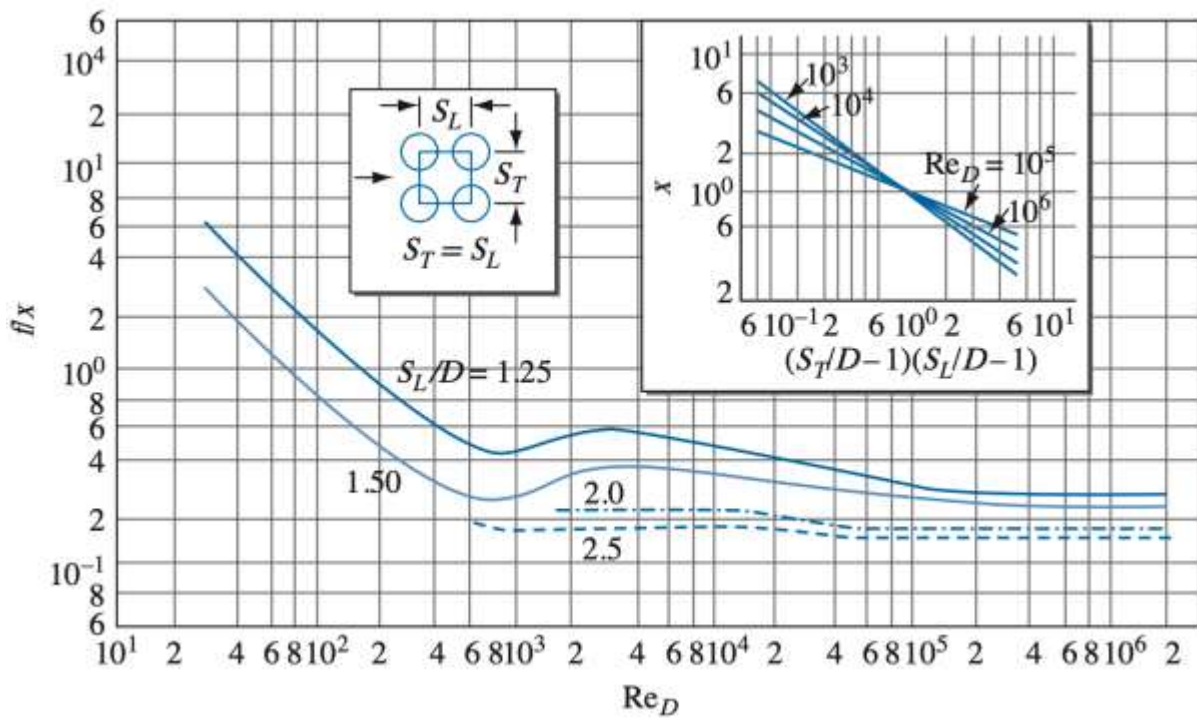


Figure 42: Graph used to find X and f values for in-line unfinned tube bundles [143].

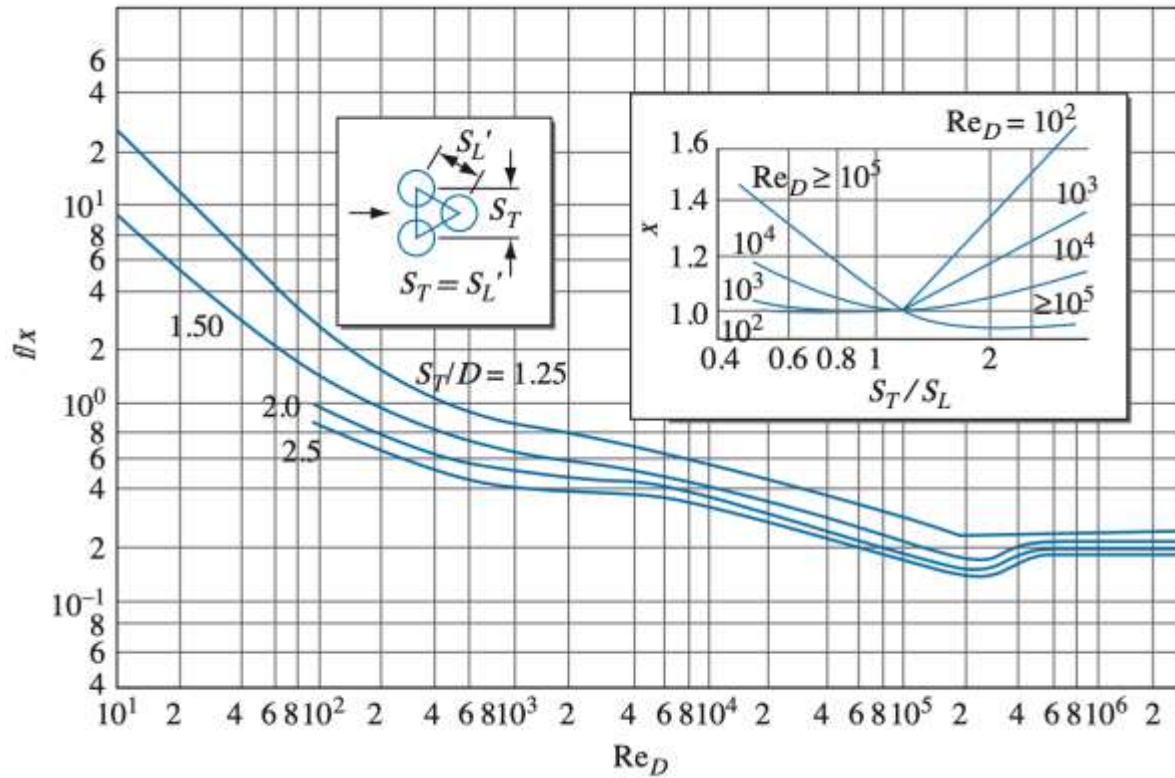


Figure 43: Graph used to find X and f values for staggered unfinned tube bundles [143].

3.10.2. Finned Thermosyphons

The following correlation is recommended for determining the Euler number for in-line finned tube bundles [143]. Equation (3.216) can then be used to determine the pressure drop.

$$Eu = 0.068\gamma^{0.5} \left(\frac{S_T}{D_o}\right)^{-0.55} \left(\frac{S_T - 1}{S_L - 1}\right)^{-0.4} \quad (3.217)$$

γ is the ratio of total surface area with fins to the surface area without fins.

For a staggered arrangement, Eu , the Euler number, is determined by correlations given in Table 18.

Table 18: Available correlations for calculation of Euler numbers over staggered tube bundles [143].

Ref.	Correlation	Condition	Equation
[143]	$Eu = 67.6Re_D^{-0.7}\gamma^{0.5}\left(\frac{S_T}{D_o}\right)^{-0.55}\left(\frac{S_L}{D_o}\right)^{-0.5}$	$100 \leq Re_D < 1,000$ $1.5 \leq \gamma \leq 16$ $1.13 \leq S_T/D_o \leq 2.0$ $1.06 \leq S_L/D_o \leq 2.0$	(3.218)
	$Eu = 3.2Re_D^{-0.25}\gamma^{0.5}\left(\frac{S_T}{D_o}\right)^{-0.55}\left(\frac{S_L}{D_o}\right)^{-0.5}$	$10^3 \leq Re_D < 10^5$ $1.9 \leq \gamma \leq 16$ $1.6 \leq S_T/D_o \leq 4.13$ $1.2 \leq S_L/D_o \leq 2.35$	(3.219)
	$Eu = 0.18\gamma^{0.5}\left(\frac{S_T}{D_o}\right)^{-0.55}\left(\frac{S_L}{D_o}\right)^{-0.5}$	$10^5 \leq Re_D < 1.4 \times 10^6$ $1.9 \leq \gamma \leq 16$ $1.6 \leq S_T/D_o \leq 4.13$ $1.2 \leq S_L/D_o \leq 2.35$	(3.220)

3.11. Radiation

Heat in the evaporator exhaust gases can also pass into the HPHE casing as well as from the condenser section to the casing as heat is transferred into it from the evaporator. This can then be lost to the atmosphere by natural convection or radiation. For this reason, HPHEs can be thermally insulated to reduce losses from the casing and it is highly recommended to do so on high temperature units where radiation plays a larger factor, not only to improve efficiency, but to also prevent contact with hot surfaces. Thermal loss calculations can be conducted using natural convection and radiation analysis to predict these losses. Due to the large variability in design, this has not been considered in this case but that units have negligible losses or are sufficiently insulated.

Radiated heat from and to the thermosyphons can also be a possible consideration at high temperatures and is an alternate heat transfer mechanism path. It was considered in this presented type of heat exchanger that the radiated heat can be neglected as the temperature ranges tested are too low for radiation to play a key factor. Work and modelling of HPHEs which recover waste pipe primarily by the mechanism of radiation have been presented by Almahmoud [57] and Delpech [93].

3.12. True Transience

True transient simulation modelling was attempted using thermosyphon capacitance and differential conservation of energy equations. However, the data available was not in a high enough frequency to obtain meaningful results and the model presented achieved a sufficient accuracy. This approach has not been reported but is available for further reading in [59][153].

3.13. Summary of Theoretical Analysis

The code created for both the steady state (MATLAB) and transient (TRNSYS) models, are provided in Appendix A and B, respectively. The TRNSYS model follows the following logic, shown in Figure 44.

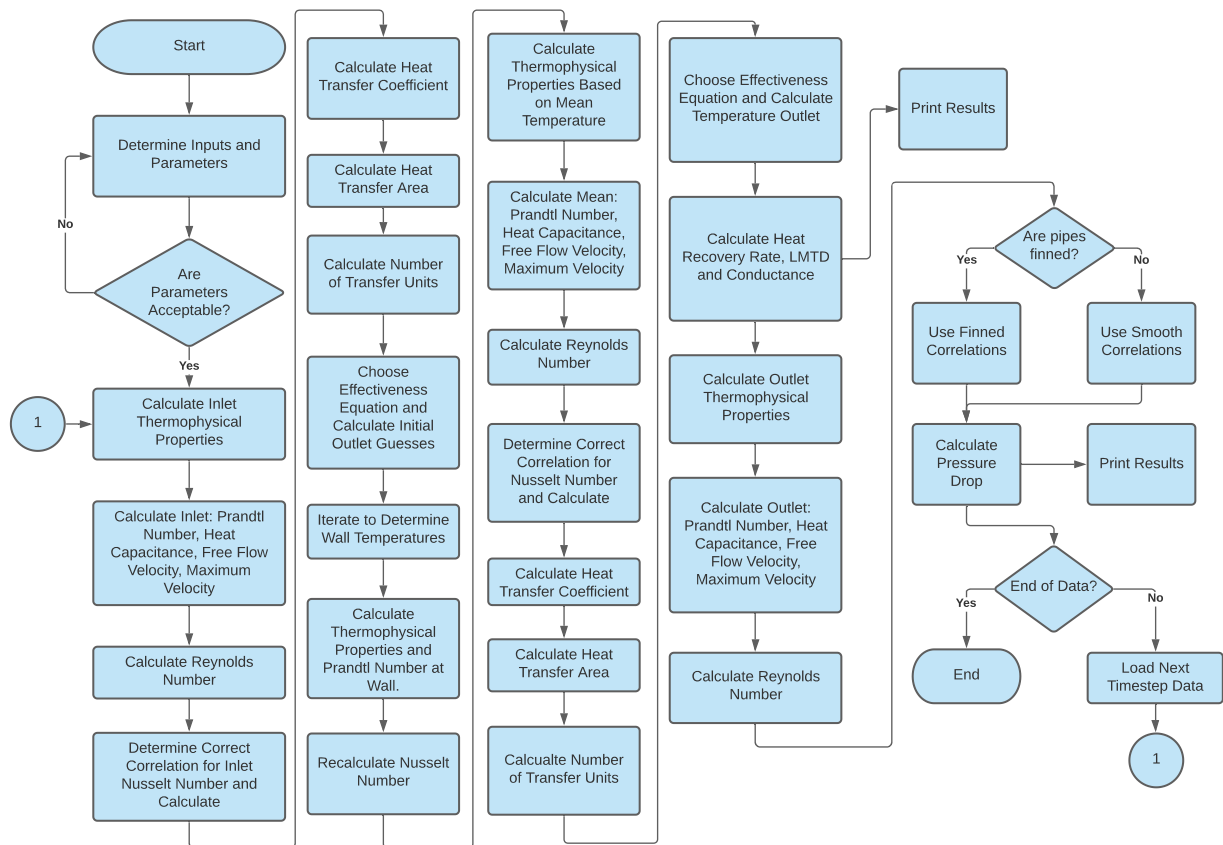


Figure 44: Flowchart of the TRNSYS code logic.

4. EXPERIMENTAL INVESTIGATION

4.1. Introduction

The experimental investigation presented was conducted using three different HPHE units of varying geometries, all of which were designed by the author's Supervisor, Prof. Hussam Jouhara, of Brunel University London. The units were manufactured under projects where the author's supervisor was the technical director, which allowed the research in this PhD to be conducted, as the author was a member of the Heat Pipe and Thermal Management Research Group at Brunel University. Data have been collected over the course of this PhD programme; some which have been requested and made available and a proportion which have been collected personally.

The design of the HPHEs, the experimental system, instrumentation and test conditions are provided for each of the units. The aim of testing multiple geometries was to provide a variety of conditions and heat sinks for the developed model, to provide greater confidence when using it to model further systems. Of the three systems, there was a laboratory-scale unit, where testing parameters could be modified, and two full-scale industrial units. With the full-scale units, other than during commissioning, the experimental data could only be collected from normal working conditions where there was little control over the system. This is due to the end users being working production facilities where their process could not be interrupted.

The first part of this chapter describes the experiments conducted on a laboratory-scale exhaust-to-water HPHE. The author analysed the experimental data, developed a TRNSYS model and drafted a paper on the results [2], parts of which have been used in this chapter. Members of the Instituto de Tecnología Cerámica (ITC), in Spain, assembled the experimental system and conducted the testing.

Secondly, data were collected from an industrial scale exhaust-to-air counterflow HPHE at a ceramic product manufacturing facility in Italy to develop a first working transient model of a HPHE that could predict performance [3]. Sections of this paper have aided development of this chapter. The initial model delivered output temperature predictions for the condenser and evaporator sections and, since then, this work has been expanded. The ability to look at further outputs of predicting HPHE performance values were added, these being: conductance, heat

transfer rate and pressure drop of both the evaporator and condenser sections. Finning is a major consideration when designing heat pipes and the model was developed to predict either finned or unfinned units. This unit has been used to test the model finning capabilities.

The third part of this chapter provides information on the testing of a full-scale industrial exhaust-to-air counterflow unit based at an aluminium die casting facility in Spain. The aluminium facility is described, the system where the unit was installed, the HPHE design and the conditions are described. This unit was also finned. In addition, pressure drop results were available for this system so these results were used to validate the pressure drop outputs of the model.

4.2. Experiment 1: Laboratory-Scale Ceramic Kiln

Initially, a HPHE designed for recovering waste heat from the exhaust gases of a laboratory-scale ceramic continuous roller kiln was tested. The photograph of the kiln is shown in Figure 45. A schematic of the kiln with the burner locations is shown in Figure 46. The kiln's naturally aspirated burners are fuelled by natural gas with roughly 20% excess air. There are eight burners that can fire on the kiln, four on each side, above and below the plane of the rollers. A control panel regulates the number of burners firing and the temperature set point between 100 and 1,200°C. To reach the temperature and flow rate conditions required for testing, only two to four burners were necessary to fire. The heat sink for the HPHE was mains water cooled using an open loop circuit.



Figure 45: Experiment 1 laboratory-scale kiln photograph.

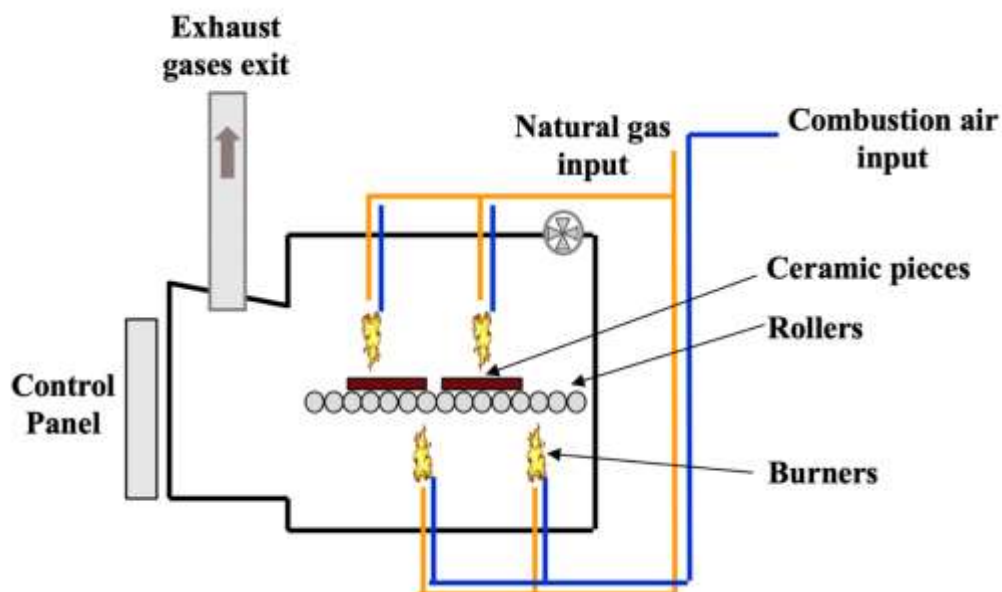


Figure 46: Diagram of the laboratory-scale kiln.

The composition of the stack exhaust gases at the pilot kiln were sampled using a Testo 350 XL combustion gas analyser in order to ensure valid specific heat capacity, c_p , values are used. Nitrogen, oxygen, carbon dioxide, carbon monoxide and water vapour were present from

excess air and natural gas combustion products. No other major relevant gases are found with negligible acidic compound precursors present that usually come from the ceramic product that is being fired in industrial kilns.

4.2.1. HPHE Design

A photograph of the HPHE unit tested is shown in Figure 47. Figure 48 and Figure 49 provide a 3D general arrangement of the unit with the design parameters, material selection and external dimensions. The casing is constructed out of carbon steel and the flange detail for connecting both the heat source and sink to the evaporator and condenser is given.



Figure 47: Experiment 1 HPHE photograph.

Figure 50 provides the detail on the separation plate between the evaporator and condenser sections and the spacing of the thermosyphons. The staggered arrangement shown is an

equilateral spacing shown by Detail A. The separation plate is made of SA516 Gr70 carbon steel which is commonly used in welded vessels operating at a low to moderate temperature.

Figure 51 shows the thermosyphon design, which is identical across the entire bank. There is a total of 100 thermosyphons in a 10 by 10 staggered arrangement. The body of the thermosyphons is made of stainless steel 304. They are 1,518 mm in length with a 28 mm outer diameter. The active evaporator section of the thermosyphons is 1,210 mm and the active condenser section 250 mm in length, with the internal working fluid being distilled water.

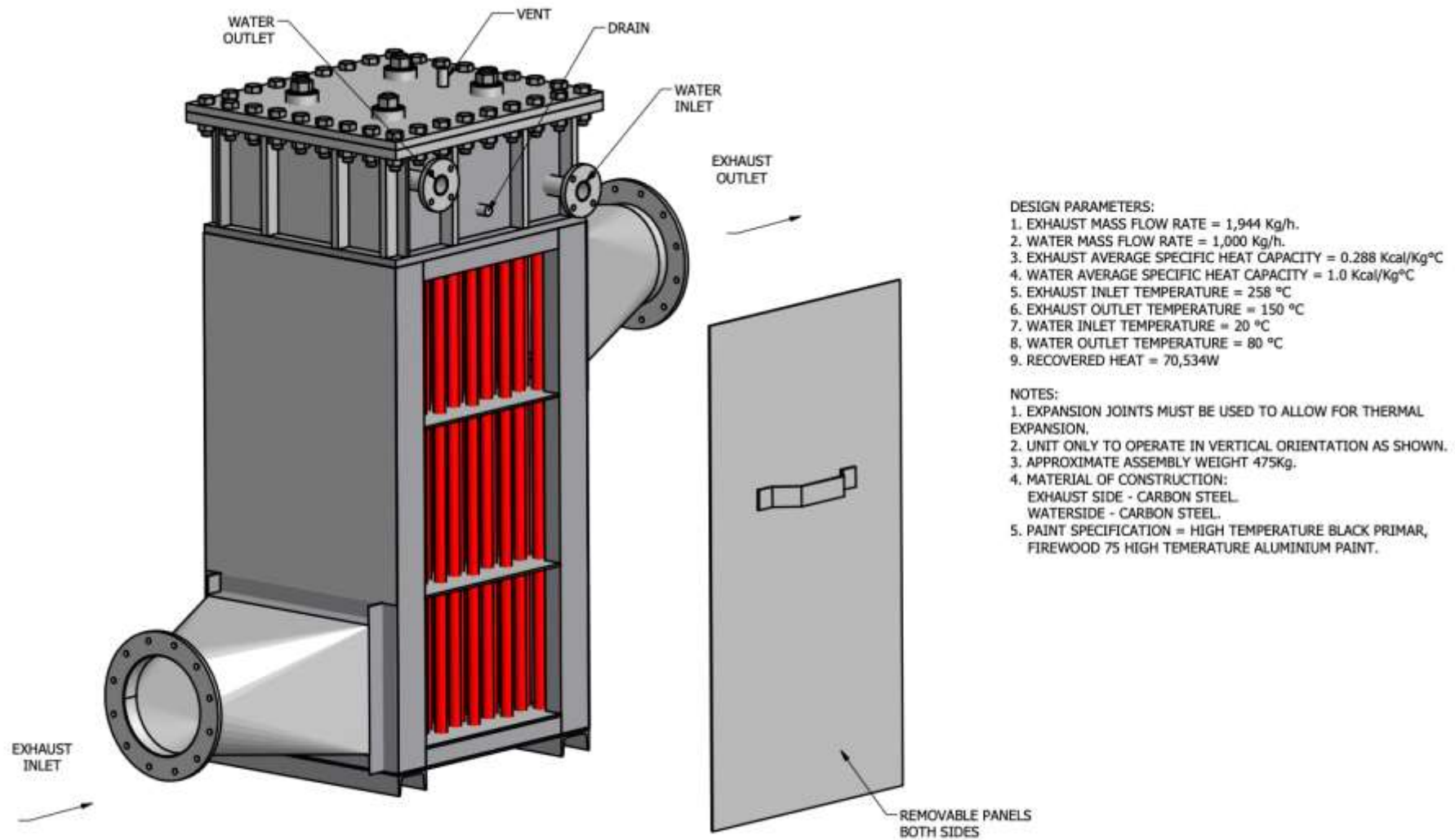


Figure 48: Experiment 1 HPHE general arrangement, showing thermosyphons and design parameters.

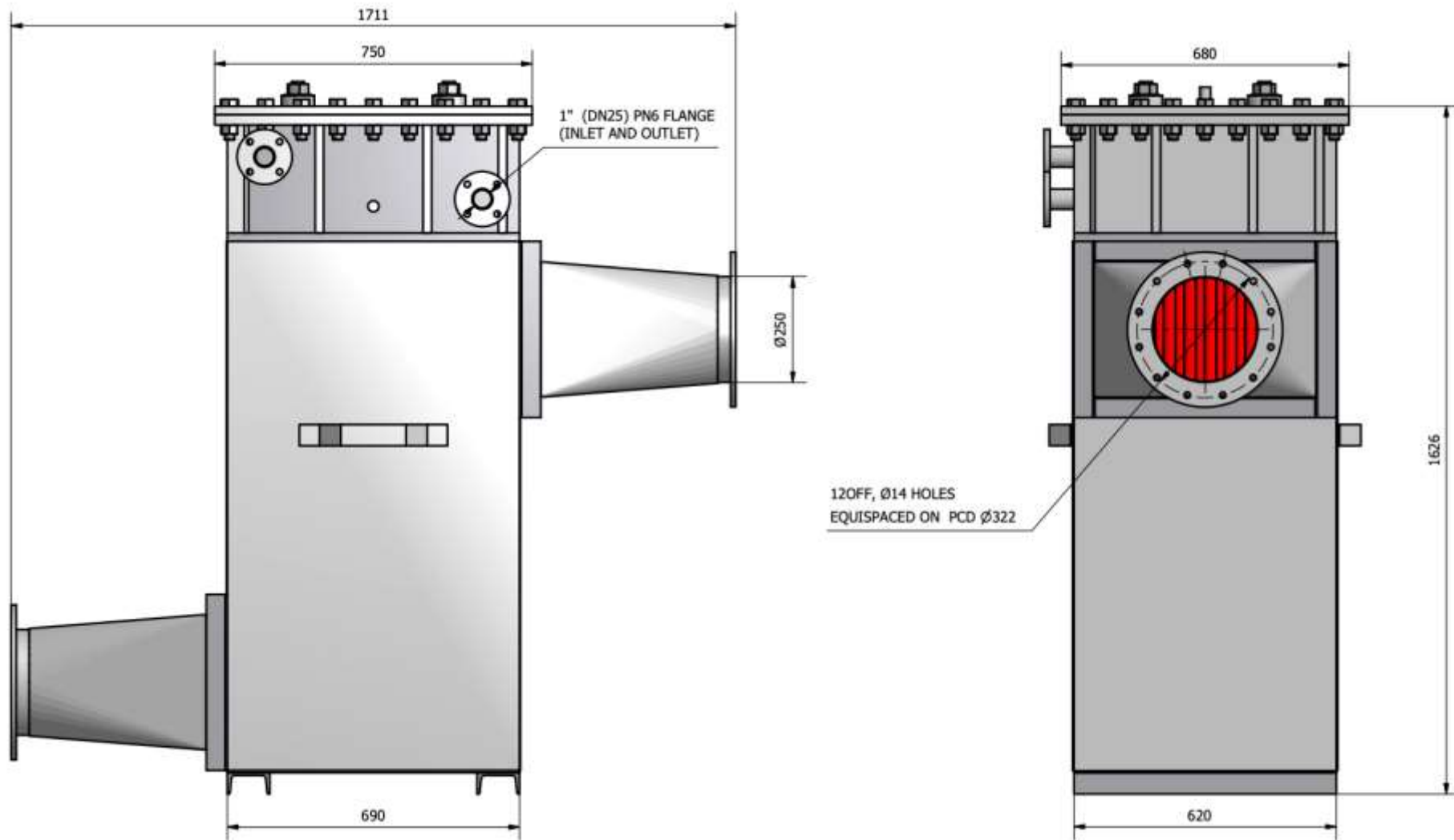


Figure 49: Experiment 1 HPHE side elevations with external dimensions and flange detail.

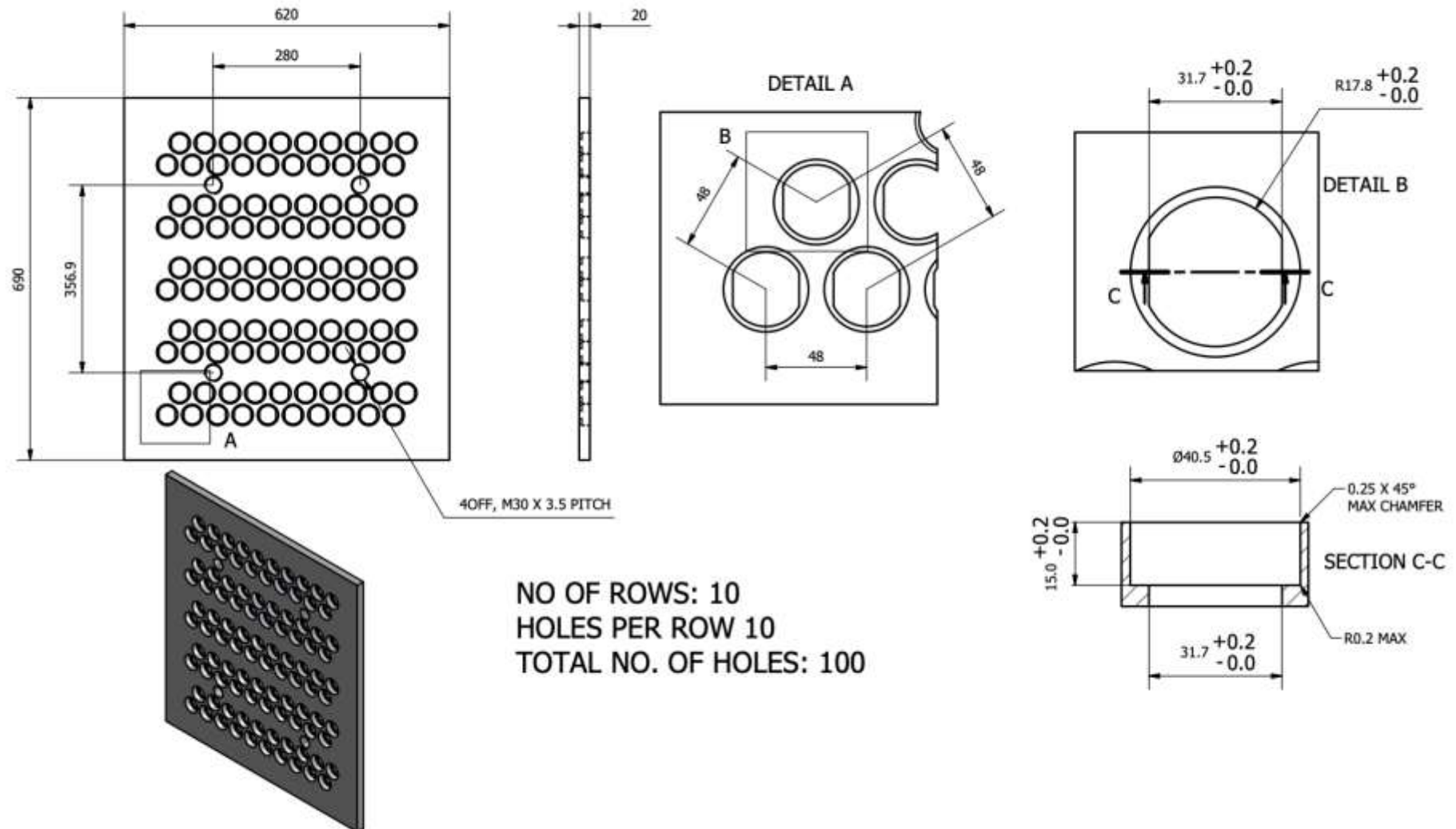


Figure 50: Experiment 1 detail of separation plate and thermosyphon spacing.

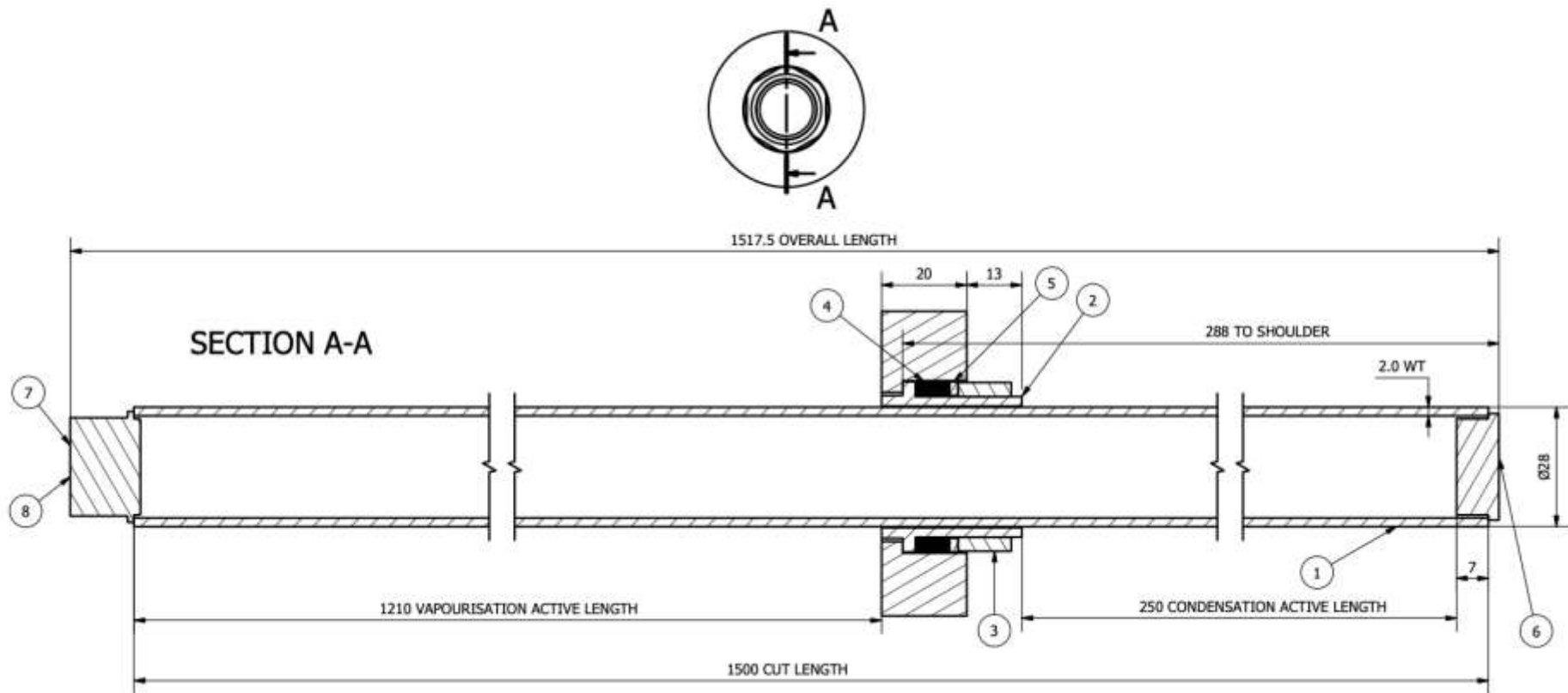


Figure 51: Experiment 1 thermosyphon detail.

4.2.2. Experimental Apparatus and Instrumentation

Figure 52 provides a P&ID (pipework and instrumentation diagram) of the experimental system. The red lines highlight the exhaust gases paths and the blue lines the water. The exhaust gases from the burners in the kiln are drawn through the evaporator section of the HPHE by a high temperature extraction fan. The mass flow rate is determined by the fan speed set by inverter driven frequency changes. These gases, once passed through the unit, are returned to the main exhaust stack. The water is pumped through the condenser section and a manual valve could be operated to restrict flow accordingly.

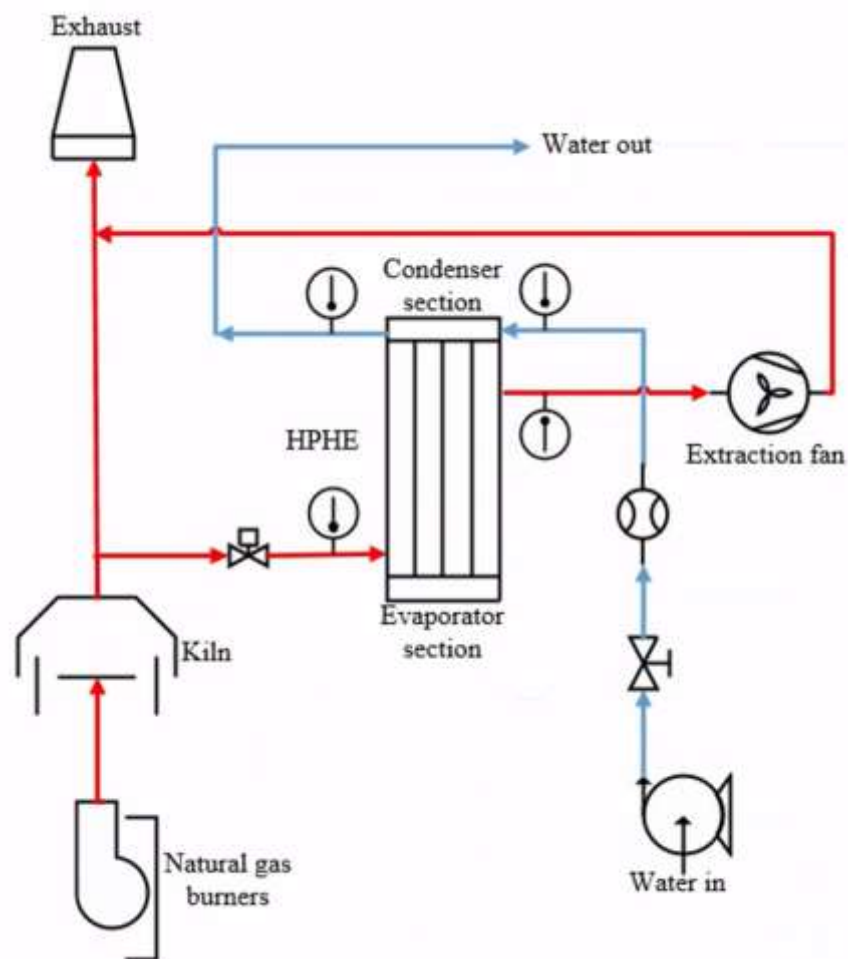


Figure 52: Experiment 1 P&ID of the installed system.

Figure 53 provides a photograph of the experimental set-up, including the kiln, HPHE, control panel, fan and heat transfer fluid entrance and exit locations.

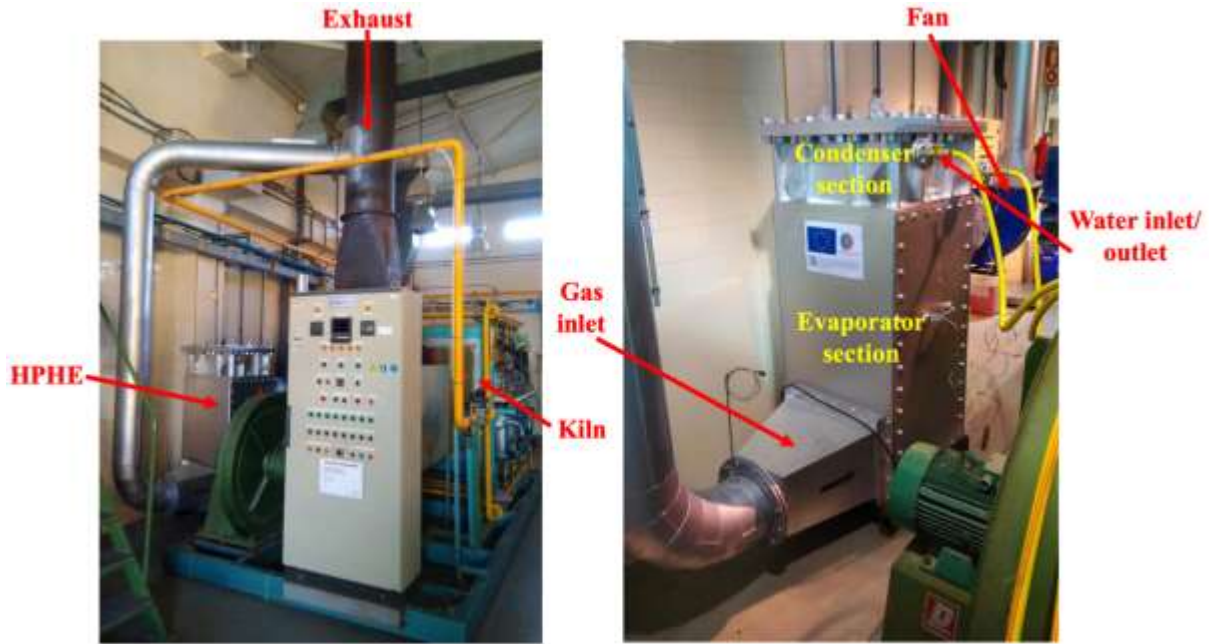


Figure 53: Experiment 1 labelled photographs of HPHE and location.

The instrumentation used in the experimental investigation consisted of thermocouples, thermistors, a rotameter and a pitot tube with manometer. Data was logged using an Omega data logger (model OM-DAQXL). Table 19 provides detail on the sensors used to measure the parameters, their location and uncertainty. Thermocouples were also present after each pass in the evaporator but these data were not required to validate the presented model.

Table 19: Experiment 1 parameters, sensors and installation location.

Parameter	Sensor	Location	Uncertainty
Temperature of exhaust gases	Thermocouple type K	Evaporator Inlet	$\pm (0.15\% \text{ Rdg} + 1.1^\circ\text{C})$
		Evaporator Outlet	
Volume flow rate of exhaust gases	Pitot tube type L and manometer	Evaporator Inlet	$\pm 5\%$
Temperature of the water	PT100 platinum thermistor probes, 4 wires	Condenser Inlet	$\pm 1^\circ\text{C}$
		Condenser Outlet	
Volume flow rate of water	Rotameter	Condenser Inlet	$\pm 2\%$

4.2.3. Test Conditions

Multiple conditions were tested in Experiment 1 by varying the set point of the exhaust gases temperature, the water flow rate to the condenser and the mass flow rate of exhaust gases. Table 20 provides the experimental conditions tested, in terms of exhaust temperature, water flow rate and the exhaust mass flow rate dictated by the fan speed.

Table 20: Experiment 1 test conditions.

Test	Exhaust Temperature Aim, °C	Water Flow Rate, kg.hr⁻¹	Fan Speeds, Hz
1	135	480	25, 30, 35, 40, 45, 50
2	230	480	25, 30, 35, 40, 45, 50
3	230	1,320	25, 35, 50
4	265	480	25, 30, 35, 40, 45
5	265	1,320	25, 35, 45, 50
6	140	480	25, 35, 45, 50
7	140	1,320	25, 35, 45, 50
8	225	480	25, 35, 45, 50
9	225	1,320	35, 45, 50

The kiln was started using the control panel with the exhaust being directed straight to the exhaust stack. The set point on the control panel was used to modulate the temperature and number of burners firing. The water mass flow rate for each test was achieved and the data-logger was then turned on. The exhaust was gradually introduced through the HPHE to initiate operation. Once the HPHE was operational, each experimental condition was aimed for until a steady state was achieved. The next experimental condition was then reached by altering the mass flow rate of the exhaust. The pitot tube and manometer were used discontinuously at each test point to ascertain the mass flow rates of the exhaust. Sometimes the tests were done in an ascending manner and sometimes descending. Certain sets of tests could not be completed on the same day so data were required to be spliced for the relevant conditions. The inlet water temperature could not be controlled but this remained very stable.

4.3. Experiment 2: Full-Scale Ceramic Continuous Roller Kiln

4.3.1. Description of the Testing Facility

A second HPHE unit has been installed at a ceramic production facility, based in Italy. The factory produces ceramic products, which require firing to reach their desired properties. The waste heat source is from an EKO continuous roller hearth kiln (Figure 54), which uses naturally aspirated burners along the length. Within the kiln there are various heating, firing and cooling stages with varying conditions and temperature profiles. The HPHE is located on a platform adjacent to the cooling exhaust stack of the kiln and a photograph of the unit is provided in Figure 55.

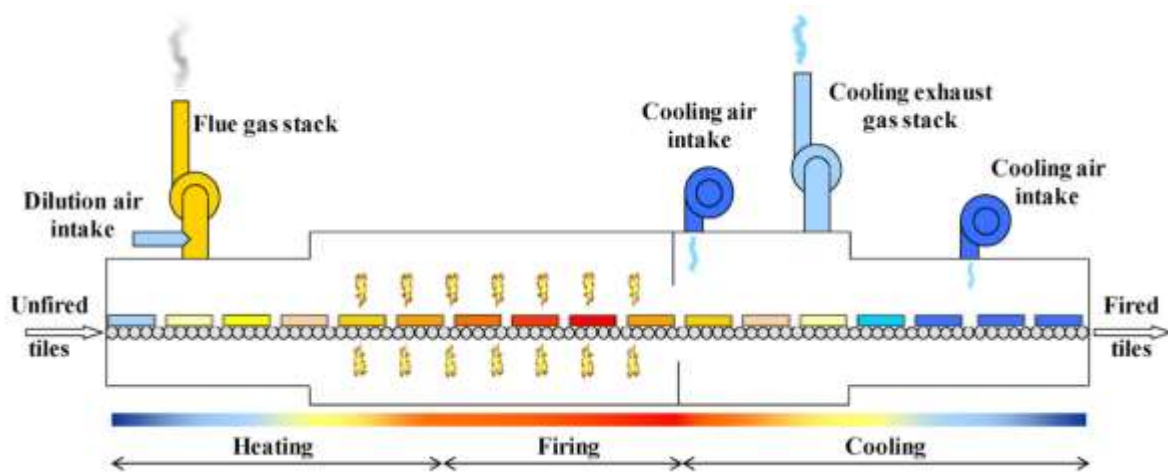


Figure 54: Diagram of a continuous roller kiln [2].



Figure 55: Experiment 2 installed HPHE photograph.

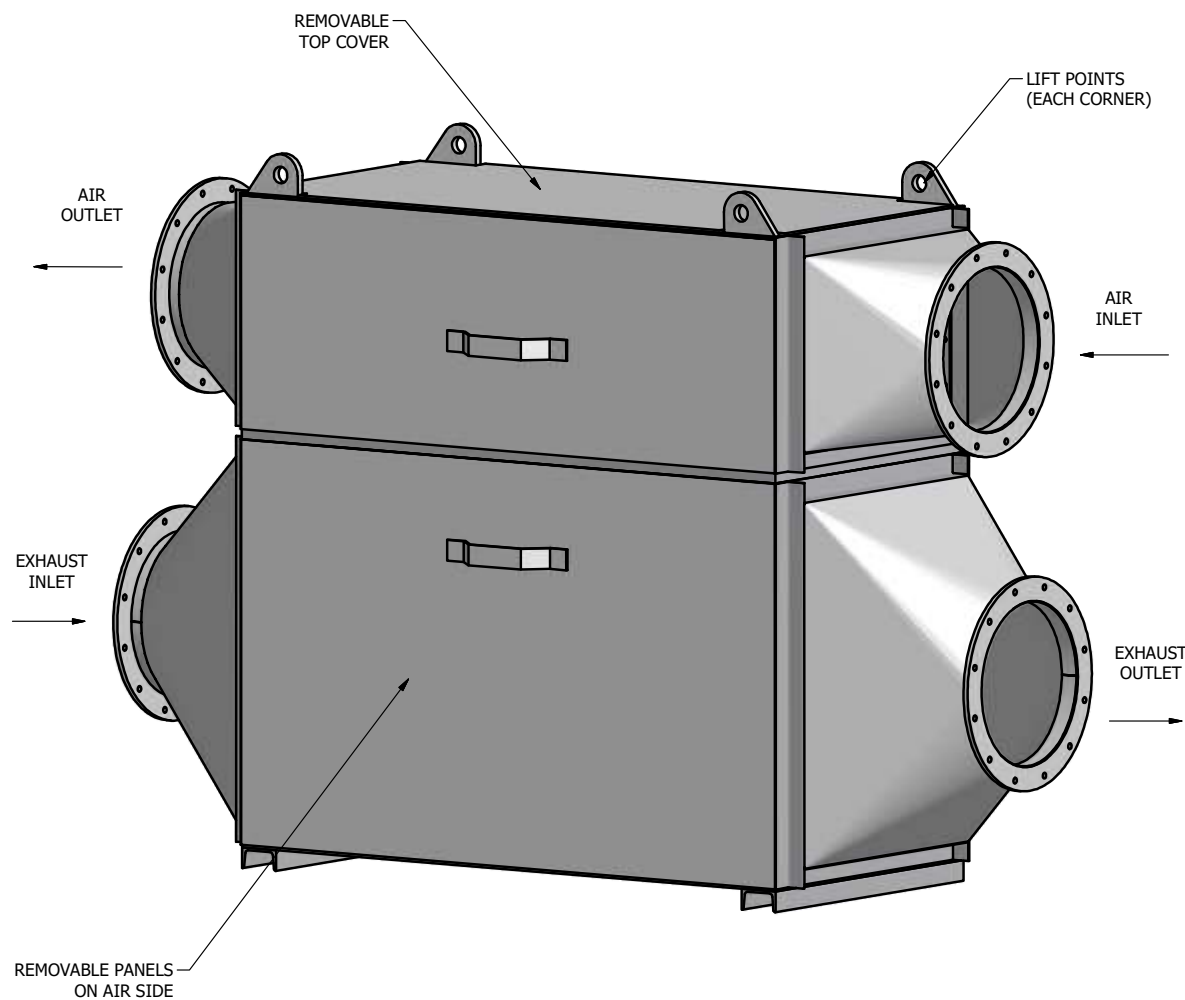
4.3.2. HPHE Design

The general arrangement, design parameters and external dimensions of the HPHE are shown in Figure 56 and Figure 57. The casing is constructed out of carbon steel and the flange detail for connecting both the heat source and sink to the evaporator and condenser is given. The unit was approximately 2.5 m long and 1.6 m high.

Figure 58 provides the detail on the separation plate between the evaporator and condenser sections and also the spacing of the thermosyphons, which are spaced in a 9 by 18 staggered equilateral arrangement. The arrangement is shown by Detail A.

Figure 59 shows the design of the 162 thermosyphons, which is identical across the entire bank. The thermosyphon casing is SA179, seamless drawn, low carbon steel. They are 1,500 mm in

total length with an outer diameter of 38 mm. The active evaporator section is 919 mm and the active condenser section 495 mm in length, with the internal working fluid being distilled water. Helical carbon steel fins are present on both the evaporator and condenser sections. The fins are 10 mm in height, 1 mm thick with a pitch of 4 mm.



DESIGN PARAMETERS:

1. AIR MASS FLOW RATE = 6,000 Kg/h.
2. AIR MASS FLOW RATE = 2,640 Kg/h.
3. AIR AVERAGE SPECIFIC HEAT CAPACITY = 0.241 Kcal/Kg°C
4. AIR AVERAGE SPECIFIC HEAT CAPACITY = 0.241 Kcal/Kg°C
5. AIR INLET TEMPERATURE = 204 °C
6. AIR OUTLET TEMPERATURE = 145 °C
7. AIR INLET TEMPERATURE = 30 °C
8. AIR OUTLET TEMPERATURE = 164 °C
9. RECOVERED HEAT = 99,299W

NOTES:

1. EXPANSION JOINTS MUST BE USED TO ALLOW FOR THERMAL EXPANSION.
2. UNIT ONLY TO OPERATE IN VERTICAL ORIENTATION AS SHOWN.
3. APPROXIMATE ASSEMBLY WEIGHT 1,800Kg.
4. MATERIAL OF CONSTRUCTION:
EXHAUST SIDE - CARBON STEEL.
AIRSIDE - CARBON STEEL.
5. PAINT SPECIFICATION = HIGH TEMPERATURE BLACK PRIMAR,
FIREWOOD 75 HIGH TEMPERATURE ALUMINIUM PAINT.

Figure 56: Experiment 2 general arrangement of the HPHE and design parameters.

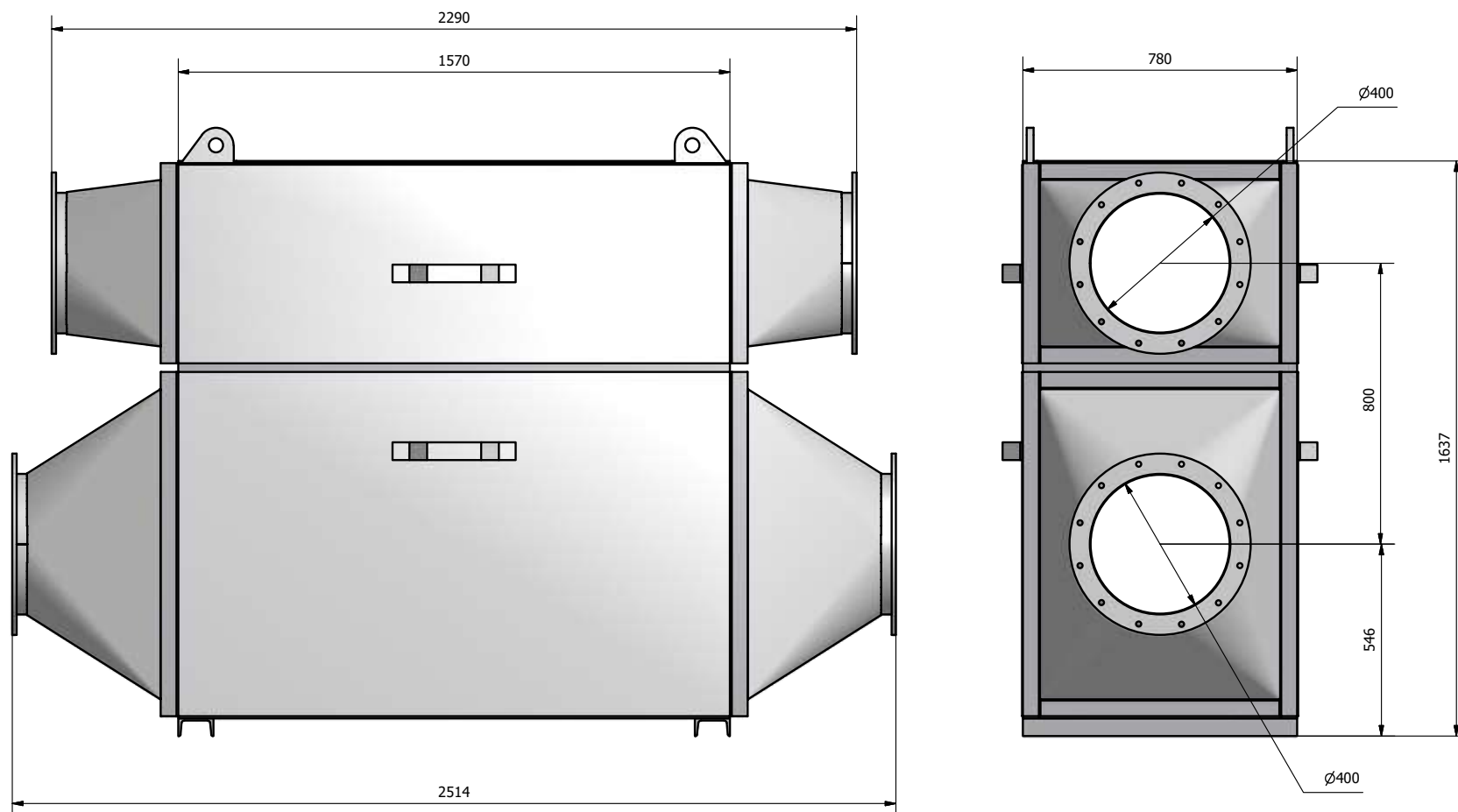


Figure 57: Experiment 2 HPHE dimensions and side elevations.

NO OF ROWS: 18
 HOLES PER ROW 9
 TOTAL NO. OF HOLES: 162

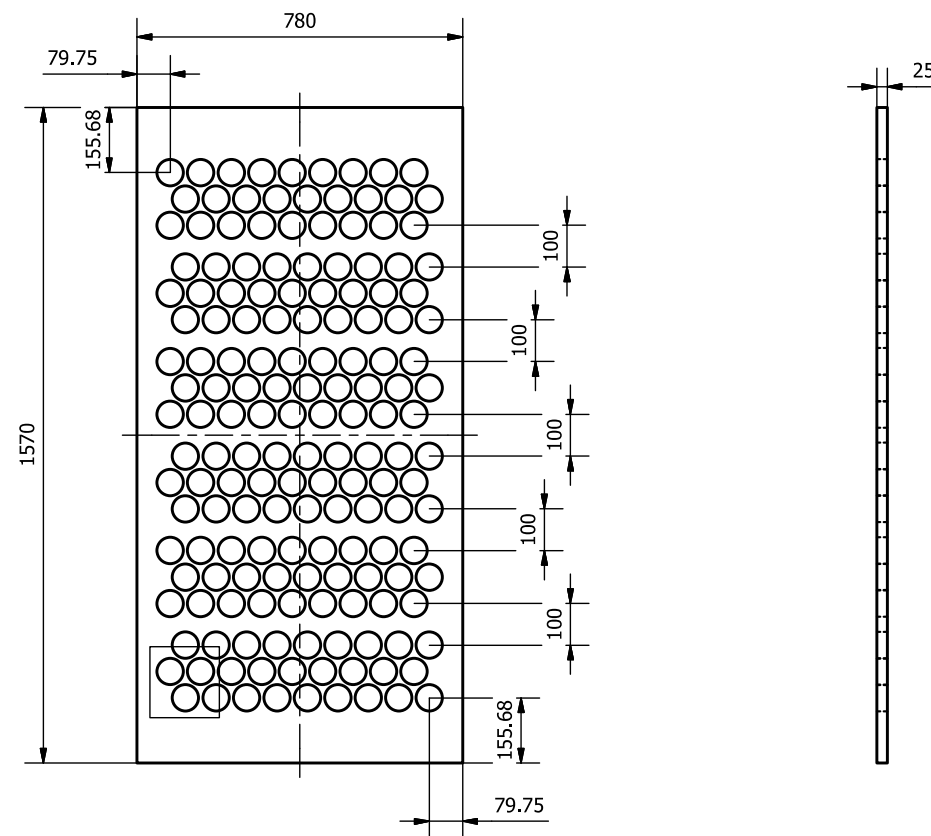
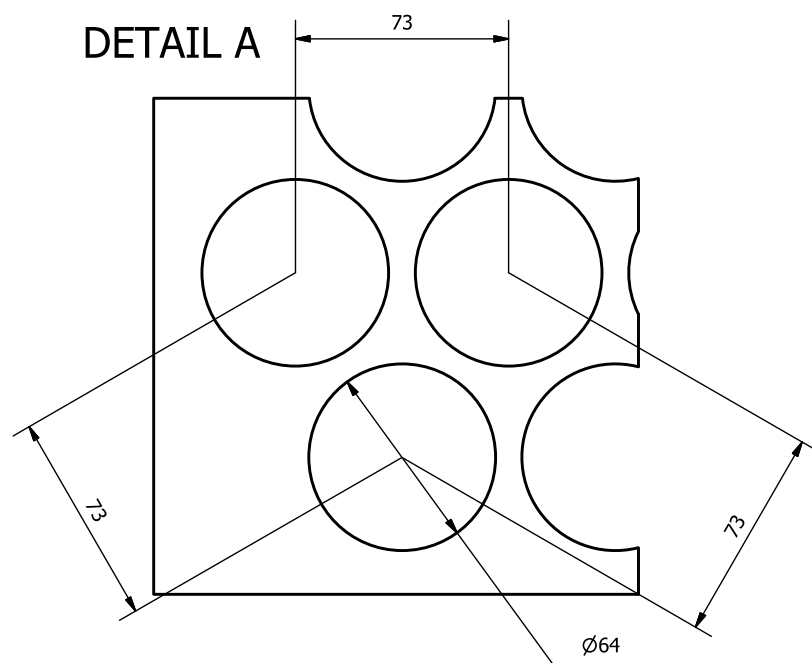


Figure 58: Experiment 2 detail of separation plate and thermosyphon arrangement.

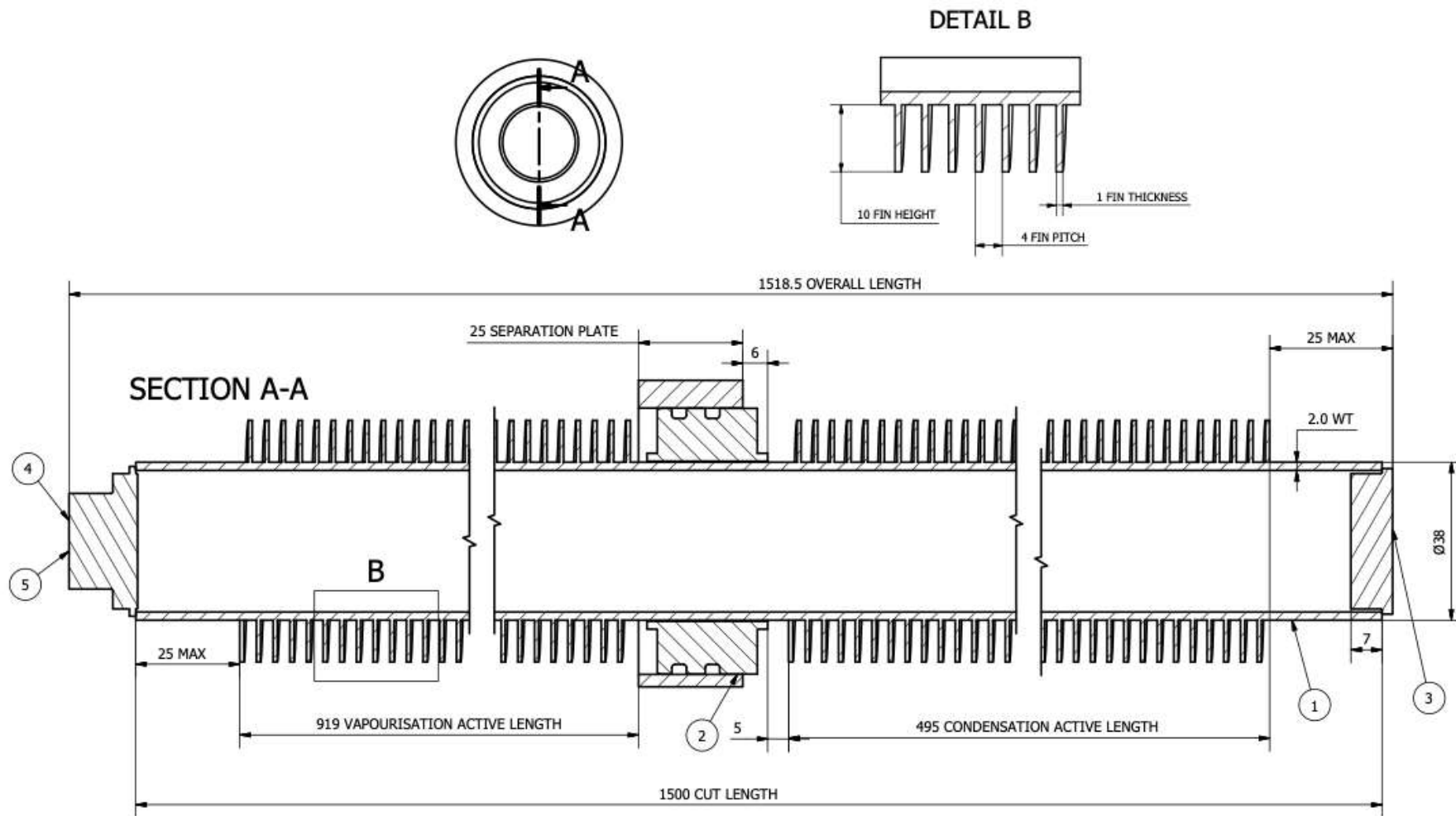


Figure 59: Experiment 2 detail of thermosyphon and finning.

4.3.3. Experimental Apparatus and Instrumentation

Figure 60 provides a P&ID of the experimental system. The exhaust gases from the burners in the kiln are pushed through the evaporator section of the HPHE by a high temperature extraction fan. The mass flow rate is determined by the fan speed set by inverter driven frequency changes. Air is pulled through the condenser section by a fan and the heated air is sent to dryers. The flow rates of the both the condenser and evaporator sections are dictated by the two fans maintaining a steady outlet temperature for the condenser. This was done to provide a steady temperature to the dryers but also to protect the thermosyphons from overheating.

Valves are present within the system to isolate the HPHE from the rest of the system if there is an issue or maintenance is required. Pressure sensors are located across the evaporator section and there are thermocouples at the inlet and outlet of each section.

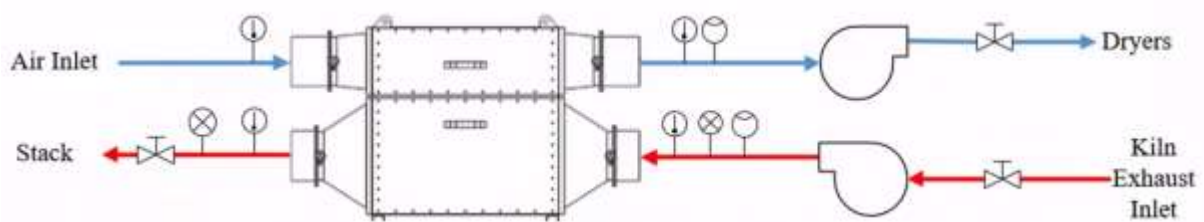


Figure 60: Experiment 2 P&ID of the installed system.

Temperature and pressure data were collected using a data-logger, which was a National Instruments (Model NI PXIe-4353). The additional uncertainty for temperature was $0.05\% \pm 0.38^\circ\text{C}$. Table 21 provides detail on the sensors used to measure the parameters, their location and uncertainty values.

Table 21: Experiment 2 parameters, sensors and installation location.

Parameter	Sensor	Location	Uncertainty
Temperature of exhaust gases	Thermocouple type K	Evaporator Inlet	$\pm (0.15\% \text{ Rdg} + 1.1^\circ\text{C})$
		Evaporator Outlet	
Temperature of air	Thermocouple type K	Condenser Inlet	
		Condenser Outlet	
Volume flow rate of exhaust gases	Pitot tube type L and manometer	Evaporator Inlet	$\pm 5\%$
Volume flow rate of air	Pitot tube type L and manometer	Condenser Outlet	$\pm 5\%$
Exhaust gases pressure	Omega PZ1009	Evaporator Inlet	$\pm 0.25\%$
		Evaporator Outlet	

As this system was installed at a functioning production facility, after commissioning, only working condition data were available for modelling purposes. The production runs as a continuous process but, beneficially, fluctuations in the input conditions are seen.

4.4. Experiment 3: Full-Scale Aluminium Heat Treatment Furnace

4.4.1. Description of the Testing Facility

The aluminium facility takes and melts or manufactures aluminium alloys and die casts them into components, primarily for the automotive industry. These components then require thermally treating to reach their desired properties. This is achieved using a solution heat treatment furnace where exhaust gases were used as the waste heat source. The furnace burners are fired by natural gas and naturally aspirated. The exhaust gases of the heat treatment furnace exited at an average temperature of 450°C but the gases were diluted, giving a temperature of 400°C prior to the HPHE, using a butterfly valve with a servomotor linked to the temperature reading.

The heat sink is air which is fed into an ageing furnace after heating in the condenser section to reduce the required primary energy consumption of the burners located in this furnace.

4.4.2. HPHE Design

A photograph of the counterflow exhaust-to-air HPHE, installed to recover waste heat from the exhaust gases of an aluminium heat treatment furnace, is shown in Figure 61. Figure 62 shows the finned thermosyphons with the inspection doors opened.



Figure 61: Experiment 3 photograph of HPHE during installation.

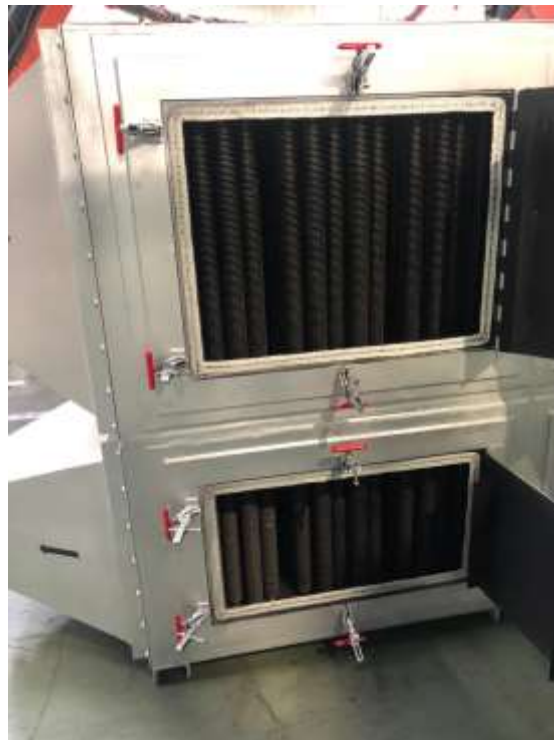


Figure 62: Experiment 3 photograph of finned thermosyphons in condenser and evaporator sections.

Figure 63 and Figure 64 provide a 3D general arrangement of the unit with the design parameters and external dimensions. The core of the heat exchanger was 2.15 m long and 1.6m high.

Figure 65 and Figure 66 provide detail on the separation plate between the evaporator and condenser sections and, also, the spacing of the thermosyphons. The HPHE is equipped with 310 thermosyphons of two different designs in a 10 by 31 staggered arrangement. Two designs of thermosyphons were chosen for this HPHE to maximise heat recovery. This was achieved by selecting a more optimum thermosyphon design as the fluids pass through the unit and the exhaust gases cool and the air heats. Considering the evaporator, the first 18 rows are SA179, low carbon steel seamless drawn, thermosyphons with Dowtherm A as the working fluid (Figure 67). The final 13 rows are stainless steel 304 with distilled water as the working fluid (Figure 68). Both sets of thermosyphons are 1,518 mm in length with a 28 mm outer diameter. The active evaporator section of the thermosyphons is 590 mm in length, the active condenser section 800 mm in length. Helical carbon steel fins are present on both the evaporator and condenser sections. For the Dowtherm thermosyphons, the fins are 10 mm in height, 1 mm thick with a pitch of 4 mm. For the distilled water the fins are 10 mm in height, 1 mm thick with a pitch of 6 mm.

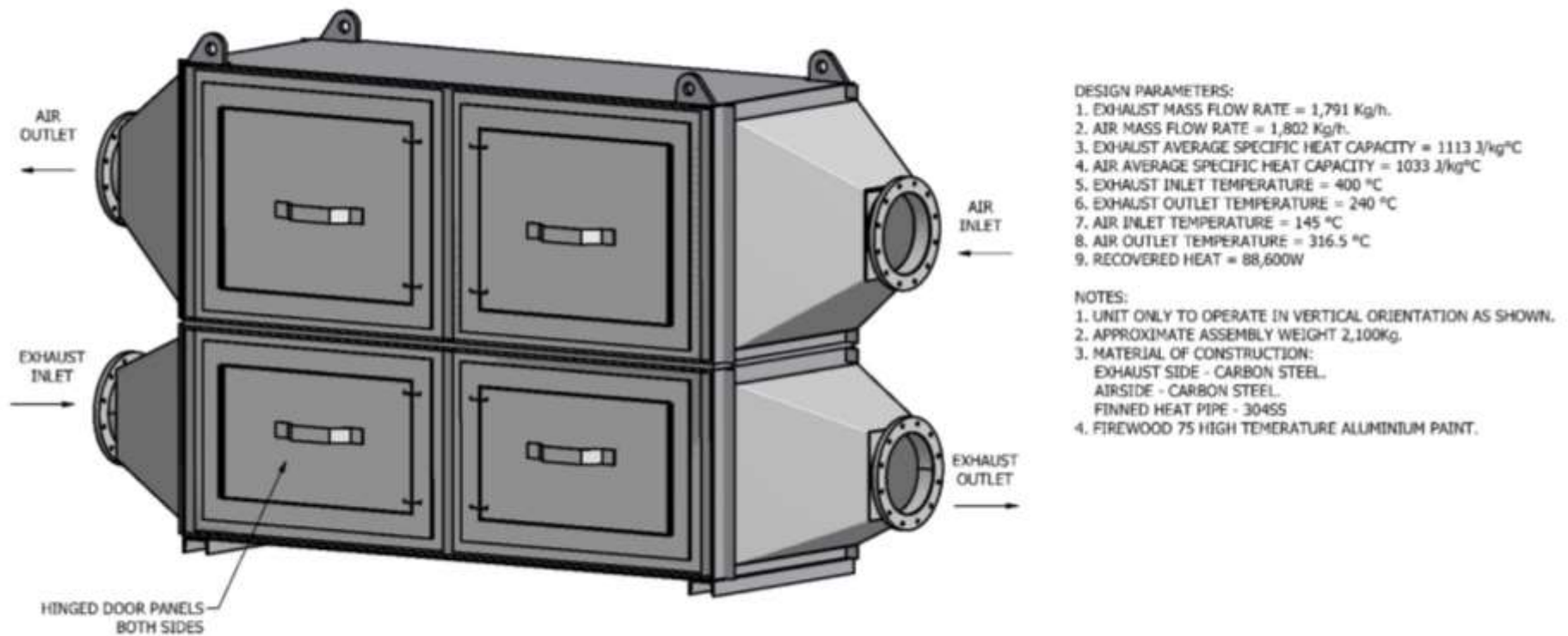


Figure 63: Experiment 3 HPHE general arrangement and design parameters.

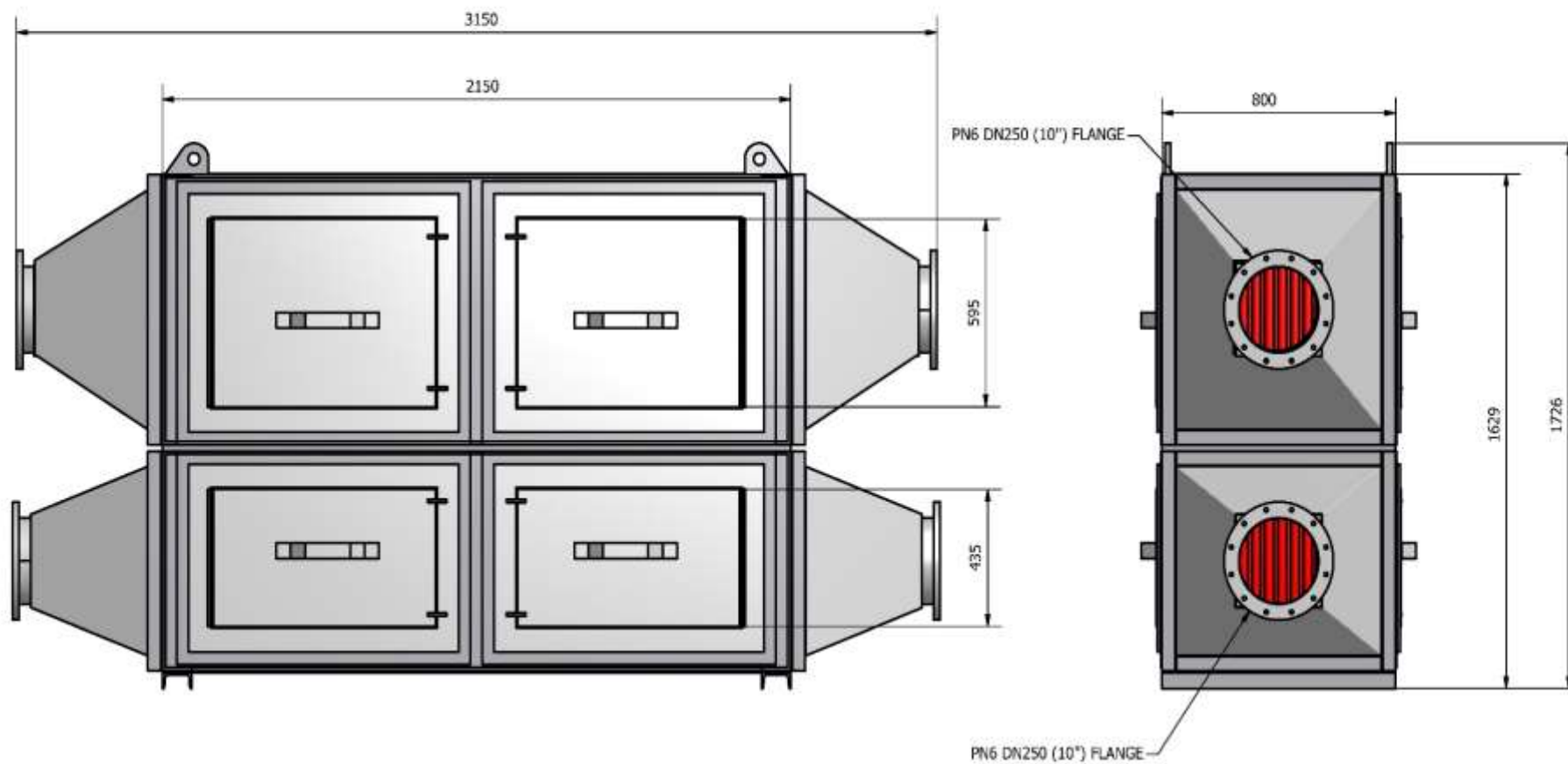
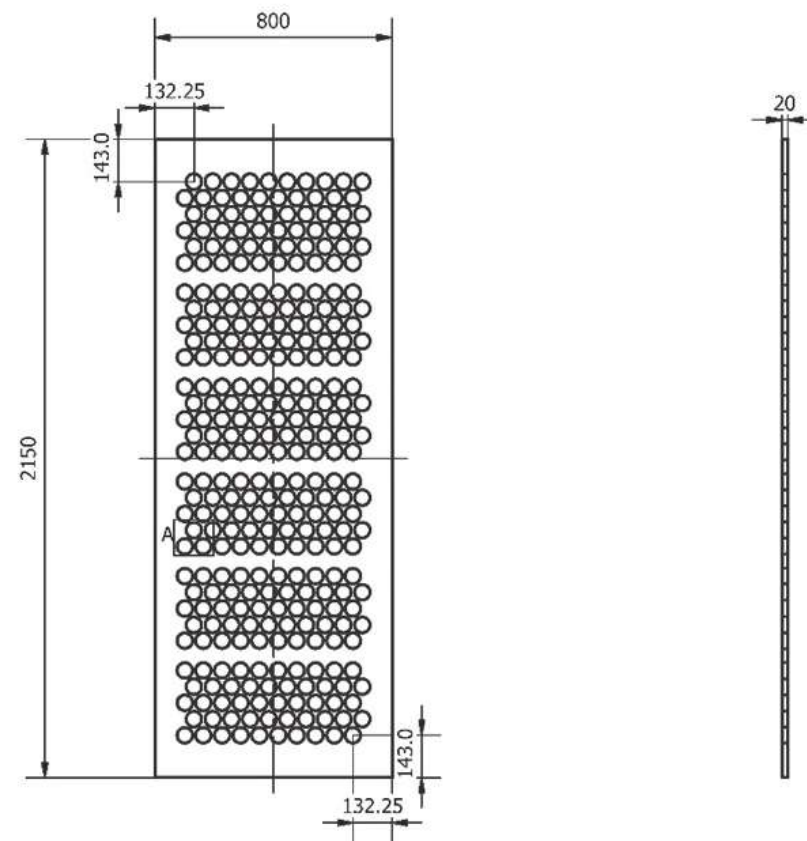
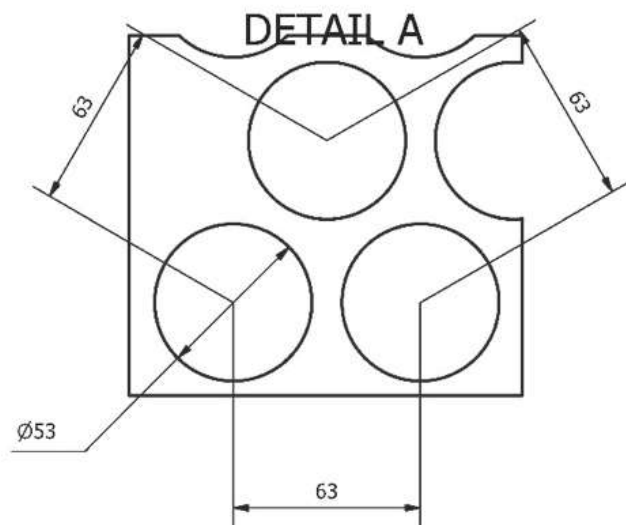
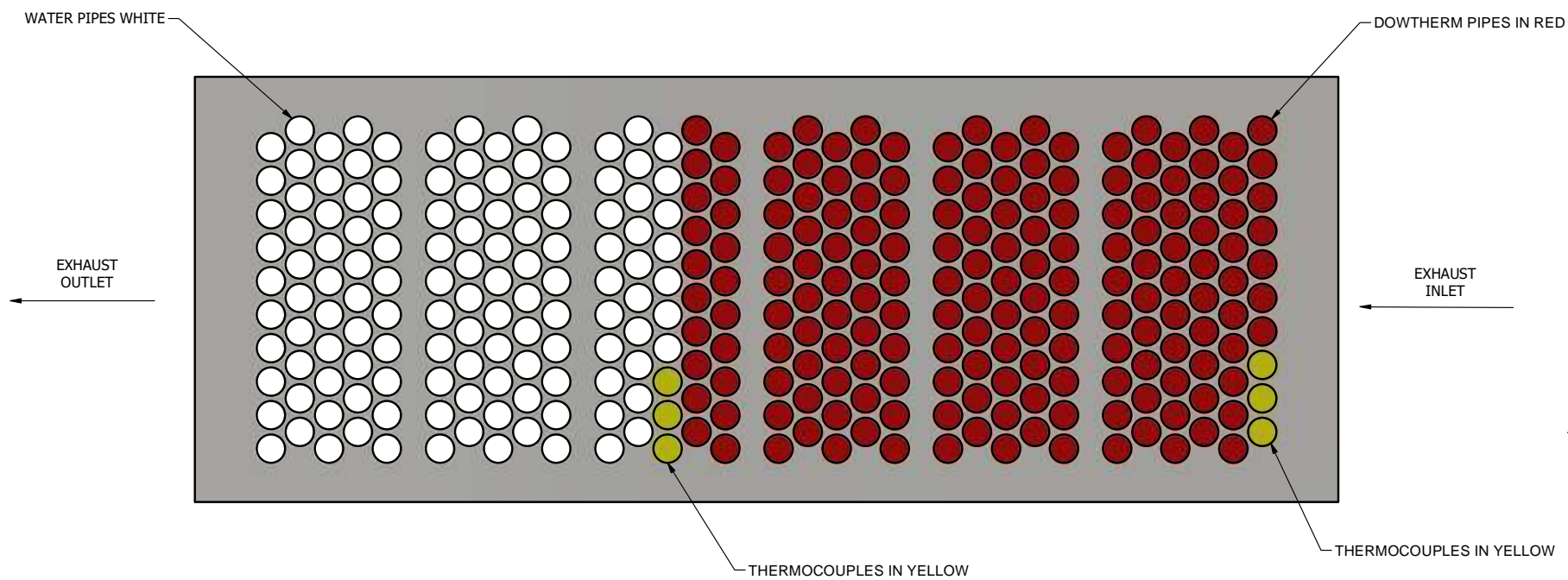


Figure 64: Experiment 3 HPHE dimensions and side elevations.



NO OF ROWS: 31
 HOLES PER ROW 10
 TOTAL NO. OF HOLES: 310

Figure 65: Experiment 3 detail of separation plate and spacing.



NO OF ROWS: 31
 HOLES PER ROW 10
 TOTAL NO. OF HOLES: 310

Figure 66: Experiment 3 detail of separation plate and thermosyphon type location.

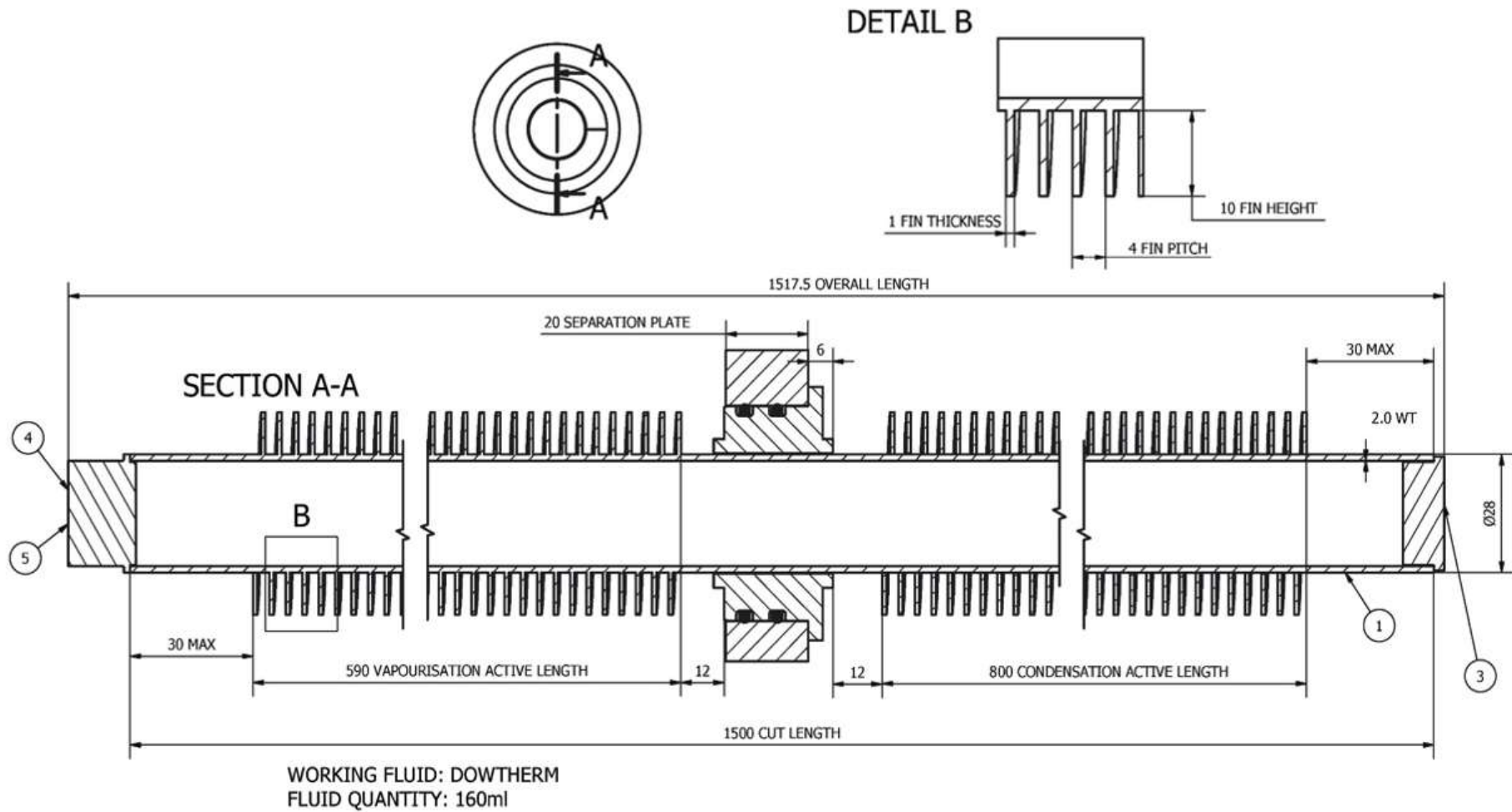


Figure 67: Experiment 3 detail of Dowtherm A thermosyphon.

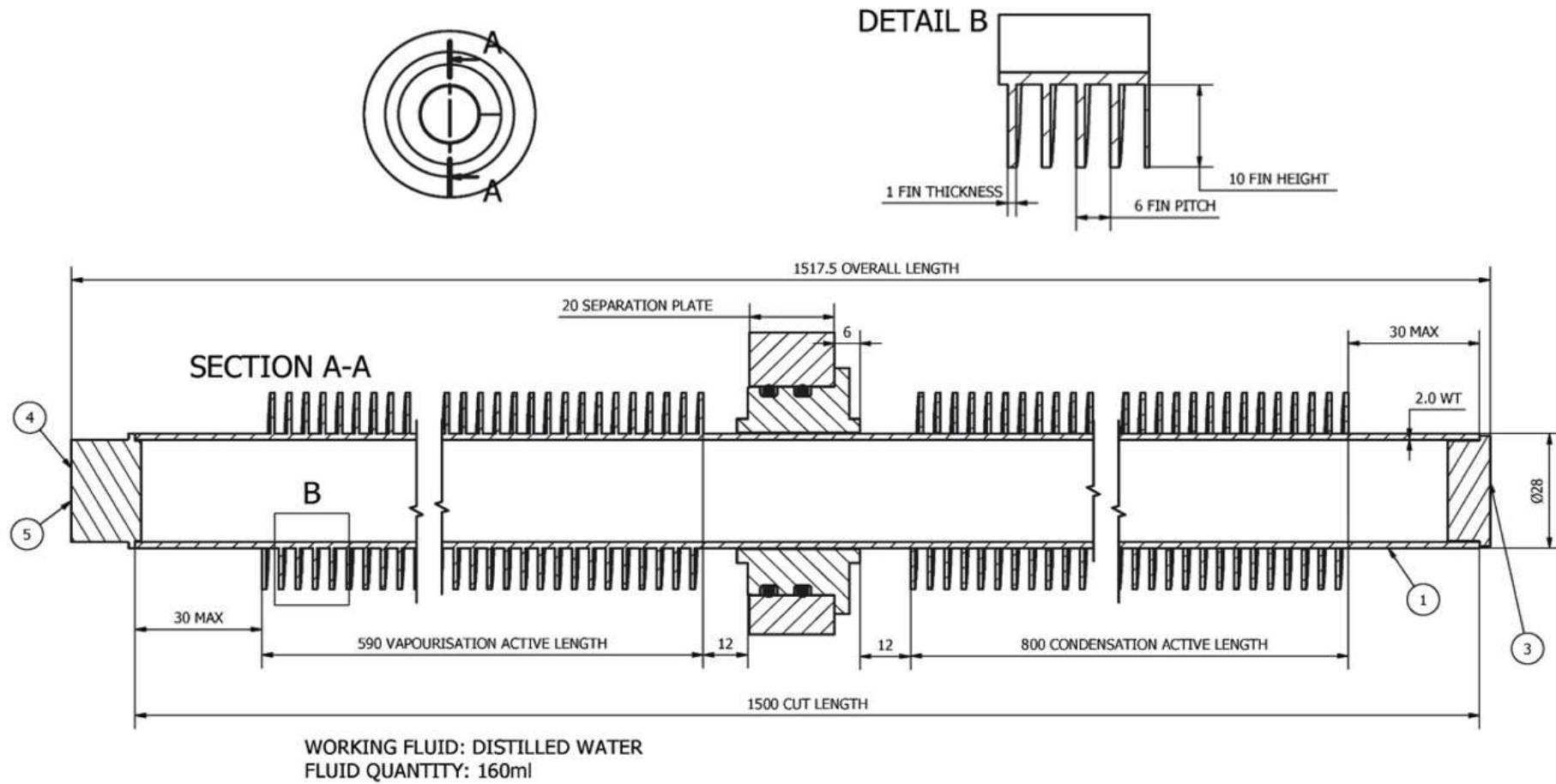


Figure 68: Experiment 3 detail of distilled water thermosyphon.

4.4.3. Experimental Apparatus and Instrumentation

Figure 69 shows a 3D schematic of the installation. The exhaust gases exit the kiln, by being drawn by a centrifugal fan. They can either bypass or enter the evaporator section of the HPHE. The air of the ageing furnace is drawn through the condenser section by an identical fan and returned to it.

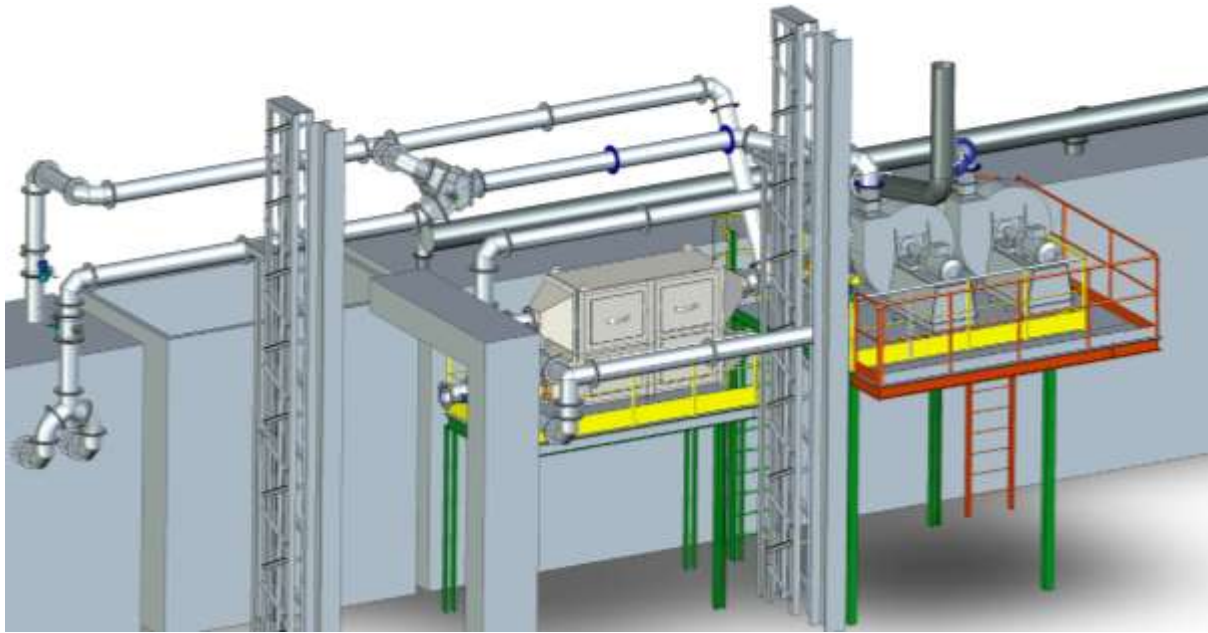


Figure 69: Experiment 3 3D of installation [214].

Figure 70 shows the path of the exhaust and air against the P&ID, whilst the HPHE is operational. Figure 71 provides a P&ID of the entire system.

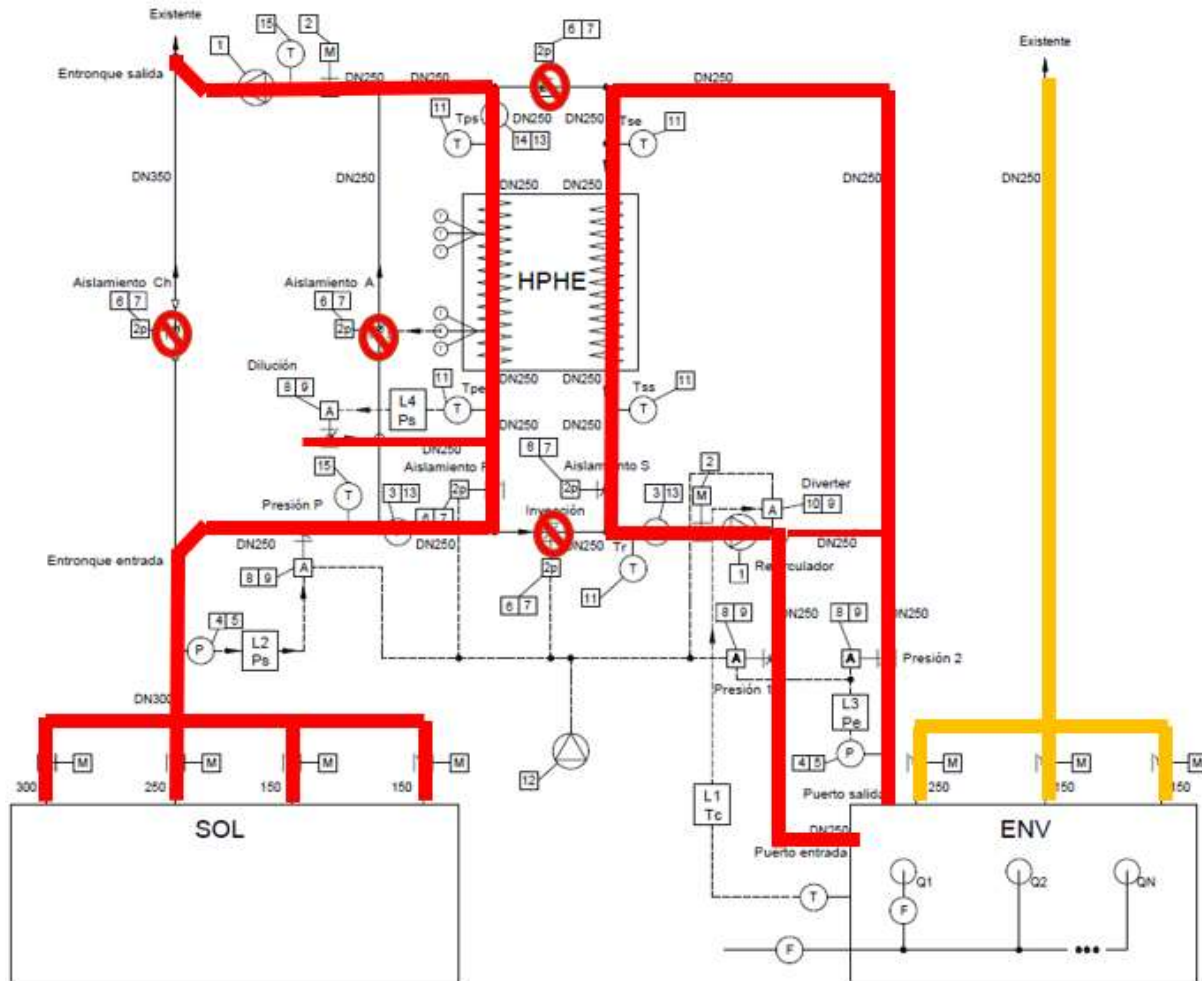


Figure 70: Schematic of heat paths during HPHE operation. SOL being the solution furnace and ENV the ageing furnace [214].

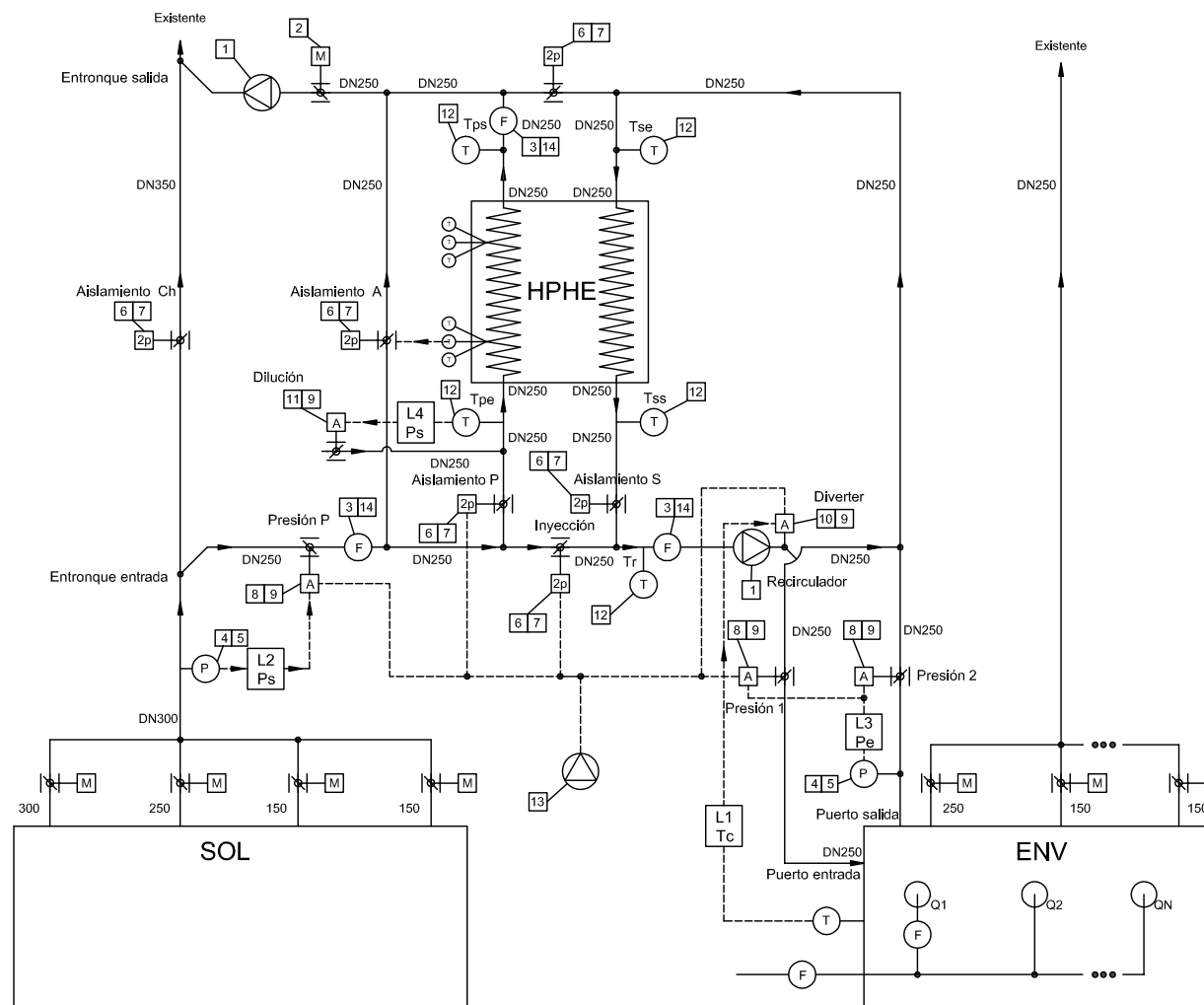


Figure 71: Experiment 3 P&ID of system installation [214].

Table 22 provides the key instrumentation that was used to collect data for the model validation. A larger variety of instrumentation was installed but the additional instruments are superfluous to requirements here. The company had a data-logging system where all measurements were recorded. Again, as the company was a production facility, data were collected from working conditions.

Table 22: Instrumentation used for Experiment 3.

Parameter	Sensor	Location	Uncertainty
Temperature of exhaust gases	J Type thermocouple, 12x500 mm	Evaporator Inlet	Greater of: $\pm 0.75\%$ Rdg or $+2.2^{\circ}\text{C}$
		Evaporator Outlet	
Temperature of the air	J Type thermocouple, 12x500 mm	Condenser Inlet	
		Condenser Outlet	
Mass flow rate of exhaust gases	Kurz 454FTB-08-HHT (-40-500°C)	Evaporator Inlet and Outlet	$\pm (3\% \text{ Rdg} + 30 \text{ SFPM})$
Mass flow rate of air	Kurz 454FTB-08-HHT (-40-500°C)	Condenser Outlet	$\pm (2\% \text{ Rdg} + 20 \text{ SFPM})$
Exhaust gases pressure	Yokogawa EJA120E-JES4J-914ED 4-20 mA, $\pm 1 \text{ mBar}$	Evaporator Inlet	$\pm 0.25\%$
		Evaporator Outlet	

5. SIMULATION STUDIES

A desktop simulation has been conducted with the personally developed transient HPHE model and results have then been compared to experimental data. Chapter 3 presents the theory used, and the current Chapter provides information on how the model was developed in TRNSYS. This section has been added to provide a greater understanding to the scientific community of how the process can be achieved. Previous versions of code and the process have been detailed by the author in [3], and the paper has been used to develop the present Chapter, with the most up to date code provided here. The complete code is provided in Appendix B.

The software TRNSYS (TRaNsient System Simulation) v17 was used to create a transient simulation with varying inputs and parameters. This simulation engine was developed by members of the Solar Energy Laboratory at the College of Engineering within the University of Wisconsin. The software is used to study thermal systems and has latterly been employed to study waste heat recovery. It is installed with a library of over 150 components. These components are used to model a transient system, which allows the user to evaluate and analyse chosen inputs and parameters and view results. An interface called ‘Simulation Studio’ is used where the system is graphically modelled using the library of components, which are known as ‘Types’. These Types are internally composed of a series of mathematical equations where inputs and parameters are converted to output values. The values and units of the inputs and parameters can be altered to provide a graphical view of the system’s functionality over a set period of time. A parameter is fixed throughout the entire simulation, but an input can be fixed or changed in each iteration step over the simulation. A transient nature can be achieved by linking an external file (.txt/.csv) as the input or linking the output of another component as the input for another, for example, data-logged real temperature profiles from a furnace or weather temperature data from cities around the world can be used.

The standard TRNSYS library with the location of the newly created HPHE Type is shown in Figure 72. The counterflow HPHE shown is a previous iteration of the code which is solely used for a counterflow HPHE. The crossflow HPHE is more versatile and can predict counterflow, crossflow and multipass HPHEs, depending on the inputs. The component needs a ‘skeleton’ where the user can change inputs and parameters, which is also the icon that can be visualised in simulation studio. It contains the internal mathematical operation, which takes

the inputs and calculates the outputs. The code provides the mathematical operation and the skeleton provides the user interface. The development of each is explained in the sections below.

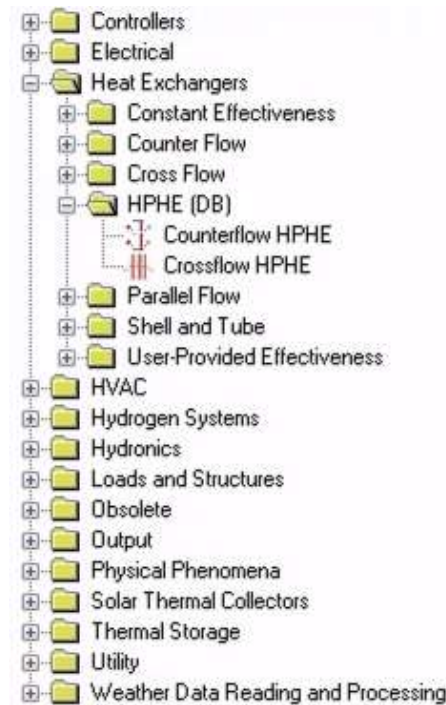


Figure 72: A view of the standard TRNSYS component library and the location of the newly developed HPHE components.

5.1. Process for Coding HPHE Component

The process for coding and including a new component in the TRNSYS library is not straightforward; it requires the use of multiple software and is coded in Fortran (FORmula TRANslation). TRNSYS was written in this language and, as such, it is required to code a Type in this language and then compile it. The Fortran language was developed by the International Business Machines (IBM) Corporation in the 1950s for the purpose of numerical computation and scientific computing specifically for engineering and scientific purposes. The first manual was released in 1956 and the first compiler was released in 1957. The idea was to ease the process of inputting equations into computers. Fortran has many iterations and releases, specifically the Fortran 90 language was used to code the Type, developed in 1991. The process for creating a new component is described in the Programmer's guide (Volume 7) [1] provided within the software. However, not all of the sections or code are required so the process for

building the novel HPHE Type is described in this section. Figure 73 provides a flowchart diagram to explain the coding process.

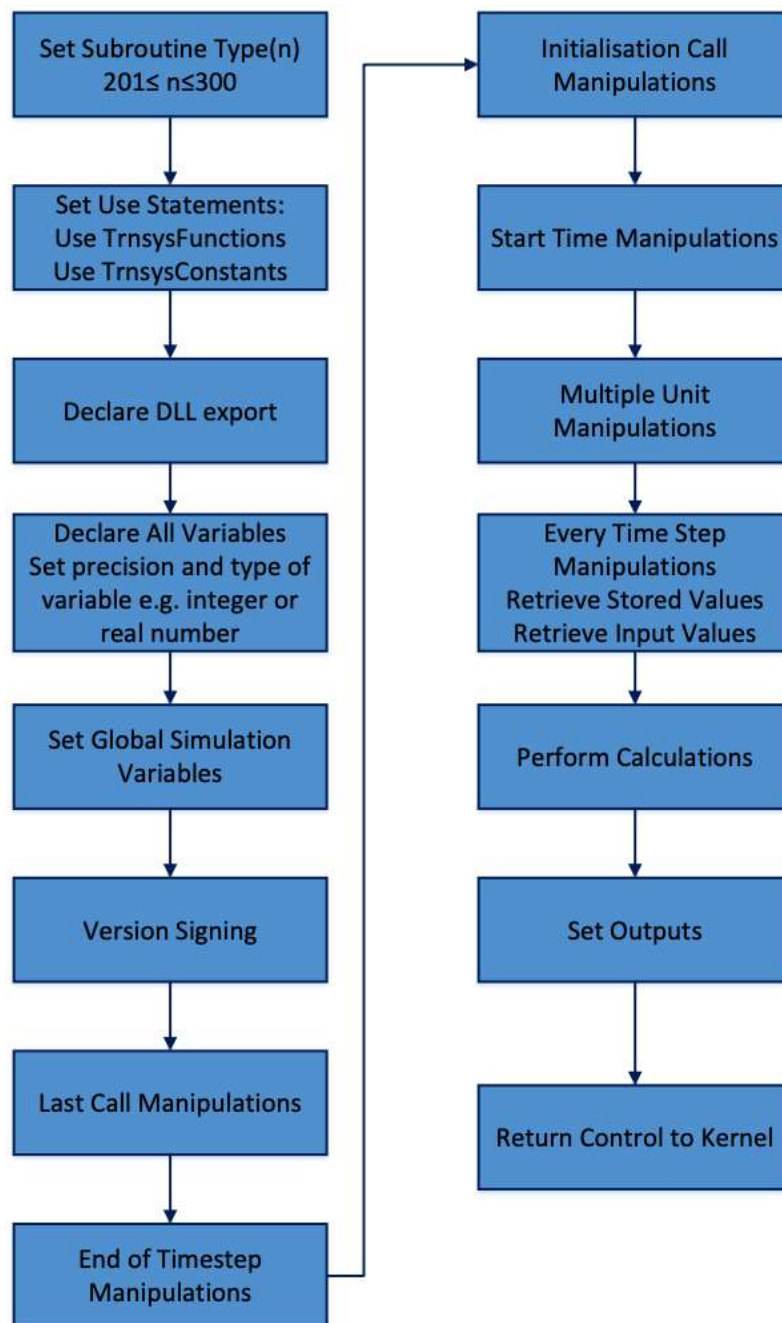


Figure 73: Flowchart of the TRNSYS component coding process.

To build a new model, TRNSYS v17 must be installed and a Fortran compiler capable of generating a 32-bit dynamic link library (DLL). Many compilers are available, but in this case Intel Parallel Studio XE 2019 with the additional Intel Visual Fortran package was used. Intel Visual Fortran is an add-on for Microsoft Visual Basic.



Figure 74: Icons of Parallel Studio XE 2019 and Visual Studio 2019.

The TRNSYS solution code is split into the kernel and the Types. The kernel provides all the background and functionality inputs to the Types. Types have the mathematical coding to perform calculations of the components used in the simulation as well as how to communicate with the kernel and call various other codes at given steps, in essence, converting inputs to outputs. Types distinguish between inputs that change with time and inputs that do not change with time. These are known as inputs and parameters, respectively. For the HPHE component, the following inputs were required, shown in Table 23.

Table 23: Inputs for HPHE TRNSYS component.

Input	Designated Symbol	Units
Source fluid inlet temperature	Thi	°C
Sink fluid inlet temperature	Tci	
Mass flow rate of evaporator fluid	FLWe	kg.s ⁻¹
Mass flow rate of condenser fluid	FLWc	

For the HPHE component, the following parameters were required, shown in Table 24.

Table 24: Parameters for HPHE TRNSYS component.

Parameter	Designated Symbol	Units
Number of evaporator longitudinal rows	Nre	Dimensionless
Number of condenser longitudinal rows	Nrc	
Outer diameter of heat pipes	Dout	m
Length of active evaporator section	Le	
Length of active condenser section	Lc	
Number of transverse evaporator thermosyphons in a row	Nte	Dimensionless
Distance between evaporator row transverse centres	STe	m
Distance between evaporator longitudinal centres	SLe	
Number of transverse condenser thermosyphons in a row	Ntc	Dimensionless
Distance between condenser heat centres in row	STc	m
Distance between condenser longitudinal centres	SLc	
Face area of evaporator	Ae	m ²
Face area of condenser	Ac	
Determining where finning is present	FinningMode	1-4
Determining heat sink fluid	Fluid Mode	1-3
Outer diameter of fins	Dofin	m
Thickness of fins	e _{fin}	
Pitch of fins	P _{fin}	
Height of fins	H _{fin}	
Pi, π	PI	Dimensionless

Within the Type, further internal calculations are carried out. Not all are required for every calculation, but the entirety are summarised in Table 25.

Table 25: Internal calculated values within HPHE component.

Value	Designated Symbol	Units
Area of condenser fins	Afc	m ²
Area of evaporator fins	Afe	
Heat capacity rate of condenser	Cc	J.K ⁻¹ .s ⁻¹
Heat capacity rate of condenser mean	Cc_m	
Heat capacity rate of condenser outlet	Cco	
Heat capacity rate of evaporator	Ce	
Heat capacity rate of evaporator mean	Ce_m	
Heat capacity rate of evaporator outlet	Ceo	
Correction factor condenser	CFc	
Correction factor evaporator	CFe	
Condenser correction factor Chi, X, for pressure drop	Chic	
Evaporator correction factor Chi, X, for pressure drop	Chie	
Smaller of Ce and CC	Cmin	J.K ⁻¹ .s ⁻¹
Smaller of Ce and CC mean	Cmin_m	
Smaller of Ce and CC outlet	Cmino	
Pressure drop condenser	dPc	Pa
Pressure drop evaporator	dPe	
Difference between Q1c and Q2c	dQ1c	W
Difference between Q1e and Q2e	dQ1e	
Difference between Q1c and Q4c	dQ2c	
Difference between Q1e and Q4e	dQ2e	
Effectiveness thermosyphon condenser	ec	Dimensionless
Effectiveness thermosyphon condenser mean	ec_m	
Effectiveness condenser row	ecn	
Effectiveness condenser row mean	ecn_m	
Effectiveness thermosyphon evaporator	ee	

Effectiveness thermosyphon evaporator mean	ee_m	
Effectiveness evaporator row	een	
Effectiveness evaporator row mean	een_m	
Efficiency of condenser fins	effc	
Efficiency of evaporator fins	effe	
Ratio between HTAc and HTAc_smooth	eratc	
Ratio between HTAe and HTAe_smooth	erate	
HPHE effectiveness	Et	
HPHE effectiveness mean	Et_m	
Euler number condenser	Euc	
Euler number evaporator	Eue	
Friction factor condenser	fxc	
Friction factor evaporator	fxe	
Core mass velocity condenser	Gc	m.s ⁻¹
Core mass velocity evaporator	Ge	
Heat transfer area condenser	HTAc	m ²
Heat transfer area bare condenser	HTAc_smooth	
Heat transfer area evaporator	HTAe	
Heat transfer area bare evaporator	HTAe_smooth	
Heat transfer coefficient condenser	HTFc	W.m ⁻² .K ⁻¹
Heat transfer coefficient condenser mean	HTFc_m	
Heat transfer coefficient evaporator	HTFe	
Heat transfer coefficient evaporator mean	HTFe_m	
Thermal conductivity of condenser fins	kfc	W.m ⁻¹ .K ⁻¹
Thermal conductivity of evaporator fins	kfe	
Thermal conductivity condenser fluid	LAMDAc	
Thermal conductivity condenser fluid mean	LAMDAc_m	
Thermal conductivity condenser fluid outlet	LAMDAc_o	
Thermal conductivity condenser fluid wall	LAMDAc_w	
Thermal conductivity evaporator fluid	LAMDAe	
Thermal conductivity evaporator fluid mean	LAMDAe_m	

Thermal conductivity evaporator fluid outlet	LAMDAeo	
Thermal conductivity evaporator fluid wall	LAMDAew	
Length of helical fin condenser	Lhlc	m
Length of helical fin evaporator	Lhle	
Logarithmic mean temperature difference	LMTD	Dimensionless
Minimum area condenser	minareac	m ²
Minimum area evaporator	minareae	
Testing minimum area between longitudinal condenser rows	minareatestc1	Dimensionless
Testing minimum area between transverse condenser rows	minareatestc2	
Testing minimum area between longitudinal condenser rows mean conditions	minareatestc_m1	
Testing minimum area between transverse condenser rows mean conditions	minareatestc_m2	
Testing minimum area between longitudinal condenser rows outlet	minareatestco1	
Testing minimum area between transverse condenser rows outlet	minareatestco2	
Testing minimum area between longitudinal evaporator rows mean conditions	minareateste_m1	
Testing minimum area between transverse evaporator rows mean conditions	minareateste_m2	
Testing minimum area between longitudinal evaporator rows outlet	minareatesteo1	
Testing minimum area between transverse c evaporator rows outlet	minareatesteo2	
Number of transfer units condenser	NTUc	
Number of transfer units condenser mean	NTUc_m	
Number of transfer units evaporator	NTUe	
Number of transfer units evaporator mean	NTUe_m	
Kinematic viscosity condenser	NUc	m ² .s ⁻¹

Kinematic viscosity condenser mean	NUc_m		
Kinematic viscosity condenser outlet	NUco		
Kinematic viscosity condenser wall	NUcw		
Kinematic viscosity evaporator	NUe		
Kinematic viscosity evaporator mean	NUe_m		
Kinematic viscosity evaporator outlet	NUeo		
Kinematic viscosity evaporator wall	NUew		
Number of iterations for wall temperature goal seek	numiterations	Dimensionless	
Nusselt number condenser	Nusc		
Nusselt number condenser mean	Nusc_m		
Nusselt number evaporator	Nuse		
Nusselt number evaporator mean	Nuse_m		
SLc/Dout	PLc		
SLe/Dout	PLe		
Prandtl number condenser	Prc		
Prandtl number condenser mean	Prc_m		
Prandtl number condenser outlet	Prco		
Prandtl number condenser wall	PrCs		
Prandtl number evaporator	Pre		
Prandtl number evaporator mean	Pre_m		
Prandtl number evaporator outlet	Preo		
Prandtl number evaporator wall	Pres		
STc/Dout	PTc		
STe/Dout	PTe		
Heat transfer rate condenser method 1	Q1c		W
Heat transfer rate evaporator method 1	Q1e		
Heat transfer rate condenser method 2	Q2c		
Heat transfer rate evaporator method 2	Q2e		
Heat transfer rate temperature balance by iterating condenser wall	Q4c		

Heat transfer rate temperature balance by iterating evaporator wall	Q4e	
Heat transfer rate output	Qdot	
Reynolds number condenser	ReDc	Dimensionless
Reynolds number condenser mean	ReDc_m	
Reynolds number condenser outlet	ReDco	
Reynolds number evaporator	ReDe	
Reynolds number evaporator mean	ReDe_m	
Reynolds number evaporator outlet	ReDeo	
Density condenser fluid	RHOc	
Density condenser fluid mean	RHOc_m	
Density condenser fluid outlet	RHOco	
Density condenser fluid wall	RHOcw	
Density evaporator fluid	RHOe	
Density evaporator fluid mean	RHOe_m	
Density evaporator fluid outlet	RHOeo	
Density evaporator fluid wall	RHOew	
Specific heat capacity condenser fluid	SHCc	J.kg ⁻¹ .K ⁻¹
Specific heat capacity condenser fluid mean	SHCc_m	
Specific heat capacity condenser fluid outlet	SHCco	
Specific heat capacity condenser fluid wall	SHCcw	
Specific heat capacity evaporator fluid	SHCe	
Specific heat capacity evaporator fluid mean	SHCe_m	
Specific heat capacity evaporator fluid outlet	SHCeo	
Specific heat capacity evaporator fluid wall	SHCew	
STc/SLc	STSLc	Dimensionless
STe/SLe	STSLe	
Mean temperature condenser fluid	Tc_m	°C
Temperature of condenser outlet	Tco	
Temperature of condenser outlet initial guess	Tcog	

Mean temperature evaporator fluid	Th_m	
Mean temperature evaporator outlet	Tho	
Temperature of evaporator outlet initial guess	Thog	
Temperature condenser wall	Twc	
Temperature condenser wall iterating down	Twc_down	
Temperature condenser wall iterating up	Twc_up	
Temperature evaporator wall	Twe	
Temperature evaporator wall iterating down	Twe_down	
Temperature evaporator wall iterating up	Twe_up	
HPHE conductance value output	UA	W.K ⁻¹
Free flow velocity condenser	vc	m.s ⁻¹
Free flow velocity condenser mean	vc_m	
Free flow velocity condenser outlet	vco	
Free flow velocity evaporator	ve	
Free flow velocity evaporator mean	ve_m	
Free flow velocity evaporator outlet	veo	
Maximum velocity condenser	Vmaxc	
Maximum velocity condenser mean	Vmaxc_m	
Maximum velocity condenser outlet	Vmaxco	
Maximum velocity evaporator	Vmaxe	
Maximum velocity evaporator mean	Vmaxe_m	
Maximum velocity evaporator outlet	Vmaxeo	
$\text{Sqrt}(2\text{HTFc}/\text{kfc}*\text{efin})$	xc	Dimensionless
$\text{Sqrt}(2\text{HTFe}/\text{kfe}*\text{efin})$	xe	

5.1.1. HPHE Coding in Intel Visual Fortran

This section explains how the Type204 code was written. The entire code for the HPHE component is provided in Appendix B. The first line of the code calls the particular subroutine to which the component in simulation studio is linked, in this case the Type number. Types201-300 are reserved for user written components and Types1-200 are reserved for the standard TRNSYS library. For this reason, Type204 was arbitrarily chosen as the code presented is the fourth iteration.

Subroutine Type204

Figure 75: Code starting the subroutine for Type204.

A TRNSYS 17 simulation requires access to global constants and functions provided in the source code. To choose which are called into the simulation is done by ‘Use’ statements. Type204 requires *TrnsysConstants* and *TrnsysFunctions*. *TrnsysConstants* is a module containing fixed values that do not change throughout a simulation, for example, declaring the maximum number of equations or outputs used in a simulation. *TrnsysFunctions* are all the functions that the subroutines can use to handle the stored data. A table of the TRNSYS constants and a full description of each function are found in Section 7.4.2 of the Programmers manual [215].

```
!-----
!Use Statements
Use TrnsysConstants
Use TrnsysFunctions
!-----
```

Figure 76: Code to call external TRNSYS constants and functions.

In previous versions of TRNSYS, Types could not exist in an external *.dll file (a dynamic link library), as it required altering the standard TRNDLL.dll. In TRNSYS 17, the Types can exist in an external *.dll. The kernel examines the contents of a user library directory to determine if any external *.dll files need to be loaded into the simulation. In this case, the Type204.dll file is an external *.dll file placed in the user library and is loaded into the memory for the duration of the simulation. The code below tells the kernel to search for Type204 in the user library and loads it into the memory.

```
!Export this subroutine for its use in external DLLs.

!DEC$ATTRIBUTES DLLEXPORT :: TYPE204
```

Figure 77: Code for exporting Type204 to an external DLL.

Declaring the variables is a section of code that comes after initially defining the subroutine, giving access to global variables and exporting the component. This is a larger section of code

where all the local variables that are used through the simulation are given. *Implicit None* is used to instruct that all variables need to be explicitly declared. If the variable is a real number, *Double precision* is used to set the variable to be a real number with twice the amount of significant decimal digits and a magnitude range of 10^{-308} to 10^{308} . This degree of accuracy is not necessary but modern computing power allows the use of it. *Integer* is used to set the variable to be an integer number. *Data* can be used before the variable to set a parameter to a fixed value, however, this command was not used for Type204. Figure 78 provides a list of the declared variables. These are visually split into inputs, parameters, internal variables and outputs.

```
!Variable Declarations
```

```
Implicit None !Force explicit declaration of local variables
```

```
!Inputs
```

```
Double precision Thi      !Temperature of source inlet fluid [deg C]
Double precision Tci      !Temperature of sink inlet fluid [deg C]
Double precision FLWe     !Mass flow rate evaporator (source) fluid [kg/s]
Double precision FLWc     !Mass flow rate condenser (sink) fluid [kg/s]
```

```
!Parameters
```

```
Integer Nre              !Number of rows in heat exchanger evaporator (longitudinal)
Integer Nrc              !Number of rows in heat exchanger condenser (longitudinal)
Double precision Dout    !Outer diameter of heat pipes [m]
Double precision Le      !Length evaporator [m]
Double precision Lc      !Length of condenser [m]
Integer Nte              !Number of tubes in evaporator row (transverse)
Integer Ntc              !Number of tubes in condenser row (transverse)
Double precision STe     !Transverse distance between evaporator row centres [m]
Double precision SLe     !Longitudinal distance between evaporator row centres [m]
Double precision STc     !Transverse distance between condenser row centres [m]
Double precision SLc     !Longitudinal distance between condenser row centres [m]
Double precision Ae      !Flow area of evaporator [m2]
Double precision Ac      !Flow area of condenser [m2]
Integer FinningMode     !(1=none, 2=con finned, 3=evap finned, 4=both)
Integer FluidMode       !Sink: 1=air 2=water 3=thermal oil
Double precision Dofin   !Outer diameter of fins [m]
Double precision efin    !Thickness of fins [m]
Double precision Pfin    !Pitch of fins [m]
Double precision Hfin    !Width of fins [m]
```

```
!Internal Variables
Double precision HTFe !Heat transfer coefficient evaporator [W/m2.K]
Double precision HTFeo !Heat transfer coefficient evaporator outlet [W/m2.K]
Double precision HTFc !heat transfer coefficient condenser [W/m2.K]
Double precision HTFco !heat transfer coefficient condenser outlet [W/m2.K]
Double precision HTAe !Heat transfer area of one evaporator row [m2]
Double precision HTAe_smooth !Heat transfer area of one evaporator row smooth [m2]
Double precision HTAc !Heat transfer area of one condenser row [m2]
Double precision HTAc_smooth !Heat transfer area of one condenser row smooth [m2]
Double precision Ce !Heat capacity rate of evaporator [j/K.s]
Double precision Ceo !Heat capacity rate of evaporator outlet [j/K.s]
Double precision Cc !Heat capacity rate of condenser [j/K.s]
Double precision Cco !Heat capacity rate of condenser outlet [j/K.s]
Double precision Cmin !Smaller or Ce and Cc [j/K.s]
Double precision Cmino !Smaller or Ce and Cc outlet [j/K.s]
Double precision Et !Overall effectiveness
Double precision Eto !Overall effectiveness outlet
Double precision een !Effectiveness of evaporator row
Double precision eeno !Effectiveness of evaporator row outlet
Double precision ecn !Effectiveness of condenser row
Double precision ecno !Effectiveness of condenser row outlet
Double precision ee !Effectiveness of evaporator
Double precision eeo !Effectiveness of evaporator outlet
Double precision ec !Effectiveness of condenser
Double precision eco !Effectiveness of condenser outlet
Double precision NTUe !Number of effectiveness units evaporator
Double precision NTUeo !Number of effectiveness units evaporator outlet
Double precision NTUc !Number of effectiveness units condenser
Double precision NTUco !Number of effectiveness units condenser outlet
Double precision Pre !Prandtl number evaporator
Double precision Preo !Prandtl number evaporator outlet
Double precision Prc !Prandtl number condenser
Double precision Prco !Prandtl number condenser outlet
```

```

Double precision Vmaxe !Maximum velocity evaporator [m/s]
Double precision Vmaxeo !Maximum velocity evaporator outlet [m/s]
Double precision Vmaxc !Maximum velocity condenser [m/s]
Double precision Vmaxco !Maximum velocity condenser outlet [m/s]
Double precision ReDe !Reynolds number evaporator
Double precision ReDeo !Reynolds number evaporator outlet
Double precision ReDc !Reynolds number condenser
Double precision ReDco !Reynolds number condenser outlet
Double precision Nuse !Nusselt number evaporator
Double precision Nuseo !Nusselt number evaporator outlet
Double precision Nusc !Nusselt number condenser
Double precision Nusco !Nusselt number condenser outlet
Double precision ve !Free flow velocity evaporator [m/s]
Double precision veo !Free flow velocity evaporator outlet [m/s]
Double precision vc !Free flow velocity condenser [m/s]
Double precision vco !Free flow velocity condenser outlet [m/s]
Double precision RHOe !Density evaporator fluid [kg/m3]
Double precision RHOeo !Density evaporator fluid outlet [kg/m3]
Double precision RHOC !Density condenser fluid [kg/m3]
Double precision RHOCO !Density condenser fluid outlet [kg/m3]
Double precision NUe !Kinematic viscosity evaporator [m2/s]
Double precision NUeo !Kinematic viscosity evaporator outlet [m2/s]
Double precision NUC !Kinematic viscosity condenser [m2/s]
Double precision NUco !Kinematic viscosity condenser outlet [m2/s]
Double precision LAMDAe !Thermal conductivity evaporator fluid [W/m.K]
Double precision LAMDAeo !Thermal conductivity evaporator fluid outlet [W/m.K]
Double precision LAMDAC !Thermal conductivity condenser fluid [W/m.K]
Double precision LAMDAco !Thermal conductivity condenser fluid outlet [W/m.K]
Double precision SHCe !Specific heat capacity evaporator fluid [J/kg.K]
Double precision SHCeo !Specific heat capacity evaporator fluid outlet [J/kg.K]

Double precision Timestep,Time !Simulation timestep and time [s]
Double precision PI !Pi, 3.1415927
Integer CurrentUnit, CurrentType

```



```

!Evaluation Of Properties At Wall Temperature
Double precision Pres !Pr evaluated at evaporator wall temperature
Double precision Prcs !Pr evaluated at condenser wall temperature
Double precision NUew !Kinematic viscosity at evaporator wall [m2/s]
Double precision NUCw !Kinematic viscosity at condenser wall [m2/s]
Double precision LAMDAew !Thermal conductivity at evaporator wall [W/m.K]
Double precision LAMDAcw !Thermal conductivity at condenser wall [W/m.K]
Double precision Twe !Iterating evap wall temperature to determine Pres [deg C]
Double precision Twc !Iterating cond wall temperature to determine Prcs [deg C]
Double precision SHCew !Specific heat capacity at evaporator wall temperature [J/kg.K]
Double precision SHCcw !Specific heat capacity at condenser wall temperature [J/kg.K]

!Goalseeking
Double precision Twe_up !Goalseek up function for Twe [deg C]
Double precision Twe_down !Goalseek down function for Twe [deg C]
Double precision Twc_up !Goalseek up function for Twc [deg C]
Double precision Twc_down !Goalseek down function for Twc [deg C]
Double precision Q1e !m.cp.dT
Double precision Q2e !((Thi-Tho)/log(Thi-Twe)/Tho-Twe)
Double precision Q4e !((Thi-Tho)/log(Thi-Twe(up/down))/Tho-Twe(up/down))
Integer numiterations
Double precision dQ1e !Q1e - Q2e
Double precision dQ2e !Q1e - Q4e
Double precision Q1c !m.cp.dT
Double precision Q2c !((Tco-Tci)/log(Tci-Tw)/Tco-Tw)
Double precision Q4c !((Tco-Tci)/log(Tci-Tw(up/down))/Tco-Tw(up/down))
Double precision dQ1c !Q1c - Q2c
Double precision dQ2c !Q1c - Q4c
Double precision Thog !Source outlet temperature initial guess [deg C]
Double precision Tcog !Sink outlet temperature initial guess [deg C]

```

```

!Finning influence
Double precision CFe !Correction factor for Nusselt equations evaporator
Double precision CFc !Correction factor for Nusselt equations condenser
Double precision efffe !Efficiency of the fin evaporator
Double precision efffc !Efficiency of the fin condenser
Double precision Afe !Heat transfer area of the evaporator fins [m2]
Double precision Afc !Heat transfer area of the condenser fins [m2]
Double precision xe !SQRT(2hfc/kfe*efffe)
Double precision xc !SQRT(2hfc/kfe*efffc)
Double precision kfe !Thermal conductivity of evaporator fin [W/m.K]
Double precision kfc !Thermal conductivity of condenser fin [W/m.K]
Double precision Lhle !Length of helical evaporator [m]
Double precision Lhlc !Length of helical condenser [m]

!Pressure Drop calculations
Double precision PLe !SLe/Dout longitudinal pitch
Double precision PLc !SLc/Dout longitudinal pitch
Double precision PTe !STe/Dout transverse pitch
Double precision PTc !STc/Dout transverse pitch
Double precision PTLc !PTc/PLc
Double precision PTLc !PTc/PLc
Double precision fe !Friction factor evaporator
Double precision fc !Friction factor condenser
Double precision fxe !Friction factor/Xe evaporator
Double precision fxc !Friction factor/Xc condenser
Double precision Chie !Correlation factor evaporator
Double precision Chic !Correlation factor condenser
Double precision Eue !Euler number evaporator
Double precision Euc !Euler number condenser
Double precision erate !Ratio of total SA with fins to bare tube SA w/o fins evaporator
Double precision eratc !Ratio of total SA with fins to bare tube SA w/o fins condenser
Double precision Ge !Core mass velocity evaporator
Double precision Gc !Core mass velocity condenser
Double precision RHOew !Density at condenser wall [kg/m3]
Double precision RHOcw !Density at condenser wall [kg/m3]
Double precision STSLe !STe/SLe
Double precision STSLc !STc/SLc

```



```
!Flow area location tests
Double precision minareateste1 !Minimum area test evaporator
Double precision minareateste2 !Minimum area test evaporator
Double precision minareateste_m1 !Minimum area test evaporator
Double precision minareateste_m2 !Minimum area test evaporator
Double precision minareatesteo1 !Minimum area test evaporator
Double precision minareatesteo2 !Minimum area test evaporator
Double precision minareatestc1 !Minimum area test condenser
Double precision minareatestc2 !Minimum area test condenser
Double precision minareatestc_m1 !Minimum area test condenser
Double precision minareatestc_m2 !Minimum area test condenser
Double precision minareatestco1 !Minimum area test condenser
Double precision minareatestco2 !Minimum area test condenser

!Means
Double precision Cc_m
Double precision Ce_m
Double precision Cmin_m
Double precision LAMDAc_m
Double precision LAMDAe_m
Double precision minareac
Double precision minareae
Double precision NUC_m
Double precision NUe_m
Double precision Nusc_m
Double precision Nuse_m
Double precision Prc_m
Double precision Pre_m
Double precision ReDc_m
Double precision ReDe_m
Double precision RHOe_m
Double precision RHOC_m
Double precision SHCe_m
Double precision SHCc_m
Double precision Tc_m
Double precision Th_m
Double precision vc_m
Double precision ve_m
Double precision Vmaxe_m
Double precision Vmaxc_m
Double precision ecn_m
Double precision een_m
Double precision ec_m
Double precision ee_m
Double precision Et_m
```

```

Double precision HTFc_m
Double precision HTFe_m
Double precision LMTD
Double precision NTUc_m
Double precision NTUe_m

!Outputs
Double precision Tho      !Temperature of source outlet fluid [deg C]
Double precision Tco      !Temperature of sink outlet fluid [deg C]
Double precision Qdot     !Energy (Heat) Transfer Rate [kW]
Double precision dPe      !Pressure drop evaporator [Pa]
Double precision dPc      !Pressure drop condenser [Pa]
Double precision UA       !Conductance value of HPHE [W/K]

```

Figure 78: Code to declare all variables that Type204 uses throughout the subroutine.

After declaring the variables, the subsequent code is the executable section. Each line is read and executed sequentially. The variables *Time*, *Timestep*, *CurrentUnit*, *CurrentType* are global variables that are required to be read during each iteration to provide the transient nature output of the simulation.

```

!-----
!Get the Global Trnsys Simulation Variables
Time = getSimulationTime()
Timestep = getSimulationTimeStep()
CurrentUnit = getCurrentUnit()
CurrentType = getCurrentType()
!-----

```

Figure 79: Code to set global simulation variables.

The code needs to be ‘version signed’. This is done to inform the kernel which version of TRNSYS and therefore the convention in which the component was written. This alters how the kernel handles the component. This allows backward compatibility with components written in earlier TRNSYS versions and allows for future compatibility with the next versions of TRNSYS. This step is vital as the simulation will call an error if the Type is not signed to a particular version.

```

!-----
!Set the Version Number for This Type
If (getIsVersionSigningTime()) Then
    Call SetTypeVersion(17)
    Return
EndIf
!-----

```

Figure 80: Code to set version of component to TRNSYS 17.

On the last run through of the code, at the end of the simulation, it may be required to perform certain actions such as closing external files before returning control to the kernel. This is known as last call manipulation. No last call functions were needed for Type204 so it was only necessary to return control to the kernel.

```

!-----
!Do All of the Last Call Manipulations Here
If (getIsLastCallofSimulation()) Then
    Return
EndIf
!-----

```

Figure 81: Code for last call manipulations.

When a particular timestep finishes, every Type in the simulation is recalled. End of timestep manipulations allows functions to occur before the Type is recalled into the simulation. No end of timestep manipulations were required for Type204 so the instruction allows the Type to be recalled.

```

!-----
!Perform Any "End of Timestep" Manipulations Here
If (getIsEndOfTimestep()) Then
    Return
EndIf
!-----

```

Figure 82: Code for end of timestep manipulations.

To operate correctly, the kernel needs to be told what Type204 is composed of. The code below informs the kernel that there are nineteen parameters, four inputs, zero derivatives and six outputs. The iteration mode tells the kernel how often the Type should be called. A value of one indicates that Type204 should be called at every timestep regardless of whether the input

values have altered from the previous iteration. Number of stored variables sets the required number of static and dynamic storage spots. Type204 completes a calculation every timestep with the inputs so no stored variables are required. No discrete controls are required.

```
!Do All of the "Very First Call of the Simulation Manipulations" Here
If(getIsFirstCallOfSimulation()) Then

!Tell the Trnsys Engine How This Type Works
  Call SetNumberOfParameters(19)
  Call SetNumberOfInputs(4)
  Call SetNumberOfDerivatives(0)
  Call SetNumberOfOutputs(6)
  Call SetIterationMode(1)
  Call SetNumberStoredVariables(0,0)
  Call SetNumberOfDiscreteControls(0)
```

Figure 83: Code to set the total number of parameters, inputs, derivatives, outputs, number of stored variables, number of discrete controls and the iteration mode.

The code assigns units to the input and output values as this is shown in Figure 84. This is an important step in order to avoid inadvertently performing calculations or connecting components with different units. An example of this is whether the component calculates using Kelvin or degrees Celsius. If an output value of one parameter is in a different unit to another, as long as the measurement type is the same (e.g. temperature), TRNSYS will convert the value to the correct unit. The programmer's manual provides a breakdown of the available measurement types, the units, the TRNSYS code and the mathematical conversion used. For the conductance value, $W.K^{-1}$ was not available so this was left as dimensionless.

```
!Set the Correct Input and Output Variable Types
  Call SetInputUnits(1,'TE1') !Thi [deg C]
  Call SetInputUnits(2,'TE1') !Tci [deg C]
  Call SetInputUnits(3,'MF2') !FLWe [kg/s]
  Call SetInputUnits(4,'MF2') !FLWc [kg/s]

  Call SetOutputUnits(1,'TE1') !Tho [deg C]
  Call SetOutputUnits(2,'TE1') !Tco [deg C]
  Call SetOutputUnits(3,'PW3') !Qdot [kW]
  Call SetOutputUnits(4,'PR3') !dPe [Pa (N/m2)]
  Call SetOutputUnits(5,'PR3') !dPc [Pa (N/m2)]
  Call SetOutputUnits(6,'DM1') !UA [W/K] !Unit N/A so dimensionless
```

Figure 84: Code to provide input and output values their unit type.

On the first run of the code there are no iterations, but the initial input and output values of the parameters are read as shown in Figure 85. The initial parameter values are read from external data files or component input values. The order within the component determines the number assigned to it. The *JFIX* function is used to ensure the number read is an integer.

```
!Do All of the "Start Time" Manipulations Here- There Are No Iterations at the Initial Time
If (getIsStartTime()) Then
!Read in the Values of the Parameters from the Input File
Nre = JFIX(getParameterValue(1))  !Number of rows evaporator
Nrc = JFIX(getParameterValue(2))  !Number of rows condenser
Dout = getParameterValue(3)      !Outer diameter of heat pipe
Le = getParameterValue(4)        !Length of evaporator
Lc = getParameterValue(5)        !Length of condenser
Nte = JFIX(getParameterValue(6)) !Number of heat pipe rows evaporator
Ntc = JFIX(getParameterValue(7)) !Number of heat pipe rows condenser
STe = getParameterValue(8)      !Distance between row centres evaporator
SLe = getParameterValue(9)      !Distance between heat pipe centres evaporator
STc = getParameterValue(10)     !Distance between row centres condenser
SLc = getParameterValue(11)     !Distance between heat pipe centres condenser
Ae = getParameterValue(12)      !Flow area evaporator
Ac = getParameterValue(13)      !Flow area condenser
FinningMode = JFIX(getParameterValue(14)) !Condenser or Evaporator finned
FluidMode = JFIX(getParameterValue(15)) !Heat sink as air, water or oil
Dofin = getParameterValue(16)   !Outer diameter of fins
efin = getParameterValue(17)    !Thickness of fins
Pfin = getParameterValue(18)    !Pitch of fins
Hfin = getParameterValue(19)    !Width of fins
```

Figure 85: Code to fetch initial values for all parameters given by user.

If an out-of-range parameter is found, to prevent erroneous and incorrect calculation, error messages were built into the code. If a parameter is out-of-range and the simulation is run, an error message pops up to alert the user (Figure 86). This is essential to ensure that all of the parameters are correctly input and results were not obtained incorrectly. Figure 87 shows the coded ranges with the error messages that are shown in a pop-up box and the results file if out of range parameters are input.

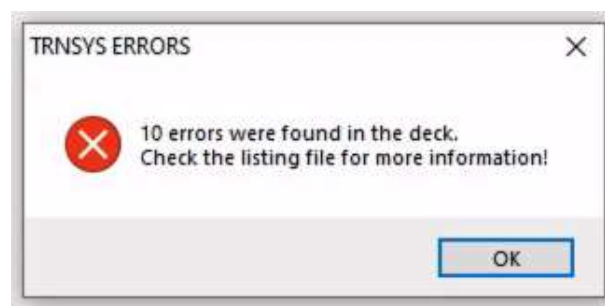


Figure 86: TRNSYS pop-up message example if parameter errors are found during the simulation.

In this case:

- The number of rows (Nre or Nrc) in the HPHE had to be greater than one. The input defaults to zero. This is to ensure that an input is entered.
- It is easy to input the outer diameter (Dout) of the pipe in millimetres or centimetres rather than metres. If Dout is over one, it is obvious that the incorrect unit and therefore input is used.
- As the initial default value of the length of the evaporator (Le) and length of the condenser (Lc) is zero, ensuring that Le and Lc are greater than zero ensures that a value is input in the initial parameters.
- To ensure the number of heat pipes in a transverse row (Nte or Ntc) is input, an error occurs if the value is less than or equal to zero.
- To ensure the distance between the heat pipes rows and the heat pipe centres in a row (STe and SLe or STc and SLc) is input in metres, a value greater than or equal to one gives an error.
- To ensure an input is given for the flow area of the evaporator and condenser (Ae and Ac), a value less than or equal to zero gives an error.
- The finning mode depends on whether the evaporator or condenser sections are finned. 1= no finning, 2= condenser finned, 3= evaporator finned, 4= both finned. Inputs outside of 1 to 4 are not allowed.
- The fluid mode tells the component which heat sink is being modelled. 1= air, 2= water 3= thermal oil. Inputs outside of 1 to 3 are not allowed.
- Errors for the finning parameters ensures that measurements are input in metres.


```

!Check Parameters for Problems
If (Nre <= 1) Call FoundBadParameter(1, 'Fatal', 'The number of evaporator rows must be positive.')
If (Nrc <= 1) Call FoundBadParameter(2, 'Fatal', 'The number of condenser rows must be positive.')
If (Dout > 1.d0) Call FoundBadParameter(3, 'Fatal', 'Ensure diameter is in metres')
If (Le <= 1.d0) Call FoundBadParameter(4, 'Fatal', 'The length evaporator must be positive.')
If (Lc <= 0.d0) Call FoundBadParameter(5, 'Fatal', 'The length condenser must be positive.')
If (Nte <= 0.d0) Call FoundBadParameter(6, 'Fatal', 'Number of heat pipes in evaporator row must be positive.')
If (Ntc <= 0.d0) Call FoundBadParameter(7, 'Fatal', 'Number of heat pipes in condenser row must be positive.')
If (STe >= 1.d0) Call FoundBadParameter(8, 'Fatal', 'Ensure distance between evaporator rows is in metres')
If (SLe >= 1.d0) Call FoundBadParameter(9, 'Fatal', 'Ensure distance between evaporator heat pipes is in metres')
If (STc >= 1.d0) Call FoundBadParameter(10, 'Fatal', 'Ensure distance between condenser rows is in metres')
If (SLc >= 1.d0) Call FoundBadParameter(11, 'Fatal', 'Ensure distance between condenser heat pipes is in metres')
If (Ae <= 0.d0) Call FoundBadParameter(12, 'Fatal', 'Ae must be positive')
If (Ac <= 0.d0) Call FoundBadParameter(13, 'Fatal', 'Ac must be positive')
If ((FinningMode <= 0) .or. (FinningMode > 4)) Call FoundBadParameter(14, 'Fatal', 'Finning mode must be between 1 and 4')
If ((FluidMode <= 0) .or. (FluidMode > 3)) Call FoundBadParameter(15, 'Fatal', 'Fluid mode must be between 1 and 3')
If (Dofin >= 1) Call FoundBadParameter(16, 'Fatal', 'Ensure fin diameter is in metres')
If (efin >= 1) Call FoundBadParameter(17, 'Fatal', 'Ensure outer fin diameter is in metres')
If (Pfin >= 1) Call FoundBadParameter(18, 'Fatal', 'Ensure pitch is in metres')
If (Hfin >= 1) Call FoundBadParameter(19, 'Fatal', 'Ensure fin height is in metres')
If (ErrorFound()) Return

```

Figure 87: Code to provide error notification if parameters are outside correct ranges for calculations to function.

Figure 88 gives an example of the error messages when the simulation is run with out-of-range parameters. The Type (204) is shown, the time step it occurred (0.000 hours) and, by clicking on the error, the parameter that is incorrect and why it occurred is shown: 'Parameter # 1, Reported Problem: The number of evaporator rows must be positive'.

Time Step	Time	Step	Type	Message
14	0.000	2	204	TRNSYS Message 125: The referenced Unit has a bad parameter value. Reported information : Parameter # 1, Reported Problem: The number of evaporator rows must be positive.
15	0.000	2	204	TRNSYS Message 125: The referenced Unit has a bad parameter value.
16	0.000	2	204	TRNSYS Message 125: The referenced Unit has a bad parameter value.
17	0.000	2	204	TRNSYS Message 125: The referenced Unit has a bad parameter value.
18	0.000	2	204	TRNSYS Message 125: The referenced Unit has a bad parameter value.
19	0.000	2	204	TRNSYS Message 125: The referenced Unit has a bad parameter value.
20	0.000	2	204	TRNSYS Message 125: The referenced Unit has a bad parameter value.
21	0.000	2	204	TRNSYS Message 125: The referenced Unit has a bad parameter value.
22	0.000	2	204	TRNSYS Message 125: The referenced Unit has a bad parameter value.
23	0.000	2	204	TRNSYS Message 125: The referenced Unit has a bad parameter value.
24	0.000	13	0	Total Fatal Errors : 10

Figure 88: Example of error messages when simulation is run with out-of-range parameters.

At the first timestep the outputs of the simulation need an initial value, the code is shown by Figure 89. In this case the output values were set to the values of Tho and Tco; temperature of the hot and cold stream outlets. The outputs for others were set at 0. For this reason, the initial time step results are not useful and are omitted from the analysis.

```

!Set the Initial Value of the Outputs
Call SetOutputValue(1, getInputValue(1))
Call SetOutputValue(2, getInputValue(2))
Call SetOutputValue(3, 0.d0)
Call SetOutputValue(4, 0.d0)
Call SetOutputValue(5, 0.d0)
Call SetOutputValue(6, 0.d0)

```

Figure 89: Code to set initial values of outputs.

In a simulation, it is possible to run multiples of the same Type, as in the case of Experiment 3, explained in Section 5.2. For example, if multiple HPHEs are in a simulation, multiple Type204 components will be put into the simulation. The simulation needs to treat these Types separately. For this reason, there is dedicated code for multiple unit manipulation (Figure 90). *If (getIsReReadParameters())* is the function used that causes the parameters list to be reread if there is more than one Type in a simulation. The parameters below the function are only read if that is true.

```

!ReRead the Parameters If Another Unit of This Type Has Been Called Last
If (getIsReReadParameters()) Then
  Nre = JFIX(getParameterValue(1))    !Number of rows evaporator
  Nrc = JFIX(getParameterValue(2))    !Number of rows condenser
  Dout = getParameterValue(3)        !Outer diameter of heat pipe
  Le = getParameterValue(4)          !Length of evaporator
  Lc = getParameterValue(5)          !Length of condenser
  Nte = JFIX(getParameterValue(6))    !Number of heat pipe rows evaporator
  Ntc = JFIX(getParameterValue(7))    !Number of heat pipe rows condenser
  STe = getParameterValue(8)         !Distance between row centres evaporator
  SLe = getParameterValue(9)         !Distance between heat pipe centres evaporator
  STc = getParameterValue(10)        !Distance between row centres condenser
  SLc = getParameterValue(11)        !Distance between heat pipe centres condenser
  Ae = getParameterValue(12)         !Flow area evaporator
  Ac = getParameterValue(13)         !Flow area condenser
  FinningMode = JFIX(getParameterValue(14)) !Condenser or Evaporator finned
  FluidMode = JFIX(getParameterValue(15)) !Heat sink as air, water or oil
  Dofin = getParameterValue(16)      !Outer diameter of fins
  efin = getParameterValue(17)       !Thickness of fins
  Pfin = getParameterValue(18)       !Pitch of fins
  Hfin = getParameterValue(19)       !Width of fins
EndIf

```

Figure 90: Code to allow multiple Type204 components to function in a simulation independently.

There are five inputs for Type204, namely: temperatures, mass flow rates and an approximate value of pi (π). Figure 91 shows the code where the input values are taken from the values entered into the component.

```
!Get the Current Inputs to the Model
Thi = getInputValue(1) !Temperature of source inlet fluid [deg C]
Tci = getInputValue(2) !Temperature of sink inlet fluid [deg C]
FLWe = getInputValue(3) !Mass flow rate evaporator (source) fluid [kg/s]
FLWc = getInputValue(4) !Mass flow rate condenser (sink) fluid [kg/s]
PI = 3.1415927
```

Figure 91: Code to set initial input values and the value used for pi.

As with the parameters, the inputs need to be in range for a successful calculation and to check that they have been entered. For this reason, error messages are coded (Figure 92) to ensure negative values return an error message and the simulation is not run.

```
If (Thi < 0.) Call foundBadInput(1, 'Fatal', 'Enter source inlet temperature')
If (Tci < 0.) Call foundBadInput(2, 'Fatal', 'Enter sink inlet temperature')
If (FLWe < 0.) Call foundBadInput(3, 'Fatal', 'Enter source inlet flow rate')
If (FLWc < 0.) Call foundBadInput(4, 'Fatal', 'Enter sink inlet flow rate')
If (ErrorFound()) Return
```

Figure 92: Code to provide an error notification if out of range inputs are entered.

The subsequent code is for all the internal calculation with Type204 that occur. See Chapter 3: Theoretical Analysis for a detailed breakdown for the origin of these equations. See Appendix B for the complete code. After the internal calculations, the output values are calculated for the outlet temperatures, the heat transfer rate and the conductance value. This is done by the equations shown in Figure 93.

```
!Outlet Results
Tho = Thi - (Et_m * (Cmin_m / Ce_m) * (Thi - Tci)) !Source outlet temperature [deg C]
Tco = Tci + (Et_m * (Cmin_m / Cc_m) * (Thi - Tci)) !Sink outlet temperature [deg C]
Qdot = FLWe * SHCe_m * (Thi - Tho) / 1000.d0 !Heat recovery rate [kW]
LMTD = ((Thi - Tco) - (Tho - Tci)) / LOG(((Thi - Tco) / (Tho - Tci))) ! Logarithmic mean temperature difference
UA = Qdot * 1000.d0 / LMTD !HPHE conductance value
```

Figure 93: Code for the equations that dictate outlet values.

The next section of code determines the pressure drop across the evaporator and condenser sections and the section of code is chosen by the input *FinningMode* as both unfinned and finned tube bundle correlations are coded.

At each iteration, to visualise the output values, the following code is used (Figure 94). These values are stored in the memory and can be used at the next timestep, be graphically displayed or exported to a .txt file.

```
!Set the Outputs from this Model
Call SetOutputValue(1,Tho) !Outlet temperature source fluid (deg C)
Call SetOutputValue(2,Tco) !Outlet temperature sink fluid (deg C)
Call SetOutputValue(3,Qdot) !Energy recovery rate
Call SetOutputValue(4,UA) !Conductance of HPHE
Call SetOutputValue(5,dPe) !Pressure drop evaporator
Call SetOutputValue(6,dPc) !Pressure drop condenser
```

Figure 94: Code to set output values.

Figure 95 shows the final code, which returns control to the kernel after all the calculations are completed and the values are stored. The subroutine for Type204 is then ended for that timestep. It is then recalled at each subsequent timestep depending upon how long the simulation has been set to run by simulation start time, simulation stop time and simulation time step in the control cards menu in simulation studio.

```
Return
End Subroutine TYPE204
```

Figure 95: Code to return control to kernel and end the subroutine for Type204.

5.1.2. Creating a *.dll File Using Intel Visual Fortran 19

The TRNSYS Programmer's Guide [215] is outdated as the manual only provides instructions on how to add a Type to the TRNDLL.dll using Intel Visual Fortran 11. This process was done using Intel Visual Fortran 19 so varied from the instructions given in the manual. The instructions to add a new project to the Ivf11.x solution is provided in this section. A flowchart for the process is provided in Figure 96.

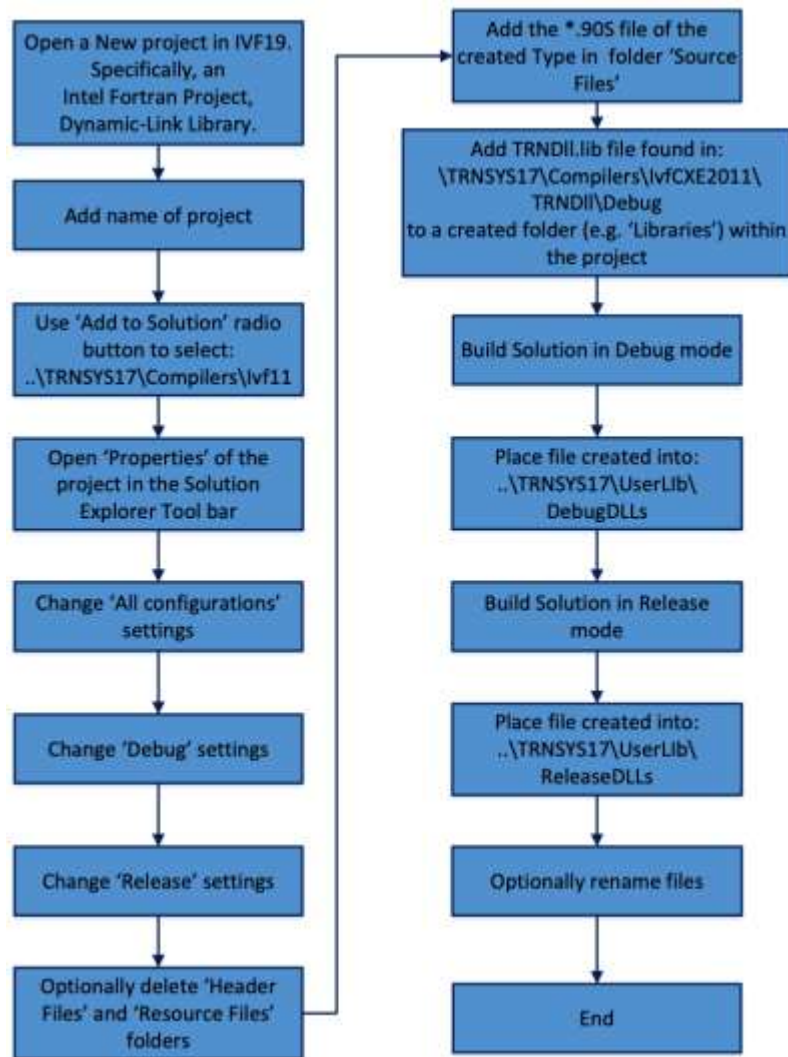


Figure 96: Flowchart for the process of compiling a component into a *.dll file to be used in TRNSYS.

Figure 97 shows a view of the Solution Explorer with the location of MyDll and the location of Type204. Figure 98 shows a view of the MyDll Property Pages. When changing the properties of the Solution, MyDll, Table 26 shows the properties that are required to be changed from Default options in the MyDll Property Pages.

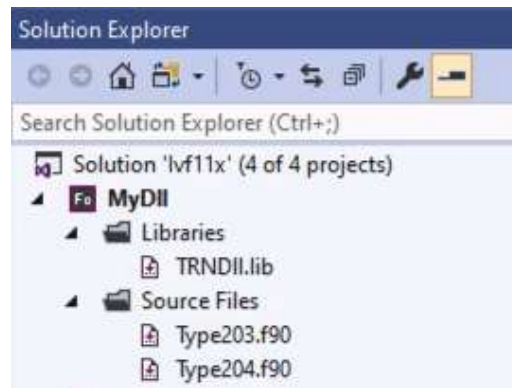


Figure 97: View of Solution Explorer tab for Type204.

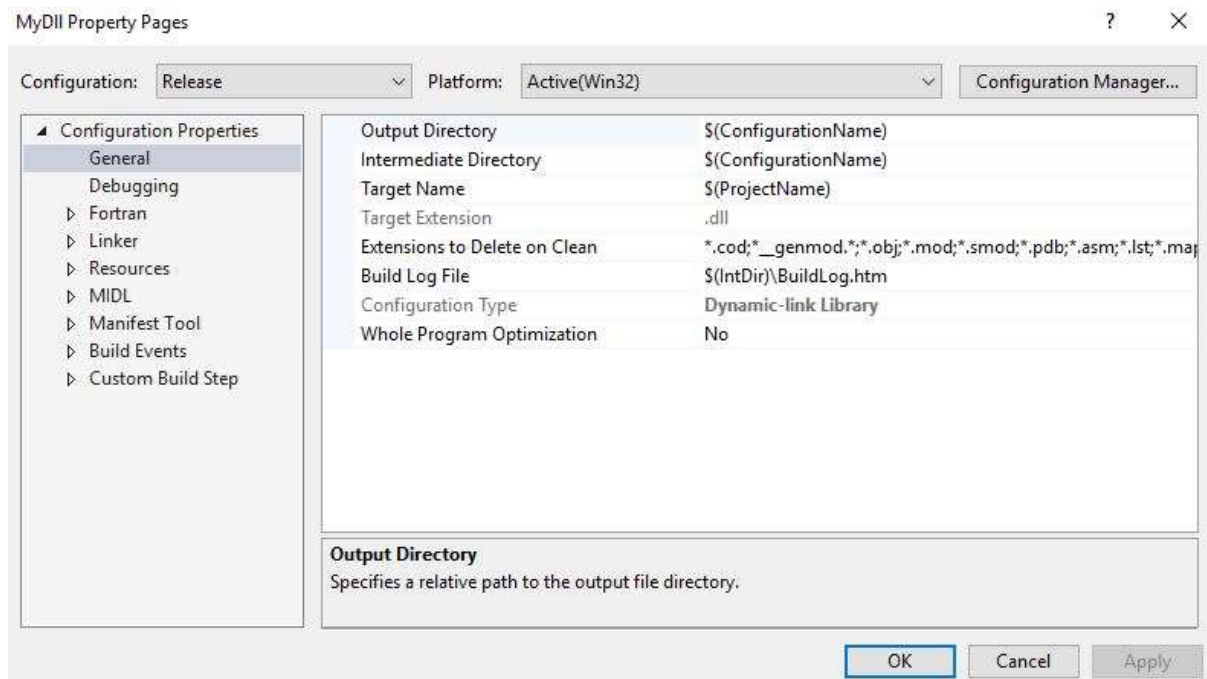


Figure 98: Property page for MyDll where properties are configured for 'All configurations', 'Debug' and 'Release' according to Table 26.

Table 26: TRNDll settings required to be changed.

Configuration mode	Branch	Category	Parameter	Value
All configurations	Fortran	General	Suppress Start-up Banner	Yes
			Optimisation	Disable
			Preprocessor Definitions	TRNSYS_MULTI_DLL; TRNSYS_WIN32; INTEL_COMPILER
		Data	Local Variable Storage	All Variables SAVE
		Floating Point	Initialise Local Saved Scalars to Zero	Yes
			Extend precision of Single-Precision Constants	Yes
		External Procedures	Calling convention	C,REFERENCE
		Libraries	Name case interpretation	Upper Case
			Runtime Library	Multithreaded
		Linker	Command Line	/ignore:4049,4217
Debug	Debugging		Command	..\..\Exe\TRNExe.exe
	Fortran	General	Preprocessor Definitions	TRNSYS_DEBUG
		Libraries	Runtime library	Debug Single-threaded DLL
		Run-time	Runtime Error Checking	All
	Build Events	Post-build Event	Command Line	Debug\TRNDll.dll ..\..\Exe\TRNDll.dll Debug\TRNDll.lib ..\..\Exe\TRNDll.lib
			Description	Copying TRNDll.dll and TRNDll.lib to the Exe folder
Release	Fortran	Libraries	Runtime library	Single-threaded DLL
		Compatibility	Use Other PowerStation Run-time Behaviour	Yes (/fpscomp:general)
	Build events	Post-build Event	Command Line	Debug\TRNDll.dll ..\..\Exe\TRNDll.dll Debug\TRNDll.lib ..\..\Exe\TRNDll.lib
			Description	Copying TRNDll.dll and TRNDll.lib to the Exe folder
	Linker	Optimization	References	Keep unreferenced data

5.1.3. Type204 Component Skeleton

A Type that is used for a simulation consists of two parts, the internal code that tells the component how to work, as detailed in Section 5.1.1, as well as the ‘skeleton’, which is used to enter the component into the simulation, link the component with other components in the simulation, house the code and provide the interface for parameter and input values. The section below deals with how the skeleton for Type 204 (HPHE) was created. The empty skeleton for Type204 (HPHE) was created in Simulation Studio by initially pressing File>New>New Component (TRNSYS TYPE).

An icon was created that is used to visualise the Type204 component in the simulation. To do this, a schematic was created in Microsoft PowerPoint, Figure 99. This was converted and sized to a *.bmp file, the format necessary for Simulation Studio, using Adobe Creative Cloud Photoshop CC.

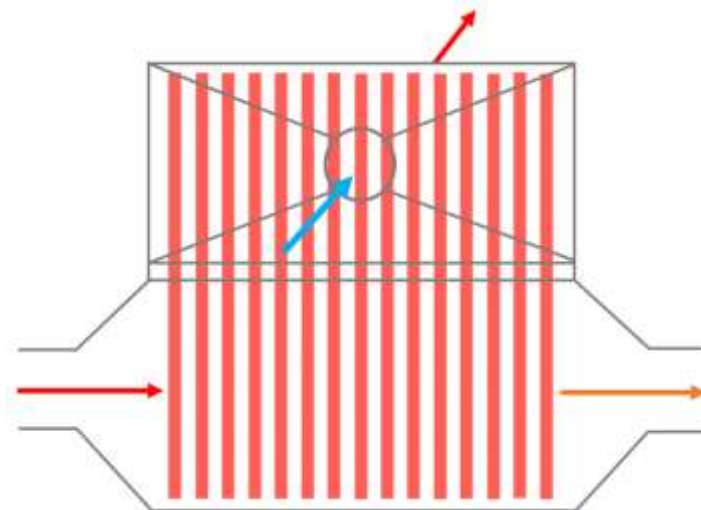


Figure 99: Schematic of Type204 HPHE created in Microsoft PowerPoint.

A view of the Type204 General, Parameter, Input and Output tab pages are provided in Figure 100, Figure 101, Figure 102 and Figure 103, respectively. The Parameter tab is where the user defines the value of the parameters that are used consistently throughout the simulation. The Input tab can have fixed user defined values or can have other Types linked to them. In this case, data files contained the source and sink fluid temperatures and flow rates at each time step.

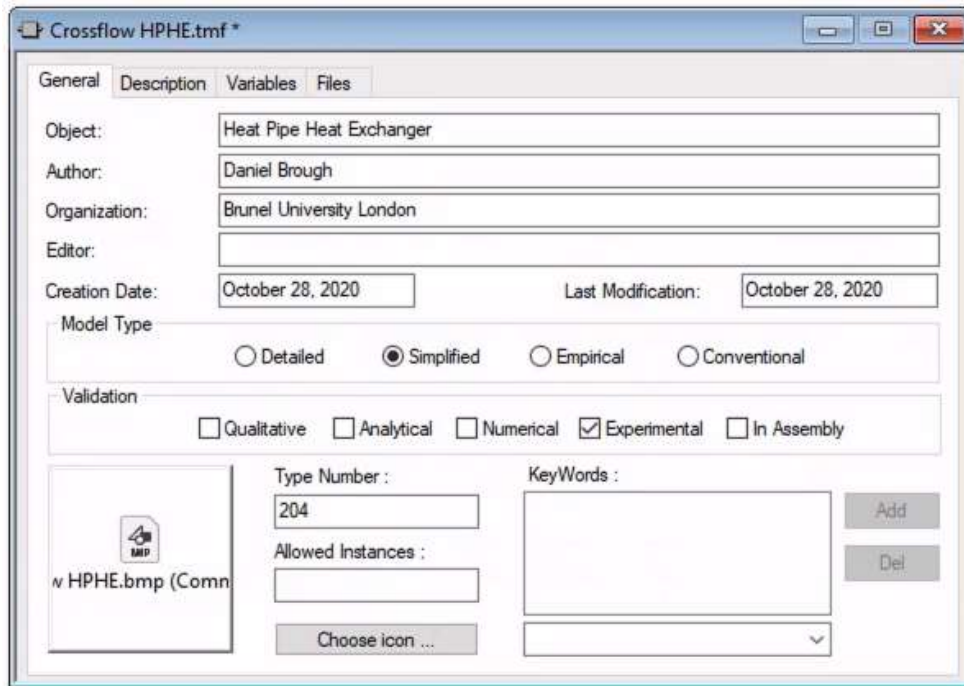


Figure 100: View of 'General' tab for HPHE component in Simulation Studio.

		Name	Value	Unit	More	Macro
1		Number of longitudinal rows in evaporator	0	-	More...	<input checked="" type="checkbox"/>
2		Number of longitudinal rows in condenser	0	-	More...	<input checked="" type="checkbox"/>
3		Outer diameter of heat pipes	0	m	More...	<input checked="" type="checkbox"/>
4		Length evaporator	0	m	More...	<input checked="" type="checkbox"/>
5		Length condenser	0	m	More...	<input checked="" type="checkbox"/>
6		Number of transverse rows evaporator	0	-	More...	<input checked="" type="checkbox"/>
7		Number of transverse rows condenser	0	-	More...	<input checked="" type="checkbox"/>

Figure 101: View of Type204 component 'Parameter' tab in Simulation Studio.

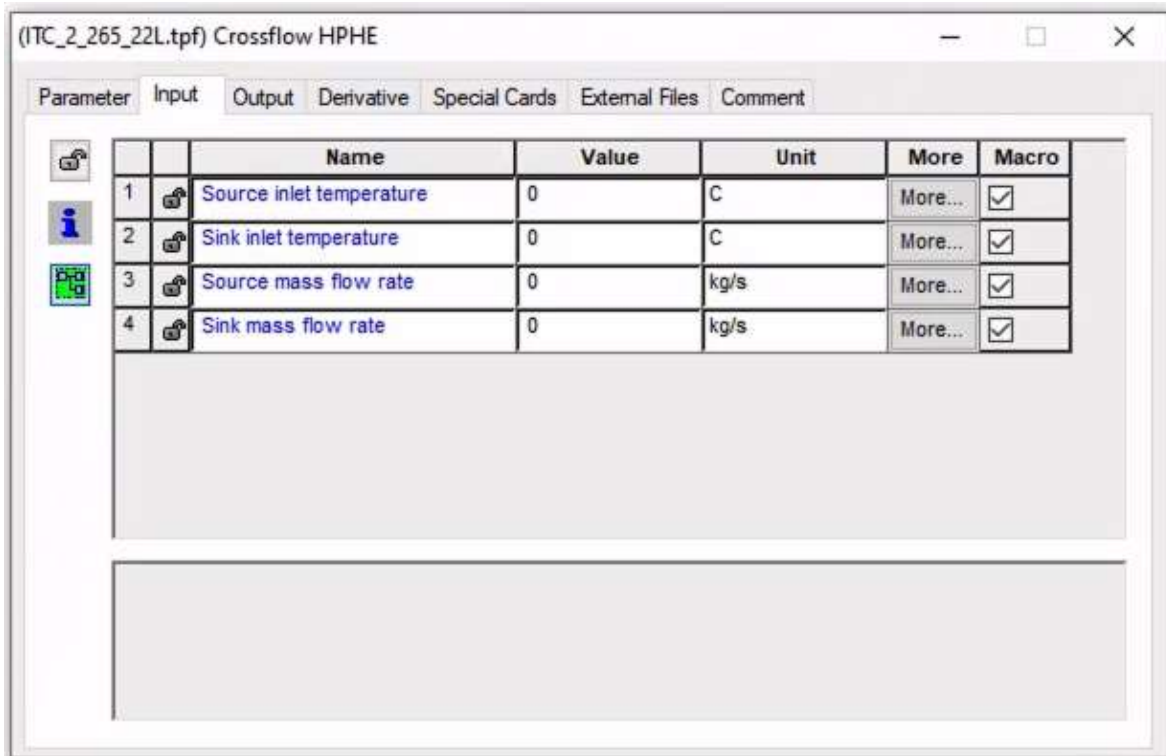


Figure 102: View of Type204 component 'Input' tab in Simulation Studio.

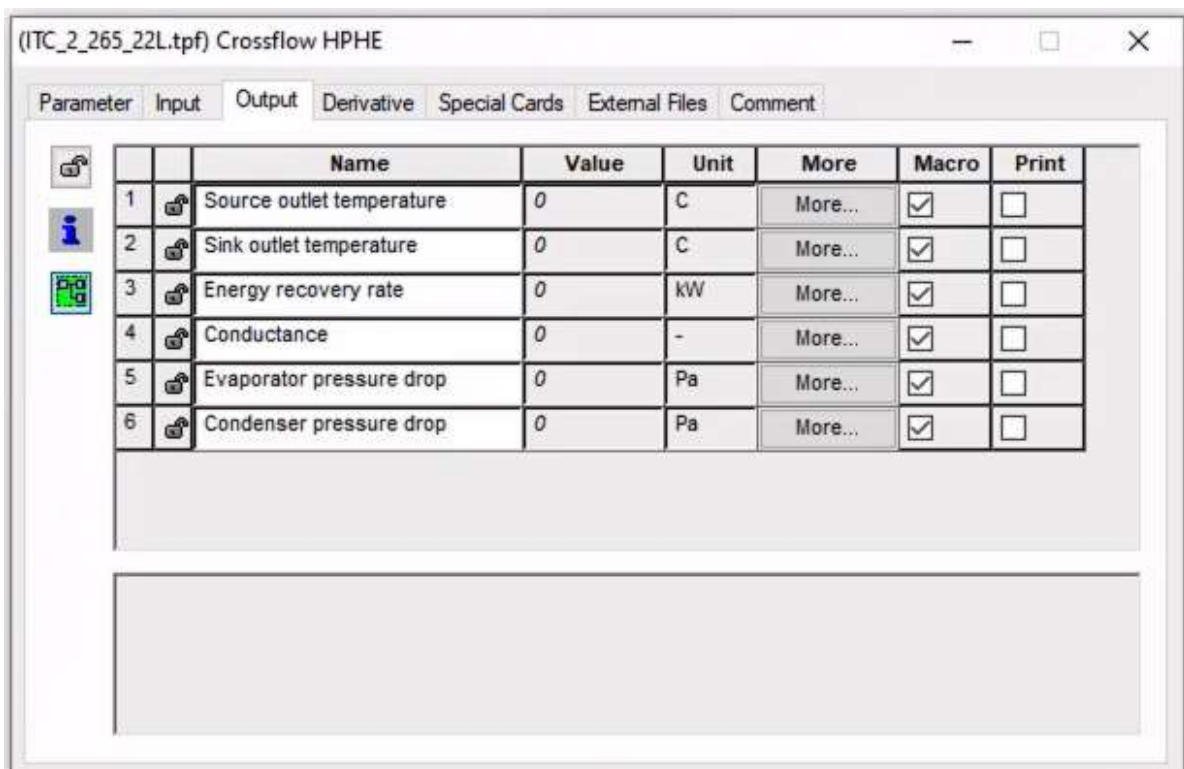


Figure 103: View of Type204 component 'Output' tab in Simulation Studio.

5.2. Using The Type in a Simulation

Figure 104 shows a view of the model in simulation studio that was used for Experiment 1 and 2, where the thermosyphons were all the same through the unit. The data input is shown on the left, the component with the internal mathematical operations is shown in the centre and the outputs are shown on the right. There is a combination of graphical outputs only and also Types that provide the outputs in a .txt file for later operations.

The lines in the simulation have been colour coded. Solid red shows inputs for the source fluid. Solid blue shows inputs for the sink fluid. Dashed lines shows where the HPHE Type has been bypassed straight to an Online Graphical Plotter. Purple shows outputs of the Type to an Online Graphical Plotter. Black shows an output to a data exporting Type. In Figure 106, a pink line shows where two HPHEs are connected. The components used, their respective type and description are provided in Table 27.

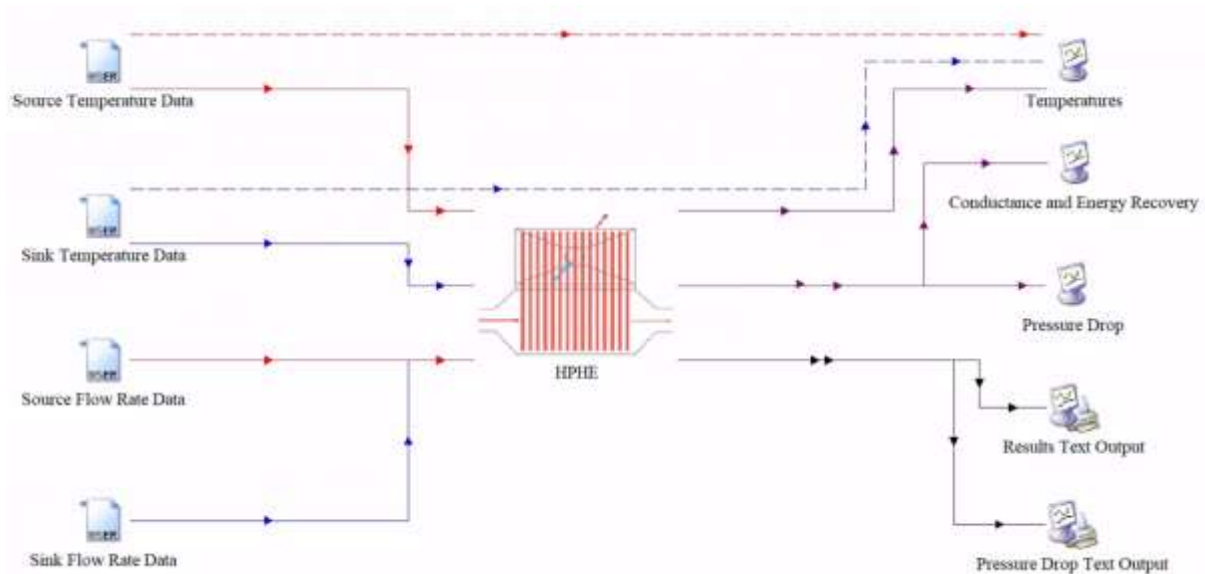


Figure 104: Model for Experiments 1 and 2.

The Types are linked by arrows. By double clicking on the lines, it opens a window where the connections can be seen. Figure 105 shows an example of these connections between the HPHE and the Temperatures Online Graphical Plotter.

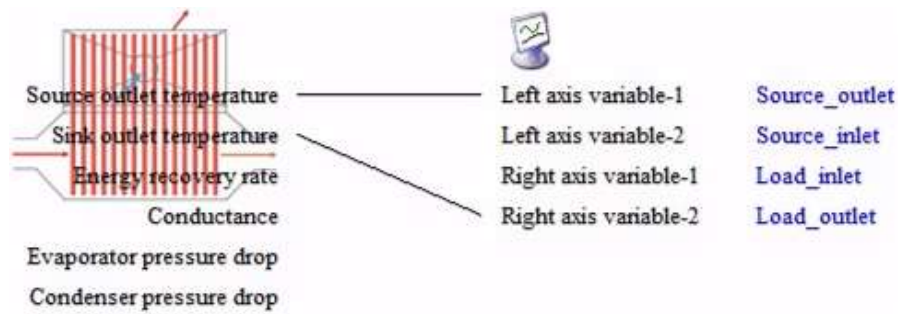


Figure 105: Connection between HPHE and Temperatures online graphical plotter.

Figure 106 shows the model for Experiment 3. There were two different types of finning present in the unit and two different working fluids in the thermosyphons. Therefore, this was modelled by treating the unit as two separate heat exchangers when, in reality, they were combined in one unit. An alteration was required as the inlet and outlet data could not be input into the same exchanger as it was counterflow. This was overcome by attaching the two components where the outputs of each HPHE is treated as inputs for the other. This is because the source fluid enters the Dowtherm A HPHE first, the sink fluid enters the water HPHE first.

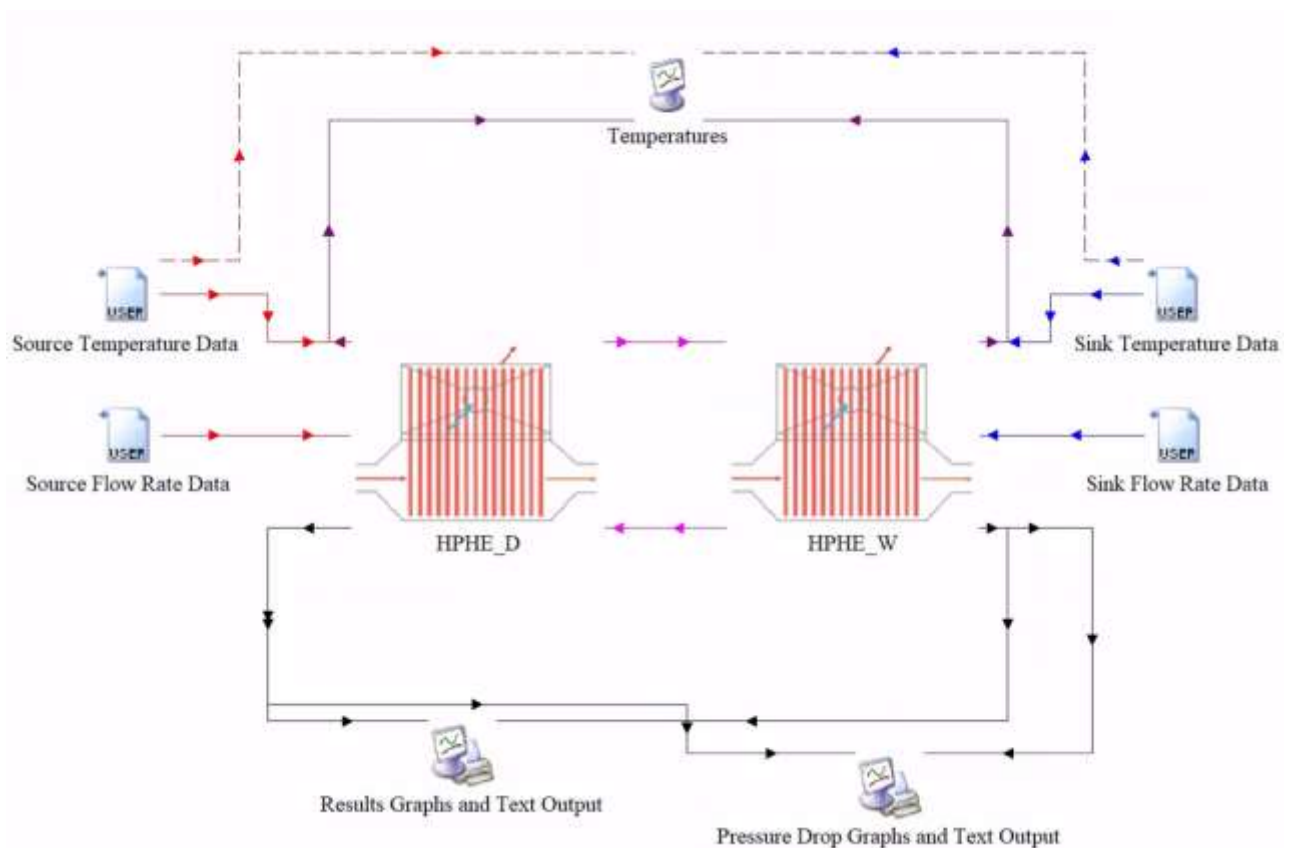

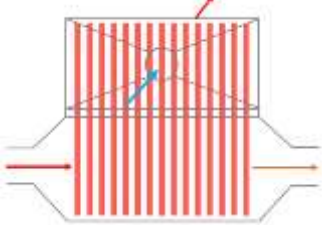




Figure 106: Model for Experiment 3.

Table 27: Components and types used in the simulations.

Component	Type	Description
	Type9a	Data reader for generic data files
	Type204	HPHE component
	Type65d	Online graphical plotter
	Type65c	Online graphical plotter with file output

5.3. Model Limitations

There are several limitations to this model. Firstly, it does not consider start-up of the heat pipes. It assumes start-up is achieved and the heat pipes are operational. In saying this, the model is used to determine recovered heat energy in a process system that would be operational, so start-up is not essential.

Secondly, HPHEs have thermal inertia. For example, there is residual heat in the casing of the HPHE and the heat pipes themselves that will be transferred to the sink fluid if the source stream is cooling down. Axial conduction through the heat pipe and conduction through the separation plate is also present. These factors are not taken into account. This means the model adapts more quickly than what would occur in reality and some heat transfer paths are not included.

The model assumes perfect insulation whereas the HPHE loses heat through the casing. As such, the model can seemingly underpredict the performance of the heat source stream or overpredict the performance of the heat sink stream. It is possible to predict temperature loss

from the HPHE casing based on the design parameters. However, it was deemed unnecessary as many additional parameters would have to be input and would make the model much more cumbersome for little return.

Currently, only helical finning is available as an option, whereas, in reality, other configurations are possible and have been presented in Chapter 3. Future work can be undertaken to validate other configurations, and the code can be updated accordingly.

6. EXPERIMENTAL AND THEORETICAL RESULTS AND DISCUSSION

This chapter presents and discusses the experimental and simulation results of experiments conducted on the three HPHE configurations and applications. The first section discusses the exhaust-to-water HPHE applied to the laboratory-scale ceramic kiln. Graphs are provided to show temperature outlet predictions from simulation against the experimental results for both the heat source and sink for each test condition. For both the simulation and experiment, the inlet and outlet temperatures and mass flow rates were identical. The heat transfer rate of the experiments is also plotted against the simulation, which is then compared. Further results from TRNSYS are given for the corresponding theoretical conductance value. Error analysis was conducted on each individual test's results showing the difference in predicted to actual heat transfer rate. Then, a combined analysis for the entire experiment is given on heat transfer rate and also temperature predictions. Pressure drop was not included as this could not be validated, though an example of the capability is given for test condition 9 of Experiment 1. Afterwards, an overall analysis on the experiment is conducted, including a statistical analysis, which displays that the experiment was conducted correctly and the results obtained were statistically significant.

The second and third sections present and discuss the results of the full-scale exhaust-to-air HPHEs applied to the full-scale ceramic kiln and then the aluminium heat treatment furnace. The same analysis is conducted as with the laboratory-scale experiment but with the added analysis on pressure drop for Experiment 3.

6.1. Experiment 1: Laboratory-Scale Ceramic Kiln

In the subsections below are the experimental and simulation results for each test condition of Experiment 1, as highlighted in Table 20 in Section 4.2.3. The sampling rate was 10 seconds for all tests except tests 4 and 5, which was 5 seconds. The water flow rate is not presented in SI units but as $\text{kg}\cdot\text{hr}^{-1}$ as is more pragmatic. The corresponding fan speed to measured mass flow rate is presented in each section.

6.1.1. Test 1

Figure 107 shows an example of the graphical output produced by TRNSYS for the temperature inlet and outlet predictions for the case of test 1. However, it was difficult to compare the simulation results against the experimental results from separate graphs. Therefore, the individual output data points of the simulation were plotted together with experimental results to produce a graph akin to Figure 108 to aid comparison. Similar TRNSYS graphs were produced for each test condition but only the combined comparison graphs have been presented to avoid unnecessary duplication of results, presented differently.

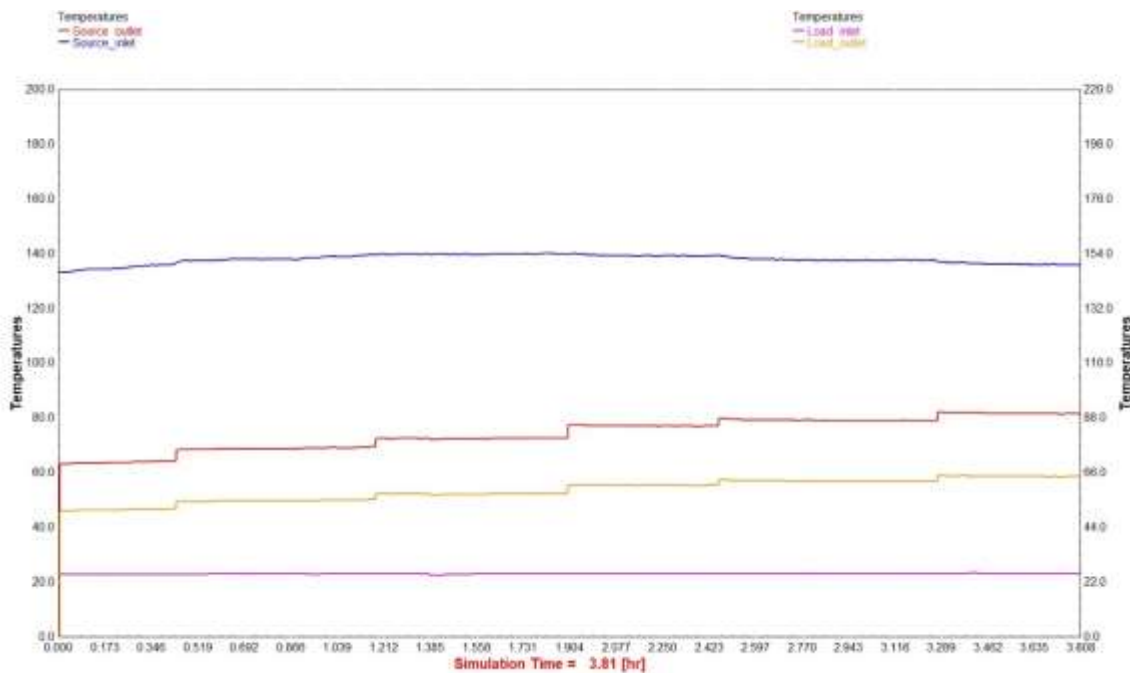


Figure 107: TRNSYS temperature output results for test 1.

Figure 108 shows the results of test 1 where the exhaust gases temperature was maintained at around 135°C and the water sink at 480 kg.hr⁻¹ over a 228-minute period. Fan speeds from 25 to 50 Hz in intervals of 5 Hz were trialled with corresponding exhaust mass flow rates between 654 and 1,284 kg.hr⁻¹.

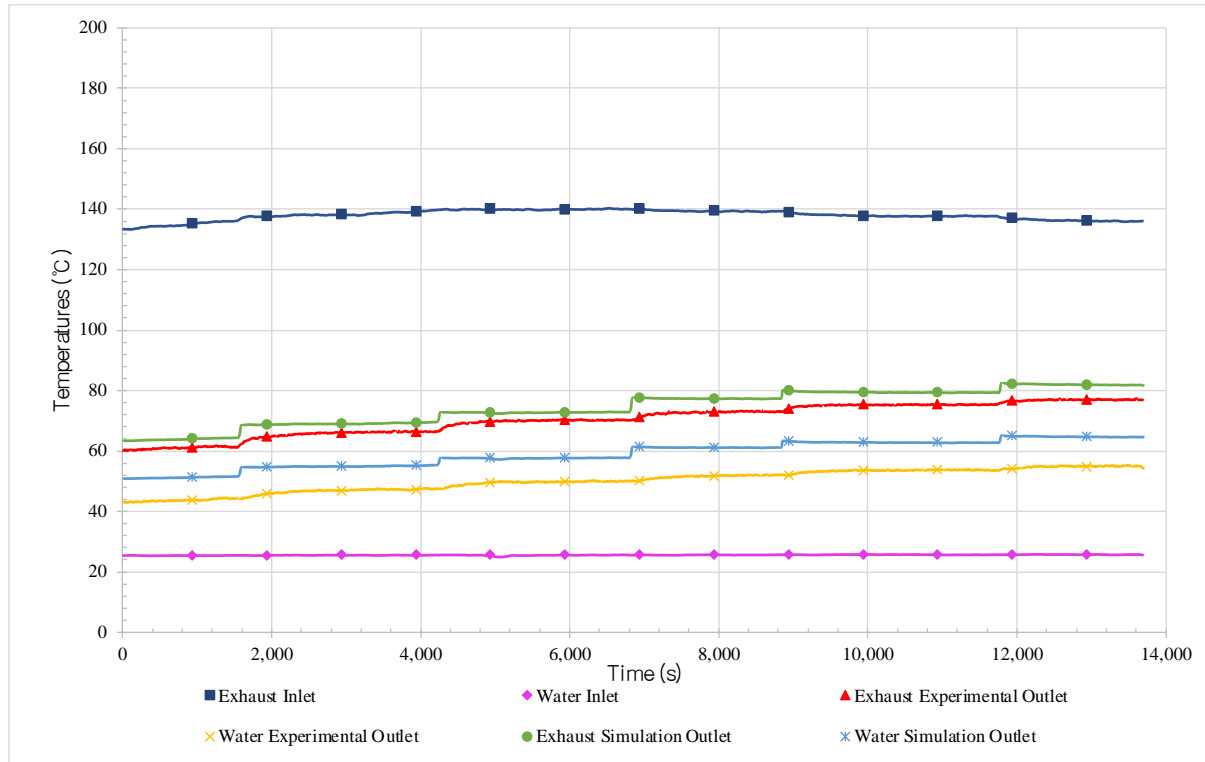


Figure 108: Transient results of test 1 showing the experimental and simulated inlet and outlet temperatures of water and exhaust streams.

As the fan speed increased, the water outlet temperature increased as more heat energy was recovered. As a higher mass flow rate of exhaust gases were directed through the heat exchanger the exhaust outlet temperature also increased. The water inlet temperature was very consistent, averaging 25.6°C. Overall, the simulation predicted a higher water outlet temperature in comparison to the experimental outlet temperature results. The results for the average temperatures and mass flow rates for test 1 are summarised for each time period and condition in Table 28. As the mass flow rate of exhaust gases increased, the outlet temperature of the exhaust increased from around 61.0 to 76.9°C, whereas the simulation predicted 63.9 to 81.9°C. The water outlet temperature was increased to between 43.6 and 54.7°C, experimentally, and 51.3 to 64.8°C by simulation.

Table 28: Test 1 average results summary.

Exhaust Gases					Water			
Fan Speed (Hz)	T _{in} (°C)	Experiment T _{out} (°C)	Simulation T _{out} (°C)	\dot{m} (kg.h ⁻¹)	\dot{m} (kg.h ⁻¹)	T _{in} (°C)	Experiment T _{out} (°C)	Simulation T _{out} (°C)
25	134.98	60.98	63.93	654	480	23.45	43.64	51.28
30	138.42	65.70	69.02	762		25.54	46.66	54.97
35	140.03	69.80	72.72	858		25.53	49.46	57.69
40	139.55	72.64	77.31	1,026		25.63	51.44	61.21
45	138.03	75.17	79.37	1,137		25.72	53.35	62.88
50	136.44	76.88	81.90	1,284		25.75	54.69	64.77

Figure 109 shows the calculated heat transfer rates for test 1 of both the experimental exhaust and water results in comparison to the simulation predictions. The red line, blue line and black line show the experimental exhaust, experimental water and simulation heat transfer rates, respectively. This colour coding is consistent across the graphs presented for each test.

Theoretically, an operating idealised heat exchanger should follow:

$$\dot{q}_{in} = \dot{q}_{out} \tag{6.1}$$

Therefore, there is only one simulation heat transfer rate. However, because there was a reasonable difference in the experimental system heat transfer rate results for the evaporator and condenser sections, both have been presented. The heat transfer rate depends on a multitude of factors, including: the mass flow rate, specific heat capacity and the difference in temperature. In this case, the simulation follows more closely the exhaust heat transfer rate than that from the water heat transfer rate. This has been attributed to potentially larger errors in the water mass flow rate measurement or increased heat losses through the casing from the condenser section as there is a higher conduction and convection heat transfer coefficient between water and the casing than for the exhaust gases and the casing. Therefore, the experimental water heat transfer rate was lower as the temperature difference between the

water inlet temperature and outlet temperature was lower than would be without thermal losses. This was not an anomaly but was consistently seen across all tests for Experiment 1. Water has a higher density, thermal conductivity, specific heat capacity and viscosity, which affect the heat transfer coefficients. The simulation matched more closely the results of the exhaust compared to the water, which was the case for all tests. For the exhaust heat transfer rate, the simulation underperformed in comparison to the experimental heat transfer rate but only in the order of a few kW. Usually, energy lost from a system is given a negative sign and energy gained has a positive sign, as heat is lost from the heat source stream and gained by the heat sink stream. However, for ease of comparison, both have been presented as positive.

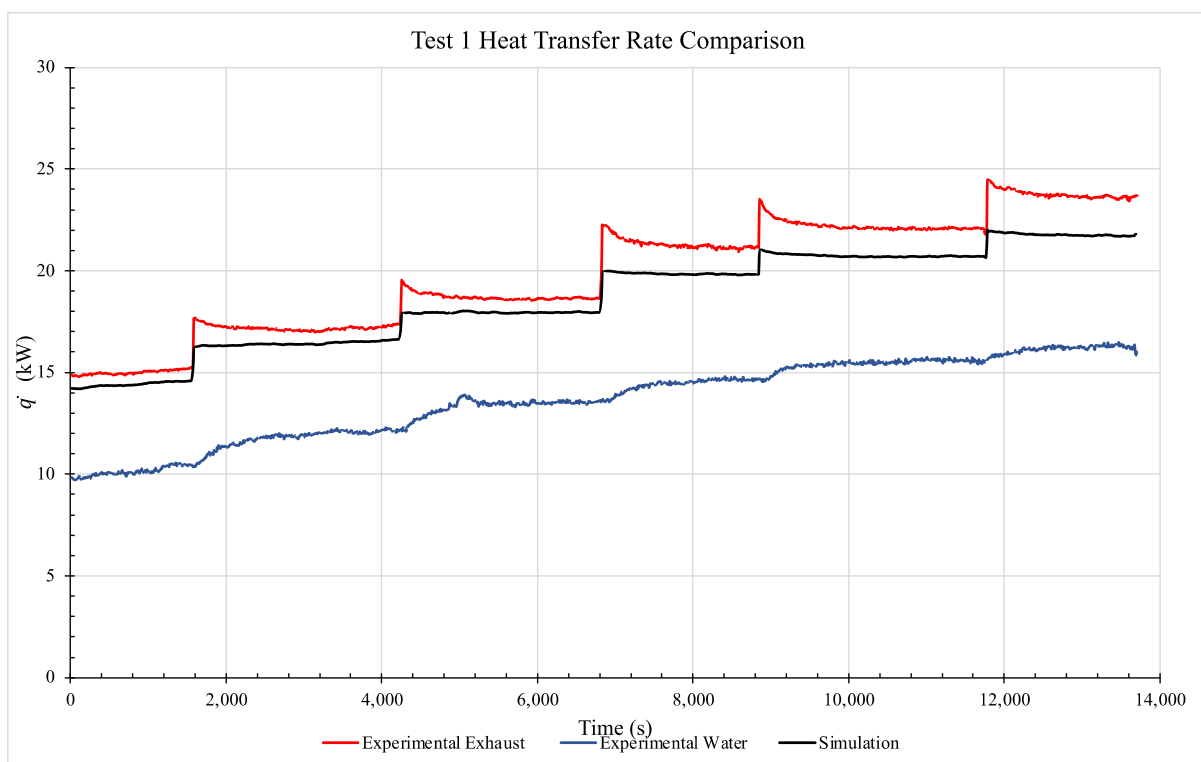


Figure 109: Heat transfer rate comparison for test 1 exhaust, water and simulation.

Figure 110 shows a comparison in the heat transfer rate between that from the experimental exhaust flow and the simulation for test 1. Due to the differences in results for heat transfer rate observed between the source and sink fluids, the exhaust heat transfer rate has been presented as it is a more accurate representation of the results. It is seen for this test that the experiment outperformed the simulation. As the exhaust mass flow rate increased, the heat transfer rate increased and the prediction was seen to deviate slightly further away from the experimental results.

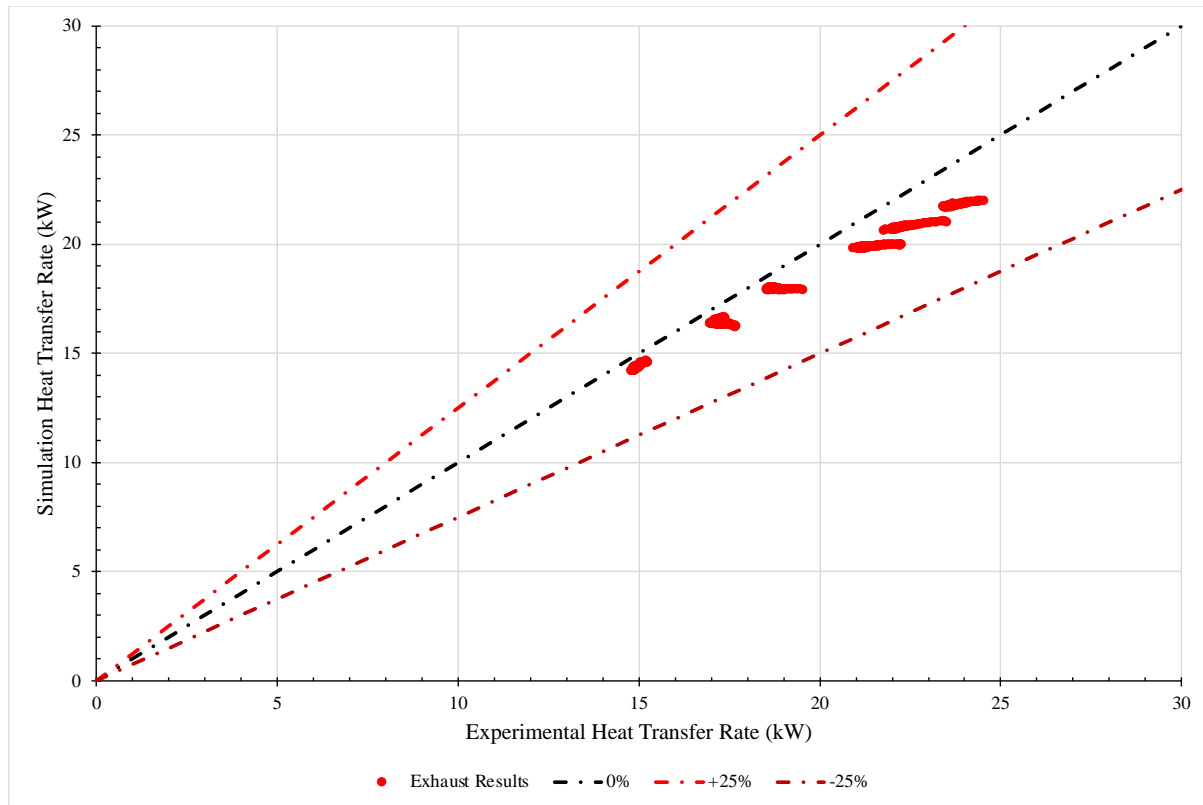


Figure 110: Heat transfer rate comparison for test 1 experimental against simulation results.

For each test condition, an error analysis was conducted on the heat transfer rate and outlet temperatures between simulation and experimental results. An overall analysis was then conducted for the combined experiment to give an indication of the accuracy of the model. These analyses are presented in Section 6.1.11.

6.1.2. Test 2

Figure 111 shows the exhaust and water inlet and outlet temperatures of the system over a 305-minute period. The exhaust gases inlet temperature was maintained at around 230°C and the water heat sink mass flow rate at 480 kg.hr⁻¹. 25 to 50 Hz fan speeds in increments of 5 Hz were tested to vary the mass flow rate of exhaust gases through the HPHE. The mass flow rate of the exhaust ranged from 595 to 1,094 kg.hr⁻¹.

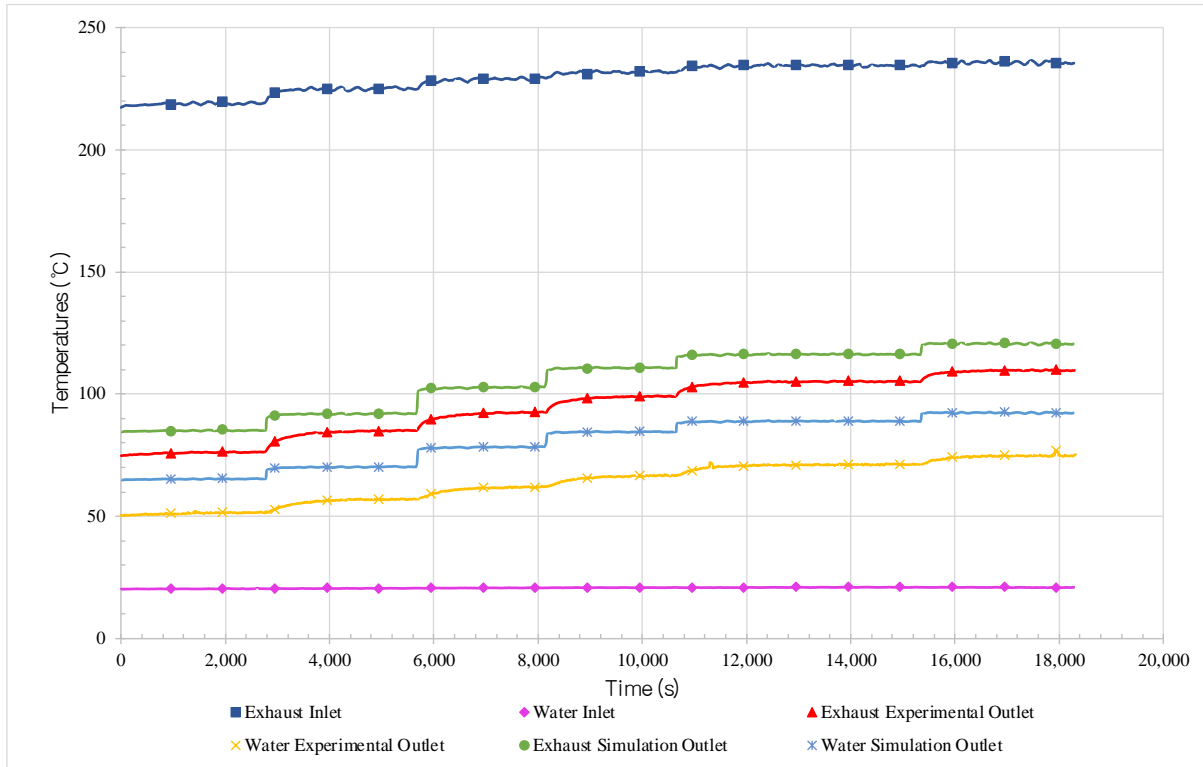


Figure 111: Transient results of test 2 showing the experimental and simulated inlet and outlet temperatures of water and exhaust streams.

It is seen from Figure 111 that, as the frequency of the fan speed is increased, the inlet and outlet temperatures of the exhaust gases increased. Furthermore, the temperature of the water outlet increased as the inlet water temperature remained fairly constant. At these higher temperatures, higher water and exhaust outlet temperatures were seen.

The average temperature results and mass flow rates for test 2 are summarised for each time period and condition in Table 29. As the mass flow rate of exhaust gases increased, the outlet temperature of the exhaust gases increased from around 75.9 to 109.3°C, the simulation predicted 85.0 to 120.6°C. The water outlet temperature was increased to between 51.2 and 74.3°C, experimentally, and 65.2 to 92.3°C by simulation.

Table 29: Test 2 average results summary.

Exhaust Gases					Water			
Fan Speed (Hz)	T _{in} (°C)	Experiment T _{out} (°C)	Simulation T _{out} (°C)	\dot{m} (kg.h ⁻¹)	\dot{m} (kg.h ⁻¹)	T _{in} (°C)	Experiment T _{out} (°C)	Simulation T _{out} (°C)
25	218.77	75.91	85.01	595	480	20.31	51.18	65.21
30	224.66	83.92	91.84	661		20.47	55.98	70.08
35	228.68	91.46	102.58	806		20.67	60.95	78.20
40	231.62	98.23	110.68	929		20.80	65.74	84.48
45	234.33	104.67	116.21	1,014		20.89	70.67	88.84
50	235.65	109.29	120.60	1,094		20.88	74.30	92.33

Figure 112 shows the calculated heat transfer rates for test 2 of both the experimental exhaust and water results in comparison to the simulation predictions. There was a larger difference seen between the simulation prediction and the water heat transfer rate than in comparison to the experimental exhaust heat transfer rate. As the mass flow rate and inlet temperature of the exhaust gases increased during the experiment, both the simulation and exhaust gases heat transfer rate increased, however, a larger difference between the simulated value and the experimental value was observed. Likewise, as the experiment progressed, the water heat transfer rate increased and there was a larger difference between the simulation and experimental heat transfer rate.

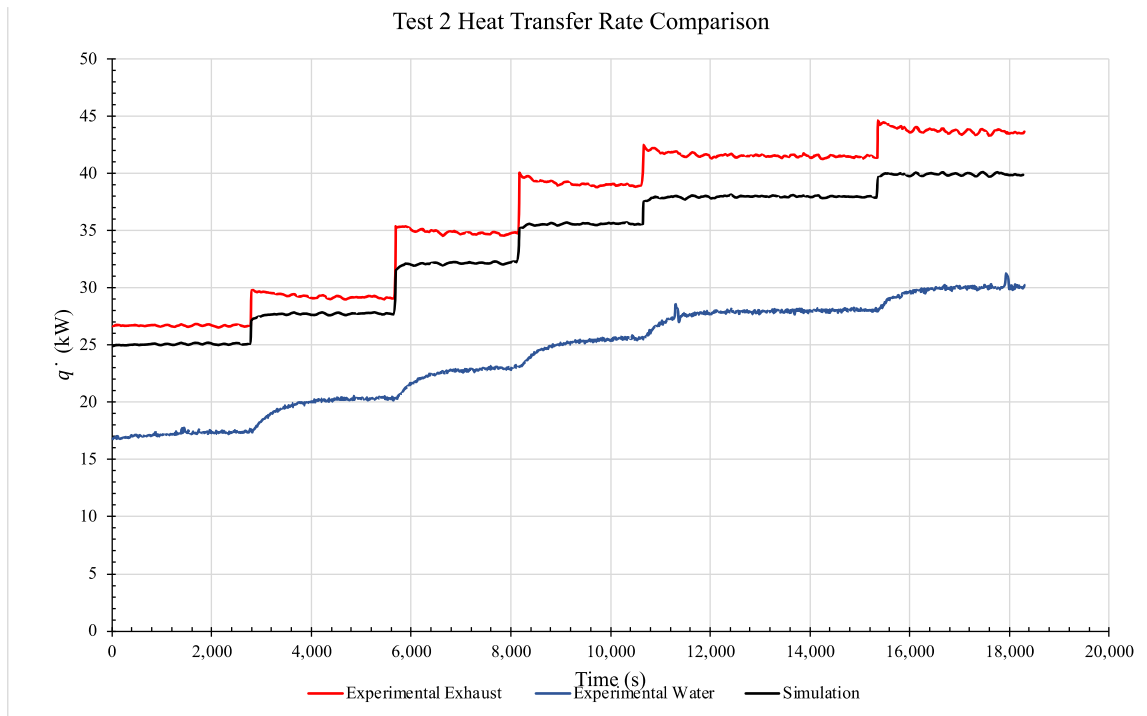


Figure 112: Heat transfer rate comparison for test 2 exhaust, water and simulation.

Figure 113 shows a comparison in the heat transfer rates for the experimental exhaust and simulation results for test 2. A reasonable underperformance in the simulation was seen for this test.

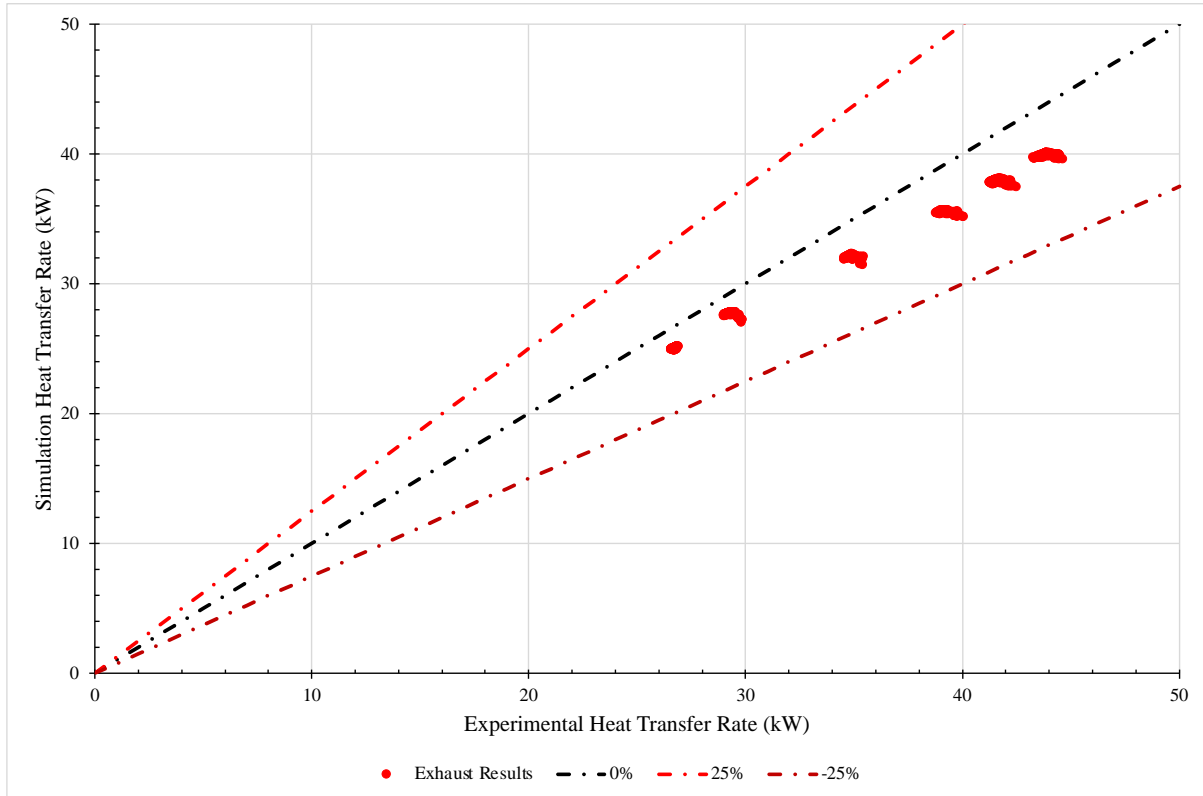


Figure 113: Heat transfer rate comparison for test 2 experimental against simulation results.

6.1.3. Test 3

Figure 114 shows the exhaust gases and water inlet and outlet temperatures of the system over the 123-minute period. The exhaust gases inlet temperature was maintained around 230°C and the water sink flow rate at 1,320 kg.hr⁻¹. 25, 35 and 50 Hz fan speeds were tested with the mass flow rate of the exhaust gases ranging from 592 to 1,132 kg.hr⁻¹.

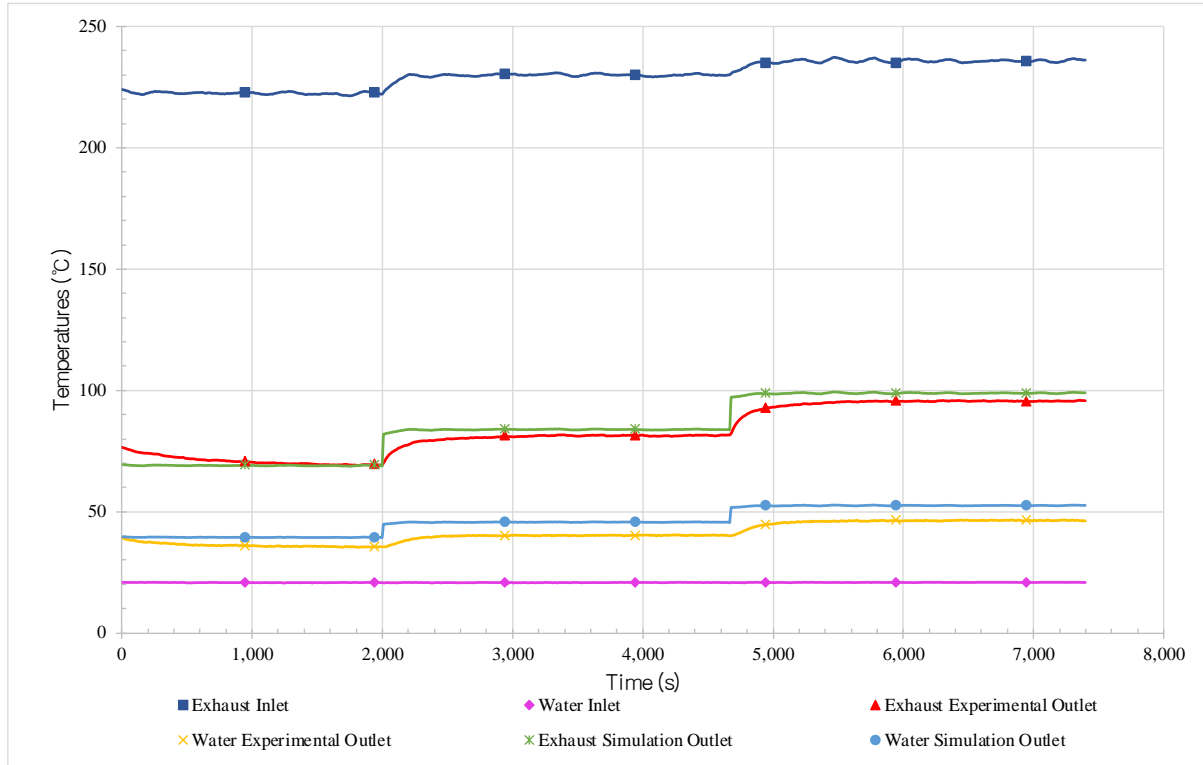


Figure 114: Transient results of test 3 showing the experimental and simulated inlet and outlet temperatures of water and exhaust streams.

The average temperature results and mass flow rates for test 3 are summarised for each time period and condition in Table 30. As the mass flow rate of exhaust gases increased, the outlet temperature of the exhaust gases increased from around 71.1 to 94.8°C, the simulation predicted 69.0 to 98.9°C. The water outlet temperature was increased to between 36.1 and 46.0°C, experimentally, and 39.3 to 52.6°C by simulation.

Table 30: Test 3 average results summary.

Exhaust Gases					Water			
Fan Speed (Hz)	T _{in} (°C)	Experiment T _{out} (°C)	Simulation T _{out} (°C)	\dot{m} (kg.h ⁻¹)	\dot{m} (kg.h ⁻¹)	T _{in} (°C)	Experiment T _{out} (°C)	Simulation T _{out} (°C)
25	222.58	71.08	69.04	592	1,320	20.68	36.14	39.30
30	229.73	80.55	83.86	832		20.68	39.88	45.61
50	235.47	94.75	98.93	1,132		20.72	45.97	52.57

Figure 115 shows the calculated heat transfer rates for test 3 of both the experimental exhaust and water results in comparison to the simulation predictions. The simulation here followed the experimental exhaust heat transfer rate results very closely. There was a similar exhaust inlet temperature to test 2 but the mass flow rate of water was higher.

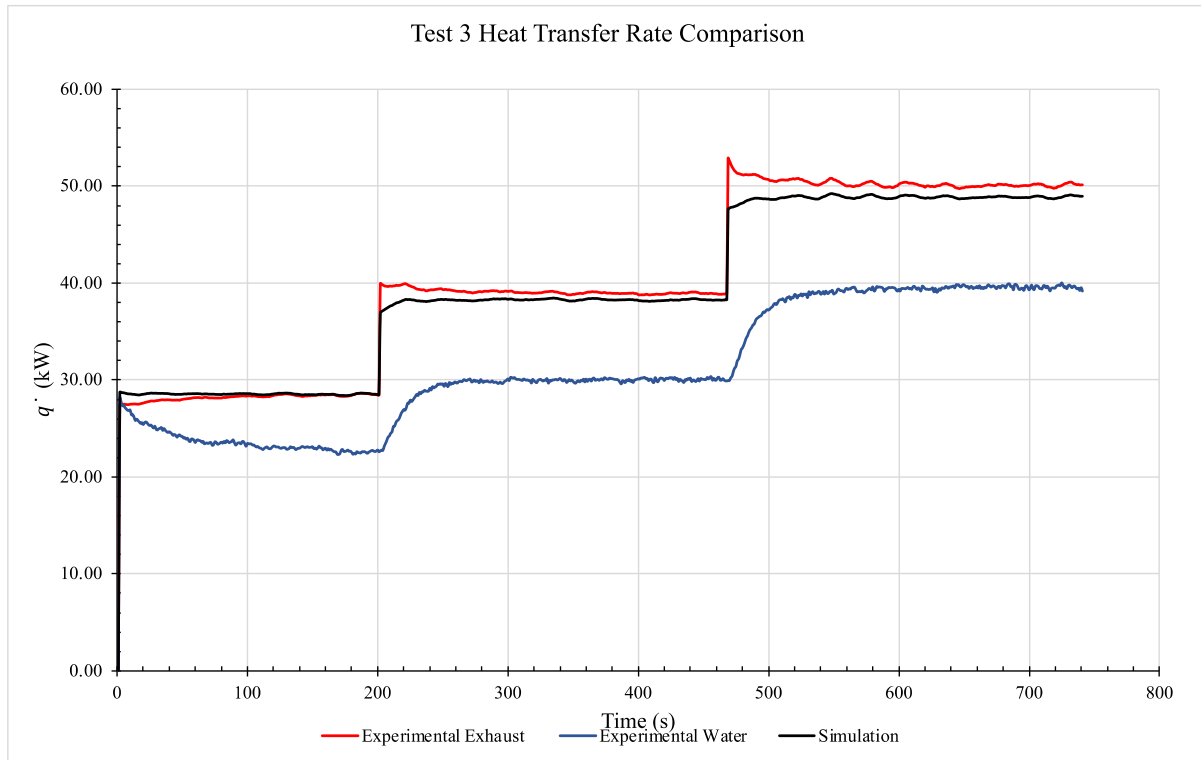


Figure 115: Heat transfer rate comparison for test 3 exhaust, water and simulation.

Figure 116 shows a comparison in the heat transfer rates for the experimental exhaust and simulation results for test 3. At the lower exhaust mass flow rates, the simulation agreed very well with the experimental results. An initial slight overprediction was seen which then fell to an underprediction. Overall, an accurate prediction is seen for this test.

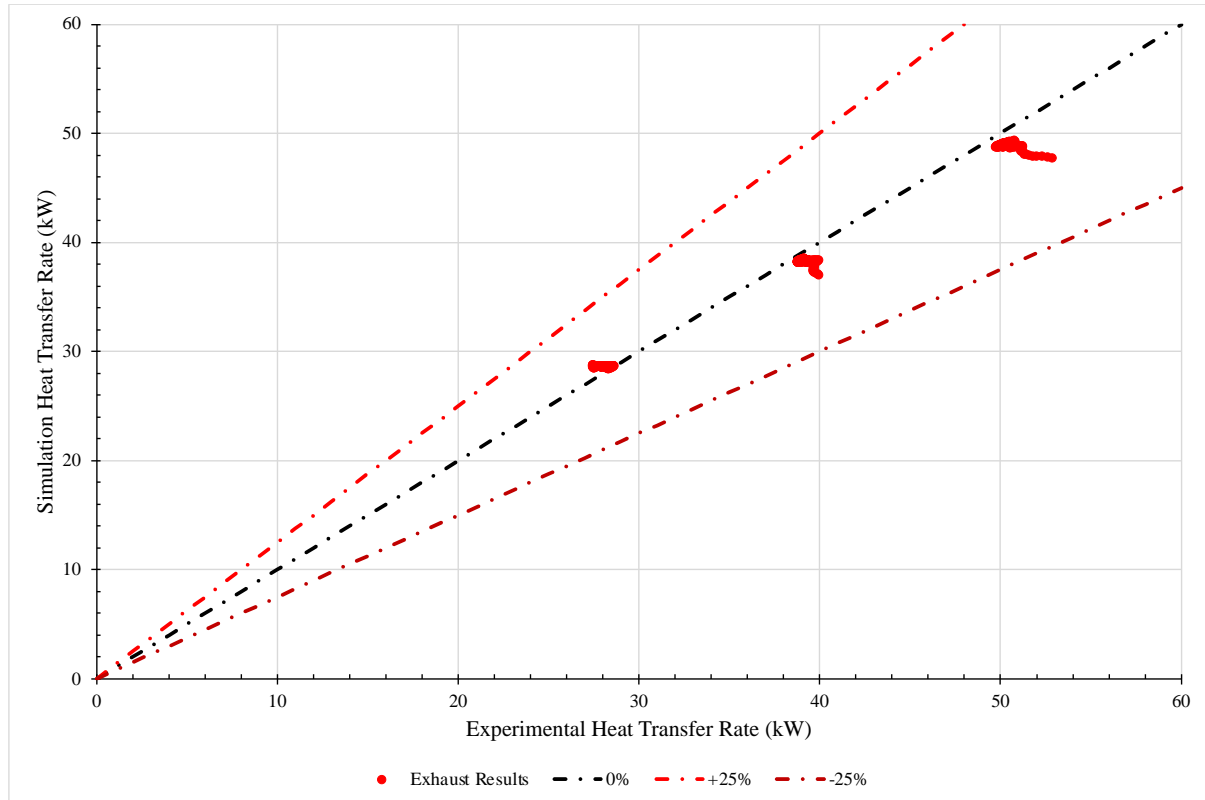


Figure 116: Heat transfer rate comparison for test 3 experimental exhaust and simulation results.

6.1.4. Test 4

Figure 117 shows inlet and outlet temperatures for the exhaust gases and water over a 206-minute period. The exhaust gases inlet temperature was maintained at around 265°C and the water sink flow rate at 480 kg.hr⁻¹. 25 to 45 Hz fan speeds in increments of 5 Hz were tested with corresponding exhaust gases mass flow rates ranging from 633 to 1,027 kg.hr⁻¹. With Experiment 4, the test conditions were not measured continuously as with the previous experiments; for this reason, the data for the different conditions were spliced when relevant conditions were seen.

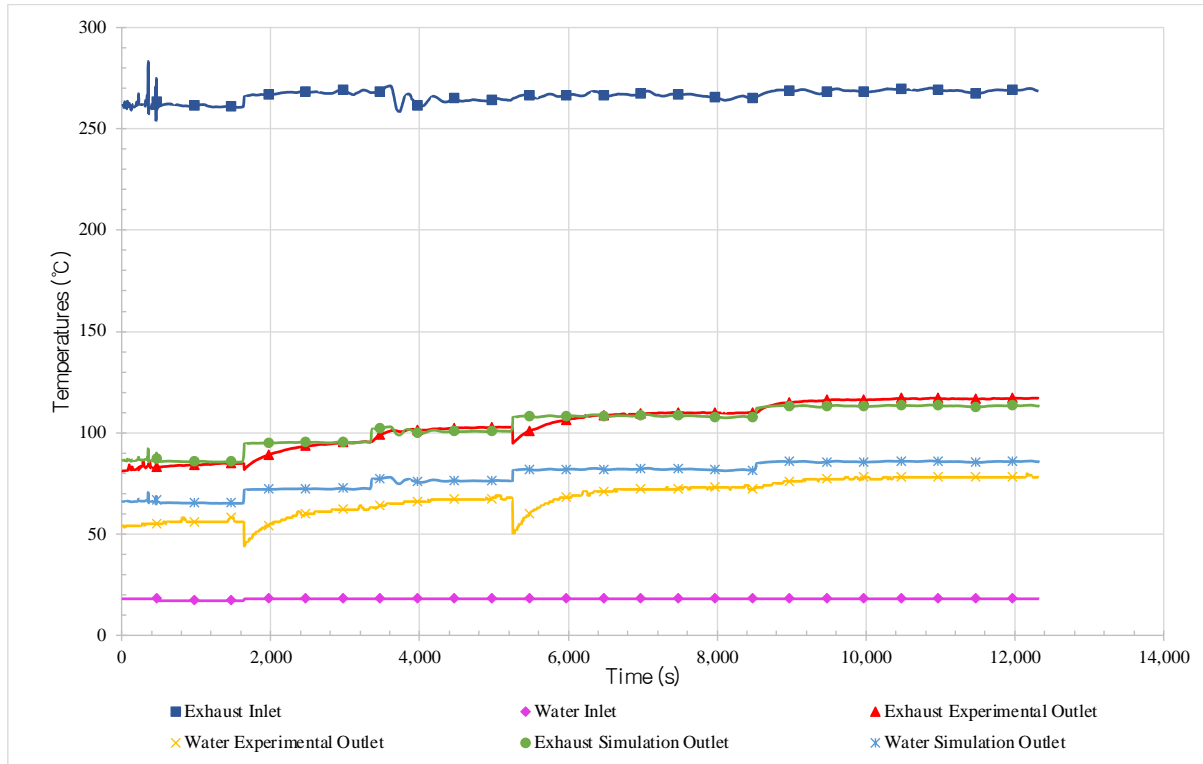


Figure 117: Transient results of test 4 showing the experimental and simulated inlet and outlet temperatures of water and exhaust streams.

The average temperature results and mass flow rates for test 4 are summarised for each time period and condition in Table 31. As the mass flow rate of exhaust gases increased, the outlet temperature of the exhaust gases increased from around 83.7 to 116.1°C, the simulation predicted 86.0 to 113.2°C. The water outlet temperature increased to between 55.6 and 77.3°C, experimentally, and 65.5 to 85.7°C by simulation.

Table 31: Test 4 average results summary.

Exhaust Gases					Water			
Fan Speed (Hz)	T _{in} (°C)	Experiment T _{out} (°C)	Simulation T _{out} (°C)	\dot{m} (kg.h ⁻¹)	\dot{m} (kg.h ⁻¹)	T _{in} (°C)	Experiment T _{out} (°C)	Simulation T _{out} (°C)
25	261.55	83.67	85.95	484	480	17.31	55.61	65.54
30	267.76	92.09	95.10	552		18.00	58.25	72.20
35	264.75	101.55	100.84	626		18.00	66.35	76.37
40	266.49	107.66	108.14	708		18.00	69.67	81.84
45	268.86	116.11	113.19	763		18.00	77.27	85.70

Figure 118 shows the calculated heat transfer rates for test 4 of both the experimental exhaust and water results in comparison to the simulation predictions. As mentioned, these results were spliced from different time periods when the testing was conducted. It shows that splicing the data is not the most effective way of obtaining valid results. However, even though the condenser section was still stabilising, interestingly, the predictions for the exhaust heat transfer rate were very accurate. The sections where splicing occurred could have been performed at more similar water outlet temperature values, leading to simulated water outlet temperature predictions more similar to experimental values. Performing the analysis in this manner has shown that the reaction time of the exhaust gases outlet temperature, the speed at which the evaporator section can react to changing load, is faster than for the condenser section. Also, removing these data would have led to an overall reduction in data points for this test condition.

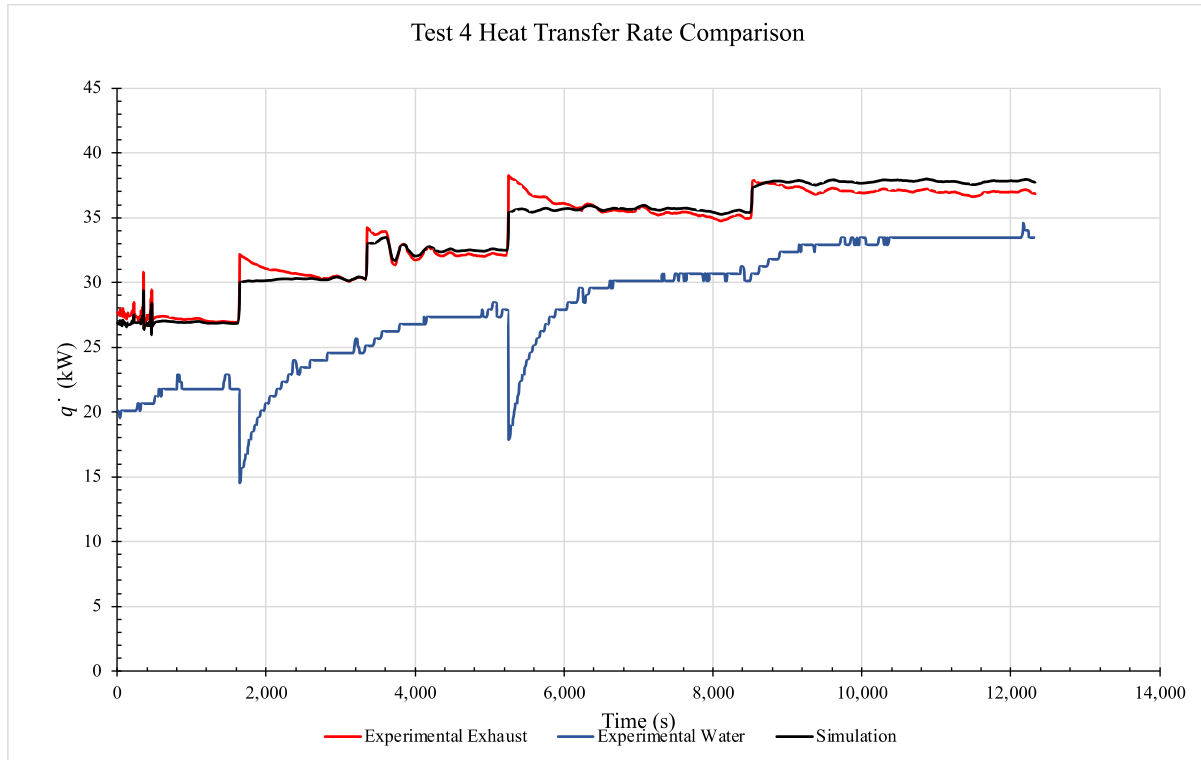


Figure 118: Heat transfer rate comparison for test 4 exhaust, water and simulation.

Figure 119 shows a comparison in the heat transfer rate between that from the experimental exhaust flow and the simulation for test 4. This test had a sampling rate of 5 seconds so it was interesting to see how the simulation would perform in comparison to other tests with a less frequent sampling rate. Test 4 had the tightest pattern between experimental exhaust and simulation heat transfer rates showing a very good agreement. This was unexpected due to this test having the highest exhaust gases inlet temperature condition. However, the HPHE was designed to recover heat from an exhaust inlet temperature of 258°C so was more in keeping with the design parameters.

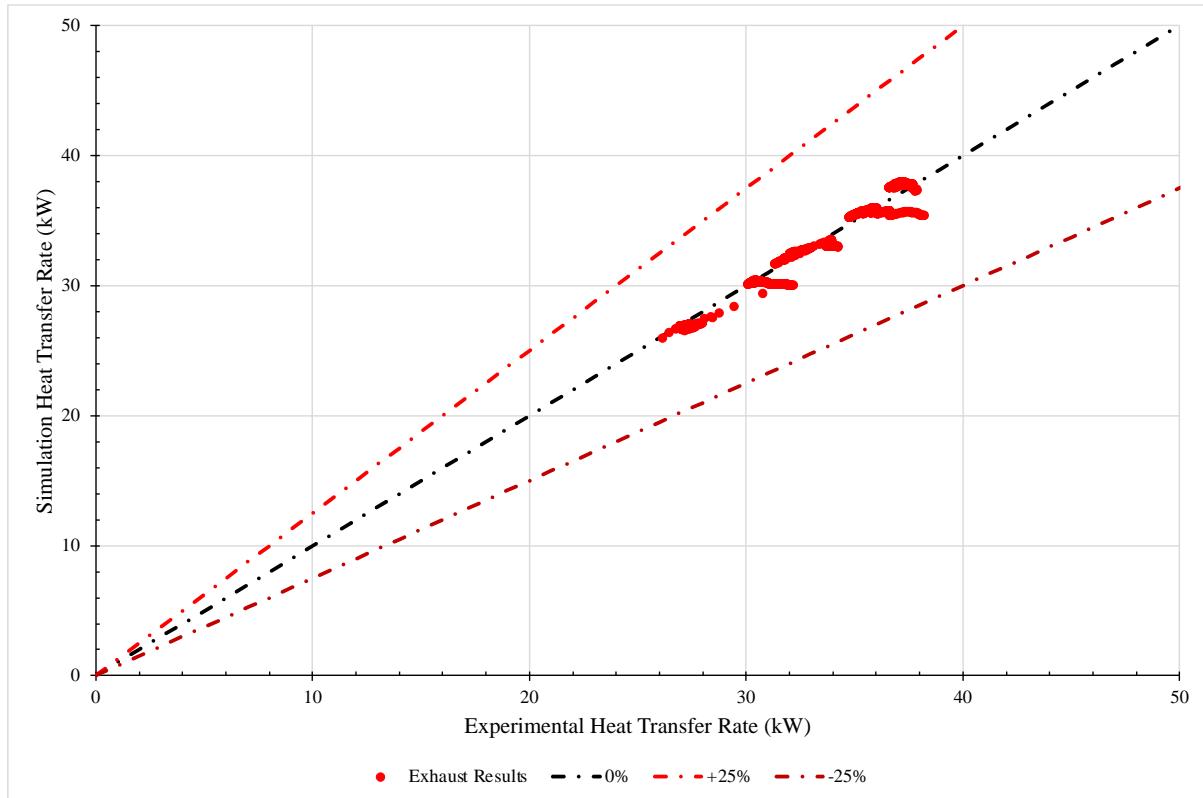


Figure 119: Heat transfer rate comparison for test 4 experimental against simulation results.

6.1.5. Test 5

Figure 120 shows the exhaust gases and water inlet and outlet temperatures of the system over a 110-minute period. The exhaust gases inlet temperature was maintained at around 265°C and the water sink mass flow rate at $1,320 \text{ kg}\cdot\text{hr}^{-1}$. 25, 35, 45 and 50 Hz fan speeds were tested. The mass flow rate of the exhaust gases ranged from 612 to $1,180 \text{ kg}\cdot\text{hr}^{-1}$. As with Experiment 4, Experiment 5 conditions were not experienced in one continuous time period. For this reason, the data were spliced from the desirable monitored period. This explains the spikes when transitioning between fan speed values seen in Figure 120.

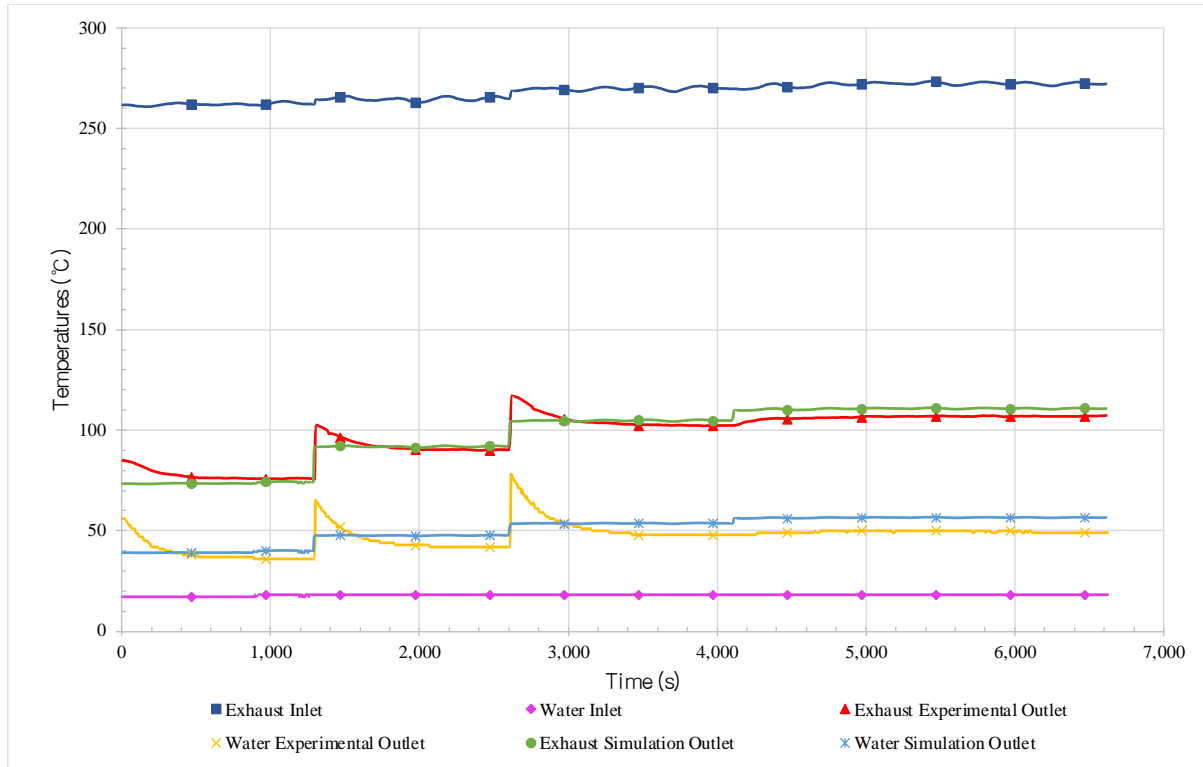


Figure 120: Transient results of test 5 showing the experimental and simulated inlet and outlet temperatures of water and exhaust streams.

The average temperature results and mass flow rates for test 5 are summarised for each time period and condition in Table 32. As the mass flow rate of exhaust gases increased, the outlet temperature of the exhaust gases increased from around 77.5 to 106.3°C, the simulation predicted 73.8 to 110.5°C. The water outlet temperature increased to between 39.2 and 49.4°C, experimentally, and 39.4 to 56.4°C by simulation.

Table 32: Test 5 average results summary.

Exhaust Gases					Water			
Fan Speed (Hz)	T _{in} (°C)	Experiment T _{out} (°C)	Simulation T _{out} (°C)	\dot{m} (kg.h ⁻¹)	\dot{m} (kg.h ⁻¹)	T _{in} (°C)	Experiment T _{out} (°C)	Simulation T _{out} (°C)
25	261.98	77.50	73.81	570	1,320	17.27	39.23	39.41
30	264.59	92.25	91.81	829		18.00	45.44	47.61
40	269.63	104.71	104.65	1,040		18.00	52.21	53.55
45	271.83	106.32	110.53	1,147		18.00	49.44	56.38

Figure 121 shows the calculated heat transfer rates for test 5 of both the experimental exhaust and water results in comparison to the simulation predictions. The same issue with splicing is seen as in the results for test 4. The simulation reacts very quickly and follows the experimental exhaust heat transfer rate results but the water heat transfer rate saw large discrepancies. It also shows how the condenser section is slower to react to changing load and to stabilise, as seen in test 4. The final condition was not spliced and a heat transfer rate was more in keeping with the simulation straight away.

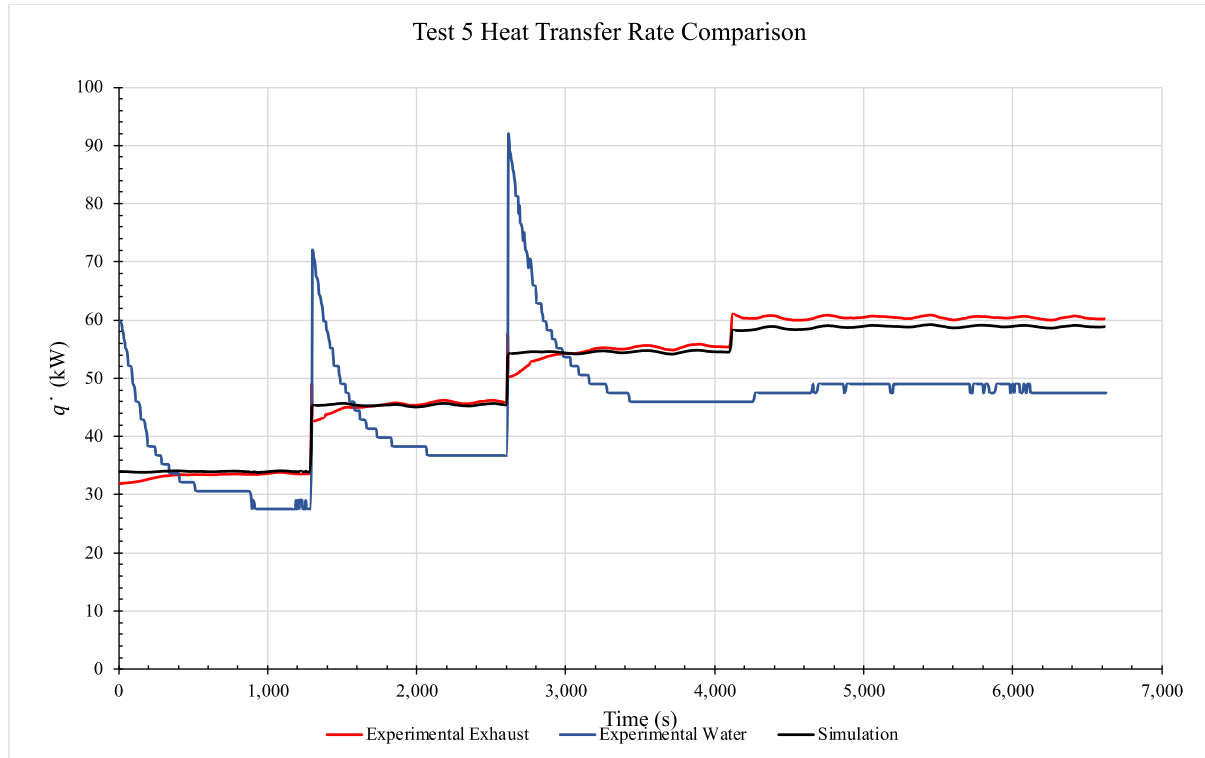


Figure 121: Heat transfer rate comparison for test 5 exhaust, water and simulation.

Figure 122 shows a comparison in the heat transfer rate between values from experimental exhaust conditions and simulation for test 5. Again, a sampling rate of 5 seconds was used for this test and the conditions were closest to the design parameters of the HPHE. A very good agreement was seen, with a slight overprediction seen, initially. As the mass flow rate of exhaust increased, an underprediction then occurred, which is in keeping with the other test conditions.

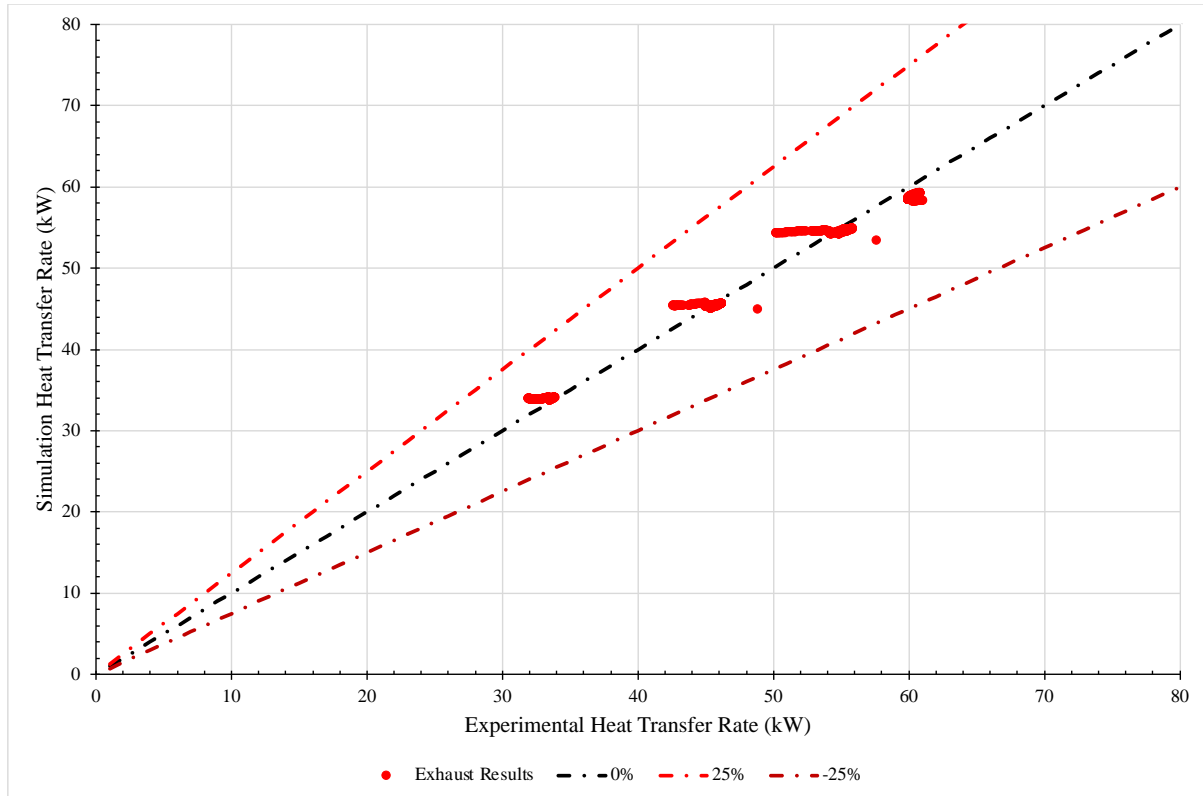


Figure 122: Heat transfer rate comparison for test 5 experimental against simulation results.

6.1.6. Test 6

Figure 123 shows the results of test 6 where the exhaust gases inlet temperature was maintained at around 140°C and the water sink mass flow rate at 480 kg.hr⁻¹ over a 108-minute period. Fan speeds at 25, 35, 45 and 50 Hz were trialled with corresponding exhaust gases mass flow rates between 609 and 1,224 kg.hr⁻¹.

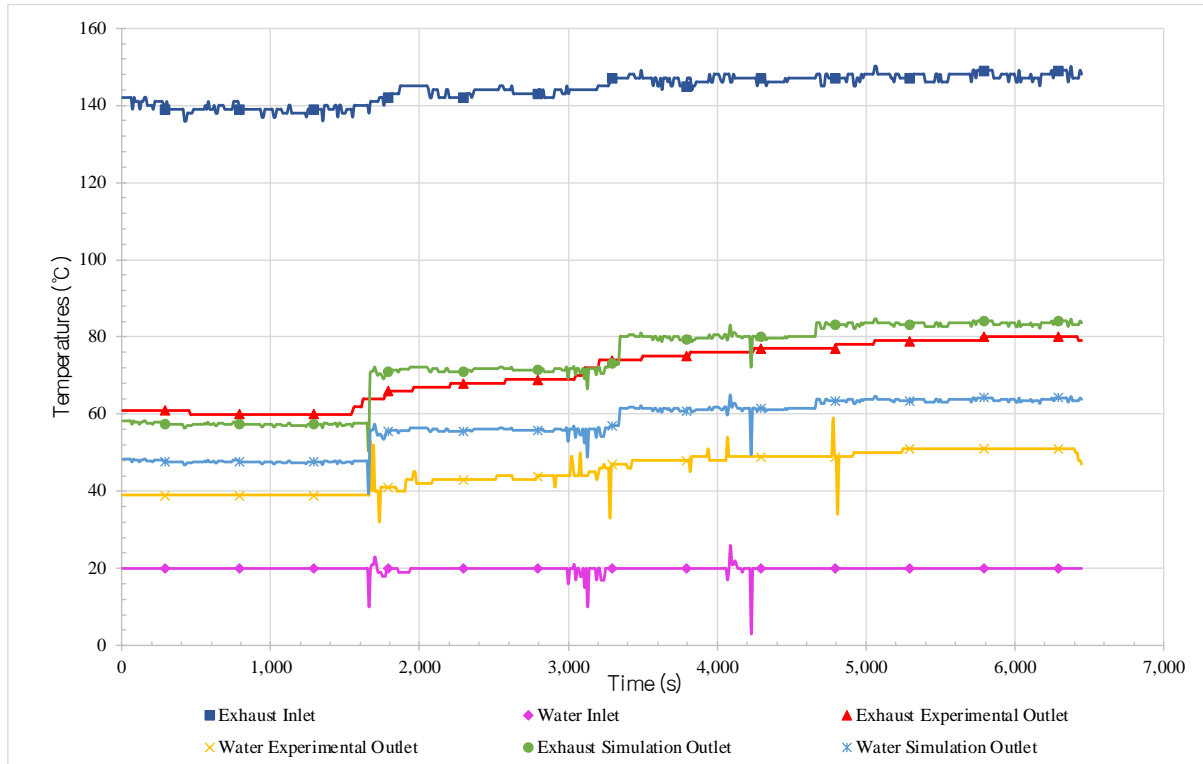


Figure 123: Transient results of test 6 showing the experimental and simulated inlet and outlet temperatures of water and exhaust streams.

The average temperature results and mass flow rates for test 6 are summarised for each time period and condition in Table 33. As the mass flow rate of exhaust gases increased, the exhaust outlet temperature increased from around 60.5 to 79.1°C, the simulation predicted 57.5 to 83.5°C. The water outlet temperature was increased to between 39.0 and 50.4°C, experimentally, and 47.6 to 63.8°C by simulation.

Table 33: Test 6 average results summary.

Exhaust Gases					Water			
Fan Speed (Hz)	T _{in} (°C)	Experiment T _{out} (°C)	Simulation T _{out} (°C)	\dot{m} (kg.h ⁻¹)	\dot{m} (kg.h ⁻¹)	T _{in} (°C)	Experiment T _{out} (°C)	Simulation T _{out} (°C)
25	139.28	60.47	57.48	609	480	19.94	39.00	47.62
35	143.58	68.48	71.56	900		19.71	43.32	55.83
45	146.64	75.85	80.04	1,115		19.92	48.49	61.37
50	147.55	79.07	83.54	1,224		20.00	50.44	63.75

Figure 124 shows the calculated heat transfer rates for test 6 of both the experimental exhaust and water results in comparison to the simulation predictions. This test saw noise in the data collection of the water inlet temperature. This was not seen in any of the other tests, where the water inlet temperature was extremely stable. Hence it is believed to be an issue with the thermocouple or, more likely, the data-logger. This could have been artificially smoothed but has been reported as collected. Interestingly, at 25 Hz, the simulation outperformed the experimental heat transfer rate, but after the fan speed was increased the simulation underperformed, as expected. Tests 6 to 9 were conducted over a year after tests 1 to 5, due to Covid-19, and the exhaust inlet temperature showed a greater instability than the smooth exhaust inlet temperatures seen in previous experiments. This was only in the order of a few degrees Celsius but caused a more fluctuating heat transfer rate in the order of a few hundred Watts for each condition. The reason for this fluctuation was that the temperature data collected were rounded to the nearest whole number, which was not the case for the previous experiments.

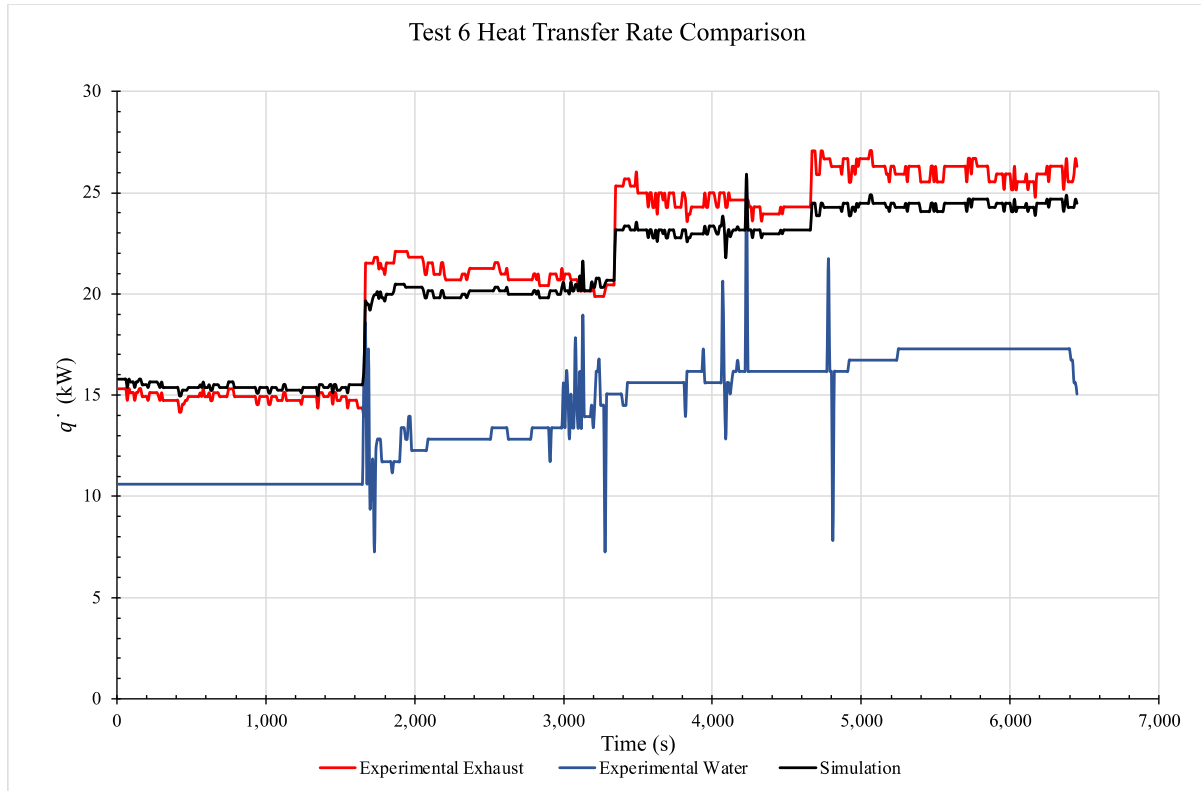


Figure 124: Heat transfer rate comparison for test 6 exhaust, water and simulation.

Figure 125 shows a comparison in the heat transfer rate between values from experimental exhaust temperatures and simulation for test 6. For tests 6 to 9, the temperature data were only to the nearest degree Celsius, therefore, a more scattered pattern was seen. The simulation heat transfer rate results followed very closely to the experimental results and an initial over prediction and then underprediction was seen as the mass flow rate of exhaust increased. Small outliers were seen due to the noise in the data-logger readings.

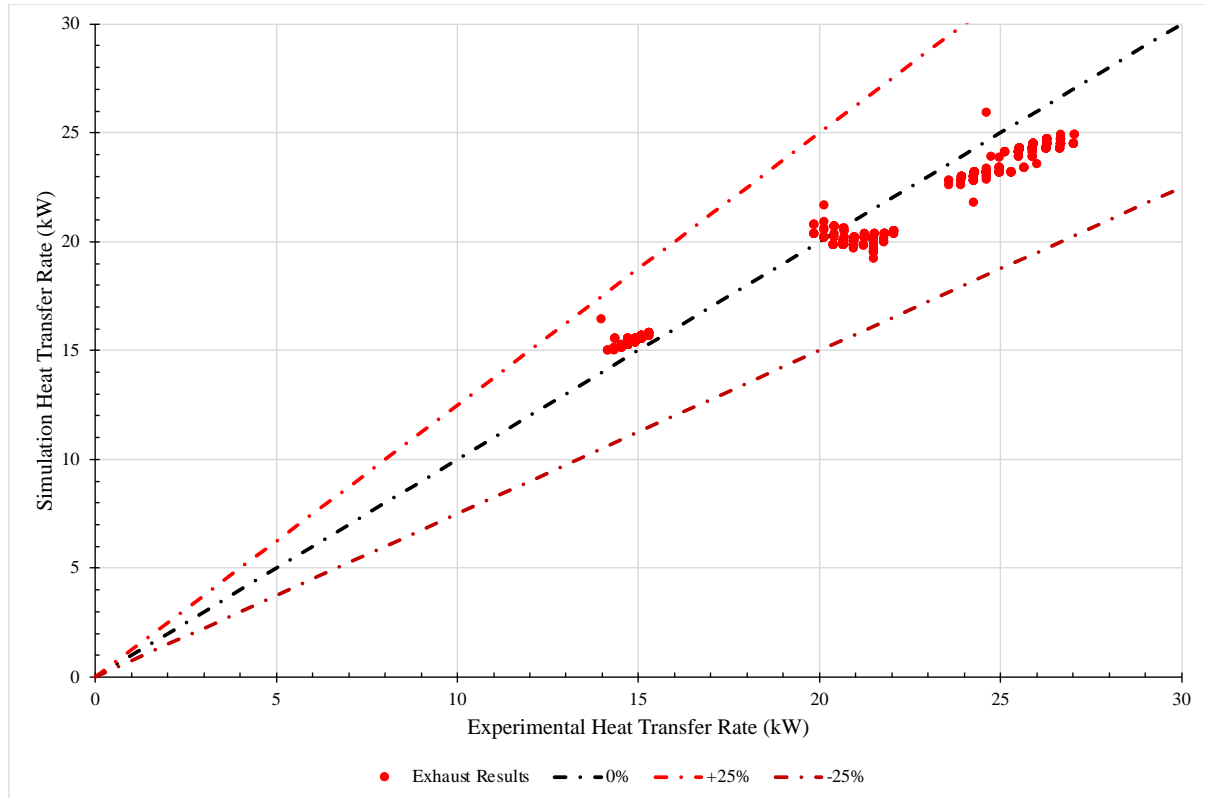


Figure 125: Heat transfer rate comparison for test 6 experimental against simulation results.

6.1.7. Test 7

Figure 126 shows the results of test 7 where the exhaust gases inlet temperature was maintained at around 140°C and the water mass flow rate at 1,320 kg.hr⁻¹ over a 111-minute period. Fan speeds at 50, 45, 35 and 25 Hz, in a descending manner, were trialled with corresponding exhaust mass flow rates between 1,224 and 649 kg.hr⁻¹.

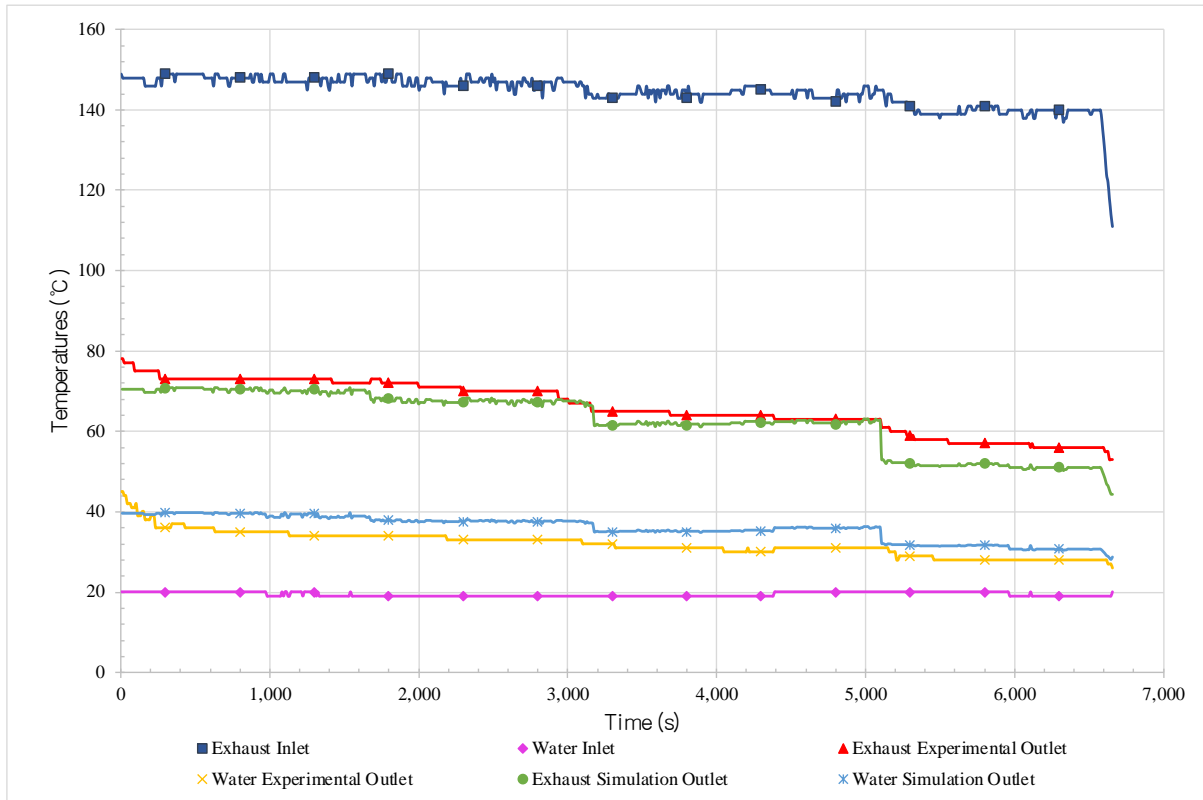


Figure 126: Transient results of test 7 showing the experimental and simulated inlet and outlet temperatures of water and exhaust streams.

The average temperature results and mass flow rates for test 7 are summarised for each time period and condition in Table 34. As the mass flow rate of exhaust gases increased, the exhaust outlet temperature increased from around 73.3 to 57.2°C, the simulation predicted 70.2 to 51.2°C. The water outlet temperature was increased to between 35.7 and 28.3°C, experimentally, and 39.3 to 31.1°C by simulation.

Table 34: Test 7 average results summary.

Exhaust Gases					Water			
Fan Speed (Hz)	T _{in} (°C)	Experiment T _{out} (°C)	Simulation T _{out} (°C)	\dot{m} (kg.h ⁻¹)	\dot{m} (kg.h ⁻¹)	T _{in} (°C)	Experiment T _{out} (°C)	Simulation T _{out} (°C)
25	147.88	73.27	70.19	1,246	1,320	19.71	35.74	39.33
35	146.83	70.21	67.44	1,159		19.00	33.29	37.64
45	144.17	63.89	62.04	969		19.37	30.90	35.48
50	139.21	57.15	51.18	649		19.56	28.28	31.10

Figure 127 shows the calculated heat transfer rates for test 7 of both the experimental exhaust and water results in comparison to the simulation predictions. This test was done in a descending manner to see if the HPHE, and hence simulation, would perform differently. A good prediction, which followed experimental results was seen, but the model overpredicted the heat transfer rate across all conditions. Test 7 and test 9 were the only tests where this was consistently seen, though the magnitude of difference between the simulation and experimental heat transfer rates was very small.

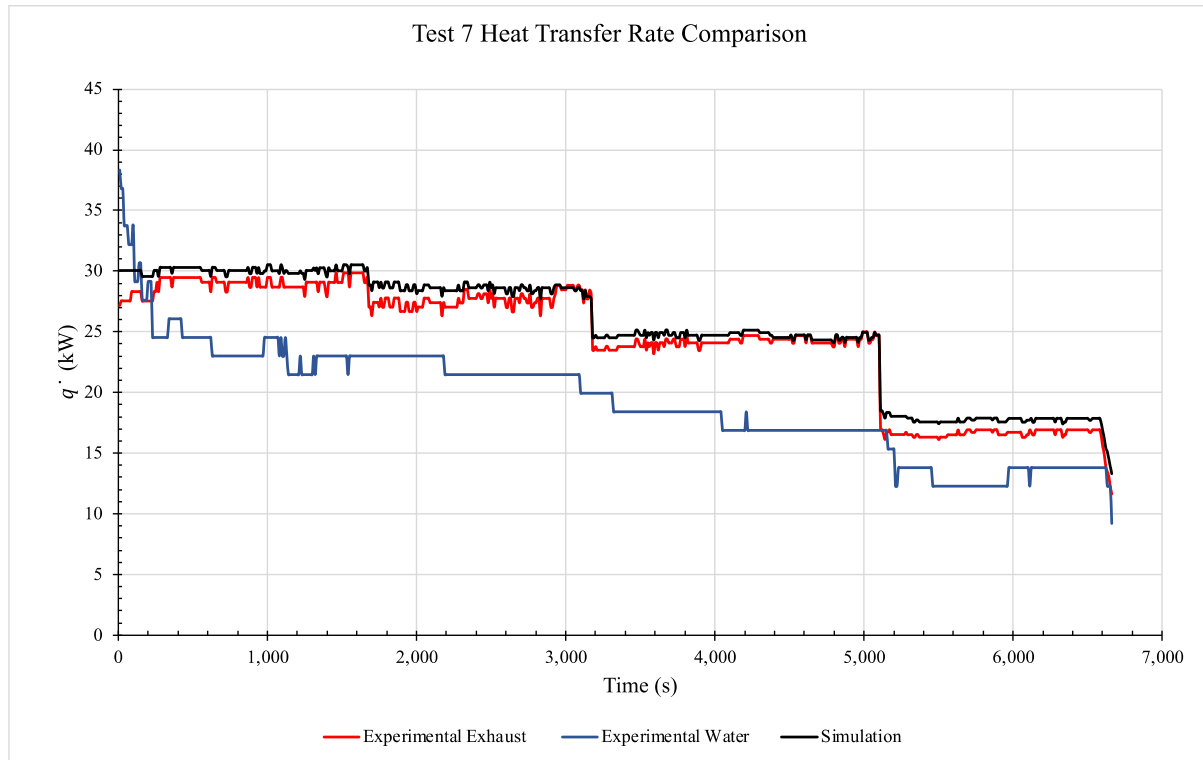


Figure 127: Heat transfer rate comparison for test 7 exhaust, water and simulation.

Figure 128 shows a comparison in the heat transfer rate between values from experimental exhaust temperature differences and simulation for test 7. For this test, a slight overprediction in the simulation was seen, with some later results at the lower exhaust mass flow rates approaching a 13% overprediction. These results also did not follow the previous test results, where a higher exhaust mass flow rate meant a larger difference between simulated and experimental heat transfer rates. The difference initially reduced as the mass flow rate of the exhaust dropped but for the lowest mass flow rate condition, an increase in difference was seen. This was the only test where this was observed.

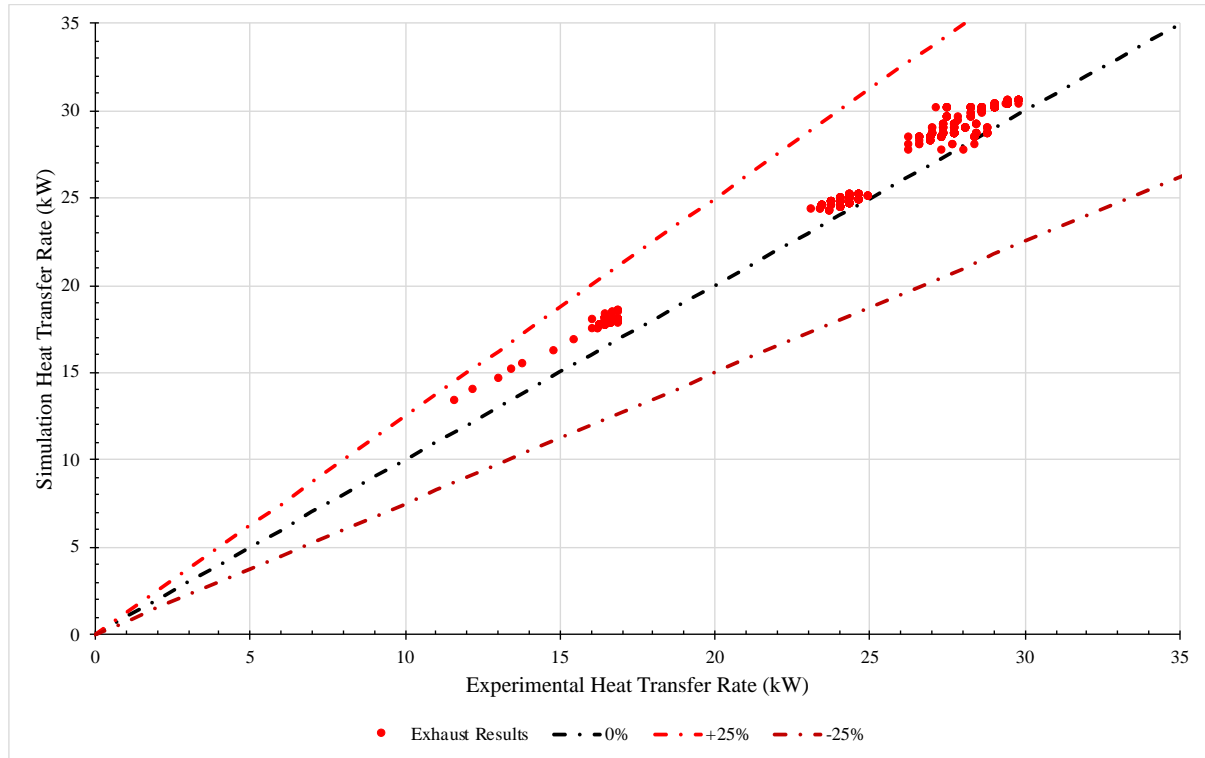


Figure 128: Heat transfer rate comparison for test 7 experimental against simulation results.

6.1.8. Test 8

Figure 129 shows the results of test 8 where the exhaust gases inlet temperature was maintained at around 225°C and the water mass flow rate at 480 kg.hr⁻¹ over a 94-minute period. Fan speeds at 25, 35, 45 and 50 Hz were trialled with corresponding exhaust mass flow rates between 591 and 1,126 kg.hr⁻¹.

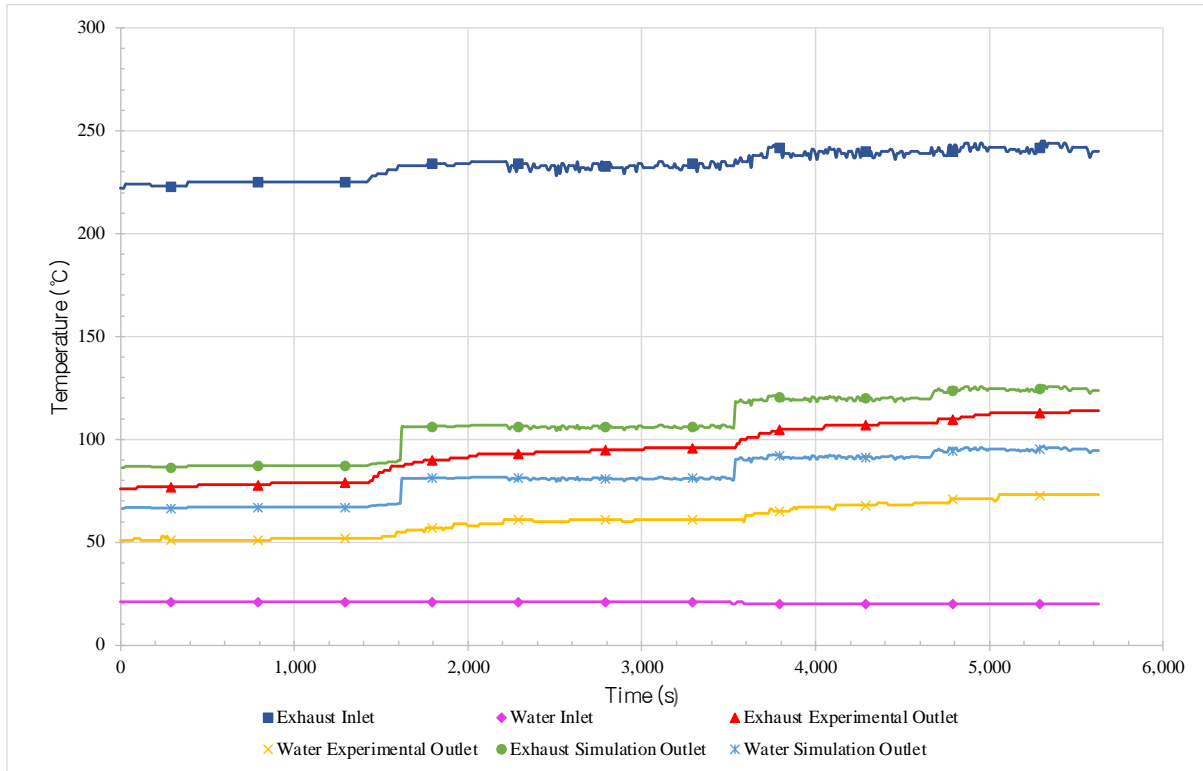


Figure 129: Transient results of test 8 showing the experimental and simulated inlet and outlet temperatures of water and exhaust streams.

The average temperature results and mass flow rates for test 8 are summarised for each time period and condition in Table 35. As the exhaust gases mass flow rate increased, the outlet temperature of the exhaust increased from around 78.7 to 112.4°C, the simulation predicted 87.2 to 124.3°C. The water outlet temperatures increased to between 51.6 and 72.0°C, experimentally, and 67.1 to 95.0°C by simulation.

Table 35: Test 8 average results summary.

Exhaust Gases					Water			
Fan Speed (Hz)	T _{in} (°C)	Experiment T _{out} (°C)	Simulation T _{out} (°C)	\dot{m} (kg.h ⁻¹)	\dot{m} (kg.h ⁻¹)	T _{in} (°C)	Experiment T _{out} (°C)	Simulation T _{out} (°C)
25	225.14	78.73	87.17	591	480	21.00	51.64	67.05
35	233.07	93.61	106.05	833		20.99	59.79	80.94
45	238.95	105.59	119.51	1,049		20.04	66.66	91.19
50	241.52	112.35	124.31	1,126		20.00	71.98	95.02

Figure 130 shows the calculated heat transfer rates for test 8 of both the experimental exhaust and water results in comparison to the simulation predictions. In contrast to test 7, test 8 showed the largest underprediction in simulation by the order of 2 to 5 kW. However, the simulation heat transfer rate results very closely followed the trend of the exhaust heat transfer rate data.

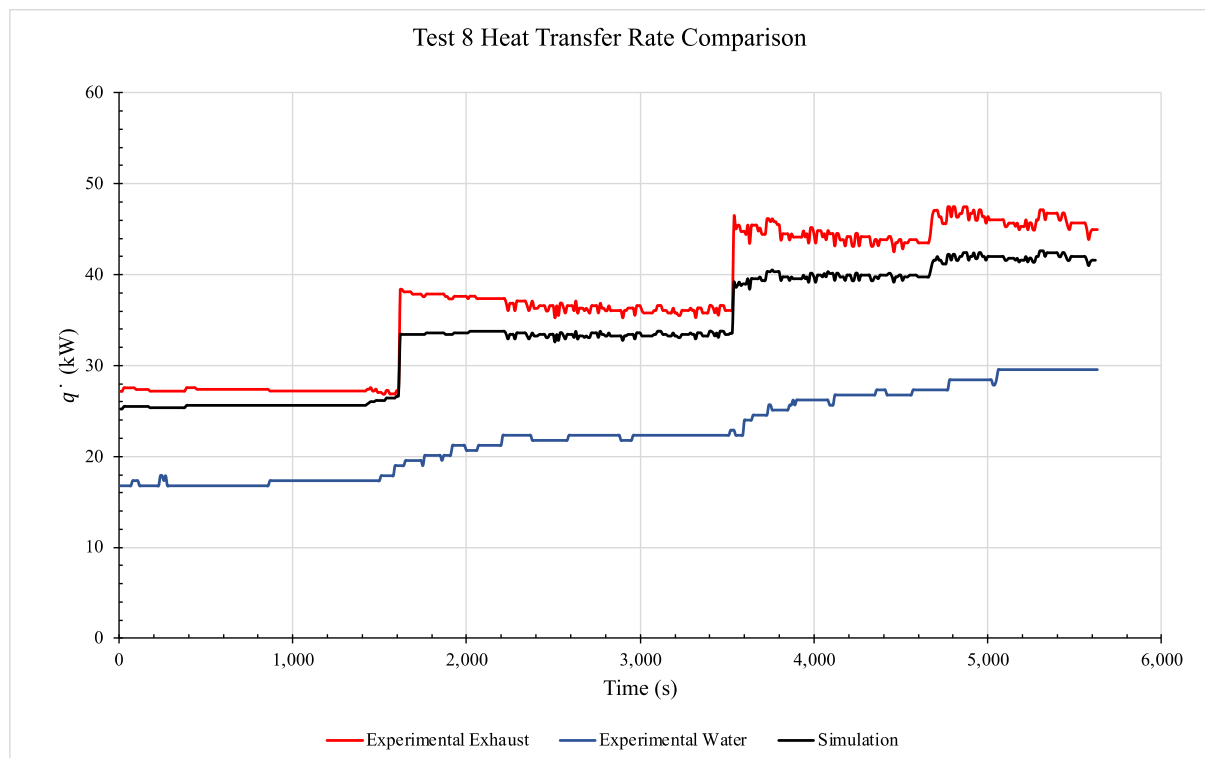


Figure 130: Heat transfer rate comparison for test 8 exhaust, water and simulation.

Figure 131 shows a comparison in the heat transfer rate between values from experimental exhaust temperature differences and simulation for test 8. An underprediction in the model was seen, which enlarged as the exhaust mass flow rate increased.

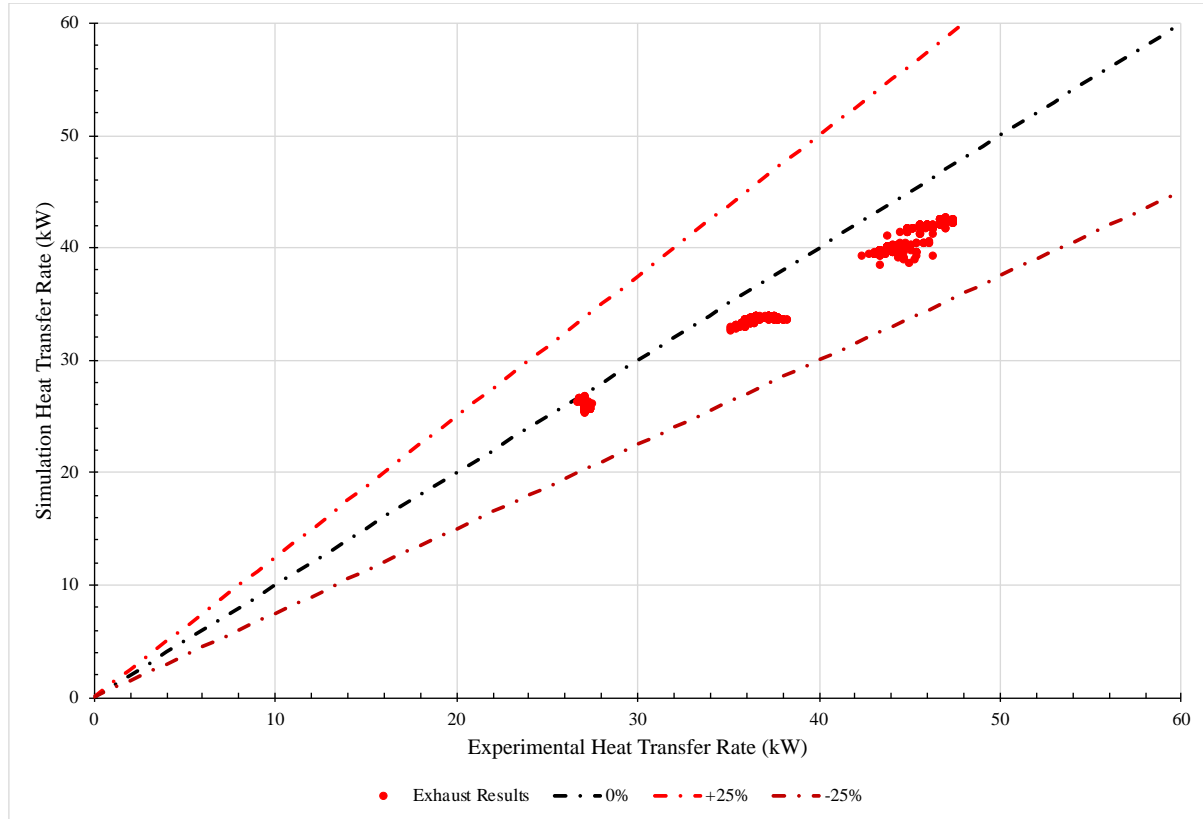


Figure 131: Heat transfer rate comparison for test 8 experimental against simulation results.

6.1.9. Test 9

Figure 132 shows the results of test 9 where the exhaust gases inlet temperature was maintained at around 225°C and the water mass flow rate at 1,320 kg.hr⁻¹ over an 85-minute period. Fan speeds at 50, 45, 35 Hz were trialled, in a descending manner, with corresponding exhaust gasses mass flow rates between 1,164 and 830 kg.hr⁻¹.

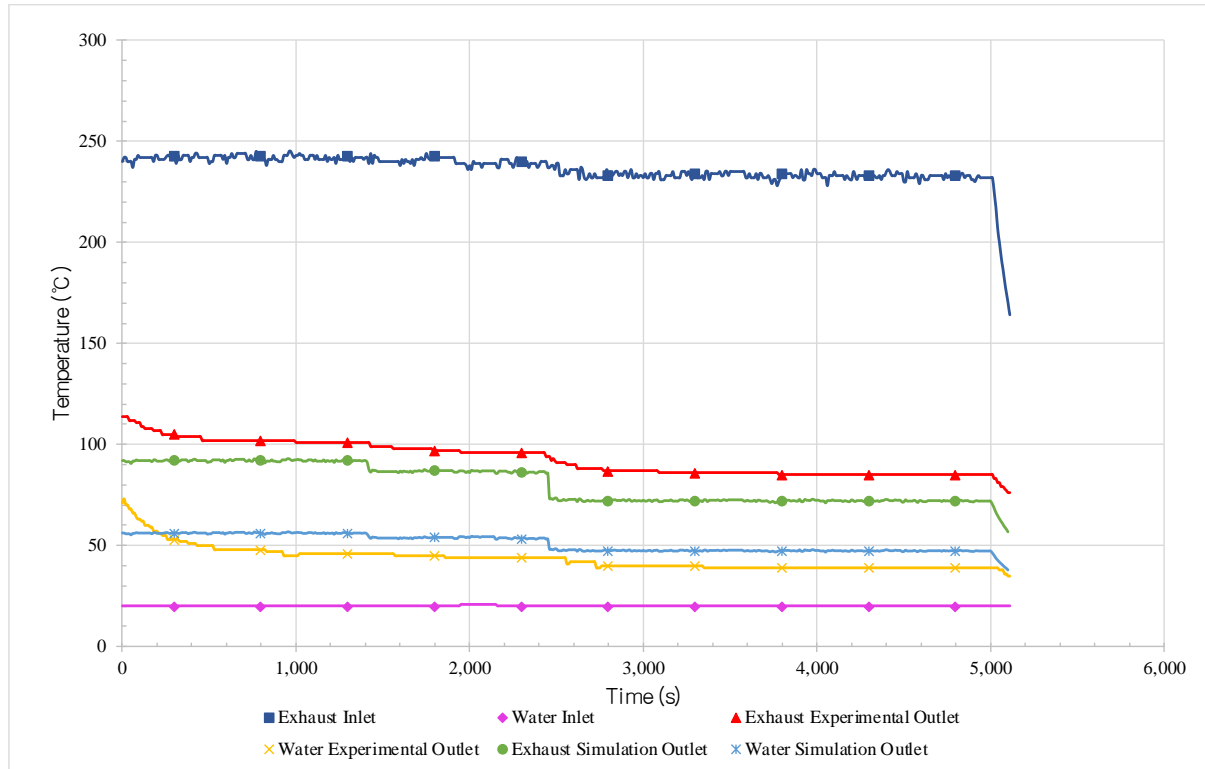


Figure 132: Transient results of test 9 showing the experimental and simulated inlet and outlet temperatures of water and exhaust streams.

The average temperature results and mass flow rates for test 9 are summarised for each time period and condition in Table 36. As the exhaust gases mass flow rate increased, the exhaust outlet temperature increased from around 103.4 to 85.8°C, the simulation predicted 91.9 to 71.8°C. The water outlet temperature increased to between 50.3 and 39.51°C, experimentally, and 56.0 to 47.2°C by simulation.

Table 36: Test 9 average results summary.

Exhaust Gases					Water			
Fan Speed (Hz)	T _{in} (°C)	Experiment T _{out} (°C)	Simulation T _{out} (°C)	\dot{m} (kg.h ⁻¹)	\dot{m} (kg.h ⁻¹)	T _{in} (°C)	Experiment T _{out} (°C)	Simulation T _{out} (°C)
50	241.86	103.36	91.87	1,164	1,320	20.00	50.34	55.96
45	239.92	96.91	86.55	1,061		20.20	44.55	53.69
35	231.57	85.79	71.82	830		20.00	39.51	47.19

Figure 133 shows the calculated heat transfer rates for test 9 of both the experimental exhaust and water results in comparison to the simulation predictions. An overprediction in the simulation was seen for this test, in the order of 4 kW; this in terms of a percentage was not a major concern. The water heat transfer rate started very high, which was due to the water outlet temperature from the condenser section stabilising.

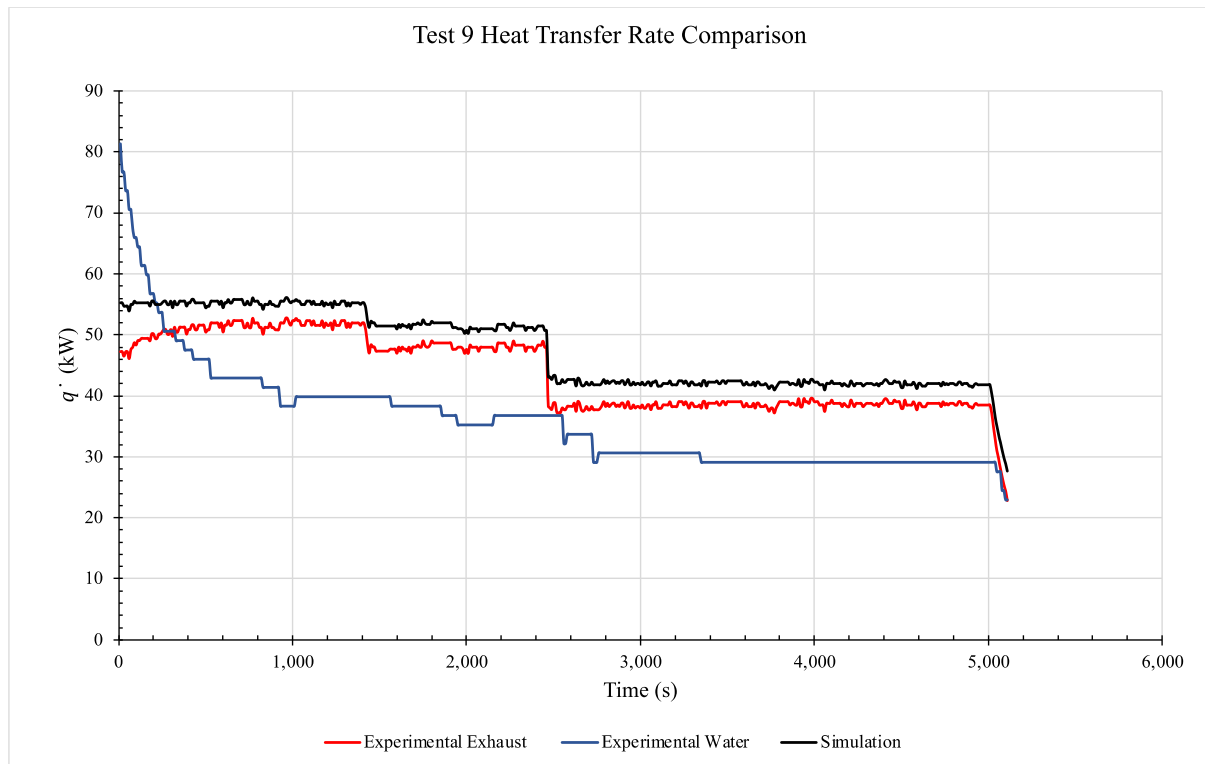


Figure 133: Heat transfer rate comparison for test 9 exhaust, water and simulation.

Figure 134 shows a comparison in the heat transfer rate between values from experimental exhaust temperature differences and simulation for test 9 where an overprediction in the model was seen. The lower heat transfer rates relate to when the HPHE operation was being ramped down. A very tight cluster was seen for these experiments indicating little fluctuation in the conditions, which was observed.

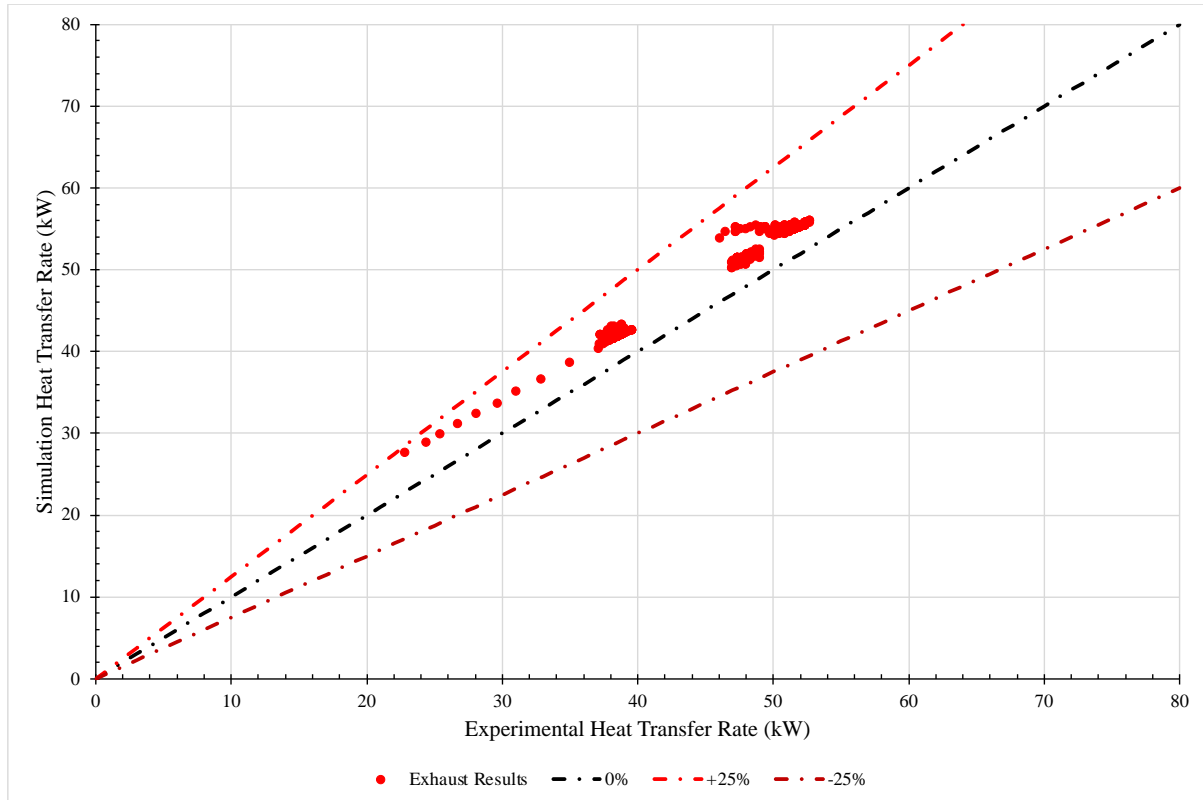


Figure 134: Heat transfer rate comparison for test 9 experimental against simulation results.

An example of the pressure drop graphical output from the TRNSYS model is provided for test 9 and it is shown in Figure 135. The simulation predicts an initial pressure drop across the evaporator section of 64 Pa, which drops to 52 Pa, and then 45 Pa as the mass flow rate of the exhaust gases is reduced. The pressure drop across the condenser was maintained around 22 Pa, which reflects the consistent water mass flow rate and inlet temperature.

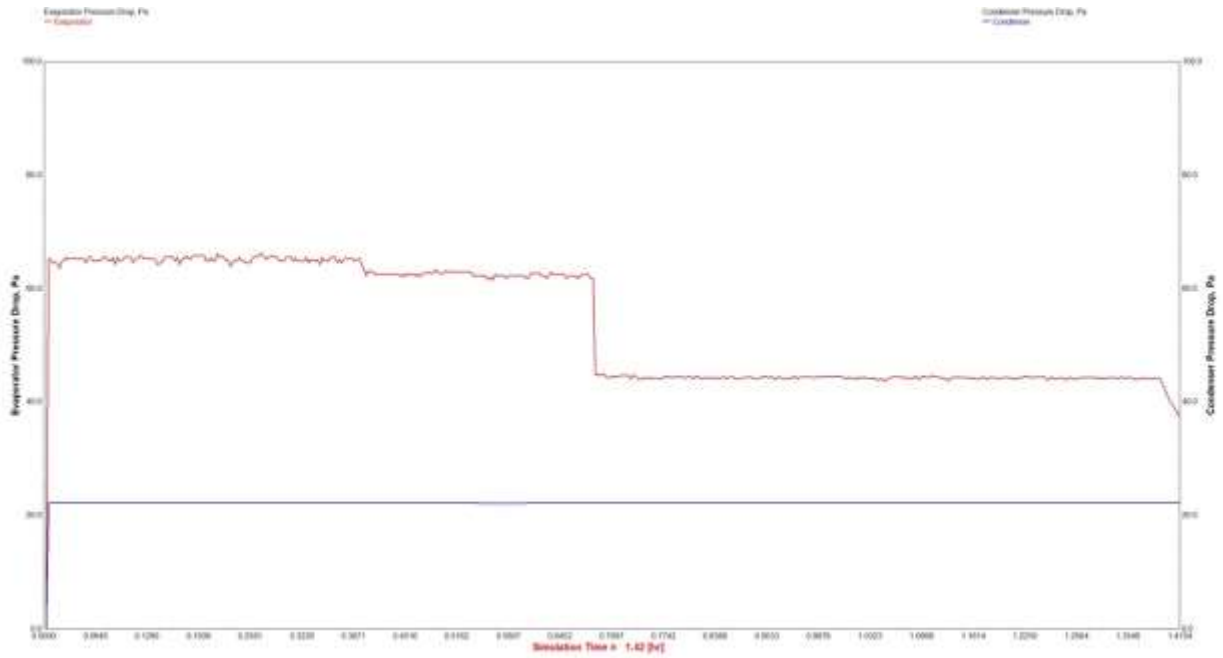
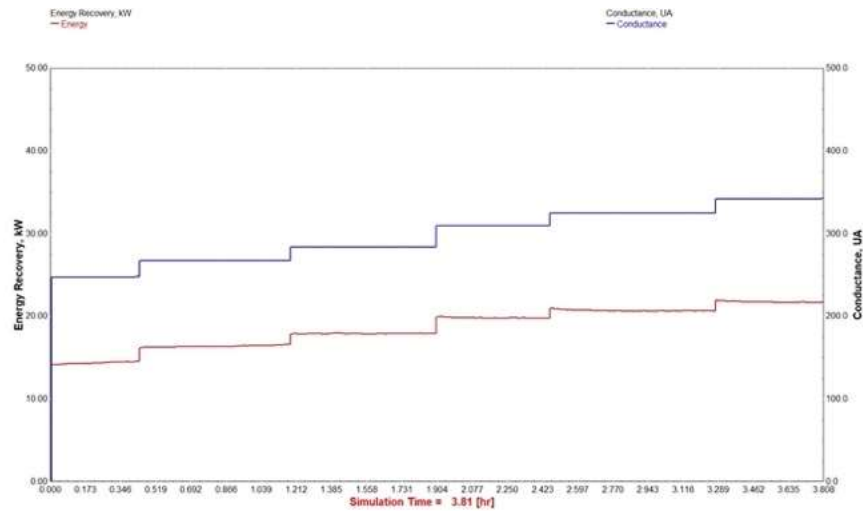


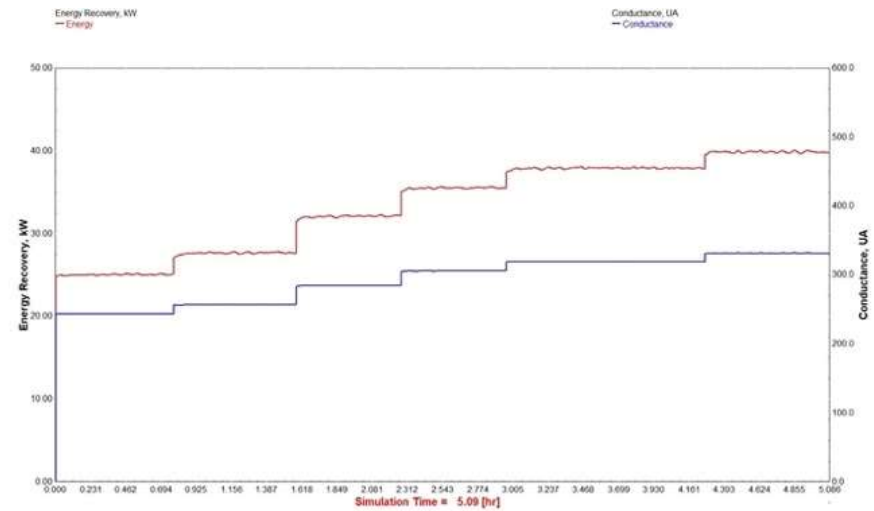
Figure 135: Pressure drop TRNSYS simulation output for test 9.

6.1.10. Graphical Heat Transfer Rate and Conductance Values

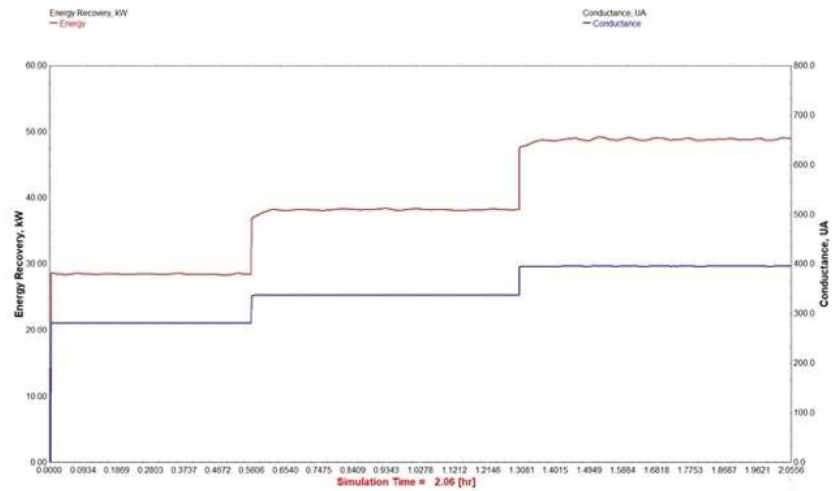
Figure 136 shows the graphical TRNSYS output of the simulated heat transfer rate and conductance value of the HPHE for each test. The conductance ranges are also given below each graph for comparison. The range in conductance value for the HPHE was between 221 and 461 W.K⁻¹ across all experiments.



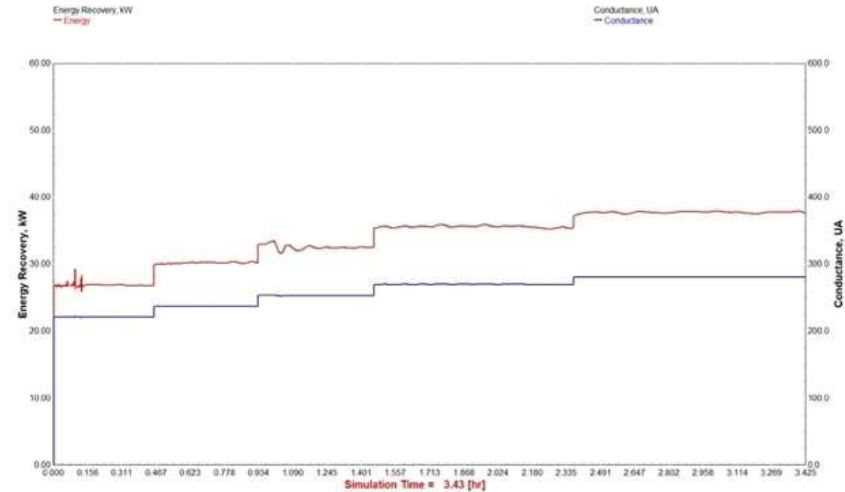
Test 1- 247 to 344 W.K⁻¹



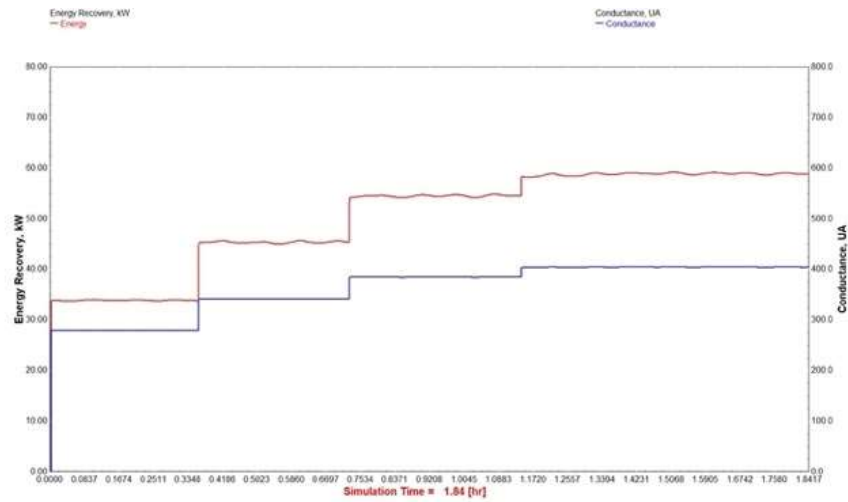
Test 2- 243 to 332 W.K⁻¹



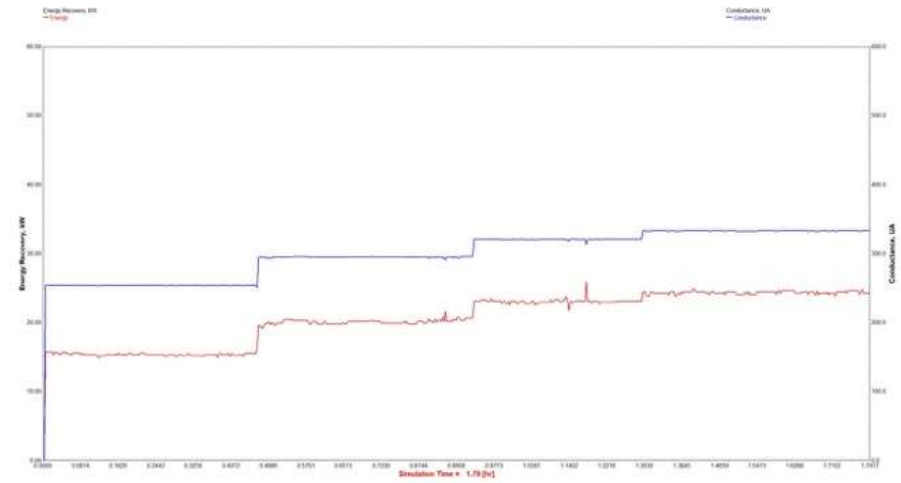
Test 3- 282 to 397 W.K⁻¹



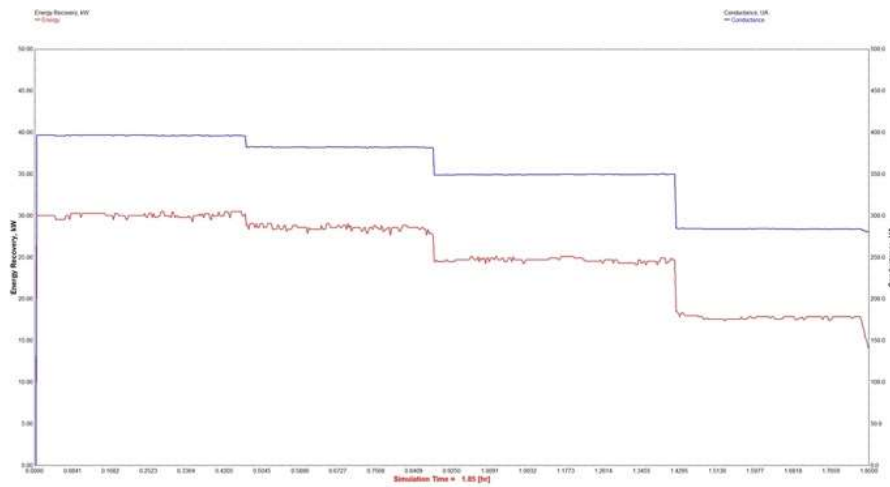
Test 4- 221 to 281 W.K⁻¹



Test 5- 280 to 405 W.K⁻¹



Test 6- 251 to 334 W.K⁻¹

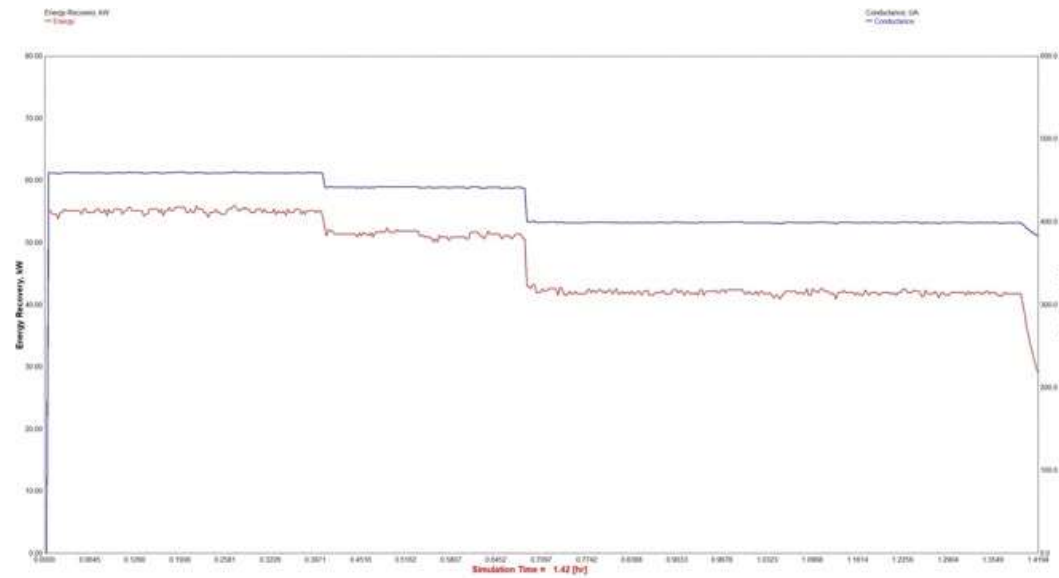


Test 7- 336 to 445 W.K⁻¹



Test 8- 243 to 338 W.K⁻¹

S

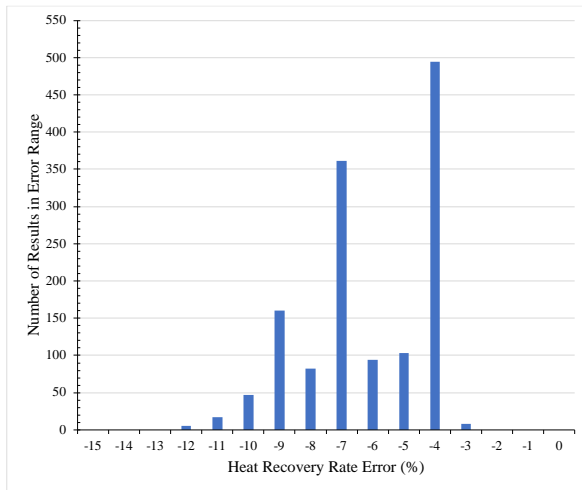


Test 9- 382 to 461 W.K⁻¹

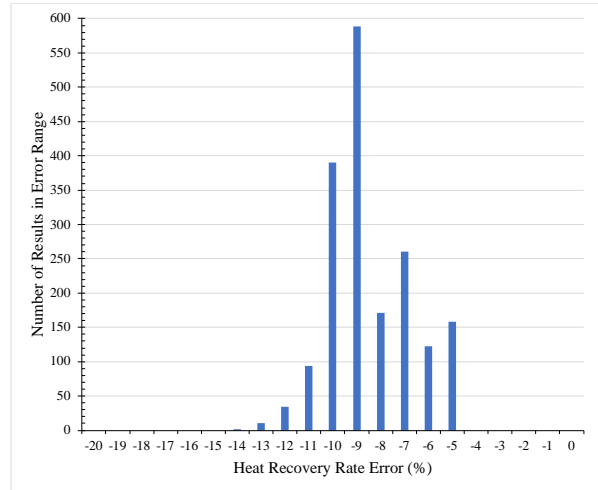
Figure 136: TRNSYS graph outputs for heat transfer rate and conductance for each test.

6.1.11. Experiment 1 Error Analysis

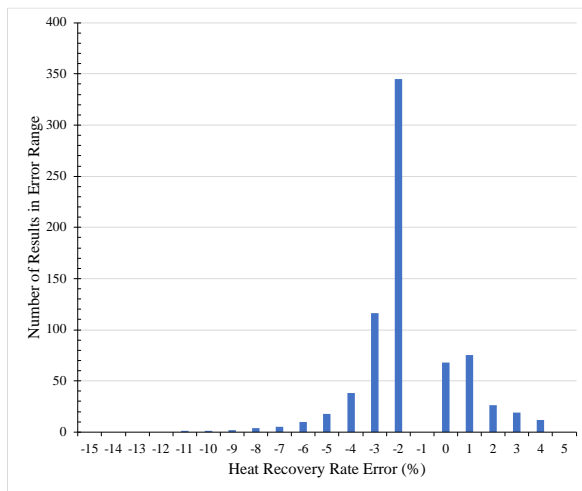
The percentage difference between the simulated heat transfer rate and experimental exhaust stream heat transfer rate was determined for each datum point. The percentage difference was rounded to the nearest whole number and all the values were aggregated and plotted in a histogram to show the spread of error for each test. As well as the error analysis between the simulated heat transfer rate and experimental exhaust heat transfer rate for each individual test, an overall analysis on the entire simulation for Experiment 1 was conducted to provide an understanding of the accuracy of the simulation for this HPHE’s performance. The histograms are provided in Figure 137 with the average percentage difference shown underneath each graph, which was calculated prior to rounding.



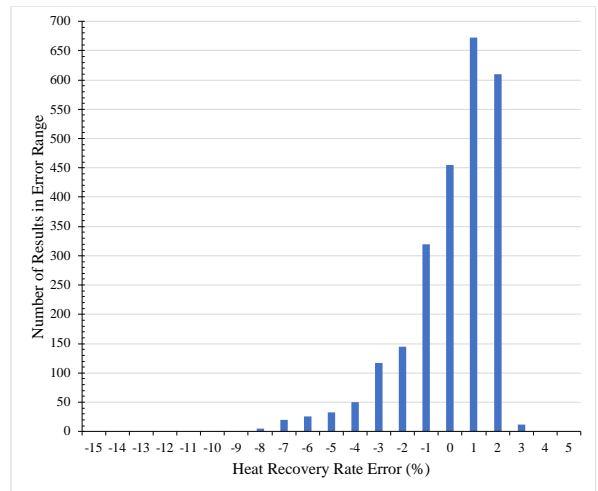
Test 1- Average -6.11%.



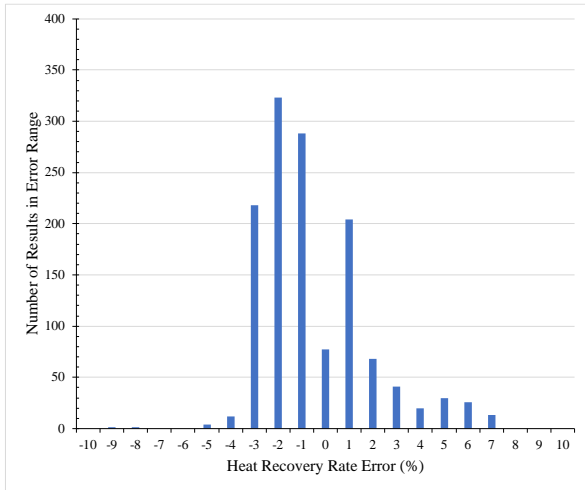
Test 2- Average -8.52%.



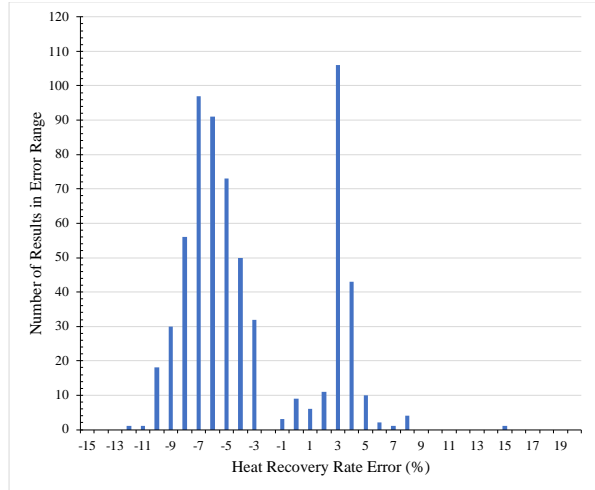
Test 3- Average -1.59%.



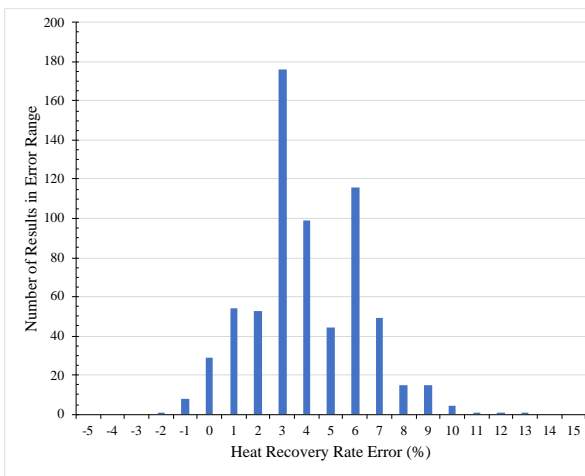
Test 4- Average -1.52%.



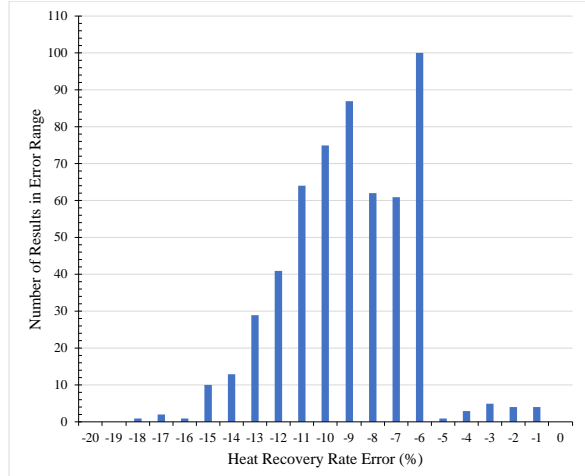
Test 5- Average +0.91%.



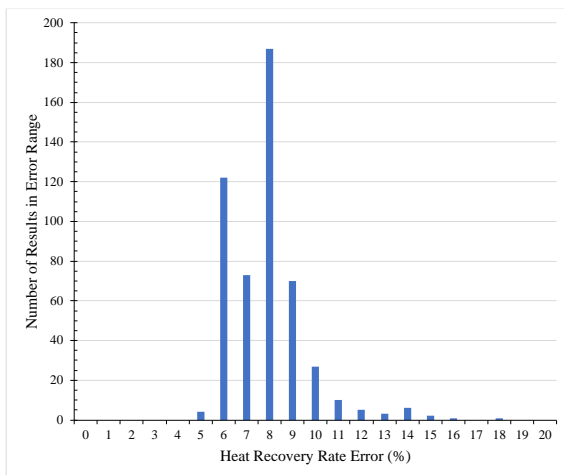
Test 6- Average -3.37%.



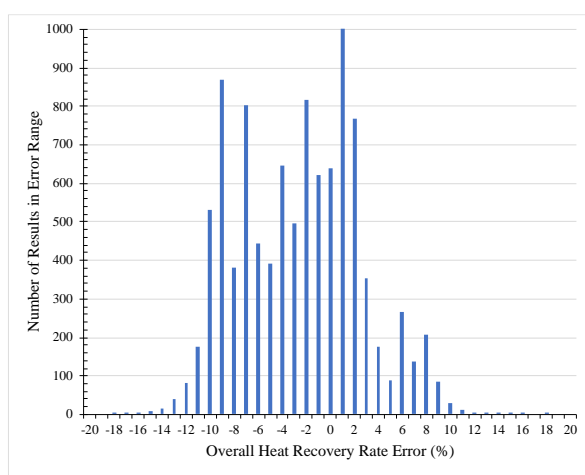
Test 7- Average +10.17%.



Test 8- Average -9.02%.



Test 9- Average +7.84%.



Combined- Average -2.39%

Figure 137: Experiment 1 heat transfer rate percentage difference between experiment and simulation.

The combined spread of heat transfer rate prediction error across Experiment 1 was between -18 and +19%. The average error of all the 10,119 individual results was -2.39%. The longer tests, where more data results were present, reflected more on the average than with the shorter tests with fewer data points. However, this spread of error is very acceptable for engineering applications and the average error gives an added confidence in the components' predictive abilities.

Calculating the heat transfer rate relies on knowing the difference between the inlet and outlet temperatures of the heat transfer fluid across the HPHE. It is also important to consider the accuracy of the outlet temperature predictions of the fluids because issues relating to condensation and corrosion, or phase change can occur. Therefore, an analysis was conducted on the percentage difference between the predicted outlet temperature of the heat transfer fluids and the experimental outlet temperature for both the evaporator and condenser sections. This percentage difference was calculated for each datum point using Equation (6.2). Figure 138 shows the percentage difference results plotted in histograms for both the exhaust gases and the water streams for all of the results obtained for Experiment 1.

$$Error (\%) = 100 \frac{Simulation T_{out}(K) - Experimental T_{out}(K)}{Simulation T_{out}(K)} \quad (6.2)$$

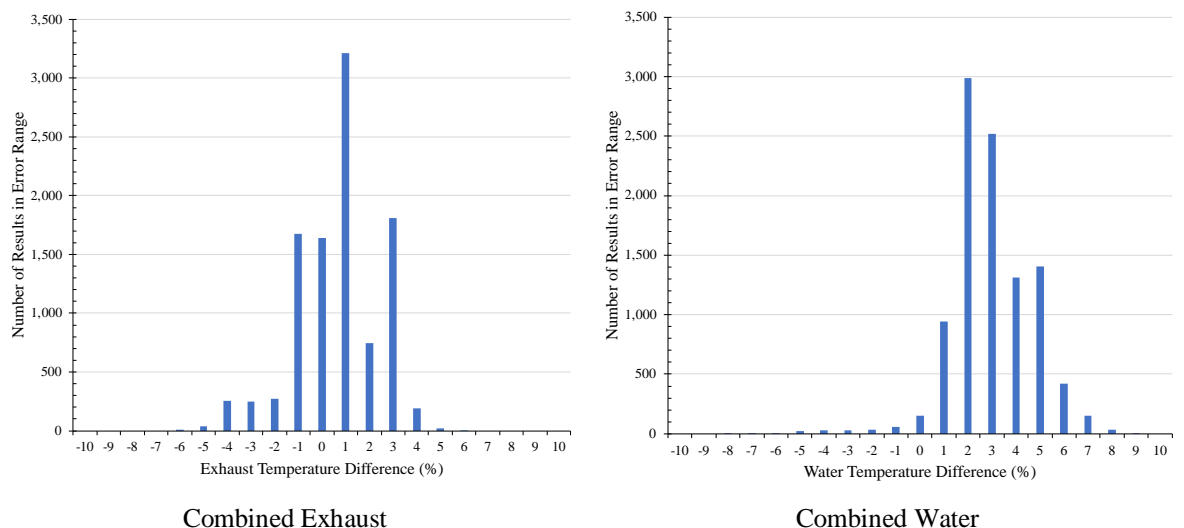


Figure 138: Experiment 1 difference in temperature between experiment and simulation outlet results histogram.

Of the 10,119 individual results, the average exhaust outlet temperature difference was +0.67% meaning that the outlet temperature for the simulation was higher than the experimental exhaust outlet temperature. Interestingly, this means that the simulation underperformed, but as losses from the casing were not considered, this is as expected. The spread of error for the exhaust percentage difference between simulation and experiment was quite small; between $\pm 6\%$. For the water outlet temperatures, this percentage error spread was slightly larger, between -8 and +9%, and the average was higher at +2.97%. This value shows that the simulated water outlet temperature was higher than the experimental water outlet temperature. This also highlights that there were more heat losses from the condenser section. With the water results, some of this error can be attributed to the water outlet temperature being more variable when the data were spliced for the experiments. This could have been counteracted by reducing the amount of data, but with more accurate splicing.

6.1.12. Statistical Analysis

The heat transfer rate results were analysed in both a linear and non-linear manner. For linear correlation analysis, Pearson correlation analysis is recommended, whereas Spearman correlation analysis is recommended for non-linear, nonparametric or monotonic relationships. Spearman correlation analysis was conducted using IBM SPSS Statistics for the experimental heat transfer rates for the exhaust and water and the results are shown in Table 37 and Table 39, respectively. Initially, the heat transfer rate of exhaust (\dot{q}_{ex}) was set as the dependent variable, with exhaust inlet temperature ($T_{ex,in}$), water inlet temperature ($T_{w,in}$), exhaust mass flow rate (\dot{m}_{ex}) and water mass flow rate (\dot{m}_w) set as the independent variables.

Table 37: Spearman correlation analysis for experimental exhaust heat transfer rate.

Variable	\dot{q}_{ex}	$T_{ex,in}$	$T_{w,in}$	\dot{m}_{ex}	\dot{m}_w
\dot{q}_{ex}	1.000	0.733	-0.304	0.347	0.396
$T_{ex,in}$	0.733	1.000	-0.762	-0.124	0.186
$T_{w,in}$	-0.304	-0.762	1.000	0.336	-0.289
\dot{m}_{ex}	0.347	-0.124	0.336	1.000	0.298
\dot{m}_w	0.396	0.186	-0.289	0.298	1.000

For \dot{q}_{ex} , it can be seen that the independent variables all have a reasonable to strong correlation, which is usually described as a value greater than 0.3 or less than -0.3. The strongest correlation was seen between the exhaust inlet temperature, $T_{ex,in}-\dot{q}_{ex}$, and the lowest between the mass flow rate of the water, $\dot{m}_w-\dot{q}_{ex}$. A $T_{ex,in}-\dot{q}_{ex}$ score of 0.733 shows that there is a strong correlation in that as the exhaust inlet temperature increases, the exhaust heat transfer rate increases. A $T_{w,in}-\dot{q}_{ex}$ score of -0.304 shows that the lower the water inlet temperature, the higher the exhaust heat transfer rate, due to there being a larger temperature differential between the two heat transfer fluids. For, $\dot{m}_{ex}-\dot{q}_{ex}$, there was a positive correlation of 0.347, meaning that increasing the exhaust gases mass flow rate, increases the exhaust gases heat transfer rate. It was also beneficial to see that the relation between $\dot{m}_w-\dot{q}_{ex}$ is 0.396 as this shows that the water heat sink is extracting energy from the thermosyphon, increasing the heat transfer rate for the exhaust gases, which follows theory as the condenser and evaporator sections are linked.

The correlations between the independent variables are also presented, which should ideally be less than 0.7 or greater than -0.7. However, on examination of the correlations, the value between the water inlet temperature and exhaust inlet temperature is -0.762. This value suggests collinearity between the values or redundancy for the predictions. This should not be observed, as the two variables should be independent, but suggests that the exhaust inlet temperature and water inlet temperature have an influence on each other. This cannot be explained by heat losses from the exhaust gases to the water as the correlation is negative. Therefore, this is left unexplained. The remaining results are acceptable. A collinearity tolerance analysis was conducted due to the unexpected potential presence of multicollinearity. The results in Table 38 show that this is not the case as the values are all greater than 0.1.

Table 38: Collinearity tolerance for Experiment 1 variables.

Independent Variable	Collinearity Tolerance
$T_{ex,in}$	0.431
$T_{w,in}$	0.362
\dot{m}_{ex}	0.718
\dot{m}_w	0.699

There were only 3 individual results for the exhaust heat transfer rate that were highlighted as serious outliers. These were all on test 6 and relate to the water inlet temperature where noise was present. Nonlinear regression analysis gave a predictive equation in the form of Equation (6.4), within the bounds of the experimental set-up and conditions. For the nonlinear regression analysis, the model expression was set as:

$$q = AT_{ex,in}^B + CT_{w,in}^D + E\dot{m}_{ex}^F + G\dot{m}_w^H + I \quad (6.3)$$

All the starting values of the coefficients, A-I, were set at 1. The estimation method was set as sequential quadratic programming. The maximum number of iterations was 999, the highest possible, and the iterations finished when the precision for each coefficient did not alter by 1×10^{-5} .

$$\dot{q}_{ex} = -683.154T_{ex,in}^{-0.09} - 0.337T_{w,in}^{0.871} + 109.145\dot{m}_{ex}^{0.117} + 2.754\dot{m}_w^{-1.510} + 219.305 \quad (6.4)$$

A R^2 value is a measure of how close the data are fitted to the regression line and is determined by:

$$R^2 = 1 - \frac{\text{Residual Sum of Squares}}{\text{Total Sum of Squares}} \quad (6.5)$$

A R^2 value of 0.919 for Equation (6.4) shows a very good relationship between the four variables and the exhaust heat transfer rate as it implies that 91.9% of the variability of the dependant variable is accounted for by the independent variables. This is a very high value; meaning that no other variables should have been or need to be considered to determine the exhaust heat transfer rate.

Table 39 shows the Spearman correlation analysis for the heat transfer rate of water (\dot{q}_w) when set as the dependent variable with exhaust inlet temperature ($T_{ex,in}$), water inlet temperature ($T_{w,in}$), exhaust mass flow rate (\dot{m}_{ex}) and water mass flow rate (\dot{m}_w) set as the independent variables.

Table 39: Spearman correlation analysis for experimental water heat transfer rate.

Variable	\dot{q}_w	$T_{ex,in}$	$T_{w,in}$	\dot{m}_{ex}	\dot{m}_w
\dot{q}_w	1.000	0.828	-0.533	0.210	0.487
$T_{ex,in}$	0.828	1.000	-0.762	-0.124	0.186
$T_{w,in}$	-0.533	-0.762	1.000	0.336	-0.289
\dot{m}_{ex}	0.210	-0.124	0.336	1.000	0.298
\dot{m}_w	0.487	0.186	-0.289	0.298	1.000

For \dot{q}_w , it can be seen that not all the independent variables have a strong correlation. The strongest correlation was seen between the exhaust inlet temperature, $T_{ex,in}-\dot{q}_w$. Interestingly, the smallest correlation was between the exhaust mass flow rate at 0.210, less than 0.3, so was, unexpectedly, not strongly correlated. A $T_{ex,in}-\dot{q}_w$ score of 0.828 shows that there is a strong correlation that as the exhaust inlet temperature increases, the water heat transfer rate increases. A $T_{w,in}-\dot{q}_w$ score of -0.553 shows that the lower the water inlet temperature, the higher the water heat transfer rate, due to being a larger temperature differential. The smallest relation was $\dot{m}_{ex}-\dot{q}_w$, where there was a positive correlation between exhaust mass flow rate and water heat transfer rate of 0.210, but this was not as strong as expected. However, $\dot{m}_w-\dot{q}_w$ was a relatively strong correlation at 0.487.

There were 152 individual results that were highlighted as serious outliers (1.5% of the total results). These were across tests 4, 5 and 6. In tests 4 and 5, the outliers occurred when there was a serious discrepancy in water heat transfer rate where the data were spliced and a significant difference was seen between the exhaust gases and water heat transfer rate. In test 6 the outliers related to the water inlet temperature where noise was present. Coefficient analysis gave a predictive equation for the water heat transfer rate in the form of Equation (6.6), within the bounds of the experimental set-up and conditions.

$$\dot{q}_w = -3871.92T_{ex,in}^{-0.009} + 944.615T_{w,in}^{-36.732} + 21.826\dot{m}_{ex}^{0.193} + 893.067\dot{m}_w^{0.010} + 2489.13 \quad (6.6)$$

An R^2 value of 0.846 shows that the four variables considered explain 84.6% of the water heat transfer rate. This is a high and respectable R^2 value but roughly 15% of the results cannot be confidently explained by the model and, hence, there were some other factors present.

6.1.13. Experiment 1 Summary

Some general conclusions can be drawn from the tests. Across all tests, by increasing the mass flow rate of exhaust gases, the higher the heat transfer rate for water and exhaust gases. The statistical analysis showed however that this was more highly correlated to inlet temperature than mass flow rate. By increasing the water mass flow rate, it was also seen experimentally and theoretically that the heat transfer rate and conductance values of the HPHE increases. This is particularly seen when comparing tests with the same exhaust inlet temperature parameters.

Interestingly, a plateau in heat transfer rate was not found, showing that the maximum heat transfer rate that the HPHE unit was capable of was not reached. Though built for variable heat, the unit design parameters were to recover heat from 258°C exhaust gases with 1,944 kg.hr⁻¹ mass flow rate and 1,000 kg.hr⁻¹ water heat sink mass flow rate. The largest mass flow rate tested for the exhaust stream was 1,284 kg.hr⁻¹ as the fan limit was reached. Increasing the frequency was possible with the inverter model, but it was deemed unnecessary to stretch outside of the fan specification. Introducing higher exhaust inlet temperatures to the HPHE was also within the kiln's ability, however, thermosyphons with water as the working fluid can only operate up to around 300°C, under the correct conditions. However, as this unit was installed abroad, if there were any failures caused by undertaking higher inlet temperature tests, the unit could not be easily repaired.

It was also observed across the tests that, the higher the exhaust inlet temperature, the higher the water and exhaust gases heat transfer rate and the larger the increase in heat sink temperature. This is expected as there is a higher energy content to recover and the process is driven by a temperature difference. The higher the temperature difference, the higher the heat transfer rate.

The overall range of heat transfer rates realised by this unit was between 13.98 and 61.01 kW; seen in test 6 and 5, respectively. This is unsurprising as test 5 had the highest exhaust inlet temperature and water mass flow rate. Test 1 had a slightly lower exhaust inlet temperature but the water inlet temperature was approximately 5 degrees higher, which is why test 6 contained the lowest heat transfer rate.

In general, the higher the exhaust inlet temperature and mass flow rate (except one condition in test 7), the larger the underprediction of the simulation. However, this is expected as the higher the inlet temperature, the larger the temperature gradient between the heat transfer fluids and the casing and, therefore, more energy will be lost to the casing from the heat transfer fluids and then through radiation or natural convection from the casing to the environment. Therefore, the heat transfer rate of the exhaust gases in the evaporator is artificially high as the energy has not been used as useful work. The true energy recovered is calculated from heat gained in the water and is related to the outlet temperature and mass flow rate of the sink fluid.

During the experiments, some experimental errors were made. Sometimes, the fan inverter frequency change was not confirmed by the operator, thereby the tests remained at the same condition when it was expected that the frequency had changed. This gave large time periods of data in the same condition, not allowing a true comparison across all experiments.

The HPHE quickly adapted to the changing conditions, but not as fast as the simulation did, introducing an error. Splicing data were an issue, as seen in the heat transfer rate comparison and by the statistical analysis, particularly for the condenser section. If conducted again, it would be beneficial to gain the results in a single test rather than across multiple attempts to, firstly, avoid this issue or, secondly, better splicing could have been undertaken.

If these tests were conducted again, rather than measuring the mass flow rates of both evaporator and condenser discontinuously, it would be more beneficial to have constant sampling, as undertaken with the other Experiments presented in this chapter. The exhaust mass flow rate adjusted very quickly, and the mass flow rate of water was assumed constant, but to confirm this, and achieve more accurate heat transfer rate calculations, a mass flow rate value for each time period would be beneficial rather than assuming it was reliably maintained. To achieve this, an extra channel in the data-logger for water would be needed, a different mass flow rate meter and a velocity measuring pitot grid in the exhaust ducting to measure traverse readings of pressure. The grid is needed as the velocity of the exhaust stream is not uniform in a duct cross section. These pieces of equipment can be expensive, especially if installed in a high temperature setting, or if made bespoke.

6.2. Experiment 2: Full-Scale Ceramic Kiln

For this experiment, the sampling frequency rate was 1 minute, which was significantly longer than for the previous laboratory-scale experiment, however, a longer period of time (1,300 minutes) was trialled. Figure 139 shows the graph produced as an output of the TRNSYS simulation and includes the inlet and outlet temperatures of the source and sink fluids.

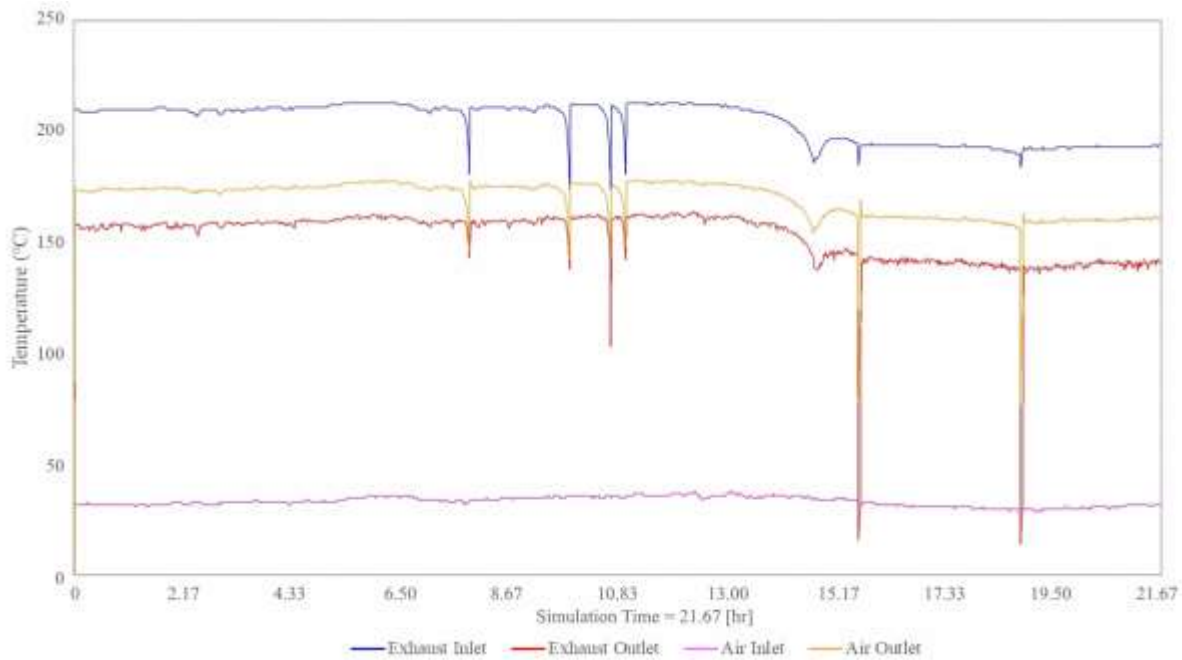


Figure 139: Experiment 2 TRNSYS temperature output results.

Figure 140 shows the experimental inlet and outlet temperature data of the installed HPHE along with the simulation inlet and outlet temperature results for comparison. The inlet temperatures were fed into the model and the experimental outlet temperatures were used for comparison against the simulation outlet temperatures to validate the component. For this experiment, the simulated air outlet temperature results were closer to the real system than the exhaust gases outlet temperature predictions. It is observed that the simulation reacts more quickly than the experimental results and the change in performance has larger spikes. The difference between the simulation outlet temperature results was of a smaller magnitude than in the experiments, suggesting that there were heat losses from the system; something which the model does not predict.

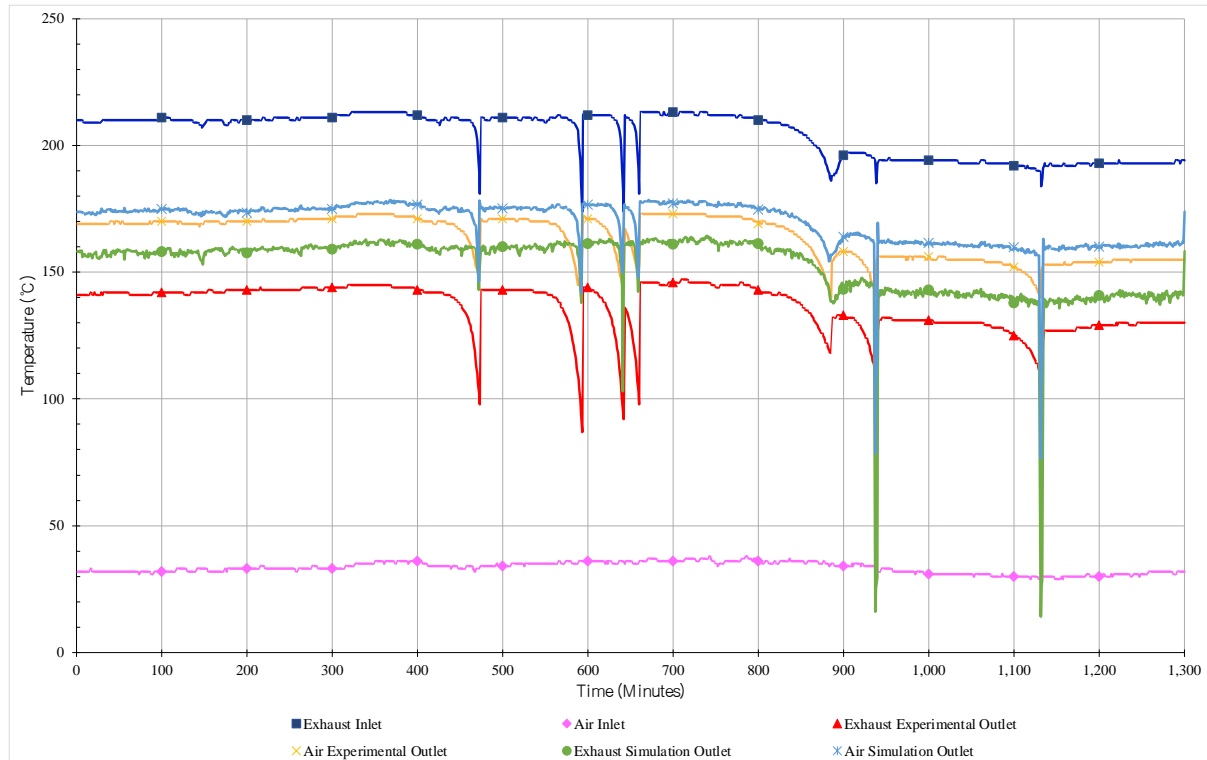


Figure 140: Experiment 2 transient results showing the experimental and simulated inlet and outlet temperatures of water and exhaust streams.

During the experiment, the air inlet temperature was roughly 35°C and remained relatively stable. The air outlet temperature increased to between 155 and 175°C and the exhaust outlet temperature reduced from between 190 and 210°C to between 130 and 145°C. The simulation used the measured air and exhaust inlet temperatures from the experiment as the temperature inlet inputs. In the simulation, the air outlet temperature increased to between 160 and 175°C and the exhaust outlet temperature reduced to between 140 and 160°C. It can be seen by comparing the graphical outlet temperature results that the simulation follows the experimental results very closely.

The system heat losses are also represented in Figure 141 where the heat transfer rates of the experiment are plotted against the simulation for comparison. The exhaust gases heat transfer rate (red line) is noticeably higher than for the air (blue line). This is artificially high as the heat transfer rate was calculated from the difference in temperature between the inlet and outlet. In the experiment, heat losses meant a larger temperature differential for the heat source, but this was not transferred into useful work. The air heat transfer rate being lower than the simulation heat transfer rate confirms that a proportion of heat from the source has not been transferred to

the sink as effective work. As the temperature of the exhaust gases at the evaporator inlet was higher than the temperature of air at the condenser inlet, there is a higher differential between them and the environment and casing so more losses are expected. In the laboratory-scale testing for Experiment 1, more losses were seen in the condenser section, but this was attributed to the fluid being a liquid whereas in this experiment, both heat transfer fluids were gaseous. Also exhibited in Figure 141 is how the exhaust gases heat transfer rate spikes upwards when a larger temperature differential between the exhaust gases inlet and outlet is seen.

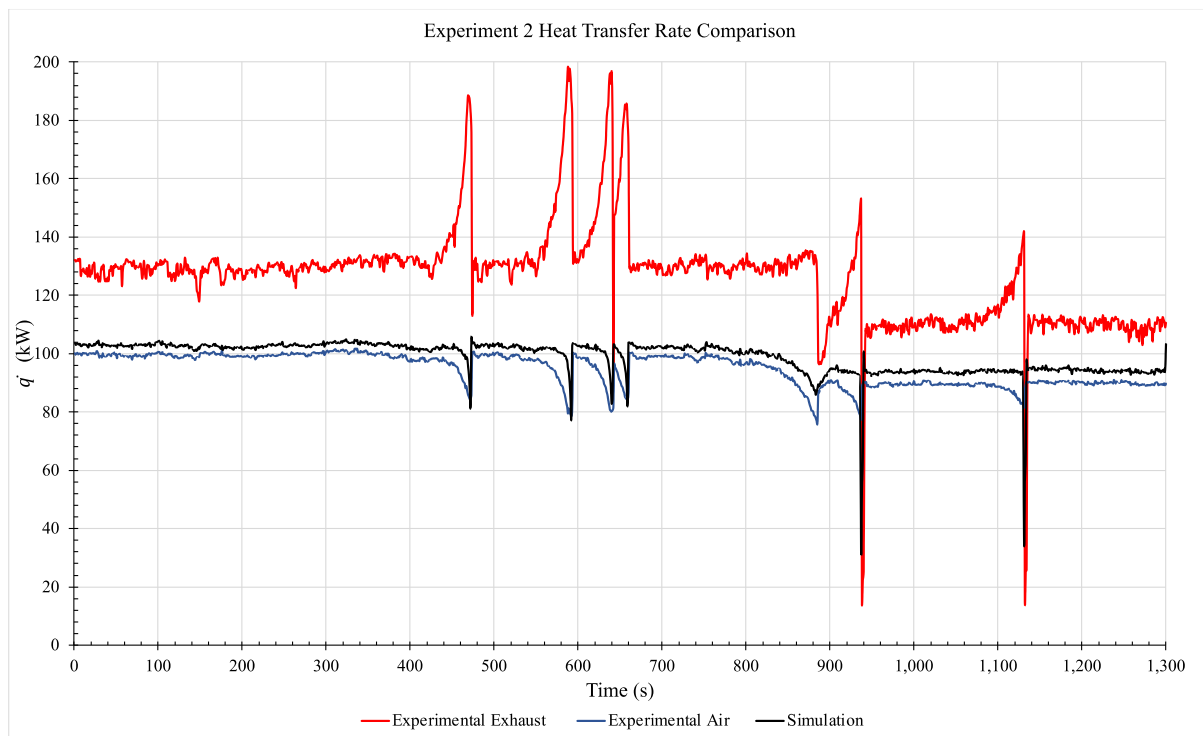


Figure 141: Experiment 2 heat transfer rate comparison for experimental and simulation results.

The experimental exhaust heat transfer rate and simulation heat transfer rate predictions spike downwards when the mass flow rate of the exhaust inputs dropped. The mass flow rates of the heat transfer fluids are shown in Figure 142. The exhaust mass flow rate fluctuated mostly around $6,200 \text{ kg}\cdot\text{hr}^{-1}$ up to 880 minutes, which then dropped to approximately $5,600 \text{ kg}\cdot\text{hr}^{-1}$. The air mass flow rate was relatively consistent and averaged at $2,600 \text{ kg}\cdot\text{hr}^{-1}$. When the mass flow rate of exhaust gases dropped, so did the heat transfer rates of the exhaust, air and simulation.

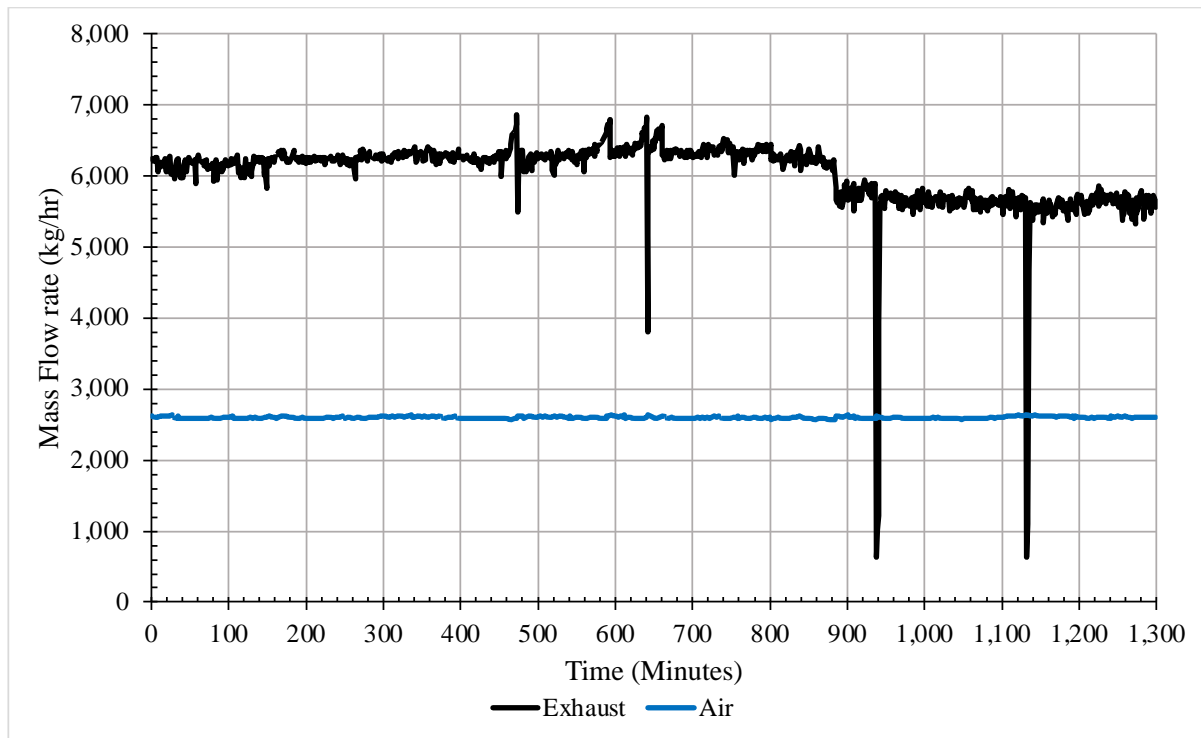


Figure 142: Experiment 2 mass flow rate measurements of exhaust gases and air.

Figure 143 shows a comparison between the experimental air heat transfer rate against the simulation heat transfer rate. The vast majority of the results were well within $\pm 25\%$ but it is observed that the majority of data points fall well within a $+15\%$ difference, with only a few outliers. There were a few major outliers predominantly caused by the faster response of the simulation compared to the experiment and lack of thermal inertia. As seen in Figure 142, the mass flow rate of the exhaust significantly dropped a few times due to the production process. This was accounted for in the simulation where a low heat transfer rate was predicted, but due to the HPHE having thermal inertia, the experimental results did not show this significant drop; explaining the results under -25% . There were two results with an over $+25\%$ difference, where the simulation reacted to peaks in the exhaust mass flow rate at 593 and 642 minutes and the system did not react as strongly.

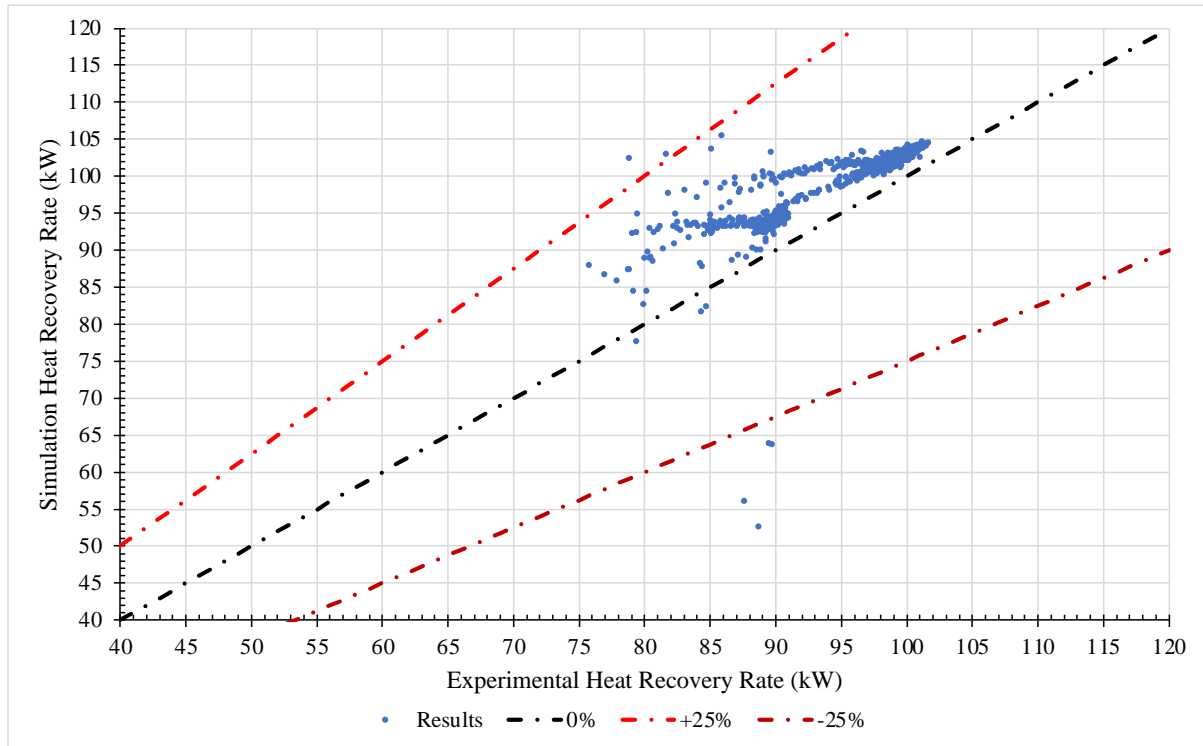


Figure 143: Experiment 2 heat transfer rate comparison for experimental against simulation results.

The simulation slightly overpredicted the performance of the HPHE, this is as expected as the model assumes perfect insulation, with no energy losses. Also, with the large number of variables and extensive calculations that need to be conducted, this performance is more than acceptable. Excluding the six major outliers, heat transfer rate error analysis conducted on the experimental and simulation heat transfer results (as Section 6.1.11), shown in Figure 144, display a range between -3 and +19%. The average error was +4.01%, with the majority of results falling within a +3 to +5% error, highlighting that the simulation overpredicted the performance, due to the aforementioned reasons.

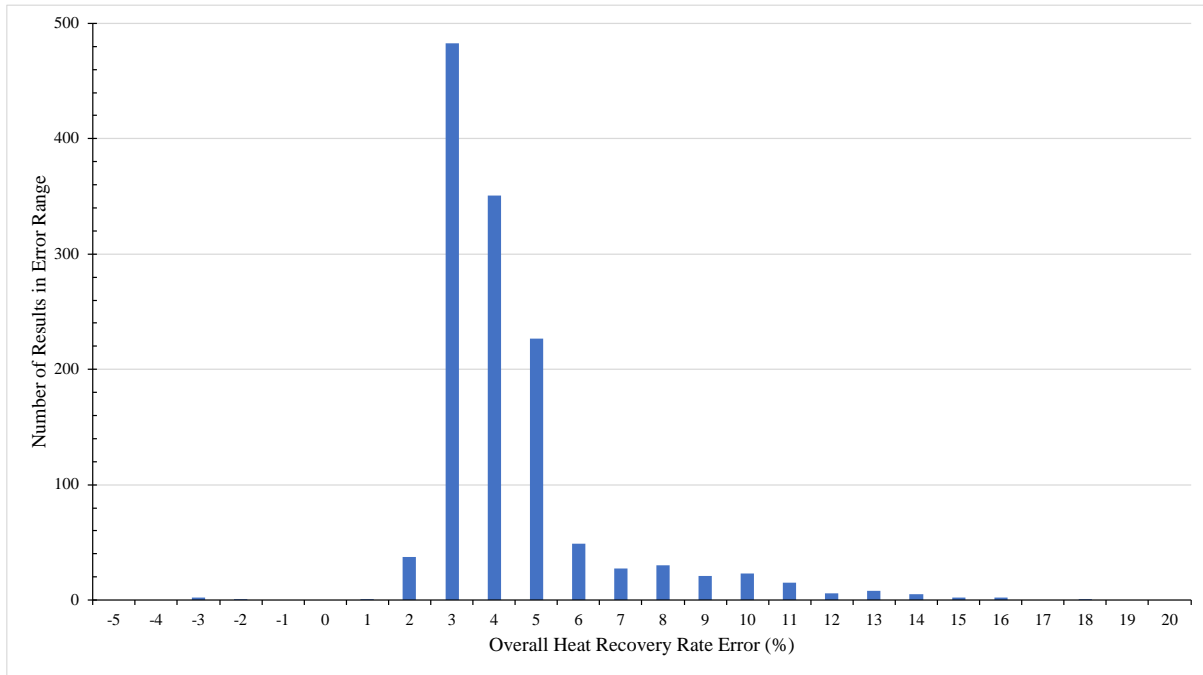


Figure 144: Experiment 2 heat transfer rate percentage difference between experimental and simulation results.

Error between the predictions of the simulation and the experimental outlet temperatures for both the exhaust and air outlet temperatures was conducted, calculated using Equation (6.2), and these results are shown in Figure 145 and Figure 146. The exhaust outlet temperature error ranged between -3 and +17%, with the average error being +3.76%. The air outlet temperature error ranged between -1 and +7%, with the average error being +1.30%. Both cases show that the simulated outlet temperatures were higher than the experimental outlet temperatures. The range between the exhaust outlet temperature error was larger than for the air outlet temperature.

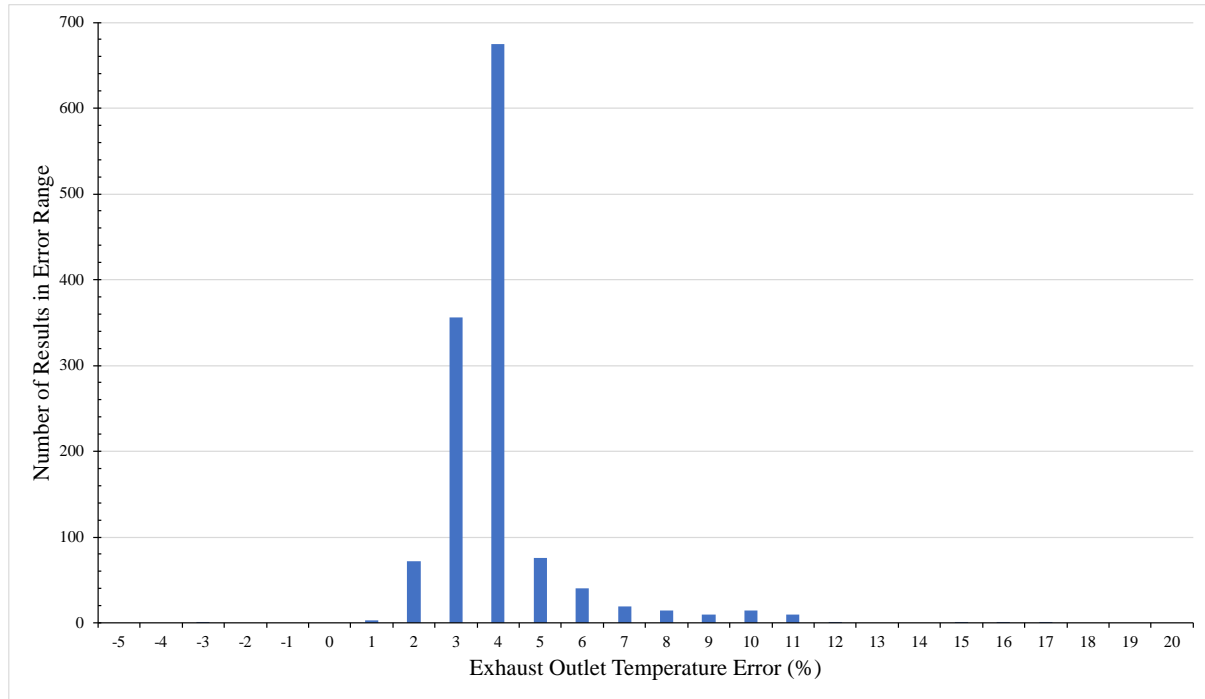


Figure 145: Experiment 2 percentage difference in outlet temperature error between experimental and simulation exhaust outlet results.

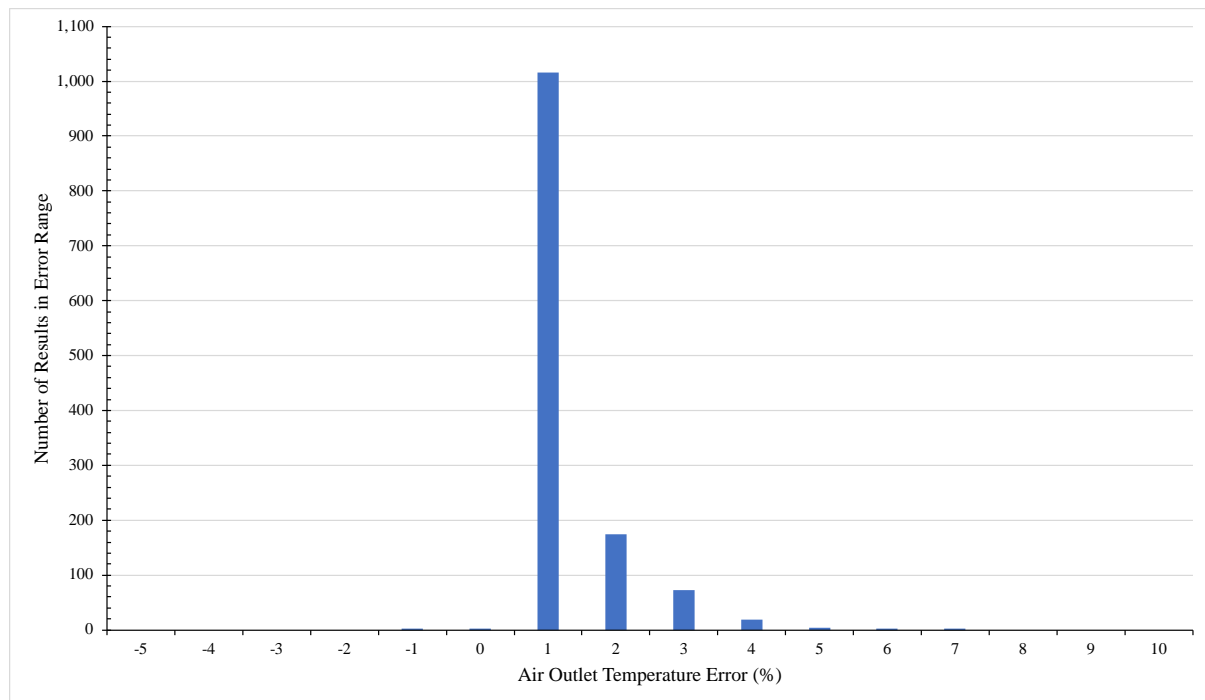


Figure 146: Experiment 2 percentage difference in outlet temperature error between experimental and simulation air outlet results.

6.2.1. Statistical Analysis

6.2.1.1. Exhaust Gases Heat Source

Spearman correlation analysis was conducted for the heat transfer rate of exhaust of the experiment, as shown in Table 40. Heat transfer rate of exhaust (\dot{q}_{ex}) was set as the dependent variable with exhaust inlet temperature ($T_{ex,in}$), air inlet temperature ($T_{air,in}$), exhaust mass flow rate (\dot{m}_{ex}) and air mass flow rate (\dot{m}_{air}) set as the independent variables.

Table 40: Spearman correlation analysis for experimental exhaust heat transfer rate.

Variable	\dot{q}_{ex}	$T_{ex,in}$	$T_{air,in}$	\dot{m}_{ex}	\dot{m}_{air}
\dot{q}_{ex}	1.000	0.625	0.635	0.843	-0.062
$T_{ex,in}$	0.625	1.000	0.709	0.747	-0.003
$T_{air,in}$	0.635	0.709	1.000	0.776	-0.141
\dot{m}_{ex}	0.843	0.747	0.776	1.000	-0.071
\dot{m}_{air}	-0.062	-0.003	-0.141	-0.071	1.000

The strongest correlation seen was between the mass flow rate of exhaust gases and the exhaust heat transfer rate, $\dot{m}_{ex}-\dot{q}_{ex}$, at 0.843. This shows that the higher the mass flow rate of exhaust, the higher the exhaust heat transfer rate. Likewise, there is a strong positive correlation between the exhaust inlet temperature and exhaust heat transfer rate, $T_{ex,in}-\dot{q}_{ex}$, at 0.625, which is to be expected.

An unexpected result observed was the relationship between the air inlet temperature and exhaust heat transfer rate $T_{air,in}-\dot{q}_{ex}$. There was a positive correlation of 0.635, suggesting that the higher the air inlet temperature, the higher the exhaust heat transfer rate. This is counterintuitive as the lower the air inlet temperature, the higher the exhaust heat transfer rate should be as there would be a larger temperature difference between the evaporator inlet and condenser inlet. However, when viewing Figure 140, it can be seen that, even though relatively consistent, there was a lower air inlet temperature for the latter part of the experiment when there was a lower mass flow rate of exhaust gases, which were also at a reduced temperature.

There was an extremely weak negative correlation between the mass flow rate of air and the exhaust heat transfer rate, $\dot{m}_{air}-\dot{q}_{ex}$. Though the mass flow rate of air should be intrinsically

linked to the exhaust heat transfer rate, it was kept extremely stable over the course of the experiment and was not an adjusted variable, therefore a strong correlation is not expected. However, a negative correlation is not expected as, when the mass flow rate of air increases, the heat transfer rate from the exhaust should increase, though the value of the correlation is very small and hence insignificant. If possible, it would be interesting to vary the mass flow rate of the air in order to expand upon the understanding of the performance of this HPHE geometry more fully.

Coefficient analysis gave a predictive equation in the form of Equation (6.7), within the bounds of this experimental set-up and conditions.

$$\dot{q}_{ex} = 30.482T_{ex,in}^{0.302} + 197.735T_{w,in}^{0.178} - 7219.29\dot{m}_{ex}^{-0.01} + 3840.338\dot{m}_w^{-1.806} + 6248.851 \quad (6.7)$$

A R^2 value of 0.547 was seen, which is high but it shows that there is the potential for other external influence on the results of the experiment. This is attributed to heat losses from the casing. There were 43 outliers out of the 1,300 results; 3.3% of the results, which is relatively insignificant. These all related to the heat transfer rate spikes seen where there were large fluctuations in conditions.

6.2.1.2. Air Heat Sink

Spearman correlation analysis was conducted for the heat transfer rate of air of the experiment, as shown in Table 41. Heat transfer rate of air (\dot{q}_{air}) was set as the dependent variable with exhaust inlet temperature ($T_{ex,in}$), air inlet temperature ($T_{air,in}$), exhaust mass flow rate (\dot{m}_{ex}) and air mass flow rate (\dot{m}_{air}) set as the independent variables.

Table 41: Spearman correlation analysis for experimental exhaust heat transfer rate.

Variable	\dot{q}_{air}	$T_{ex,in}$	$T_{air,in}$	\dot{m}_{ex}	\dot{m}_{air}
\dot{q}_{air}	1.000	0.737	0.242	0.427	0.290
$T_{ex,in}$	0.737	1.000	0.709	0.747	-0.003
$T_{air,in}$	0.242	0.709	1.000	0.776	-0.141
\dot{m}_{ex}	0.427	0.747	0.776	1.000	-0.071
\dot{m}_{air}	0.290	-0.003	-0.141	-0.071	1.000

The strongest correlation seen against the heat transfer rate of the air was with exhaust inlet temperature, followed by the exhaust mass flow rate. The air mass flow rate followed with a weaker correlation and then a weak correlation for air inlet temperature. These results are not in keeping with theory as the air heat transfer rate should be linked more directly with the variables seen in the condenser section of the HPHE and all the correlations were positive.

A $T_{ex,in}-\dot{q}_{air}$ value of 0.737 shows that the higher the exhaust gases inlet temperature, the higher the air heat transfer rate. This fits very well as the higher the exhaust inlet temperature, the higher the air heat transfer rate should be. A $\dot{m}_{ex}-\dot{q}_{air}$ value of 0.427, shows that the higher the exhaust gases mass flow rate, the higher the air heat transfer rate.

Two unexpected results were obtained for the condenser section. Firstly, there was a positive $T_{air,in}-\dot{q}_{air}$ correlation of 0.242, meaning that the higher the air inlet temperature, the higher the air heat transfer rate. Secondly, a $\dot{m}_{air}-\dot{q}_{air}$ value of 0.290 is unexpected as it implies that there is little correlation between the mass flow rate of air and the air heat transfer rate. This should not be the case, but is explained in the exhaust gases analysis above. Mainly this is due to a lack in variability of the air mass flow rate and inlet temperature so the analysis was mostly determined by fluctuating conditions in the exhaust. However, this shows that a full characterisation of the performance has not been completed.

Coefficient analysis gave a predictive equation in the form of Equation (6.8), within the bounds of this experimental set-up and conditions.

$$\dot{q}_{air} = 1.568E - 5T_{ex,in}^{2.828} + 308.7047T_{w,in}^{-0.241} + 1502.097\dot{m}_{ex}^{-0.002} - 196.577\dot{m}_w^{-439.984} - 1563.423 \quad (6.8)$$

A R^2 value for the model was 0.835, which is higher than for the exhaust analysis showing that the results were more in keeping with the predictors. This also explains why the simulation was more in keeping with the air-side, condenser, results.

There were 42 outliers; 3.2% of the total results. This, again, related to the peaks in conditions. The number of outliers was expected to be less as the condenser conditions did not fluctuate as greatly as the evaporator conditions, but this shows that both sections are linked and depend upon each other, which is expected.

6.2.2. Experiment 2 Summary

Experiment 2 was from a full-scale installation and, therefore, could not be tested to the same extent as Experiment 1. Two overarching conditions were seen, stemming from the evaporator section, and the model predicted exhaust and air outlet temperatures and heat transfer rates very well. The percentage error in temperature outlet predictions was low and the predicted heat transfer rate was well within $\pm 25\%$ of experimental results, with the vast majority of results falling well within a $+15\%$ difference. The average difference between simulated and experimental heat transfer rates was $+4.1\%$ showing that the simulation overpredicted performance. There were a few outliers due to thermal inertia but not to the extent to cause concern. The overall heat transfer rate for air for the unit ranged between 75.7 and 101.6 kW and averaged 94.7 kW. The model predicted the HPHE to have an average performance of 98.9 kW. To this end, the model has shown that it is capable of predicting performance for this exhaust-to-air application, even if slightly overpredicting.

6.3. Experiment 3: Full-Scale Aluminium Heat Treatment Furnace

For this experiment, the sampling frequency rate was set at 5 seconds. This, along with a longer period of time, 2.3 days, meant that a significant amount of data were available. Figure 147 shows the graph produced as an output of the TRNSYS simulation and includes the inlet and outlet temperatures of the source and sink fluids.

Figure 148 shows the experimental inlet and outlet temperature data of the installed HPHE along with the simulation results for comparison. The exhaust and air inlet temperatures were fed into the model and the experimental outlet temperatures were compared against the simulation to validate the component in terms of the calculated heat transfer rate and difference in temperature. In this case, the simulated air outlet temperature predictions were closer to the real system than the exhaust gases outlet temperature predictions. The difference between the simulation outlet temperature results was of a smaller magnitude than observed for the experiments and both experimental outlet temperatures were lower than the simulated values. This shows that there were heat losses from the system, which the model does not predict. An analysis is conducted in Section 6.3.3 to rationalise this difference.

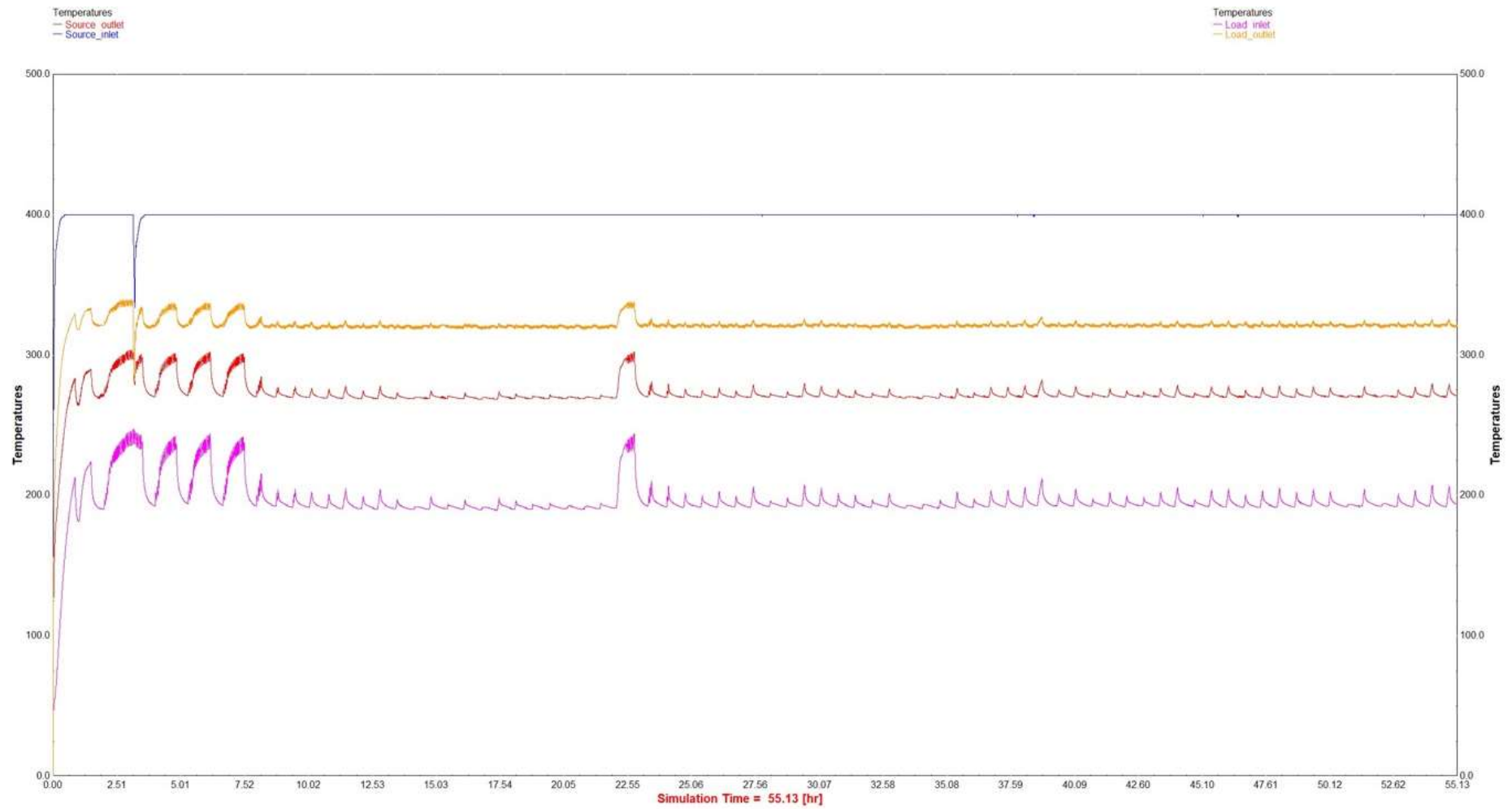


Figure 147: Experiment 3 TRNSYS temperature output results.

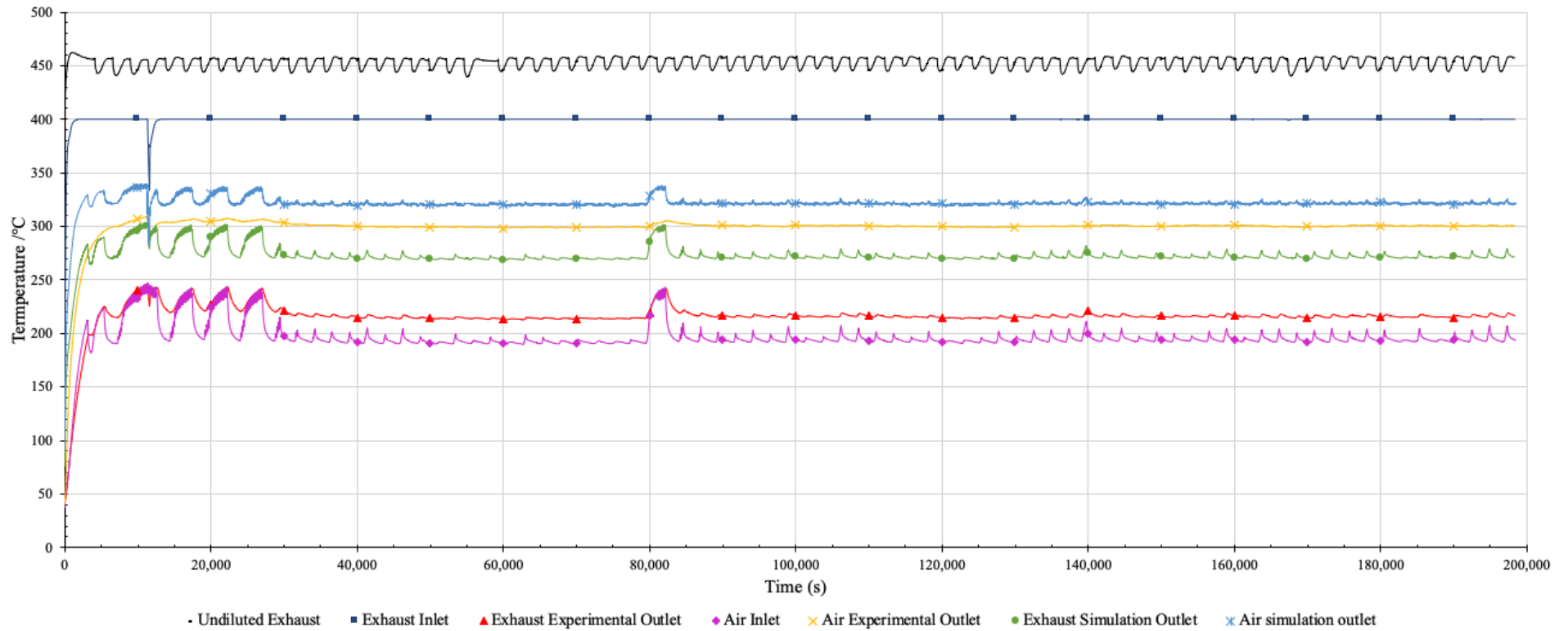


Figure 148: Experiment 3 transient results showing the experimental and simulated inlet and outlet temperatures of exhaust and air streams.

The undiluted exhaust gases temperature was measured from the furnace and is shown to visualise the exhaust inlet temperature prior to dilution to 400°C. In the experiments, the air inlet temperature is roughly 195°C, which remained relatively stable and only varied by roughly 10°C. The air outlet temperature stayed around 299°C and the exhaust outlet temperature around 216°C; both depending on the inlet conditions. The air and exhaust inlet temperatures from experiment were used as the inputs for the simulation. The simulation air temperature was raised to between 321°C at the outlet and the exhaust temperature reduced to 273°C at the outlet. It can be seen by comparing the graphs that there was some discrepancy between the simulation and experimental outlet results.

The system heat losses are also represented in Figure 149, where the heat transfer rate of the experiment is plotted against the simulation heat transfer rate (black line) for comparison. The heat transfer rate of the exhaust gases (red line) is much higher than the air heat transfer rate (blue line). The exhaust heat transfer rate is misleadingly high and the air heat transfer rate is low as the heat transfer rate was calculated from the difference in temperature between the inlet and outlet of each stream. In the experiment, heat losses meant a larger temperature differential across the HPHE for the heat source fluid, but this was not transferred into useful heat exchange work. Also, there were heat losses from the air condenser side, which is confirmed by the experimental air heat transfer rate being lower than the simulated heat transfer rate; the heat from the source has not been transferred to the sink as effective work and some has been lost. The inlet temperatures for this experiment were much higher than seen in the previous experiments, leading to more thermal losses to the environment.

At the start of the heat transfer rate results shown in Figure 149, it can be seen that there are large spikes between 0 and around 10,000 seconds. This is attributed to the HPHE warming up to stable operating conditions where a proportion of heat is being transferred into the casing and the thermosyphons. This caused the exhaust gases outlet temperature and air outlet temperature to be reduced, causing artificially high and low heat transfer rates, respectively. After this period of reaching operating conditions, the system remained very stable with only a minor deviation observed at around 80,000 seconds.

Figure 150 shows the mass flow rate measurements of the exhaust gases and air streams. The air mass flow rate fluctuated mostly around $1,774 \text{ kg}\cdot\text{hr}^{-1}$. The exhaust mass flow rate was relatively consistent and averaged at $1,500 \text{ kg}\cdot\text{hr}^{-1}$, with slightly more fluctuation.

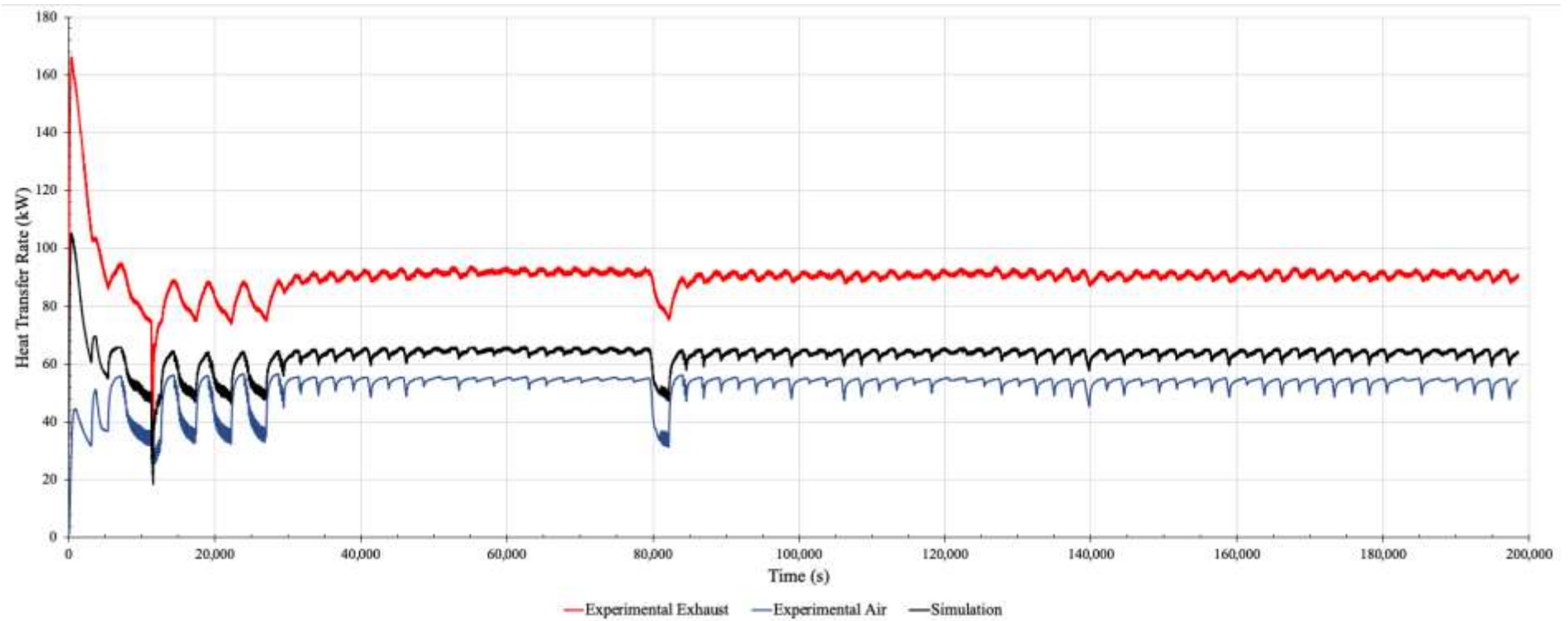


Figure 149: Experiment 3 heat transfer rate comparison for experimental and simulation results.

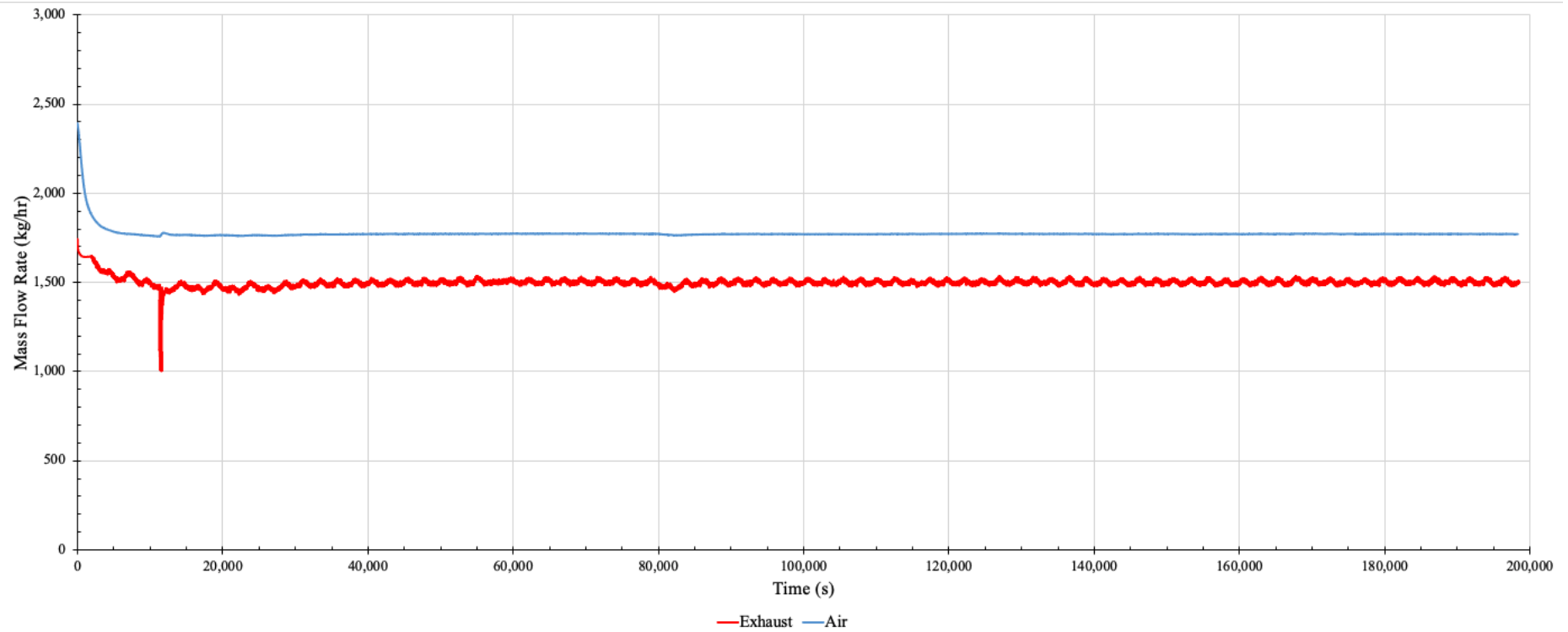


Figure 150: Experiment 3 mass flow rate measurements of exhaust gases and air.

Figure 151 shows a comparison between the experimental air heat transfer rate and the simulation heat transfer rate. The results from 0 to 20,000 seconds were removed as this was when the heat exchanger was reaching operating conditions and, due to the high number of results, caused the graph to be unreadable. The majority of the simulated air heat transfer rate results were within +25% of the experimental heat transfer rate results but there were many outliers. The Figure also shows how there is a large perceived difference between the exhaust and air heat transfer rates. The majority of the simulated exhaust heat transfer rate results did not fall within $\pm 25\%$ of the simulated values. The simulation, in this case, did not predict the performance of the HPHE to a high enough accuracy, which is expected as the model assumes perfect insulation with no energy losses.

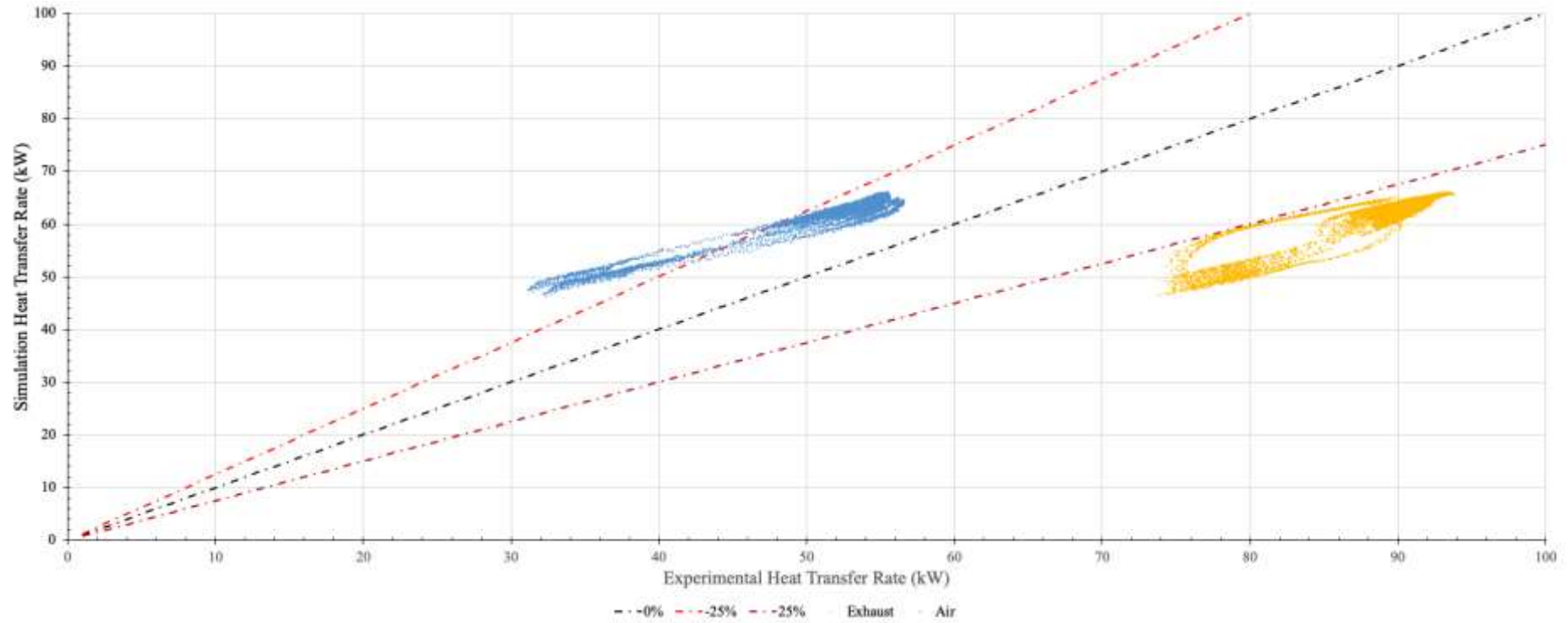


Figure 151: Experiment 3 heat transfer rate comparison for experimental against simulation results.

Error analysis conducted on the percentage difference between the experimental air heat transfer rate and simulation heat transfer rate results, not including the start-up period, are shown in Figure 152, and display a range between +11 and +37%. The average error was +17.05%. In other words, the simulated heat transfer rate was consistently predicted to be higher than the observed experimental heat transfer rate.

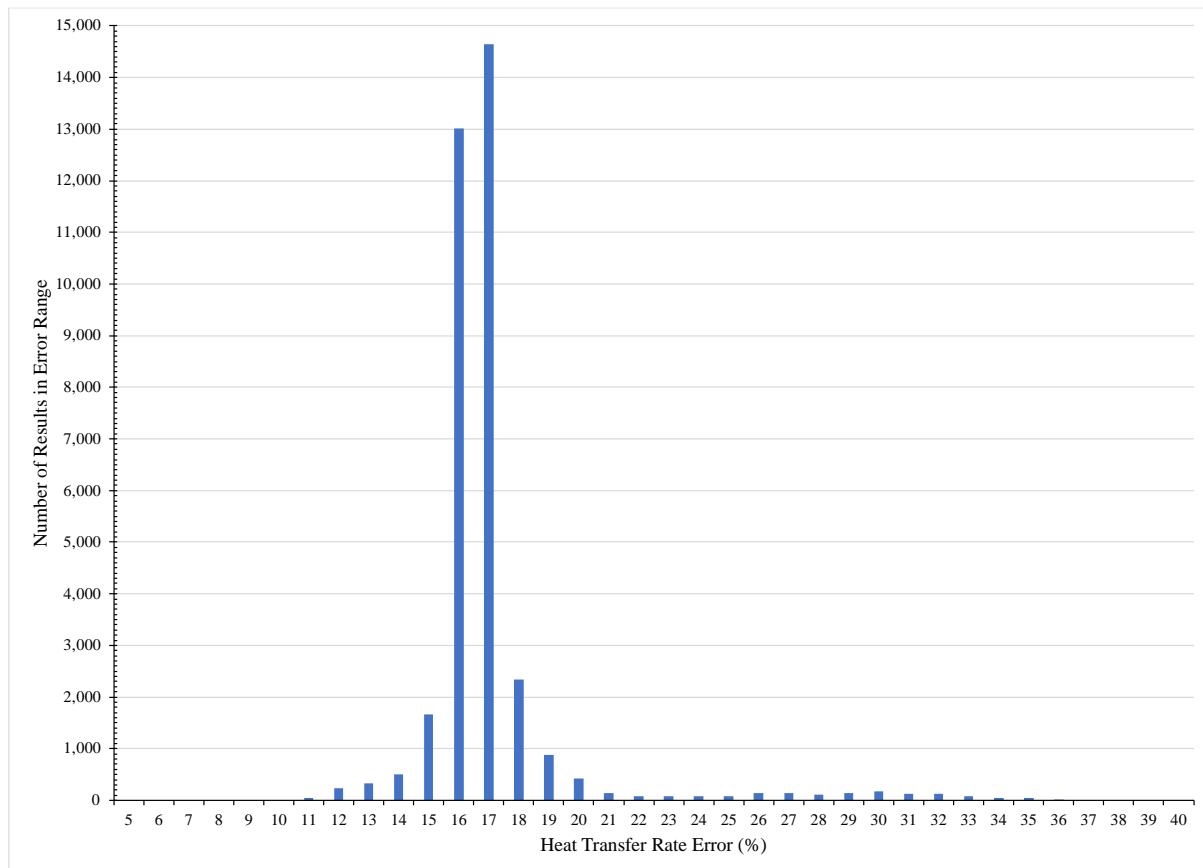


Figure 152: Experiment 3 heat transfer rate percentage difference between experimental and simulation results.

Percentage error difference between the simulated and experimental exhaust and air outlet temperatures was conducted, calculated using Equation (6.2), and these results are shown in Figure 153 and Figure 154. The simulated exhaust outlet temperature error ranged between +3 and +12% higher than the experimental exhaust outlet temperature, with the average being +10.17%. The simulated air outlet temperature error ranged between +2 and +6% higher than the experimental air outlet temperature, with the average error being +3.55%. The spread between the exhaust temperature error results was larger than seen with the air temperature error results.

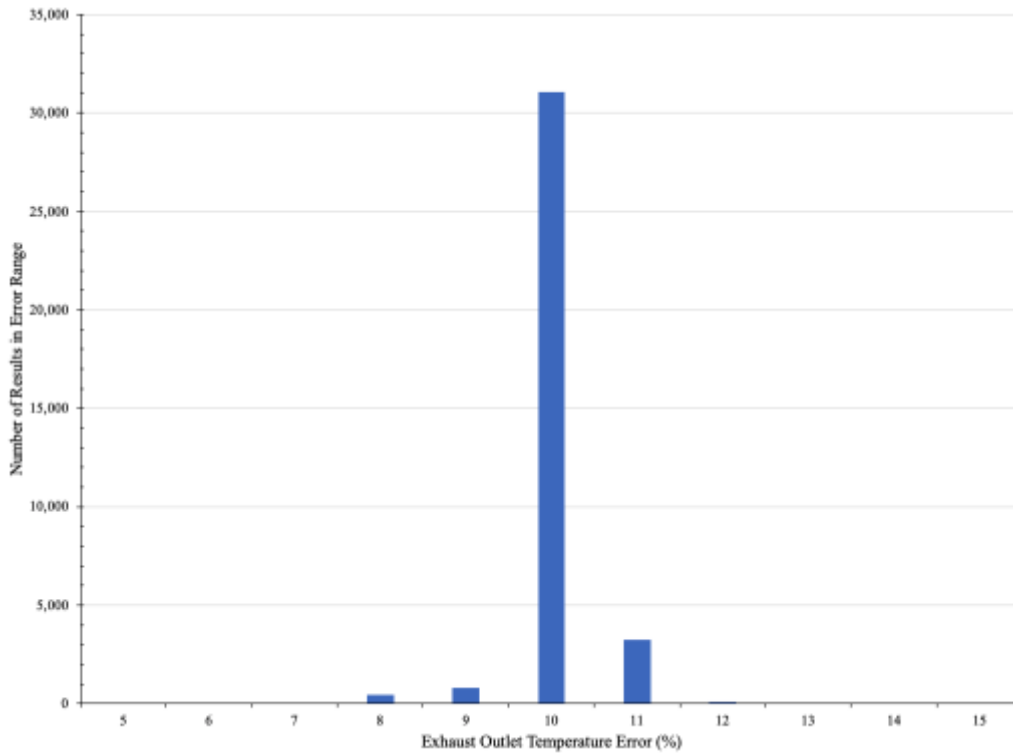


Figure 153: Experiment 3 difference in temperature error between experimental and simulation exhaust outlet results.

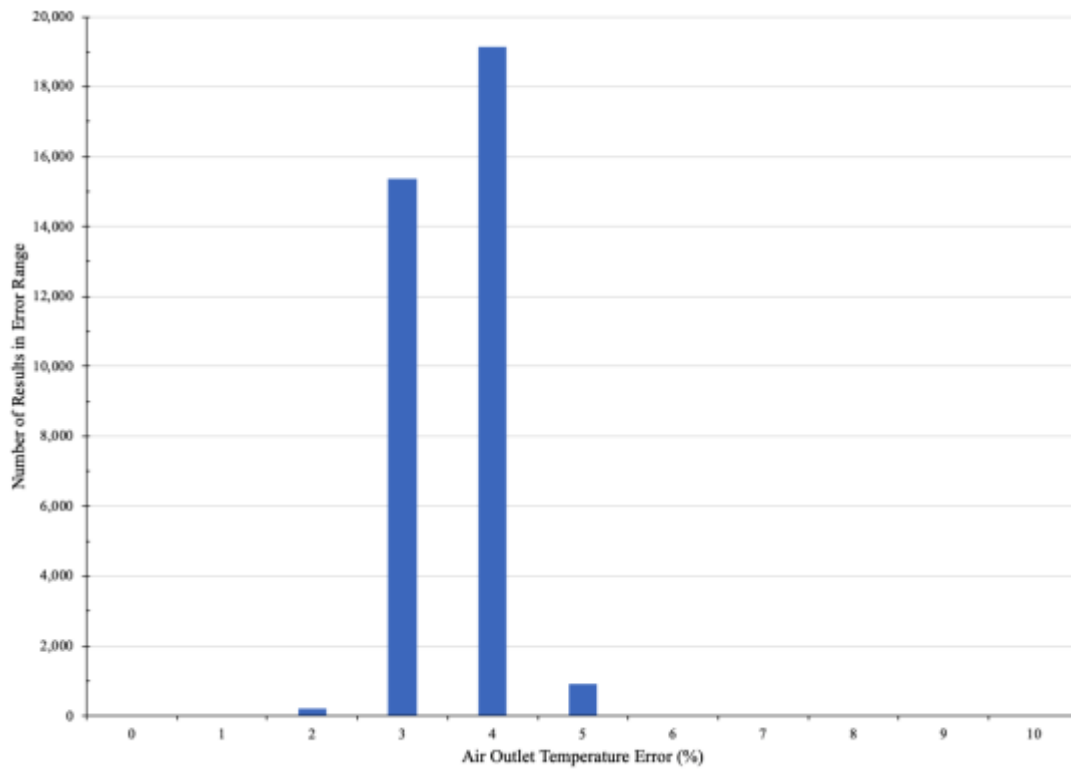


Figure 154: Experiment 3 air temperature difference error between experimental and simulation results.

6.3.1. Statistical Analysis

For the statistical analysis, the start-up period of the HPHE is removed, such that results prior to 20,000 seconds are discounted. Overall, there were 35,693 data points.

6.3.1.1. Exhaust Gases Heat Source

Spearman correlation analysis was conducted for the experimental exhaust heat transfer rate, as shown in Table 42. Exhaust heat transfer rate (\dot{q}_{ex}) was set as the dependent variable with exhaust inlet temperature ($T_{ex,in}$), air inlet temperature ($T_{air,in}$), exhaust mass flow rate (\dot{m}_{ex}) and air mass flow rate (\dot{m}_{air}) set as the independent variables.

Table 42: Spearman correlation analysis for experimental exhaust heat transfer rate.

Variable	\dot{q}_{ex}	$T_{ex,in}$	$T_{air,in}$	\dot{m}_{ex}	\dot{m}_{air}
\dot{q}_{ex}	1.000	-0.007	-0.832	0.885	0.712
$T_{ex,in}$	-0.007	1.000	0.003	-0.025	-0.007
$T_{air,in}$	-0.832	0.003	1.000	-0.654	-0.602
\dot{m}_{ex}	0.885	-0.025	-0.654	1.000	0.441
\dot{m}_{air}	0.712	-0.007	-0.602	0.441	1.000

The strongest correlation seen was between the exhaust mass flow rate and the exhaust heat transfer rate, $\dot{m}_{ex}-\dot{q}_{ex}$, at 0.885. This shows that the higher the mass flow rate of the exhaust, the higher the exhaust heat transfer rate.

There is a very strong negative correlation between the air inlet temperature and exhaust heat transfer rate, $T_{air,in}-\dot{q}_{ex}$, at -0.832. Likewise, there is a very strong positive correlation between the air mass flow rate and exhaust heat transfer rate, $\dot{m}_{air}-\dot{q}_{ex}$, at 0.712. Both of these results are expected as, the higher the exhaust mass flow rate, the more energy content available. The lower the air inlet temperature, the more capacity for extracting heat and higher temperature differential between source and sink inlet temperature.

A very unexpected, counterintuitive, result was the relationship between the exhaust inlet temperature and the exhaust heat transfer rate, $T_{ex,in}-\dot{q}_{ex}$. There is an extremely weak negative correlation of -0.007 suggesting that the exhaust inlet temperature has very little to no effect

on the exhaust heat transfer rate. However, when viewing Figure 140, it can be seen that the exhaust inlet temperature was kept so consistent, with such little deviation, that it does not play a critical part in the analysis.

Coefficient analysis gave a predictive equation in the form of Equation (6.9), within the bounds of this experimental set-up and conditions.

$$\dot{q}_{ex} = 1.166T_{ex,in}^{1.359} + 1990.984T_{w,in}^{-0.41} - 0.069\dot{m}_{ex}^{-7.998} - 0.275\dot{m}_w^{-24.988} - 5531.689 \quad (6.9)$$

A R^2 value of 0.774 was seen, which is very high. There were 840 outliers out of the 35,693 results; 2.35% of the results, which is relatively insignificant. All the outliers relate to the heat transfer rate spikes seen between 20,000 to 30,000 seconds, where there were fluctuating conditions, which could have been removed from the analysis.

6.3.1.2. Air Heat Sink

Spearman correlation analysis was conducted for the air heat transfer rate of the experiment, as shown in Table 43. Air heat transfer rate (\dot{q}_{air}) was set as the dependent variable with exhaust inlet temperature ($T_{ex,in}$), air inlet temperature ($T_{air,in}$), exhaust mass flow rate (\dot{m}_{ex}) and air mass flow rate (\dot{m}_{air}) set as the independent variables.

Table 43: Spearman correlation analysis for experimental exhaust heat transfer rate.

Variable	\dot{q}_{air}	$T_{ex,in}$	$T_{air,in}$	\dot{m}_{ex}	\dot{m}_{air}
\dot{q}_{air}	1.000	0.000	-0.890	0.595	0.281
$T_{ex,in}$	0.000	1.000	0.003	-0.025	-0.007
$T_{air,in}$	-0.890	0.003	1.000	-0.654	-0.602
\dot{m}_{ex}	0.595	-0.025	-0.654	1.000	0.441
\dot{m}_{air}	0.281	-0.007	-0.602	0.441	1.000

As with the exhaust heat transfer rate, the strongest correlation seen was between the air inlet temperature and the air heat transfer rate, $T_{air,in}-\dot{q}_{air}$, at -0.890. This shows that the lower the inlet temperature of the air, the higher the air heat transfer rate.

There is a positive correlation between the exhaust mass flow rate and air heat transfer rate, $\dot{m}_{ex}-\dot{q}_{air}$, at 0.595. There is a weak positive correlation between the air mass flow rate and exhaust heat transfer rate, $\dot{m}_{air}-\dot{q}_{air}$, of 0.281.

Again, there is a negligible correlation between the exhaust inlet temperature and air heat transfer rate, $T_{ex,in}-\dot{q}_{air}$, of 0.000 because the exhaust inlet temperature was kept very consistent.

Coefficient analysis gave a predictive equation in the form of Equation (6.10), within the bounds of this experimental set-up and conditions. Note that the exhaust inlet temperature had a coefficient of 0.000, which means it was negated.

$$\dot{q}_{air} = -1.3667T_{w,in}^{0.843} + 1129.970\dot{m}_{ex}^{-0.001} - 82.705\dot{m}_{air}^{0.373} + 392.099 \quad (6.10)$$

The highest R^2 value for the model was seen in this experiment at 0.999. This is confirmed by there only being 12 outliers; 0.03% of the total results. The R^2 value is higher than for the exhaust analysis showing that the air heat transfer rate results were more in keeping with the predictors.

6.3.2. Pressure Drop Analysis

Figure 155 shows the graphical pressure drop output from TRNSYS. In this HPHE, there are two different types of finning on the thermosyphons depending on whether they were filled with Dowtherm A or distilled water. The pitch was the only difference at 4 and 6 mm respectively. For the evaporator section, the Dowtherm A heat pipes with a pitch of 4 mm would have been encountered first by the exhaust gases stream. For the condensers section, the water heat pipes with a pitch of 6mm would be encountered first by the air stream. Interestingly, even though the exhaust mass flow rate was less by roughly $275 \text{ kg}\cdot\text{hr}^{-1}$, the pressure drop was predicted to be higher by roughly 10 Pa. The condenser section face area was larger than the evaporator face area, which also reflects why the condenser pressure drop was higher.

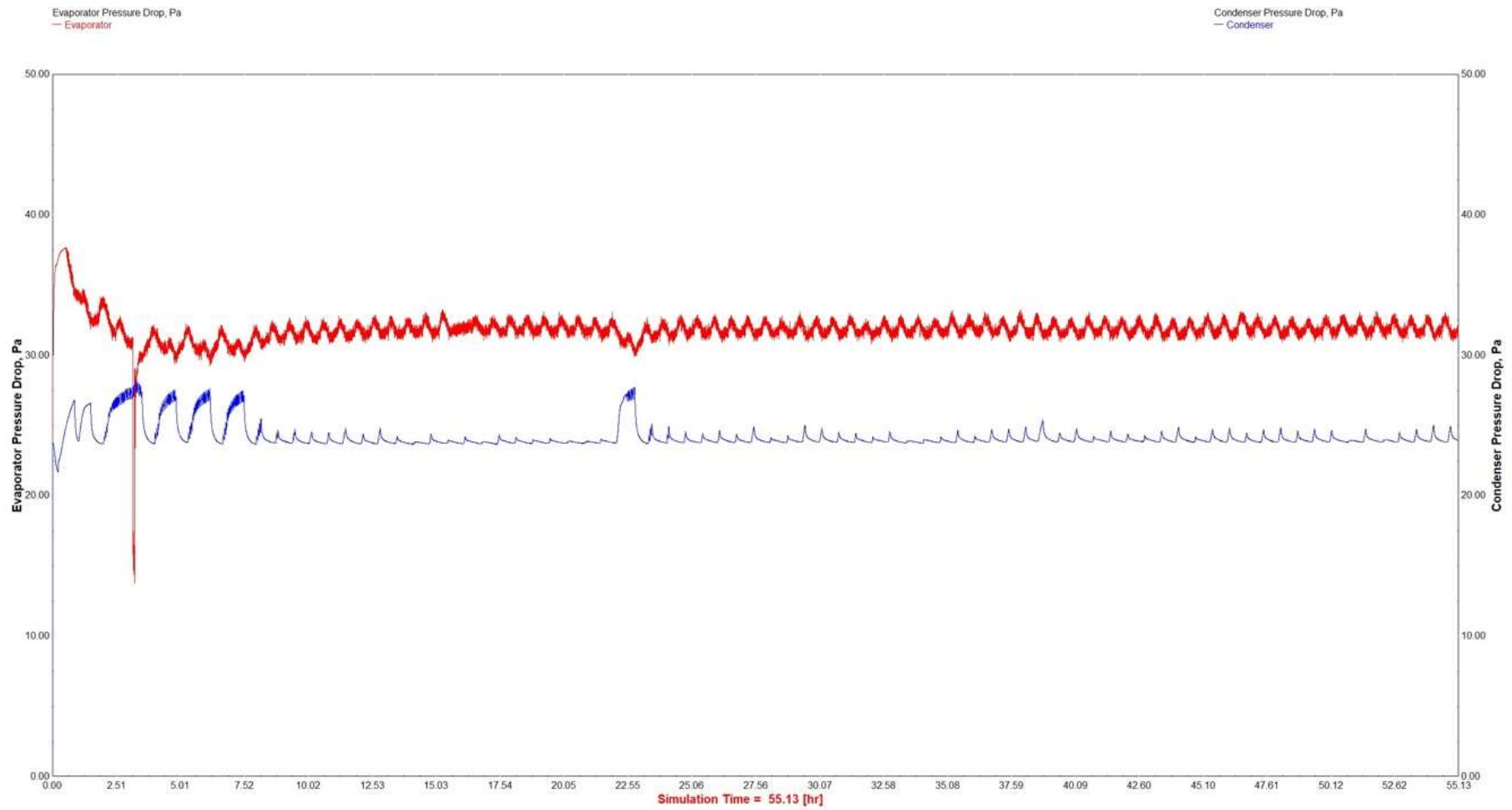


Figure 155: Experiment 3 simulation pressure drop TRNSYS output.

Figure 156 shows the pressure drop measurements across the HPHE for both the condenser and evaporator sections. The line of best fit shows a pressure drop of around 93 Pa at 1,500 kg.hr⁻¹ for the evaporator section. The simulation predicted around 32-33 Pa, which is in the same order or magnitude. For the condenser section, the line of best fit shows a pressure drop of 60.5 Pa for 1,775 kg.hr⁻¹ for the condenser section. The simulation predicted around 24 to 25 Pa, which is in the same order or magnitude. Both these results are acceptable in terms of pressure drop predictions, which are notoriously inaccurate.

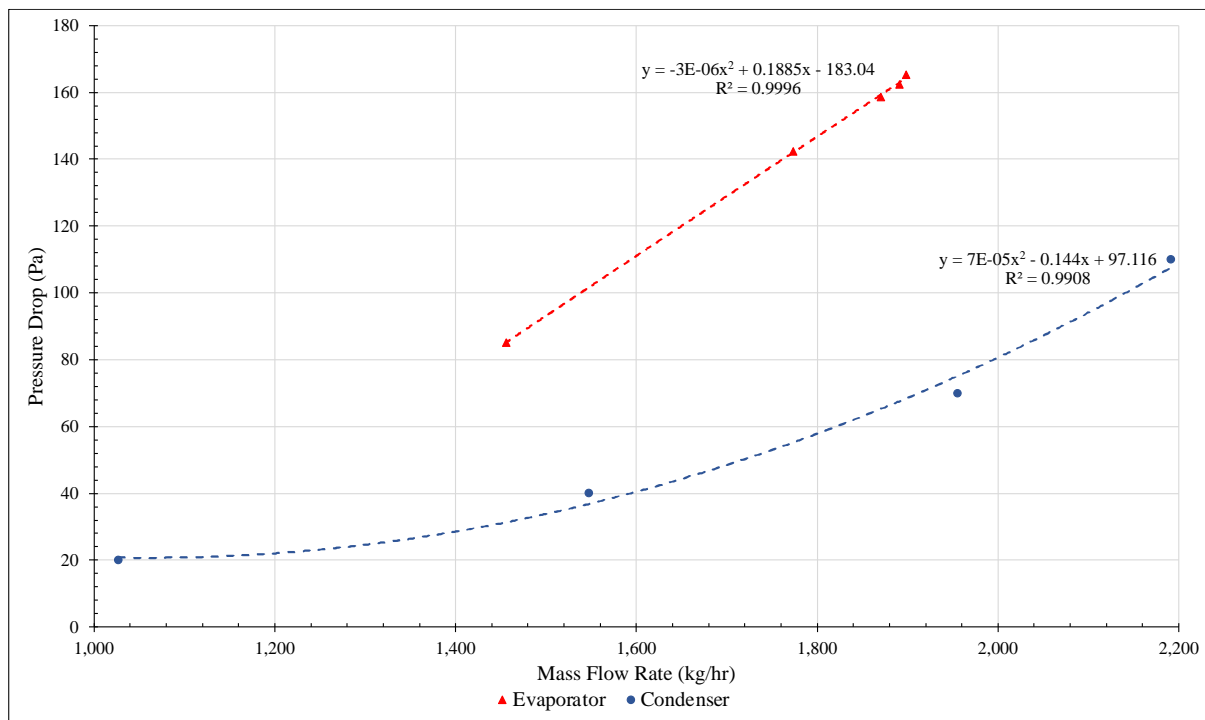


Figure 156: Experiment 3 evaporator and condenser pressure drop measurements.

The results confirmed that the evaporator section experienced a greater pressure drop as seen in the simulation. The pressure drop here is so small in comparison to other technologies that the results are acceptable even if they underpredicted by a margin.

6.3.3. Heat Loss Analysis

Due to the large difference seen between the simulation and experimental heat transfer rate results for Experiment 3, natural convection and radiation analysis was conducted to see if the losses of this magnitude could be explained. The ambient temperature was 20°C and the casing temperature of the evaporator and condenser sections were measured in four different

locations. The combined losses of radiation and natural convection at these operating conditions was predicted at approximately 35 kW and the calculations are provided in Appendix D. If these losses were present, the unit should have been better insulated, and this was an outcome that was to be rectified during the project. Secondly, the order of magnitude of losses explains the difference between the simulation and experimental heat transfer rate and outlet temperature differences.

6.3.4. Experiment 3 Summary

The largest difference between simulation and experimental heat transfer rate results was seen for Experiment 3. The percentage difference between simulated outlet temperature and outlet temperature results were also higher than desired meaning the calculated heat transfer rates were not well within $\pm 25\%$, with many results falling outside. There were many outliers, which were seen to be from the start-up process. The experimental air heat transfer rate was between 31.2 and 66.1 kW and averaged 53.4 kW, whereas the model predicted an average heat transfer rate of 64.3 kW. Therefore, the model has been shown to not adequately predict performance for this exhaust-to-air application, especially when significant heat losses are present, the inlet temperatures are higher and thermal insulation is not sufficiently present. Heat loss analysis on the HPHE showed calculated losses of 35 kW from natural convection and radiation. This value fits relatively well with the presented results.

Pressure drop analysis showed a reasonable agreement in the order of magnitude predicted. The simulated pressure drop results were lower than the experiment results but were close enough to not warrant any concerns.

The HPHE in this application was designed for a performance of 88.6 kW. This was not achieved for three main reasons: firstly, the heat losses mentioned, secondly, the air inlet temperature averaged 196°C, whereas it was designed for an air inlet temperature of 145°C, meaning that the temperature differential between heat transfer fluids was less. However, the exhaust inlet temperature followed the design parameter very well. Thirdly, the experimental average exhaust mass flow rate of 1,500 kg.hr⁻¹ was not matched extremely closely to the design parameters of 1,802 kg.hr⁻¹; 16.8% less. The air mass flow rate was very close, with an experimental average of 1,775 kg.hr⁻¹ and design parameter of 1,791 kg.hr⁻¹.

7. CONCLUSIONS AND FUTURE WORK

In this Chapter, the conclusions drawn from the work conducted are collated and contribution to knowledge is highlighted. In addition, recommendations for future work are suggested.

7.1. Conclusions

The main objective of this work was to develop a transient tool for predicting performance of HPHEs equipped with vertical thermosyphons that recover waste heat from industrial exhaust gases. The research was conducted using three different experimental conditions with three different HPHEs with varying geometries. This work was conducted both on laboratory-scale and full-scale HPHEs. As described in Chapter 1, five objectives were specified. These objectives are restated here with the conclusions drawn.

Objective 1: Develop a working knowledge of the heat transfer processes within a HPHE.

Chapter 3 provides a thorough development of theory behind singular heat pipe performance, which is then applied to a HPHE, where the thermosyphons are working in parallel. The ϵ -NTU method was used as a basis for the model with additional information provided on the thermal network analysis, which can be implemented.

Objective 2: Develop a novel and versatile model for predicting transient behaviour of HPHEs.

The theory gained from Objective 1 has been applied to obtain transient results in a novel manner. Initially a steady state code was developed in MATLAB, which has then been converted into the Fortran language for use in TRNSYS simulations. The coding process has been described in Chapter 5, along with how the user can interact with the tool. Furthermore, the code is provided in Appendices A and B for use by the wider scientific community with the ability to be altered for the desired purpose. The limitations are also highlighted. In terms of versatility, a number of heat sink options have been coded along with many applicable correlations to allow a large range of input conditions to be determined. Multiple HPHE geometries of any scale can be modelled.

Objective 3: Demonstrate the advantage of the model over existing models.

No other available tool can provide transient results in this manner. Very reasonable predictions are obtained, when taking into account the differences caused by heat losses. This tool can now be confidently used for larger system simulations or other HPHE performance predictions when performance over time is required.

Objective 4: Validate the model using experimental results from a laboratory-scale installation.

Results from Experiment 1 on a laboratory-scale HPHE were compared with simulation results. Very reasonable agreements were seen for heat transfer rate and outlet temperature predictions of both the heat source and heat sink fluids. The exhaust outlet temperature prediction was on average +0.67% higher than the experimental results with a spread of $\pm 6\%$. On average, the water outlet temperature was +2.97% higher than the experimental results with a spread of -8 to +9%. The simulated heat transfer rate across the entire results was between -18 and +19% different in comparison to the experimental results. The average error was -2.39% showing that, overall, the model underpredicted the heat transfer rate, which can be attributed to heat losses.

Objective 5: Validate the model using experimental results from a full-scale installation.

Results from Experiment 2 and 3 on full-scale HPHEs were compared with the simulation results. Reasonable agreements were seen for heat transfer rate and outlet temperature predictions of both the heat source and heat sink. Heat losses were an issue at this larger scale and for higher temperature inlets. The HPHE for Experiment 3 was not as thermally insulated as required. It is shown by heat loss analysis from radiative and natural convection that more accurate results would have been obtained if the unit was more adequately thermally insulated.

When comparing the temperature outlets between simulation predictions and experimental results for the ceramic kiln exhaust-to-air full-scale unit, the component returned on average exhaust outlet temperatures +3.76% higher than the experimental results and air outlet temperatures +1.30% higher. In other words, the outlet temperatures were higher for the simulation than for the experiment. The air heat transfer rate predictions were on average +4.1% higher for the simulation than those seen experimentally.

For the aluminium furnace exhaust-to-air finned full-scale demonstration, the results were less accurate, with the simulation exhaust outlet temperature being on average +10.17% higher than the experimental exhaust outlet temperature. The simulation air outlet temperatures were +3.55% higher than the experimental air outlet temperatures. However, thermal losses had a larger influence with higher inlet temperatures, with a reduction in the experimental outlet temperatures. The air heat transfer rate prediction was on average +17.05% higher than the experimental heat transfer rate with a spread of 11 to 37%.

7.2. Recommendations for Future Work

It is considered that the thermosyphons used in the HPHEs are well designed and that the operating limits described in Section 2.4 are not applicable when using the developed model. It is feasible for the model to provide errors when heat pipe operating limits are reached. This would need additional inputs concerning the heat pipe design such as material selection and working fluid selection. This could also have the benefit of more accurately predicting performance of smaller units as the model presented exploits the fact that overall HPHE resistance tends towards zero, the more heat pipes and rows that are introduced.

It would be possible to develop further models for different configurations of HPHE, such as parallel or through flow, though these HPHEs are seen less frequently. All three HPHEs tested had a staggered arrangement of thermosyphons, whereas it is possible for the thermosyphons to be in an in-line arrangement. The model has the ability to predict the performance of HPHEs with in-line thermosyphons, but this is yet to be validated. Helical finning is currently the only available option. Annular finning or other options can be added and validated.

The model is in fact quasi-transient. It would be interesting to see what the smallest temporal period is, to which the model can react accurately. No analysis has been conducted or considered on the temporal spacing of the data. 5 seconds to 1-minute intervals of data have been trialled, which has shown to be sufficient.

Furthermore, differential calculus can be used to theoretically determine the rate of change in a heat pipe's heat transfer rate. An individual heat pipe can quickly adapt by increasing and decreasing its heat transfer rate depending on the fluctuating conditions present. This knowledge can theoretically be used to adjust the HPHE model presented; the author postulates

that this would give more accurate predictions and can be used to determine differences over a smaller period of time. This would be an extremely complex calculation process and the benefits may not be significant overall.

As presented, the attached code can be neatened and structured in a more efficient way, reducing the total number of lines. As it stands, the calculations do not take an extortionate amount of time, so the decision was made to leave the code in a linear fashion to reflect the order of calculations as well as to increase comprehension by third parties. For example, the thermophysical properties and Nusselt calculations are coded multiple times to recalculate the values when initially guessed parameters have been derived. To prevent this, repetitive code could be revisited and the values replaced.

The presented code uses Nusselt number correlations to determine the heat transfer coefficient of forced convection. Another method is possible that would be attractive to study. Correlations presented for calculating heat transfer coefficients for boiling and condensation can be coded and, instead of treating the heat pipes as superconductors, the thermal network analysis can be used to determine the thermal resistance of each heat pipe, then row, then the HPHE overall. The author believes this would be particularly beneficial for smaller units.

It was highlighted during the experimental and theoretical results, particularly for Experiment 3, that heat losses did play a larger factor than anticipated. The units could be insulated more appropriately and the analyses then repeated. Indeed, insulation was an action of the project for Experiment 3 and these results will be made available.

8. REFERENCES

- [1] Brough D, Jouhara H. The aluminium industry: A review on state-of-the-art technologies, environmental impacts and possibilities for waste heat recovery. *Int J Thermofluids* 2020;1–2. doi:10.1016/J.IJFT.2019.100007.
- [2] Brough D, Mezquita A, Ferrer S, Segarra C, Chauhan A, Almahmoud S, et al. An experimental study and computational validation of waste heat recovery from a lab scale ceramic kiln using a vertical multi-pass heat pipe heat exchanger. *Energy* 2020;208. doi:10.1016/j.energy.2020.118325.
- [3] Brough D, Ramos J, Delpech B, Jouhara H. Development and validation of a TRNSYS type to simulate heat pipe heat exchangers in transient applications of waste heat recovery. *Int J Thermofluids* 2021;9:100056. doi:10.1016/j.ijft.2020.100056.
- [4] Jouhara H, Almahmoud S, Brough D, Guichet V, Delpech B, Chauhan A, et al. Experimental and theoretical investigation of the performance of an air to water multi-pass heat pipe-based heat exchanger. *Energy* 2021;219:119624. doi:10.1016/j.energy.2020.119624.
- [5] Venturelli M, Brough D, Milani M, Montorsi L, Jouhara H. Comprehensive Numerical Model for the Analysis of Potential Heat Recovery Solutions in a Ceramic Industry. *Int J Thermofluids* 2021;10:100080. doi:10.1016/j.ijft.2021.100080.
- [6] European Commission. Energy-intensive industries n.d. https://ec.europa.eu/growth/industry/policy/energy-intensive-industries_en (accessed June 8, 2020).
- [7] United Nations Treaty Collection. Paris Agreement. 2015.
- [8] European Commission. 2030 climate & energy framework n.d. https://ec.europa.eu/clima/policies/strategies/2030_en (accessed August 19, 2019).
- [9] European Commission. Energy Roadmap 2050. *Luxemb Publ Off Eur Union* 2012;20. doi:10.2833/10759.
- [10] Department for Business Energy & Industrial Strategy, Skidmore C. UK becomes first major economy to pass net zero emissions law 2019. <https://www.gov.uk/government/news/uk-becomes-first-major-economy-to-pass-net-zero-emissions-law>.
- [11] Central Intelligence Agency. *The World Factbook 2016-17*. 2018.
- [12] Jouhara H, Olabi AG. Editorial: Industrial waste heat recovery. *Energy* 2018;160:1–2.

- doi:10.1016/j.energy.2018.07.013.
- [13] Agathokleous R, Panayiotou G, Aresti L, Argyrou MC, Georgiou GS, Jouhara H, et al. Waste Heat Recovery in the EU industry and proposed new technologies. *Energy Procedia* 2019;161:489–96. doi:10.1016/J.EGYPRO.2019.02.064.
- [14] Conference UCC. COP26 The Glasgow Climate Pact. 2021.
- [15] Hammond GP, Norman JB. Heat recovery opportunities in UK industry. *Appl Energy* 2014;116:387–97. doi:10.1016/j.apenergy.2013.11.008.
- [16] Johnson, Ilona ; Choate, William T. ; Davidson A. Waste Heat Recovery: Technology Opportunities in the US Industry - prepared by Bcs, Incorporated. US Dep Energy - Ind Technol Progr 2008:1–112.
- [17] Atreya A, Everest D. Highly Preheated Combustion Air Furnace with Oxygen Enrichment for Metal Processing to Significantly Improve Enrgy Efficiency and Reduce Emissions. 2003.
- [18] State of Green. District Energy, Green heating and cooling for urban areas. 2020.
- [19] Yu M, Gudjonsdottir MS, Valdimarsson P, Saevarsdottir G. Waste heat recovery from aluminum production. *Miner Met Mater Ser* 2018;Part F6:165–78. doi:10.1007/978-3-319-72362-4_14.
- [20] Simeoni P, Ciotti G, Cottes M, Meneghetti A. Integrating industrial waste heat recovery into sustainable smart energy systems. *Energy* 2019;175:941–51. doi:10.1016/J.ENERGY.2019.03.104.
- [21] Arink T, Hassan MI. Metal Scrap Preheating using Flue Gas Waste Heat. *Energy Procedia* 2017;105:4788–95. doi:10.1016/J.EGYPRO.2017.03.945.
- [22] Dell'Oste EF. Procedure and means for preheating scrap to be charged into a smelting furnace. 4559629A US, 1985.
- [23] U.S. Department of Energy. Energy Tips - Process Heating. *Combust Technol Man* 2007.
- [24] Migchielsen JM, De Groot JD. Design Consideration for Charge Preheating Ovens. *Miner Met Mater Soc Annu Meetign Ans Exhib* 2006:737–40.
- [25] Schlesinger ME. *Aluminium Recycling*. New Editio. Taylor & Francis Inc; 2013.
- [26] Evans R, Guest G. *The Aluminium Decoating Handbook* 2002.
- [27] Capuzzi S, Timelli G. Preparation and Melting of Scrap in Aluminum Recycling: A Review. *Metals (Basel)* 2018;8:24. doi:10.3390/met8040249.
- [28] Sung T, Yun E, Kim HD, Yoon SY, Choi BS, Kim K, et al. Performance characteristics

- of a 200-kW organic Rankine cycle system in a steel processing plant. *Appl Energy* 2016;183:623–35. doi:10.1016/J.APENERGY.2016.09.018.
- [29] Júnior EPB, Arrieta MDP, Arrieta FRP, Silva CHF. Assessment of a Kalina cycle for waste heat recovery in the cement industry. *Appl Therm Eng* 2019;147:421–37. doi:10.1016/J.APPLTHERMALENG.2018.10.088.
- [30] Ramirez M, Epelde M, De Arteché MG, Panizza A, Hammerschmid A, Baresi M, et al. Performance evaluation of an ORC unit integrated to a waste heat recovery system in a steel mill. *Energy Procedia* 2017;129:535–42. doi:10.1016/j.egypro.2017.09.183.
- [31] Jouhara H, Khordehghah N, Almahmoud S, Delpech B, Chauhan A, Tassou SA. Waste heat recovery technologies and applications. *Therm Sci Eng Prog* 2018;6:268–89. doi:10.1016/J.TSEP.2018.04.017.
- [32] Børset MT, Wilhelmsen Ø, Kjelstrup S, Burheim OS. Exploring the potential for waste heat recovery during metal casting with thermoelectric generators: On-site experiments and mathematical modeling. *Energy* 2017;118:865–75. doi:10.1016/J.ENERGY.2016.10.109.
- [33] Peris B, Navarro-Esbrí J, Molés F, Mota-Babiloni A. Experimental study of an ORC (organic Rankine cycle) for low grade waste heat recovery in a ceramic industry. *Energy* 2015;85:534–42. doi:10.1016/J.ENERGY.2015.03.065.
- [34] Incropera FP, Prescott PJ, Voelkel DD. Hybrid systems for furnace waste heat recovery: I. Use of a radiation recuperator with a Rankine cycle. *J Heat Recover Syst* 1985;5:321–30. doi:10.1016/0198-7593(85)90006-2.
- [35] Precott PJ, Incropera FP. Hybrid systems for furnace waste heat recovery: II. Use of a convective recuperator with a Rankine cycle. *J Heat Recover Syst* 1985;5:331–9.
- [36] Caglayan H, Caliskan H. Energy, exergy and sustainability assessments of a cogeneration system for ceramic industry. *Appl Therm Eng* 2018;136:504–15. doi:10.1016/J.APPLTHERMALENG.2018.02.064.
- [37] Montorsi L, Milani M, Stefani M, Terzi S. Numerical analysis of the exhaust gases recovery from a turbine CHP unit to improve the energy efficiency of a ceramic kiln. *Therm Sci Eng Prog* 2018;5:444–53. doi:10.1016/J.TSEP.2018.01.013.
- [38] Casi Á, Araiz M, Catalán L, Astrain D. Thermoelectric heat recovery in a real industry: From laboratory optimization to reality. *Appl Therm Eng* 2021;184. doi:10.1016/j.applthermaleng.2020.116275.
- [39] Jouhara H. Heat Pipes. *Compr Energy Syst* 2018;4:70–97. doi:10.1016/b978-0-12-

- 809597-3.00403-x.
- [40] Reay DA, Kew PA, McGlen RJ. Heat Pipes. Theory, Design and Applications. Sixth Edit. Oxford: Butterworth-Heinemann; 2013.
- [41] Reay DA. The Perkins Tube- A Noteworthy Contribution to Heat Exchanger Tecnology. Heat Recover Syst 1982;2:173–87.
- [42] Silva DDO. Experimental Investigation Of The Thermal Performance Of Screen Mesh Wick Heat Pipes Operating In Mid-Level Temperatures 2018.
- [43] Gay F. Heat transfer means. 1725906, 1942.
- [44] Grover GM, Cotter TP, Erickson GF. Structures of very high thermal conductance. J Appl Phys 1964;35:1990–1. doi:10.1063/1.1713792.
- [45] Faghri A. Heat Pipes: Review, Opportunities and Challenges. Front Heat Pipes 2014;5. doi:10.5098/fhp.5.1.
- [46] Jouhara H, Chauhan A, Nannou T, Almahmoud S, Delpech B, Wrobel LC. Heat pipe based systems - Advances and applications. Energy 2017;128:729–54. doi:10.1016/j.energy.2017.04.028.
- [47] Groll M. Heat pipe research and development in Western Europe. Heat Recover Syst 1989;9:19–66.
- [48] Terdtoon P et al. Investigation of effect of inclination angle on heat transfer characteristics of closed two-phase thermosyphons. Proc. 7th Int. Heat Pipe Conf., Minsk: n.d.
- [49] Corp CM. Heat Pipe n.d. <https://www.coolermastercorp.com/technology/design/heatpipe/> (accessed September 25, 2021).
- [50] Nam Y, Sharratt S, Cha G, Ju YS. Characterization and modeling of the heat transfer performance of nanostructured Cu micropost wicks. J Heat Transfer 2011;133. doi:10.1115/1.4004168.
- [51] Solomon AB, Ramachandran K, Pillai BC. Thermal performance of a heat pipe with nanoparticles coated wick. Appl Therm Eng 2012;36:106–12. doi:10.1016/j.applthermaleng.2011.12.004.
- [52] Dunn P, Reay DA. Heat Pipes. 3rd ed. Pergamon Press; 1982.
- [53] Kiseev V, Sazhin O. Heat transfer enhancement in a loop thermosyphon using nanoparticles/water nanofluid. Int J Heat Mass Transf 2019;132:557–64. doi:10.1016/j.ijheatmasstransfer.2018.11.109.

-
- [54] Kim J, Kim SJ. Experimental investigation on working fluid selection in a micro pulsating heat pipe. *Energy Convers Manag* 2020;205:112462. doi:10.1016/j.enconman.2019.112462.
- [55] Heat Transfer Committee. ESDU 80017. Thermophysical properties of heat pipe working fluids: operating range between -60°C and 300°C. London: 1980.
- [56] Heat Transfer Committee. Convective Heat Transfer During Forced Crossflow of Fluids Over a Circular Cylinder, Including Free Convection Effects. ESDU 69004a. 1970.
- [57] Almahmoud S. Experimental and theoretical investigation of a radiative flat heat pipe based heat exchanger for waste recovery in the steel industry. Brunel University London, 2019.
- [58] Bezrodyni M., Alekseenko D. Investigation of the critical region of heat and mass transfer in low-temperature wickless heat pipes. *High Temp Sci* 1977;15:309–13.
- [59] Faghri A. *Heat Pipe Science and Technology*. 2nd ed. Global Digital Press; 2016.
- [60] Noie SH. Heat transfer characteristics of a two-phase closed thermosyphon. *Appl Therm Eng* 2005;25:495–506. doi:10.1016/j.applthermaleng.2004.06.019.
- [61] Faghri A, Chen M., Morgan M. Heat Transfer in Two-Phase Closed Conventional and Concentric Annular Thermosyphon. *ASME J Heat Mass Transf* 1989;111:611–8.
- [62] Rohsenow Editor WM, Hartnett Editor JR, Cho Editor YI, San NY, Washington F, Auckland DC, et al. *Handbook of heat transfer*. 1998.
- [63] Imura H, Sasaguchi K, Kozai H, Numata S. Critical heat flux in a closed two-phase thermosyphon. *Int J Heat Mass Transf* 1983;26:1181–8. doi:10.1016/S0017-9310(83)80172-0.
- [64] Busse CA. Theory of the ultimate heat transfer limit of cylindrical heat pipes. *Int J Heat Mass Transf* 1973;16:169–86. doi:10.1016/0017-9310(73)90260-3.
- [65] Kays WM, London AL. *Compact Heat Exchangers*. New York: 1964.
- [66] Zohuri B. *Heat pipe design and technology: Modern applications for practical thermal management*. Second. 2016. doi:10.1007/978-3-319-29841-2.
- [67] Shabgard H, Allen MJ, Sharifi N, Benn SP, Faghri A, Bergman TL. Heat pipe heat exchangers and heat sinks: Opportunities, challenges, applications, analysis, and state of the art. *Int J Heat Mass Transf* 2015;89:138–58. doi:10.1016/j.ijheatmasstransfer.2015.05.020.
- [68] ESDU. *Heat Pipes - General Information on Their Use, Operation, and Design*. 80013. Eng Sci Data Unit, Data Items 1980.

-
- [69] Ramos JAGSB. Experimental Investigation and CFD Modelling of a Thermosyphon-Equipped Heat Exchanger Used in Low-Grade Waste Heat Recovery. University of South Wales, 2016.
- [70] Kerrigan K, Jouhara H, O'Donnell GE, Robinson AJ. Heat pipe-based radiator for low grade geothermal energy conversion in domestic space heating. *Simul Model Pract Theory* 2011;19:1154–63. doi:10.1016/j.simpat.2010.05.020.
- [71] Ayompe LM, Duffy A, Mc Keever M, Conlon M, McCormack SJ. Comparative field performance study of flat plate and heat pipe evacuated tube collectors (ETCs) for domestic water heating systems in a temperate climate. *Energy* 2011;36:3370–8. doi:10.1016/j.energy.2011.03.034.
- [72] Jouhara H, Nannou T, Ghazal H, Kayyali R, Tassou SA, Lester S. Temperature and energy performance of open refrigerated display cabinets using heat pipe shelves. *Energy Procedia* 2017;123:273–80. doi:10.1016/J.EGYPRO.2017.07.240.
- [73] Mehmood A, Waqas A, Said Z, Rahman SMA, Akram M. Performance evaluation of solar water heating system with heat pipe evacuated tubes provided with natural gas backup. *Energy Reports* 2019;5:1432–44. doi:10.1016/j.egyr.2019.10.002.
- [74] Hussein HMS. Theoretical and experimental investigation of wickless heat pipes flat plate solar collector with cross flow heat exchanger. *Energy Convers Manag* 2007;48:1266–72. doi:10.1016/j.enconman.2006.09.021.
- [75] Jouhara H, Milko J, Danielewicz J, Sayegh MA, Szulgowska-Zgrzywa M, Ramos JB, et al. The performance of a novel flat heat pipe based thermal and PV/T (photovoltaic and thermal systems) solar collector that can be used as an energy-active building envelope material. *Energy* 2016;108:148–54. doi:10.1016/j.energy.2015.07.063.
- [76] Budihardjo I, Morrison GL. Performance of water-in-glass evacuated tube solar water heaters. *Sol Energy* 2009;83:49–56. doi:10.1016/j.solener.2008.06.010.
- [77] Noie-Baghban SH, Majideian GR. Waste heat recovery using heat pipe heat exchanger (HPHE) for surgery rooms in hospitals. *Appl Therm Eng* 2000;20:1271–82. doi:10.1016/S1359-4311(99)00092-7.
- [78] Yau YH. Theoretical determination of effectiveness for heat pipe heat exchangers operating in naturally ventilated tropical buildings. *Proc Inst Mech Eng Part A J Power Energy* 2001;215:389–98. doi:10.1243/0957650011538604.
- [79] Yau YH. The use of a double heat pipe heat exchanger system for reducing energy consumption of treating ventilation air in an operating theatre-A full year energy

- consumption model simulation. *Energy Build* 2008;40:917–25. doi:10.1016/j.enbuild.2007.07.006.
- [80] Yau YH, Tucker AS. The performance study of a wet six-row heat-pipe heat exchanger operating in tropical buildings. *Int J Energy Res* 2003;27:187–202. doi:10.1002/er.867.
- [81] Jouhara H, Meskimmon R. Experimental investigation of wraparound loop heat pipe heat exchanger used in energy efficient air handling units. *Energy* 2010;35:4592–9. doi:10.1016/j.energy.2010.03.056.
- [82] Jouhara H, Anastasov V, Khamis I. Potential of heat pipe technology in nuclear seawater desalination. *Desalination* 2009;249:1055–61. doi:10.1016/j.desal.2009.05.019.
- [83] Zhang X, Liu Y, Wen X, Li C, Hu X. Low-grade waste heat driven desalination with an open loop heat pipe. *Energy* 2018;163:221–8. doi:10.1016/j.energy.2018.08.121.
- [84] Zhou F, Chen J, Ma G, Liu Z. Energy-saving analysis of telecommunication base station with thermosyphon heat exchanger. *Energy Build* 2013;66:537–44. doi:10.1016/j.enbuild.2013.06.020.
- [85] Jouhara H, Meskimmon R. Heat pipe based thermal management systems for energy-efficient data centres. *Energy* 2014;77:265–70. doi:10.1016/j.energy.2014.08.085.
- [86] Wu XP, Mochizuki M, Mashiko K, Nguyen T, Nguyen T, Wuttijumnong V, et al. Cold Energy Storage Systems Using Heat Pipe Technology for Cooling Data Centers. *Front Heat Pipes* 2011;2. doi:10.5098/fhp.v2.1.3005.
- [87] Mochizuki M, Nguyen T, Mashiko K, Saito Y, Singh R, Nguyen T, et al. Prevention Possibility of Nuclear Power Reactor Meltdown By Use of Heat Pipes for Passive Cooling of Spent Fuel. *Front Heat Pipes* 2013;4. doi:10.5098/fhp.v4.1.3001.
- [88] Vasiliev LL. Heat pipes in modern heat exchangers. *Appl Therm Eng* 2005;25:1–19. doi:10.1016/J.APPLTHERMALENG.2003.12.004.
- [89] Kim TY, Hyun BS, Lee JJ, Rhee J. Numerical study of the spacecraft thermal control hardware combining solid-liquid phase change material and a heat pipe. *Aerosp Sci Technol* 2013;27:10–6. doi:10.1016/j.ast.2012.05.007.
- [90] Almahmoud S, Jouhara H. Experimental and theoretical investigation on a radiative flat heat pipe heat exchanger. *Energy* 2019;174:972–84. doi:10.1016/j.energy.2019.03.027.
- [91] I-ThERM n.d. <http://www.itherm-project.eu/> (accessed April 26, 2020).
- [92] Delpech B, Axcell B, Jouhara H. Experimental investigation of a radiative heat pipe for waste heat recovery in a ceramics kiln. *Energy* 2018;170:636–51. doi:10.1016/j.energy.2018.12.133.

-
- [93] Delpech B. Experimental and theoretical investigation of a radiative heat pipe ceiling for uniform cooling and heat recovery in a ceramic roller hearth kiln. Brunel University London, 2020.
- [94] Lukitobudi AR, Akbarzadeh A, Johnson PW, Hendy P. Design, construction and testing of a thermosyphon heat exchanger for medium temperature heat recovery in bakeries. *Heat Recover Syst CHP* 1995;15:481–91. doi:10.1016/0890-4332(95)90057-8.
- [95] Yodrak. Waste Heat Recovery by Heat Pipe Air-Preheater to Energy Thrift from the Furnace in a Hot Forging Process. *Am J Appl Sci* 2010;7:675–81. doi:10.3844/ajassp.2010.675.681.
- [96] Egilegor B, Jouhara H, Zuazua J, Al-Mansour F, Plesnik K, Montorsi L, et al. ETEKINA: Analysis of the potential for waste heat recovery in three sectors: aluminium low pressure die casting, steel sector and ceramic tiles manufacturing sector. *Int J Thermofluids* 2019:100002. doi:https://doi.org/10.1016/j.ijft.2019.100002.
- [97] Delpech B, Milani M, Montorsi L, Boscardin D, Chauhan A, Almahmoud S, et al. Energy efficiency enhancement and waste heat recovery in industrial processes by means of the heat pipe technology: Case of the ceramic industry. *Energy* 2018;158:656–65. doi:10.1016/j.energy.2018.06.041.
- [98] Econotherm Ltd. Gas to Oil unit n.d. <https://www.econotherm.co.uk/project-4> (accessed August 27, 2021).
- [99] Jouhara H, Nannou T, Delpech B, Almahmoud S, Chauhan A, Boocock M, et al. Heat Pipe Based Heat Exchanger For Clean Yerba Mate Drying Process. SEEP2017, Bled, Slovenia: n.d.
- [100] Chi SW. *Heat Pipe Theory and Practice*. New York: Hemisphere; 1976.
- [101] Chisholm D. *The Heat Pipe*. London: Mills & Boone; 1971.
- [102] Faghri A, Harley C. Transient Lumped Heat Pipe Analyses. *Heat Recover Syst CHP* 1994;14:351–63.
- [103] Deverall JE, Kemme JE, Florschuetz LW. *Sonic Limitations and Startup Problems of Heat Pipes*. Los Alamos: 1970.
- [104] Colwell GT. *Modeling of Transient Heat Pipe Operation*. Hampton, Virginia: 1989.
- [105] Yang L, Ling X, Peng H, Duan LF, Chen X. Starting characteristics of a novel high temperature flat heat pipe receiver in solar power tower plant based of “Flat-front” Startup model. *Energy* 2019;183:936–45. doi:10.1016/j.energy.2019.07.007.
- [106] Hall ML, Doster JM. A sensitivity study of the effects of evaporation/condensation

- accommodation coefficients on transient heat pipe modeling. *Int J Heat Mass Transf* 1990;33:465–81. doi:10.1016/0017-9310(90)90182-T.
- [107] Ochterbeck J. Modeling of a Room-Temperature Heat Pipe Start-up from the Frozen State. *J Thermophys Heat Transf* 1997;11:165–72.
- [108] Brocheny P. Modeling of the Transient Behavior of Heat Pipes With Room-Temperature Working Fluids. Clemson University, 2006.
- [109] Beam J. Transient Heat Pipe Analysis. 20th AIAA Thermophys. Conf., Williamsburg, Virginia: 1985.
- [110] Ambrose J., Chow L., Beam J. Transient Heat Pipe Response and Rewetting Behaviour. *J Thermophys Heat Transf* 1987;1:222–7.
- [111] Kuramae M, Ito M. The Physical Models of a Heat Pipe for Analyzing Dynamic Heat Transfer Characteristics. *Int Chem Eng* 1992;32:336–44.
- [112] Ivanovskii MN, Sorokin VP, Yagodkin IV. The Physical Principles of Heat Pipes. Oxford Uni. 1982.
- [113] Cullimore B. Modeling of Transient Heat Pipe Effects Using a Generalized Thermal Analysis Program. 20th AIAA Thermophys. Conf., Williamsburg, Virginia: 1985.
- [114] Zuo ZJ, Faghri A. A network thermodynamic analysis of the heat pipe. *Int J Heat Mass Transf* 1998;41:1473–84. doi:10.1016/S0017-9310(97)00220-2.
- [115] El-Genk MS, Huang L. An Experimental Investigation of Water Heat Pipe. *Int J Heat Mass Transf* 1993;36:3823–30.
- [116] Tournier JM, El-Genk MS. A heat pipe transient analysis model. *Int J Heat Mass Transf* 1994;37:753–62. doi:10.1016/0017-9310(94)90113-9.
- [117] Huang L, El-Genk MS, Tournier JM. Transient performance of an inclined water heat pipe with a screen wick. *Am Soc Mech Eng Heat Transf Div HTD* 1993;236:87–92.
- [118] El-Genk MS, Huang L, Tournier JM. Transient Experiments of an Inclined Copper-Water Heat Pipe. *J Therm* 1995;9:109–16.
- [119] Ramos J, Chong A, Jouhara H. Experimental and numerical investigation of a cross flow air-to-water heat pipe-based heat exchanger used in waste heat recovery. *Int J Heat Mass Transf* 2016;102:1267–81. doi:10.1016/j.ijheatmasstransfer.2016.06.100.
- [120] Zuo ZJ, Faghri A. A Boundary Element Approach to Transient Heat Pipe Analysis. *Numer Heat Transf* 1997;32.
- [121] Cao Y, Faghri A. Transient multidimensional analysis of nonconventional heat pipes with uniform and nonuniform heat distributions. *J Heat Transfer* 1991;113:995–1002.

-
- [122] Amode J., Feldman K. Preliminary analysis of heat pipe heat exchangers for heat recovery. *Am. Soc. Mech. Eng.*, 1975.
- [123] Lee Y, Bedrossian A. The characteristics of heat exchangers using heat pipes or thermosyphons. *Int J Heat Mass Transf* 1978;21:221–9. doi:10.1016/0017-9310(78)90226-0.
- [124] Huang BJ, Tsuei JT. A method of analysis for heat pipe heat exchangers. *Int J Heat Mass Transf* 1985;28:553–62. doi:10.1016/0017-9310(85)90178-4.
- [125] Çengel Y. *Heat Transfer: A Practical Approach*. Second. Mcgraw-Hill (Tx); 2002.
- [126] Çengel YA. *Heat Transfer: A Practical Approach*. New York McGraw-Hill 2003:785–841. doi:10.1017/CBO9781107415324.004.
- [127] Weierman C, Taborek J, Marner WJ. Comparison of the Performance of Inline and Staggered Banks of Tubes with Segmented Fins. *AIChE Chem Eng Prog Symp Ser* 1978;74:39–46.
- [128] Mroue H, Ramos JB, Wrobel LC, Jouhara H. Experimental and numerical investigation of an air-to-water heat pipe-based heat exchanger. *Appl Therm Eng* 2015;78:339–50. doi:10.1016/j.applthermaleng.2015.01.005.
- [129] Krishnan K., Rao K. Analysis and Design of a Heat Pipe Heat Exchanger. *Proc. 5th Int. Heat Pipe Conf.*, Tsukuba Science City, Japan: 1984, p. 152–6.
- [130] Chaudrone S. Modelization and Optimization of Heat Pipe Heat Exchangers. *Proc. 5th Int. Heat Pipe Conf.*, Tsukuba Science City, Japan: 1984, p. 53–8.
- [131] Azad E, Geoola F. A design procedure for gravity-assisted heat pipe heat exchanger. *J Heat Recover Syst* 1984;4:101–11. doi:10.1016/0198-7593(84)90014-6.
- [132] Rich DG. The effects of fin spacing on the heat transfer and friction performance of multi-row smooth plate fin-and-tube heat exchanger. *ASHRAE Trans* 1973;79:137–45.
- [133] Azad E, Mohammadi F, Moztarzadeh F. Thermal Performance of Heat Pipe Heat Recovery System. *Heat Recover Syst* 1985;5:561–70.
- [134] Tan JO, Liu CY. Predicting the performance of a heat-pipe heat exchanger, using the effectiveness- NTU method. *Int J Heat Fluid Flow* 1990;11:376–9. doi:10.1016/0142-727X(90)90062-G.
- [135] Whitaker S. Forced convection heat transfer correlations flow in pipes, past flat plates, single cylinders, single spheres, and for flow packed beds and tube bundles. *Am Inst Chem Eng* 1972;18:361–71.
- [136] Shariah A, Shalabi B. Optimal design for a thermosyphon solar water heater. *Renew*

- Energy 1997;11:351–61. doi:10.1016/S0960-1481(97)00005-0.
- [137] Kalogirou SA, Papamarcou C. Modelling of a thermosyphon solar water heating system and simple model validation. *Renew Energy* 2000;21:471–93. doi:10.1016/S0960-1481(00)00086-0.
- [138] Budihardjo I, Morrison GL, Behnia M. Development of TRNSYS Models for Predicting the Performance of Water-in-Glass Evacuated Tube Solar Water Heaters in Australia. *Sch. Mech. Manuf. Eng.*, vol. i, 2003, p. 10.
- [139] Ayompe LM, Duffy A, McCormack SJ, Conlon M. Validated TRNSYS model for forced circulation solar water heating systems with flat plate and heat pipe evacuated tube collectors. *Appl Therm Eng* 2011;31:1536–42. doi:10.1016/j.applthermaleng.2011.01.046.
- [140] Yau YH. Energy savings in tropical HVAC systems using heat pipe heat exchangers (HPHXs). University of Canterbury, 2004.
- [141] Ahmadzadehtalatapeh M. An air-conditioning system performance enhancement by using heat pipe based heat recovery technology. *Sci Iran* 2013;20:329–36. doi:10.1016/j.scient.2013.02.004.
- [142] Ahmadzadehtalatapeh M. Feasibility study of a water-to-air heat pipe based heat exchanger for cooling load reduction and energy saving in the office buildings: A simulation study. *Sci Iran* 2017;24:1040–50. doi:10.24200/sci.2017.4087.
- [143] Kreith F, Manglik RM, Bohn MS. Principles of heat transfer. 7th ed. Stamford: Cengage Learning, Inc; 2011.
- [144] Khan WA, Culham JR, Yovanovich MM. Convection heat transfer from tube banks in crossflow: Analytical approach. *Int J Heat Mass Transf* 2006;49:4831–8. doi:10.1016/j.ijheatmasstransfer.2006.05.042.
- [145] Kuntysh V., Stenin N. Heat Transfer and Pressure Drop in Cross Flow through Mixed In-Line Staggered Finned Tube Bundles. *Therm Eng* 1993;40.
- [146] Žukauskas A. Convective Heat Transfer In Cross Flow, Vilnius, USSR: Academy of Sciences of the Lithuanian SSR; n.d., p. 1–45.
- [147] Shiraishi M, Kikuchi K, Yamanishi T. Investigation of heat transfer characteristics of a two-phase closed thermosyphon. *J Heat Recover Syst* 1981;1:287–97. doi:10.1016/0198-7593(81)90039-4.
- [148] Marek R, Straub J. Analysis of the evaporation coefficient and the condensation coefficient of water. *Int J Heat Mass Transf* 2001;44:39–53. doi:10.1016/S0017-

- 9310(00)00086-7.
- [149] Paul B. Compilation of Evaporation Coefficients 1962. doi:10.2514/8.6277.
- [150] Finkelstein Y, Tamir A. Interfacial heat transfer coefficients of various vapors in direct contact condensation. *Chem Eng J* 1976;12:199–209. doi:10.1016/0300-9467(76)87013-X.
- [151] Park YJ, Kang HK, Kim CJ. Heat transfer characteristics of a two-phase closed thermosyphon to the fill charge ratio. *Int J Heat Mass Transf* 2002;45:4655–61. doi:10.1016/S0017-9310(02)00169-2.
- [152] Guichet V, Almahmoud S, Jouhara H. Nucleate pool boiling heat transfer in wickless heat pipes (two-phase closed thermosyphons): A critical review of correlations. *Therm Sci Eng Prog* 2019;13. doi:10.1016/j.tsep.2019.100384.
- [153] Bergman TL, Lavine AS, Incropera FP, Dewitt DP. *Fundamentals of Heat and Mass Transfer*. 7th ed. John Wiley & Sons, Inc; 2011.
- [154] Noie SH. Investigation of thermal performance of an air-to-air thermosyphon heat exchanger using ε -NTU method. *Appl Therm Eng* 2006;26:559–67. doi:10.1016/J.APPLTHERMALENG.2005.07.012.
- [155] Jouhara H, Merchant H. Experimental investigation of a thermosyphon based heat exchanger used in energy efficient air handling units. *Energy* 2012;39:82–9. doi:10.1016/j.energy.2011.08.054.
- [156] Jouhara H, Robinson AJ. Experimental investigation of small diameter two-phase closed thermosyphons charged with water, FC-84, FC-77 and FC-3283. *Appl Therm Eng* 2010;30:201–11. doi:10.1016/j.applthermaleng.2009.08.007.
- [157] Shah RK, Sekulić DP. *Fundamentals of heat exchanger design*. vol. 4. John Wiley & Sons, Inc; 2003.
- [158] Mohan Jagadeesh Kumar M, Kaushik SC, Garg SN. Thermodynamic performance evaluation of an air-air heat pipe heat exchanger. *Therm Sci* 2014;18:1343–53. doi:10.2298/TSCI121214123K.
- [159] Sukarno R, Putra N, Hakim II, Rachman FF, Mahlia TMI. Multi-stage heat-pipe heat exchanger for improving energy efficiency of the HVAC system in a hospital operating room 1. *Int J Low-Carbon Technol* 2020;1–9. doi:10.1093/ijlct/ctaa048.
- [160] Thulukkanam K. *Heat Exchanger Design Handbook*, 2nd Edition. 2013.
- [161] Golobič I, Gašperšič B. Corresponding states correlation for maximum heat flux in two-phase closed thermosyphon. *Int J Refrig* 1997;20:402–10. doi:10.1016/S0140-

- 7007(97)00019-4.
- [162] Colburn AP. A method of correlating forced convection heat transfer data and a comparison with fluid friction. *Trans Am Inst Chem Eng* 1933;29:174–210.
- [163] Grimison ED. Correlation and utilization of new data on flow resistance and heat transfer for cross flow of gases over tube banks. *Trans ASME* 1937;59:583–94.
- [164] Holman JP. *Heat Transfer*. 7th ed. New York: McGraw-Hill; 1992.
- [165] Hausen H. *Heat Transfer in Counter Flow, Parallel Flow and Cross Flow*. New York: McGraw-Hill; 1983.
- [166] Zukauskas A. Heat transfer from tubes in crossflow. *Adv Heat Transf* 1972;8:93–160.
- [167] Stasiulevicius J, Skrinska A. *Heat Transfer of Finned Tube Bundles in Crossflow*. Washington, D.C.: Hemisphere Publishing; 1988.
- [168] Yudin V., Tochtarova LS. *Heat Transfer of Finned Tube Bundles in Crossflow*. Washington, D.C.: Hemisphere Publishing; 1988.
- [169] Schmidt T. *Heat Transfer of Finned Tube Bundles in Crossflow*. Washington, D.C.: Hemisphere Publishing; 1988.
- [170] Briggs D., Young E. Convection Heat Transfer and Pressure Drop of Air Flowing across Triangular Pitch Banks of Finned Tubes. *Chem Eng Prog Symp Ser* 1963;59:1–10.
- [171] Pongsoi P, Pikulkajorn S, Wongwiset S. Heat transfer and flow characteristics of spiral fin-and-tube heat exchangers: A review. *Int J Heat Mass Transf* 2014;79:417–31. doi:10.1016/j.ijheatmasstransfer.2014.07.072.
- [172] Andros F. Heat transfer characteristics of the two-phase closed thermosyphon (wickless heat pipe) including direct flow observation. Arizona State University, 1980.
- [173] Kruzhilin GN. Free-convection transfer of heat from a horizontal plate and boiling liquid. *Dokl AN SSSR (Reports USSR Acad Sci)* 1947;58:1657–60.
- [174] Rohsenow WM. A method of correlating heat-transfer data for surface boiling of liquids. 1952.
- [175] McNelly MJ. A correlation of rates of heat transfer to nucleate boiling of liquids. *J Imp Coll Chem Eng Soc* 1953;7:18–34.
- [176] Forster HK, Zuber N. Dynamics of vapor bubbles and boiling heat transfer. *AIChE J* 1955;1:531–5.
- [177] Tien CL. A hydrodynamic model for nucleate pool boiling. *Int J Heat Mass Transf* 1962;5:533–40. doi:10.1016/0017-9310(62)90164-3.
- [178] Mostinski IL. Application of the rule of corresponding states for calculation of heat

- transfer and critical heat flux. *Teploenergetika* 1963;4:66–71.
- [179] Labuntsov DA. Heat transfer problems with nucleate boiling of liquids. *Therm Eng(USSR)(Engl Transl)*, v 19, No 9, Pp 21-28 1973.
- [180] Imura H, Kusuda H, Ogata J-I, Miyazaki T, Sakamoto N. Heat transfer in two-phase closed-type thermosyphons. *JSME Trans* 1979;45:712–22.
- [181] Stephan K, Abdelsalam M. Heat-transfer correlations for natural convection boiling. *Int J Heat Mass Transf* 1980;23:73–87. doi:10.1016/0017-9310(80)90140-4.
- [182] Bier K, Schmadl J, Gorenflo D. Influence of heat flux and saturation pressure on pool boiling heat transfer of binary mixtures. *VT VERFAHRENSTECHNIK* 1982;16:708–10.
- [183] Nishikawa K, Fujita Y, Ohta H, Hidaka S. Effect of the surface roughness on the nucleate boiling heat transfer over the wide range of pressure. *Heat Transf. Proc. Int. Heat Transf. Conf.*, Hemisphere Publ Corp; 1982, p. 61–6.
- [184] Cooper MG. Saturation nucleate pool boiling - A simple correlation. *Inst Chem Eng Symp Ser* 1984;2.86:785–93. doi:10.1016/B978-0-85295-175-0.50013-8.
- [185] Ueda T, Miyashita T, Chu P-H. Heat transport characteristics of a closed two-phase thermosyphon. vol. 54. 1988. doi:10.1299/kikaib.54.2848.
- [186] Kutateladze SS. *Heat Transfer and Hydrodynamic Resistance: Handbook (in Russian)*, Chapter 12.7 1990.
- [187] Groß U. Pool Boiling Heat Transfer inside a Two-Phase Thermosyphon (Correlation of Experimental Data). *Proc. 9th Int. Heat Transf. Conf.*, 1990, vol. 2, 1990, p. 57–62.
- [188] Kaminaga F, Okamoto Y, Suzuki T, Ma T. Study on boiling heat transfer correlation in a closed two-phase thermosyphon. *Proc. 8th Int. Heat Pipe Conf. Beijing*, 1992.
- [189] Chowdhury FM, Kaminaga F, Goto K, Matsumura K. Boiling heat transfer in a small diameter tube below atmospheric pressure on a natural circulation condition. *J Japan Assoc Heat Pipe* 1997;16:14–6.
- [190] El-Genk MS, Saber HH. Heat transfer correlations for small, uniformly heated liquid pools. *Int J Heat Mass Transf* 1997;41:261–74. doi:10.1016/S0017-9310(97)00143-9.
- [191] Kiatsiriroat T, Nuntaphan A, Tiansuwan J. Thermal performance enhancement of thermosyphon heat pipe with binary working fluids. *Exp Heat Transf* 2000;13:137–52. doi:10.1080/089161500269517.
- [192] Jensen M., Memmel G. Evaluation of bubble departure diameter correlations. *Proc. 8th Int. Heat Transf. Conf.* vol. 4, 1986, p. 1907–12.

-
- [193] Kopchikov I., Voronin G., Kolach T., Labuntsov D., Lebedev P. Liquid boiling in a thin film. *Int J Heat Mass Transf* 1969;12:791–6. doi:doi:10.1016/0017-9310(69)90182-3.
- [194] Chun K., Seban R. Heat transfer to evaporating liquid films. *J Heat Transfer* 1971;93:391–6. doi:doi:10.1115/1.3449836.
- [195] El-Genk MS, Saber HH. Determination of operation envelopes for closed, two-phase thermosyphons. *Int J Heat Mass Transf* 1999;42:889–903. doi:doi:10.1016/S0017-9310(98)00212-9.
- [196] Gogonin I. The dependance of boiling heat transfer on the properties and geometric parameters of heat-transfer wall. *High Temp* 2006;44:913–21.
- [197] Guichet V, Jouhara H. Condensation, evaporation and boiling of falling films in wickless heat pipes (two-phase closed thermosyphons): A critical review of correlations. *Int J Thermofluids* 2020;1–2:100001. doi:10.1016/j.ijft.2019.100001.
- [198] Nusselt W. The condensation of steam on cooled surfaces. *Z Ver Dtsch Ing* 1916;60:541–6.
- [199] McAdams WH. *Heat Transmission - Second Edition* 1942.
- [200] Rohsenow WM. Heat transfer and temperature distribution in laminar film condensation. *Trans Asme* 1956;78:1645–8.
- [201] Kutateladze SS. *Heat transfer theory fundamentals*. Atomizdat, Moscow./E. Arnold Publishers, London, Academic Press Inc, New York; 1963.
- [202] Butterworth C. *Condensers: Basic heat transfer and fluid flow*. Kakaç, S; Bergles, AE; Mayinger, F *Heat Exch Therm Fundam Des Washingt Hemisph* 1981:289–313.
- [203] Gross U. Reflux condensation heat transfer inside a closed thermosyphon. *Int J Heat Mass Transf* 1992;35:279–94. doi:10.1016/0017-9310(92)90267-V.
- [204] Schnabel G, Palen JW. *Wärmeübergang an senkrechten berieselten Flächen*. Springer-Verlag Sect Md, Berlin 1998.
- [205] Uehara H, Kusuda H, NAKAORA T, Yamada M. Filmwise condensation for turbulent flow in a vertical plate. *Heat Transf Japanese Res* 1983;12:85–96.
- [206] Chun MH, Kim KT. A natural convection heat transfer correlation for laminar and turbulent film condensation on a vertical surface. *3rd ASME/JSME Therm. Eng. Jt. Conf.*, 1991, p. 459–64.
- [207] Nozhat WM. The effect of free surface curvature on the heat transfer coefficient of thin liquid films. *Fourth Am. Soc. Mech. Eng. Soc. Mech. Eng. Therm. Eng. Jt. Conf. Maui, Hawaii*, vol. 2, 1995, p. 171–8.

-
- [208] Hashimoto H, Kaminaga F. Heat transfer characteristics in a condenser of closed two-phase thermosyphon: Effect of entrainment on heat transfer deterioration. *Heat Transf Res* 2002;31:212–25. doi:10.1002/htj.10030.
- [209] Labuntsov DA. Heat transfer in film condensation of pure steam on vertical surfaces and horizontal tubes. *Teploenergetika* 1957;4:72–9.
- [210] Sanaye S, Modarrespoor D. Thermal-economic multiobjective optimization of heat pipe heat exchanger for energy recovery in HVAC applications using genetic algorithm. *Energy Syst Improv Lab Mech Eng Dep Iran Univ Sci Technol* n.d.
- [211] Domański T, Kmicik K. Load-bearing capacity of the steel-to-timber connections in fire temperature. *MATEC Web Conf* 2019;262. doi:10.1051/mateconf/201926209005.
- [212] Hammock GL. Cross-Flow, Staggered-Tube Heat Exchanger Analysis for High Enthalpy Flows 2011:111.
- [213] Lokshin V., Fomina V. Correlation of Experimental Data on Finned Tubbe Bundles. *Teploenergetika* 1978;6:36–9.
- [214] Etekina Project- Grant Agreement ID: 768772 (2017-2022). n.d.
- [215] Solar Energy Laboratory U of W-M. TRNSYS 17, Volume 7, Programmer’s Guide n.d.
- [216] Engineers Field. Flue Gases Properties n.d. <https://engineersfield.com/flue-gases-properties-table-density-viscosity/> (accessed July 16, 2020).
- [217] The Engineering ToolBox. Dry Air Properties n.d. https://www.engineeringtoolbox.com/dry-air-properties-d_973.html (accessed July 16, 2020).
- [218] Evans P. Properties of water at atmospheric pressure. *Eng Mindset* 2015. <https://theengineeringmindset.com/properties-of-water-atmospheric-pressure-saturated-liquid/> (accessed July 16, 2020).
- [219] Solutia. Therminol 66 n.d. <http://tw.t.mpei.ac.ru/TTHB/HEDH/HTF-66.PDF> (accessed July 16, 2020).
- [220] Churchill S. *Heat Exchanger Design Handbook: Free Convection Around Immersed Bodies*. Hemisphere; 1983.

9. APPENDICES

A. MATLAB Code For HPHE

MATLAB_R2019b was initially used to draft write the code to test the equations used for the TRNSYS components. This was initially done as the MATLAB code did not require the input of specific TRNSYS functions or linking with external libraries. This code was the foundation by which the Fortran TRNSYS code was expanded upon. This code is capable of completing calculations for steady state or averaged parameters but does not work transiently over time. To achieve this, the language was converted to Fortran and the TRNSYS functionalities were added to formulate the final transient code. On running the code below, a text box appears (Figure 157) which prompts the user to input the parameters needed for the calculations. It provides the values of all the internal variables, allowing a thorough evaluation of the equations. The command line then presents the six outputs of the model:

- Source outlet temperature (°C)
- Sink outlet temperature (°C)
- Energy recovery rate (kW)
- Conductance, UA, of the HPHE (W.K^{-1})
- Evaporator pressure drop (Pa)
- Condenser pressure drop (Pa)

Input parameters

Source temperature in? (deg C):

Sink temperature in? (deg C):

Mass flow rate evaporator? (kg/s):

Mass flow rate condenser? (kg/s):

Number of heat pipe longitudinal rows in evaporator?:

Number of heat pipe longitudinal rows in condenser?:

Outer diameter of heat pipe? (m):

Length of evaporator? (m):

Length of condenser? (m):

Number of heat pipes in evaporator transverse row?:

Transverse distance between evaporator heat pipes centres? (m):

Longitudinal distance between evaporator heat pipes centres? (m):

Number of heat pipes in condenser transverse row?:

Transverse distance between condenser heat pipes centres? (m):

Longitudinal distance between evaporator heat pipes centres? (m):

Face area of evaporator? (m2):

Face area of condenser? (m2):

Finning mode (1=none, 2=cond, 3=evap, 4=both):

Fluid mode (1=Air, 2=Water, 3=Thermal oil):

Outer diameter of fins (m):

Thickness of fins (m):

Pitch of fins (m):

Height of fins (m):

OK Cancel

Figure 157: The prompt box that appears to enter the parameters in MATLAB.

The complete MATLAB code for the counterflow HPHE is presented below:

```
% Code for predicting the performance of a counterflow, crossflow or
% multipass HPHE using the E-NTU method.
% Outputs of source and sink temperature out, energy recovery rate,
% conductance and pressure drop in both the evaporator and condenser
% sections
%
% Can predict pressure drop for finned or unfinned units
% Amended thermophysical properties for SHC thermal oil/ NUC thermal oil
% 01/20 DJB- Initial version (Type 202)
% 06/20 DJB- Counterflow model (Type 203)
%           Increased number of available models for finning
%           Temperature inputs converted to Celsius
%           Nusselt correlations present for finned units
%           Wall temperatures now goal-seeked
%           Averaged thermal properties equations used
%           Added water and thermal oil as heat sinks
% 10/20 DJB- Crossflow model (Type 204)
%           Split evaporator and condenser sections so transverse and
%           longitudinal rows can be different values
% 11/21 DJB- Counterflow, crossflow or multipass (Type 204 improved)
%           Combined different geometries
%           Finned Nusselt correlations expanded
%           Zukauskas method and Yudin model added for pressure drop
%           predictions

%Assumptions: Same geometry of finning for both evaporator and condenser
%           Helical fins only
%           No axial conduction
%           No thermal losses
%           Carbon steel fins
%           Staggered arrangement assumed equilateral for pressure drop
%           Start-up achieved

% Enter fixed inlet parameters
prompt= {'Source temperature in? (deg C):', ...
        'Sink temperature in? (deg C):', ...
        'Mass flow rate evaporator? (kg/s):', ...
        'Mass flow rate condenser? (kg/s):', ...
```

```

'Number of heat pipe longitudinal rows in evaporator?:', ...
'Number of heat pipe longitudinal rows in condenser?:', ...
'Outer diameter of heat pipe? (m):', ...
'Length of evaporator? (m):', ...
'Length of condenser? (m):', ...
'Number of heat pipes in evaporator transverse row?:', ...
'Transverse distance between evaporator heat pipes centres? (m):', ...
'Longitudinal distance between evaporator heat pipes centres? (m):',...
'Number of heat pipes in condenser transverse row?:', ...
'Transverse distance between condenser heat pipes centres? (m):', ...
'Longitudinal distance between evaporator heat pipes centres? (m):',...
'Face area of evaporator? (m2):', ...
'Face area of condenser? (m2):', ...
'Finning mode? (1=none, 2=cond, 3=evap, 4=both:', ...
'Fluid mode? (1=Air, 2=Water, 3=Thermal oil', ...
'Outer diameter of fins? (m)', ...
'Thickness of fins? (m)', ...
'Pitch of fins? (m)', ...
'Height of fins? (m)'};

dlgtitle= 'Input parameters';
dims= [1 23];
answer=inputdlg(prompt,dlgtitle);

%-----

%Convert string to numerals
%Inputs
Thi=str2num(answer{1}); %Temperature of source inlet fluid [deg C]
Tci=str2num(answer{2}); %Temperature of sink inlet fluid [deg C]
FLWe=str2num(answer{3}); %Mass flow rate evaporator (source) fluid [kg/s]
FLWc=str2num(answer{4}); %Mass flow rate condenser (sink) fluid [kg/s]

%Parameters
Nre= str2num(answer{5}); %Number of evaporator longitudinal rows
Nrc= str2num(answer{6}); %Number of condenser longitudinal rows
Dout= str2num(answer{7}); %Outer diameter of heat pipe [m]
Le= str2num(answer{8}); %Length of evaporator [m]
Lc= str2num(answer{9}); %Length of condenser [m]
Nte= str2num(answer{10}); %Number of evaporator transverse rows

```

```

STe= str2num(answer{11}); %Distance between evaporator row centres [m]
SLe= str2num(answer{12}); %Distance between evaporator heat pipe centres[m]
Ntc= str2num(answer{13}); %Number of tubes in condenser row (transverse)
STc= str2num(answer{14}); %Distance between condenser row centres [m]
SLc= str2num(answer{15}); %Distance between condenser row centres [m]
Ae= str2num(answer{16}); %Face area of evaporator [m2]
Ac= str2num(answer{17}); %Face area of condenser [m2]
FinningMode= str2num(answer{18}); % (1=none, 2=con finned, 3=evap finned,
4=both)
FluidMode= str2num(answer{19}); %Sink: 1=air 2=water 3=thermal oil
Dofin= str2num(answer{20}); %Outer diameter of fins [m]
efin= str2num(answer{21}); %Thickness fins [m]
Pfin= str2num(answer{22}); %Pitch of fins [m]
Hfin= str2num(answer{23}); %Width of fins [m]

PI=3.1415927;

%-----

%Check Parameters for Problems
if (Nre <= 1)
    error('The number of rows must be positive.')
end
if (Nrc <= 1)
    error('The number of rows must be positive.')
end
if (Dout > 1)
    error('Ensure diameter is in metres')
end
if (Le <= 0)
    error('The length evaporator must be positive.')
end
if (Lc <= 0)
    error('The length condenser must be positive.')
end
if (Nte<= 0)
    error('Number of heat pipes in row must be positive.')
end
if (Ntc <= 0)
    error('Number of heat pipes in row must be positive.')

```

```
end
if (STe >= 1)
    error('Ensure distance between rows is in metres')
end
if (SLe >= 1)
    error('Ensure distance between heat pipes is in metres')
end
if (STc >= 1)
    error('Ensure distance between rows is in metres')
end
if (SLc >= 1)
    error('Ensure distance between heat pipes is in metres')
end
if (Ae <= 0)
    error('Ae must be positive')
end
if (Ac <= 0)
    error('Ac must be positive')
end
if ((FinningMode <= 0) || (FinningMode > 4))
    error('Finning mode must be between 1 and 4')
end
if ((FluidMode <= 0) || (FluidMode > 3))
    error('FluidMode must be between 1-3')
end
if (Dofin >= 1)
    error('Ensure fin diameter is in metres')
end
if (efin >= 1)
    error('Ensure outer fin diameter is in metres')
end
if (Pfin >= 1)
    error('Ensure pitch is in metres')
end
if (Hfin >= 1)
    error('Ensure fin height is in metres')
end
if (Thi < 0.)
    error('Enter source inlet temperature')
end
if (Tci < 0.)
```

```

    error('Enter sink inlet temperature')
end
if (FLWe < 0.)
    error('Enter source inlet flow rate')
end
if (FLWc < 0.)
    error('Enter sink inlet flow rate')
end

%-----

%Perform All of the Calculations Here

%Densities Inlet (kg/m3)
RHOe = 1.08622+(-0.00234)*Thi+(2.7773E-6)*Thi^2 ... %Natural gas exhaust
      +(-1.60009E-9)*Thi^3+3.48272E-13*Thi^4;

if (FluidMode == 1) %Air
    RHOc = 0.16103+0.34473*exp(-Tci/103.23714)+0.78857* ...
          exp(-Tci/512.29169);

elseif (FluidMode == 2) %Water
    RHOc = exp(2.2467*(1-((Tci+273.15)/647.25))^(1/3)-2.09405* ...
              (1-((Tci+273.15)/647.25))^(2/3)+2.737*(1-((Tci+273.15)/647.25)) ...
              -1.7475*(1-((Tci+273.15)/647.25))^(4/3))*315.5;

else %Thermal oil
    RHOc = ((-0.614254*(Tci))- (0.000321*((Tci)^2))+1020.62);

end

%-----

%Dynamic Viscosities Inlet (m2/s)
NUe = (1.51901E-5+3.7842E-8*Thi-8.96178E-12*Thi^2 ... %Natural gas exhaust
      +1.57382E-15*Thi^3);

if (FluidMode == 1) %Air
    NUc = (1.70899E-5+4.6117E-8*Tci-2.07642E-11*Tci^2 ...

```

```

+5.40458E-15*Tci^3);

elseif (FluidMode == 2) %Water
    NUC = (exp(-10.1083+1.39621*(1/((Tci+273.15)/647.25)-1)^(1/3) ...
    +0.48431*(1/((Tci+273.15)/647.25)-1)^(4/3)+0.71019* ...
    (1/((Tci+273.15)/647.25)-1)^(7/3)));

else %Thermal oil
    NUC = (exp((586.375/(Tci+62.5)-2.2809)))*RHOC/1000000;
end

%-----

%Thermal Conductivities Inlet (W/m.K)
LAMDAe = 0.02272+7.19522E-5*Thi-4.70107E-9*Thi^2; %Natural gas exhaust

if (FluidMode == 1) %Air
    LAMDAc = 0.02411+7.71055E-5*Tci-2.81463E-8*Tci^2 ...
    +6.36061E-12*Tci^3;

elseif (FluidMode == 2) %Water
    LAMDAc = -1.63975+11.1421*((Tci+273.15)/647.25)+-20.0805* ...
    ((Tci+273.15)/647.25)^(2)+16.7447*((Tci+273.15)/647.25) ...
    ^ (3)+-5.78763*((Tci+273.15)/647.25)^(4);

else %Thermal oil
    LAMDAc = (1E-11*Tci^3)-(2E-7*Tci^2)-(3E-5*Tci)+0.1182;
end

%-----

%Specific Heat Capacities Inlet (J/kg.K)
SHCe = 1083.52006+0.33081*Thi+(-3.15922E-5)*Thi^2 ... %Natural gas exhaust
    +(-1.66552E-8)*Thi^3;

if (FluidMode == 1) %Air
    SHCc = (1.00224+3.33594E-5*Tci+5.415E-7*Tci^2- ...
    6.31148E-10*Tci^3+2.86052E-13*Tci^4-4.66306E-17 ...
    *Tci^5)*1000;

```

```

elseif (FluidMode == 2) %Water
SHCc = -14995*(1+0.088*(1-((Tci+273.15)/647.25))^( -2 / 3) ...
      +(-0.682)*(1-((Tci+273.15)/647.25))^( -1/3)+(-0.705)* ...
      (1-((Tci+273.15)/647.25))^(1/3));

else %Thermal oil
SHCc = ((1E-9*Tci^3)+(3E-7*Tci^2)+(0.0034*Tci)+1.4943)*1000;
end

%-----

%Prandtl Numbers
Pre = SHCe*NUe/LAMDAe;

Prc = SHCc*NUc/LAMDAC;

%-----

%Do Calculations Here
%Heat Capacitance and Minimum (W/K)
Ce = SHCe*FLWe;

Cc = SHCc*FLWc;

Cmin = min(Ce,Cc);

%-----

%Free Flow Velocities (m/s)
ve = FLWe/(Ae*RHOe);
vc = FLWc/(Ac*RHOc);

%-----

%Maximum Velocities (m/s)
Vmaxe = (STe/(STe-Dout))*ve;
minareae = ((Ae/Le)-(Nte*Dout))*Le;

```

```

%Minimum area test condenser
minareatestc1 = sqrt(((STc/2)^2)+(SLc^2));
minareatestc2 = (STc+Dout)/2;

if (minareatestc1 > minareatestc2)
    Vmaxc = (STc/(STc-Dout))*vc;

    minareac= Ac-(Lc*Ntc*Dout);
else
    Vmaxc = (vc/(sqrt(1+((2*(SLc/STc))^2)-(2*(Dout/STc)))));

    minareac = ((Ac/Lc)-(((Ntc-1)*STc)+Dout)+((sqrt((STc/2)^2-SLc^2) ...
        -Dout)*(Ntc+1)))*Lc;

end

%-----

%Reynolds Numbers
ReDe = (Vmaxe*Dout*RHOe)/NUe;

ReDc = (minareac*Dout*RHOc)/NUc;

%-----

%Nusselt Numbers
%This Section provides a correction factor if the number of rows <16
if ((Nre >= 14) && (Nre <= 16))
    CFe = 0.995;
elseif (Nre == 13)
    CFe = 0.99;
elseif ((Nre >= 11) && (Nre <= 12))
    CFe = 0.985;
elseif (Nre == 10)
    CFe = 0.98;
elseif (Nre == 7)
    CFe = 0.96;
elseif (Nre == 6)

```

```
    CFe = 0.945;
elseif (Nre == 5)
    CFe = 0.93;
elseif (Nre == 4)
    CFe = 0.89;
elseif (Nre == 3)
    CFe = 0.84;
elseif (Nre == 2)
    CFe = 0.76;
elseif (Nre == 1)
    CFe = 0.64;
else
    CFe = 1; %(Nre > 16)
end

if ((Nrc >= 14) && (Nrc <= 16))
    CFc = 0.995;
elseif (Nrc == 13)
    CFc = 0.99;
elseif ((Nrc >= 11) && (Nrc <= 12))
    CFc = 0.985;
elseif (Nrc == 10)
    CFc = 0.98;
elseif (Nrc == 7)
    CFc = 0.96;
elseif (Nrc == 6)
    CFc = 0.945;
elseif (Nrc == 5)
    CFc = 0.93;
elseif (Nrc == 4)
    CFc = 0.89;
elseif (Nrc == 3)
    CFc = 0.84;
elseif (Nrc == 2)
    CFc = 0.76;
elseif (Nrc == 1)
    CFc = 0.64;
else
    CFc = 1; %(Nrc > 16)
end
```

```

%-----

%Nusselt Correlations
%Evaporator smooth
if ((FinningMode == 1) || (FinningMode == 2))

    if (ReDe <= 500)
        Nuse = CFe*1.04*(ReDe^0.4)*(Pre^0.36)*(1.1^0.25);

    elseif (ReDe <= 1000)
        Nuse = CFe*0.71*(ReDe^0.5)*(Pre^0.36)*(1.1^0.25);

    elseif (ReDe <= 20000)
        Nuse = CFe*0.35*((STe/SLe)^0.2)*(ReDe^0.6)*(Pre^0.36) ...
            *(1.1^0.25);

    else
        Nuse = CFe*0.031*((STe/SLe)^0.2)*(ReDe^0.8)*(Pre^0.36) ...
            *(1.1^0.25);
    end

% Evaporator finned correlations
else
    if (ReDe <= 20000)
        Nuse= 0.192*(ReDe^0.65)*(Pre^0.36)*((STe/SLe)^0.2)*((Pfin/Dout) ...
            ^0.18)*((Hfin/Dout)^-0.14)*(1.1^0.25);

    elseif (ReDe <= 200000)
        Nuse = 0.0507*(ReDe^0.8)*(Pre^0.4)*((STe/SLe)^0.2)*((Pfin/Dout) ...
            ^0.18)*((Hfin/Dout)^-0.14)*(1.1^0.25);

    else
        Nuse = 0.0081*(ReDe^0.95)*(Pre^0.4)*((STe/SLe)^0.2)*((Pfin/Dout)
        ...
            ^0.18)*((Hfin/Dout)^-0.14)*(1.1^0.25);
    end
end

```

```

%-----

%Condenser smooth
if ((FinningMode == 1) || (FinningMode == 3))

    if (ReDc <= 500)
        Nusc = CFc*1.04*(ReDc^0.4)*(Prc^0.36)*(1.1^0.25);

    elseif (ReDc <= 1000)
        Nusc = CFc*0.71*(ReDc^0.5)*(Prc^0.36)*(1.1^0.25);

    elseif (ReDc <= 20000)
        Nusc = CFc*0.35*((STc/SLc)^0.2)*(ReDc^0.6)*(Prc^0.36) ...
            *(1.1^0.25);

    else
        Nusc = CFc*0.031*((STc/SLc)^0.2)*(ReDc^0.8)*(Prc^0.36) ...
            *(1.1^0.25);
    end

end

%Condenser finned
else
    if (ReDc <= 10000)
        Nusc = CFc*0.192*(ReDc^0.65)*(Prc^0.36)*((STc/SLc)^0.2) ...
            *((Pfin/Dout)^0.18)*((Hfin/Dout)^-0.14)*(1.1^0.25);

    elseif (ReDc <= 100000)
        Nusc= CFc*0.0507*(ReDc^0.8)*(Prc^0.4)*((STc/SLc)^0.2) ...
            *((Pfin/Dout)^0.18)*((Hfin/Dout)^-0.14)*(1.1^0.25);

    else
        Nusc = CFc*0.0081*(ReDc^0.95)*(Prc^0.4)*((STc/SLc)^0.2) ...
            *((Pfin/Dout)^0.18)*((Hfin/Dout)^-0.14)*(1.1^0.25);
    end
end

%-----

%Heat Transfer Coefficients (W/m2.K)

```

```

HTFe = (Nuse*LAMDAe)/Dout;

HTFc = (Nusc*LAMDAc)/Dout;

%-----

%Heat Transfer Areas (m2)
%Evaporator smooth
if ((FinningMode == 1) || (FinningMode == 2))
    HTAe = PI*Dout*Le*Nte;

%Evaporator finned
else
    HTAe_smooth = PI*Dout*Le*Nte;
    kfe = (-0.0333*((Thi+Tci)/2)+53.902);
    Lhle = (Le/Pfin)*sqrt(((PI*(Dout+Dofin)/2)^2)+Pfin^2);
    Afe = 2*Hfin*Lhle*Nte;
    xe = sqrt((2*HTFe)/(kfe*efin));
    efffe = (tanh(xe*Hfin))/(xe*Hfin);
    HTAe = ((PI*Dout*Le*(1-efin*1/Pfin))*Nte)+(efffe*Afe);
end

%Condenser smooth
if ((FinningMode == 1) || (FinningMode == 3))
    HTAc = PI*Dout*Lc*Ntc;

%Condenser finned
else
    HTAc_smooth = PI*Dout*Le*Ntc;
    kfc = (-0.0333*((Thi+Tci/2))+53.902);
    Lhlc = (Lc/Pfin)*sqrt(((PI*(Dout+Dofin)/2)^2)+Pfin^2);
    Afc = 2*Hfin*Lhlc*Ntc;
    xc = sqrt((2*HTFc)/(kfc*efin));
    efffc = (tanh(xc*Hfin))/(xc*Hfin);
    HTAc = ((PI*Dout*Lc*(1-efin*1/Pfin))*Ntc)+(efffc*Afc);
end

%-----

```

```

%Number of Transfer Units
NTUe = (HTFe*HTAe)/Ce;

NTUc = (HTFc*HTAc)/Cc;

%-----

%Effectiveness
ee = 1-exp(-NTUe);
ec = 1-exp(-NTUc);

een = 1-((1-ee)^Nre);
ecn = 1-((1-ec)^Nrc);

%-----

%Choose Overall Effectiveness
if (Ce > Cc)
    Et = (((1/ecn)+(Cc/Ce)/een)^-1);
else
    Et = (((1/een)+(Ce/Cc)/ecn)^-1);
end

%-----

%Initial Outlet Temperature Guesses
Thog = Thi-(Et*(Cmin/Ce)*(Thi-Tci));
Tcog = Tci+(Et*(Cmin/Cc)*(Thi-Tci));

%-----

%Temperature at Evaporator Wall Iterations
Twe = (Thi+Thog)/2;
Q1e = FLWe*SHCe*(Thi-Thog);
Q2e = HTFe*HTAe*((Thi-Thog)/log(Thi-Twe)/(Thog-Twe));
dQ1e = Q1e-Q2e;
Twe_up = Twe+0.001;

```

```

Twe_down = Twe-0.001;
Q4e = HTFe*HTAe*((Thi-Thog)/log(Thi-Twe_up)/(Thog-Twe_up));
dQ2e = Q1e-Q4e;

numiterations = 0;

if (dQ2e < dQ1e)
    while ((dQ2e > 0.000001) && (numiterations < 1000000))
        Twe_up = Twe_up+0.001;
        Q4e = HTFe*HTAe*((Thi-Thog)/log(Thi-Twe_up)/(Thog-Twe_up));
        dQ2e = Q1e-Q4e;
        numiterations = numiterations+1;
        Twe = Twe_up;
    end
else
    while ((dQ2e < -0.000001) && (numiterations < 1000000))
        Twe_down = Twe_down -0.001;
        Q4e = HTFe*HTAe*((Thi-Thog)/log(Thi-Twe_down)/(Thog-Twe_down));
        dQ2e = Q1e-Q4e;
        numiterations = numiterations+1;
        Twe = Twe_down;
    end
end

%-----

%Temperature at Condenser Wall Iterations
Twc = (Tci+Tcog)/2;
Q1c = FLWc*SHCc*(Tcog-Tci);
Q2c = HTFc*HTAc*((Tcog-Tci)/log(Tci-Twc)/(Tcog-Twc));
dQ1c = Q1c-Q2c;
Twc_up = Twc+0.001;
Twc_down = Twc-0.001;
Q4c = HTFc*HTAc*((Tcog-Tci)/log(Tcog-Twc_up)/(Tci-Twc_up));
dQ2c = Q1c-Q4c;
numiterations = 0;

if (dQ2c < dQ1c)
    while ((dQ2c > 0.000001) && (numiterations < 1000000))
        Twc_up = Twc_up+0.001;

```

```

    Q4c = HTFc*HTAc*((Tcog-Tci)/log(Tcog-Twc_up)/(Tci-Twc_up));
    dQ2c= Q1c-Q4c;
    numiterations = numiterations+1;
    Twc = Twc_up;
end
else
    while ((dQ2c < -0.000001) && (numiterations < 1000000))
        Twc_down = Twc_down -0.001;
        Q4c = HTFc*HTAc*((Tcog-Tci)/log(Tcog-Twc_down)/(Tci-Twc_down));
        dQ2c = Q1c-Q4c;
        numiterations = numiterations+1;
        Twc = Twc_down;
    end
end

%-----

%Wall Calculations
%Densities at Walls (kg/m3)
RHOew = 1.08622+(-0.00234)*Twe+(2.7773E-6)*Twe^2 ...
        +(-1.60009E-9)*Twe^3+3.48272E-13*Twe^4;

if (FluidMode == 1) %Air
    RHOcw = 0.16103+0.34473*exp(-Twc/103.23714)+0.78857* ...
            exp(-Twc/512.29169);

elseif (FluidMode == 2) %Water
    RHOcw = exp(2.2467*(1-((Twc+273.15)/647.25))^(1/3)-2.09405* ...
            (1-((Twc+273.15)/647.25))^(2/3)+2.737*(1-((Twc+273.15)/647.25)) ...
            -1.7475*(1-((Twc+273.15)/647.25))^(4/3))*315.5;

else %Thermal oil
    RHOcw = ((-0.614254*(Twc))- (0.000321*((Twc)^2))+1020.62);

end

%Dynamic Viscosity at Walls (W/m.K)
NUew = (1.51901E-5+3.7842E-8*Twe-8.96178E-12*Twe^2 ...
        +1.57382E-15*Twe^3);

```

```

if (FluidMode == 1) %Air
    NUcw = (1.70899E-5+4.6117E-8*Twc-2.07642E-11*Twc^2 ...
            +5.40458E-15*Twc^3);

elseif (FluidMode == 2) %Water
    NUcw = (exp(-10.1083+1.39621*(1/((Twc+273.15)/647.25)-1)^(1/3) ...
            +0.48431*(1/((Twc+273.15)/647.25)-1)^(4/3)+0.71019* ...
            (1/((Twc+273.15)/647.25)-1)^(7/3)));

else %Thermal oil
    NUcw = (exp((586.375/(Twc+62.5)-2.2809)))*RHOcw/1000000;
end

%Thermal Conductivities at Walls (W/m.K)
LAMDAew = 0.02272+7.19522E-5*Twe-4.70107E-9*Twe^2;

if (FluidMode == 1) %Air
    LAMDAcw = 0.02411+7.71055E-5*Twc-2.81463E-8*Twc^2 ...
            +6.36061E-12*Twc^3;

elseif (FluidMode == 2) %Water
    LAMDAcw = -1.63975+11.1421*((Twc+273.15)/647.25)+-20.0805* ...
            ((Twc+273.15)/647.25)^(2)+16.7447*((Twc+273.15)/647.25) ...
            ^ (3)+-5.78763*((Twc+273.15)/647.25)^(4);

else %Thermal oil
    LAMDAcw = (1E-11*Twc^3)-(2E-7*Twc^2)-(3E-5*Twc)+0.1182;
    if (LAMDAcw <= 0)
        LAMDAcw = 0.01;
    end
end

%Specific Heat Capacities at Walls
SHCew = 1083.52006+0.33081*Twe+(-3.15922E-5)*Twe^2 ...
        +(-1.66552E-8)*Twe^3;

if (FluidMode == 1) %Air
    SHCcw = (1.00224+3.33594E-5*Twc+5.415E-7*Twc^2- ...
            6.31148E-10*Twc^3+2.86052E-13*Twc^4-4.66306E-17 ...
            *Twc^5)*1000;

```



```

elseif (FluidMode == 2) %Water
    SHCcw = -14995*(1+0.088*(1-((Twc+273.15)/647.25))^-2/3) ...
        +(-0.682)*(1-((Twc+273.15)/647.25))^-1/3)+(-0.705)* ...
        (1-((Twc+273.15)/647.25))^(1/3));
else %Thermal oil
    SHCcw = ((1E-9*Twc^3)+(3E-7*Twc^2)+(0.0034*Twc)+1.4943)*1000;
end

%-----

%Prandtl Number at Walls
Pres = SHCew*NUew/LAMDAew;

PrCs = SHCcw*NUcw/LAMDACw;

%-----

%Nusselt Correlations
%Evaporator smooth

if ((FinningMode == 1) || (FinningMode == 2))

    if (ReDe <= 500)
        Nuse = CFe*1.04*(ReDe^0.4)*(Pre^0.36)*((Pre/Pres)^0.25);

    elseif (ReDe <= 1000)
        Nuse = CFe*0.71*(ReDe^0.5)*(Pre^0.36)*((Pre/Pres)^0.25);

    elseif (ReDe <= 20000)
        Nuse = CFe*0.35*((STe/SLe)^0.2)*(ReDe^0.6)*(Pre^0.36) ...
            *((Pre/Pres)^0.25) ;

    else
        Nuse = CFe*0.031*((STe/SLe)^0.2)*(ReDe^0.8)*(Pre^0.36) ...
            *((Pre/Pres)^0.25) ;
    end
end

```

```

%Evaporator finned
else
    if (ReDe <= 10000)
        Nuse= 0.192*(ReDe^0.65)*(Pre^0.36)*((STe/SLe)^0.2)*((Pfin/Dout) ...
            ^0.18)*((Hfin/Dout)^-0.14)*((Pre/Pres)^0.25);

    elseif (ReDe <= 100000)
        Nuse = 0.0507*(ReDe^0.8)*(Pre^0.4)*((STe/SLe)^0.2)*((Pfin/Dout) ...
            ^0.18)*((Hfin/Dout)^-0.14)*((Pre/Pres)^0.25);

    else
        Nuse = 0.0081*(ReDe^0.95)*(Pre^0.4)*((STe/SLe)^0.2)*((Pfin/Dout)
        ...
            ^0.18)*((Hfin/Dout)^-0.14)*((Pre/Pres)^0.25);
    end
end

%-----

%Condenser smooth
if ((FinningMode == 1) || (FinningMode == 3))

    if (ReDc <= 500)
        Nusc = CFc*1.04*(ReDc^0.4)*(Prc^0.36)*((Prc/PrCs)^0.25);

    elseif (ReDc <= 1000)
        Nusc = CFc*0.71*(ReDc^0.5)*(Prc^0.36)*((Prc/PrCs)^0.25);

    elseif (ReDc <= 20000)
        Nusc = CFc*0.35*((STc/SLc)^0.2)*(ReDc^0.6)*(Prc^0.36) ...
            *((Prc/PrCs)^0.25);

    else
        Nusc = CFc*0.031*((STc/SLc)^0.2)*(ReDc^0.8)*(Prc^0.36) ...
            *((Prc/PrCs)^0.25);
    end

%Condenser finned
else

```

```

if (ReDc <= 20000)
    Nusc = 0.192*(ReDc^0.65)*(Prc^0.36)*((STc/SLc)^0.2) ...
        *((Pfin/Dout)^0.18)*((Hfin/Dout)^-0.14)*((Prc/PrCs)^0.25);

elseif (ReDc <= 200000)
    Nusc= 0.0507*(ReDc^0.8)*(Prc^0.4)*((STc/SLc)^0.2) ...
        *((Pfin/Dout)^0.18)*((Hfin/Dout)^-0.14)*((Prc/PrCs)^0.25);

else
    Nusc = 0.0081*(ReDc^0.95)*(Prc^0.4)*((STc/SLc)^0.2) ...
        *((Pfin/Dout)^0.18)*((Hfin/Dout)^-0.14)*((Prc/PrCs)^0.25);
end
end

%-----

%Mean Thermal Properties
Th_m = (Thi+Thog)/2;
Tc_m = (Tci+Tcog)/2;

%Densities Mean (kg/m3)
RHOe_m = 1.08622+(-0.00234)*Th_m+(2.7773E-6)*Th_m^2 ... %Natural gas exhaust
        +(-1.60009E-9)*Th_m^3+3.48272E-13*Th_m^4;

if (FluidMode == 1) %Air
    RHOc_m = 0.16103+0.34473*exp(-Tc_m/103.23714)+0.78857* ...
        exp(-Tc_m/512.29169);

elseif (FluidMode == 2) %Water
    RHOc_m = exp(2.2467*(1-((Tc_m+273.15)/647.25))^(1/3)-2.09405* ...
        (1-((Tc_m+273.15)/647.25))^(2/3)+2.737* ...
        (1-((Tc_m+273.15)/647.25))-1.7475* ...
        (1-((Tc_m+273.15)/647.25))^(4/3))*315.5;

else %Thermal oil
    RHOc_m = ((-0.614254*(Tc_m))-(0.000321*((Tc_m)^2))+1020.62);
end

%-----

```

```

%Dynamic Viscosities Mean (m2/s)
NUe_m = (1.51901E-5+3.7842E-8*Th_m-8.96178E-12*Th_m^2 ... %Natural gas
exhaust
+1.57382E-15*Th_m^3);

if (FluidMode == 1) %Air
    NUC_m = (1.70899E-5+4.6117E-8*Tc_m-2.07642E-11*Tc_m^2 ...
+5.40458E-15*Tc_m^3);

elseif (FluidMode == 2) %Water
    NUC_m = (exp(-10.1083+1.39621*(1/((Tc_m+273.15)/647.25)-1)^(1/3) ...
+0.48431*(1/((Tc_m+273.15)/647.25)-1)^(4/3)+0.71019* ...
(1/((Tc_m+273.15)/647.25)-1)^(7/3)));

else %Thermal oil

    NUC_m = (exp((586.375/(Tc_m+62.5)-2.2809)))*RHOC_m/1000000;
end

%-----

%Thermal Conductivities Mean(W/m.K)
LAMDAe_m = 0.02272+7.19522E-5*Th_m-4.70107E-9*Th_m^2; %Natural gas exhaust

if (FluidMode == 1) %Air
    LAMDAc_m = 0.02411+7.71055E-5*Tc_m-2.81463E-8*Tc_m^2 ...
+6.36061E-12*Tc_m^3;

elseif (FluidMode == 2) %Water
    LAMDAc_m = -1.63975+11.1421*((Tc_m+273.15)/647.25)+-20.0805* ...
((Tc_m+273.15)/647.25)^(2)+16.7447*((Tc_m+273.15)/647.25) ...
^(3)+-5.78763*((Tc_m+273.15)/647.25)^(4);

else %Thermal oil
    LAMDAc_m = (1E-11*Tc_m^3)-(2E-7*Tc_m^2)-(3E-5*Tc_m)+0.1182;
end

%-----

```

```

%Specific Heat Capacities Mean (J/kg.K)
SHCe_m = 1083.52006+0.33081*Th_m+(-3.15922E-5)*Th_m^2 ... %Natural gas
exhaust
    +(-1.66552E-8)*Th_m^3;

if (FluidMode == 1) %Air
SHCc_m = (1.00224+3.33594E-5*Tc_m+5.415E-7*Tc_m^2- ... %Natural gas exhaust
    6.31148E-10*Tc_m^3+2.86052E-13*Tc_m^4-4.66306E-17 ...
    *Tc_m^5)*1000;

elseif (FluidMode == 2) %Water
SHCc_m = -14995*(1+0.088*(1-((Tc_m+273.15)/647.25))^(2/3)) ...
    +(-0.682)*(1-((Tc_m+273.15)/647.25))^(1/3)+(-0.705)* ...
    (1-((Tc_m+273.15)/647.25))^(1/3));

else %Thermal oil
SHCc_m = ((1E-9*Tc_m^3)+(3E-7*Tc_m^2)+(0.0034*Tc_m)+1.4943)*1000;
end

%-----

%Prandtl Numbers
Pre_m = SHCe_m*NUe_m/LAMDAe_m;

Prc_m = SHCc_m*NUc_m/LAMDAC_m;

%-----

%Heat Capacitance and Minimum (W/K)
Ce_m = SHCe_m*FLWe;

Cc_m = SHCc_m*FLWc;

Cmin_m = min(Ce_m,Cc_m);

%-----

```

```

%Free Flow Velocities (m/s)
ve_m = FLWe/(Ae*RHOe_m);
vc_m = FLWc/(Ac*RHOc_m);

%-----

%Maximum Velocities (m/s)
%Minimum area test evaporator
minareateste_m1 = sqrt(((STe/2)^2)+(SLe^2));
minareateste_m2 = (STe+Dout)/2;

if (minareateste_m1 > minareateste_m2)
    Vmaxe_m = (STe/(STe-Dout))*ve_m;

else
    Vmaxe_m = (ve_m/(sqrt(1+((2*(SLe/STe))^2)-(2*(Dout/STe)))));
end

%Minimum area test condenser
minareatestc_m1 = sqrt(((STc/2)^2)+(SLc^2));
minareatestc_m2 = (STc+Dout)/2;

if (minareatestc_m1 > minareatestc_m2)
    Vmaxc_m = (STc/(STc-Dout))*vc_m;

else
    Vmaxc_m = (vc_m/(sqrt(1+((2*(SLc/STc))^2)-(2*(Dout/STc)))));
end

%-----

%Reynolds Numbers
ReDe_m = (Vmaxe_m*Dout*RHOe_m)/NUe_m;

ReDc_m = (minareac*Dout*RHOc_m)/NUc_m;

%-----

```

```

%This section provides the correlations for staggered smooth tube bundles
%Evaporator smooth
if ((FinningMode == 1) || (FinningMode == 2))

    if (ReDe_m <= 500)
        Nuse_m = CFe*1.04*(ReDe_m^0.4)*(Pre_m^0.36)*((Pre_m/Pres)^0.25);

    elseif (ReDe_m <= 1000)
        Nuse_m = CFe*0.71*(ReDe_m^0.5)*(Pre_m^0.36)*((Pre_m/Pres)^0.25);

    elseif (ReDe_m <= 20000)
        Nuse_m = CFe*0.35*((STe/SLe)^0.2)*(ReDe_m^0.6)*(Pre_m^0.36) ...
            *((Pre_m/Pres)^0.25) ;

    else
        Nuse_m = CFe*0.031*((STe/SLe)^0.2)*(ReDe_m^0.8)*(Pre_m^0.36) ...
            *((Pre_m/Pres)^0.25) ;
    end

%Evaporator finned
else
    if (ReDe_m <= 20000)
        Nuse_m=
0.192*(ReDe_m^0.65)*(Pre_m^0.36)*((STe/SLe)^0.2)*((Pfin/Dout) ...
            ^0.18)*((Hfin/Dout)^-0.14)*((Pre_m/Pres)^0.25);

    elseif (ReDe_m <= 200000)
        Nuse_m
=
0.0507*(ReDe_m^0.8)*(Pre_m^0.4)*((STe/SLe)^0.2)*((Pfin/Dout) ...
            ^0.18)*((Hfin/Dout)^-0.14)*((Pre_m/Pres)^0.25);

    else
        Nuse_m
=
0.0081*(ReDe_m^0.95)*(Pre_m^0.4)*((STe/SLe)^0.2)*((Pfin/Dout) ...
            ^0.18)*((Hfin/Dout)^-0.14)*((Pre_m/Pres)^0.25);
    end
end

%-----

```

```

%Condenser smooth
if ((FinningMode == 1) || (FinningMode == 3))

    if (ReDc_m <= 500)
        Nusc_m = CFC*1.04*(ReDc_m^0.4)*(Prc_m^0.36)*((Prc_m/PrCs)^0.25);

    elseif (ReDc_m <= 1000)
        Nusc_m = CFC*0.71*(ReDc_m^0.5)*(Prc_m^0.36)*((Prc_m/PrCs)^0.25);

    elseif (ReDc_m <= 20000)
        Nusc_m = CFC*0.35*((STc/SLc)^0.2)*(ReDc_m^0.6)*(Prc_m^0.36) ...
            *((Prc_m/PrCs)^0.25);

    else
        Nusc_m = CFC*0.031*((STc/SLc)^0.2)*(ReDc_m^0.8)*(Prc_m^0.36) ...
            *((Prc_m/PrCs)^0.25);
    end

end

%Condenser finned
else
    if (ReDc_m <= 10000)
        Nusc_m = 0.192*(ReDc_m^0.65)*(Prc_m^0.36)*((STc/SLc)^0.2) ...
            *((Pfin/Dout)^0.18)*((Hfin/Dout)^-0.14)*((Prc_m/PrCs)^0.25);

    elseif (ReDc_m <= 100000)
        Nusc_m= 0.0507*(ReDc_m^0.8)*(Prc_m^0.4)*((STc/SLc)^0.2) ...
            *((Pfin/Dout)^0.18)*((Hfin/Dout)^-0.14)*((Prc_m/PrCs)^0.25);

    else
        Nusc_m = 0.0081*(ReDc_m^0.95)*(Prc_m^0.4)*((STc/SLc)^0.2) ...
            *((Pfin/Dout)^0.18)*((Hfin/Dout)^-0.14)*((Prc_m/PrCs)^0.25);
    end

end

%-----

%Heat Transfer Coefficients (W/m2.K)
HTFe_m = (Nusc_m*LAMDAe_m)/Dout;

```

```

HTFc_m = (Nusc_m*LAMDAc_m)/Dout;

%-----

%Number of Transfer Units
NTUe_m = (HTFe_m*HTAe)/Ce_m;

NTUc_m = (HTFc_m*HTAc)/Cc_m;

%-----

%Effectiveness
ee_m = 1-exp(-NTUe_m);
ec_m = 1-exp(-NTUc_m);

een_m = 1-((1-ee_m)^Nre);
ecn_m = 1-((1-ec_m)^Nrc);

%-----

%Choose Overall Effectiveness
if (Ce_m > Cc_m)
    Et_m = (((1/ecn_m)+(Cc_m/Ce_m)/een_m)^-1);
else
    Et_m = (((1/een_m)+(Ce_m/Cc_m)/ecn_m)^-1);
end

%-----

%Outlet Results
Tho = Thi-(Et_m*(Cmin_m/Ce_m)*(Thi-Tci)) %Source outlet temperature [deg C]
Tco = Tci+(Et_m*(Cmin_m/Cc_m)*(Thi-Tci)) %Sink outlet temperature [deg C]
Qdot = FLWe*SHCe_m*(Thi-Tho)/1000 %Heat recovery rate [kW]
LMTD = ((Thi-Tco)-(Tho-Tci))/log(((Thi-Tco)/(Tho-Tci))); %LMTD
UA = Qdot*1000/LMTD %Conductance value of HPHE [W/K]

%-----

```

```

%Outlet Thermal Properties
%Densities Mean (kg/m3)
RHOeo = 1.08622+(-0.00234)*Tho+(2.7773E-6)*Tho^2 ... %Natural gas exhaust
        +(-1.60009E-9)*Tho^3+3.48272E-13*Tho^4;

if (FluidMode == 1) %Air
    RHOco = 0.16103+0.34473*exp(-Tco/103.23714)+0.78857* ...
            exp(-Tco/512.29169);

elseif (FluidMode == 2) %Water
    RHOco = exp(2.2467*(1-((Tco+273.15)/647.25))^(1/3)-2.09405* ...
            (1-((Tco+273.15)/647.25))^(2/3)+2.737* ...
            (1-((Tco+273.15)/647.25))-1.7475* ...
            (1-((Tco+273.15)/647.25))^(4/3))*315.5;

else %Thermal oil
    RHOco = ((-0.614254*(Tco))- (0.000321*(Tco)^2))+1020.62);
end

%-----

%Dynamic Viscosities Mean (m2/s)
NUeo = (1.51901E-5+3.7842E-8*Tho-8.96178E-12*Tho^2 ... %Natural gas exhaust
        +1.57382E-15*Tho^3);

if (FluidMode == 1) %Air
    NUco = (1.70899E-5+4.6117E-8*Tco-2.07642E-11*Tco^2 ...
            +5.40458E-15*Tco^3);

elseif (FluidMode == 2) %Water
    NUco = (exp(-10.1083+1.39621*(1/((Tco+273.15)/647.25)-1))^(1/3) ...
            +0.48431*(1/((Tco+273.15)/647.25)-1)^(4/3)+0.71019* ...
            (1/((Tco+273.15)/647.25)-1)^(7/3)));

else %Thermal oil

    NUco = (exp((586.375/(Tco+62.5)-2.2809)))*RHOco/1000000;
end

```

```

%-----

%Thermal Conductivities Mean (W/m.K)
LAMDAeo = 0.02272+7.19522E-5*Tho-4.70107E-9*Tho^2; %Natural gas exhaust

if (FluidMode == 1) %Air
    LAMDAco = 0.02411+7.71055E-5*Tco-2.81463E-8*Tco^2 ...
        +6.36061E-12*Tco^3;

elseif (FluidMode == 2) %Water
    LAMDAco = -1.63975+11.1421*((Tco+273.15)/647.25)+-20.0805* ...
        ((Tco+273.15)/647.25)^2+16.7447*((Tco+273.15)/647.25) ...
        ^3+-5.78763*((Tco+273.15)/647.25)^4);

else %Thermal oil
    LAMDAco = (1E-11*Tco^3)-(2E-7*Tco^2)-(3E-5*Tco)+0.1182;
end

%-----

%Specific Heat Capacities Mean (J/kg.K)
SHCeo = 1083.52006+0.33081*Tho+(-3.15922E-5)*Tho^2 ... %Natural gas exhaust
    +(-1.66552E-8)*Tho^3;

if (FluidMode == 1) %Air
    SHCco = (1.00224+3.33594E-5*Tco+5.415E-7*Tco^2- ... %Natural gas exhaust
        6.31148E-10*Tco^3+2.86052E-13*Tco^4-4.66306E-17 ...
        *Tco^5)*1000;

elseif (FluidMode == 2) %Water
    SHCco = -14995*(1+0.088*(1-((Tco+273.15)/647.25))^-2/3) ...
        +(-0.682)*(1-((Tco+273.15)/647.25))^-1/3)+(-0.705)* ...
        (1-((Tco+273.15)/647.25))^(1/3));

else %Thermal oil
    SHCco = ((1E-9*Tco^3)+(3E-7*Tco^2)+(0.0034*Tco)+1.4943)*1000;
end

```

```

%-----

%Prandtl Numbers
Preo = SHCeo*NUeo/LAMDAeo;

Prco = SHCco*NUco/LAMDAco;

%-----

%Heat Capacitance and Minimum (W/K)
Ceo = SHCeo*FLWe;

Cco = SHCco*FLWc;

Cmino = min(Ceo,Cco);

%-----

%Free Flow Velocities (m/s)
veo = FLWe/(Ae*RHOeo);
vco = FLWc/(Ac*RHOco);

%-----

%Maximum Velocities (m/s)
%Minimum area test evaporator
minareatesteo1 = sqrt(((STe/2)^2)+(SLe^2));
minareatesteo2 = (STe+Dout)/2;

if (minareatesteo1 > minareatesteo2)
    Vmaxeo = (STe/(STe-Dout))*veo;

else
    Vmaxeo = (veo/(sqrt(1+((2*(SLe/STe))^2)-(2*(Dout/STe)))));

end

%Minimum area test condenser

```

```

minareatestco1 = sqrt(((STc/2)^2)+(SLc^2));
minareatestco2 = (STc+Dout)/2;

if (minareatestco1 > minareatestco2)
    Vmaxco = (STc/(STc-Dout))*vco;

else
    Vmaxco = (vco/(sqrt(1+((2*(SLc/STc))^2)-(2*(Dout/STc)))));

end

%-----

%Reynolds Numbers
ReDeo = (Vmaxeo*Dout*RHOeo)/NUeo;

ReDco = (minareac*Dout*RHOco)/NUco;

%-----

%Pressure Drop Calculations
%(1 = no finning, 2 = condenser finned, 3 = evaporator finned, 4 = both
finned)
PTe = STe/Dout;
PTc = STc/Dout;
PLe = SLe/Dout;
PLc = SLc/Dout;
STSLe = STe/SLe;
STSLc = STc/SLc;
if ((FinningMode == 1) || (FinningMode == 2))

%Calculating X (Chi)
if (ReDe<550)
    if (STSLe<1.2)
        Chie=1;
    else
        Chie=0.055476370223*STSLe^6-0.807737327822*STSLe^5+4.791061335894
...
        *STSLe^4-14.775008015945*STSLe^3+24.848044479172*STSLe^2 ...

```

```

-21.13587970328*STSLe+8.030267420326;
end

elseif (ReDe<5500)
    Chie=-0.006582510659882*STSLe^6+0.086512756111735*STSLe^5 ...
        -0.429365023037395*STSLe^4+0.967477501402558*STSLe^3 ...
        -0.87746851708403*STSLe^2+0.174439100478289*STSLe+1.09714274629842;
elseif (ReDe<55000)
    Chie=0.008671843104707*STSLe^6-0.119491431144033*STSLe^5 ...
        +0.667459785818119*STSLe^4-1.93997806035734*STSLe^3 ...
        +3.11719768511303*STSLe^2-2.60629695221346*STSLe+1.88881954700185;
else
    Chie= 0.01090483478788*STSLe^5-0.088732136558723*STSLe^4 ...
        +0.180975740557806*STSLe^3+0.233839225186575*STSLe^2 ...
        -1.13914487426972*STSLe+1.88969439044012;
end

if (PTe<1.375)

    if (ReDe<55)
        fxe = 0.00000000304672310189*ReDe^6-0.00000090695882490676* ...
            ReDe^5+0.000109425635603455*ReDe^4-0.00691792826131564* ...
            ReDe^3+0.247530159394677*ReDe^2-5.05542618913993*ReDe+ ...
            57.605423373848;
    elseif (ReDe<550)
        fxe = 0.00000000000000083215*ReDe^6-0.00000000000238158711* ...
            ReDe^5+0.000000027363655918*ReDe^4-0.00000162360038933978 ...
            *ReDe^3+0.000532828876206208*ReDe^2-0.0960643479984688*ReDe ...
            +9.61786287906493;
    elseif (ReDe<5500)
        fxe = -0.0000000000000000244*ReDe^5+0.0000000000000289881* ...
            ReDe^4-0.0000000017798752675*ReDe^3+0.00000060405096862192 ...
            *ReDe^2-0.00112347015674636*ReDe+1.76762993138187;
    elseif (ReDe<55000)
        fxe = 0.0000000000000000047*ReDe^4-0.00000000000002865962* ...
            ReDe^3+0.0000000105603407663*ReDe^2-0.0000258664220503753 ...
            *ReDe+0.875546721856801;
    elseif (ReDe<550000)
        fxe = -0.0000000000000001787*ReDe^3+0.0000000000740106679* ...
            ReDe^2-0.00000190891762195942*ReDe+0.569096588296964;
    end
end

```

```

elseif (ReDe<5500000)
    fxe = -0.000000000000000000000003*ReDe^3+0.000000000000010117251 ...
        *ReDe^2-0.00000016357781964993*ReDe+0.33256305725565;
else
    fxe = 0.242224797365682;
end

elseif (PTe<1.75)

    if (ReDe<55)
        fxe = 0.00000000114868524973*ReDe^6-0.00000034638165718312* ...
            ReDe^5+0.0000421418078584364*ReDe^4-0.00266761574594401 ...
            *ReDe^3+0.0945654639576471*ReDe^2-1.88762853451537*ReDe ...
            +21.4428342470075;
    elseif (ReDe<550)
        fxe = 0.000000000000000015255*ReDe^6- 0.000000000000046615345* ...
            ReDe^5+0.00000000057851437448*ReDe^4-0.00000037608117844575* ...
            ReDe^3+0.000137635189258499*ReDe^2-0.0284194584882274*ReDe ...
            +3.79362252312672;
    elseif (ReDe<5500)
        fxe = -0.000000000000000000174*ReDe^5+0.00000000000001935299* ...
            ReDe^4-0.00000000011108837479*ReDe^3+0.00000035587470947408 ...
            *ReDe^2-0.00064621859209747*ReDe+1.15054329015104;
    elseif (ReDe<55000)
        fxe = 0.000000000000000000039*ReDe^4-0.00000000000002138387* ...
            ReDe^3+0.00000000069719534679*ReDe^2-0.0000161315082414622* ...
            ReDe+0.630319186014919;
    elseif (ReDe<550000)
        fxe = -0.00000000000000001842*ReDe^3+0.00000000000699952338* ...
            ReDe^2-0.00000166932528414058*ReDe+0.451192894189153;
    elseif (ReDe<5500000)
        fxe = -0.00000000000000000006*ReDe^3+0.00000000000020142234* ...
            ReDe^2-0.00000032669280227272*ReDe+0.367180244544361;
    else
        fxe = 0.216498811988182;
    end

elseif (PTe<2.25)

    if (ReDe<550)

```

```

fxe = 0.0000000000000000910*ReDe^6-0.00000000000003658734* ...
      ReDe^5+0.00000000006021195169*ReDe^4-0.00000005263723839061* ...
      ReDe^3+0.0000265381828685591*ReDe^2-0.00789168282494227*ReDe ...
      +1.8355926726513;
elseif (ReDe<5500)
fxe = -0.0000000000000000101*ReDe^5+0.0000000000001160338* ...
      ReDe^4-0.0000000006873699553*ReDe^3+0.00000022365809450496 ...
      *ReDe^2-0.000400804319671022*ReDe+0.814130211150491;
elseif (ReDe<55000)
fxe = -0.0000000000000000011*ReDe^4+0.0000000000001049493* ...
      ReDe^3-0.000000004273588584*ReDe^2+0.00000477262161487613* ...
      ReDe+0.427538350478811;
elseif (ReDe<550000)
fxe = -0.00000000000000000553*ReDe^3+0.00000000000371124399* ...
      ReDe^2-0.00000122526204810312*ReDe+0.38293963530156;
elseif (ReDe<5500000)
fxe = 0.0000000000006263317*ReDe^2-0.00000014855615788396* ...
      ReDe+0.259742394917818;
else
fxe = 0.198895782982392;
end

else

if (ReDe<550)
fxe = 0.0000000000000000982*ReDe^6-0.00000000000003765112* ...
      ReDe^5+0.0000000005871185134*ReDe^4-0.00000004816240180048* ...
      ReDe^3+0.0000225707909619934*ReDe^2-0.00626113799921795* ...
      ReDe+1.45138423197786;
elseif (ReDe<5500)
fxe = -0.0000000000000000046*ReDe^5+0.0000000000000604261* ...
      ReDe^4-0.0000000004171156554*ReDe^3+0.00000015915610209495* ...
      ReDe^2-0.000324266250554968*ReDe+0.682593897519661;
elseif (ReDe<55000)
fxe = -0.0000000000000000016*ReDe^4+0.0000000000001077911* ...
      ReDe^3-0.00000000037498237585*ReDe^2+0.00000413491976991877* ...
      ReDe+0.367963674275565;
elseif (ReDe<550000)
fxe = - 0.00000000000000001457*ReDe^3+0.00000000000535808696* ...
      ReDe^2-0.00000127208886715665*ReDe+0.352068277778896;

```



```

elseif (ReDe<5500000)
    fxe = -0.00000000000000000002*ReDe^3+0.0000000000001004569* ...
        ReDe^2-0.00000017832626843352*ReDe+0.255079372314046;
else
    fxe = 0.185330984133629;
end
end

%-----

fe = fxe*Chie;
dPe = fe*Nre*((Vmaxe^2)*RHOe)/2

else %Evaporator finned correction factor
    erate = HTAe/HTAe_smooth;

    if (ReDe <= 1000)
        Eue = 67.6*(ReDe^-0.7)*(erate^0.5)*((STe/Dout)^-0.55) ...
            *((SLe/Dout)^-0.5);
    elseif (ReDe <= 100000)
        Eue = 3.2*(ReDe^-0.25)*(erate^0.5)*((STe/Dout)^-0.55) ...
            *((SLe/Dout)^-0.5);
    else
        Eue = 0.18*(ReDe^0)*(erate^0.5)*((STe/Dout)^-0.55) ...
            *((SLe/Dout)^-0.5);
    end

    Ge = ((RHOe+RHOeo)/2)*((Vmaxe+Vmaxeo)/2); %Core mass velocity
    RHOew = 1.08622+(-0.00234)*Twe+(2.7773E-6)*Twe^2 ...
        +(-1.60009E-9)*Twe^3+3.48272E-13*Twe^4;
    dPe = Ge^2/(2*RHOe)*(Eue*Nre*RHOe*(1/RHOew)+(2*(RHOe/RHOeo)-1))
end

%Condenser smooth
if ((FinningMode == 1) || (FinningMode == 3))
    if (ReDc<550)
        if (STSLc<1.2)
            Chic=1;
        else

```

```

Chic=0.055476370223*STSLc^6-0.807737327822*STSLc^5+4.791061335894
...
    *STSLc^4-14.775008015945*STSLc^3+24.848044479172*STSLc^2 ...
    -21.13587970328*STSLc+8.030267420326;
end

elseif (ReDc<5500)
    Chic=-0.006582510659882*STSLc^6+0.086512756111735*STSLc^5 ...
        -0.429365023037395*STSLc^4+0.967477501402558*STSLc^3 ...
        -0.87746851708403*STSLc^2+0.174439100478289*STSLc+1.09714274629842;
elseif (ReDc<55000)
    Chic=0.008671843104707*STSLc^6-0.119491431144033*STSLc^5 ...
        +0.667459785818119*STSLc^4-1.93997806035734*STSLc^3 ...
        +3.11719768511303*STSLc^2-2.60629695221346*STSLc+1.88881954700185;
else
    Chic= 0.01090483478788*STSLc^5-0.088732136558723*STSLc^4 ...
        +0.180975740557806*STSLc^3+0.233839225186575*STSLc^2 ...
        -1.13914487426972*STSLc+1.88969439044012;
end

if (PTc<1.375)

    if (ReDc<55)
        fxc = 0.00000000304672310189*ReD^6-0.00000090695882490676* ...
            ReDc^5+0.000109425635603455*ReDc^4-0.00691792826131564* ...
            ReDc^3+0.247530159394677*ReDc^2-5.05542618913993*ReDc+ ...
            57.605423373848;
    elseif (ReDc<550)
        fxc = 0.00000000000000083215*ReDc^6-0.00000000000238158711* ...
            ReDc^5+0.000000027363655918*ReDc^4-0.00000162360038933978 ...
            *ReDc^3+0.000532828876206208*ReDc^2-0.0960643479984688*ReDc ...
            +9.61786287906493;
    elseif (ReDc<5500)
        fxc = -0.0000000000000000244*ReDc^5+0.0000000000000289881* ...
            ReDc^4-0.0000000017798752675*ReDc^3+0.00000060405096862192 ...
            *ReDc^2-0.00112347015674636*ReDc+1.76762993138187;
    elseif (ReDc<55000)
        fxc = 0.0000000000000000047*ReDc^4-0.00000000000002865962* ...
            ReDc^3+0.00000000105603407663*ReDc^2-0.0000258664220503753 ...
            *ReDc+0.875546721856801;
    elseif (ReDc<550000)

```

```

    fxc = -0.00000000000000001787*ReDc^3+0.00000000000740106679* ...
        ReDc^2-0.00000190891762195942*ReDc+0.569096588296964;
elseif (ReDc<550000)
    fxc = -0.0000000000000000003*ReDc^3+0.00000000000010117251 ...
        *ReDc^2-0.00000016357781964993*ReDc+0.33256305725565;
else
    fxc = 0.242224797365682;
end

elseif (PTc<1.75)

    if (ReDc<55)
        fxc = 0.00000000114868524973*ReDc^6-0.00000034638165718312* ...
            ReDc^5+0.0000421418078584364*ReDc^4-0.00266761574594401 ...
            *ReDc^3+0.0945654639576471*ReDc^2-1.88762853451537*ReDc ...
            +21.4428342470075;
    elseif (ReDc<550)
        fxc = 0.000000000000000015255*ReDc^6- 0.00000000000046615345* ...
            ReDc^5+0.00000000057851437448*ReDc^4-0.00000037608117844575* ...
            ReDc^3+0.000137635189258499*ReDc^2-0.0284194584882274*ReDc ...
            +3.79362252312672;
    elseif (ReDc<5500)
        fxc = -0.00000000000000000174*ReDc^5+0.00000000000001935299* ...
            ReDc^4-0.00000000011108837479*ReDc^3+0.00000035587470947408 ...
            *ReDc^2-0.00064621859209747*ReDc+1.15054329015104;
    elseif (ReDc<55000)
        fxc = 0.00000000000000000039*ReDc^4-0.000000000000002138387* ...
            ReDc^3+0.00000000069719534679*ReDc^2-0.0000161315082414622* ...
            ReDc+0.630319186014919;
    elseif (ReDc<550000)
        fxc = -0.000000000000000001842*ReDc^3+0.00000000000699952338* ...
            ReDc^2-0.00000166932528414058*ReDc+0.451192894189153;
    elseif (ReDc<5500000)
        fxc = -0.0000000000000000006*ReDc^3+0.00000000000020142234* ...
            ReDc^2-0.00000032669280227272*ReDc+0.367180244544361;
    else
        fxc = 0.216498811988182;
    end

elseif (PTc<2.25)

```

```

if (ReDc<550)
    fxc = 0.0000000000000000910*ReDe^6-0.0000000000003658734* ...
        ReDc^5+0.0000000006021195169*ReDc^4-0.00000005263723839061* ...
        ReDc^3+0.0000265381828685591*ReDc^2-0.00789168282494227*ReDc ...
        +1.8355926726513;
elseif (ReDc<5500)
    fxc = -0.0000000000000000101*ReDc^5+0.0000000000001160338* ...
        ReDc^4-0.0000000006873699553*ReDc^3+0.00000022365809450496 ...
        *ReDc^2-0.000400804319671022*ReDc+0.814130211150491;
elseif (ReDc<55000)
    fxc = -0.0000000000000000011*ReDc^4+0.0000000000001049493* ...
        ReDc^3-0.0000000004273588584*ReDc^2+0.00000477262161487613* ...
        ReDc+0.427538350478811;
elseif (ReDc<550000)
    fxc = -0.00000000000000000553*ReDc^3+0.00000000000371124399* ...
        ReDc^2-0.00000122526204810312*ReDc+0.38293963530156;
elseif (ReDc<5500000)
    fxc = 0.00000000000006263317*ReDc^2-0.00000014855615788396* ...
        ReDc+0.259742394917818;
else
    fxc = 0.198895782982392;
end

else

if (ReDc<550)
    fxc = 0.0000000000000000982*ReDc^6-0.0000000000003765112* ...
        ReDc^5+0.0000000005871185134*ReDc^4-0.00000004816240180048* ...
        ReDc^3+0.0000225707909619934*ReDc^2-0.00626113799921795* ...
        ReDc+1.45138423197786;
elseif (ReDc<5500)
    fxc = -0.0000000000000000046*ReDc^5+0.0000000000000604261* ...
        ReDc^4-0.0000000004171156554*ReDc^3+0.00000015915610209495* ...
        ReDc^2-0.000324266250554968*ReDc+0.682593897519661;
elseif (ReDc<55000)
    fxc = -0.0000000000000000016*ReDc^4+0.0000000000001077911* ...
        ReDc^3-0.00000000037498237585*ReDc^2+0.00000413491976991877* ...
        ReDc+0.367963674275565;
elseif (ReDc<550000)

```

```

    fxc = -0.00000000000000001457*ReDc^3+0.00000000000535808696* ...
        ReDc^2-0.00000127208886715665*ReDc+0.352068277778896;
elseif (ReDc<5500000)
    fxc = -0.0000000000000000002*ReDc^3+0.0000000000001004569* ...
        ReDc^2-0.00000017832626843352*ReDc+0.255079372314046;
else
    fxc = 0.185330984133629;
end
end
fc = fxc*Chic;
dPc = fc*Nrc*((Vmaxc^2)*RHOC)/2

else
    eratc = HTAc/HTAc_smooth;

    if (ReDc <= 1000)
        Euc = 67.6*(ReDc^-0.7)*(eratc^0.5)*((STc/Dout)^-0.55) ...
            *((SLc/Dout)^-0.5);
    elseif (ReDc <= 100000)
        Euc = 3.2*(ReDc^-0.25)*(eratc^0.5)*((STc/Dout)^-0.55) ...
            *((SLc/Dout)^-0.5);
    else
        Euc = 0.18*(ReDc^0)*(eratc^0.5)*((STc/Dout)^-0.55) ...
            *((SLc/Dout)^-0.5);
    end

    Gc = ((RHOC+RHOCO)/2)*((Vmaxc+Vmaxco)/2);

    dPc= Gc^2/(2*RHOCw)*(Euc*Nrc*RHOC*(1/RHOCw)+(2*(RHOC/RHOCO)-1))

end
%-----

```

B. Fortran Code for Type204 TRNSYS Component

Subroutine Type204

```
!*****
```

```
! This routine simulates a HPHE component providing outlet
! temperatures of source and sink streams, pressure drop, conductance
! and energy recovery rate using the Effectiveness NTU method.
```

```
!*****
```

```
!-----
```

```
!Use Statements
```

```
Use TrnsysConstants
```

```
Use TrnsysFunctions
```

```
!-----
```

```
!Export this subroutine for its use in external DLLs.
```

```
!DEC$ATTRIBUTES DLLEXPORT :: TYPE204
```

```
!-----
```

```
!Variable Declarations
```

```
Implicit None !Force explicit declaration of local variables
```

```
!Inputs
```

```
Double precision Thi !Temperature of source inlet fluid [deg C]
```

```
Double precision Tci !Temperature of sink inlet fluid [deg C]
```

```
Double precision FLWe !Mass flow rate evaporator (source) fluid [kg/s]
```

Double precision FLWc !Mass flow rate condenser (sink) fluid [kg/s]

!Parameters

Integer Nre !Number of rows in heat exchanger evaporator (longitudinal)

Integer Nrc !Number of rows in heat exchanger condenser (longitudinal)

Double precision Dout !Outer diameter of heat pipes [m]

Double precision Le !Length evaporator [m]

Double precision Lc !Length of condenser [m]

Integer Nte !Number of tubes in evaporator row (transverse)

Integer Ntc !Number of tubes in condenser row (transverse)

Double precision STe !Transverse distance between evaporator row centres [m]

Double precision SLc !Longitudinal distance between evaporator row centres [m]

Double precision STc !Transverse distance between condenser row centres [m]

Double precision SLc !Longitudinal distance between condenser row centres [m]

Double precision Ae !Flow area of evaporator [m²]

Double precision Ac !Flow area of condenser [m²]

Integer FinningMode !(1=none, 2=con finned, 3=evap finned, 4=both)

Integer FluidMode !Sink: 1=air 2=water 3=thermal oil

Double precision Dofin !Outer diameter of fins [m]

Double precision efin !Thickness of fins [m]

Double precision Pfin !Pitch of fins [m]

Double precision Hfin !Width of fins [m]

!Internal Variables

Double precision HTFe !Heat transfer coefficient evaporator [W/m².K]

Double precision HTFeo !Heat transfer coefficient evaporator outlet [W/m².K]

Double precision HTFc !Heat transfer coefficient condenser [W/m².K]

Double precision HTFco !Heat transfer coefficient condenser outlet [W/m².K]

Double precision HTAe !Heat transfer area of one evaporator row [m²]

Double precision HTAe_smooth !Heat transfer area of one evaporator row smooth [m²]

Double precision HTAc !Heat transfer area of one condenser row [m²]

Double precision HTAc_smooth !Heat transfer area of one condenser row smooth [m²]

Double precision Ce !Heat capacity rate of evaporator [j/K.s]

Double precision C_{eo} !Heat capacity rate of evaporator outlet [j/K.s]

Double precision C_c !Heat capacity rate of condenser [j/K.s]

Double precision C_{co} !Heat capacity rate of condenser outlet [j/K.s]

Double precision C_{min} !Smaller or C_e and C_c [j/K.s]

Double precision C_{mino} !Smaller or C_e and C_c outlet [j/K.s]

Double precision E_t !Overall effectiveness

Double precision E_{to} !Overall effectiveness outlet

Double precision e_{en} !Effectiveness of evaporator row

Double precision e_{eno} !Effectiveness of evaporator row outlet

Double precision e_{cn} !Effectiveness of condenser row

Double precision e_{cno} !Effectiveness of condenser row outlet

Double precision e_e !Effectiveness of evaporator

Double precision e_{eo} !Effectiveness of evaporator outlet

Double precision e_c !Effectiveness of condenser

Double precision e_{co} !Effectiveness of condenser outlet

Double precision NTU_e !Number of effectiveness units evaporator

Double precision NTU_{eo} !Number of effectiveness units evaporator outlet

Double precision NTU_c !Number of effectiveness units condenser

Double precision NTU_{co} !Number of effectiveness units condenser outlet

Double precision Pr_e !Prandtl number evaporator

Double precision Pr_{eo} !Prandtl number evaporator outlet

Double precision Pr_c !Prandtl number condenser

Double precision Pr_{co} !Prandtl number condenser outlet

Double precision V_{maxe} !Maximum velocity evaporator [m/s]

Double precision V_{maxeo} !Maximum velocity evaporator outlet [m/s]

Double precision V_{maxc} !Maximum velocity condenser [m/s]

Double precision V_{maxco} !Maximum velocity condenser outlet [m/s]

Double precision $ReDe$!Reynolds number evaporator

Double precision $ReDeo$!Reynolds number evaporator outlet

Double precision $ReDc$!Reynolds number condenser

Double precision $ReDco$!Reynolds number condenser outlet

Double precision Nu_e !Nusselt number evaporator

Double precision Nu_{eo} !Nusselt number evaporator outlet

Double precision Nusc !Nusselt number condenser
 Double precision Nusco !Nusselt number condenser outlet
 Double precision ve !Free flow velocity evaporator [m/s]
 Double precision veo !Free flow velocity evaporator outlet [m/s]
 Double precision vc !Free flow velocity condenser [m/s]
 Double precision vco !Free flow velocity condenser outlet [m/s]
 Double precision RHOe !Density evaporator fluid [kg/m3]
 Double precision RHOeo !Density evaporator fluid outlet [kg/m3]
 Double precision RHOC !Density condenser fluid [kg/m3]
 Double precision RHOCO !Density condenser fluid outlet [kg/m3]
 Double precision NUe !Kinematic viscosity evaporator [m2/s]
 Double precision NUeo !Kinematic viscosity evaporator outlet [m2/s]
 Double precision NUc !Kinematic viscosity condenser [m2/s]
 Double precision NUco !Kinematic viscosity condenser outlet [m2/s]
 Double precision LAMDAe !Thermal conductivity evaporator fluid [W/m.K]
 Double precision LAMDAeo !Thermal conductivity evaporator fluid outlet [W/m.K]
 Double precision LAMDAC !Thermal conductivity condenser fluid [W/m.K]
 Double precision LAMDACO !Thermal conductivity condenser fluid outlet [W/m.K]
 Double precision SHCe !Specific heat capacity evaporator fluid [J/kg.K]
 Double precision SHCeO !Specific heat capacity evaporator fluid outlet [J/kg.K]
 Double precision SHCc !Specific heat capacity condenser fluid [J/kg.K]
 Double precision SHCCO !Specific heat capacity condenser fluid outlet [J/kg.K]
 Double precision Timestep,Time !Simulation timestep and time [s]
 Double precision PI !Pi, 3.1415927
 Integer CurrentUnit, CurrentType

!Evaluation Of Pr At Wall Temperature

Double precision Pres !Pr evaluated at evaporator wall temperature
 Double precision Prcs !Pr evaluated at condenser wall temperature
 Double precision NUew !Kinematic viscosity at evaporator wall [m2/s]
 Double precision NUcw !Kinematic viscosity at condenser wall [m2/s]
 Double precision LAMDAew !Thermal conductivity at evaporator wall [W/m.K]
 Double precision LAMDACw !Thermal conductivity at condenser wall [W/m.K]

```

Double precision Twe  !Iterating evap wall temperature to determine Pres [deg C]
Double precision Twc  !Iterating cond wall temperature to determine Prcs [deg C]
Double precision SHCew !Specific heat capacity at evaporator wall temperature [J/kg.K]
Double precision SHCcw !Specific heat capacity at condenser wall temperature [J/kg.K]

!Goalseeking
Double precision Twe_up !Goalseek up function for Twe [deg C]
Double precision Twe_down !Goalseek down function for Twe [deg C]
Double precision Twc_up !Goalseek up function for Twc [deg C]
Double precision Twc_down !Goalseek down function for Twc [deg C]
Double precision Q1e  !m.cp.dT
Double precision Q2e  !((Thi-Tho)/log(Thi-Twe)/Tho-Twe))
Double precision Q4e  !((Thi-Tho)/log(Thi-Twe(up/down))/Tho-Twe(up/down)))
Integer numiterations
Double precision dQ1e !Q1e - Q2e
Double precision dQ2e !Q1e - Q4e
Double precision Q1c  !m.cp.dT
Double precision Q2c  !((Tco-Tci)/log(Tci-Tw)/Tco-Tw))
Double precision Q4c  !((Tco-Tci)/log(Tci-Tw(up/down))/Tco-Tw(up/down)))
Double precision dQ1c !Q1c - Q2c
Double precision dQ2c !Q1c - Q4c
Double precision Thog !Source outlet temperature initial guess [deg C]
Double precision Tcog !Sink outlet temperature initial guess [deg C]

!Finning influence
Double precision CFfe !Correction factor for Nusselt equations evaporator
Double precision CFfc !Correction factor for Nusselt equations condenser
Double precision efffe !Efficiency of the fin evaporator
Double precision efffc !Efficiency of the fin condenser
Double precision Afe  !Heat transfer area of the evaporator fins [m2]
Double precision Afc  !Heat transfer area of the condenser fins [m2]
Double precision xe  !SQRT(2hfc/kfe*efffe)
Double precision xc  !SQRT(2hfc/kfe*efffc)

```

Double precision kfe !Thermal conductivity of evaporator fin [W/m.K]
 Double precision kfc !Thermal conductivity of condenser fin [W/m.K]
 Double precision Lhle !Length of helical evaporator [m]
 Double precision Lhlc !Length of helical condenser [m]

!Pressure Drop calculations

Double precision PLe !SLe/Dout longitudinal pitch
 Double precision PLc !SLc/Dout longitudinal pitch
 Double precision PTe !STe/Dout transverse pitch
 Double precision PTc !STc/Dout transverse pitch
 Double precision fe !Friction factor evaporator
 Double precision fc !Friction factor condenser
 Double precision fxe !Friction factor/Xe evaporator
 Double precision fxc !Friction factor/Xc condenser
 Double precision Chie !Correlation factor evaporator
 Double precision Chic !Correlation factor condenser
 Double precision Eue !Euler number evaporator
 Double precision Euc !Euler number condenser
 Double precision erate !Ratio of total SA with fins to bare tube SA w/o fins evaporator
 Double precision eratc !Ratio of total SA with fins to bare tube SA w/o fins condenser
 Double precision Ge !Core mass velocity evaporator
 Double precision Gc !Core mass velocity condenser
 Double precision RHOew !Density at condenser wall [kg/m3]
 Double precision RHOcw !Density at condenser wall [kg/m3]
 Double precision STSLe !STe/SLe
 Double precision STSLc !STc/SLc

!Flow area location tests

Double precision minareateste1 !Minimum area test evaporator
 Double precision minareateste2 !Minimum area test evaporator
 Double precision minareateste_m1 !Minimum area test evaporator
 Double precision minareateste_m2 !Minimum area test evaporator
 Double precision minareatesteo1 !Minimum area test evaporator

Double precision minareatesteo2 !Minimum area test evaporator
Double precision minareatestc1 !Minimum area test condenser
Double precision minareatestc2 !Minimum area test condenser
Double precision minareatestc_m1 !Minimum area test condenser
Double precision minareatestc_m2 !Minimum area test condenser
Double precision minareatestco1 !Minimum area test condenser
Double precision minareatestco2 !Minimum area test condenser

!Means

Double precision Cc_m
Double precision Ce_m
Double precision Cmin_m
Double precision LAMDAc_m
Double precision LAMDAe_m
Double precision minareac
Double precision minareae
Double precision NUC_m
Double precision NUe_m
Double precision Nusc_m
Double precision Nuse_m
Double precision Prc_m
Double precision Pre_m
Double precision ReDc_m
Double precision ReDe_m
Double precision RHOe_m
Double precision RHOc_m
Double precision SHCe_m
Double precision SHCc_m
Double precision Tc_m
Double precision Th_m
Double precision vc_m
Double precision ve_m
Double precision Vmaxe_m

Double precision Vmaxc_m
Double precision ecn_m
Double precision een_m
Double precision ec_m
Double precision ee_m
Double precision Et_m
Double precision HTFc_m
Double precision HTFe_m
Double precision LMTD
Double precision NTUc_m
Double precision NTUe_m

!Outputs

Double precision Tho !Temperature of source outlet fluid [deg C]
Double precision Tco !Temperature of sink outlet fluid [deg C]
Double precision Qdot !Energy (Heat) Transfer Rate [kW]
Double precision dPe !Pressure drop evaporator [Pa]
Double precision dPc !Pressure drop condenser [Pa]
Double precision UA !Conductance value of HPHE [W/K]

!-----

!Get the Global Trnsys Simulation Variables

Time = getSimulationTime()
Timestep = getSimulationTimeStep()
CurrentUnit = getCurrentUnit()
CurrentType = getCurrentType()

!-----

!Set the Version Number for This Type

If (getIsVersionSigningTime()) Then

 Call SetTypeVersion(17)

 Return

EndIf

!-----

!Do All of the Last Call Manipulations Here

If (getIsLastCallofSimulation()) Then

 Return

EndIf

!-----

!Perform Any "End of Timestep" Manipulations Here

If (getIsEndOfTimestep()) Then

 Return

EndIf

!-----

!Do All of the "Very First Call of the Simulation Manipulations" Here

If(getIsFirstCallofSimulation()) Then

!Tell the Trnsys Engine How This Type Works

 Call SetNumberOfParameters(19)

 Call SetNumberOfInputs(4)

 Call SetNumberOfDerivatives(0)

 Call SetNumberOfOutputs(6)

 Call SetIterationMode(1)

 Call SetNumberStoredVariables(0,0)

 Call SetNumberOfDiscreteControls(0)

!Set the Correct Input and Output Variable Types

Call SetInputUnits(1,'TE1') !Thi [deg C]

Call SetInputUnits(2,'TE1') !Tci [deg C]

Call SetInputUnits(3,'MF2') !FLWe [kg/s]

Call SetInputUnits(4,'MF2') !FLWc [kg/s]

Call SetOutputUnits(1,'TE1') !Tho [deg C]

Call SetOutputUnits(2,'TE1') !Tco [deg C]

Call SetOutputUnits(3,'PW3') !Qdot [kW]

Call SetOutputUnits(4,'PR3') !dPe [Pa (N/m²)]

Call SetOutputUnits(5,'PR3') !dPc [Pa (N/m²)]

Call SetOutputUnits(6,'DM1') !UA [W/K] !Unit N/A so dimensionless

Return

EndIf

!-----

!Do All of the "Start Time" Manipulations Here- There Are No Iterations at the Initial Time

If (getIsStartTime()) Then

!Read in the Values of the Parameters from the Input File

Nre = JFIX(getParameterValue(1)) !Number of rows evaporator

Nrc = JFIX(getParameterValue(2)) !Number of rows condenser

Dout = getParameterValue(3) !Outer diameter of heat pipe

Le = getParameterValue(4) !Length of evaporator

Lc = getParameterValue(5) !Length of condenser

Nte = JFIX(getParameterValue(6)) !Number of heat pipe rows evaporator

Ntc = JFIX(getParameterValue(7)) !Number of heat pipe rows condenser

STe = getParameterValue(8) !Distance between row centres evaporator

SLe = getParameterValue(9) !Distance between heat pipe centres evaporator

STc = getParameterValue(10) !Distance between row centres condenser

SLc = getParameterValue(11) !Distance between heat pipe centres condenser

```

Ae = getParameterValue(12)    !Flow area evaporator
Ac = getParameterValue(13)    !Flow area condenser
FinningMode = JFIX(getParameterValue(14)) !Condenser or Evaporator finned
FluidMode = JFIX(getParameterValue(15)) !Heat sink as air, water or oil
Dofin = getParameterValue(16) !Outer diameter of fins
efin = getParameterValue(17) !Thickness of fins
Pfin = getParameterValue(18) !Pitch of fins
Hfin = getParameterValue(19) !Width of fins

!-----

!Check Parameters for Problems
If (Nre <= 1) Call FoundBadParameter(1, 'Fatal', 'The number of evaporator rows must be
positive.')
If (Nrc <= 1) Call FoundBadParameter(2, 'Fatal', 'The number of condenser rows must be
positive.')
If (Dout > 1.d0) Call FoundBadParameter(3, 'Fatal', 'Ensure diameter is in metres')
If (Le <= 0.d0) Call FoundBadParameter(4, 'Fatal', 'The length evaporator must be positive.')
If (Lc <= 0.d0) Call FoundBadParameter(5, 'Fatal', 'The length condenser must be positive.')
If (Nte <= 0.d0) Call FoundBadParameter(6, 'Fatal', 'Number of heat pipes in evaporator row
must be positive.')
If (Ntc <= 0.d0) Call FoundBadParameter(7, 'Fatal', 'Number of heat pipes in condenser row
must be positive.')
If (STe >= 1.d0) Call FoundBadParameter(8, 'Fatal', 'Ensure distance between evaporator rows
is in metres')
If (SLe >= 1.d0) Call FoundBadParameter(9, 'Fatal', 'Ensure distance between evaporator heat
pipes is in metres')
If (STc >= 1.d0) Call FoundBadParameter(10, 'Fatal', 'Ensure distance between condenser rows
is in metres')
If (SLc >= 1.d0) Call FoundBadParameter(11, 'Fatal', 'Ensure distance between condenser heat
pipes is in metres')
If (Ae <= 0.d0) Call FoundBadParameter(12, 'Fatal', 'Ae must be positive')
If (Ac <= 0.d0) Call FoundBadParameter(13, 'Fatal', 'Ac must be positive')

```

If ((FinningMode <= 0) .or. (FinningMode > 4)) Call FoundBadParameter(14, 'Fatal', 'Finning mode must be between 1 and 4')

If ((FluidMode <= 0) .or. (FluidMode > 3)) Call FoundBadParameter(15, 'Fatal', 'Fluid mode must be between 1 and 3')

If (Dofin >= 1) Call FoundBadParameter(16, 'Fatal', 'Ensure fin diameter is in metres')

If (efin >= 1) Call FoundBadParameter(17, 'Fatal', 'Ensure outer fin diameter is in metres')

If (Pfin >= 1) Call FoundBadParameter(18, 'Fatal', 'Ensure pitch is in metres')

If (Hfin >= 1) Call FoundBadParameter(19, 'Fatal', 'Ensure fin height is in metres')

If (ErrorFound()) Return

!-----

!Set the Initial Value of the Outputs

Call SetOutputValue(1, getInputValue(1))

Call SetOutputValue(2, getInputValue(2))

Call SetOutputValue(3, 0.d0)

Call SetOutputValue(4, 0.d0)

Call SetOutputValue(5, 0.d0)

Call SetOutputValue(6, 0.d0)

Return

EndIf

!-----

!ReRead the Parameters If Another Unit of This Type Has Been Called Last

If (getIsReReadParameters()) Then

Nre = JFIX(getParameterValue(1)) !Number of rows evaporator

Nrc = JFIX(getParameterValue(2)) !Number of rows condenser

Dout = getParameterValue(3) !Outer diameter of heat pipe

Le = getParameterValue(4) !Length of evaporator

Lc = getParameterValue(5) !Length of condenser

Nte = JFIX(getParameterValue(6)) !Number of heat pipe rows evaporator

```

Ntc = JFIX(getParameterValue(7)) !Number of heat pipe rows condenser
STe = getParameterValue(8) !Distance between row centres evaporator
SLe = getParameterValue(9) !Distance between heat pipe centres evaporator
STc = getParameterValue(10) !Distance between row centres condenser
SLc = getParameterValue(11) !Distance between heat pipe centres condenser
Ae = getParameterValue(12) !Flow area evaporator
Ac = getParameterValue(13) !Flow area condenser
FinningMode = JFIX(getParameterValue(14)) !Condenser or Evaporator finned
FluidMode = JFIX(getParameterValue(15)) !Heat sink as air, water or oil
Dofin = getParameterValue(16) !Outer diameter of fins
efin = getParameterValue(17) !Thickness of fins
Pfin = getParameterValue(18) !Pitch of fins
Hfin = getParameterValue(19) !Width of fins

EndIf

!-----

!Get the Current Inputs to the Model
Thi = getInputValue(1) !Temperature of source inlet fluid [deg C]
Tci = getInputValue(2) !Temperature of sink inlet fluid [deg C]
FLWe = getInputValue(3) !Mass flow rate evaporator (source) fluid [kg/s]
FLWc = getInputValue(4) !Mass flow rate condenser (sink) fluid [kg/s]
PI = 3.1415927

If (Thi < 0.) Call foundBadInput(1, 'Fatal', 'Enter source inlet temperature')
If (Tci < 0.) Call foundBadInput(2, 'Fatal', 'Enter sink inlet temperature')
If (FLWe < 0.) Call foundBadInput(3, 'Fatal', 'Enter source inlet flow rate')
If (FLWc < 0.) Call foundBadInput(4, 'Fatal', 'Enter sink inlet flow rate')
If (ErrorFound()) Return

!-----

!Perform All of the Calculations Here

```

!Densities Inlet(kg/m3)

$$\text{RHOe} = 1.08622 + (-0.00234) * \text{Thi} + (2.7773\text{E-}6) * \text{Thi}^{**2.d0} \& \text{!Natural gas exhaust} \\ + (-1.60009\text{E-}9) * \text{Thi}^{**3.d0} + 3.48272\text{E-}13 * \text{Thi}^{**4.d0}$$

If (FluidMode == 1) Then !Air

$$\text{RHOC} = 0.16103 + 0.34473 * \text{EXP}(-\text{Tci}/103.23714) + 0.78857 * \& \\ \text{EXP}(-\text{Tci}/512.29169)$$

ElseIf (FluidMode == 2) Then !Water

$$\text{RHOC} = \text{EXP}(2.2467 * (1.d0 - ((\text{Tci} + 273.15) / 647.25)))^{**}(1.d0/3.d0) - 2.09405 * \& \\ (1.d0 - ((\text{Tci} + 273.15) / 647.25))^{**}(2.d0/3.d0) + 2.737 * (1.d0 - ((\text{Tci} + 273.15) / 647.25)) \& \\ - 1.7475 * (1.d0 - ((\text{Tci} + 273.15) / 647.25))^{**}(4.d0/3.d0) * 315.5$$

Else !Thermal oil

$$\text{RHOC} = ((-0.614254 * (\text{Tci})) - (0.000321 * ((\text{Tci})^{**2.d0})) + 1020.62)$$

EndIf

!-----

!Dynamic Viscosities Inlet(m2/s)

$$\text{NUe} = (1.51901\text{E-}5 + 3.7842\text{E-}8 * \text{Thi} - 8.96178\text{E-}12 * \text{Thi}^{**2.d0} \& \text{!Natural gas exhaust} \\ + 1.57382\text{E-}15 * \text{Thi}^{**3.d0})$$

If (FluidMode == 1) Then !Air

$$\text{NUc} = (1.70899\text{E-}5 + 4.6117\text{E-}8 * \text{Tci} - 2.07642\text{E-}11 * \text{Tci}^{**2.d0} \& \\ + 5.40458\text{E-}15 * \text{Tci}^{**3.d0})$$

ElseIf (FluidMode == 2) Then !Water

$$\text{NUc} = (\text{EXP}(-10.1083 + 1.39621 * (1.d0 / ((\text{Tci} + 273.15) / 647.25) - 1.d0))^{**}(1.d0/3.d0) \& \\ + 0.48431 * (1.d0 / ((\text{Tci} + 273.15) / 647.25) - 1.d0)^{**}(4.d0/3.d0) + 0.71019 * \& \\ (1.d0 / ((\text{Tci} + 273.15) / 647.25) - 1.d0)^{**}(7.d0/3.d0)))$$

Else !Thermal oil

$$NUc = (\text{EXP}((586.375/(Tci+62.5))-2.2809)) * RHOC / 1000000.d0$$

EndIf

!-----

!Thermal Conductivities Inlet(W/m.K)

$$LAMD Ae = 0.02272 + 7.19522E-5 * Thi - 4.70107E-9 * Thi ** 2.d0 \text{ !Natural gas exhaust}$$

If (FluidMode == 1) Then !Air

$$LAMD Ac = 0.02411 + 7.71055E-5 * Tci - 2.81463E-8 * Tci ** 2.d0 \& \\ + 6.36061E-12 * Tci ** 3.d0$$

ElseIf (FluidMode == 2) Then !Water

$$LAMD Ac = -1.63975 + 11.1421 * ((Tci + 273.15) / 647.25) + -20.0805 * \& \\ ((Tci + 273.15) / 647.25) ** (2.d0) + 16.7447 * ((Tci + 273.15) / 647.25) \& \\ ** (3.d0) + -5.78763 * ((Tci + 273.15) / 647.25) ** (4.d0)$$

Else !Thermal oil

$$LAMD Ac = (1E-11 * Tci ** 3.d0) - (2E-7 * Tci ** 2.d0) - (3E-5 * Tci) + 0.1182$$

EndIf

!-----

!Specific Heat Capacities Inlet(J/kg.K)

$$SHC e = 1083.52006 + 0.33081 * Thi + (-3.15922E-5) * Thi ** 2.d0 \& \text{ !Natural gas exhaust} \\ + (-1.66552E-8) * Thi ** 3.d0$$

If (FluidMode == 1) Then !Air

$$SHC c = (1.00224 + 3.33594E-5 * Tci + 5.415E-7 * Tci ** 2.d0 - \& \\ 6.31148E-10 * Tci ** 3.d0 + 2.86052E-13 * Tci ** 4.d0 - 4.66306E-17 \& \\ * Tci ** 5.d0) * 1000.d0$$

ElseIf (FluidMode == 2) Then !Water

$$\text{SHCc} = -14995.\text{d}0 * (1.\text{d}0 + 0.088 * (1.\text{d}0 - ((\text{Tci} + 273.15) / 647.25))^{**}(-2.\text{d}0 / 3.\text{d}0)) \&$$

$$+ (-0.682) * (1.\text{d}0 - ((\text{Tci} + 273.15) / 647.25))^{**}(-1.\text{d}0 / 3.\text{d}0) + (-0.705) * \&$$

$$(1.\text{d}0 - ((\text{Tci} + 273.15) / 647.25))^{**}(1.\text{d}0 / 3.\text{d}0))$$

Else !Thermal oil

$$\text{SHCc} = ((1\text{E}-9 * \text{Tci}^{**}3.\text{d}0) + (3\text{E}-7 * \text{Tci}^{**}2.\text{d}0) + (0.0034 * \text{Tci}) + 1.4943) * 1000.\text{d}0$$

EndIf

!-----

!Prandtl Numbers

$$\text{Pre} = \text{SHCe} * \text{NUe} / \text{LAMDAe}$$

$$\text{Prc} = \text{SHCc} * \text{NUc} / \text{LAMDAc}$$

!-----

!Do Calculations Here

!Heat Capacitance and Minimum (W/K)

$$\text{Ce} = \text{SHCe} * \text{FLWe}$$

$$\text{Cc} = \text{SHCc} * \text{FLWc}$$

$$\text{Cmin} = \text{MIN}(\text{Ce}, \text{Cc})$$

!-----

!Free Flow Velocities (m/s)

$$\text{ve} = \text{FLWe} / (\text{Ae} * \text{RHOe})$$

$$\text{vc} = \text{FLWc} / (\text{Ac} * \text{RHOC})$$

```

!-----
!Maximum Velocities (m/s)
Vmaxe = (STe/(STe-Dout))*ve
minareae = ((Ae/Le)-(Nte*Dout))*Le
!Minimum area test condenser
minareatestc1 = SQRT(((STc/2.d0)**2.d0)+(SLc**2.d0))
minareatestc2 = (STc+Dout)/2.d0

If (minareatestc1 > minareatestc2) Then
    Vmaxc = (STc/(STc-Dout))*vc

    minareac= Ac-(Lc*Ntc*Dout)
Else
    Vmaxc = (vc/(SQRT(1.d0+((2.d0*(SLc/STc))**2.d0)-(2.d0*(Dout/STc))))

    minareac = ((Ac/Lc)-(((Ntc-1.d0)*STc)+Dout)+((SQRT((STc/2.d0)**2.d0-SLc**2.d0) &
        -Dout)*(Ntc+1.d0)))*Lc

EndIf

!-----

!Reynolds Numbers
ReDe = (Vmaxe*Dout*RHOe)/NUe

ReDc = (minareac*Dout*RHOc)/NUc

!-----

!Nusselt Numbers
!This Section provides a correction factor If the number of rows <16
If ((Nre >= 14) .and. (Nre <= 16)) Then

```

```
CFe = 0.995
ElseIf (Nre == 13) Then
    CFe = 0.99
ElseIf ((Nre >= 11) .and. (Nre <= 12)) Then
    CFe = 0.985
ElseIf (Nre == 10) Then
    CFe = 0.98
ElseIf (Nre == 7) Then
    CFe = 0.96
ElseIf (Nre == 6) Then
    CFe = 0.945
ElseIf (Nre == 5) Then
    CFe = 0.93
ElseIf (Nre == 4) Then
    CFe = 0.89
ElseIf (Nre == 3) Then
    CFe = 0.84
ElseIf (Nre == 2) Then
    CFe = 0.76
ElseIf (Nre == 1) Then
    CFe = 0.64
Else
    CFe = 1.d0 !(Nre > 16)
EndIf
```

```
If ((Nrc >= 14) .and. (Nrc <= 16)) Then
    CFc = 0.995
ElseIf (Nrc == 13) Then
    CFc = 0.99
ElseIf ((Nrc >= 11) .and. (Nrc <= 12)) Then
    CFc = 0.985
ElseIf (Nrc == 10) Then
```

```

    CFc = 0.98
ElseIf (Nrc == 7) Then
    CFc = 0.96
ElseIf (Nrc == 6) Then
    CFc = 0.945
ElseIf (Nrc == 5) Then
    CFc = 0.93
ElseIf (Nrc == 4) Then
    CFc = 0.89
ElseIf (Nrc == 3) Then
    CFc = 0.84
ElseIf (Nrc == 2) Then
    CFc = 0.76
ElseIf (Nrc == 1) Then
    CFc = 0.64
Else
    CFc = 1.d0 !(Nrc > 16)
EndIf
!-----

!This section provides the correlations for staggered smooth tube bundles
!Evaporator

If ((FinningMode == 1) .or. (FinningMode == 2)) Then

    If (ReDe <= 500.d0) Then
        Nusc = CFe*1.04*(ReDe**0.4)*(Pre**0.36)*(1.1**0.25)

    ElseIf (ReDe <= 1000.d0) Then
        Nusc = CFe*0.71*(ReDe**0.5)*(Pre**0.36)*(1.1**0.25)

    ElseIf (ReDe <= 20000.d0) Then
        Nusc = CFe*0.35*((STe/SLe)**0.2)*(ReDe**0.6)*(Pre**0.36) &

```


$*(1.1^{**0.25})$

Else

$Nuse = CFe*0.031*((STe/SLe)^{**0.2})*(ReDe^{**0.8})*(Pre^{**0.36}) \&$
 $*(1.1^{**0.25})$

EndIf

Else

If (ReDe <= 10000.d0) Then

$Nuse = 0.192*(ReDe^{**0.65})*(Pre^{**0.36})*((STe/SLe)^{**0.2})*((Pfin/Dout) \&$
 $^{**0.18})*((Hfin/Dout)^{**-0.14})*(1.1^{**0.25})$

ElseIf (ReDe <= 100000.d0) Then

$Nuse = 0.0507*(ReDe^{**0.8})*(Pre^{**0.4})*((STe/SLe)^{**0.2})*((Pfin/Dout) \&$
 $^{**0.18})*((Hfin/Dout)^{**-0.14})*(1.1^{**0.25})$

Else

$Nuse = 0.0081*(ReDe^{**0.95})*(Pre^{**0.4})*((STe/SLe)^{**0.2})*((Pfin/Dout) \&$
 $^{**0.18})*((Hfin/Dout)^{**-0.14})*(1.1^{**0.25})$

EndIf

EndIf

!-----

!Condenser

If ((FinningMode == 1) .or. (FinningMode == 3)) Then

If (ReDc <= 500.d0) Then

$Nusc = CFc*1.04*(ReDc^{**0.4})*(Prc^{**0.36})*(1.1^{**0.25})$

ElseIf (ReDc <= 1000.d0) Then

$Nusc = CFc*0.71*(ReDc^{**0.5})*(Prc^{**0.36})*(1.1^{**0.25})$

ElseIf (ReDc <= 20000.d0) Then

$$\text{Nusc} = \text{CFc} * 0.35 * ((\text{STc}/\text{SLc})^{**0.2}) * (\text{ReDc}^{**0.6}) * (\text{Prc}^{**0.36}) \& \\ * (1.1^{**0.25})$$

Else

$$\text{Nusc} = \text{CFc} * 0.031 * ((\text{STc}/\text{SLc})^{**0.2}) * (\text{ReDc}^{**0.8}) * (\text{Prc}^{**0.36}) \& \\ * (1.1^{**0.25})$$

EndIf

Else

If (ReDc <= 10000.d0) Then

$$\text{Nusc} = \text{CFc} * 0.192 * (\text{ReDc}^{**0.65}) * (\text{Prc}^{**0.36}) * ((\text{STc}/\text{SLc})^{**0.2}) \& \\ * ((\text{Pfin}/\text{Dout})^{**0.18}) * ((\text{Hfin}/\text{Dout})^{**-0.14}) * (1.1^{**0.25})$$

ElseIf (ReDc <= 100000.d0) Then

$$\text{Nusc} = \text{CFc} * 0.0507 * (\text{ReDc}^{**0.8}) * (\text{Prc}^{**0.4}) * ((\text{STc}/\text{SLc})^{**0.2}) \& \\ * ((\text{Pfin}/\text{Dout})^{**0.18}) * ((\text{Hfin}/\text{Dout})^{**-0.14}) * (1.1^{**0.25})$$

Else

$$\text{Nusc} = \text{CFc} * 0.0081 * (\text{ReDc}^{**0.95}) * (\text{Prc}^{**0.4}) * ((\text{STc}/\text{SLc})^{**0.2}) \& \\ * ((\text{Pfin}/\text{Dout})^{**0.18}) * ((\text{Hfin}/\text{Dout})^{**-0.14}) * (1.1^{**0.25})$$

EndIf

EndIf

!-----

!Heat Transfer Coefficients (W/m2.K)

$$\text{HTFe} = (\text{Nuse} * \text{LAMDAe}) / \text{Dout}$$

$$\text{HTFc} = (\text{Nusc} * \text{LAMDAc}) / \text{Dout}$$

!-----

!Heat Transfer Areas (m2)

!Evaporator

If ((FinningMode == 1) .or. (FinningMode == 2)) Then

$$HTAe = PI * Dout * Le * Nte$$

Else

$$HTAe_smooth = PI * Dout * Le * Nte$$

$$kfe = (-0.0333 * ((Thi + Tci) / 2) + 53.902)$$

$$Lhle = (Le / Pfin) * SQRT(((PI * (Dout + Dofin) / 2.d0) ** 2.d0) + Pfin ** 2.d0)$$

$$Afe = 2.d0 * Hfin * Lhle * Nte$$

$$xe = SQRT((2.d0 * HTFe) / (kfe * efin))$$

$$efffe = (TANH(xe * Hfin)) / (xe * Hfin)$$

$$HTAe = ((PI * Dout * Le * (1.d0 - efin * 1.d0 / Pfin)) * Nte) + (efffe * Afe)$$

EndIf

!Condenser

If ((FinningMode == 1) .or. (FinningMode == 3)) Then

$$HTAc = PI * Dout * Lc * Ntc$$

Else

$$HTAc_smooth = PI * Dout * Lc * Ntc$$

$$kfc = (-0.0333 * ((Thi + Tci / 2.d0)) + 53.902)$$

$$Lhlc = (Lc / Pfin) * SQRT(((PI * (Dout + Dofin) / 2.d0) ** 2.d0) + Pfin ** 2.d0)$$

$$Afc = 2.d0 * Hfin * Lhlc * Ntc$$

$$xc = SQRT((2.d0 * HTFc) / (kfc * efin))$$

$$efffc = (TANH(xc * Hfin)) / (xc * Hfin)$$

$$HTAc = ((PI * Dout * Lc * (1.d0 - efin * 1.d0 / Pfin)) * Ntc) + (efffc * Afc)$$

EndIf

!-----

!Number of Transfer Units

$$NTUe = (HTFe * HTAe) / Ce$$

$$NTUc = (HTFc * HTAc) / Cc$$

!-----

!Effectiveness

$$ee = 1.d0-EXP(-NTUe)$$

$$ec = 1.d0-EXP(-NTUc)$$

$$een = 1.d0-((1.d0-ee)**Nre)$$

$$ecn = 1.d0-((1.d0-ec)**Nrc)$$

!-----

!Choose Overall Effectiveness

If (Ce > Cc) Then

$$Et = (((1.d0/ecn)+(Cc/Ce)/een)**-1.d0)$$

Else

$$Et = (((1.d0/een)+(Ce/Cc)/ecn)**-1.d0)$$

EndIf

!-----

!Initial Outlet Temperature Guesses

$$Thog = Thi-(Et*(Cmin/Ce)*(Thi-Tci))$$

$$Tcog = Tci+(Et*(Cmin/Cc)*(Thi-Tci))$$

!-----

!Temperature at Evaporator Wall Iterations

$$Twe = (Thi+Thog)/2.d0$$

$$Q1e = FLWe*SHCe*(Thi-Thog)$$

$$Q2e = HTFe*HTAe*((Thi-Thog)/log(Thi-Twe)/(Thog-Twe))$$

```

dQ1e = Q1e-Q2e
Twe_up = Twe+0.001
Twe_down = Twe-0.001
Q4e = HTFe*HTAe*((Thi-Thog)/log(Thi-Twe_up)/(Thog-Twe_up))
dQ2e = Q1e-Q4e

numiterations = 0

If (dQ2e < dQ1e)
  while ((dQ2e > 0.000001) .and. (numiterations < 1000000))
    Twe_up = Twe_up+0.001
    Q4e = HTFe*HTAe*((Thi-Thog)/log(Thi-Twe_up)/(Thog-Twe_up))
    dQ2e = Q1e-Q4e
    numiterations = numiterations+1
    Twe = Twe_up
  end
Else
  while ((dQ2e < -0.000001) .and. (numiterations < 1000000))
    Twe_down = Twe_down -0.001
    Q4e = HTFe*HTAe*((Thi-Thog)/log(Thi-Twe_down)/(Thog-Twe_down))
    dQ2e = Q1e-Q4e
    numiterations = numiterations+1
    Twe = Twe_down
  end
end

!-----

!Temperature at Condenser Wall Iterations
Twc = (Tci+Tcog)/2.d0
Q1c = FLWc*SHCc*(Tcog-Tci)
Q2c = HTFc*HTAc*((Tcog-Tci)/log(Tci-Twc)/(Tcog-Twc))
dQ1c = Q1c-Q2c

```

```

Twc_up = Twc+0.001
Twc_down = Twc-0.001
Q4c = HTFc*HTAc*((Tcog-Tci)/log(Tcog-Twc_up)/(Tci-Twc_up))
dQ2c = Q1c-Q4c
numiterations = 0

If (dQ2c < dQ1c)
  while ((dQ2c > 0.000001) .and. (numiterations < 1000000))
    Twc_up = Twc_up+0.001
    Q4c = HTFc*HTAc*((Tcog-Tci)/log(Tcog-Twc_up)/(Tci-Twc_up))
    dQ2c= Q1c-Q4c
    numiterations = numiterations+1
    Twc = Twc_up
  end
Else
  while ((dQ2c < -0.000001) .and. (numiterations < 1000000))
    Twc_down = Twc_down -0.001
    Q4c = HTFc*HTAc*((Tcog-Tci)/log(Tcog-Twc_down)/(Tci-Twc_down))
    dQ2c = Q1c-Q4c
    numiterations = numiterations+1
    Twc = Twc_down
  end
end

!-----
!Wall Calculations
!Densities at Walls (kg/m3)
RHOew = 1.08622+(-0.00234)*Twe+(2.7773E-6)*Twe**2.d0 &
+(-1.60009E-9)*Twe**3.d0+3.48272E-13*Twe**4.d0

If (FluidMode == 1) Then !Air
  RHOcw = 0.16103+0.34473*EXP(-Twc/103.23714)+0.78857* &
  EXP(-Twc/512.29169)

```

ElseIf (FluidMode == 2) Then !Water

$$\begin{aligned} \text{RHOcw} = & \text{EXP}(2.2467*(1.d0-((\text{Twc}+273.15)/647.25))^{**}(1.d0/3.d0)-2.09405* & \\ & (1.d0-((\text{Twc}+273.15)/647.25))^{**}(2.d0/3.d0)+2.737*(1.d0-((\text{Twc}+273.15)/647.25)) & \\ & -1.7475*(1.d0-((\text{Twc}+273.15)/647.25))^{**}(4.d0/3.d0))*315.5 \end{aligned}$$

Else !Thermal oil

$$\text{RHOcw} = ((-0.614254*(\text{Twc}))-0.000321*((\text{Twc})^{**}2.d0))+1020.62)$$

EndIf

!Dynamic Viscosity at Walls (W/m.K)

$$\begin{aligned} \text{NUew} = & (1.51901\text{E-}5+3.7842\text{E-}8*\text{Twe}-8.96178\text{E-}12*\text{Twe}^{**}2.d0 & \\ & +1.57382\text{E-}15*\text{Twe}^{**}3.d0) \end{aligned}$$

If (FluidMode == 1) Then !Air

$$\begin{aligned} \text{NUcw} = & (1.70899\text{E-}5+4.6117\text{E-}8*\text{Twc}-2.07642\text{E-}11*\text{Twc}^{**}2.d0 & \\ & +5.40458\text{E-}15*\text{Twc}^{**}3.d0) \end{aligned}$$

ElseIf (FluidMode == 2) Then !Water

$$\begin{aligned} \text{NUcw} = & (\text{EXP}(-10.1083+1.39621*(1.d0/((\text{Twc}+273.15)/647.25)-1.d0))^{**}(1.d0/3.d0) & \\ & +0.48431*(1.d0/((\text{Twc}+273.15)/647.25)-1.d0)^{**}(4.d0/3.d0)+0.71019* & \\ & (1.d0/((\text{Twc}+273.15)/647.25)-1.d0)^{**}(7.d0/3.d0))) \end{aligned}$$

Else !Thermal oil

$$\text{NUcw} = (\text{EXP}((586.375/(\text{Twc}+62.5)-2.2809)))*\text{RHOcw}/1000000.d0$$

EndIf

!Thermal Conductivities at Walls (W/m.K)

$$\text{LAMDAew} = 0.02272+7.19522\text{E-}5*\text{Twe}-4.70107\text{E-}9*\text{Twe}^{**}2.d0$$

If (FluidMode == 1) Then !Air

$$\begin{aligned} \text{LAMDAcw} = & 0.02411+7.71055\text{E-}5*\text{Twc}-2.81463\text{E-}8*\text{Twc}^{**}2.d0 & \\ & +6.36061\text{E-}12*\text{Twc}^{**}3.d0 \end{aligned}$$

ElseIf (FluidMode == 2) Then !Water

$$\begin{aligned} \text{LAMDAcw} = & -1.63975+11.1421*((\text{Twc}+273.15)/647.25)+-20.0805* \& \\ & ((\text{Twc}+273.15)/647.25)**(2.\text{d}0)+16.7447*((\text{Twc}+273.15)/647.25) \& \\ & *(3.\text{d}0)+-5.78763*((\text{Twc}+273.15)/647.25)**(4.\text{d}0) \end{aligned}$$

Else !Thermal oil

$$\text{LAMDAcw} = (1\text{E}-11*\text{Twc}**3.\text{d}0)-(2\text{E}-7*\text{Twc}**2.\text{d}0)-(3\text{E}-5*\text{Twc})+0.1182$$

If (LAMDAcw <= 0.d0) Then

$$\text{LAMDAcw} = 0.01$$

EndIf

EndIf

!Specific Heat Capacities at Walls

$$\begin{aligned} \text{SHCew} = & 1083.52006+0.33081*\text{Twe}+(-3.15922\text{E}-5)*\text{Twe}**2.\text{d}0 \& \\ & +(-1.66552\text{E}-8)*\text{Twe}**3.\text{d}0 \end{aligned}$$

If (FluidMode == 1) Then !Air

$$\begin{aligned} \text{SHCcw} = & (1.00224+3.33594\text{E}-5*\text{Twc}+5.415\text{E}-7*\text{Twc}**2.\text{d}0- \& \\ & 6.31148\text{E}-10*\text{Twc}**3.\text{d}0+2.86052\text{E}-13*\text{Twc}**4.\text{d}0-4.66306\text{E}-17 \& \\ & *\text{Twc}**5.\text{d}0)*1000.\text{d}0 \end{aligned}$$

ElseIf (FluidMode == 2) Then !Water

$$\begin{aligned} \text{SHCcw} = & -14995.\text{d}0*(1.\text{d}0+0.088*(1.\text{d}0-((\text{Twc}+273.15)/647.25))**(-2.\text{d}0/3.\text{d}0) \& \\ & +(-0.682)*(1.\text{d}0-((\text{Twc}+273.15)/647.25))**(-1.\text{d}0/3.\text{d}0)+(-0.705)* \& \\ & (1.\text{d}0-((\text{Twc}+273.15)/647.25))**(1.\text{d}0/3.\text{d}0)) \end{aligned}$$

Else !Thermal oil

$$\text{SHCcw} = ((1\text{E}-9*\text{Twc}**3.\text{d}0)+(3\text{E}-7*\text{Twc}**2.\text{d}0)+(0.0034*\text{Twc})+1.4943)*1000.\text{d}0$$

EndIf

!-----

!Prandtl Number at Walls

$$\text{Pres} = \text{SHCew}*\text{NUew}/\text{LAMDAew}$$

$$\text{PrCs} = \text{SHCCw} * \text{NUcw} / \text{LAMDAcw}$$

!-----

!This section provides the correlations for staggered smooth tube bundles

!Evaporator

If ((FinningMode == 1) .or. (FinningMode == 2)) Then

 If (ReDe <= 500.d0) Then

$$\text{Nuse} = \text{CFe} * 1.04 * (\text{ReDe}^{**0.4}) * (\text{Pre}^{**0.36}) * ((\text{Pre}/\text{Pres})^{**0.25})$$

 ElseIf (ReDe <= 1000.d0) Then

$$\text{Nuse} = \text{CFe} * 0.71 * (\text{ReDe}^{**0.5}) * (\text{Pre}^{**0.36}) * ((\text{Pre}/\text{Pres})^{**0.25})$$

 ElseIf (ReDe <= 20000.d0) Then

$$\text{Nuse} = \text{CFe} * 0.35 * ((\text{STe}/\text{SLe})^{**0.2}) * (\text{ReDe}^{**0.6}) * (\text{Pre}^{**0.36}) * ((\text{Pre}/\text{Pres})^{**0.25})$$

 Else

$$\text{Nuse} = \text{CFe} * 0.031 * ((\text{STe}/\text{SLe})^{**0.2}) * (\text{ReDe}^{**0.8}) * (\text{Pre}^{**0.36}) * ((\text{Pre}/\text{Pres})^{**0.25})$$

 EndIf

Else

 If (ReDe <= 10000.d0) Then

$$\text{Nuse} = 0.192 * (\text{ReDe}^{**0.65}) * (\text{Pre}^{**0.36}) * ((\text{STe}/\text{SLe})^{**0.2}) * ((\text{Pfin}/\text{Dout})^{**0.18}) * ((\text{Hfin}/\text{Dout})^{**-0.14}) * ((\text{Pre}/\text{Pres})^{**0.25})$$

 ElseIf (ReDe <= 100000.d0) Then

$$\text{Nuse} = 0.0507 * (\text{ReDe}^{**0.8}) * (\text{Pre}^{**0.4}) * ((\text{STe}/\text{SLe})^{**0.2}) * ((\text{Pfin}/\text{Dout})^{**0.18}) * ((\text{Hfin}/\text{Dout})^{**-0.14}) * ((\text{Pre}/\text{Pres})^{**0.25})$$

```

Else
    Nusc = 0.0081*(ReDe**0.95)*(Pre**0.4)*((STe/SLe)**0.2)*((Pfin/Dout) &
        **0.18)*((Hfin/Dout)**-0.14)*((Pre/Pres)**0.25)
EndIf
EndIf

```

!-----

!Condenser

```

If ((FinningMode == 1) .or. (FinningMode == 3)) Then

```

```

    If (ReDc <= 500.d0) Then

```

$$Nusc = CFC * 1.04 * (ReDc^{0.4}) * (Prc^{0.36}) * ((Prc/Prs)^{0.25})$$

```

    ElseIf (ReDc <= 1000.d0) Then

```

$$Nusc = CFC * 0.71 * (ReDc^{0.5}) * (Prc^{0.36}) * ((Prc/Prs)^{0.25})$$

```

    ElseIf (ReDc <= 20000.d0) Then

```

$$Nusc = CFC * 0.35 * ((STc/SLc)^{0.2}) * (ReDc^{0.6}) * (Prc^{0.36}) * ((Prc/Prs)^{0.25})$$

```

    Else

```

$$Nusc = CFC * 0.031 * ((STc/SLc)^{0.2}) * (ReDc^{0.8}) * (Prc^{0.36}) * ((Prc/Prs)^{0.25})$$

```

    EndIf

```

```

Else

```

```

    If (ReDc <= 10000.d0) Then

```

$$Nusc = 0.192 * (ReDc^{0.65}) * (Prc^{0.36}) * ((STc/SLc)^{0.2}) * ((Pfin/Dout)^{0.18}) * ((Hfin/Dout)^{-0.14}) * ((Prc/Prs)^{0.25})$$

```

ElseIf (ReDc <= 100000.d0) Then
  Nusc= 0.0507*(ReDc**0.8)*(Prc**0.4)*((STc/SLc)**0.2) &
    *((Pfin/Dout)**0.18)*((Hfin/Dout)**-0.14)*((Prc/PrCs)**0.25)

Else
  Nusc = 0.0081*(ReDc**0.95)*(Prc**0.4)*((STc/SLc)**0.2) &
    *((Pfin/Dout)**0.18)*((Hfin/Dout)**-0.14)*((Prc/PrCs)**0.25)
EndIf
EndIf

!-----

!Mean Thermal Properties
Th_m = (Thi+Thog)/2.d0
Tc_m = (Tci+Tcog)/2.d0
!Densities Mean (kg/m3)
RHOe_m = 1.08622+(-0.00234)*Th_m+(2.7773E-6)*Th_m**2.d0 & !Natural gas exhaust
  +(-1.60009E-9)*Th_m**3.d0+3.48272E-13*Th_m**4.d0

If (FluidMode == 1) Then !Air
  RHOc_m = 0.16103+0.34473*EXP(-Tc_m/103.23714)+0.78857* &
    EXP(-Tc_m/512.29169)

ElseIf (FluidMode == 2) Then !Water
  RHOc_m = EXP(2.2467*(1.d0-((Tc_m+273.15)/647.25))**(1.d0/3.d0)-2.09405* &
    (1.d0-((Tc_m+273.15)/647.25))**(2.d0/3.d0)+2.737* &
    (1.d0-((Tc_m+273.15)/647.25))-1.7475* &
    (1.d0-((Tc_m+273.15)/647.25))**(4.d0/3.d0))*315.5

Else !Thermal oil
  RHOc_m = ((-0.614254*(Tc_m))-0.000321*((Tc_m)**2.d0))+1020.62)
EndIf

```

!-----

!Dynamic Viscosities Mean (m2/s)

$$\text{NUe}_m = (1.51901\text{E-}5 + 3.7842\text{E-}8 * \text{Th}_m - 8.96178\text{E-}12 * \text{Th}_m^{**2} + 1.57382\text{E-}15 * \text{Th}_m^{**3}) \& \text{!Natural gas exhaust}$$

If (FluidMode == 1) Then !Air

$$\text{NUc}_m = (1.70899\text{E-}5 + 4.6117\text{E-}8 * \text{Tc}_m - 2.07642\text{E-}11 * \text{Tc}_m^{**2} + 5.40458\text{E-}15 * \text{Tc}_m^{**3}) \&$$

ElseIf (FluidMode == 2) Then !Water

$$\begin{aligned} \text{NUc}_m = & (\text{EXP}(-10.1083 + 1.39621 * ((\text{Tc}_m + 273.15) / 647.25) - 1.0) ** (1.0 / 3.0)) \& \\ & + 0.48431 * ((\text{Tc}_m + 273.15) / 647.25) - 1.0) ** (4.0 / 3.0) + 0.71019 * \& \\ & (1.0 / ((\text{Tc}_m + 273.15) / 647.25) - 1.0) ** (7.0 / 3.0)) \end{aligned}$$

Else !Thermal oil

$$\text{NUc}_m = (\text{EXP}((586.375 / (\text{Tc}_m + 62.5) - 2.2809))) * \text{RHOC}_m / 1000000.0$$

EndIf

!-----

!Thermal Conductivities Mean(W/m.K)

$$\text{LAMDAe}_m = 0.02272 + 7.19522\text{E-}5 * \text{Th}_m - 4.70107\text{E-}9 * \text{Th}_m^{**2} \& \text{!Natural gas exhaust}$$

If (FluidMode == 1) Then !Air

$$\begin{aligned} \text{LAMDAc}_m = & 0.02411 + 7.71055\text{E-}5 * \text{Tc}_m - 2.81463\text{E-}8 * \text{Tc}_m^{**2} \& \\ & + 6.36061\text{E-}12 * \text{Tc}_m^{**3} \end{aligned}$$

ElseIf (FluidMode == 2) Then !Water

$$\begin{aligned} \text{LAMDAc}_m = & -1.63975 + 11.1421 * ((\text{Tc}_m + 273.15) / 647.25) + -20.0805 * \& \\ & ((\text{Tc}_m + 273.15) / 647.25) ** (2.0) + 16.7447 * ((\text{Tc}_m + 273.15) / 647.25) \& \\ & ** (3.0) + -5.78763 * ((\text{Tc}_m + 273.15) / 647.25) ** (4.0) \end{aligned}$$

Else !Thermal oil

$$\text{LAMD}Ac_m = (1E-11 * Tc_m^{**3.d0}) - (2E-7 * Tc_m^{**2.d0}) - (3E-5 * Tc_m) + 0.1182$$

EndIf

!-----

!Specific Heat Capacities Mean (J/kg.K)

$$\text{SHCe}_m = 1083.52006 + 0.33081 * Th_m + (-3.15922E-5) * Th_m^{**2.d0} \& \text{!Natural gas exhaust} \\ + (-1.66552E-8) * Th_m^{**3.d0}$$

If (FluidMode == 1) Then !Air

$$\text{SHCc}_m = (1.00224 + 3.33594E-5 * Tc_m + 5.415E-7 * Tc_m^{**2.d0} - \& \text{!Natural gas exhaust} \\ 6.31148E-10 * Tc_m^{**3.d0} + 2.86052E-13 * Tc_m^{**4.d0} - 4.66306E-17 \& \\ * Tc_m^{**5.d0}) * 1000.d0$$

ElseIf (FluidMode == 2) Then !Water

$$\text{SHCc}_m = -14995.d0 * (1.d0 + 0.088 * (1.d0 - ((Tc_m + 273.15) / 647.25))^{**(-2.d0/3.d0)} \& \\ + (-0.682) * (1.d0 - ((Tc_m + 273.15) / 647.25))^{**(-1.d0/3.d0)} + (-0.705) * \& \\ (1.d0 - ((Tc_m + 273.15) / 647.25))^{**(1.d0/3.d0)})$$

Else !Thermal oil

$$\text{SHCc}_m = ((1E-9 * Tc_m^{**3.d0}) + (3E-7 * Tc_m^{**2.d0}) + (0.0034 * Tc_m) + 1.4943) * 1000.d0$$

EndIf

!-----

!Prandtl Numbers

$$\text{Pre}_m = \text{SHCe}_m * \text{NUe}_m / \text{LAMD}Ae_m$$

$$\text{Prc}_m = \text{SHCc}_m * \text{NUc}_m / \text{LAMD}Ac_m$$

!-----

!Heat Capacitance and Minimum (W/K)

$$Ce_m = SHCe_m * FLWe$$

$$Cc_m = SHCc_m * FLWc$$

$$Cmin_m = MIN(Ce_m, Cc_m)$$

!-----

!Free Flow Velocities (m/s)

$$ve_m = FLWe / (Ae * RHOe_m)$$

$$vc_m = FLWc / (Ac * RHOc_m)$$

!-----

!Maximum Velocities (m/s)

!Minimum area test evaporator

$$minareateste_m1 = \sqrt{((STe/2.d0)**2.d0) + (SLe**2.d0)}$$

$$minareateste_m2 = (STe + Dout) / 2.d0$$

If (minareateste_m1 > minareateste_m2) Then

$$Vmaxe_m = (STe / (STe - Dout)) * ve_m$$

Else

$$Vmaxe_m = (ve_m / (\sqrt{1.d0 + ((2.d0 * (SLe / STe)) ** 2.d0)} - (2.d0 * (Dout / STe))))$$

EndIf

!Minimum area test condenser

$$minareatestc_m1 = \sqrt{((STc/2.d0)**2.d0) + (SLc**2.d0)}$$

$$minareatestc_m2 = (STc + Dout) / 2.d0$$

```

If (minareatestc_m1 > minareatestc_m2) Then
  Vmaxc_m = (STc/(STc-Dout))*vc_m

Else
  Vmaxc_m = (vc_m/(SQRT(1.d0+((2.d0*(SLc/STc))**2.d0)-(2.d0*(Dout/STc))))

EndIf

!-----

!Reynolds Numbers
ReDe_m = (Vmaxe_m*Dout*RHOe_m)/NUe_m

ReDc_m = (minareac*Dout*RHOc_m)/NUc_m

!-----

!This section provides the correlations for staggered smooth tube bundles
!Evaporator

If ((FinningMode == 1) .or. (FinningMode == 2)) Then

  If (ReDe_m <= 500.d0) Then
    Nuse_m = CFe*1.04*(ReDe_m**0.4)*(Pre_m**0.36)*((Pre_m/Pres)**0.25)

  ElseIf (ReDe_m <= 1000.d0) Then
    Nuse_m = CFe*0.71*(ReDe_m**0.5)*(Pre_m**0.36)*((Pre_m/Pres)**0.25)

  ElseIf (ReDe_m <= 20000.d0) Then
    Nuse_m = CFe*0.35*((STe/SLe)**0.2)*(ReDe_m**0.6)*(Pre_m**0.36) &
      *((Pre_m/Pres)**0.25)

  Else

```

```

Nuse_m = CFe*0.031*((STe/SLe)**0.2)*(ReDe_m**0.8)*(Pre_m**0.36) &
*((Pre_m/Pres)**0.25)
EndIf

Else
If (ReDe_m <= 10000.d0) Then
Nuse_m= 0.192*(ReDe_m**0.65)*(Pre_m**0.36)*((STe/SLe)**0.2)*((Pfin/Dout) &
**0.18)*((Hfin/Dout)**-0.14)*((Pre_m/Pres)**0.25)

ElseIf (ReDe_m <= 100000.d0) Then
Nuse_m = 0.0507*(ReDe_m**0.8)*(Pre_m**0.4)*((STe/SLe)**0.2)*((Pfin/Dout) &
**0.18)*((Hfin/Dout)**-0.14)*((Pre_m/Pres)**0.25)

Else
Nuse_m = 0.0081*(ReDe_m**0.95)*(Pre_m**0.4)*((STe/SLe)**0.2)*((Pfin/Dout) &
**0.18)*((Hfin/Dout)**-0.14)*((Pre_m/Pres)**0.25)
EndIf
EndIf

!-----

!Condenser

If ((FinningMode == 1) .or. (FinningMode == 3)) Then

If (ReDc_m <= 500.d0) Then
Nusc_m = CFc*1.04*(ReDc_m**0.4)*(Prc_m**0.36)*((Prc_m/Prcs)**0.25)

ElseIf (ReDc_m <= 1000.d0) Then
Nusc_m = CFc*0.71*(ReDc_m**0.5)*(Prc_m**0.36)*((Prc_m/Prcs)**0.25)

ElseIf (ReDc_m <= 20000.d0) Then
Nusc_m = CFc*0.35*((STc/SLc)**0.2)*(ReDc_m**0.6)*(Prc_m**0.36) &

```


$$*((Pr_c_m/Pr_c_s)**0.25)$$

Else

$$Nusc_m = C_{Fc} * 0.031 * ((ST_c/SL_c)**0.2) * (Re_{Dc_m}**0.8) * (Pr_c_m**0.36) & \\ *((Pr_c_m/Pr_c_s)**0.25)$$

EndIf

Else

If (ReDc_m <= 10000.d0) Then

$$Nusc_m = 0.192 * (Re_{Dc_m}**0.65) * (Pr_c_m**0.36) * ((ST_c/SL_c)**0.2) & \\ *((P_{fin}/D_{out})**0.18) * ((H_{fin}/D_{out})**-0.14) * ((Pr_c_m/Pr_c_s)**0.25)$$

ElseIf (ReDc_m <= 100000.d0) Then

$$Nusc_m = 0.0507 * (Re_{Dc_m}**0.8) * (Pr_c_m**0.4) * ((ST_c/SL_c)**0.2) & \\ *((P_{fin}/D_{out})**0.18) * ((H_{fin}/D_{out})**-0.14) * ((Pr_c_m/Pr_c_s)**0.25)$$

Else

$$Nusc_m = 0.0081 * (Re_{Dc_m}**0.95) * (Pr_c_m**0.4) * ((ST_c/SL_c)**0.2) & \\ *((P_{fin}/D_{out})**0.18) * ((H_{fin}/D_{out})**-0.14) * ((Pr_c_m/Pr_c_s)**0.25)$$

EndIf

EndIf

!-----

!Heat Transfer Coefficients (W/m².K)

$$HTFe_m = (Nusc_m * LAMDAe_m) / D_{out}$$

$$HTFc_m = (Nusc_m * LAMDAc_m) / D_{out}$$

!-----

!Number of Transfer Units

$$NTUe_m = (HTFe_m * HTAe) / C_{e_m}$$

$$NTUc_m = (HTFc_m * HTAc) / Cc_m$$

!-----

!Effectiveness

$$ee_m = 1.d0 - \text{EXP}(-NTUe_m)$$

$$ec_m = 1.d0 - \text{EXP}(-NTUc_m)$$

$$een_m = 1.d0 - ((1.d0 - ee_m) ** Nre)$$

$$ecn_m = 1.d0 - ((1.d0 - ec_m) ** Nrc)$$

!-----

!Choose Overall Effectiveness

If (Ce_m > Cc_m) Then

$$Et_m = (((1.d0 / ecn_m) + (Cc_m / Ce_m) / een_m) ** -1.d0)$$

Else

$$Et_m = (((1.d0 / een_m) + (Ce_m / Cc_m) / ecn_m) ** -1.d0)$$

EndIf

!-----

!Outlet Results

$$Tho = Thi - (Et_m * (Cmin_m / Ce_m) * (Thi - Tci)) \quad \text{!Source outlet temperature [deg C]}$$

$$Tco = Tci + (Et_m * (Cmin_m / Cc_m) * (Thi - Tci)) \quad \text{!Sink outlet temperature [deg C]}$$

$$Qdot = FLWe * SHCe_m * (Thi - Tho) / 1000.d0 \quad \text{!Heat recovery rate [kW]}$$

$$LMTD = ((Thi - Tco) - (Tho - Tci)) / \text{LOG}(((Thi - Tco) / (Tho - Tci)))$$

$$UA = Qdot * 1000.d0 / LMTD$$

!-----

!Outlet Thermal Properties

!Densities Mean (kg/m3)

$$\text{RHOeo} = 1.08622 + (-0.00234) * \text{Tho} + (2.7773\text{E-}6) * \text{Tho}^{**2.d0} \& \text{!Natural gas exhaust} \\ + (-1.60009\text{E-}9) * \text{Tho}^{**3.d0} + 3.48272\text{E-}13 * \text{Tho}^{**4.d0}$$

If (FluidMode == 1) Then !Air

$$\text{RHOco} = 0.16103 + 0.34473 * \text{EXP}(-\text{Tco}/103.23714) + 0.78857 * \& \\ \text{EXP}(-\text{Tco}/512.29169)$$

ElseIf (FluidMode == 2) Then !Water

$$\text{RHOco} = \text{EXP}(2.2467 * (1.d0 - ((\text{Tco} + 273.15) / 647.25))^{**}(1.d0/3.d0) - 2.09405 * \& \\ (1.d0 - ((\text{Tco} + 273.15) / 647.25))^{**}(2.d0/3.d0) + 2.737 * \& \\ (1.d0 - ((\text{Tco} + 273.15) / 647.25)) - 1.7475 * \& \\ (1.d0 - ((\text{Tco} + 273.15) / 647.25))^{**}(4.d0/3.d0)) * 315.5$$

Else !Thermal oil

$$\text{RHOco} = ((-0.614254 * (\text{Tco})) - (0.000321 * ((\text{Tco})^{**2.d0})) + 1020.62)$$

EndIf

!-----

!Dynamic Viscosities Mean (m2/s)

$$\text{NUeo} = (1.51901\text{E-}5 + 3.7842\text{E-}8 * \text{Tho} - 8.96178\text{E-}12 * \text{Tho}^{**2.d0} \& \text{!Natural gas exhaust} \\ + 1.57382\text{E-}15 * \text{Tho}^{**3.d0})$$

If (FluidMode == 1) Then !Air

$$\text{NUco} = (1.70899\text{E-}5 + 4.6117\text{E-}8 * \text{Tco} - 2.07642\text{E-}11 * \text{Tco}^{**2.d0} \& \\ + 5.40458\text{E-}15 * \text{Tco}^{**3.d0})$$

ElseIf (FluidMode == 2) Then !Water

$$\text{NUco} = (\text{EXP}(-10.1083 + 1.39621 * (1.d0 / ((\text{Tco} + 273.15) / 647.25) - 1.d0))^{**}(1.d0/3.d0) \& \\ + 0.48431 * (1.d0 / ((\text{Tco} + 273.15) / 647.25) - 1.d0)^{**}(4/3) + 0.71019 * \&$$

$$(1.d0/((Tco+273.15)/647.25)-1.d0)**(7.d0/3.d0))$$

Else !Thermal oil

$$NUco = (EXP((586.375/(Tco+62.5)-2.2809)))*RHOco/1000000.d0$$

EndIf

!-----

!Thermal Conductivities Mean(W/m.K)

$$LAMDAeo = 0.02272+7.19522E-5*Tho-4.70107E-9*Tho**2.d0 !Natural gas exhaust$$

If (FluidMode == 1) Then !Air

$$LAMDAco = 0.02411+7.71055E-5*Tco-2.81463E-8*Tco**2.d0 & \\ +6.36061E-12*Tco**3.d0$$

ElseIf (FluidMode == 2) Then !Water

$$LAMDAco = -1.63975+11.1421*((Tco+273.15)/647.25)+-20.0805* & \\ ((Tco+273.15)/647.25)**(2.d0)+16.7447*((Tco+273.15)/647.25) & \\ *(3.d0)+-5.78763*((Tco+273.15)/647.25)**(4.d0)$$

Else !Thermal oil

$$LAMDAco = (1E-11*Tco**3.d0)-(2E-7*Tco**2.d0)-(3E-5*Tco)+0.1182$$

EndIf

!-----

!Specific Heat Capacities Mean (J/kg.K)

$$SHCe0 = 1083.52006+0.33081*Tho+(-3.15922E-5)*Tho**2.d0 & !Natural gas exhaust \\ +(-1.66552E-8)*Tho**3.d0$$

If (FluidMode == 1) Then !Air

$$SHCco = (1.00224+3.33594E-5*Tco+5.415E-7*Tco**2.d0- & !Natural gas exhaust$$

$$6.31148E-10 * T_{co}^{**3} + 2.86052E-13 * T_{co}^{**4} - 4.66306E-17 * T_{co}^{**5} * 1000$$

ElseIf (FluidMode == 2) Then !Water

$$SHC_{co} = -14995 * (1 + 0.088 * ((T_{co} + 273.15) / 647.25))^{**(-2/3)} + (-0.682) * (1 - ((T_{co} + 273.15) / 647.25))^{**(-1/3)} + (-0.705) * (1 - ((T_{co} + 273.15) / 647.25))^{**(1/3)}$$

Else !Thermal oil

$$SHC_{co} = ((1E-9 * T_{co}^{**3}) + (3E-7 * T_{co}^{**2}) + (0.0034 * T_{co}) + 1.4943) * 1000$$

EndIf

!-----

!Prandtl Numbers

$$Pr_{eo} = SHC_{eo} * NU_{eo} / LAMDA_{eo}$$

$$Pr_{co} = SHC_{co} * NU_{co} / LAMDA_{co}$$

!-----

!Heat Capacitance and Minimum (W/K)

$$C_{eo} = SHC_{eo} * FLW_e$$

$$C_{co} = SHC_{co} * FLW_c$$

$$C_{mino} = \text{MIN}(C_{eo}, C_{co})$$

!-----

!Free Flow Velocities (m/s)

$$v_{eo} = FLW_e / (A_e * RHO_{eo})$$

$$v_{co} = FLW_c / (A_c * RHO_{co})$$

!-----

!Maximum Velocities (m/s)

!Minimum area test evaporator

$$\text{minareatesteo1} = \text{SQRT}(((\text{STe}/2.\text{d0})^{**2}.\text{d0})+(\text{SLe}^{**2}.\text{d0}))$$

$$\text{minareatesteo2} = (\text{STe}+\text{Dout})/2.\text{d0}$$

If (minareatesteo1 > minareatesteo2) Then

$$\text{Vmaxeo} = (\text{STe}/(\text{STe}-\text{Dout}))\cdot\text{veo}$$

Else

$$\text{Vmaxeo} = (\text{veo}/(\text{SQRT}(1.\text{d0}+((2.\text{d0}\cdot(\text{SLe}/\text{STe}))^{**2}.\text{d0}))-2.\text{d0}\cdot(\text{Dout}/\text{STe}))))$$

EndIf

!Minimum area test condenser

$$\text{minareatestco1} = \text{SQRT}(((\text{STc}/2.\text{d0})^{**2}.\text{d0})+(\text{SLc}^{**2}.\text{d0}))$$

$$\text{minareatestco2} = (\text{STc}+\text{Dout})/2.\text{d0}$$

If (minareatestco1 > minareatestco2) Then

$$\text{Vmaxco} = (\text{STc}/(\text{STc}-\text{Dout}))\cdot\text{vco}$$

Else

$$\text{Vmaxco} = (\text{vco}/(\text{SQRT}(1.\text{d0}+((2.\text{d0}\cdot(\text{SLc}/\text{STc}))^{**2}.\text{d0}))-2.\text{d0}\cdot(\text{Dout}/\text{STc}))))$$

EndIf

!-----

!Reynolds Numbers

$$\text{ReDeo} = (\text{Vmaxeo}\cdot\text{Dout}\cdot\text{RHOeo})/\text{NUeo}$$

$$\text{ReDco} = (\text{minareac} * \text{Dout} * \text{RHOco}) / \text{NUco}$$

!-----

!Pressure Drop Calculations

!(1 = no finning, 2 = condenser finned, 3 = evaporator finned, 4 = both finned)

$$\text{PTe} = \text{STe} / \text{Dout}$$

$$\text{PTc} = \text{STc} / \text{Dout}$$

$$\text{PLe} = \text{SLe} / \text{Dout}$$

$$\text{PLc} = \text{SLc} / \text{Dout}$$

$$\text{STSLe} = \text{STe} / \text{SLe}$$

$$\text{STSLc} = \text{STc} / \text{SLc}$$

If ((FinningMode == 1) .or. (FinningMode == 2)) Then

!Calculating X (Chi)

If (ReDe < 550.d0) Then

 If (STSLe < 1.2) Then

$$\text{Chie} = 1.d0$$

 Else

$$\text{Chie} = 0.055476370223 * \text{STSLe}^{**6}.d0 -$$

$$0.807737327822 * \text{STSLe}^{**5}.d0 + 4.791061335894 \&$$

$$* \text{STSLe}^{**4}.d0 - 14.775008015945 * \text{STSLe}^{**3}.d0 + 24.848044479172 * \text{STSLe}^{**2}.d0 \&$$

$$- 21.13587970328 * \text{STSLe} + 8.030267420326$$

 EndIf

ElseIf (ReDe < 5500.d0) Then

$$\text{Chie} = -0.006582510659882 * \text{STSLe}^{**6}.d0 + 0.086512756111735 * \text{STSLe}^{**5}.d0 \&$$

$$- 0.429365023037395 * \text{STSLe}^{**4}.d0 + 0.967477501402558 * \text{STSLe}^{**3}.d0 \&$$

$$- 0.87746851708403 * \text{STSLe}^{**2}.d0 + 0.174439100478289 * \text{STSLe} + 1.09714274629842$$

ElseIf (ReDe < 55000.d0) Then

$$\text{Chie} = 0.008671843104707 * \text{STSLe}^{**6}.d0 - 0.119491431144033 * \text{STSLe}^{**5}.d0 \&$$

$$+ 0.667459785818119 * \text{STSLe}^{**4}.d0 - 1.93997806035734 * \text{STSLe}^{**3}.d0 \&$$

$$+ 3.11719768511303 * \text{STSLe}^{**2}.d0 - 2.60629695221346 * \text{STSLe} + 1.88881954700185$$

Else

$$\text{Chie} = 0.01090483478788 * \text{STSLe}^{**5}.d0 - 0.088732136558723 * \text{STSLe}^{**4}.d0 \&$$

+0.180975740557806*STSLe**3.d0+0.233839225186575*STSLe**2.d0 &
-1.13914487426972*STSLe+1.88969439044012

EndIf

If (P_{Te}<1.375) Then

If (ReDe<55.d0) Then

fxe = 0.00000000304672310189*ReDe**6.d0-0.00000090695882490676* &
ReDe**5.d0+0.000109425635603455*ReDe**4.d0-0.00691792826131564* &
ReDe**3.d0+0.247530159394677*ReDe**2.d0-5.05542618913993*ReDe+ &
57.605423373848

ElseIf (ReDe<550.d0) Then

fxe = 0.000000000000000083215*ReDe**6.d0-0.0000000000238158711* &
ReDe**5.d0+0.0000000027363655918*ReDe**4.d0-0.00000162360038933978 &
*ReDe**3.d0+0.000532828876206208*ReDe**2.d0-0.0960643479984688*ReDe &
+9.61786287906493

ElseIf (ReDe<5500.d0) Then

fxe = -0.0000000000000000244*ReDe**5.d0+0.000000000000289881* &
ReDe**4.d0-0.00000000017798752675*ReDe**3.d0+0.00000060405096862192 &
*ReDe**2.d0-0.00112347015674636*ReDe+1.76762993138187

ElseIf (ReDe<55000.d0) Then

fxe = 0.0000000000000000047*ReDe**4.d0-0.0000000000002865962* &
ReDe**3.d0+0.00000000105603407663*ReDe**2.d0-0.0000258664220503753 &
*ReDe+0.875546721856801

ElseIf (ReDe<550000.d0) Then

fxe = -0.00000000000000001787*ReDe**3.d0+0.00000000000740106679* &
ReDe**2.d0-0.00000190891762195942*ReDe+0.569096588296964

ElseIf (ReDe<5500000.d0) Then

fxe = -0.0000000000000000003*ReDe**3.d0+0.00000000000010117251 &
*ReDe**2.d0-0.00000016357781964993*ReDe+0.33256305725565

Else

fxe = 0.242224797365682

EndIf

ElseIf (PTe<1.75) Then

If (ReDe<55.d0) Then

$$\begin{aligned} \text{fxe} = & 0.00000000114868524973 * \text{ReDe}^{**6} \cdot \text{d0} - 0.00000034638165718312 * \& \\ & \text{ReDe}^{**5} \cdot \text{d0} + 0.0000421418078584364 * \text{ReDe}^{**4} \cdot \text{d0} - 0.00266761574594401 \& \\ & * \text{ReDe}^{**3} \cdot \text{d0} + 0.0945654639576471 * \text{ReDe}^{**2} \cdot \text{d0} - 1.88762853451537 * \text{ReDe} \& \\ & + 21.4428342470075 \end{aligned}$$

ElseIf (ReDe<550.d0) Then

$$\begin{aligned} \text{fxe} = & 0.000000000000000015255 * \text{ReDe}^{**6} \cdot \text{d0} - 0.00000000000046615345 * \& \\ & \text{ReDe}^{**5} \cdot \text{d0} + 0.00000000057851437448 * \text{ReDe}^{**4} \cdot \text{d0} - 0.00000037608117844575 * \& \\ & \text{ReDe}^{**3} \cdot \text{d0} + 0.000137635189258499 * \text{ReDe}^{**2} \cdot \text{d0} - 0.0284194584882274 * \text{ReDe} \& \\ & + 3.79362252312672 \end{aligned}$$

ElseIf (ReDe<5500.d0) Then

$$\begin{aligned} \text{fxe} = & -0.00000000000000000174 * \text{ReDe}^{**5} \cdot \text{d0} + 0.0000000000001935299 * \& \\ & \text{ReDe}^{**4} \cdot \text{d0} - 0.00000000011108837479 * \text{ReDe}^{**3} \cdot \text{d0} + 0.00000035587470947408 \& \\ & * \text{ReDe}^{**2} \cdot \text{d0} - 0.00064621859209747 * \text{ReDe} + 1.15054329015104 \end{aligned}$$

ElseIf (ReDe<55000.d0) Then

$$\begin{aligned} \text{fxe} = & 0.00000000000000000039 * \text{ReDe}^{**4} \cdot \text{d0} - 0.0000000000002138387 * \& \\ & \text{ReDe}^{**3} \cdot \text{d0} + 0.00000000069719534679 * \text{ReDe}^{**2} \cdot \text{d0} - 0.0000161315082414622 * \& \\ & \text{ReDe} + 0.630319186014919 \end{aligned}$$

ElseIf (ReDe<550000.d0) Then

$$\begin{aligned} \text{fxe} = & -0.000000000000000001842 * \text{ReDe}^{**3} \cdot \text{d0} + 0.00000000000699952338 * \& \\ & \text{ReDe}^{**2} \cdot \text{d0} - 0.00000166932528414058 * \text{ReDe} + 0.451192894189153 \end{aligned}$$

ElseIf (ReDe<5500000.d0) Then

$$\begin{aligned} \text{fxe} = & -0.00000000000000000006 * \text{ReDe}^{**3} \cdot \text{d0} + 0.0000000000020142234 * \& \\ & \text{ReDe}^{**2} \cdot \text{d0} - 0.00000032669280227272 * \text{ReDe} + 0.367180244544361 \end{aligned}$$

Else

$$\text{fxe} = 0.216498811988182$$

EndIf

ElseIf (PTe<2.25) Then

If (ReDe<550.d0) Then

$$\begin{aligned} \text{fxe} = & 0.0000000000000000910 * \text{ReDe}^{**6.d0} - 0.0000000000003658734 * \& \\ & \text{ReDe}^{**5.d0} + 0.0000000006021195169 * \text{ReDe}^{**4.d0} - 0.0000005263723839061 * \& \\ & \text{ReDe}^{**3.d0} + 0.0000265381828685591 * \text{ReDe}^{**2.d0} - 0.00789168282494227 * \text{ReDe} \& \\ & + 1.8355926726513 \end{aligned}$$

ElseIf (ReDe<5500.d0) Then

$$\begin{aligned} \text{fxe} = & -0.0000000000000000101 * \text{ReDe}^{**5.d0} + 0.0000000000001160338 * \& \\ & \text{ReDe}^{**4.d0} - 0.0000000006873699553 * \text{ReDe}^{**3.d0} + 0.00000022365809450496 \& \\ & * \text{ReDe}^{**2.d0} - 0.000400804319671022 * \text{ReDe} + 0.814130211150491 \end{aligned}$$

ElseIf (ReDe<55000.d0) Then

$$\begin{aligned} \text{fxe} = & -0.0000000000000000011 * \text{ReDe}^{**4.d0} + 0.0000000000001049493 * \& \\ & \text{ReDe}^{**3.d0} - 0.0000000004273588584 * \text{ReDe}^{**2.d0} + 0.00000477262161487613 * \& \\ & \text{ReDe} + 0.427538350478811 \end{aligned}$$

ElseIf (ReDe<550000.d0) Then

$$\begin{aligned} \text{fxe} = & -0.00000000000000000553 * \text{ReDe}^{**3.d0} + 0.00000000000371124399 * \& \\ & \text{ReDe}^{**2.d0} - 0.00000122526204810312 * \text{ReDe} + 0.38293963530156 \end{aligned}$$

ElseIf (ReDe<5500000.d0) Then

$$\begin{aligned} \text{fxe} = & 0.000000000000006263317 * \text{ReDe}^{**2.d0} - 0.00000014855615788396 * \& \\ & \text{ReDe} + 0.259742394917818 \end{aligned}$$

Else

$$\text{fxe} = 0.198895782982392$$

EndIf

Else

If (ReDe<550.d0) Then

$$\begin{aligned} \text{fxe} = & 0.0000000000000000982 * \text{ReDe}^{**6.d0} - 0.0000000000003765112 * \& \\ & \text{ReDe}^{**5.d0} + 0.0000000005871185134 * \text{ReDe}^{**4.d0} - 0.00000004816240180048 * \& \\ & \text{ReDe}^{**3.d0} + 0.0000225707909619934 * \text{ReDe}^{**2.d0} - 0.00626113799921795 * \& \\ & \text{ReDe} + 1.45138423197786 \end{aligned}$$

ElseIf (ReDe<5500.d0) Then

$$\begin{aligned} \text{fxe} = & -0.0000000000000000046 * \text{ReDe}^{**5.d0} + 0.000000000000604261 * \& \\ & \text{ReDe}^{**4.d0} - 0.0000000004171156554 * \text{ReDe}^{**3.d0} + 0.00000015915610209495 * \& \end{aligned}$$

```

    ReDe**2.d0-0.000324266250554968*ReDe+0.682593897519661
ElseIf (ReDe<55000.d0) Then
    fxe = -0.00000000000000000016*ReDe**4.d0+0.0000000000001077911* &
        ReDe**3.d0-0.00000000037498237585*ReDe**2.d0+0.00000413491976991877* &
        ReDe+0.367963674275565
ElseIf (ReDe<550000.d0) Then
    fxe = - 0.000000000000000001457*ReDe**3.d0+0.00000000000535808696* &
        ReDe**2.d0-0.00000127208886715665*ReDe+0.352068277778896
ElseIf (ReDe<5500000.d0) Then
    fxe = -0.00000000000000000002*ReDe**3.d0+0.000000000001004569* &
        ReDe**2.d0-0.00000017832626843352*ReDe+0.255079372314046
Else
    fxe = 0.185330984133629
EndIf
EndIf

!-----

fe = fxe*Chie
dPe = fe*Nre*(((Vmaxe**2.d0)*RHOe)/2.d0)

Else !Evaporator finned correction factor
    erate = HTAe/HTAe_smooth

    If (ReDe <= 1000.d0) Then
        Eue = 67.6*(ReDe**-.7)*(erate**0.5)*((STe/Dout)**-.55) &
            *((SLe/Dout)**-.5)
    ElseIf (ReDe <= 100000.d0) Then
        Eue = 3.2*(ReDe**-.25)*(erate**0.5)*((STe/Dout)**-.55) &
            *((SLe/Dout)**-.5)
    Else
        Eue = 0.18*(1.d0)*(erate**0.5)*((STe/Dout)**-.55) &

```

```

        *((SLe/Dout)**-0.5)
    EndIf

    Ge = ((RHOe+RHOeo)/2.d0)*((Vmaxe+Vmaxeo)/2.d0) !Core mass velocity
    RHOew = 1.08622+(-0.00234)*Twe+(2.7773E-6)*Twe**2.d0 &
        +(-1.60009E-9)*Twe**3.d0+3.48272E-13*Twe**4.d0
    dPe = Ge**2.d0/(2.d0*RHOe)*(Eue*Nre*RHOe*(1.d0/RHOew)+(2.d0*(RHOe/RHOeo)-
    1.d0))
    EndIf

!Condenser
If ((FinningMode == 1) .or. (FinningMode == 3)) Then
    If (ReDc<550.d0) Then
        If (STSLc<1.2) Then
            Chic=1.d0
        Else
            Chic=0.055476370223*STSLc**6.d0-
0.807737327822*STSLc**5.d0+4.791061335894 &
                *STSLc**4.d0-14.775008015945*STSLc**3.d0+24.848044479172*STSLc**2.d0 &
                -21.13587970328*STSLc+8.030267420326
        EndIf

    ElseIf (ReDc<5500.d0) Then
        Chic=-0.006582510659882*STSLc**6.d0+0.086512756111735*STSLc**5.d0 &
            -0.429365023037395*STSLc**4.d0+0.967477501402558*STSLc**3.d0 &
            -0.87746851708403*STSLc**2.d0+0.174439100478289*STSLc+1.09714274629842
    ElseIf (ReDc<55000.d0) Then
        Chic=0.008671843104707*STSLc**6.d0-0.119491431144033*STSLc**5.d0 &
            +0.667459785818119*STSLc**4.d0-1.93997806035734*STSLc**3.d0 &
            +3.11719768511303*STSLc**2.d0-2.60629695221346*STSLc+1.88881954700185
    Else
        Chic= 0.01090483478788*STSLc**5.d0-0.088732136558723*STSLc**4.d0 &
            +0.180975740557806*STSLc**3.d0+0.233839225186575*STSLc**2.d0 &

```

-1.13914487426972*STSLc+1.88969439044012

EndIf

If (PTc<1.375) Then

If (ReDc<55.d0) Then

fxc = 0.00000000304672310189*ReDc**6.d0-0.00000090695882490676* &
 ReDc**5.d0+0.000109425635603455*ReDc**4.d0-0.00691792826131564* &
 ReDc**3.d0+0.247530159394677*ReDc**2.d0-5.05542618913993*ReDc+ &
 57.605423373848

ElseIf (ReDc<550.d0) Then

fxc = 0.000000000000000083215*ReDc**6.d0-0.00000000000238158711* &
 ReDc**5.d0+0.0000000027363655918*ReDc**4.d0-0.00000162360038933978 &
 *ReDc**3.d0+0.000532828876206208*ReDc**2.d0-0.0960643479984688*ReDc &
 +9.61786287906493

ElseIf (ReDc<5500.d0) Then

fxc = -0.00000000000000000244*ReDc**5.d0+0.000000000000289881* &
 ReDc**4.d0-0.0000000017798752675*ReDc**3.d0+0.00000060405096862192 &
 *ReDc**2.d0-0.00112347015674636*ReDc+1.76762993138187

ElseIf (ReDc<55000.d0) Then

fxc = 0.00000000000000000047*ReDc**4.d0-0.0000000000002865962* &
 ReDc**3.d0+0.00000000105603407663*ReDc**2.d0-0.0000258664220503753 &
 *ReDc+0.875546721856801

ElseIf (ReDc<550000.d0) Then

fxc = -0.000000000000000001787*ReDc**3.d0+0.00000000000740106679* &
 ReDc**2.d0-0.00000190891762195942*ReDc+0.569096588296964

ElseIf (ReDc<5500000) Then

fxc = -0.00000000000000000003*ReDc**3.d0+0.00000000000010117251 &
 *ReDc**2.d0-0.00000016357781964993*ReDc+0.33256305725565

Else

fxc = 0.242224797365682

EndIf

ElseIf (PTc<1.75) Then

If (ReDc<55.d0) Then

$$\begin{aligned} \text{fxc} = & 0.00000000114868524973 * \text{ReDc}^{**6.d0} - 0.00000034638165718312 * \& \\ & \text{ReDc}^{**5.d0} + 0.0000421418078584364 * \text{ReDc}^{**4.d0} - 0.00266761574594401 * \& \\ & * \text{ReDc}^{**3.d0} + 0.0945654639576471 * \text{ReDc}^{**2.d0} - 1.88762853451537 * \text{ReDc} \& \\ & + 21.4428342470075 \end{aligned}$$

ElseIf (ReDc<550.d0) Then

$$\begin{aligned} \text{fxc} = & 0.000000000000000015255 * \text{ReDc}^{**6.d0} - 0.00000000000046615345 * \& \\ & \text{ReDc}^{**5.d0} + 0.00000000057851437448 * \text{ReDc}^{**4.d0} - 0.00000037608117844575 * \& \\ & \text{ReDc}^{**3.d0} + 0.000137635189258499 * \text{ReDc}^{**2.d0} - 0.0284194584882274 * \text{ReDc} \& \\ & + 3.79362252312672 \end{aligned}$$

ElseIf (ReDc<5500.d0) Then

$$\begin{aligned} \text{fxc} = & -0.00000000000000000174 * \text{ReDc}^{**5.d0} + 0.0000000000001935299 * \& \\ & \text{ReDc}^{**4.d0} - 0.0000000011108837479 * \text{ReDc}^{**3.d0} + 0.00000035587470947408 * \& \\ & * \text{ReDc}^{**2.d0} - 0.00064621859209747 * \text{ReDc} + 1.15054329015104 \end{aligned}$$

ElseIf (ReDc<55000.d0) Then

$$\begin{aligned} \text{fxc} = & 0.00000000000000000039 * \text{ReDc}^{**4.d0} - 0.0000000000002138387 * \& \\ & \text{ReDc}^{**3.d0} + 0.00000000069719534679 * \text{ReDc}^{**2.d0} - 0.0000161315082414622 * \& \\ & \text{ReDc} + 0.630319186014919 \end{aligned}$$

ElseIf (ReDc<550000.d0) Then

$$\begin{aligned} \text{fxc} = & -0.000000000000000001842 * \text{ReDc}^{**3.d0} + 0.00000000000699952338 * \& \\ & \text{ReDc}^{**2.d0} - 0.00000166932528414058 * \text{ReDc} + 0.451192894189153 \end{aligned}$$

ElseIf (ReDc<5500000.d0) Then

$$\begin{aligned} \text{fxc} = & -0.0000000000000000006 * \text{ReDc}^{**3.d0} + 0.0000000000020142234 * \& \\ & \text{ReDc}^{**2.d0} - 0.00000032669280227272 * \text{ReDc} + 0.367180244544361 \end{aligned}$$

Else

$$\text{fxc} = 0.216498811988182$$

EndIf

ElseIf (PTc<2.25) Then

If (ReDc<550.d0) Then

$$\text{fxc} = 0.000000000000000000910 * \text{ReDe}^{**6.d0} - 0.0000000000003658734 * \&$$

ReDc**5.d0+0.00000000006021195169*ReDc**4.d0-0.00000005263723839061* &
 ReDc**3.d0+0.0000265381828685591*ReDc**2.d0-0.00789168282494227*ReDc &
 +1.8355926726513

ElseIf (ReDc<5500.d0) Then

fxc = -0.0000000000000000101*ReDc**5.d0+0.00000000000001160338* &
 ReDc**4.d0-0.0000000006873699553*ReDc**3.d0+0.00000022365809450496 &
 *ReDc**2.d0-0.000400804319671022*ReDc+0.814130211150491

ElseIf (ReDc<55000.d0) Then

fxc = -0.0000000000000000011*ReDc**4.d0+0.00000000000001049493* &
 ReDc**3.d0-0.0000000004273588584*ReDc**2.d0+0.00000477262161487613* &
 ReDc+0.427538350478811

ElseIf (ReDc<550000.d0) Then

fxc = -0.00000000000000000553*ReDc**3.d0+0.00000000000371124399* &
 ReDc**2.d0-0.00000122526204810312*ReDc+0.38293963530156

ElseIf (ReDc<5500000.d0) Then

fxc = 0.000000000000006263317*ReDc**2.d0-0.00000014855615788396* &
 ReDc+0.259742394917818

Else

fxc = 0.198895782982392

EndIf

Else

If (ReDc<550.d0) Then

fxc = 0.00000000000000000982*ReDc**6.d0-0.0000000000003765112* &
 ReDc**5.d0+0.00000000005871185134*ReDc**4.d0-0.00000004816240180048* &
 ReDc**3.d0+0.0000225707909619934*ReDc**2.d0-0.00626113799921795* &
 ReDc+1.45138423197786

ElseIf (ReDc<5500.d0) Then

fxc = -0.0000000000000000046*ReDc**5.d0+0.0000000000000604261* &
 ReDc**4.d0-0.0000000004171156554*ReDc**3.d0+0.00000015915610209495* &
 ReDc**2.d0-0.000324266250554968*ReDc+0.682593897519661

ElseIf (ReDc<55000.d0) Then

```

fxc = -0.000000000000000000016*ReDc**4.d0+0.00000000000001077911* &
    ReDc**3.d0-0.00000000037498237585*ReDc**2.d0+0.00000413491976991877* &
    ReDc+0.367963674275565
ElseIf (ReDc<550000) Then
    fxc = -0.00000000000000000001457*ReDc**3.d0+0.000000000000535808696* &
        ReDc**2.d0-0.00000127208886715665*ReDc+0.352068277778896
ElseIf (ReDc<5500000.d0) Then
    fxc = -0.000000000000000000002*ReDc**3.d0+0.0000000000001004569* &
        ReDc**2.d0-0.00000017832626843352*ReDc+0.255079372314046
Else
    fxc = 0.185330984133629
EndIf
EndIf
fc = fxc*Chic
dPc = fc*Nrc*(((Vmaxc**2.d0)*RHOC)/2.d0)

Else
    eradc = HTAc/HTAc_smooth

    If (ReDc <= 1000.d0) Then
        Euc = 67.6*(ReDc**-0.7)*(eradc**0.5)*((STc/Dout)**-0.55) &
            *((SLc/Dout)**-0.5)
    ElseIf (ReDc <= 100000.d0) Then
        Euc = 3.2*(ReDc**-0.25)*(eradc**0.5)*((STc/Dout)**-0.55) &
            *((SLc/Dout)**-0.5)
    Else
        Euc = 0.18*(1.d0)*(eradc**0.5)*((STc/Dout)**-0.55) &
            *((SLc/Dout)**-0.5)
    EndIf

    !dPc = Euc*(RHOC*Vmaxc**2*Nrc)*Cz
    Gc = ((RHOC+RHOCO)/2.d0)*((Vmaxc+Vmaxco)/2.d0)

```

```
dPc=  
Gc**2.d0/(2.d0*RHOcw)*(Euc*Nrc*RHOc*(1.d0/RHOcw)+(2.d0*(RHOc/RHOco)-1.d0))  
  
EndIf  
!-----  
  
!-----  
  
!Set the Outputs from this Model  
Call SetOutputValue(1,Tho) !Outlet temperature source fluid (deg C)  
Call SetOutputValue(2,Tco) !Outlet temperature sink fluid (deg C)  
Call SetOutputValue(3,Qdot) !Energy recovery rate  
Call SetOutputValue(4,UA) !Conductance of HPHE  
Call SetOutputValue(5,dPe) !Pressure drop evaporator  
Call SetOutputValue(6,dPc) !Pressure drop condenser  
  
!-----  
  
Return  
End Subroutine TYPE204
```

C. Thermophysical Properties

C1. Natural Gas Combustion Products

The thermophysical properties tables for natural gas post-combustion exhaust gases were obtained from [216]. The data was graphically plotted and the trendline equations were extracted.

Table 44: Thermophysical properties of exhaust gases from natural gas combustion [216].

Temperature, °C	Density, kg.m ⁻³	Kinematic viscosity, ν mm ² .s ⁻¹	Specific heat capacity, C_p kJ.kg ⁻¹ .K ⁻¹	Thermal conductivity, λ W.m ⁻¹ .K ⁻¹
0	1.295	12.2	1.042	1.083
100	0.95	21.54	1.068	1.116
200	0.748	32.8	1.097	1.148
300	0.617	45.81	1.122	1.179
400	0.525	60.38	1.151	1.209
500	0.457	76.3	1.185	1.238
600	0.405	93.61	1.214	1.267
700	0.363	112.1	1.239	1.293
800	0.33	131.8	1.264	1.319
900	0.301	152.5	1.29	1.343
1000	0.275	174.3	1.306	1.366
1100	0.257	197.1	1.323	1.387
1200	0.24	221	1.34	1.406

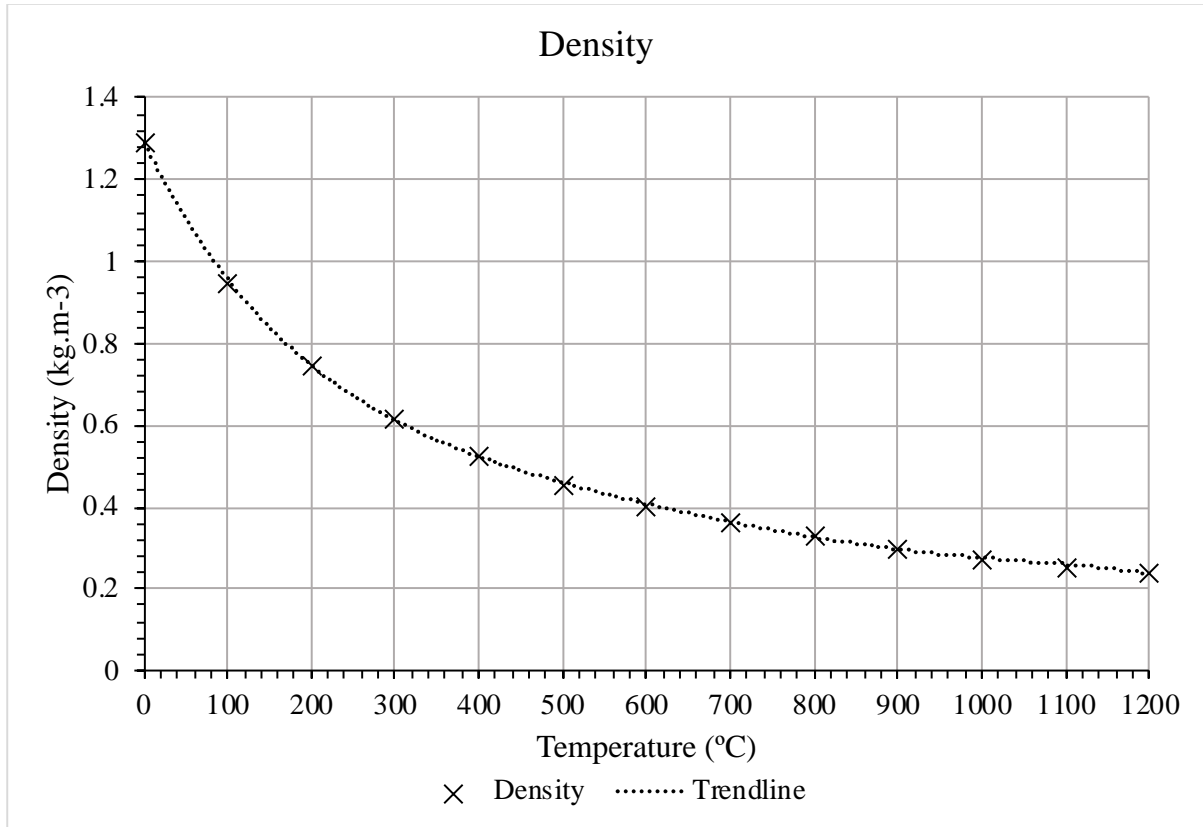


Figure 158: Density of exhaust gases against temperature.

$$\rho_{ex} = (3.48272E - 13 \times T^4) - (1.60009E - 9 \times T^3) + (2.7773E - 6 \times T^2) - (0.00234 \times T) + 1.08622 \quad (9.1)$$

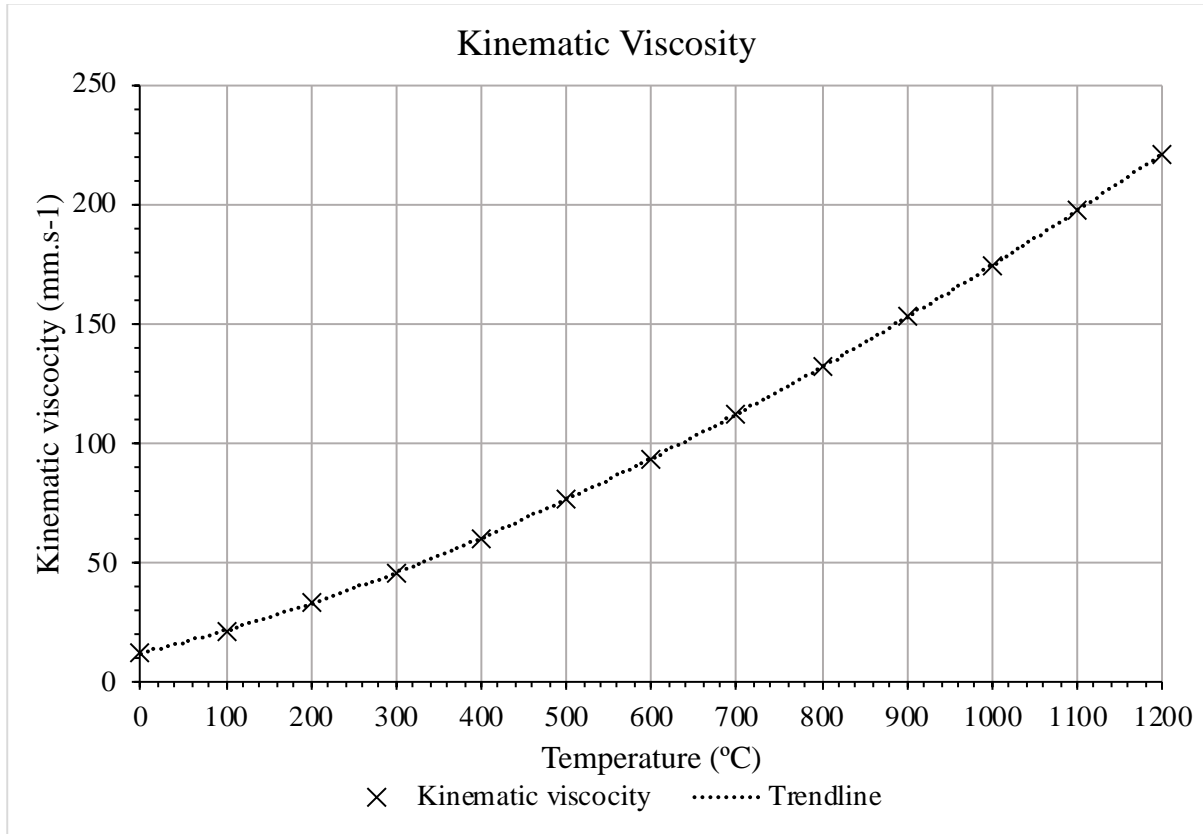


Figure 159: Kinematic viscosity of exhaust gases against temperature.

$$v_{ex} = (1.57382E - 15 \times T^3) - (8.96178E - 12 \times T^2) + (3.7842E - 8 \times T) + 1.51901E - 5 \quad (9.2)$$

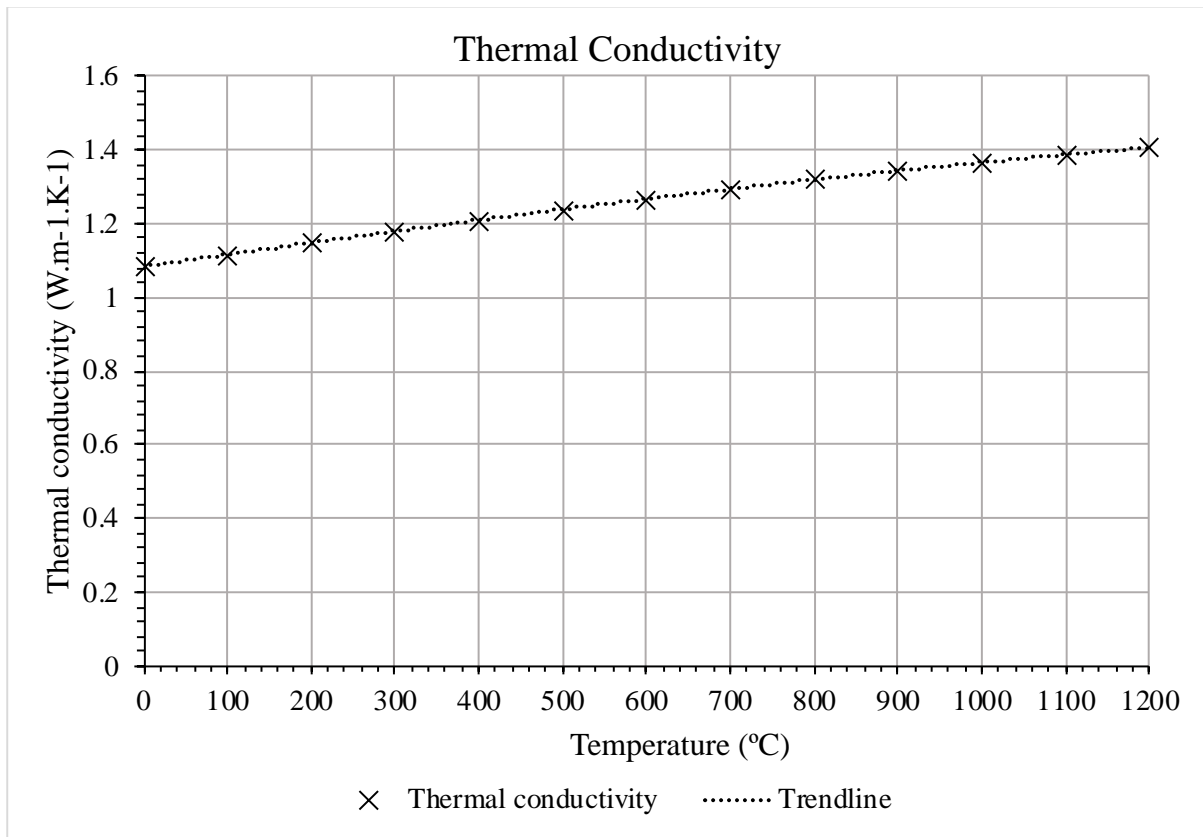


Figure 160: Thermal conductivity of exhaust gases against temperature.

$$\lambda_{ex} = (-4.70107E - 9 \times T^2) + (7.19522E - 5 \times T) + 0.02272 \quad (9.3)$$

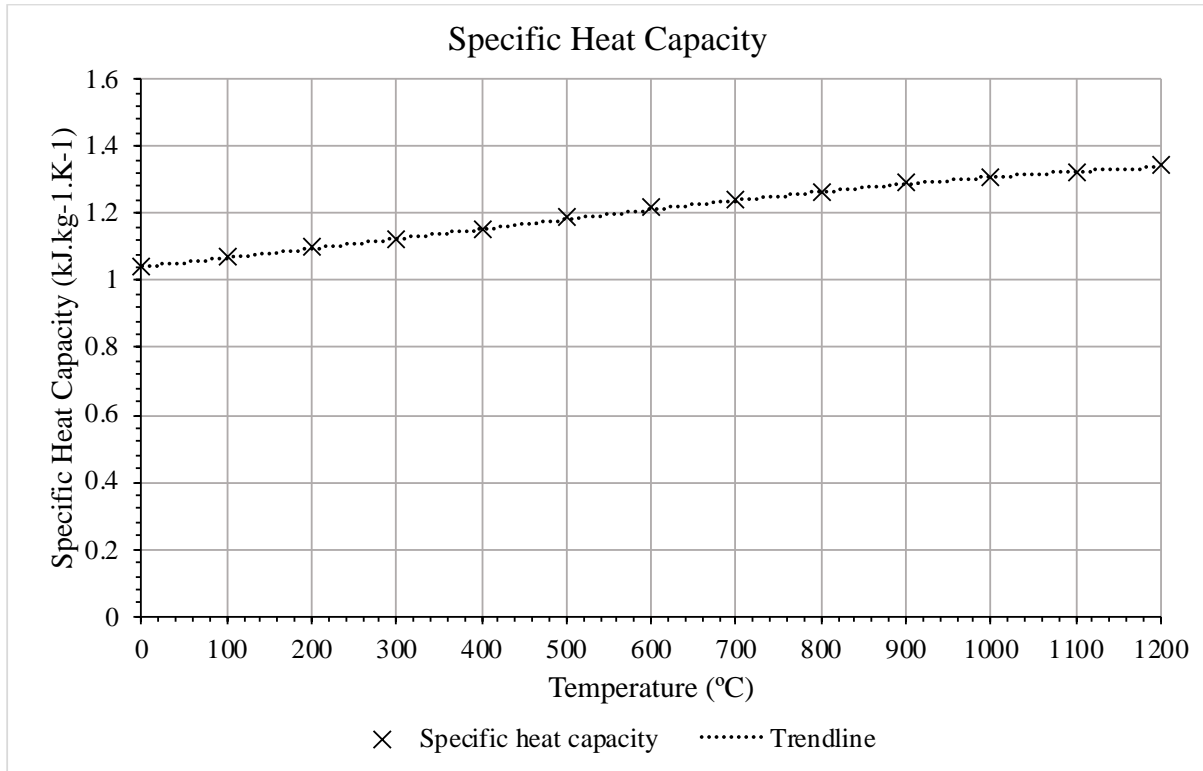


Figure 161: Specific heat capacity of exhaust gases against temperature.

$$c_{p,ex} = (-1.66552E - 8 \times T^3) - (3.15922E - 5 \times T^2) + (0.33081 \times T) + 1083.52006 \tag{9.4}$$

C2. Air

The thermophysical properties tables for air were obtained from [217]. The data was graphically plotted and the trendline equations were extracted.

Table 45: Thermophysical properties of air [217].

Temperature, °C	Density, kg.m ⁻³	Kinematic viscosity, mm ² .s ⁻¹	Specific heat capacity, kJ.kg ⁻¹ .K ⁻¹	Thermal conductivity, W.m ⁻¹ .K ⁻¹
-23	1.412	1.132	1.0031	2.227
2	1.284	1.343	1.0038	2.428
27	1.177	1.568	1.0049	2.624
52	1.086	1.807	1.0063	2.816
77	1.009	2.056	1.0082	3.003
102	0.9413	2.317	1.0106	3.186
127	0.8824	2.591	1.0135	3.365
177	0.7844	3.168	1.0206	3.71
227	0.706	3.782	1.0295	4.041
277	0.6418	4.439	1.0398	4.357
327	0.5883	5.128	1.0511	4.661
377	0.543	5.853	1.0629	4.954
427	0.5043	6.607	1.075	5.236
477	0.4706	7.399	1.087	5.509
527	0.4412	8.214	1.0987	5.774
577	0.4153	9.061	1.1101	6.03
627	0.3922	9.936	1.1209	6.276
677	0.3716	10.83	1.1313	6.52
727	0.353	11.76	1.1411	6.754
777	0.3362	12.72	1.1502	6.985
827	0.3209	13.7	1.1589	7.209
877	0.3069	14.7	1.167	7.427
927	0.2941	15.73	1.1746	7.64
977	0.2824	16.77	1.1817	7.849

1027	0.2715	17.85	1.1884	8.054
1077	0.2615	18.94	1.1946	8.253
1127	0.2521	20.06	1.2005	8.45

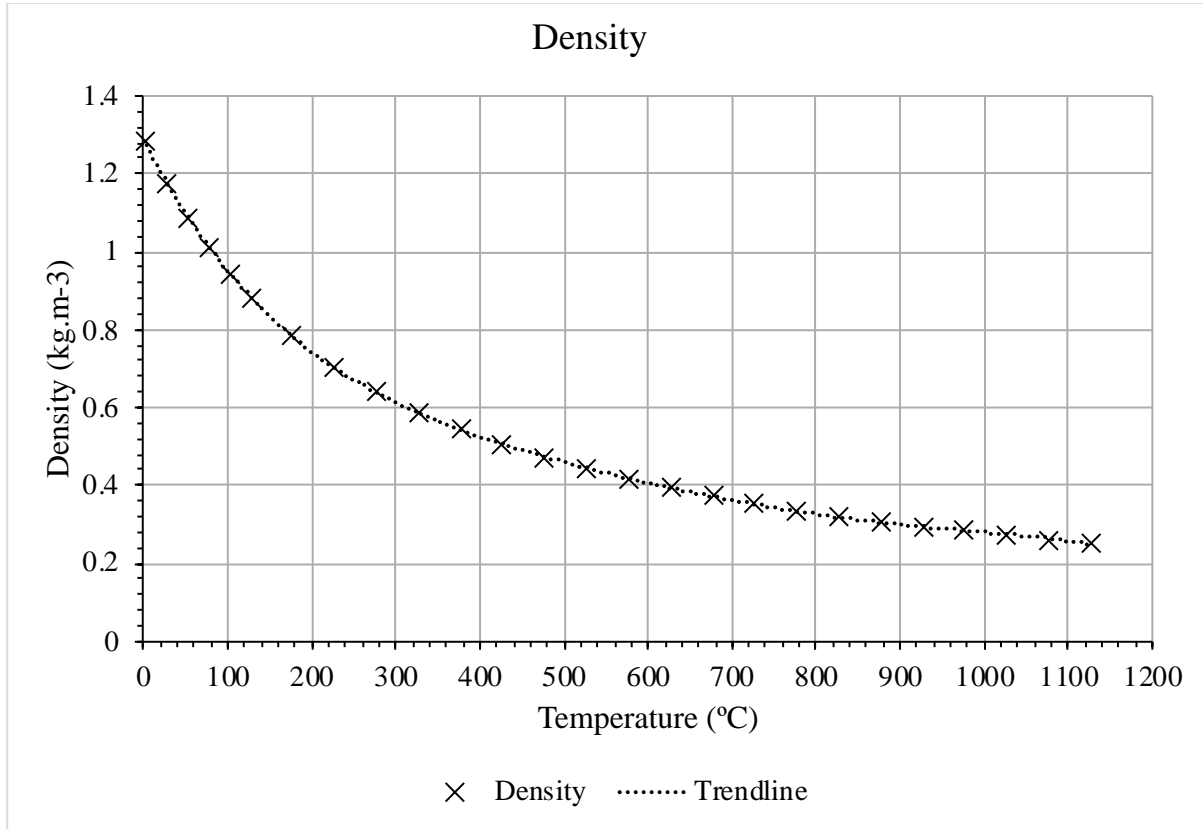


Figure 162: Density of air against temperature.

$$\rho_{air} = 0.16103 + 0.34473 \times e^{\left(\frac{-T}{103.23714}\right)} + 0.78857 \times e^{\left(\frac{-T}{512.29169}\right)} \quad (9.5)$$

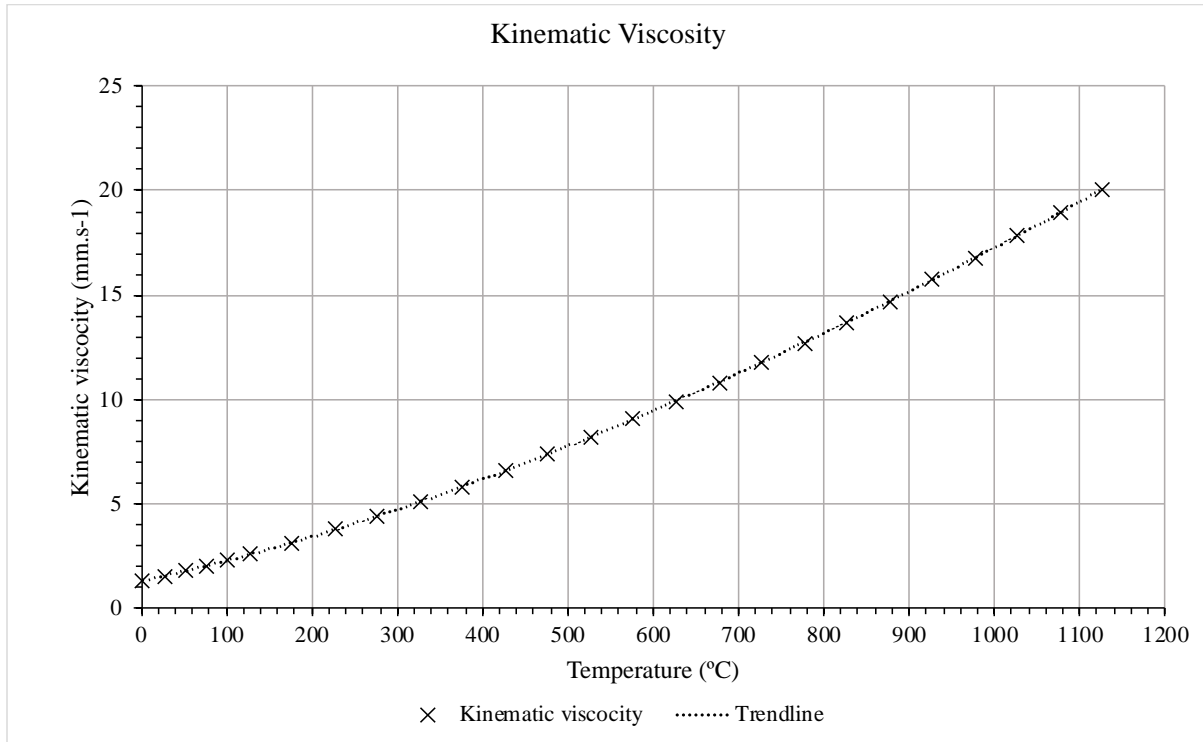


Figure 163: Kinematic viscosity of air against temperature.

$$v_{air} = (5.40458E - 15 \times T^3) - (2.07642E - 11 \times T^2) + (4.6117E - 8 \times T) + 1.70899E - 5 \quad (9.6)$$

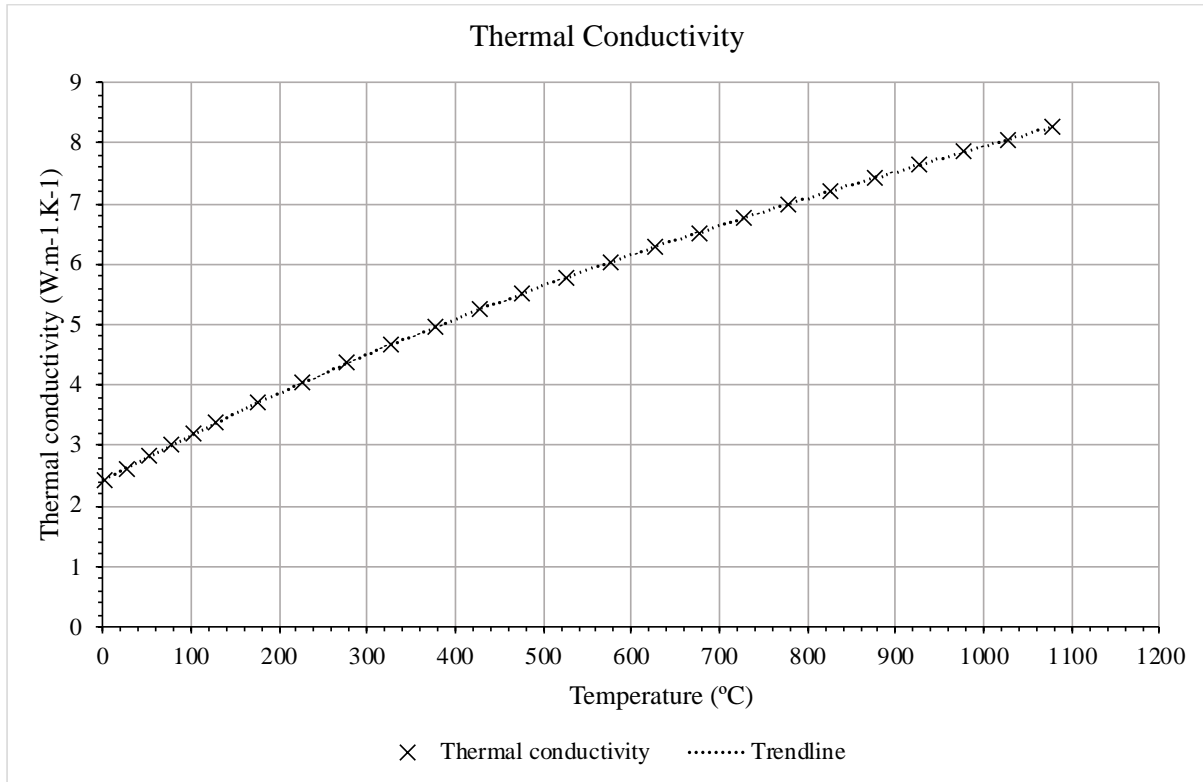


Figure 164: Thermal conductivity of air against temperature.

$$\lambda_{air} = (6.36061E - 12 \times T^3) - (2.81463E - 8 \times T^2) + (7.71055E - 5 \times T) + 0.02411 \quad (9.7)$$

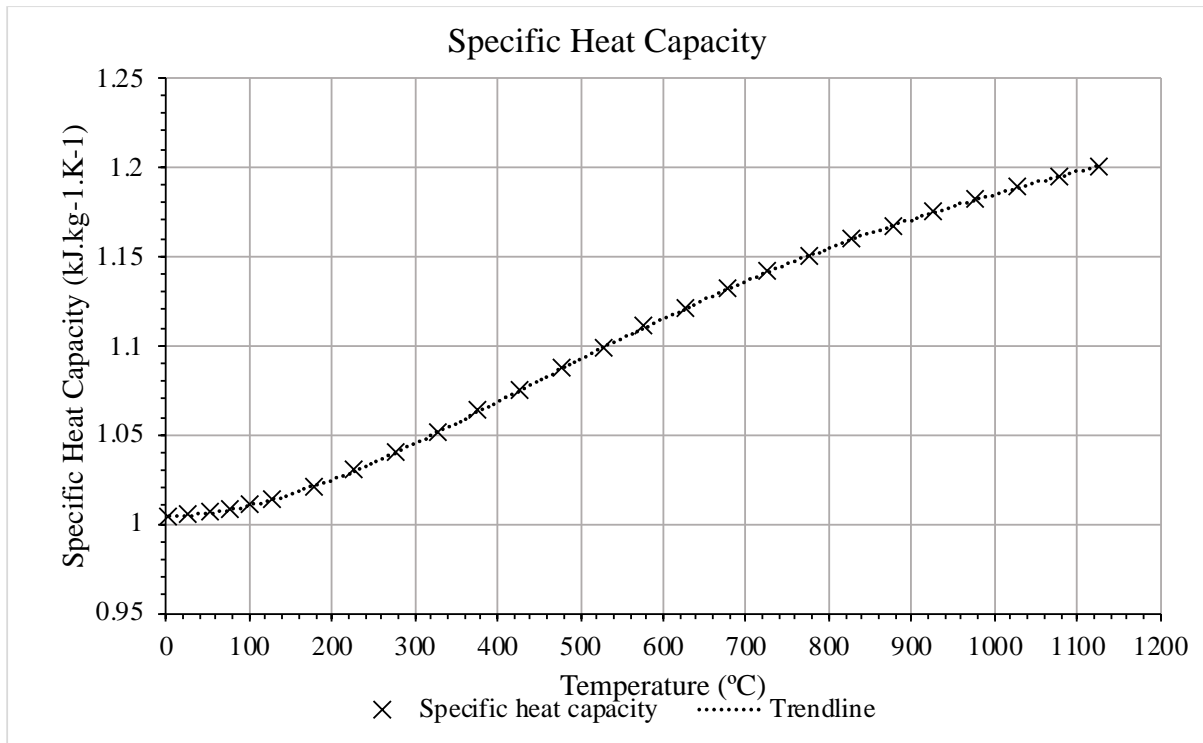


Figure 165: Specific heat capacity of air against temperature.

$$\begin{aligned}
 c_{p,air} = 1000 \times & ((-4.66306E - 17 - 17 \times T^5) + (2.86052E - 13 \times T^4) \\
 & - (6.31148E - 10 \times T^3) + (5.415E - 7 \times T^2) \\
 & + (3.33594E - 5 \times T) + 1.00224)
 \end{aligned}
 \tag{9.8}$$

C3. Water

The thermophysical properties tables for water were obtained from [218]. The data was graphically plotted and the trendline equations were extracted.

Table 46: Thermophysical properties of water [218].

Temperature, °C	Density, kg.m⁻³	Kinematic viscosity, mm².s⁻¹	Specific heat capacity, kJ.kg⁻¹.K⁻¹	Thermal conductivity, W.m⁻¹.K⁻¹
0	999.84	1.792	4.219	0.561
5	999.97	1.518	4.205	0.571
10	999.7	1.306	4.195	0.58
15	999.1	1.139	4.189	0.589
20	998.21	1.003	4.185	0.598
25	997.05	0.893	4.182	0.607
30	995.65	0.801	4.18	0.616
35	994.04	0.724	4.179	0.623
40	992.22	0.658	4.179	0.631
45	990.22	0.602	4.179	0.637
50	988.05	0.553	4.18	0.644
55	985.71	0.511	4.181	0.649
60	983.21	0.474	4.183	0.654
65	980.57	0.442	4.185	0.659
70	977.78	0.413	4.188	0.663
75	974.86	0.387	4.192	0.667
80	971.8	0.365	4.196	0.67
85	968.62	0.344	4.2	0.673
90	965.32	0.326	4.205	0.675
95	961.9	0.309	4.211	0.677
100	958.43	0.294	4.217	0.679

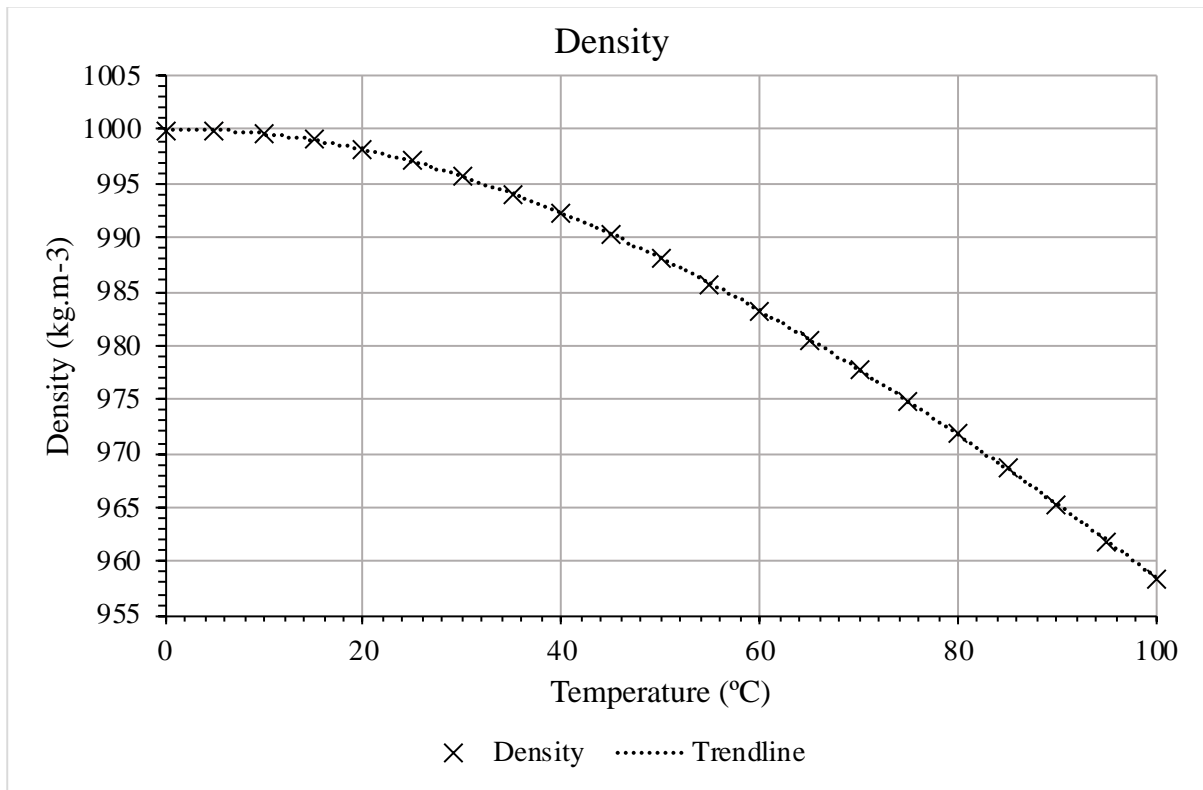


Figure 166: Density of water against temperature.

$$\rho_w = (1.56544853569E - 5 \times T^3) - (5.894798260414E - 3 \times T^2) + (1.801825875236E - 2 \times T) + 999.9993929984 \quad (9.9)$$

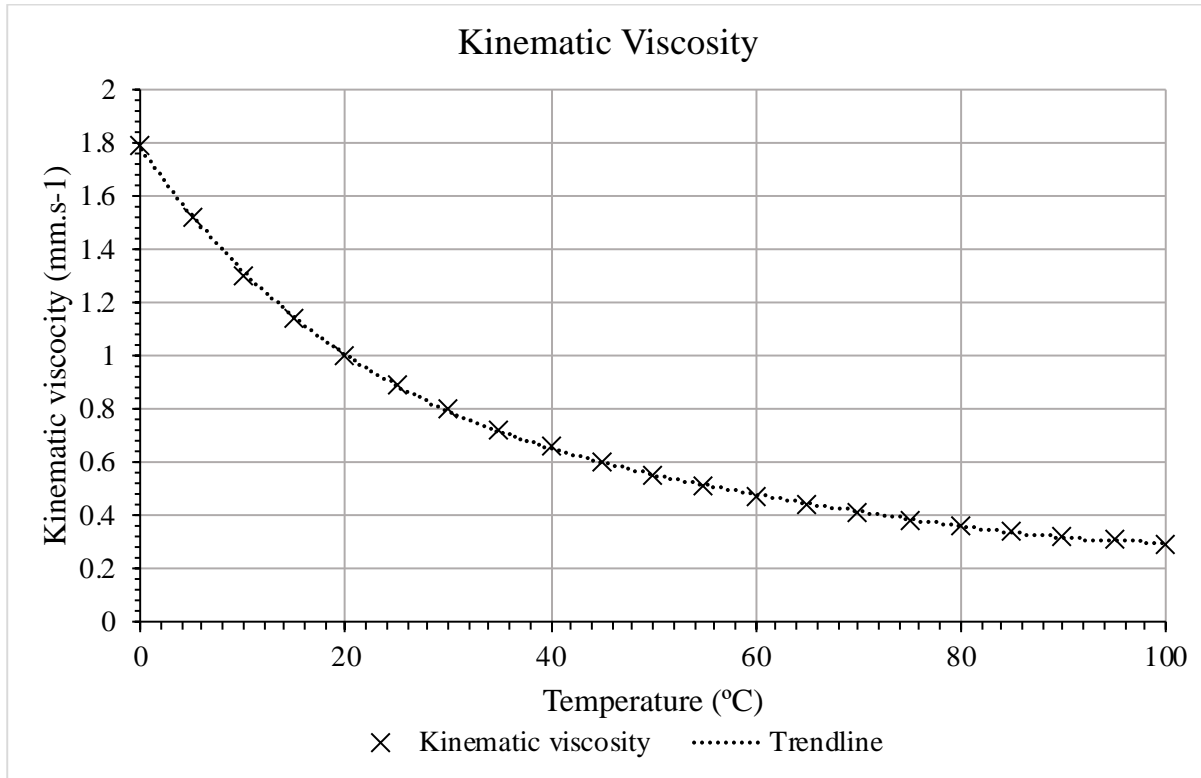


Figure 167: Kinematic viscosity of water against temperature.

$$\begin{aligned}
 \nu_w = & (3.295455565211E - 8 \times T^4) - (9.144070489074E - 6 \times T^3) \\
 & + (9.889667165667E - 4 \times T^2) - (5.551894120217E - 2 \times T) \quad (9.10) \\
 & + 1.779195445135
 \end{aligned}$$

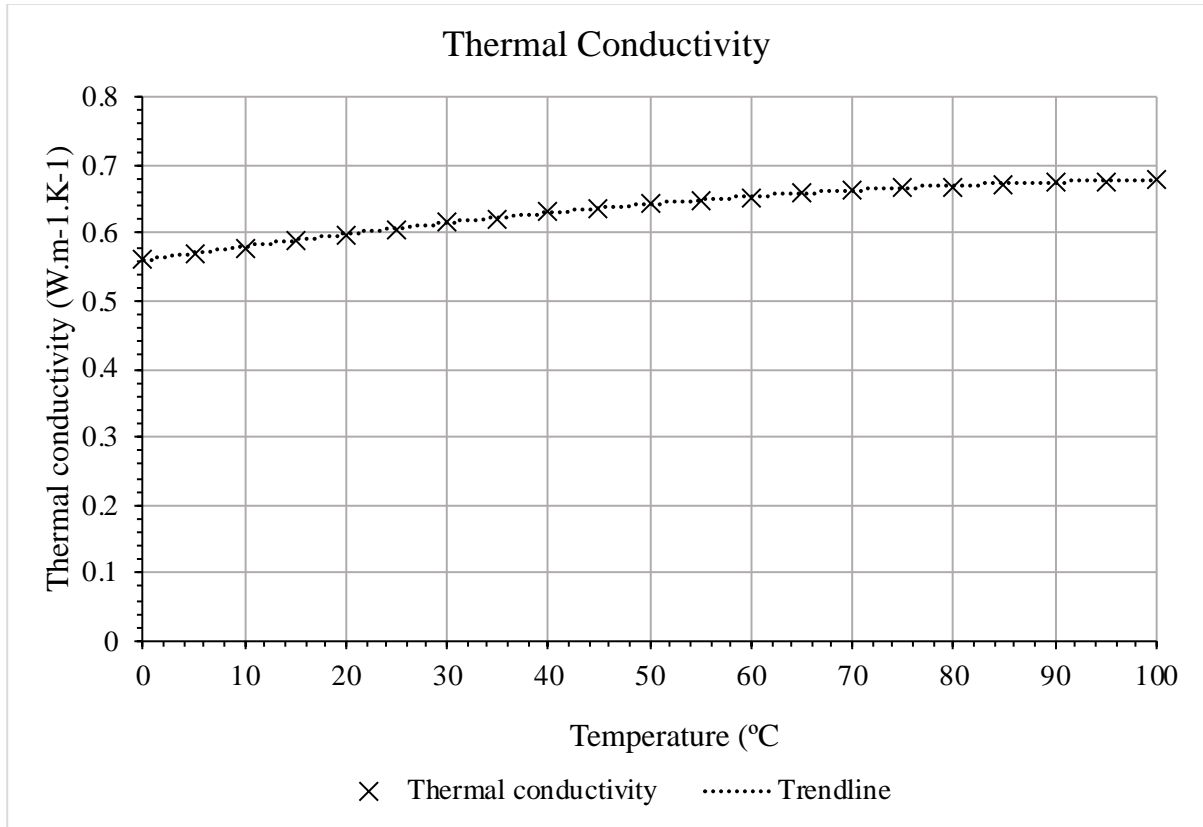


Figure 168: Thermal conductivity of water against temperature.

$$\lambda_w = (-7966776845593E - 9 \times T^3) - (8.323245531447E - 6 \times T^2) + (2.091674233891E - 2 \times T) + 50.603738942218 \quad (9.11)$$

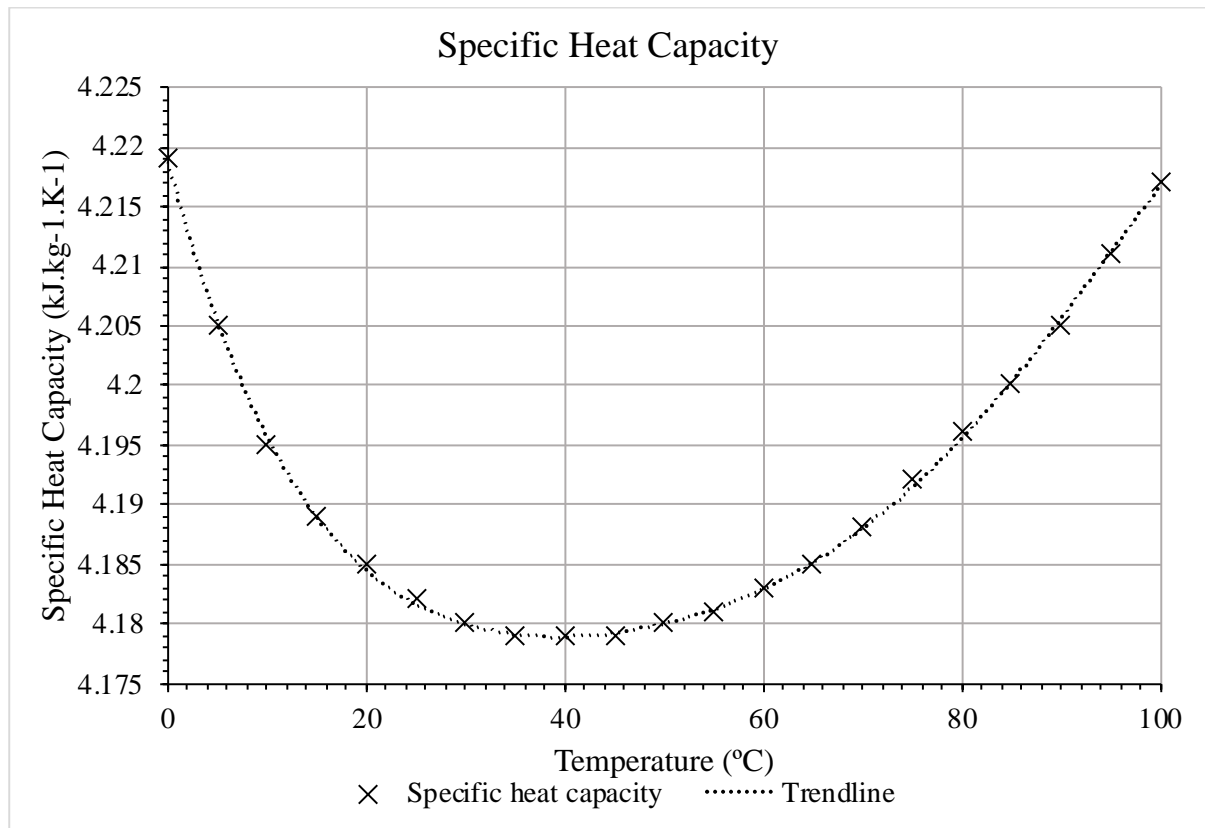


Figure 169: Specific heat capacity of water against temperature.

$$\begin{aligned}
 c_{p,w} = & (-4.496032533226E - 11 \times T^5) + (1.372909857E - 8 \times T^4) \\
 & - (1.596068924914E - 6 \times T^3) \\
 & + (9.852380006592E - 5 \times T^2) \\
 & - (2.144025268853E - 3 \times T) + 4.21868683073889
 \end{aligned}
 \tag{9.12}$$

C4. Thermal Oil

The thermophysical properties tables for thermal oil, specifically the commonly available and used therminol-66, were obtained from [219]. The data was graphically plotted and the trendline equations were extracted.

Table 47: Thermophysical properties of therminol-66 oil [219].

Temperature, °C	Density, kg.m⁻³	Thermal conductivity, W.m⁻¹.K⁻¹	Specific heat capacity, kJ.kg⁻¹.K⁻¹	Kinematic viscosity, mm².s⁻¹
0	1021.5	0.118	1.495	1297.01
10	1014.9	0.118	1.529	339.2
20	1008.4	0.118	1.562	122.45
30	1001.8	0.117	1.596	55.51
40	995.2	0.117	1.63	29.64
50	988.6	0.116	1.665	17.84
60	981.9	0.116	1.699	11.74
70	975.2	0.115	1.733	8.26
80	968.5	0.115	1.768	6.12
90	961.8	0.114	1.803	4.73
100	955	0.114	1.837	3.77
110	948.2	0.113	1.873	3.08
120	941.4	0.112	1.908	2.58
130	934.5	0.111	1.943	2.19
140	927.6	0.111	1.978	1.89
150	920.6	0.11	2.014	1.65
160	913.6	0.109	2.05	1.46
170	906.6	0.108	2.086	1.3
180	899.5	0.107	2.122	1.17
190	892.3	0.107	2.158	1.06
200	885.1	0.106	2.195	0.97
210	877.8	0.105	2.231	0.89
220	870.4	0.104	2.268	0.82

230	863	0.103	2.305	0.77
240	855.5	0.102	2.342	0.71
250	847.9	0.1	2.379	0.67
260	840.3	0.099	2.417	0.63
270	832.5	0.098	2.455	0.59
280	824.6	0.097	2.492	0.56
290	816.6	0.096	2.531	0.54
300	808.5	0.095	2.569	0.51
310	800.3	0.093	2.608	0.49
320	783.5	0.092	2.647	0.47
330	774.8	0.091	2.686	0.45
340	765.9	0.089	2.726	0.43
350	756.9	0.088	2.766	0.42
360	756.9	0.086	2.806	0.41
370	747.7	0.085	2.847	0.39
380	738.2	0.084	2.889	0.38

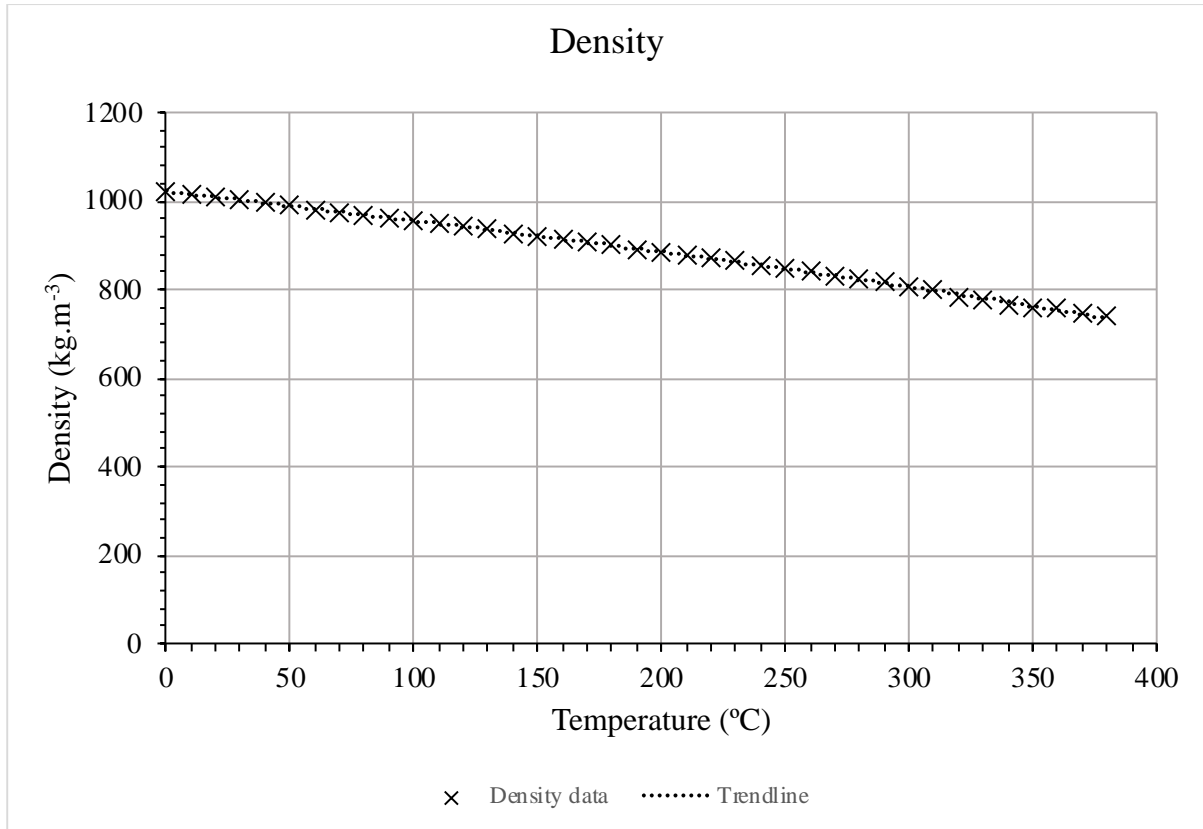


Figure 170: Density of thermal oil against temperature.

$$\rho_{oil} = (-6.05817133E - 7 \times T^3) - (5.39266926E - 5 \times T^2) - (6.45601396E - 1 \times T) + 1021.09262039 \quad (9.13)$$

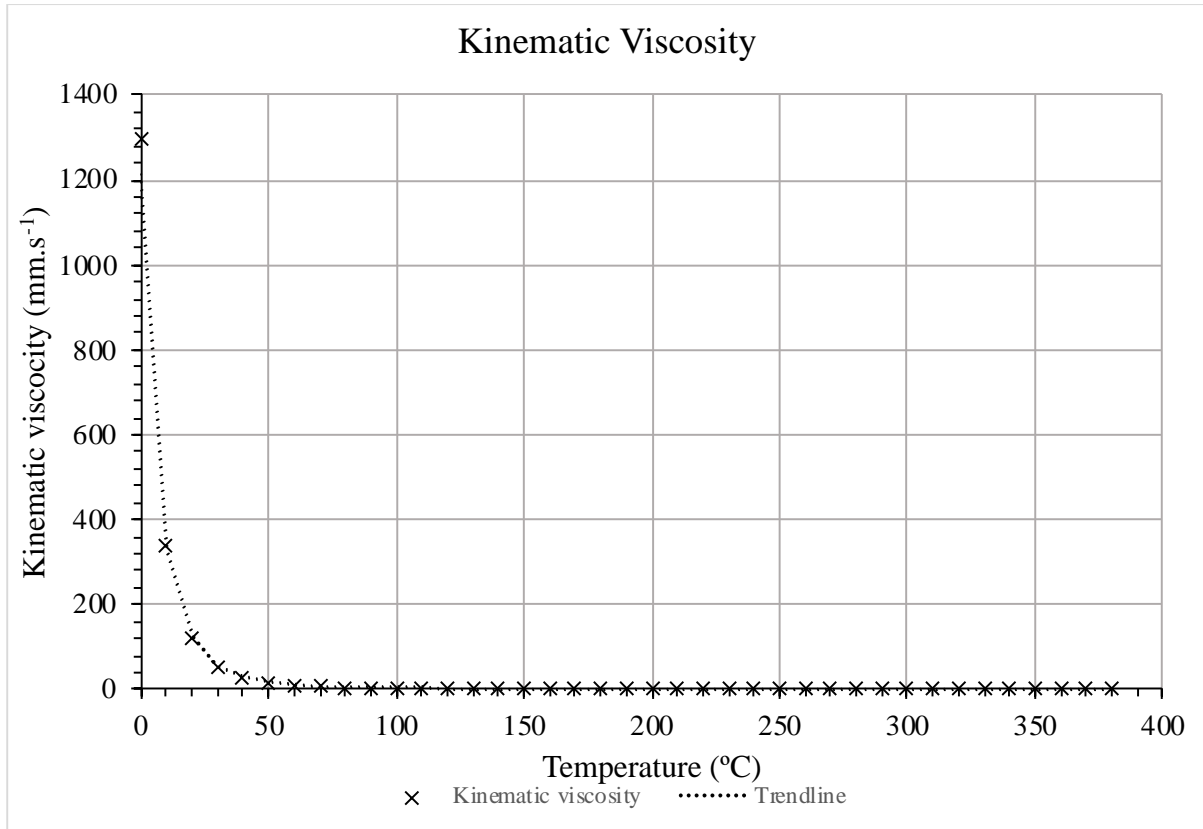


Figure 171: Kinematic viscosity of thermal oil against temperature.

$$v_{oil} = e^{\left(\frac{586.375}{T+62.5} - 2.2809\right)} \tag{9.14}$$

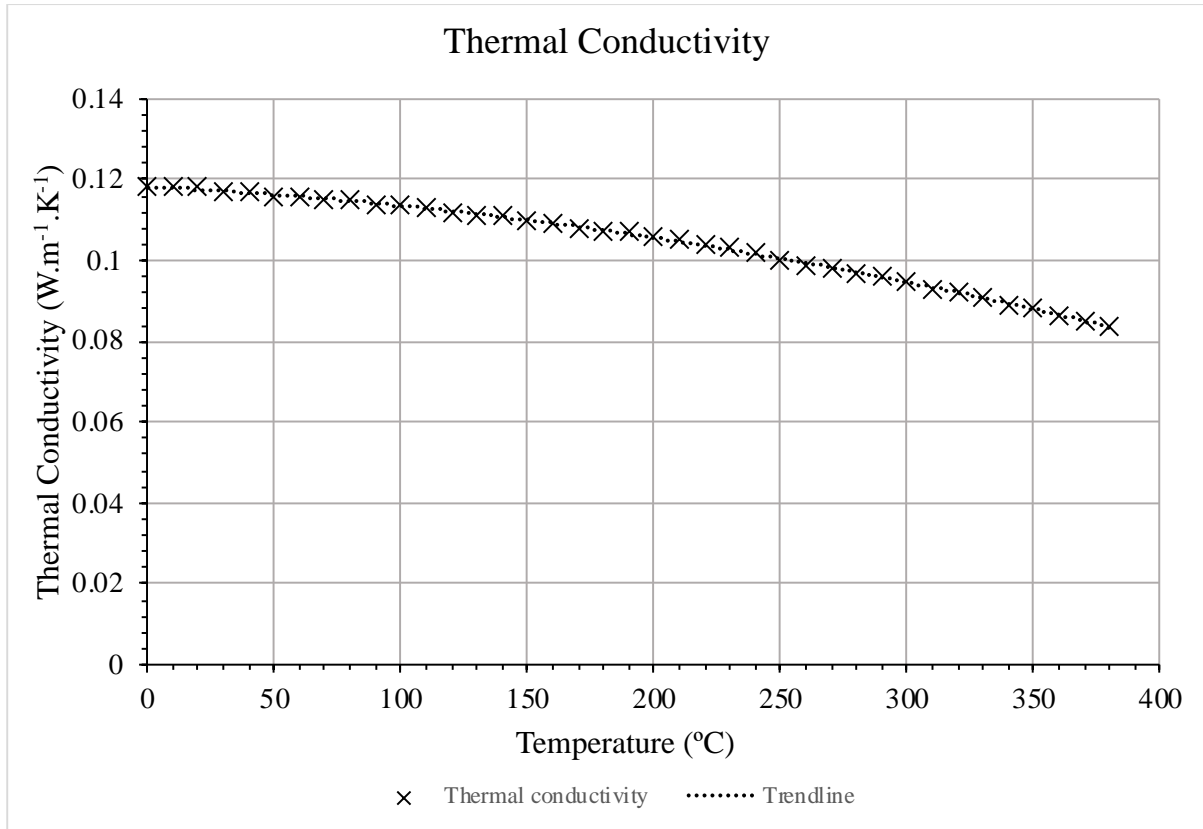


Figure 172: Thermal conductivity of thermal oil against temperature.

$$\begin{aligned}
 \lambda_{oil} = & (1.361586727359E - 11 \times T^3) && (9.15) \\
 & - (1.651340290616E - 7 \times T^2) \\
 & - (3.051156963224E - 5 \times T) \\
 & + 0.1182482801751
 \end{aligned}$$

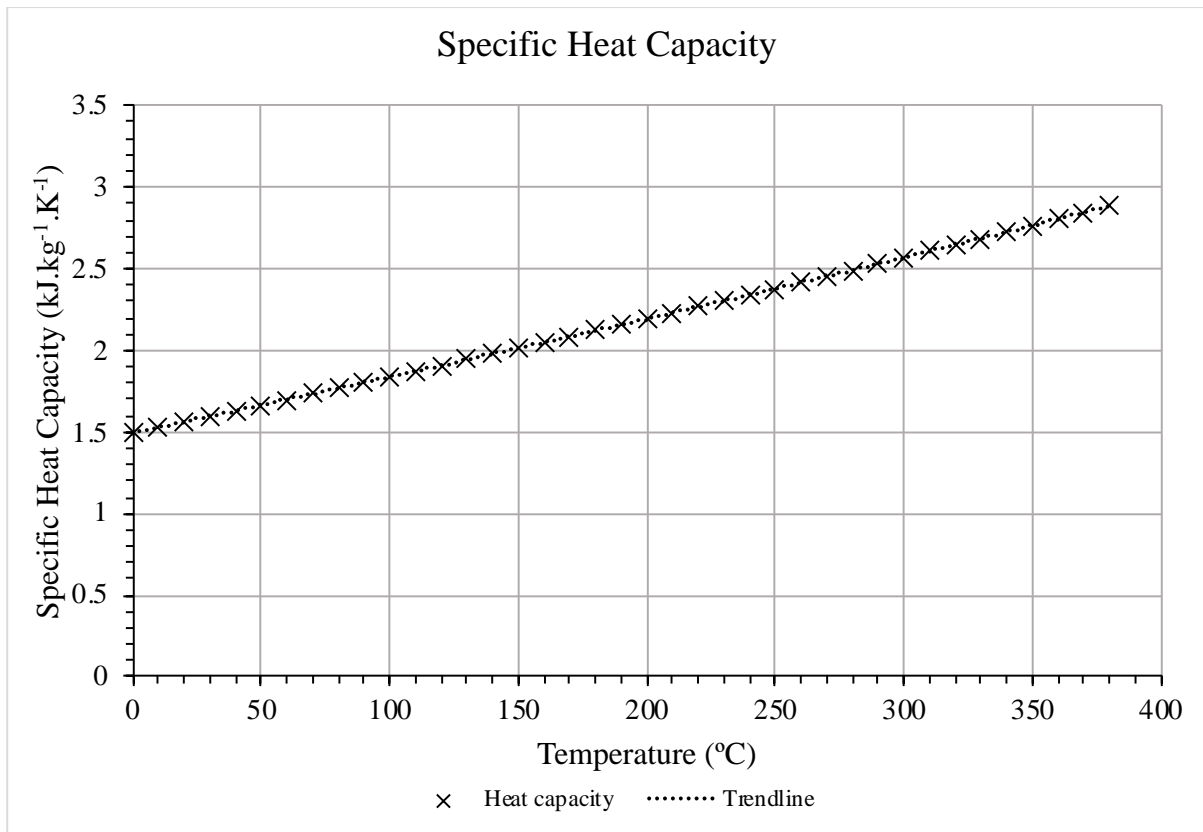


Figure 173: Specific heat capacity of thermal oil against temperature.

$$\begin{aligned}
 c_{p,oil} = & (1.004460568002E - 9 \times T^3) + (3.445669427699E - 7 \times T^2) & (9.16) \\
 & + (3.390395821911E - 3 \times T) + 1.494315509694
 \end{aligned}$$

D. Thermal Losses Calculations for Experiment 3

For the calculations, both convection and radiation analysis was conducted. Four external temperatures were measured during operation at the centre of each door. The heat exchanger was then split into four respective sections to simplify the equations. These being: the evaporator inlet and transition duct (e,1); the evaporator outlet and transition duct (e,2); the condenser inlet and transition duct (c,1); the condenser outlet and transition duct (c,2).

Temperature measured at evaporator inlet door, $T_{e,1} = 521.15$ K

Temperature measured at evaporator outlet door, $T_{e,2} = 421.15$ K

Temperature measured at condenser inlet door, $T_{c,1} = 405.15$ K

Temperature measured at condenser outlet door, $T_{c,2} = 411.15$ K

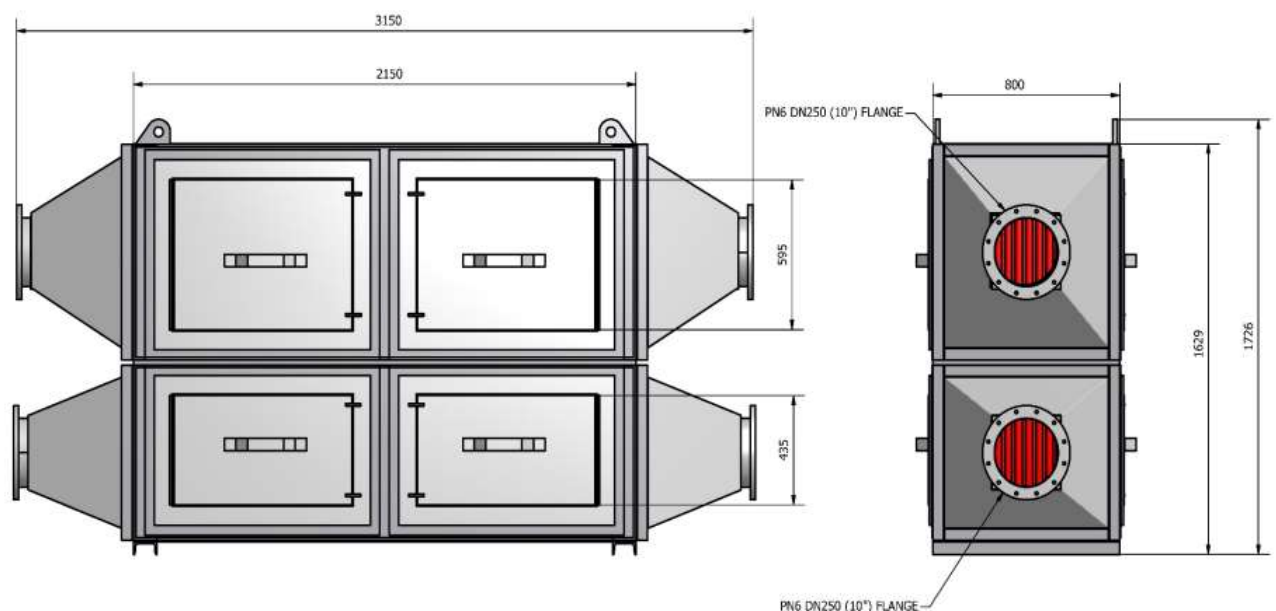


Figure 174: External dimensions of Experiment 3 HPHE.

Additional measurements needed for the calculations are below. Figure 174 provides a schematic of some external dimensions of the HPHE.

- Dimensions of HPHE core: 1,629 (h) x 800 (w) x 2,150 (d)
- Length of evaporator section with ducts = 3,174 mm
- Length of condenser section with ducts = 3,150 mm
- Height of evaporator section = 734 mm
- Height of condenser section = 895 mm

- Inclined length of evaporator lateral ducts= 570 mm
- Inclined length of evaporator vertical ducts = 570 mm
- Inclined length of condenser lateral ducts = 561 mm
- Inclined length of condenser vertical ducts = 547 mm
- Lengths at condenser duct transition= 290 x 290 mm
- Lengths at evaporator duct transition = 300 x 300 mm

The above was used to calculation the surface area of each section:

- Area evaporator inlet core and duct, $A_{e,1} = 3.65 \text{ m}^2$
- Area evaporator outlet core and duct, $A_{e,2} = 3.65 \text{ m}^2$
- Area condenser inlet core and duct, $A_{c,1} = 4.05 \text{ m}^2$
- Area condenser outlet core and duct, $A_{c,2} = 4.05 \text{ m}^2$

Constants used in the calculations include:

- Stefan-Boltzman constant, $\sigma_{SB} = 5.6696 \times 10^{-8} \text{ (W.m}^{-2}.\text{K}^{-4})$
- Emissivity value, $\varepsilon = 0.7$ (conservative value for metallic paint)
- Ambient temperature, $T_{\infty} = 293.15 \text{ K}$

The radiation equation for heat transfer rate is:

$$\dot{q}_{rad} = A\varepsilon\sigma_{SB}(T^4 - T_{\infty}^4) \quad (9.17)$$

Therefore,

$$\dot{q}_{e,1,rad} = A_{e,1}\varepsilon\sigma_{SB}(T_{e,1}^4 - T_{\infty}^4) = 9,626 \text{ W}$$

$$\dot{q}_{e,2,rad} = A_{e,2}\varepsilon\sigma_{SB}(T_{e,2}^4 - T_{\infty}^4) = 3,491 \text{ W}$$

$$\dot{q}_{c,1,rad} = A_{c,1}\varepsilon\sigma_{SB}(T_{c,1}^4 - T_{\infty}^4) = 3,140 \text{ W}$$

$$\dot{q}_{c,2,rad} = A_{c,2}\varepsilon\sigma_{SB}(T_{c,2}^4 - T_{\infty}^4) = 3,402 \text{ W}$$

$$\dot{q}_{total,rad} = \mathbf{19.66 \text{ kW}}$$

The natural convection equation for heat transfer rate is:

$$\dot{q}_{conv} = Ah(T - T_{\infty}) \quad (9.18)$$

The natural convection heat transfer coefficient, h is found by rearranging the Nusselt number Equation (3.8), which is found by [220]:

$$Nu = \left[Nu_0^{\frac{1}{2}} + \left[\frac{\frac{GrPr}{300}}{\left[1 + \left(\frac{0.5}{Pr} \right)^{\frac{9}{16}} \right]^{\frac{16}{9}}} \right]^{\frac{1}{6}} \right]^2 \quad (9.19)$$

The Grashof number is found by Equation (3.18). The Prandtl number is considered to be 0.70. Nu_0 is considered to be 0.67 [220].

$h = 7.139 \text{ W.m}^{-2}.\text{K}^{-1}$ at the mean temperature, $T_m = \frac{(T_w + T_\infty)}{2}$ (3664 K).

Therefore,

$$\dot{q}_{e,1,conv} = A_{e,1} h (T_{e,1} - T_\infty) = 5,948 \text{ W}$$

$$\dot{q}_{e,2,conv} = A_{e,2} h (T_{e,2} - T_\infty) = 3,339 \text{ W}$$

$$\dot{q}_{c,1,conv} = A_{c,1} h (T_{c,1} - T_\infty) = 3,235 \text{ W}$$

$$\dot{q}_{c,2,conv} = A_{c,2} h (T_{c,2} - T_\infty) = 3,408 \text{ W}$$

$$\dot{q}_{total,conv} = 15.93 \text{ kW}$$

Total losses are determined by:

$$\dot{q}_{losses} = \dot{q}_{rad} + \dot{q}_{conv} \quad (9.20)$$

Therefore,

$$\dot{q}_{losses} = 35.59 \text{ kW}$$